

Lecture Notes in Civil Engineering

Anurag Mudgal · Philip Davies ·  
Maria Kennedy · Guillermo Zaragoza ·  
Kiho Park *Editors*

# Advances in Water Treatment and Management

Select Proceedings of ICAWTM 2023

 Springer

# Lecture Notes in Civil Engineering

Volume 536

## Series Editors

Marco di Prisco, Politecnico di Milano, Milano, Italy

Sheng-Hong Chen, School of Water Resources and Hydropower Engineering,  
Wuhan University, Wuhan, China

Ioannis Vayas, Institute of Steel Structures, National Technical University of  
Athens, Athens, Greece

Sanjay Kumar Shukla, School of Engineering, Edith Cowan University, Joondalup,  
Australia

Anuj Sharma, Iowa State University, Ames, USA

Nagesh Kumar, Department of Civil Engineering, Indian Institute of Science  
Bangalore, Bengaluru, India

Chien Ming Wang, School of Civil Engineering, The University of Queensland,  
Brisbane, Australia

Zhen-Dong Cui, China University of Mining and Technology, Xuzhou, China

Xinzheng Lu, Department of Civil Engineering, Tsinghua University, Beijing,  
China

**Lecture Notes in Civil Engineering (LNCE)** publishes the latest developments in Civil Engineering—quickly, informally and in top quality. Though original research reported in proceedings and post-proceedings represents the core of LNCE, edited volumes of exceptionally high quality and interest may also be considered for publication. Volumes published in LNCE embrace all aspects and subfields of, as well as new challenges in, Civil Engineering. Topics in the series include:

- Construction and Structural Mechanics
- Building Materials
- Concrete, Steel and Timber Structures
- Geotechnical Engineering
- Earthquake Engineering
- Coastal Engineering
- Ocean and Offshore Engineering; Ships and Floating Structures
- Hydraulics, Hydrology and Water Resources Engineering
- Environmental Engineering and Sustainability
- Structural Health and Monitoring
- Surveying and Geographical Information Systems
- Indoor Environments
- Transportation and Traffic
- Risk Analysis
- Safety and Security

To submit a proposal or request further information, please contact the appropriate Springer Editor:

- Pierpaolo Riva at [pierpaolo.riva@springer.com](mailto:pierpaolo.riva@springer.com) (Europe and Americas);
- Swati Meherishi at [swati.meherishi@springer.com](mailto:swati.meherishi@springer.com) (Asia—except China, Australia, and New Zealand);
- Wayne Hu at [wayne.hu@springer.com](mailto:wayne.hu@springer.com) (China).

**All books in the series now indexed by Scopus and EI Compendex database!**

Anurag Mudgal · Philip Davies · Maria Kennedy ·  
Guillermo Zaragoza · Kiho Park  
Editors

# Advances in Water Treatment and Management

Select Proceedings of ICAWTM 2023

 Springer

*Editors*

Anurag Mudgal  
School of Technology  
Pandit Deendayal Energy University  
Gandhinagar, Gujarat, India

Philip Davies  
University of Birmingham  
Edgbaston, UK

Maria Kennedy  
IHE Delft Institute for Water Education  
Delft, The Netherlands

Guillermo Zaragoza  
Environment and Technology Research  
Centre for Energy  
Madrid, Spain

Kiho Park  
Department of Chemical Engineering  
Hanyang University  
Seoul, Korea (Republic of)

ISSN 2366-2557

ISSN 2366-2565 (electronic)

Lecture Notes in Civil Engineering

ISBN 978-981-97-5954-5

ISBN 978-981-97-5955-2 (eBook)

<https://doi.org/10.1007/978-981-97-5955-2>

© The Editor(s) (if applicable) and The Author(s), under exclusive license to Springer Nature Singapore Pte Ltd. 2024

This work is subject to copyright. All rights are solely and exclusively licensed by the Publisher, whether the whole or part of the material is concerned, specifically the rights of translation, reprinting, reuse of illustrations, recitation, broadcasting, reproduction on microfilms or in any other physical way, and transmission or information storage and retrieval, electronic adaptation, computer software, or by similar or dissimilar methodology now known or hereafter developed.

The use of general descriptive names, registered names, trademarks, service marks, etc. in this publication does not imply, even in the absence of a specific statement, that such names are exempt from the relevant protective laws and regulations and therefore free for general use.

The publisher, the authors and the editors are safe to assume that the advice and information in this book are believed to be true and accurate at the date of publication. Neither the publisher nor the authors or the editors give a warranty, expressed or implied, with respect to the material contained herein or for any errors or omissions that may have been made. The publisher remains neutral with regard to jurisdictional claims in published maps and institutional affiliations.

This Springer imprint is published by the registered company Springer Nature Singapore Pte Ltd. The registered company address is: 152 Beach Road, #21-01/04 Gateway East, Singapore 189721, Singapore

If disposing of this product, please recycle the paper.

# Organization

## Program Committee Chairs

Anurag Mudgal, Professor, Department of Mechanical Engineering, School of Technology (SoT), Pandit Deendayal Energy University (PDEU), India  
Kiho Park, Professor (Associate), Department of Chemical Engineering, Hanyang University, 222 Wangsimni-ro, Seongdong-gu, Seoul 04763, Republic of Korea

## Program Committee Members

Anurag Mudgal, Professor, Department of Mechanical Engineering, School of Technology (SoT), Pandit Deendayal Energy University (PDEU), India  
Kiho Park, Professor (Associate), Department of Chemical Engineering, Hanyang University, 222 Wangsimni-ro, Seongdong-gu, Seoul 04763, Republic of Korea

## Contributors

Jaeseok An, Chonnam National University, 77 Yongbong-ro, Buk-gu, Gwangju, 61186, Republic of Korea  
Dipak Ankoliya, Pandit Deendayal Energy University, Gandhinagar, Gujarat, India  
Pravesh Chandra, Assistant Professor, MIT Moradabad, Uttar Pradesh, India  
Gyusang Cho  
Jingyeong Im Chonnam National University, 77 Yongbong-ro, Buk-gu, Gwangju, 61186, Republic of Korea  
Jeong, Yuhyeok, Chonnam National University, 77 Yongbong-ro, Buk-gu, Gwangju, 61186, Republic of Korea  
Heun Se Kim

Gunyoung Kim

Dong Gi Lee, Chonnam National University, 77 Yongbong-ro, Buk-gu, Gwangju, 61186, Republic of Korea

Vima Mali, Pandit Deendayal Energy University, Gandhinagar, Gujarat, India

Varsha Mudgal, Pandit Deendayal Energy University, Mechanical Engineering, Gandhinagar, India

Anurag Mudgal, Professor, Department of Mechanical Engineering, School of Technology (SoT), Pandit Deendayal Energy University (PDEU), India

Sunyoung Oh, Chonnam National University, 77 Yongbong-ro, Buk-gu, Gwangju, 61186, Republic of Korea

Dhaval Patel, Pandit Deendayal Energy University, Mechanical Engineering, Gandhinagar, India

Milan Raninga, Pandit Deendayal Energy University, Gandhinagar, Gujarat, India

Suji Son

Yinseo Song

Soowon Son

# Preface

This book consists of selected papers presented at the 2nd International Conference on Advances in Water Treatment and Management (ICAWTM 23), held on March 11–12, 2023, at Pandit Deendayal Energy University (PDEU), Gandhinagar, Gujarat India. The papers represent the research work in the water treatment fields using the technologies of constructed wetland, membrane technologies, adsorption, coagulation, electrocoagulation and photo-assisted degradation of contaminants. It contains the treatment and management of wastewater from textile industry, domestic wastewater, landfill leachate and dairy industry. It focuses on the water contaminants including heavy metals, Chlorpyrifos, endocrine disrupting chemicals and Toluene, the bio-based adsorbent like aerial roots of banyan tree, banana peel and agricultural waste-derived activated carbon ash. It also highlights the machine learning tool for the water quality assessment and indexing and environment impact using life cycle assessment tool. Apart from water and wastewater treatment, it also includes water resources management analysis, flood risk management, watershed analysis and geo-thermal system. The papers were presented by the academicians, research scientists and experts from the reputed institutions and universities in the field of water treatment and management.

Gandhinagar, India  
Edgbaston, UK  
Delft, The Netherlands  
Madrid, Spain  
Seoul, Korea (Republic of)

Anurag Mudgal  
Philip Davies  
Maria Kennedy  
Guillermo Zaragoza  
Kiho Park

# Contents

<b>Treatment of Domestic and Industrial Wastewater with Constructed Wetland—A Review</b> .....	1
Varsha Mudgal, Milan Raninga, Dhaval Patel, Dipak Ankoliya, Anurag Mudgal, Jatin Patel, Vivek Patel, Rajeev Srivastava, Suphiya Khan, and Dinesh Kumar	
<b>Synthesis and Characterization of Amine-Functionalized Zeolite 4A for Wastewater Treatment</b> .....	19
Megha Parmar, Mahuya Bandyopadhyay, Rama Gaur, and Syed Shahabuddin	
<b>Flood Risk Management Using HecRAS Model for the Planning of Artificial Levees as a Structural Measure: A Case Study of Upper Sabarmati River Basin, Gujarat, India</b> .....	31
Shibani Chourushi, Pradeep P. Lodha, and Indra Prakash	
<b>Modification of Graphene as an Effective Photo-Driven Catalyst for Photo-Assisted Degradation of Chlorpyrifos</b> .....	49
Jinal Patel, Syed Shahabuddin, and Rama Gaur	
<b>Air Quality Index Management of Medium-Sized Community Space in Gurugram, Haryana</b> .....	61
Vivek Jaiswal, Shubham Singh, and Sanjay Maurya	
<b>Application of MOFs in Membrane Modification for Treatment of Wastewater: A Review</b> .....	69
Sapna Ajay Gawali, Sunskrati Pandey, Het Tilala, Kashyap Tailor, Swapnil Dharaskar, Nagarjuna Reddy Paluvai, Swapna P. Reddy, Manish Kumar Sinha, and Surendra Sasi Kumar Jampa	
<b>Identification of Sensitive Region by Short Term Shoreline Change Analysis Over Gulf of Khambhat, Gujarat</b> .....	97
Keval H. Jodhani, Dhruvesh Patel, and N. Madhavan	

<b>Water Consciousness and Indian Cinema: A Critical Discourse Analysis of Select Hindi Language Movies</b> .....	115
Amrita Chakraborty and Sunayan Bhattacharjee	
<b>Characteristic Analysis of Oil-Field-Produced Water</b> .....	129
Om Patel, Arth Padaria, Akshay Gupta, Balasubramanian Ragunathan, and S. Vinod Kumar	
<b>Treatment of Wastewater Using Conducting Polymer/Magnetite (Fe<sub>3</sub>O<sub>4</sub>) Based Magnetic Adsorbent Materials</b> .....	141
Krunal Baria, Krunal Parekh, and Syed Shahabuddin	
<b>Potential Impacts of Landfill Leachate on the Quality of Groundwater Bodies</b> .....	159
Jagriti Patel, Sanskriti Mujumdar, and Vijay Kumar Srivastava	
<b>Batch Reverse Osmosis: Evolution from the Concept to the Technology</b> .....	175
Dhaval Patel, Dipak Ankoliya, Milan Raninga, Anurag Mudgal, Vivek Patel, Jatin Patel, Varsha Mudgal, and Himanshu Choksi	
<b>Breaking of Butyric Acid–Water Azeotrope: Experimental Analysis on Air Gap Membrane Distillation</b> .....	201
Rajeshwar Kholapure, Kailash Singh, Sushant Upadhyaya, and Divya Gaur	
<b>Life Cycle Assessment of Electrocoagulation Pilot Unit for Dairy Wastewater Treatment</b> .....	211
Dipak Ankoliya, Milan Raninga, Dhaval Patel, Varsha Mudgal, Prashanthi Vallamsetty, Anurag Mudgal, Manish Kumar Sinha, Vivek K. Patel, Jatin Patel, Himanshu Choksi, and Prasanta Dey	
<b>Presence of Endocrine-Disrupting Chemicals (EDCs) in Water, Health Impacts, and Its Treatability—A Review</b> .....	225
Dipti Christian, M. A. Shabiimam, Hetvi Dani, and Jesic Patadiya	
<b>Electrochemical Coagulation of Wastewater Using Aerial Roots of Banyan Tree as Adsorbent</b> .....	239
Sachin Mane and Pratiksha P. Patil	
<b>Analysis of Groundwater Quality in the Coastal Stretch of Bhavnagar, Gujarat</b> .....	249
Nayankumar P. Soni, S. D. Dhiman, and Singh Garima Shailendra	
<b>Surface Water Quality Assessment of Lakhisarai Stretch of Kiul River in Bihar</b> .....	267
Gaurav Kumar and Neeta Kumari	

<b>Decolorization of Textile Wastewater Using the Electrocoagulation Process</b> .....	279
M. A. Shabiiimam and Tirtha Trivedi	
<b>Membrane Desalination of Wastewater for the Contaminant Removal and Reduction of Fouling</b> .....	303
S. Vinod Kumar, Balasubramanian Ragunathan, and K. Nishant	
<b>Emerging Water Desalting Technologies: Current Status, Challenges, and Future Trends</b> .....	313
M. A. Shabiiimam, Jay Dhorawala, and Tirtha Trivedi	
<b>A Conceptual Model of the Tulsishyam Hot Springs' Geothermal System, Gujarat, India</b> .....	333
Namrata Bist, Kriti Yadav, and Anirbid Sircar	
<b>Extraction of Geothermal Water Using Directed Energy Method of Millimeter-Wave Technology</b> .....	341
Anirbid Sircar, Abhishek Nair, Namrata Bist, Kriti Yadav, Vaishnavi Pandey, Neel Shah, and Bhavy Chotaliya	
<b>Machine Learning-Based Predictive Models for Water Quality Index—An Analysis and Comparison</b> .....	355
Vaishvi Shah, Ashwini Ramanuj, Krishna Patel, Shruti Jethloja, Debabrata Swain, and Manish Kumar	
<b>Evaluation of Groundwater Quality in an Urbanized Watershed with a Special Reference to Heavy Metal Concentration</b> .....	369
Apurva Marathe and Prakash Samnani	
<b>Identifying Climate Hotspots from Spatiotemporal Variation of Exposure Indicators for Southern Agro-Climatic Zone in Gujarat State, India</b> .....	385
Daksh H. Soni and Geeta S. Joshi	
<b>Utilizing Agricultural Waste-Derived Activated Carbon Ash with Rapid Microwave Digestion Method to Treat Industrial Waste Water</b> .....	409
Khushbu G. Patel, Pranav Saraswat, Nirendra M. Misra, and Tarun M. Patel	
<b>Integrated Assessment of Groundwater of Dudhwada Village of Padra Taluka with Special Reference to Industrial Pollution</b> .....	425
Dhruvi Rana and Sanskriti Mujumdar	

<b>Toluene–Water Removal from Synthetic Water Using Air Gap Membrane Distillation</b> .....	435
Divya Gaur, Sushant Upadhyaya, Kailash Singh, and Rajeshwar Kholapure	
<b>Experimental Study for Removal of Pb and Cu from Industrial Wastewater by Using Low-Cost Adsorbent (Banana Peel)</b> .....	449
Sachin Mane, Sanjana Hibare, and Pooja Kumbhare	

## About the Editors

**Prof. Anurag Mudgal** is a professor at the Mechanical Engineering Department at Pandit Deendayal Energy University (PDEU), Gujarat, India. He has more than 26 years of teaching and research experience and more than four years of experience in the industry. He is a mechanical engineer with a Master's degree in Thermal Engineering. He also completed his MBA in operation management. He was awarded his Ph.D. in 2010 from the Indian Institute of Technology (IIT) Delhi. His research interests include water desalination, application of renewable energy, Heat transfer systems, cooling, food preservation, and other sustainable environmental issues. He published more than 45 papers in journals and conferences. He handled more than nine projects from DST, DBT, and various institutes across India.

**Prof. Philip Davies** is currently a professor of water technology and professorial researcher at the School of Engineering, University of Birmingham, UK, where he is pursuing research topics and innovations in the areas of water purification and the water-energy-food nexus. He qualified with a B.Sc. (First Class Honours) in Mechanical Engineering from Imperial College. He gained D.Phil. in biomedical engineering at the University of Oxford. He has extensive publications and leading R&D projects. He has over 35 years of academic and industrial research experience. His research areas include desalination and water reuse, solar-powered cooling using seawater, seawater greenhouse technology, and negative emissions technologies. He participates in several international collaborations in regions including North Africa, the Middle East, and the Indian subcontinent.

**Prof. Maria Kennedy** [B.Sc. (Hons.) in Industrial Chemistry and Ph.D. from the University of Limerick, Ireland] is a professor of water treatment technology at IHE Delft Institute for Water Education. She has 11 years of research experience and currently specializes in research and development in the field of membrane technology, including microfiltration, ultrafiltration, reverse osmosis, and electro dialysis for potable and industrial water treatment and water reuse. Her main research areas of interest are membrane fouling (indices), membrane scaling, and cleaning. Professor

Kennedy is also involved in international training projects in Israel (West Bank) in the field of desalination of brackish/seawater.

**Dr. Guillermo Zaragoza** is a senior researcher in Centre for Energy, Environment and Technology Research (CIEMAT), at the Department of Energy of CIEMAT, where he is the head of the Solar Thermal Applications R&D unit of Plataforma Solar de Almería (PSA), Spain. He obtained Ph.D. in Physics (University of Granada, 1996). At PSA, he leads the research group of solar desalination, and his particular expertise is on the topic of membrane distillation. He leads the Working Group on Renewable Energy Desalination at the Water Europe platform. He is an editorial board member of the *Journal of Water Process Engineering*.

**Dr. Kiho Park** is currently an assistant professor at Chonnam National University, South Korea. He was awarded his B.S., master, and Ph.D. in Chemical and Biological Engineering from Korea University. He worked as research fellow at the Department of Civil Engineering, University of Birmingham, and a research professor at Korea University. He was honoured with Hoimyung Graduate Research Award at KICChE in 2017 Fall Meeting. He published more than 41 research papers in journals and conferences. He has more than five years of teaching and research experience. His research interests include desalination, crystallization, water purification technologies, seawater desalination, membranes, membrane distillation, and modelling.

# Treatment of Domestic and Industrial Wastewater with Constructed Wetland—A Review



Varsha Mudgal , Milan Raninga, Dhaval Patel, Dipak Ankoliya, Anurag Mudgal, Jatin Patel, Vivek Patel, Rajeev Srivastava, Suphiya Khan, and Dinesh Kumar

## 1 Introduction

Developed countries treat about 70%, developing countries treat 38–28%, and low-income countries treat only 8% of the wastewater (WW) they generate. Globally about 80% of all WW discharged without proper treatment [1]. This untreated domestic wastewater (DWW) and industrial wastewater (IWW) pollute the water bodies and disturb sustainability of the aquatic flora and fauna which affects human health [2]. To achieve sustainable development (proper sanitization along with wastewater treatment (WWT) and reuse of treated water) in small and rural areas, decentralized WWT systems is economically good option for domestic, agriculture, and industrial WWT [3–5]. Constructed wetlands (CW) perform excellent for DWW as well as IWW treatment in decentralized sanitation concepts. Warm climate supports growth of plants, microbes, and processes inside wetland [6]. CWs can efficiently remove suspended solids, dissolved organic and inorganic pollutants, and pathogens [7]. CWs are simple to operate with changing water flow and number of pollutants and can produce an economically valuable crop as an additional benefit [8]. Almost 70% of all freshwaters globally used in the agriculture sector, and the

---

V. Mudgal (✉) · M. Raninga · D. Patel · D. Ankoliya · A. Mudgal · J. Patel · V. Patel  
Pandit Deendayal Energy University, Gandhinagar, Gujarat, India  
e-mail: [varsha.mudgal@sot.pdpu.ac.in](mailto:varsha.mudgal@sot.pdpu.ac.in)

A. Mudgal  
e-mail: [anurag.mudgal@sot.pdpu.ac.in](mailto:anurag.mudgal@sot.pdpu.ac.in)

R. Srivastava  
GB Pant Agricultural University, Pantnagar, Uttarakhand, India

S. Khan  
Banasthali University, Rajasthan, India

D. Kumar  
Central University of Gujarat, Gandhinagar, Gujarat, India

production of crops need to expand approximately 70% by 2050 [9]. Reuse of treated WW is now essential to cope with increasing demand of water for irrigation.

CW is a sustainable and low-cost solution for domestic and industrial WWT. This review discussed about plant, media, hydraulic loading rate (HLR), hydraulic retention time (HRT), and effectiveness of microorganisms, along with cost analysis. Author compared more than 80 research studies from around the world, in various ways to find the best possible solution for domestic and industrial WWT (winery, textile, paper, and dairy) with CW.

CWs divided into three categories (Fig. 1), namely surface flow (SFCW), subsurface flow (SSFCW), and hybrid (HCW). In SFCW, the WW flooded on the surface (20–40 cm) [10, 11]. In SSFCW, water flows beneath the surface through porous media, plant roots, and attached microbes [12, 13]. SSFCW can treat raw sewage with integrated sludge management, useful in decentralized WWT [6]. SSFCW further classified into horizontal flow (HFCW) and vertical flow (VFCW). HFCW is easy to run and maintain but required large space. In VFCW water discharged on entire wetland surface evenly, and with batch feeding of water more oxygen available to microbes, which favours removal of nitrogen, Biochemical Oxygen Demand (BOD) and Chemical Oxygen Demand (COD). It requires less space than HFCW but is expensive to run and maintain. In hybrid CW, combinations of different CWs used to get benefit of more than one type of wetland and to treat different type of wastes [11]. CWs have three components: filter media, plant, and microorganism.

Media consists of layers of gravel and sand to support the plant roots. The size of particle and the porosity of the substrate should be such that it supports the required HRT, and microorganisms can take advantage of oxygen in rhizosphere of plants and maintain hydraulic conductivity in the filter systems [13]. Ion-exchange substrates used to enhance removal of ammonium nitrogen, e.g. biochar [14], zeolite [15], vermiculite [16], and rice husk [14].

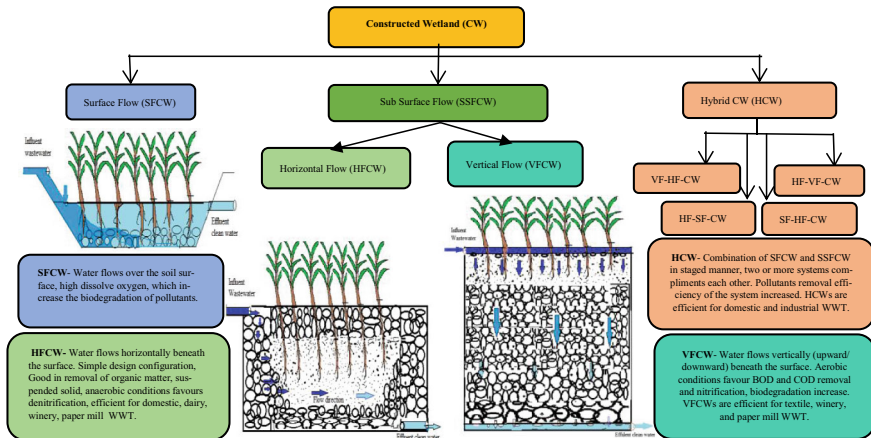


Fig. 1 Types of constructed wetlands

Removal of phosphorus takes place mainly by the substrate used in the CW. Phosphorus either adsorbed or precipitated by the chemical or minerals present in the media of the filter bed. Media which contain minerals of aluminium, iron, and calcium ( $\text{Fe}_2\text{O}_3$ ,  $\text{CaO}$ ,  $\text{MgO}$ ,  $\text{Al}_2\text{O}_3$ , and  $\text{CaCO}_3$ ) enhance phosphorus removal in CW [15, 17], like light expanded clay aggregates (LECA) [18], ceramsite [4, 19], and drinking water treatment sludge composite substrate (DWTSCS) [20]. A ceramsite substrate prepared from coal fly ash (CFA), waterworks sludge (WS), and oyster shell (OS).  $\text{Al}_2\text{O}_3$  content of WS may promote the formation of high strength mullite, while oxides of calcium, iron, magnesium, and sulphur of CFA may reduce the sintering temperature. It increased the phosphorus absorption in CW up to 90% [4]. Waste materials like alum sludge, tyre chips, and crushed red/fly-ash brick [21] are alternative substrates to increase the phosphorus absorption and for better waste disposal. DWTSCS prepared with drinking water treatment sludge (DWTS), bentonite, zeolite, and fly ash and increases the phosphorus removal up to 68% in CW at 1 day HRT [20].

Pollutant removals efficiency (PRE) for BOD, COD, nitrogen, phosphorus, and other pollutants determined by the equation

$$\text{PRE} = [(C_i - C_e)/C_i] \times 100\%$$

where  $C_i$  is the concentration of the pollutant in the influent (mg/L), and  $C_e$  is the concentration of the pollutant in the effluent (mg/L) [4]. Vegetation type plays a vital role on PRE. Around oxygenated area of the root, microbes digest the organic material and utilize it for their growth. The higher removal of organic matter by the cattails than common reed is due to a more vigorous root system [10, 16, 22–24]. Plants also improve aesthetic value of the area. Harvesting of plant biomass is necessary to maintain the PRE of CW and to prepare valuable products from the biomass.

Microbes are the real factor of biological pollutant removal inside CW. Various bacteria take part in decomposition and biodegradation of pollutants. These are alpha-proteobacteria (from Rhizobiales, Rhodospirillales order), beta-proteobacteria (from Burkholderiales, Rhodocyclales order), and gamma-proteobacteria (from Pseudomonadales, Enterobacteriales, and Xanthomonadales order) [25]. Microorganisms can use organic compounds in the WW as a nutrient, through enzymatic reactions [26]. Bacterial strains *Microbacterium arborescens* TYSI04 and *Bacillus pumilus* PIRI30 are useful in textile WW degradation and support the plant growth in VFCW [27]. Gradual increment in the WW concentration helps to increase the microbial tolerance for the toxic substances [28].

Various factors affecting performance of CW are temperature, HLR, and HRT. Biological degradation of pollutant takes place with the help of plants and microbes which in turn require a specific temperature for survival, growth, and activity. Thus, temperature plays an important role in PRE of CW. Seasonal variation in nitrogen removal efficiency of the wetlands linked with temperature.

Author observed 6 to 11% higher nitrogen removal in CW during summer than in winter [29]. Ammonification and nitrification decreased at low temperature [30].

Removal of nitrogen lower 27% in winters than in summers, and activity of denitrifying bacteria slow down below 10 °C and almost stops below 6 °C [31]. The rate of ammonification increased 1–3.5 times with every 10 °C rise in temperature, from 0 °C to 30 °C, and denitrification rates almost double with every 10 °C rise [32]. PRE of CW at low temperature can be increased with insulation, artificial aeration, and augmentation with suitable microbes [33]. Temperature above 15 °C supports the growth and functioning of microbes which are responsible for removal of total Kjeldahl nitrogen (TKN) and ammonia nitrogen [22]. Continuous high temp during the summer causes higher water losses via evapotranspiration. This leads to increase the salinity inside CW. Selection of plants is important to minimize the evapotranspiration. Local wetland plants with low transpiration and high biomass productivity should be preferred to grow in CWs, in such areas [6].

Plants were providing a buffer against hydraulic loading increment; hence, systems can achieved higher nitrogen and organics removal even at high organic loading [15]. Lower HLR and higher HRT improved the PRF of CW [33]. Author suggested that HLR should be less than 0.1 m/day for SFCW (5–30 days HRT) and less than 0.5 m/day for SSFCW (2–5 days HRT) [5]. HRT is the duration, water resides in the CW. It is an important variable in designing and evaluating the treatment performance of a CW system [34]. The nitrate and TKN removal increased up to 3 times when retention time increased from 1 to 2 days [35]. On comparing PRE for tertiary effluent of STP with SFCW at four different HRTs (0.3, 0.8, 2.3, and 9.3 days), found that PRE of the system enhanced with increasing the HRT [36]. PRE decreases as the loading increases and HRT decreases [22]. PRE of CW treating winery WW increases with increasing HRT. COD removal increased from 60 to 80% with increased HRT from 7 to 14 days [37]. Nitrogen removing capacity of a ditch wetland compared at three HRTs (0.5, 1, and 2 days) and found that on increasing HRT from 0.5 to 2 days, nitrate and COD removal efficiency increased from 50% to 98% and 20% to 80%, respectively [19]. COD and phosphorus removal increased by 4% and 9%, respectively, as HRT increased from 1 to 5 days, in a slope wetland, to treat polluted river water [38].

## 2 Role of CW in Treatment of Domestic and Different Industrial Wastewaters

CW can be used for sewage, sludge dewatering, agricultural runoff, landfill leachate, acid mine drainage, and industrial effluent of oil mills, fisheries, piggyery, textile, abattoir, tannery, sugar industry, winery, rubber industry, pulp and paper mills, dairy, seafood processing, potato processing, steel processing, olive mills, petroleum refineries for secondary or tertiary treatment of their WW, removal of azo dyes, and endocrine disrupting chemicals [39] and also for removing of hormones and pharmaceutical compounds [40]. In coastal regions, seawater infiltrate into sewage system and TDS of DWW become high. CW with *Typha* spp. achieved constant high PRE in DWW treatment at such places [41]. CW requires a sedimentation or septic tank as pre-treatment unit, for effective treatment of WW. CW effluent satisfies the safe

discharge of WW and its reuse regulations [42]. Effluent of centralized ETP (CETP) contains high refractory organic matter and low biological degradable contents. PRE of the HCW for treatment of secondary effluent of CETP shows good nitrifying and denitrifying capacity [43]. Table 1 shows that CW can efficiently treat DWW and different IWW.

## 2.1 Treatment of Domestic Wastewater

SFCW planted with *Cyperus* investigated at 4 days HRT, to treat STP effluent. The system reduces up to 83% COD and 81% nitrate [24]. STP effluent treated with VFCW under varying conditions (planted/unplanted, gravel/vermiculite, and continuous/batch mode). PRE of planted beds (76% COD and 85% BOD) was more than unplanted one (29% COD and 37% BOD). Batch feeding with vermiculite media support ammonia and phosphorus removal [16]. Municipal WW treated with an up-flow anaerobic filter (UAF) followed by a HFCW, planted with *Canna* and *Strelitzia*. System removed 85% COD, 79% BOD, 30% total nitrogen (TN), and 24% total phosphorus (TP), at 3 days HRT. In this system, UAF helps to reduce area requirement for HFCW [34]. VFCW planted with *Phragmites* to treat DWW investigated at 3 days HRT and found the system reduced 86% COD and 85% BOD and the treated water used for irrigation [10]. Gravel with zeolite or ceramsite were good substrate for nitrogen removal from municipal sewage, gradually increment in WW strength helpful for microbial enrichment [19]. CW can treat DWW efficiently and remove total suspended solids (TSS), COD, BOD, total nitrogen (TN), total phosphorus (TP), and bacteria up to 87%, 89%, 93%, 70%, 72%, and 4.0 log<sub>10</sub>, respectively [40]. On comparing results of different researches, it is found that for DWW and STP effluent treatment, HFCW is more efficient than VFCW, at 3–4 days HRT. Efficiency of VFCW to treat DWW increased with batch feeding, vermiculite media, and coupling with HFCW.

## 2.2 Treatment of Textile Industry Wastewater

The WW from textile mills contains colours and organic chemicals related to dyeing and finishing of the fabric. It is very toxic due to presence of heavy metals like copper, arsenic, lead, cadmium, mercury, nickel, and cobalt [44]. HCW (two VFCW and a HFCW) with coarse and fine sand examined for colour and PRE of textile WW, at two days HRT and found 90% decolourisation and high PRE for COD (84%), total organic carbon (TOC) (89%), and sulphate (88%) [45]. Bacteria support the plant growth and textile effluent degradation as more COD, BOD, and colour removed in inoculated units [27]. 90–94% colour removed from textile WW in CW with rice husk biochar and microbes and planted with *Prescaria* [14].

**Table 1** Constructed wetlands and wastewater treatment

S. No	WW type	Wetland type	Plant	Media	BOD (mg/l)		COD (mg/l)		NH <sub>4</sub> -N (mg/l)		Reference
					In	Out	In	Out	In	Out	
1	STPE	SFCW	<i>Cyperus</i>	S	–	–	484	75.5	68	38	[24]
2	STPE	HFCW	<i>Canna</i> and <i>Sireltzia</i>	Tezontle	243.84	47.63	537.77	76.88	–	–	[34]
3	STPE	VFCW	<i>Phragmites</i>	G or vermiculite	253	38	465	110	33	21	[16]
4	DWW	VFCW	<i>Phragmites</i>	G + S	145.5	19.8	281	38.4	89.9	16	[10]
5	STPE	HFCW	<i>Canna</i>	G + zeolite/ceramsite/volcanic rock	–	–	200	30	20	12	[19]
6	ICETP	HCW (VF + HF)	<i>Phragmites</i>	G	–	–	36	24	2.46	0.42	[43]
7	Textile	HCW (VF + HF)	<i>Phragmites</i>	S	198	66	771	122	2.4	10	[45]
8	Textile	HCW (VF + HF)	<i>Phragmites</i> , <i>Dracaena</i>	Sugarcane Bagasse	2705	134	12,625	1430	158	30	[46]
9	Textile	VFCW	<i>Typha</i>	G + S + Soil + Coconut	207	47	410	85	–	–	[27]
10	Textile	VFCW	<i>Prescaria</i>	Soil + Rice husk + microbes (90% CR) Soil + biochar of Rice husk + microbes (94% CR)	–	–	–	–	–	–	[14]
11	Textile	VFCW	<i>Phragmites</i>	G	–	–	167	93	–	–	
12	Textile	TEWS Tank1— <i>Eichhornia</i> Tank 2— <i>Hydrilla</i> , Tank 3— <i>Pistia</i>		5 cm at bottom, Tank1 + 2—lake sediments, tank 3—fine sand (76% CR)	–	–	292	57	30.2	17	[47]
13	Dairy	VFCW	<i>Typha</i>	G	52–160	9–17	108–193	10–13	34–46	0.41–00	[35]
14	Dairy	HCW (VF + VF + HFCW)	<i>Phragmites</i>	G + S	1574	138	4425	323	77	22	[51]
15	Dairy	HFCW	<i>Phragmites</i>	G	–	–	2368	559	16.39	4.09	[52]

(continued)

Table 1 (continued)

S. No	WW type	Wetland type	Plant	Media	BOD (mg/l)		COD (mg/l)		NH <sub>4</sub> -N (mg/l)		Reference
					In	Out	In	Out	In	Out	
16	Dairy	HFCW	<i>Typha</i>	Clay aggregate	-	-	157	23	17.3	0.48	[18]
17	Dairy	VFCW	<i>Phragmites</i>	G + S	-	-	2100	134	-	-	[54]
18	Dairy	VFCW	<i>Juncaceae</i>	G + S	-	-	2100	154	-	-	[54]
19	Dairy	HFCW	<i>Typha</i>	G	90	35	269	81	86	60	[55]
20	Winery	HFCW	<i>Typha + Scirpus + Phragmites</i>	G	-	-	14,000	500	-	-	[57]
21	Winery	HF + HFCW	<i>Typha, Scirpus</i>	G	522	116	1183	260	-	-	[23]
22	Winery	HCW (HF + VFCW)	unplanted	S + sediments of CW treating winery ww	-	-	15,800	180	-	-	[28]
23	Winery	HCW (FR + HF + SFCW)	<i>Phragmites</i>	G	-	-	3777	67	-	-	[59]
24	Winery	HCW (VF + HF + SFCW)	VF— <i>Phragmites</i> HF— <i>Canna</i> SF— <i>Iris, Scirpus</i>	G	1243	65	2020	94	3.7	0.3	[60]
25	Paper	HFCW	<i>Typha + canna</i> 84–92% CR	CS	337	51	1,070	136	-	-	[64]
26	Paper	HFCW	<i>Canna</i>	G + S	248	17	1011	122	-	-	[65]
27	Paper	VFCW	<i>Phragmites</i>	G + S	230	58	981	265	-	-	[66]
28	Paper	VFCW	<i>Typha</i>	G + S	230	51	981	193	-	-	[66]
29	Paper	VFCW	<i>Typha</i>	G + S	276	25	342	27	-	-	[67]
30	Paper	CW	<i>Scirpus</i>	Gravel + Sand (55% CR)	-	-	110	39	-	-	[68]

CR—colour removed, CS—coarse sand, DW—domestic wastewater, G—gravel, S—sand, STPE—sewage treatment plant effluent, IGETP—Industrial common effluents treatment plant, HFCW—horizontal flow CW, VFCW—vertical flow CW, HCW—hybrid CW, TEWS—tri-phasic engineered wetland system

Two HCW (VFCW with sugarcane bagasse + HFCW with Sylhet sand) evaluated for textile WWT, under high hydraulic loadings with HRTs of 0.2–1.8 days for VFCW and 0.7–7.1 days for HFCW. The results show that the VFCW removed BOD (79%) and ammonia (66%), while HFCW facilitated efficient colour removal (91%). The carbon (C) of sugarcane bagasse in VFCW helps in denitrification [46]. VFCW planted with *Phragmites* was efficient in colour (85–100%) and COD (80%) removal at low loading rate with high resting time (2–4 days) for textile WW [47]. A tri-phasic (3 tanks) engineered wetland system (TEWS) designed to treat textile WW with continuous feeding mode. First tank was anaerobic facilitate denitrification, second tank was aerobic and helps in nitrification and third tank for final water polishing. Complete TEWS removed 76% colour and 87% COD [48]. In the view of above researches, it is concluded that hybrid CWs with plants, when operated at low HLR and high HRT (4 days), are good to treat textile WW. Augmentation of specific microbes helps to increase colour, COD, and heavy metals removal.

### 2.3 Treatment of Milk Processing Plant Effluent

WW in food industry especially in dairy industry changed according to the product (e.g. pasteurized milk, sweet whey, curd, butter, cheese, and sweet). Main constituents of dairy WW are proteins (casein), sugar (lactose), and fat along with waste from washing and cleaning line (inorganic salts, detergents, and sanitizers). Dairy wastes undergo rapid fermentation and form lactic acid due to which it becomes acidic. All these components contribute towards their high BOD and COD [49].

VFCW evaluated for tertiary treatment of dairy WW at four different HRTs, efficiency of the system increased from 16 to 84% for BOD, 15% to 89% for COD, and 11.61% to 46.36% for phosphate, as the HRT increased from 1 to 4 days [35]. Hybrid CW system showed satisfactory results in dairy WW treatment and removes 83–96% COD; 65–92% nitrogen; 52–99% phosphorus. HFCW also shows good pollutant removal efficiency with dairy WW [50]. Hybrid SSFCW system built with a configuration of VF-VF-HF beds in series for the treatment of 4.5 m<sup>3</sup>/d WW from dairy unit in continuous flow mode. The hybrid system efficiently removes pollutant (reduced 88% COD and 89% BOD), even during winter and with variable loading rate [51]. HFCW studied to reduce area and clogging caused by highly polluted dairy effluent, with gravel and plastic substrate. Units with plastic media show better performance even with higher hydraulic load and reduce the area requirements by 75% [52]. Performance of HFCW evaluated for dairy WW at seven days HRT and planted with *Phragmites* and *Typha*, and the main media was LECA, which has high porosity and low cost. Wetland removes 75% COD and 96% NH<sub>4</sub>-N, and *Typha* plants are more efficient for effluent of dairy industry [18]. Removal of organic pollutants increased in lab-scale VFCW, planted with *Canna*, contains *Eisenia fetida* (common composting earthworm), and did not clog with synthetic dairy WW [53]. Dairy WW treatment efficiency of VFCW compared in three units: (1) unplanted, (2) planted with *Phragmites*, and (3) planted with rushes (*Juncaea* spp.), with 6 days HRT.

Planted beds remove pollutant more efficiently, as 67.62%, 93.62%, and 92.33% reduction in COD, observed in beds number 1, 2, and 3, respectively [54]. A pilot-scale HFCW planted with *Typha* investigated, for tertiary treatment of dairy WW, at 7 days HRT. System removed 78.4%, 57.9%, and 68.7% suspended solids, BOD, and COD, respectively [55]. It is concluded from the studied researches that, after pre-treatment, dairy WW can efficiently treated (68–93% COD removal) with SSFCW at 4–7 days HRT.

## 2.4 Treatment of Winery Wastewater

One litre of wine generates 0.2–4 L of WW. The main chemical responsible for high COD in wineries WW is ethanol, short-chain volatile fatty acids, and phenolic compounds. The concentration of sodium was higher in the growing season of grapes, while organic compounds were higher during harvest season [56]. CW reduced more than 90% COD in winery effluent at 14 days HRT, and the treated water provides enough nutrition to cabbage fields [57]. The planted bed of CW in greenhouse treats winery and sugarcane WW and reduces COD 70% and 78% for 2.5- and 5-days HRT, respectively, after 3 weeks of growth, reduced 80% of COD. Field experiment also replicates the greenhouse findings [23]. *Typha*, *Juncus*, and *Scirpus* plants have higher ability to absorb sodium and can grow in WW with high COD. All these qualities help them to perform better in phytoremediation of winery WW [58]. Incremental priming (slowly increase the WW concentration) is helpful in acclimatization of microbial populations and increases the tolerance of the residing microbial consortia for potentially toxic substances even at higher concentrations during the treatment of winery WW. CWs were bi-weekly inundate with winery WW and followed by drainage. Primed system reduced COD 98% while unprimed system 81% [28]. Winery WW treated with a unique combination of four-stage hybrid CW, in which WW enters in French Reed Bed, then in HFCW followed by SFCW and finally in sand filter. HRT of the system varies (6–7 days) according to load. These all together reduced COD up to 96% and *Phragmites* flourished well without any toxic effect [59]. Winery WW treated with hybrid CW—VFCW (with *Phragmites*) + HFCW (with *Canna*) + SFCW (with *Iris*, *Nymphaea*, and *Scirpus*). Hybrid system has HRTs of 0.16, 4.5, 3.75 days for VFCW, HFCW, and SFCW, respectively. This system reduces 81%, 69%, 56%, 38% of COD, TSS, TN, and phosphate, respectively. CW effluent used to irrigate adjacent green area and growing plants did not show any phytotoxic effect [60]. Studied researches indicate that hybrid CWs perform better in removal of ethanol, volatile fatty acids, and phenolic compounds of the winery WW with 70–99% COD removal and HRT usually more than six days.

## 2.5 Treatment of Pulp and Paper Industry Wastewater

Pulp and paper industry effluent contains compounds of sodium, calcium, and magnesium which causes high BOD, COD, and pH. Approximately 240–450 m<sup>3</sup> water required for one tonne of the paper. The brown colour of effluent is due to lignin compounds [61]. After bleaching process, chlorolignin compounds discharged in first extraction effluent, due to which it is highly coloured and causes 80% colour, 30% BOD, and 60% COD of paper mills effluent. Aquatic flora and fauna of the stream adversely affected by this polluted coloured effluent [62]. Lignin and its derivatives release phenols after degradation. SSFCW planted with *Phragmites* and *papyrus* under varying HRT (3 and 5 days) with batch loading, studied to remove phenol from pre-treated effluent of pulp and paper industry. The removal efficiencies of SSFCW for phenol were higher at 3-days (77%) than 5 days (66%) HRT [63]. HFCW planted with *Typha* and *Canna* assessed for the treatment of paper mill effluent and operated at three different HRTs (1.5, 3.5, and 6.5 days) and found that PRE increased along with HRT, but after 3.5 days, increase in efficiency was insignificant [64]. HFCW at 5.9 days of HRT and planted with *Canna* removes 89% organic halides, 99% hazardous bleaching agents cholophenolics, 89% COD, 93% BOD, and 96% colour removed from pulp and paper WW [65]. VFCW planted with *Typha*, *Erianthus*, and *Phragmites* is efficient in heavy metals removal from pulp and paper industry effluent, with 24 h HRT. The removal efficiencies for the heavy metals varied between 70 and 74% and were in the order of Cu > Fe > Cd > Ni > Zn > Mn and reduced 75–79% BOD and 69–75% COD [66]. Paper mill WW treated in a lab scale HFCW, planted with *Typha*. The system effectively reduced BOD (75–79%) and COD (69–75%) of the WW [67]. Planted (*Scirpus*) SSFCW at 5 days HRT removed 3.6% more COD and 11.4% more colour than unplanted units, from pulp and paper mill WW [68]. In the view of studied researches concluded that HFCW and VFCW perform excellent in reduction of COD (66–88%) and colour (up to 96%) with 1–7 days HRT for paper mills effluent and remove organic halides, cholophenolics, and various heavy metals.

## 3 Techniques to Increase Treatment Efficiency of CW

Performance of constructed wetland depends on many parameters like design, operation, and maintenance factors. Design parameter includes type of constructed wetland, plants, and substrate used for treatment. Operational parameters are type of dosing, HLR, and HRT. Maintenance parameters include plant harvest and its economic use. Microbes play a key role in treatment process, so augmentation of suitable and beneficial microbe is now new area of research. Research in all the above areas is required to increase treatment efficiency of CW [69, 70]. Pollutant removal efficiency of the system can be increased with additional oxygen supply. Intermittent aeration increases in microbial diversity and nitrogen functional genes

[71]. Continuous supply of oxygen inhibits denitrification, so intermittent oxygen supply is a viable choice to enhance nitrification/denitrification and TN removal efficiency of the system [72]. Treatment efficiency of VFCW compared for dairy WW, under different recirculation rates—25%, 50%, and 75%, in CW1, CW2, and CW3, respectively. Author found that removal of BOD, TP, and TN increased with increase in recirculation rates [73]. Nitrogen removal efficiency of towery hybrid constructed wetland (THCW) increased due to cascade overflow in second stage, which increases the aeration of the wetland [74].

DWW treated with a modified HFCW, in which 30 perforated PVC pipes arranged vertically in a rectangular form to form bio-racks, which support the *Phragmites* plants and provide sufficient surface area for the microbes. This system efficiently degrades pollutants (75% COD, 86% BOD<sub>5</sub>), in the DWW at 10 h HRT and reduces the retention time and area requirement of the CW [75]. PRE of the system treating swine WW, increased above 93.9% when some quantity of treated water recirculates again back into influent WW in a circular-flow corridor (CFC) wetland. This arrangement maintains its efficiency in winter as well [76]. Vertical baffles along the width of the wetland provide longer path and more retention time to WW, and hence, the performance of the system increased [77]. Two VFCWs connected in series, with palm mulch media and continuous feeding fulfil the required pollutant removal limits regarding COD, BOD, and TSS, even with high HLR [78].

Augmentation of specific microbe in the system enhances PRE for specific WW. Aerobic bacteria of the order Burkholderiales (*Delftia acidovorans*, *Delftia tsuruhatensis*, and *Delftia* sp.) enhance degradation of organic substances in dairy WW. Anaerobic bacteria of the order Lactobacillales (*Carnobacterium maltaromaticum*), Clostridiales (*Clostridium tyrobutyricum*, *Clostridium cellulovorans*, and *Clostridium argentinense*) help to metabolize lactose, fat, and proteins of dairy WW [79]. Microbial consortium (*Providencia rettgeri* strain HSL1 and *Pseudomonas* sp. SUK1) at pH 7.5 and 30 °C temperature showed up to 99% decolourization of different azo dyes (Reactive Black 5, Reactive Orange 16, Disperse Red 78 and Direct Red 81) at 100 mg·L<sup>-1</sup> concentration within 12 – 30 h [80]. Bacterial community in biological reactor treating winery wastewater is Actinobacteria (up to 50%), Alpha-proteobacteria (13–14%), and Flavobacteria (10–12%). *Candida*, *Trichosporon*, and *Fusarium* are the main fungal communities. Augmentation of these microbes in the CW will improve the PRE of the CW [81].

## 4 Cost of CW

Budget of a subsurface CW include cost of land, liner, media, plants, plumbing and piping material, fencing and payments to engineer, contractor, labour, and legal persons for their services. On comparing cost of sequential batch reactors (SBR) and SSFCW for the treatment of 100,000 gallons of WW per day, capital cost is around 1,104,500 USD for SBR and only 466,700 USD for SSFCW, while operation and maintenance cost is around 106,600 USD/yr. for SBR and only 6,000 USD/

yr. for SSFCW. Money required to treat per thousand gallons of WW for SSFCW is 0.73 USD, which is far less than that of SBR (3.06 USD) [82]. On comparing the capital (246–657 USD/m<sup>3</sup>) and maintenance (0.1151–0.246 USD/m<sup>3</sup>) cost for conventional WWT plant with that for CW (164–460 USD/m<sup>3</sup> and 0.0082–0.039 USD/m<sup>3</sup>, respectively), found that wetland can constructed at 1/3<sup>rd</sup> cost and can be maintained at 1/5<sup>th</sup> to 1/6<sup>th</sup> cost [83]. Similar observation for capital and maintenance cost recorded by [84] and [85]. Capital cost of HFCW, treating DWW, compared in different countries and found that it may be as low as 29 USD per m<sup>2</sup> in India in year 1999, to as expensive as 257 EUR per m<sup>2</sup> in Belgium in year 2004 [39]. Cost and performance for waste stabilization ponds (WSP) and HFCW compared and found that HFCW required 1/3<sup>rd</sup> land in comparison with WSP [86]. Decision of constructing a wetland in place of a sequencing batch reactor compared with the help of replacement cost methodology (RCM) and life cycle assessment (LCA) and found that total \$282 million saved over the project's lifetime (30 years) [87]. Two VFCW connected in series, to treat sewage of single household, reduced COD and BOD efficiently up to 90% and 84%, respectively, and it reduces the area requirement to 0.79 m<sup>2</sup>/person. Authors also reported that for tropical climate, the area requirement can further reduce to 0.5 m<sup>2</sup>/person [88].

## 5 Conclusion

Pollutants can remove with either SFCW, SSFCW, or hybrid CW. They are only different in level of efficiency, and hybrid CW is the most efficient. Higher temperature favours the plant and microbe growth; thus, CW are good option for decentralize WWT in tropical and sub-tropical countries. For DWW treatment, HFCW at 3–4 days HRT is efficient. VFCW with batch feeding and specialized media or coupling with HFCW in hybrid CW are good for DWW. After pre-treatment, planted VFCW and hybrid CW can treat textile WW efficiently, with low HLR and high HRT (1–4 days). Addition of specific microbes enhances the system performance to remove colour, COD, and heavy metals. Hybrid CWs at 4–7 days HRT efficiently degrade the pollutants of dairy, winery, and paper mills WW. To reduce the capital, operation, and maintenance cost of WWT, it is necessary to popularize the use of CW as a mean of decentralized domestic, industrial, and municipal WWT in different configurations and combinations with engineering optimization techniques.

**Acknowledgements** This study has been carried out under the project 'Low Cost- Renewable Energy Driven (LC-RED) Water Treatment Solution Centre', grant No 'DST/TM/WTI/WIC/2K17/124' extended by the Department of Science and Technology (DST), Government of India, under Water Technology Initiative (WTI) scheme. Authors are also thankful to Pandit Deendayal Energy University for providing facilities and necessary infrastructure to bring out this study.

## References

1. UN World Water Development Report: Wastewater: The Untapped Resource (2017). <https://reliefweb.int/report/world/2017-un-world-water-development-report-wastewater-untapped-resource>
2. Saeed T, Khan T (2018) Constructed wetlands for industrial wastewater treatment: alternative media, input biodegradation ratio and unstable loading. *J Environ Chem Eng* 7:103042. <https://doi.org/10.1016/j.jece.2019.103042>
3. Wu S, Lyu T, Zhao Y, Vymazal J, Arias CA, Brix H (2018) Rethinking intensification of constructed wetlands as a green eco-technology for wastewater treatment. *Environ Sci Technol* 52:1693–1694. <https://doi.org/10.1021/acs.est.8b00010>
4. Cheng G, Li Q, Su Z, Sheng S, Fu J (2018) Preparation, optimization, and application of sustainable ceramsite substrate from coal fly ash/waterworks sludge/oyster shell for phosphorus immobilization in constructed wetlands. *J Clean Prod* 175:572–581. <https://doi.org/10.1016/j.jclepro.2017.12.102>
5. Rahman ME et al (2020) Design, operation and optimization of constructed wetland for removal of pollutant. *Int J Environ Res Public Health* 17:1–40. <https://doi.org/10.3390/ijerph17228339>
6. Stefanakis AI (2020) Constructed wetlands for sustainable wastewater treatment in hot and arid climates: opportunities, challenges and case studies in the Middle East. *Water* 12:1665. <https://doi.org/10.3390/w12061665>
7. Rozman U, Klun B, Kalčíková G (2023) Distribution and removal of microplastics in a horizontal sub-surface flow laboratory constructed wetland and their effects on the treatment efficiency. *Chem Eng J* 461:142076. <https://doi.org/10.1016/j.cej.2023.142076>
8. García-Ávila F et al (2023) Application of ornamental plants in constructed wetlands for wastewater treatment: a scientometric analysis. *Case Stud Chem Environ Eng* 7:100307. <https://doi.org/10.1016/j.csee.2023.100307>
9. World Bank Organization (2020). <https://www.worldbank.org/en/topic/water-in-agriculture>
10. Rahi MA et al (2020) Biochemical performance modelling of non-vegetated and vegetated vertical subsurface-flow constructed wetlands treating municipal wastewater in hot and dry climate. *J Water Process Eng* 33:101003. <https://doi.org/10.1016/j.jwpe.2019.101003>
11. Vymazal J (2022) The historical development of constructed wetlands for wastewater treatment. *Land* 11(2):174. <https://doi.org/10.3390/land11020174>
12. Thalla AK, Devatha CP, Anagh K, Sony E (2019) Performance evaluation of horizontal and vertical flow constructed wetlands as tertiary treatment option for secondary effluents. *Appl Water Sci* 9:1–9. <https://doi.org/10.1007/s13201-019-1014-9>
13. Wijaya DS (2016) A review on sub-surface flow constructed wetlands in tropical and subtropical countries. *Open Sci J* 1:1–11. <https://doi.org/10.23954/osj.v1i2.415>
14. Saba B, Jabeen M, Mahmood T, Aziz I (2014) Treatment comparison efficiency of microbial amended agro-waste biochar constructed wetlands for reactive black textile dye. *Int Proc Chem Biol Environ Eng* 65:13–16
15. Stefanakis AI, Tsihrintzis VA (2012) Effects of loading, resting period, temperature, porous media, vegetation and aeration on performance of pilot-scale vertical flow constructed wetlands. *Chem Eng J* 181–182:416–430. <https://doi.org/10.1016/j.cej.2011.11.108>
16. Abdelhakeem SG, Abouloos SA, Kamel MM (2016) Performance of a vertical subsurface flow constructed wetland under different operational conditions. *J Adv Res* 7:803–814. <https://doi.org/10.1016/j.jare.2015.12.002>
17. Vohla C, Kõiv M, Bavor HJ, Chazarenc F, Mander Ü (2011) Filter materials for phosphorus removal from wastewater in treatment wetlands—a review. *Ecol Eng* 37:70–89. <https://doi.org/10.1016/j.ecoleng.2009.08.003>
18. Schierano MC, Panigatti MC, Maine MA (2018) Horizontal subsurface flow constructed wetlands for tertiary treatment of dairy wastewater. *Int J Phytoremediation* 20:895–900. <https://doi.org/10.1080/15226514.2018.1438361>
19. Wang W, Chi ZYY (2020) Nitrogen removal in Ditch Wetland systems: effects of hydraulic retention time (HRT) and spatial configuration. *Fresenius Environ Bull* 29:3230–3239

20. Gao J et al (2020) Preparation of a new low-cost substrate prepared from drinking water treatment sludge (DWTS)/bentonite/zeolite/fly ash for rapid phosphorus removal in constructed wetlands. *J Clean Prod* 261:121110. <https://doi.org/10.1016/j.jclepro.2020.121110>
21. Yang Y, Zhao Y, Liu R, Morgan D (2018) Global development of various emerged substrates utilized in constructed wetlands. *Bioresour Technol* 261:441–452. <https://doi.org/10.1016/j.biortech.2018.03.085>
22. Akratos CS, Tsihrintzis VA (2007) Effect of temperature, HRT, vegetation and porous media on removal efficiency of pilot-scale horizontal subsurface flow constructed wetlands. *Ecol Eng* 29:173–191. <https://doi.org/10.1016/j.ecoleng.2006.06.013>
23. Grismer ME, Shepherd HL (2011) Plants in constructed wetlands help to treat agricultural processing wastewater. *Calif Agric* 65:73–79. <https://doi.org/10.3733/ca.v065n02p73>
24. Ebrahimi A et al (2013) Efficiency of constructed wetland vegetated with *Cyperus alternifolius* applied for municipal wastewater treatment. *J Environ Public Health* 815962:1–6. <https://doi.org/10.1155/2013/815962>
25. Arroyo P et al (2010) Comparative analysis of the composition of bacterial communities from two constructed wetlands for municipal and swine wastewater treatment. *J Water Health* 8:147–157. <https://doi.org/10.2166/wh.2009.123>
26. Dong Q, Chen Q, Li, Z, Zeng S (2017) Application of microbial technology in wastewater treatment. *Prog Appl Microbiol*, 3–6
27. Shehzadi M, Afzal M, Khan MU, Islam E, Mobin A, Anwar S, Khan QM (2014) Enhanced degradation of textile effluent in constructed wetland system using *Typha domingensis* and textile effluent-degrading endophytic bacteria. *Water Res* 58:152–159. <https://doi.org/10.1016/j.watres.2014.03.064>
28. Welz PJ, Ramond JB, Cowan DA, Prins A, Burton SG (2011) Ethanol degradation and the benefits of incremental priming in pilot-scale constructed wetlands. *Ecol Eng* 37:1453–1459. <https://doi.org/10.1016/j.ecoleng.2011.03.009>
29. Tunçsiper B (2009) Nitrogen removal in a combined vertical and horizontal subsurface-flow constructed wetland system. *Desalination* 247:466–475. <https://doi.org/10.1016/j.desal.2009.03.003>
30. Huang J, Cai W, Zhong Q, Wang S (2013) Influence of temperature on micro-environment, plant eco-physiology and nitrogen removal effect in subsurface flow constructed wetland. *Ecol Eng* 60:242–248. <https://doi.org/10.1016/j.ecoleng.2013.07.023>
31. Yan Y, Xu J (2014) Improving winter performance of constructed wetlands for wastewater treatment in northern china: a review. *Wetlands* 34:243–253. <https://doi.org/10.1007/s13157-013-0444-7>
32. Ng WJ, Gunaratne G (2011) Design of tropical constructed wetlands. In *Wetlands for tropical applications*, pp 69–93. [https://doi.org/10.1142/9781848162983\\_0005](https://doi.org/10.1142/9781848162983_0005)
33. Varma M, Gupta AK, Ghosal PS, Majumder A (2020) A review on performance of constructed wetlands in tropical and cold climate: insights of mechanism, role of influencing factors, and system modification in low temperature. *Sci Total Environ* 755(2):142540. <https://doi.org/10.1016/j.scitotenv.2020.142540>
34. Merino-Solís M, Villegas E, de Anda J, López-López A (2015) The effect of the hydraulic retention time on the performance of an ecological wastewater treatment system: an anaerobic filter with a constructed wetland. *Water* 7:1149–1163. <https://doi.org/10.3390/w7031149>
35. Ghosh D, Gopal B (2010) Effect of hydraulic retention time on the treatment of secondary effluent in a subsurface flow constructed wetland. *Ecol Eng* 36:1044–1051. <https://doi.org/10.1016/j.ecoleng.2010.04.017>
36. Toet S, Van Logtestijn RSP, Kampf R, Schreijer M, Verhoeven JTA (2005) The effect of hydraulic retention time on the removal of pollutants from sewage treatment plant effluent in a surface-flow wetland system. *Wetlands* 25:375–391
37. Mulidzi AR (2010) Winery and distillery wastewater treatment by constructed wetland with shorter retention time. *Water Sci Technol* 61:2611–2615. <https://doi.org/10.2166/wst.2010.206>
38. Wang J, Gu Y, Wang H, Li Z (2021) Investigation on the treatment effect of slope wetland on pollutants under different hydraulic retention times. *Environ Sci Pollut Res* 28:9107–9119. <https://doi.org/10.1007/s11356-020-11292-z>

39. Vymazal J, Kröpfelová L (2008) Wastewater treatment in constructed wetlands with horizontal sub-surface flow. Springer Science + Business Media, Dordrecht
40. Moreira FD, Dias EHO (2020) Constructed wetlands applied in rural sanitation: a review. *Environ Res* 190:110016. <https://doi.org/10.1016/j.envres.2020.110016>
41. Valipour A, Hamnabard N, Woo K-S, Ahn Y-H (2014) Performance of high-rate constructed phytoremediation process with attached growth for domestic wastewater treatment: effect of high TDS and Cu. *J Environ Manage* 145:1–8. <https://doi.org/10.1016/j.jenvman.2014.06.009>
42. World Health Organization: Guidelines on Sanitation and Health (2018). <https://apps.who.int/iris/bitstream/handle/10665/274939/9789241514705-eng.pdf>
43. Xu M, Liu W, Li C, Xiao C, Ding L, Xu K, Geng J, Ren H (2016) Evaluation of the treatment performance and microbial communities of a combined constructed wetland used to treat industrial park wastewater. *Environ Sci Pollut Res* 23:10990–11001. <https://doi.org/10.1007/s11356-016-6181-8>
44. Kant R (2012) Textile dyeing industry an environmental hazard. *Nat Sci* 04:22–26. <https://doi.org/10.4236/ns.2012.41004>
45. Bulc TG, Ojstršek A (2008) The use of constructed wetland for dye-rich textile wastewater treatment. *J Hazard Mater* 155:76–82. <https://doi.org/10.1016/j.jhazmat.2007.11.068>
46. Saeed T, Sun G (2013) A lab-scale study of constructed wetlands with sugarcane bagasse and sand media for the treatment of textile wastewater. *Bioresour Technol* 128:438–447. <https://doi.org/10.1016/j.biortech.2012.10.052>
47. Hussein A, Scholz M (2018) Treatment of artificial wastewater containing two azo textile dyes by vertical-flow constructed wetlands. *Environ Sci Pollut Res* 25:6870–6889. <https://doi.org/10.1007/s11356-017-0992-0>
48. Yeruva DK, Ranadheer P, Kiran Kumar A, Venkata Mohan S (2019) Tri-phasic engineered wetland system for effective treatment of azo dye-based wastewater. *npj Clean Water* 2:1–8. <https://doi.org/10.1038/s41545-019-0037-y>
49. Shete BS, Shinkar NP (2013) Dairy industry wastewater sources, characteristics & its effects on environment. *Int J Curr Eng Technol* 3(5):1611–1615. <http://inpressco.com/category/ijcet/vol-3no-5dec-2013/>
50. Stefanakis A, Akrotas CS, Tsihrintzis VA (2014) Vertical flow constructed wetlands: eco-engineering systems for wastewater and sludge treatment. *Newnes*
51. Sharma PK, Inoue T, Kato K, Ietsugu H, Tomita K, Nagasawa T (2011) Potential of hybrid constructed wetland system in treating milking parlor wastewater under cold climatic conditions in northern Hokkaido, Japan. *Water Pract Technol* 6(3). <https://doi.org/10.2166/wpt.2011.052>
52. Tatoulis T, Akrotas CS, Tekerlekopoulou AG, Vayenas DV, Stefanakis AI (2017) A novel horizontal subsurface flow constructed wetland: reducing area requirements and clogging risk. *Chemosphere* 186:257–268. <https://doi.org/10.1016/j.chemosphere.2017.07.151>
53. Samal K, Dash RR, Bhunia P (2017) Performance assessment of a *Canna indica* assisted vermifilter for synthetic dairy wastewater treatment. *Process Saf Environ Prot* 111:363–374. <https://doi.org/10.1016/j.psep.2017.07.027>
54. Yazdani V, Golestani HA (2019) Advanced treatment of dairy industrial wastewater using vertical flow constructed wetlands. *Desalin Water Treat* 162:149–155. <https://doi.org/10.5004/dwt.2019.24335>
55. Schierano MC, Panigatti MC, Maine MA, Griffa CA, Boglione R (2020) Horizontal subsurface flow constructed wetland for tertiary treatment of dairy wastewater: removal efficiencies and plant uptake. *J Environ Manage* 272:111094. <https://doi.org/10.1016/j.jenvman.2020.111094>
56. Welz PJ, Holtman G, Haldenwang R, Le Roes-Hill M (2016) Characterisation of winery wastewater from continuous flow settling basins and waste stabilisation ponds over the course of 1 year: implications for biological wastewater treatment and land application. *Water Sci Technol* 74:2036–2050. <https://doi.org/10.2166/wst.2016.226>
57. Mulidzi AR (2007) Winery wastewater treatment by constructed wetlands and the use of treated wastewater for cash crop production. *Water Sci Technol* 56:103–109. <https://doi.org/10.2166/wst.2007.478>

58. Zingelwa NS, Wooldridge J (2009) Tolerance of macrophytes and grasses to sodium and chemical oxygen demand in Winery wastewater. *South African J Enol Vitic* 30:117–123. <https://doi.org/10.21548/30-2-1431>
59. Masi F, Bresciani R, Bracali M (2015) A new concept of multistage treatment wetland for winery wastewater treatment: long term evaluation of performances. In: Vymazal J (ed) *The role of natural and constructed wetlands in nutrient cycling and retention on the landscape*. Springer, Cham. [https://doi.org/10.1007/978-3-319-08177-9\\_13](https://doi.org/10.1007/978-3-319-08177-9_13)
60. Milani M et al (2020) Treatment of winery wastewater with a multistage constructed wetland system for irrigation reuse. *Water* 12(5):1260. <https://doi.org/10.3390/W12051260>
61. Chhonkar PK, Datta SP, Joshi HC, Pathak H (2000) Impact of industrial effluents on soil health and agriculture—Indian experience: part I—distillery and paper mill effluents. *J Sci Ind Res (India)* 59:350–361
62. Bajpai P, Bajpai PK (1994) Biological colour removal of pulp and paper mill wastewaters. *J Biotechnol* 33:211–220. [https://doi.org/10.1016/0168-1656\(94\)90069-8](https://doi.org/10.1016/0168-1656(94)90069-8)
63. Abira MA, van Bruggen JJA, Denny P (2005) Potential of a tropical subsurface constructed wetland to remove phenol from pre-treated pulp and papermill wastewater. *Water Sci Technol* 51:173–176. <https://doi.org/10.2166/wst.2005.0312>
64. Rani N, Maheshwari RC, Kumar V, Vijay VK (2011) Purification of pulp and paper mill effluent through *Typha* and *Canna* using constructed wetlands technology. *J Water Reuse Desalin* 1:237–242. <https://doi.org/10.2166/wrd.2011.045>
65. Choudhary AK, Kumar S, Sharma C (2012) Removal of chlorophenolics from pulp and paper mill wastewater through constructed wetland. *Water Environ Res* 85(1):54–62. <https://doi.org/10.2175/106143012x13415215907419>
66. Arivoli A, Mohanraj R, Seenivasan R (2015) Application of vertical flow constructed wetland in treatment of heavy metals from pulp and paper industry wastewater. *Environ Sci Pollut Res* 22:13336–13343. <https://doi.org/10.1007/s11356-015-4594-4>
67. Prasanna K, Sudarsan JS, Nithiyantham S (2017) Wastewater treatment using combined biological and constructed wetlands technique in paper mills. *Sustain Water Resour Manag* 3:431–439. <https://doi.org/10.1007/s40899-017-0108-5>
68. Md Yusoff MF et al (2019) Performance of continuous pilot subsurface constructed wetland using *Scirpus grossus* for removal of COD, colour and suspended solid in recycled pulp and paper effluent. *Environ Technol Innov* 13:346–352. <https://doi.org/10.1016/j.eti.2018.12.008>
69. Wu S, Kuschk P, Brix H, Vymazal J, Dong R (2014) Development of constructed wetlands in performance intensifications for wastewater treatment: a nitrogen and organic matter targeted review. *Water Res* 57:40–55. <https://doi.org/10.1016/j.watres.2014.03.020>
70. Kumar S, Dutta V (2019) Efficiency of constructed wetland microcosms (CWMs) for the treatment of domestic wastewater using aquatic macrophytes. In: Sobti R, Arora N, Kothari R (eds) *Environmental biotechnology: for sustainable future*. Springer, Singapore
71. Liu F et al (2019) Intensified nitrogen transformation in intermittently aerated constructed wetlands: removal pathways and microbial response mechanism. *Sci Total Environ* 650:2880–2887. <https://doi.org/10.1016/j.scitotenv.2018.10.037>
72. Wu H, Zhang J, Ngo HH, Guo W, Hu Z, Liang S, Fan J, Liu H (2015) A review on the sustainability of constructed wetlands for wastewater treatment: design and operation. *Bioresour Technol* 175:594–601. <https://doi.org/10.1016/j.biortech.2014.10.068>
73. Sharma PK, Minakshi D, Rani A, Malaviya P (2018) Treatment efficiency of vertical flow constructed wetland systems operated under different recirculation rates. *Ecol Eng* 120:474–480. <https://doi.org/10.1016/j.ecoleng.2018.07.004>
74. Ye F, Li Y (2009) Enhancement of nitrogen removal in towery hybrid constructed wetland to treat domestic wastewater for small rural communities. *Ecol Eng* 35(7):1043–1050. <https://doi.org/10.1016/j.ecoleng.2009.03.009>
75. Valipour A, Kalyan Raman V, Ghole VS (2009) A new approach in wetland systems for domestic wastewater treatment using *Phragmites* sp. *Ecol Eng* 35(12):1797–1803. <https://doi.org/10.1016/j.ecoleng.2009.08.004>

76. Peng J, Song Y, Liu Z, Gao H, Yu H (2012) Performance of a novel circular-flow corridor wetland toward the treatment of simulated high-strength swine wastewater. *Ecol Eng* 49:1–9. <https://doi.org/10.1016/j.ecoleng.2012.08.005>
77. Tee HC, Lim PE, Seng CE, Nawi MAM (2012) Newly developed baffled subsurface-flow constructed wetland for the enhancement of nitrogen removal. *Bioresour Technol* 104:235–242. <https://doi.org/10.1016/j.biortech.2011.11.032>
78. Herrera-Melián JA et al (2018) Effect of substrate, feeding mode and number of stages on the performance of hybrid constructed wetland systems. *Water* 10(1):39. <https://doi.org/10.3390/w10010039>
79. Custodio M, Peñaloza R, Espinoza C, Espinoza W, Mezarina J (2022) Treatment of dairy industry wastewater using bacterial biomass isolated from eutrophic lake sediments for the production of agricultural water. *Bioresour Technol Rep* 17:100891. <https://doi.org/10.1016/j.biteb.2021.100891>
80. Lade H, Govindwar S, Paul D (2015) Mineralization and detoxification of the carcinogenic Azo Dye Congo red and real textile effluent by a polyurethane foam immobilized microbial consortium in an upflow column bioreactor. *Int J Environ Res Public Health* 12(6):6894–6918. <https://doi.org/10.3390/ijerph120606894>
81. De Beer DM, Botes M, Cloete TE (2018) The microbial community of a biofilm contact reactor for the treatment of winery wastewater. *J Appl Microbiol* 124(2):598–610. <https://doi.org/10.1111/jam.13654>
82. USEPA (2000) Wastewater technology fact sheet: wetlands: subsurface flow. Environ Prot Agency, 1–7
83. Liu D et al (2009) Constructed wetlands in China: recent developments and future challenges. *Front Ecol Environ* 7:261–268. <https://doi.org/10.1890/070110>
84. Wang L, Peng I, Wang B, Yang L (2006) Design and operation of an eco-system for municipal wastewater treatment and utilization. *Water Sci Technol* 54:429–436. <https://doi.org/10.2166/wst.2006.923>
85. Zhang DQ et al (2014) Application of constructed wetlands for wastewater treatment in developing countries—a review of recent developments (2000–2013). *J Environ Manage* 141:116–131. <https://doi.org/10.1016/j.jenvman.2014.03.015>
86. Mburu N et al (2013) Performance comparison and economics analysis of waste stabilization ponds and horizontal subsurface flow constructed wetlands treating domestic wastewater: a case study of the Juja sewage treatment works. *J Environ Manage* 128:220–225. <https://doi.org/10.1016/j.jenvman.2013.05.031>
87. Dimuro JL et al (2014) Financial and environmental analysis of constructed wetlands for industrial wastewater treatment. *J Ind Ecol* 18(5):631–640. <https://doi.org/10.1111/jiec.12129>
88. Yadav A, Chazarenc F, Mutnuri S (2018) Development of the “French system” vertical flow constructed wetland to treat raw domestic wastewater in India. *Ecol Eng* 113:88–93. <https://doi.org/10.1016/j.ecoleng.2018.01.001>

# Synthesis and Characterization of Amine-Functionalized Zeolite 4A for Wastewater Treatment



Megha Parmar, Mahuya Bandyopadhyay, Rama Gaur,  
and Syed Shahabuddin

## 1 Introduction

India is among the most populated countries, and to meet the demand of this huge population is a task. This increases the load on various industries. This leads to the directly dumping of the effluents and hazardous chemicals like heavy metals, dyes, and organic pollutants into river bodies that contaminate the river water, aquatic life, and human life as well. Exposing environment to these chemicals and harmful gases will have negative impact on environment. Wastewater treatment is one of the major problems that our country is facing today. Various wastewater treatment technologies are available nowadays like reverse osmosis [1], adsorption [2], chemical precipitation [3], electrodialysis [4], etc. These treatment technologies have several disadvantages like production of large amount of sludge, toxic by-products hard to dispose and manage. As compared to the other techniques, photocatalysis [5] and adsorption are the most reliable techniques because it offers several advantages like cost-effectiveness and sustainability over other techniques. There are various materials available that can act as adsorbents like activated carbon [5], clay minerals [6], biochar [7], etc. These adsorbents like activated carbon and biochar have disadvantage of cost [8] and require high calcination temperature [9]. These adsorbents are made from different precursors; hence, the products have different chemical composition. These problems can be overcome using adsorbent materials synthesized from natural precursors, following sustainable routes of synthesis. Zeolites synthesized from sustainable and natural precursors, such as, coal fly ash, clay, and industrial

---

M. Parmar · R. Gaur · S. Shahabuddin (✉)

Department of Chemistry, School of Energy Technology, Pandit Deendayal Energy University,  
Gandhinagar, Gujarat 382426, India

e-mail: [Syed.shahabuddin@sot.pdpu.ac.in](mailto:Syed.shahabuddin@sot.pdpu.ac.in)

M. Bandyopadhyay

Department of Basic Sciences, Institute of Infrastructure, Technology, Research and Management,  
Maninagar, Ahmedabad, India

waste, can be an excellent choice, which greatly reduces the cost of preparation and applications. The method also contributes to managing waste. Raw zeolites without much modification have great potential, and compared to costly adsorbent materials, zeolites are the aluminosilicate crystalline materials that have negative framework. Zeolites have large surface area and porous structure, due to which they can be used as an adsorbent material to remove pollutants from wastewater [10]. Zeolites are made up of two units, primary and secondary units.  $\text{TO}_4$  represents the primary unit, where T is for silicon or aluminum. The primary units are connected by the bridged oxygen atoms and form the secondary unit. The framework of zeolite processes negative charge [11]. The reason of processing negative charge is isomorphic substitution [12], that means replacement of  $\text{Si}^{+4}$  by  $\text{Al}^{+3}$ . The chemical formula that is used for the representation of zeolite is  $\text{Mx/n} [(\text{AlO}_2) \times (\text{SiO}_2) y] \cdot z\text{H}_2\text{O}$ . Zeolite has porous structure. The channel and pore size can also be uniform, that makes it a good candidate for making filters and membranes. Zeolites can be used to adsorb pollutants like heavy metals [13], dyes [14], and radioactive elements [15] from wastewater. Metals have positive charge, and zeolite has negative framework which leads to the metals getting incorporated and stuck into the intercrystallite structure of zeolite. Various methods are there to synthesize zeolite like hydrothermal method [16], solvothermal method [17], microwave assisted [18], and solvent-free synthesis [19]. Zeolite synthesis basically requires silica source and an alumina source. Zeolite synthesis requires costly chemicals and templates, longer time durations, and high temperature for crystallization. Various natural sources like rice husk [20], kaolin clay [21], coal fly ash [22], industrial waste [23], bauxite [24], red mud [25], windshield waste [26], etc., have been used to synthesize zeolite. Modifying zeolite by inserting metal and functionalizing it may increase the adsorption and photocatalytic activity of zeolite. Zeolite exhibits tremendous activity in terms of ion exchange. This property makes it a good material to use it in the application of water softening and catalysis. Zeolite has the potential to act as the leading adsorbent material having variety of application. Zeolite has been synthesized using different synthetic and natural precursors. In this study, two catalysts, namely raw zeolite 4A and amine-F-4A, have been explored for the adsorption of methylene blue dye.

## 2 Experimental Section

### 2.1 Materials

Zeolite 4A (Procured from Dr. Syed Shahabuddin research group, Department of Chemistry, Pandit Deendayal Energy University), sodium hydroxide (Merck chemicals), distilled water, methanol (Finar chemicals, India), and methylene blue dye.

## 2.2 Preparation of Amine-Functionalized Zeolite 4A

Zeolite 4A (1 g) that was acting as support catalyst was first dried in oven at 80 °C for 3 h. Zeolite and amino propyl triethoxy silane (APTES) were added into the round bottom flask in the ratio of 1:1. Then, 50 ml of toluene was added into it, and the mixture was left for stirring at 120 °C for 11 h. The product was then filtered and thoroughly washed with toluene followed by drying in oven.

## 2.3 Characterization

The synthesized materials were characterized using XRD, FE-SEM, and FTIR. XRD was used to evaluate the crystallinity, FTIR to know about the functional groups and molecular structure, and FE-SEM was performed to check the morphology. Data of XRD was taken using PANalytical X<sup>+</sup> pert Pro diffractometer at 40 kV and 30 Ma utilizing copper K $\alpha$  radiation, 2 $\theta$  range in 5–50° having step size of 1° per min. FT-IR analysis was performed using Perkin Elmer spectrum having two FT-IR spectrometers. The spectra are recorded in the region of 4000–400 cm<sup>-1</sup>. FE-SEM analysis was done using Zeiss ultra 55 instruments. The samples that are non-conductive were coated using gold layer with LEICA EM ACE200. This will make the samples conductive. UV–vis spectrometer was used for the analysis of absorption spectra of the samples between 200 and 800 nm ranges utilizing LABINDIA model UV 3000 +.

## 2.4 Adsorption Studies

Dye adsorption studies using raw zeolite 4A and amine-functionalized 4A were carried out in batch mode. The experiments were carried out in 20 ml of dye solution and rotatory shaker. After adding adsorbent into the dye solution, the beaker was rotated in shaker for different time intervals followed by UV–vis analysis to find the equilibrium time. Variables such as dosage and adsorption time were analyzed and kinetics were plotted using following equations are used

$$\text{Removal \%} = \frac{C_o - C_e}{100} * 100$$

where  $C_o$  (mg/l) and  $C_e$  (mg/l) are the initial and final concentration of dye, respectively.  $Q_e$  (mg/g) and  $Q_t$  (mg/g) are adsorption capacity at equilibrium and time  $t$ , respectively, using following equations.

$$Q_t = \frac{(C_o - C_t)}{M} * V$$

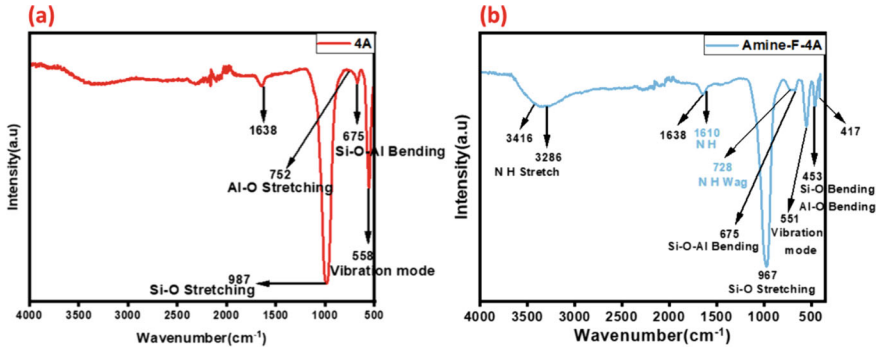


**Fig. 1** FT-IR analysis of **a** zeolite 4A and **b** amine-functionalized zeolite 4A

$$Q_e = \frac{(C_o - C_e)}{M} * V$$

where  $C_t$  and  $C_e$  are the concentration of dye solution at a particular time  $t$  and at equilibrium.  $M$  is the mass of adsorbent, and  $V$  is the total volume of dye solution.

### 3 Result and Discussion

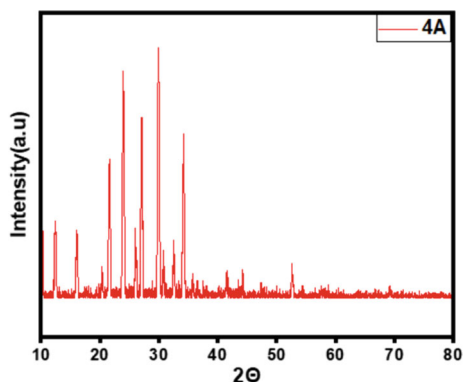
#### 3.1 FT-IR Analysis

Figure 1 shows the FT-IR analysis of (a) zeolite 4A and (b) amine-functionalized 4A. The characteristic peak of zeolite 4A appeared at  $675\text{ cm}^{-1}$ ,  $752\text{ cm}^{-1}$ , and  $987\text{ cm}^{-1}$ , that are attributed to Si–O–Al bending, Al–O stretching, and Si–O stretching, respectively. The characteristic peak of amine (N–H) appeared at  $1610\text{ cm}^{-1}$  and  $728\text{ cm}^{-1}$  as shown in Fig. 1b. The characteristic peaks of amine and zeolite 4A are visible in the FTIR spectra of amine-F-4A.

#### 3.2 XRD Analysis

Figure 2 depicts the XRD analysis of zeolite 4A. As depicted in Fig. 2, all the peaks are crisp and sharp having good pattern of diffraction, proving that the zeolite has high percentage of crystallinity and ordered structure. Zeolite 4A exhibits characteristic sharp peaks at  $2\theta = 10.08^\circ$ ,  $12.36^\circ$ ,  $16.06^\circ$ , and  $21.64^\circ$  indicating the formation of zeolite 4A.

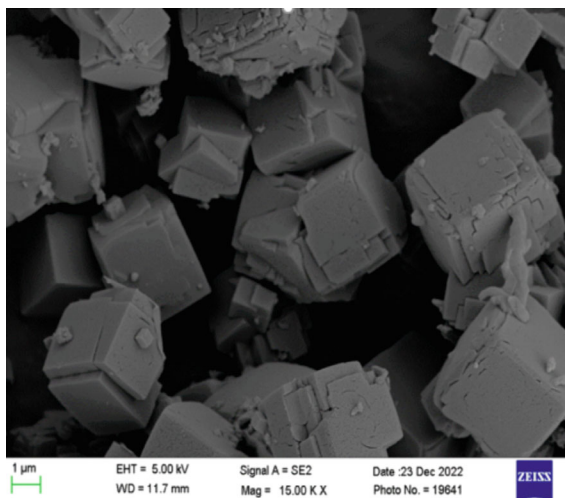
**Fig. 2** XRD analysis of zeolite 4A



### 3.3 FE-SEM Analysis

Figure 3 depicts the morphological analysis of zeolite 4A. It shows the morphology of zeolite 4A. As depicted in the figure, zeolite 4A has cubical structure. Cubical morphology is corresponding to higher surface area. Zeolite 4A having high surface area and cubical particle structure has formed properly.

**Fig. 3** FE-SEM analysis of zeolite 4A



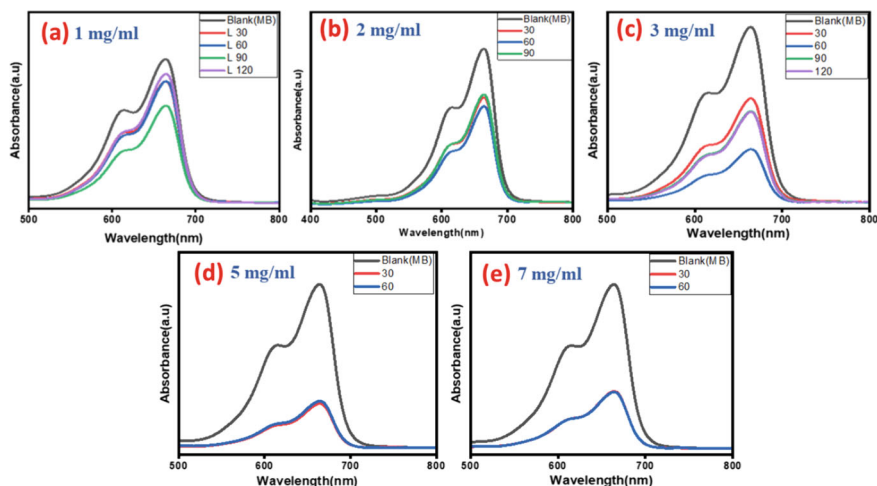


Fig. 4 Methylene blue UV–vis absorption spectra having different dosage of catalyst (mg/ml) a 1, b 2, c 3, d 5 and e 7

## 4 Adsorption Studies

### 4.1 Adsorption Studies of Methylene Blue Dye Using Raw Zeolite 4A

10 ppm of 10 ml methylene blue dye has been used. Different dosage of catalyst was evaluated to find out the best dosage that will give maximum adsorption. The dosage of catalyst that has been evaluated is 1 mg/ml, 2 mg/ml, 3 mg/ml, 5 mg/ml, and 7 mg/ml, and the adsorption percentage that the dosage of catalyst has given was 33%, 38%, 71%, 74%, and 66%, respectively. Out of all the dosage, the optimum dosage showing maximum adsorption of 74% is 5 mg per ml. There is a minor difference between 3 mg per ml and 5 mg per ml adsorption efficiency. 3 mg/ml was showing 71% adsorption, and 5 mg/ml was showing 74% adsorption. Figure 4 describes the UV–Vis spectra of methylene blue dye using zeolite 4A. In (c), (d), and (e), after 60 min, the adsorption–desorption equilibria came.

### 4.2 Adsorption Studies of Methylene Blue Dye Using Amine-Functionalized Zeolite 4A

10 ppm of methylene blue dye has been used, and different dosage of catalyst has been examined to test the efficiency of catalyst as adsorbent. The following dosage of catalyst (mg/ml) has been evaluated, 0.1, 0.2, 0.5, 0.7, and 1 that shows the following

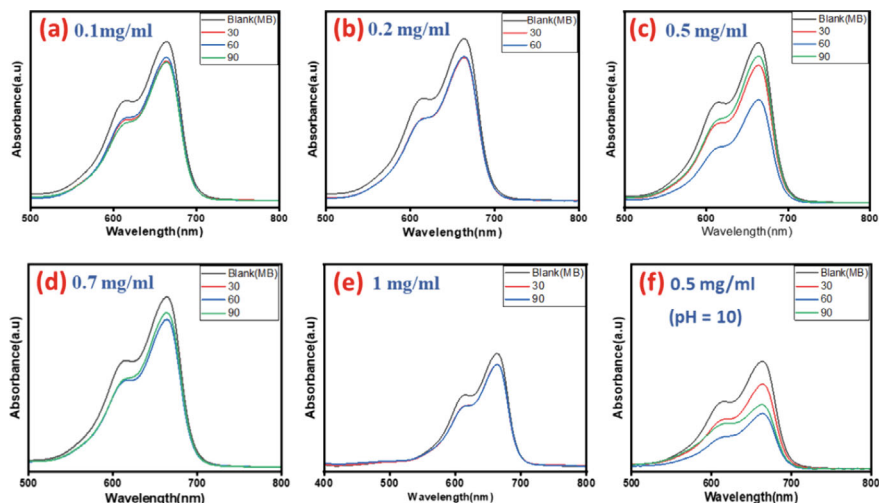


**Fig. 5** UV–vis analysis of amine-F-4A for methylene blue dye removal having different dosage of catalyst (mg/ml). **a** 0.1, **b** 0.2, **c** 0.5, **d** 0.7, **e** 1 and **f** 0.5—pH = 10.5

absorption efficiency, 16%, 12%, 36%, 14% and 9%, respectively. Figure 5f shows the UV–vis analysis of 5 mg/ml dosage of catalyst having pH of the solution as 10.5 and adsorption percentage as 50%. As the pH increases, the absorption efficiency of the catalyst also increased as negative framework will easily adsorb cationic methylene blue dye. As the dosage of catalyst increased, the adsorption efficiency decreases because it was leading to the formation of suspension. Figure 5 describes the adsorption efficiency of amine-F-4A for the removal of methylene blue dye using UV–vis analysis.

Figure 6 represents the bar graph showing adsorption percentage of zeolite 4A and amine-F-4A. In raw zeolite 4A, as the dosage of catalyst increased, the adsorption percentage also increased, but in amine-F-4A, as the dosage of catalyst increased, the adsorption efficiency decreased because of the formation of suspension of the mixture and catalyst–catalyst interaction.

### 4.3 Adsorption Kinetics

In this study, following kinetics models, first order, second order, pseudo first order, pseudo second order, and Elovich models are investigated and plotted, depicted in Table 1.

Figure 7 shows kinetic plots of different models applied on 4A. Zeolite 4A follows pseudo-first-order kinetics. This model supposes that rate of adsorption is dependent proportionally on difference between adsorption capacity and amount adsorbed at equilibrium.

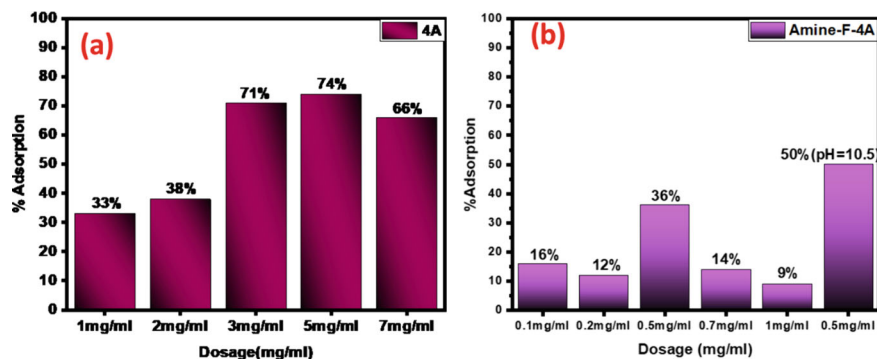


Fig. 6 Bar graph depicting adsorption % of different dosage of catalyst. **a** zeolite 4A and **b** amine-F-4A

Table 1 Equations of different kinetic models

Kinetic model	Linear equation
First order	$\ln C_e = -k_1 t + \ln C_0$
Second order	$1/C_e = k_2 t + \ln C_0$
Pseudo first order	$\ln(Q_e - Q_t) = \ln Q_e - k_3 t$
Pseudo second order	$t/Q_t = 1/k_4 Q_e^2 + t/Q_e$
Elovich model	$Q_t = 1/\beta \ln(\alpha\beta) + 1/\beta \ln t$

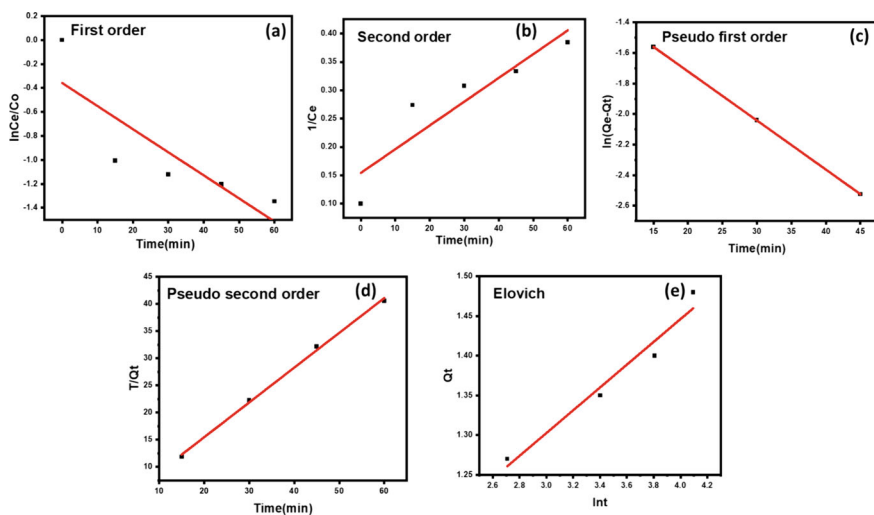
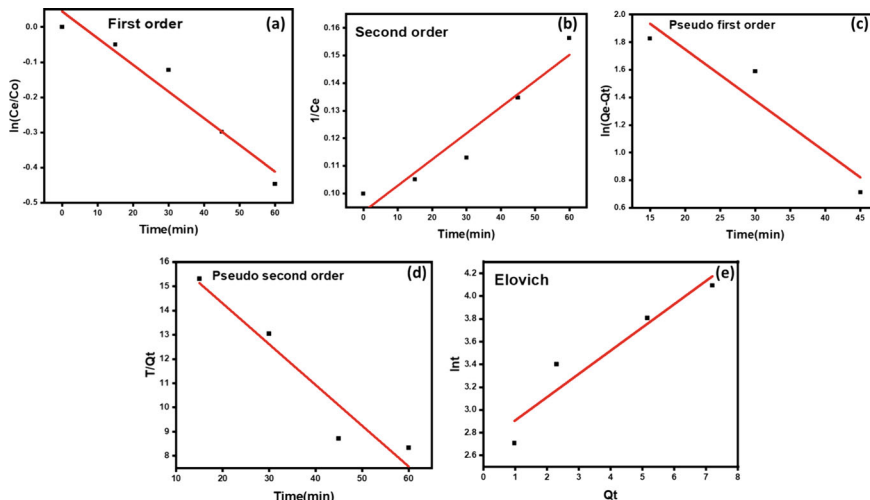


Fig. 7 Kinetic plots representing different kinetic models for 4A. **a** First order, **b** second order, **c** pseudo first order, **d** pseudo second order and **e** Elovich



**Fig. 8** Kinetic plots representing different kinetic models for functionalized 4A. **a** First order, **b** second order, **c** pseudo first order, **d** pseudo second order and **e** Elovich

**Table 2** Parameters of different kinetic models applied on raw 4A and functionalized 4A

Code	Parameters	First order	Second order	Pseudo first order	Pseudo second order	Elovich
4A	$R^2$	0.94672	0.92439	0.99999	0.9977	0.95961
F-4A	$R^2$	0.94672	0.92439	0.90164	0.92251	0.90869

Figure 8 depicts the kinetic plots of functionalized 4A. It follows first-order kinetics, which states that the rate of adsorption is dependent on the amount of adsorbate adsorbed.

Table 2 contains values of correlation coefficient for both zeolite 4A and functionalized 4A. The value of correlation coefficient ranges between 0 and 1. Closer the value to 1, more appropriate the model is.

## 5 Conclusion

Here, two catalysts, zeolite 4A and amine-F-4A, have been explored for the adsorption of methylene blue dye. Different dosage study has been performed. In raw zeolite, as the dosage of catalyst was increased, the adsorption efficiency also increased. 5 mg/ml was showing 74% of adsorption in 60 min. In amine-F-4A, as the dosage of catalyst increased, the adsorption efficiency decreased because the solution was forming suspension. 0.5 mg/ml having pH of the solution as 10.5 was showing good adsorption percentage of 50%. From the present study, we concluded that raw zeolite has

more adsorption efficiency toward methylene blue dye as compared to the functionalized zeolite. Hence, raw zeolite without any chemical treatment and modification can directly be used as an adsorbent material.

**Acknowledgements** Author would like to thank Solar Research and Development Centre, SRDC, Department of chemistry, PDEU, for instrumentation facility.

## References

1. Ismail F, Khulbe KC, Matsuura T (2018) Reverse osmosis. Elsevier
2. Ruthven DM (1987) Principles of adsorption and adsorption processes. Wiley
3. Wang LK et al (2005) Chemical precipitation. In: Physicochemical treatment processes, pp 141–197
4. Valero F, Barceló A, Arbós R (2011) Electrodialysis technology: theory and applications. *Desalin Trends Technol* 28:3–20
5. Serpone N (2000) Photocatalysis. In: Kirk-Othmer encyclopedia of chemical technology
6. Zhang D et al (2010) Synthesis of clay minerals. *Appl Clay Sci* 50(1):1–11
7. Jha S et al (2022) Kinetic and isothermal investigations on the use of low-cost coconut fiber-polyaniline composites for the removal of chromium from wastewater. *Polymers* 14(20):4264
8. Lazaratou C, Vayenas D, Papoulis D (2020) The role of clays, clay minerals and clay-based materials for nitrate removal from water systems: a review. *Appl Clay Sci* 185:105377
9. Kalló D (2001) Applications of natural zeolites in water and wastewater treatment. *Rev Mineral Geochem* 45(1):519–550
10. Jha B et al (2016) Basics of zeolites. In: Fly ash zeolites: innovations, applications, and directions, pp 5–31
11. De Vries AH et al (1999) Zeolite structure and reactivity by combined quantum-chemical—classical calculations. *J Phys Chem B* 103(29):6133–6141
12. Okulik NB, Diez RP, Jubert AH (2003) Topological study of the effect of the isomorphic substitution of silicon by aluminum on the zeolite structure and its interaction with methane. *J Phys Chem A* 107(32):6225–6230
13. Darban Z et al (2022) Hydrogel-based adsorbent material for the effective removal of heavy metals from wastewater: a comprehensive review. *Gels* 8(5):263
14. Sodha V et al (2023) Synthesis of zeolite-doped polyaniline composite for photocatalytic degradation of methylene blue from aqueous solution. *Environ Sci Pollut Res* 30(16):46159–46174
15. Abbas TK, Rashid KT, Alsahy QF (2022) NaY zeolite-polyethersulfone-modified membranes for the removal of cesium-137 from liquid radioactive waste. *Chem Eng Res Des* 179:535–548
16. Mirfendereski M, Mohammadi T (2011) Investigation of hydrothermal synthesis parameters on characteristics of T type zeolite crystal structure. *Powder Technol* 206(3):345–352
17. Jamil AK, Muraza O, Al-Amer AM (2016) Microwave-assisted solvothermal synthesis of ZSM-22 zeolite with controllable crystal lengths. *Particuology* 24:138–141
18. Zhang R et al (2020) Sequential microwave-assisted dealumination and hydrothermal alkaline treatments of Y zeolite for preparing hierarchical mesoporous zeolite catalysts. *Top Catal* 63:340–350
19. Luo W et al (2017) Synthesis of ZSM-5 aggregates made of zeolite nanocrystals through a simple solvent-free method. *Micropor Mesopor Mater* 243:112–118
20. Wang Y et al (2020) Synthesis of La and Ce modified X zeolite from rice husk ash for carbon dioxide capture. *J Market Res* 9(3):4368–4378
21. He Y et al (2021) Research progress on green synthesis of various high-purity zeolites from natural material-kaolin. *J Clean Prod* 306:127248

22. Yadav VK et al (2022) A noble and economical method for the synthesis of low-cost zeolites from coal fly ash waste. *Adv Mater Process Technol* 8(sup2):301–319
23. Zhang L et al (2021) The effect and mechanism of Si/Al ratio on microstructure of zeolite modified ceramsite derived from industrial wastes. *Micropor Mesopor Mater* 311:110667
24. Guo Y et al (2019) A prospective process for alumina extraction via the co-treatment of coal fly ash and bauxite red mud: investigation of the process. *Hydrometallurgy* 186:98–104
25. Quyen DTN et al (2017) Synthesis of adsorbent with zeolite structure from red mud and rice husk ash and its properties. In: *AIP conference proceedings*. AIP Publishing LLC
26. Siddika A et al (2021) Roles of waste glass and the effect of process parameters on the properties of sustainable cement and geopolymer concrete—a state-of-the-art review. *Polymers* 13(22):3935

# Flood Risk Management Using HecRAS Model for the Planning of Artificial Levees as a Structural Measure: A Case Study of Upper Sabarmati River Basin, Gujarat, India



Shibani Chourushi , Pradeep P. Lodha , and Indra Prakash 

## 1 Introduction

A flood is a natural phenomenon that occurs mostly during the monsoon season in river basins and lakes due to rise of water levels. Overtopping of the banks of water bodies causes flooding of the surrounding areas. The main causes of floods include high intensity and duration of rainfall, heavy snow melt from glaciers, and sudden release of reservoir water due to excessive rains, dam failures, and cyclones. In coastal areas, tidal effect and tsunamis, besides cyclones are responsible for coastal floods. In this study, we have considered riverine floods, which cause loss of life, heavy damages to infrastructure, and adversely affect socioeconomic condition of a region in inland areas. River flood plain areas are most vulnerable to flooding requiring proper flood management. As it is difficult to prevent flooding, attempts can be made to control floods by adopting proper flood management techniques using new technologies like remote sensing, geographical information system (GIS) and hydraulic modeling.

The integration of GIS technology with Hydrologic Engineering Center's River Analysis System (HecRAS) is vital to geospatial analysis for the preparation of probable flood inundation maps and in identifying locations of vulnerable sections from which river flood water can enter in surrounding areas. This type of study helps in

---

S. Chourushi (✉)

Government Engineering College, Rajkot 360005, India

e-mail: [sschourushi@gecrajkot.ac.in](mailto:sschourushi@gecrajkot.ac.in)

P. P. Lodha

Government Engineering College, Bharuch 392002, India

I. Prakash

Geological Survey of India, Gandhinagar 382010, India

accurately identifying flood vulnerable areas, thus in cost saving of flood management [18, 19]. Similar study was conducted for Shetrunji River Basin in Gujarat [17]. Other versions such as HecHMS and HecGeoRAS are also used together with HecRAS for flood risk analysis [1, 2, 13]. HecRAS 2D is a hydraulic model which is used to simulate water flowing through rivers, open channels [3, 16] and helps in providing best method for flood control and management to design a weir [12]. Recent advancement in geospatial techniques, especially in remote sensing, GIS, 3D hydrological models, and machine learning (ML) algorithms have revolutionized the methodology of flood analysis [8]. In the present study, we have used HecRAS 1D model for the planning of artificial levees as structural measure in upper part of Sabarmati River basin, Gujarat, India, using GIS technology. RAS Mapper and GIS tools were used for the data analysis and visualization.

### ***1.1 Flood Management Measures***

Flood management measures are implemented to prevent and control floods. According to research [21], flood mitigation measures can be classified into five categories: (1) prevention, (2) prediction, (3) proofing, (4) physical control, and (5) insurance. However, flood management measures can also be broadly classified into two types based on the nature of the work and flood protection measures as described below:

- (1) **Engineering /Structural Measures:** The engineering measures for flood control are physical structures constructed for managing floods. In another way, they are the structures that are constructed to keep floods away from people to save their lives. The huge structures are dams, reservoirs, embankments, channels, drainage works, diversion headworks, levees, floodways, floodwalls, etc. [6, 9, 14].
- (2) **Administrative / Non-structural Measures:** Administrative measures are activities that are planned to mitigate flood damages. In another way, they are measures taken to keep people away from floods to save their lives. The non-structural measures are flood forecasting methods, flood warning technologies, flood plain zoning schemes, flood fighting measures, flood proofing techniques, flood insurance policies, relief camps and rehabilitation centers in emergency, etc. [4, 7].

Many researchers have studied structural measures and non-structural measures for flood risk mitigation. Structural measures include prevention of erosion in the river basin, plantation of trees, stabilization of soil, and construction of structures such as dams, weirs, levees, and flood walls. Non-structural measures include plantation, land use planning, awareness, etc. [11, 14, 15]. Flood proofing is structural/ non-structural methods, which helps in reduction of damage to building, etc., from flooding.

## 2 Study Area

The study area (Fig. 1) comprises the Upper Sabarmati River basin (72°35–73°45' East longitudes and 23°35–24°55' North latitudes), extending from Southern part of Rajasthan to Northern part of Gujarat States, India, covering about 6114 Sq.km area. The Sabarmati River originates from Aravalli ranges in Udaipur, Rajasthan to Gulf of Khambhat, Gujarat. There is steep slope in Udaipur region, whereas slope is mild in Gujarat region. For the development flood model, we have selected part of river basin from Dharoi dam (above 150 m elevation) to Derol bridge (about 80 m elevation) covering about 58 km length. Distance from the origin Point of Sabarmati River to Derol Bridge is about 138 km.

### 2.1 HecRAS Model

The US Army Corps of Engineers, Hydrologic Engineering Center, developed a User's manual for Hydrologic Engineering Center's River Analysis System (HecRAS) which supports steady and unsteady flow water surface profile calculations, sediment transport computations, and water quality analysis [5]. The software also contains tools for performing inundation mapping directly using DEM and hydraulic data [5]. The RAS Mapper is an effective tool in HecRAS, which can be

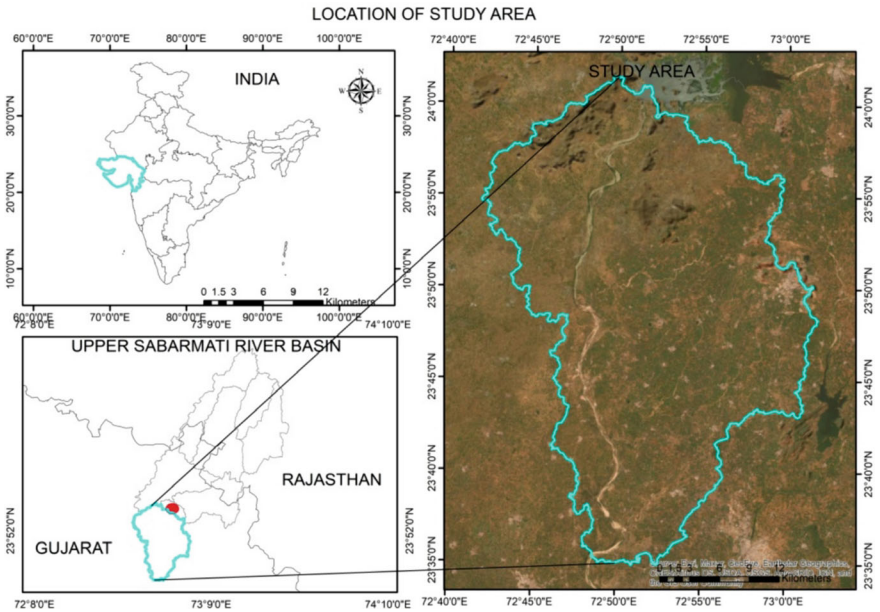


Fig. 1 Location map of study area (red dot indicates Dharoi dam)

**Table 1** Various HecRAS model scenarios generated based on different discharge data

HecRAS model scenarios	Discharge data (cumec)	Various water surface elevation profiles generated
H1	32,000	PF1
H2	23,000	PF2
H3	17,000	PF3
H4	8000	PF4

utilized for inundation of the study area [10]. The HecRAS model when coupled with remotely sensed data such as digital elevation model (DEM) plays a vital role in geospatial analysis such as inundation mapping, watershed, and flood plain delineation. The maps produced by this model are useful for the development planning and disaster management [20].

### 3 Methodology of HecRAS 1D Model

The DEM was used to extract basin boundary, topography, and hydrology thematic maps. In this study, the HecRAS model project was created, and in total thirteen cross-sections/ profiles were generated using the RAS Mapper tool. Then 1D steady flow analysis was performed using four different HecRAS model scenarios. Based on the topographical profiles (sections), artificial levee structures were added to the vulnerable cross-sections. After that, steady flow analysis was performed again after the addition of the artificial levee structures on the Sabarmati River at different probable sites based on 13 cross-sections of river basin between Dharoi dam and Derol Bridge.

Table 1 represents four different HecRAS model scenarios based on the assumed discharge data. The various model scenarios were used for generating various water surface elevation profiles: PF1, PF2, PF3, and PF4.

### 4 Results and Discussions

Using the RAS mapper tool in the HecRAS model, a total of 13 cross-sections were generated in the downstream region of the Dharoi dam within the study area. The model study revealed that the top six nearby cross-sections are more vulnerable to flood-like situations than the other cross-sections due to meandering stages of a river and heavy discharge flow directly from the dam, as shown in Fig. 2. As a result, levees have been proposed at these six cross-sections to mitigate the risk of flooding, as illustrated in Fig. 2.

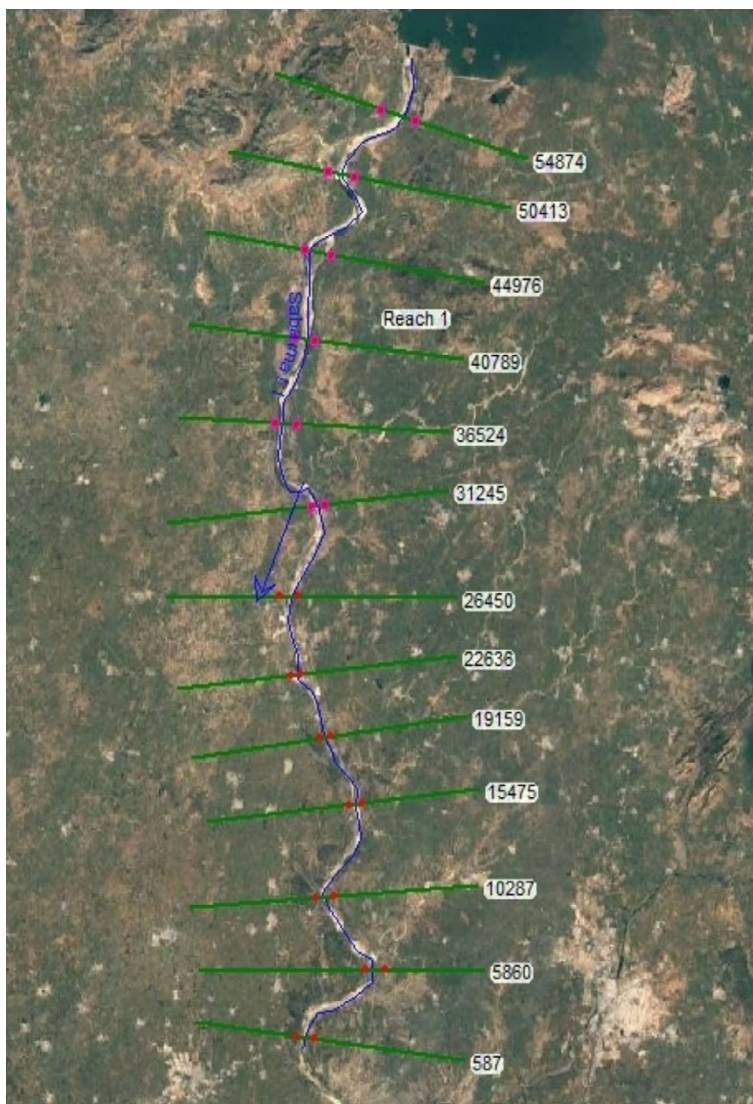


**Fig. 2** Map showing river line, bank stations, various cross-sections, and levees at 6 cross-sections

In Fig. 2, the blue line represents the river centreline, the red dots represent river banks, the green lines represent various cross-sections on the river, and the pink dots indicate levees at 6 cross-sections.

Table 2 shows the left as well as right side elevation details of levees proposed at six cross-sections out of all thirteen cross-sections up to Derol gauge station to reduce flood inundation in the downstream region. This table also represents the water surface elevation based on the various profiles such as PF1, PF2, PF3, and PF4

before and after the addition of levees. This indicates that the addition of artificial levees in the model resulted in an increase of approximately 1 m in the water level, only. The height of the levees is fixed with respect to PF1 (as per 2006 August month), which can be reduced for other profiles, respectively, as per the situation.

The main channel ground elevation profile from the Dharoi dam to Derol Bridge is the same before (Fig. 3a) and after the addition of artificial levees (Fig. 5b). This Figure represents the ground level and levee elevation profiles.

Figures 4, 5, 6, 7, 8, 9, 10, 11, 12, 13, 14, 15, and 16 show various river cross-sections without and with addition of levees. The first six cross-sections show that the water level rises in the main channel elevations and flood inundation occurs in nearby low-lying areas. After the addition of levees in these six cross-sections, the water level rises but within river channel, thus not spreading beyond banks. This measure may help in preventing and reducing flooding in low-lying areas of the downstream part of the basin.

Figures 17, 18, 19, and 20 show X-Y-Z perspectives of four profiles, respectively, before and after the addition of levees. The X-Y-Z perspectives represent various cross-sections in three dimensions which show six vulnerable cross-sections after steady flow analysis. Hence, the vulnerable cross-sections are identified, levees are added, and the steady flow analysis is performed again which shows flood mitigations in the identified six vulnerable cross-sections.

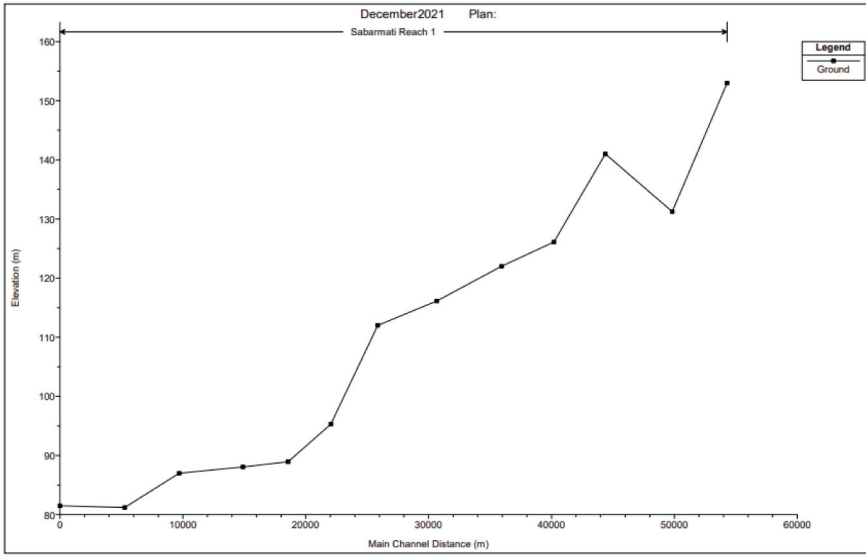
Figure 21 illustrates that Chandap, A village located in the Saurashtra region of Gujarat in western India, is at high risk of flooding based on data from the 2006 flood. However, the model study suggests that by constructing levees in this area, it could be protected from future flooding. The height and length of the levees may be adjusted based on future probable floods in this section of the Sabarmati River basin to ensure maximum safety.

## 5 Conclusions

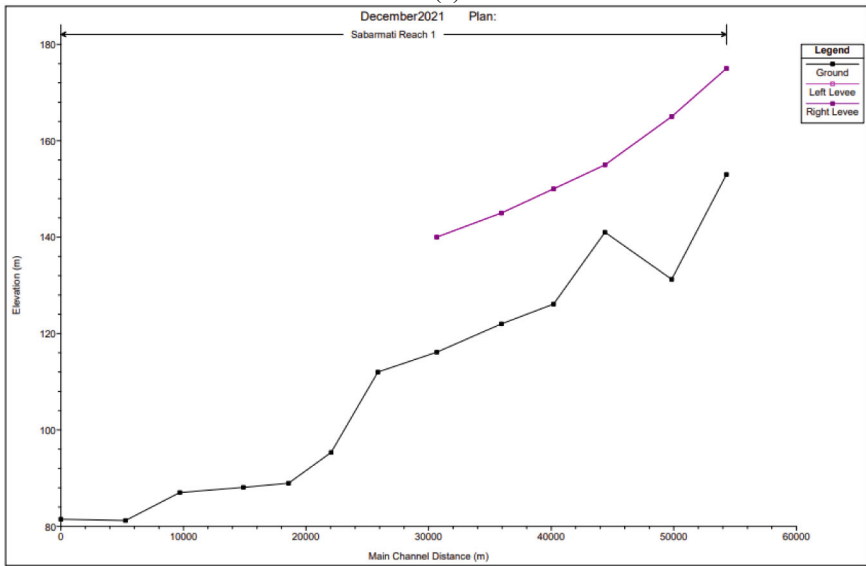
The primary objective of this study is to identify areas at risk of flooding and potential sites for the construction of artificial levees as a structural measure for effective flood risk management in the downstream region of the study area, using the HecRAS-1D model. The model was run using monthly peak data from 2006, and a steady flow analysis was performed to generate flood inundation maps. These maps were used to identify Chandap Village as a high-risk area within the study area. As a remedial measure, flood protection levees were proposed at six cross-sections in six locations. A steady flow analysis was performed in two stages: first without levees, to identify probable flood areas, and second with the addition of levees, to mitigate flooding. The analysis produced water surface elevation profiles and their X-Y-Z perspectives for four profiles, both with and without the addition of artificial structures (levees) to mitigate flood risk in the downstream area based on flood inundation maps. After adding levees at vulnerable sections in the HecRAS model, low-lying areas of Chandap Village appear to be safe from flooding. However, the length

**Table 2** Water surface elevation details before and after addition of levees with various profiles

Cross-section numbers	River stations	Main channel elevation (RL's) (m)	Right & Left Levee elevation (m)	Water surface elevation-PF1 (m)	Water surface elevation-PF1 (m) after addition of levees	Water surface elevation-PF2 (m)	Water surface elevation-PF2 (m) after addition of levees	Water surface elevation-PF3 (m)	Water surface elevation-PF3 (m) after addition of levees	Water surface elevation-PF4 (m)	Water surface elevation-PF4 (m) after addition of levees
1	54,874	153.00	175	161.71	162.69	160.79	161.51	159.84	160.69	158.53	158.61
2	50,413	131.25	165	155.46	156.21	154.12	154.58	152.94	153.20	150.11	150.04
3	44,976	141.00	155	151.26	151.16	150.20	150.14	148.98	148.93	147.43	147.43
4	40,789	126.11	150	142.93	143.59	141.34	141.79	140.01	140.28	136.51	136.53
5	36,524	122.00	145	140.22	140.58	138.01	138.31	136.15	136.34	131.55	131.56
6	31,245	116.12	140	135.31	135.31	132.83	132.83	130.92	130.92	127.18	127.18
7	26,450	112.00		126.17		124.06		122.32		119.21	
8	22,636	95.32		117.08		113.75		111.06		105.86	
9	19,159	88.95		112.79		109.80		107.35		102.14	
10	15,475	88.07		110.00		107.34		105.18		100.39	
11	10,287	87.00		106.07		103.86		102.08		97.29	
12	5860	81.20		103.86		100.91		99.09		94.38	
13	587	81.49		98.61		96.33		94.41		90.51	



(a)



(b)

Fig. 3 Ground longitudinal profile plots before a and after addition of levees b

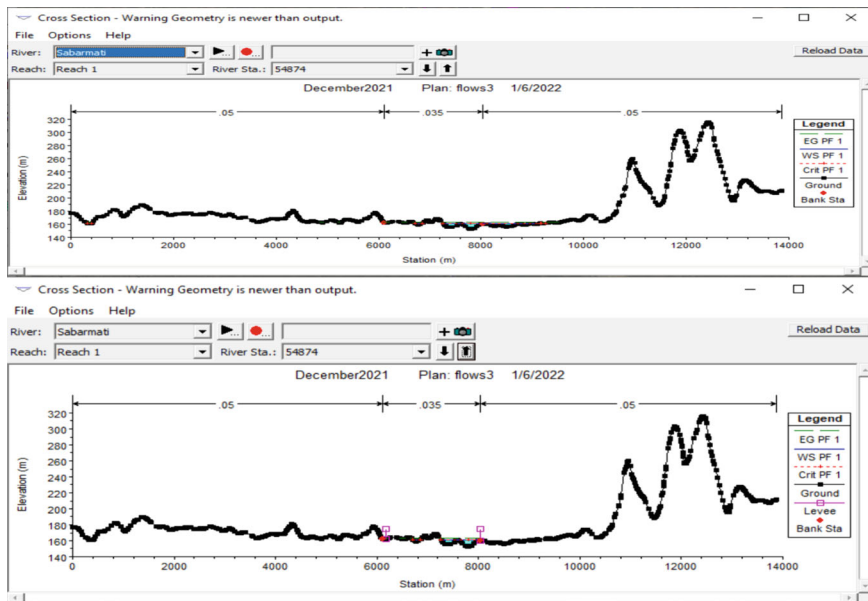


Fig. 4 Cross-Sect. 1 before and after the addition of levees

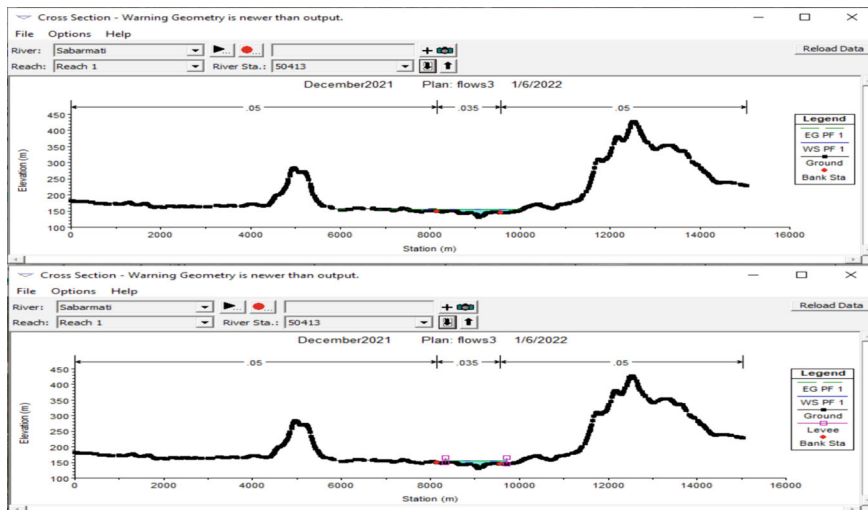


Fig. 5 Cross-Sect. 2 before and after the addition of levees

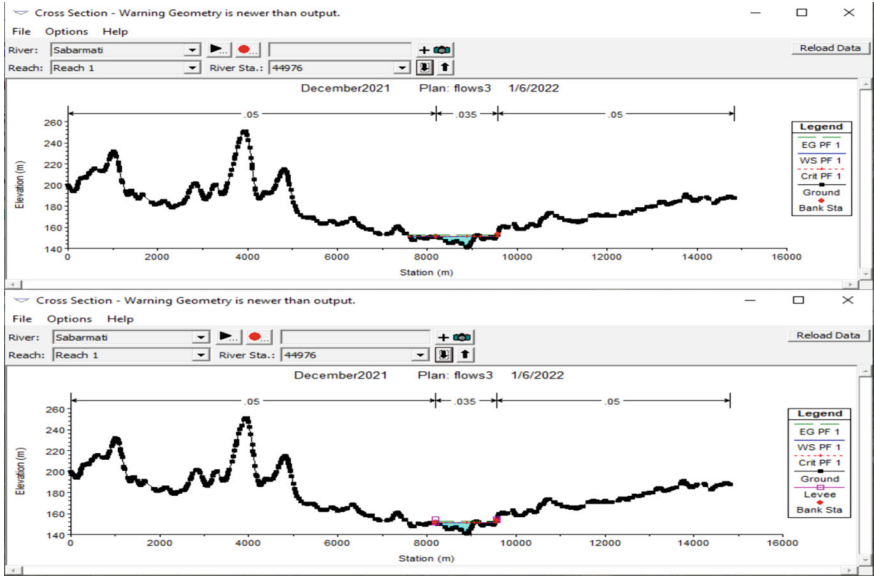


Fig. 6 Cross-Sect. 3 before and after the addition of levees

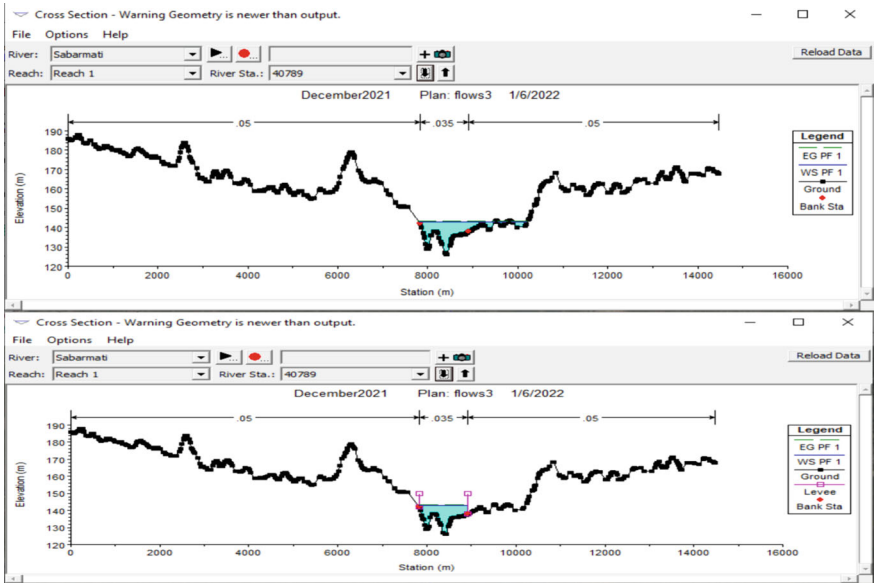


Fig. 7 Cross-Sect. 4 before and after the addition of levees

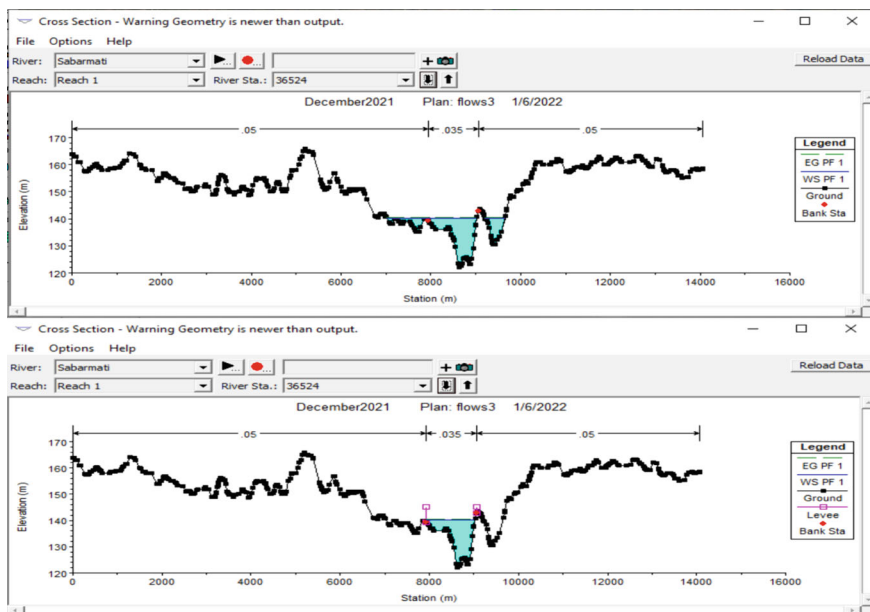


Fig. 8 Cross-Sect. 5 before and after the addition of levees

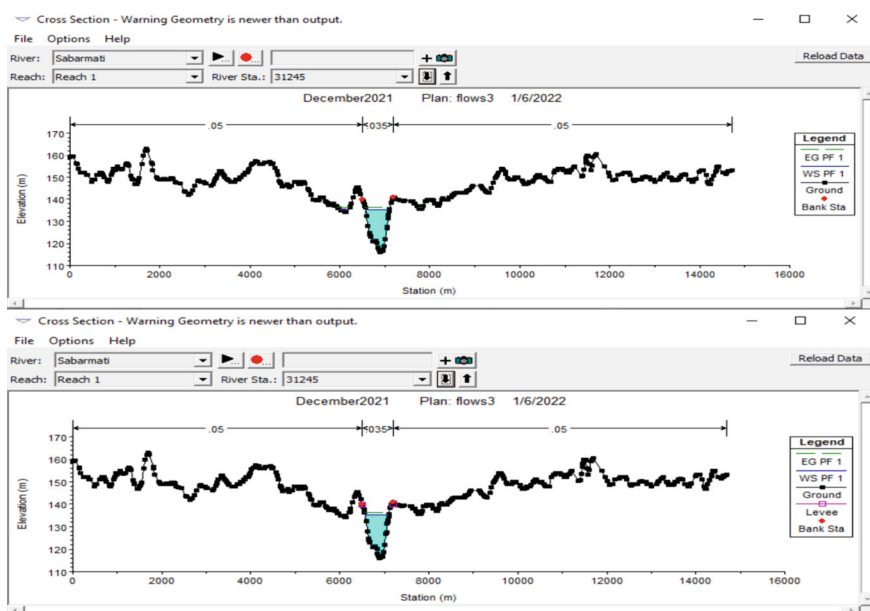


Fig. 9 Cross-Sect. 6 before and after the addition of levees

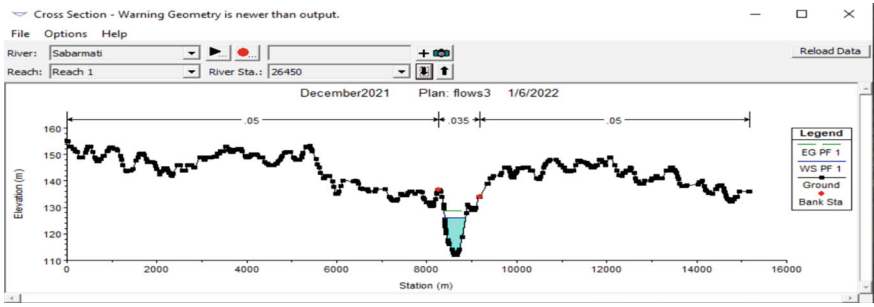


Fig. 10 Cross-Sect. 7

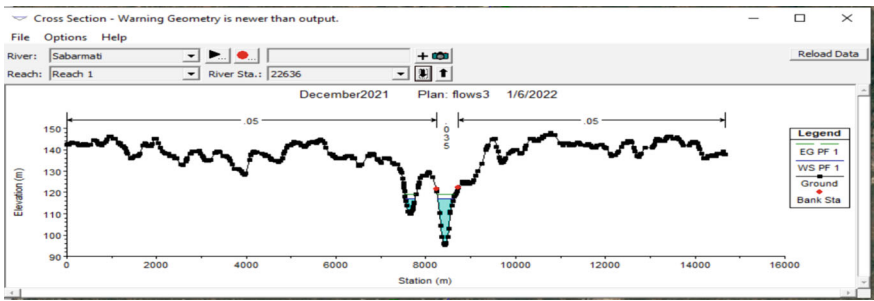


Fig. 11 Cross-Sect. 8

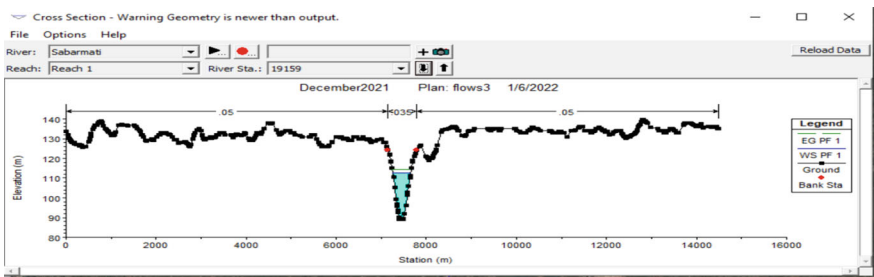


Fig. 12 Cross-Sect. 9

and height of the levees will need to be determined based on future model studies that consider different flood scenarios. This study can be applied to other areas for flood mitigation and management, depending on local topographical, hydrological, and geo-environmental conditions. It is proposed that the results of this model are compared with those of other advanced models for future improvement, if any.

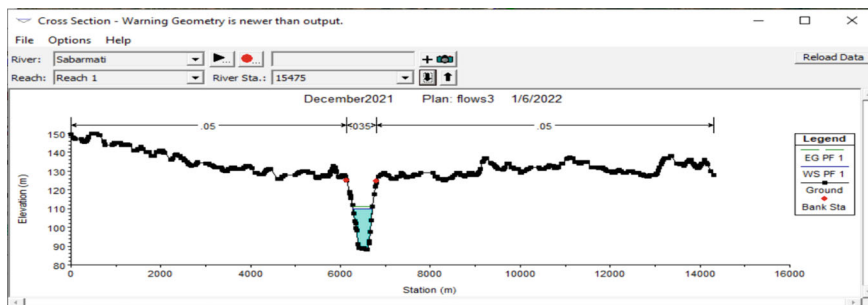


Fig. 13 Cross-Sect. 10

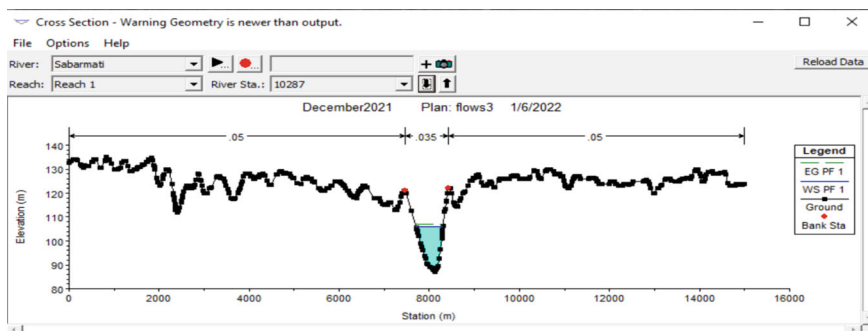


Fig. 14 Cross-Sect. 11

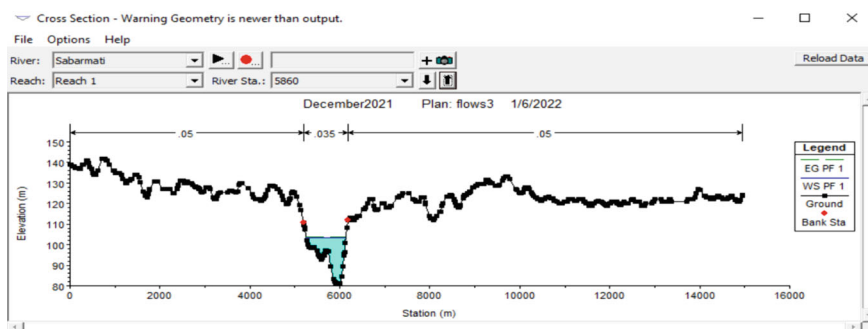


Fig. 15 Cross-Sect. 12

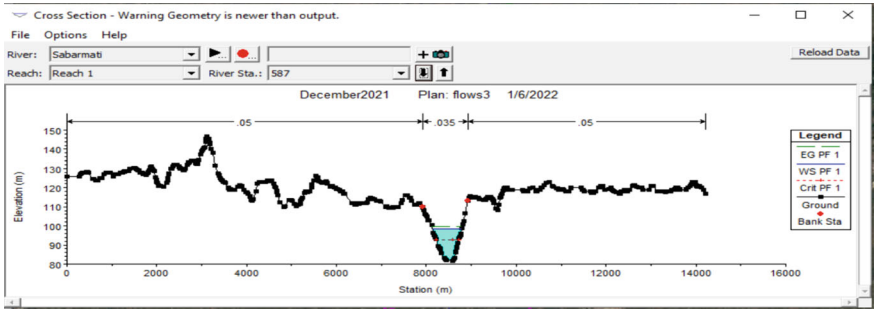


Fig. 16 Cross-Sect. 13

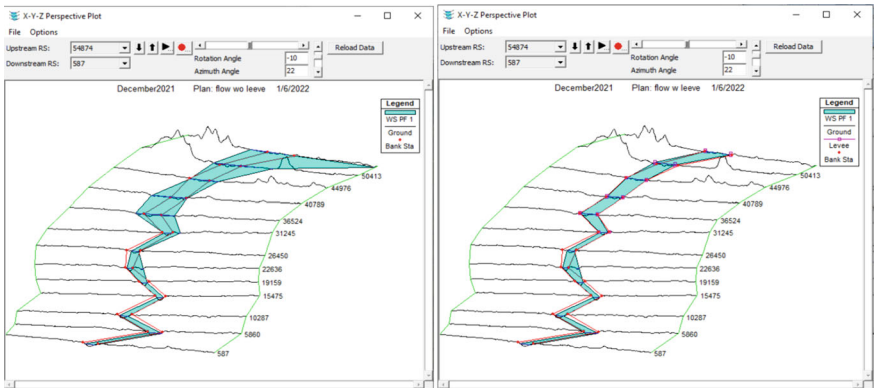


Fig. 17 Map showing X-Y-Z perspectives of profile 1 before and after addition of levees

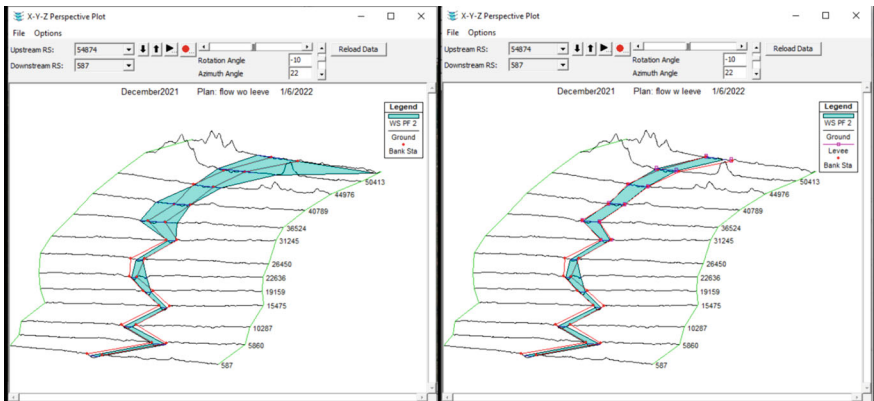


Fig. 18 Map showing X-Y-Z perspectives of profile 2 before and after addition of levees

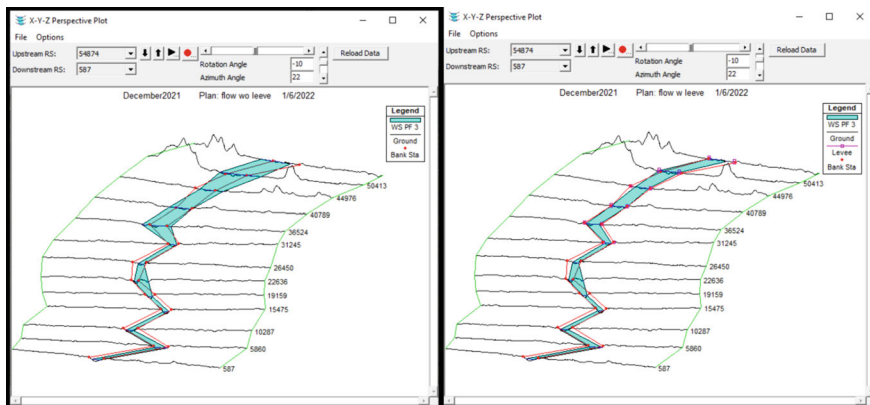


Fig. 19 Map showing X-Y-Z perspectives of profile 3 before and after addition of levees

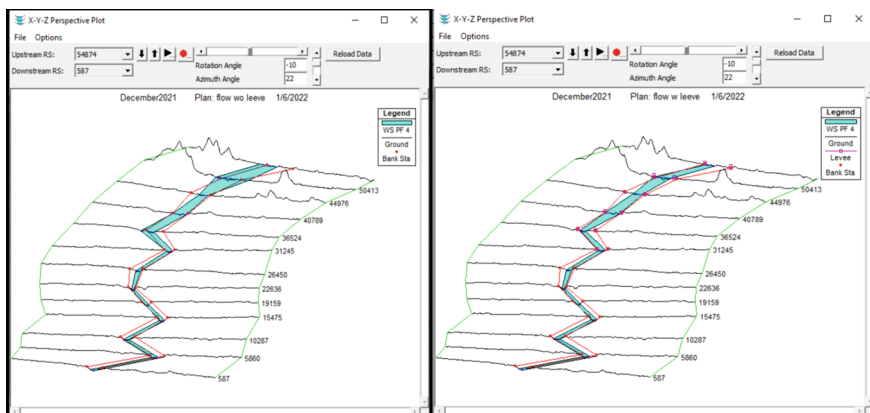
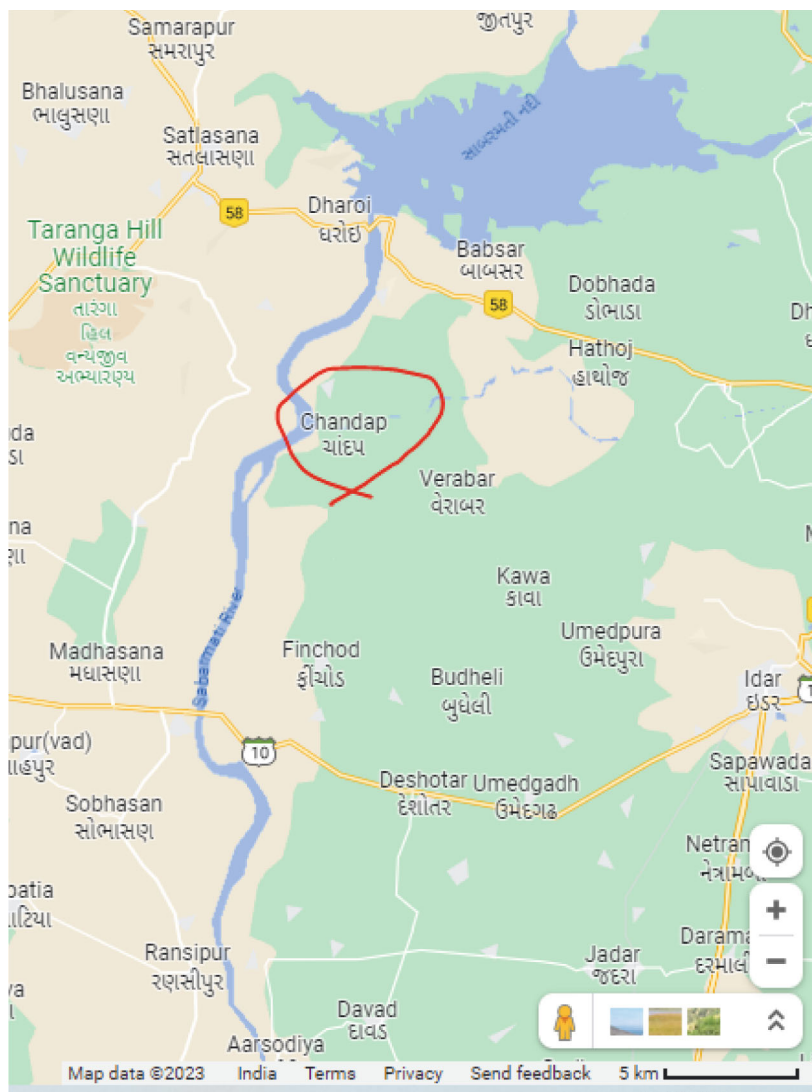


Fig. 20 Map showing X-Y-Z perspectives of profile 4 before and after addition of levees



(Source: <https://www.google.com/maps/@23.9112074,72.6900449,11z?entry=ttu>)

**Fig. 21** Location map of Chandap village at flood risk

## References

1. Al-Hussein AA, Khan S, Ncibi K, Hamdi N, Hamed Y (2022) Flood analysis using HEC-RAS and HEC-HMS: a case study of Khazir River (Middle East—Northern Iraq). *Water* 14(22):3779
2. Al-Zahrani M, Ahmed Al-Areeq A and Shareef H (2016) Flood analysis using HEC-RAS model: a case study for Hafir Al-Batin, Saudi Arabia. “Flood risk 2016—3rd European conference on flood risk management. Europe: Flood risk 2016—3rd European conference on flood risk management, pp 1–5
3. Awad T, Mayur B, Raju C, Ranjeet B, Shivamurti BK (2022) Flood management by using Hec-RAS software. *Int Res J Mod Eng Technol Sci* 4(6):148–154
4. Bakker MHN, Hegger D, Dieperink C, Driessen PPI, Raadgever GT and Wiering MA (2013) Flood risk management strategies across boundaries: a research approach. TWAM 2013, International conference and workshop. TWAM 2013, International conference and workshop, pp 1–5
5. Brunner GW (2020) Hec-RAS River analysis system user’s manual version 6.0 Beta. User’s manual, Hec-RAS river analysis system, US: US Army Corps of Engineers, Hydrologic Engineering Center
6. Choden T (2018) Research report for flood protection structures. Flood Engineering and management division, Dept Eng Serv Ministry Works Human Settl, pp 1–62
7. Conitz F, Zingraff-Hamed A, Lupp G, Pauleit S (2021) Non-structural flood management in European rural mountain areas—are scientists supporting implementation? *Hydrology* 8(4):167
8. Diaconu DC, Costache R, Popa MC (2021) An overview of flood risk analysis methods. *Water* 13(4):474
9. Ginige K, Mendis K, Thayaparan M (2022) An assessment of structural measures for risk reduction of hydrometeorological disasters in Sri Lanka. *Progress Disaster Sci* 1(14):100232
10. Khan A, Pathan I, Agnihotri PG (2020) 2 D Unsteady flow modelling and inundation mapping for lower region of purna basin using HEC-RAS. *Nat Environ Pollut Technol J* 19(1):277–285
11. Kryzanowski A, Brilly M, Rusjan S, Schnabl S (2014) Structural flood-protection measures referring to several European case studies. *Nat Hazards Earth Syst Sci* 14(1):135–142
12. Mahdi TW and Hillo AN (2021) Flood control by weir design using HecRAS model: the case of Al-Musandaq Escape. *IOP Conference series: earth and environmental science journal*, pp 1–11
13. Marina I, Josub M, Oana H, Romanescu GH (2015) The use of Hec-RAS modeliiing in flood risk analysis *Alexandru Ioan Cuza*. *Univ Faculty Geogr Carol* 20:315–322
14. Minea G, Zaharia L (2011) Structural and non-structural measures for flood risk mitigation in the Basca River catchment (Romania). *Forum Geogr J* 10(1):157–166
15. Ogie RI, Adam C, Perez P (2020) A review of structural approach to flood management in coastal megacities of developing nations: current research and future directions. *J Environ Plan Manag* 63(2):127–147
16. Ogras S, Onen F (2020) Flood analysis with HEC-RAS: a case study of Tigris river. *Adv Civil Eng* 2020(1):6131982
17. Patel AD, Dhruvesh DP and Prakash I (2016) Flood modelling using HecRAS and Geoinformatics technology in lower reaches of Shetrunji river, Gujarat, India. National conference on water resources and flood management with special reference to flood modelling. SVNIT Surat: National conference on water resources and flood management with special reference to flood modelling, pp 1–11
18. Patel CG, Gundaliya PJ (2016) Floodplain delineation using HecRAS model- a case study of smart city. *Open J Mod Hydrol* 6:34–42
19. Singh SK, Kanga S, Đurin B, Kranjčič N, Chaurasia R, Markovinović D (2021) Flood risk modeling using HEC-RAS and geospatial techniques. *E-ZBORNİK Electron Collect Pap Fac Civ Eng* 1(11):20–36

20. Thol T, Kim L, Ly S, Heng S and Sun S (2016) Applications of HEC-RAS for a flood study of a river reach in Cambodia. Proceedings of 4th international young researchers workshop on river basin environment and management. Vietnam: Proceedings of 4th International Young Researchers workshop on river basin environment and management, pp 16–20
21. Yevjevich V (1994) Chapter-28: Classification and description of flood mitigation measures. In: Coping with floods, by G. et al. Rossi, pp 573–584

# Modification of Graphene as an Effective Photo-Driven Catalyst for Photo-Assisted Degradation of Chlorpyrifos



Jinal Patel, Syed Shahabuddin, and Rama Gaur

## 1 Introduction

Agrochemicals are being used in agriculture for the protection of crops from pests and to enhance the crop yield to meet the current food demands [1]. The non-stop use of agrochemicals results in water pollution and degrades the water quality [2]. These chemicals ultimately enter the food cycle and have an adverse effect on aquatic fauna and human health. Agrochemicals and their metabolites are reported to be carcinogenic, genotoxic, and cytotoxic and cause a number of health-related issues in human beings. These agrochemicals are purposely used not only to kill several types of pests, but in addition, they also render a poisonous effect on non-target creatures [1]. So, these toxic pollutants must be removed from the wastewater for a better and safe environment. There are number of methods that have been used to eliminate pollutants from wastewater such as adsorption, reverse osmosis, hydrolysis, membrane filtration, and many more [3]. Amongst all the reported methods for waste water treatment, photocatalysis is the most suitable method for the removal of pollutants. Photocatalytic mechanism gives an advantages like light absorption, high surface area, cost-effective, reusable, and no secondary by-products [4].

In the present scenario, the photocatalysts become main key because of their great potential efficiency to help the environment problems. All the researchers and scientists are getting more and more attracted toward the graphene, and its derivatives are potential candidates due to their special characteristics of high surface area, high adsorption capacity, and electron mobility [5, 6]. GO and rGO show the different chemical, mechanical, and electrical properties due to their chemical and structural

---

J. Patel · S. Shahabuddin (✉) · R. Gaur (✉)  
Department of Chemistry, School of Energy Technology, Pandit Deendayal Energy University,  
Gandhinagar, Gujarat 382426, India  
e-mail: [syed.shahabuddin@sot.pdpu.ac.in](mailto:syed.shahabuddin@sot.pdpu.ac.in)

R. Gaur  
e-mail: [rama.gaur@sot.pdpu.ac.in](mailto:rama.gaur@sot.pdpu.ac.in)

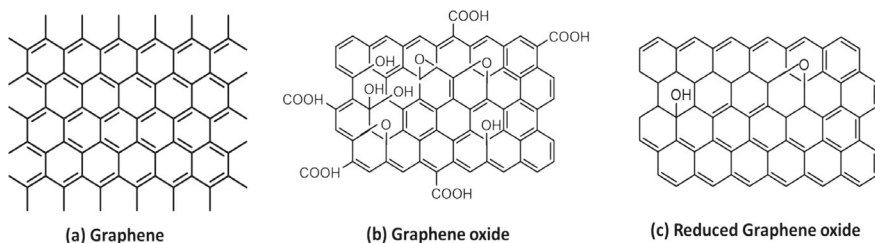


**Fig. 1** Chemical structure of graphene, GO and rGO

differences. Reduced graphene oxide shows similar properties of pristine graphene. But graphene has some limitations; it suffers from zero band gap and short-lived charge carriers, so modified in their chemical functionality which is important parameter in deciding the photocatalytic activity. Photocatalytic performance of catalyst depends on its electronic structure and band gap energy. Abid et al., have reported a 2.2 eV and 1.69 eV band gap for GO and rGO, respectively [7]. For an efficient photocatalyst, the rGO has smaller band gap to extend the light absorption in visible region.

Figure 1 represents the chemical structure of graphene and its derivatives and graphene structure arranged in carbon atoms joined by covalent bonds. During oxidation process of graphite, there is addition of oxygenated groups such as carboxyl, hydroxyl, and epoxy groups on the carbon basal planes and edges resulting in formation of graphene oxide (GO). In rGO structure through reduction process, oxygenated groups are removed, and bandgap can be adjusted by managing the oxygen present in GO [8]. The removal of oxygenated groups leads to a high surface area of rGO compared to GO. This study showing the comparison of graphene and its derivatives used as photo-driven catalyst for photocatalytic degradation of chlorpyrifos and its metabolites.

Several reports are available regarding the utilization of graphene, GO, and rGO as photocatalysts for the elimination of dyes, agrochemicals, and heavy metals. However, the present investigation aims to compare the efficacy of graphene, GO, and rGO in the process of photocatalytic degradation of chlorpyrifos. In the current study, we successfully synthesized GO and rGO using a modified Hummers method and a chemical reduction method. The current study demonstrates that rGO, when employed as a photocatalyst, exhibits a superior photocatalytic efficiency in the degradation of chlorpyrifos in comparison with both graphene and GO. Furthermore, the study highlights the significance of chemical functionality as a crucial parameter in determining photocatalytic activity.

## 2 Materials and Methods

Potassium permanganate (Avra 98%), sodium nitrate (Avra 99%), sulfuric acid (Finar 98%), hydrochloric acid (Finar 37%), ammonia solution (Finar 99%), ethanol, chloroform (Merck 99%), ascorbic acid (Avra 98%), hydrogen peroxide (Merck 30%), graphene nano powder multilayer flakes: (AO-4 G supermarket), graphite fine powder (HPLC), chlorpyrifos-CPY commercial (SUPER-D 50% purity) all chemicals, and DI water were used for the synthesis of GO, rGO, and photocatalytic studies.

### 2.1 *Synthesis of Graphene Oxide (GO) by Modified Hummer's Method*

Graphene oxide is prepared by the oxidation of graphite layers. For the synthesis of GO a mixture of 1 gm graphite, 1 gm  $\text{NaNO}_3$  and 50 ml  $\text{H}_2\text{SO}_4$  were taken in the beaker, and the mixture was stirred in ice bath for 15 min at  $8^\circ$ . After 15 min, 3 gm of  $\text{KMnO}_4$  powder was added into the solution slowly with continuous stirring for 30 min maintaining temperature below  $20^\circ$ . After this, the mixture was heated up to  $35^\circ$  for 30 min. Then distilled water was added, and temperature was raised maintained to  $90^\circ$ . After 30 min, distilled water and 30% of  $\text{H}_2\text{O}_2$  were added into the beaker to end the reaction. The washing was done by using 5% HCL solution and DI water until pH became 7. The product was dried in oven at  $80^\circ$  for 1 day [9].

### 2.2 *Synthesis of Reduced Graphene Oxide (rGO) by Chemical Reduction*

Reduced graphene oxide was synthesized via chemical reduction method using ascorbic acid as reducing agent. 400 mg of graphene oxide was added in beaker and dissolved in distilled water. After the complete suspension of GO, 4 gm ascorbic acid was added into beaker and stirred for 30 min at  $60^\circ$ . After the reaction, the solution was centrifuged for complete separation. Then 30 wt. %  $\text{H}_2\text{O}_2$  was added in the solution to oxidize the remaining ascorbic acid, and the solution was stirred for half hour at  $60^\circ$ . After the completion of the reaction, the solution was centrifuged and washed with ethanol and followed by washing with distilled water till pH becomes 7. The sample dried in oven at  $120^\circ\text{C}$  for 1 day [10].

### 3 Characterization

The as prepared samples graphene, GO and rGO were analyzed for identification of functional group, phase, and structural characterization. The functional group analysis was carried out using FT-IR spectroscopy Spectrum 2 Perkin Elmer spectrum instrument in a range of 400–4000  $\text{cm}^{-1}$ . The vibrational modes Raman analysis was carried out using a Renishaw spectrometer in a range of 300–3500  $\text{cm}^{-1}$ . The phase analysis was carried out using powder XRD, and the patterns were captured using PANalytical X'Pert Pro diffractometer at 30 mA and 40 kV using filtered Cu  $K\alpha$  radiation ( $\lambda = 1.53 \text{ \AA}$ ) in 10–50°s  $2\Theta$  range with a goniometer speed and step size of 1° per minute.

### 4 Photocatalytic Studies

Photocatalytic studies were conducted using a UV–Visible spectrometer (LABINDIA, UV 3000) in the range of 190–800 nm. For photocatalytic studies, 1 mg/ml photocatalyst was added into aqueous solution of CPY (10 PPM) and sonicated for uniform dispersion. The solution was kept in dark for half hour to attain adsorption–desorption equilibrium. Three drops of  $\text{H}_2\text{O}_2$  were added after 30 min as an initiator. After that the solution was kept in visible lamp (450 Watts HPMVL VIS Lamp High-Pressure Lamp) for 90 min with constant stirring. 3 ml of solution were withdrawn and centrifuged at regular time intervals for kinetic studies. The solution was analyzed using a UV–Visible spectrometer in a quartz cuvette.

## 5 Results and Discussion

### 5.1 FT-IR Analysis

FT-IR spectra of graphene, GO and rGO are shown in Fig. 2a. The vibrational peak at 1616  $\text{cm}^{-1}$  in the spectrum of the graphene indicates the C=C stretch from unoxidized graphitic domain [11]. After the oxidation of graphite, two additional peaks appeared at around 1039 and 1718  $\text{cm}^{-1}$ . The peak at around 1039  $\text{cm}^{-1}$  indicating the presence of C–O stretching vibrations of C–O–C and another peak at around 1718  $\text{cm}^{-1}$  is attributed to C=O stretch of carboxyl group. The broad peak between 280 and 3500  $\text{cm}^{-1}$  which indicates the carboxyl O–H stretching (3395  $\text{cm}^{-1}$ ) due to presence of water molecules and alcohol groups. The presence of ether, hydroxyl, and carbonyl groups in the chemical structure of the treated graphite is shown by these spectral modifications, which indicates that GO has been successfully produced [12]. In rGO spectra, the oxygenated group's peak intensities were decreased as compared to GO intensities which indicate the successful reduction of GO by ascorbic acid.

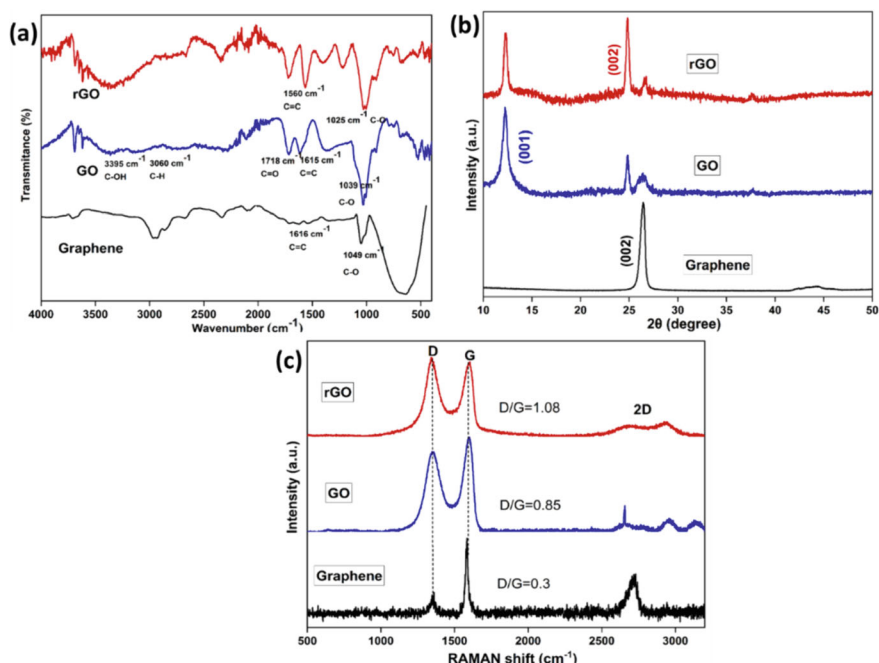


Fig. 2 a FT-IR spectra, b XRD pattern, and c RAMAN spectra of graphene, GO, and rGO

## 5.2 XRD Analysis

Figure 2b shows the XRD pattern of graphene, GO, and rGO. XRD pattern of graphene exhibits a strong reflection at 26.48°, which correspond to the (002) plane clearly describe the graphene structure with a 3.37 nm interlayer spacing (JCPDS-01-0646) [6]. During the oxidation process of graphite, the insertion of oxygenated groups (–OH, –COOH) between the graphite layers in GO pattern showed a larger interlayer spacing (7.36 nm) than graphene. The reflection at 26° there is decrease in peak intensity of GO and rGO it may be partial oxidation- reduction or unreacted graphene. In the reduction process, a layer-to-layer distance decreases from 7.36 nm (GO) to 3.58 nm (rGO) which confirms that the oxygenated groups were removed efficiently [13]. An additional low intensity peak at 38° which shows the disordered carbon material [8]. The d-spacing and average crystallite size of graphene, GO and rGO, were calculated using 26.48°, 12°, and 24.8° reflection using Bragg's equation and Scherer's equation. The obtained values are given in Table 1.

**Table 1** D-spacing and crystallite size values of graphene, GO, and rGO

Samples	Graphene	GO	rGO
Crystallite size (Å)	13.84	8.33	20.46
D-spacing (nm)	3.37	7.36	3.58

### 5.3 RAMAN Analysis

The study of carbon disorder and defects in crystal structure for graphene, GO and rGO, are confirmed by RAMAN spectroscopy (Fig. 2c). The *D* band at  $1345\text{ cm}^{-1}$ ,  $1349\text{ cm}^{-1}$ , and  $1341\text{ cm}^{-1}$  and *G* band at  $1580\text{ cm}^{-1}$ ,  $1598\text{ cm}^{-1}$ , and  $1593\text{ cm}^{-1}$  for graphene, GO, and rGO, respectively. In graphene, the 2D band at  $2730\text{ cm}^{-1}$  shows the rings and chain, indicating the presence of multilayer nature of graphene structure. In GO, the *D* band is widened due to reduction in size of the  $sp^2$  domains by formation of defects, and *G* band is shifted to the higher wavenumber which indicates formation of  $sp^3$  carbon atoms during the oxidation of graphite [14]. In the rGO, the *G* band intensity is less than *D* band due to the increased number of  $sp^2$  carbon atoms and shifted to lower wavenumber. Higher *D/G* intensity ratio confirmed the presence of more defects and disorder in the structure [13]. Increased *D/G* intensity ratio indicates that the *D/G* value increased after the oxidation of graphite and reduction of GO. The increase of *D/G* intensity ratio from 0.85 to 1.08 during the formation of GO to rGO points towards the structural disorder and also confirms the attachment of oxygenated groups. rGO has higher *D/G* ratio than graphite due to  $sp^2$  domains which are again formed through the reduction process [12].

### 5.4 Photocatalytic Studies of Graphene and Derivatives of Graphene

Figure 3a shows the UV–Visible spectrum depicting the adsorption and degradation studies using graphene, GO, and rGO for the degradation of chlorpyrifos (peak at 295 nm). Graphene shows the only adsorption while in the case of GO there is no change after adsorption it shows saturation. In rGO, it shows the decrease in peak intensity, but in the presence of light, there is a shift in the peak which indicates that new species are formed. From the literature, it was confirmed that the new species formed was chlorpyrifos-oxon showing absorbance maxima at 280 nm [15]. Figure 3b shows the C/Co versus time graph which indicates as the time increases there is increase in the degradation efficiency for graphene and rGO. Among all of them, rGO shows the highest degradation efficiency of 85%. GO shows saturation at one point; there is no decrease in the peak intensity. Figure 3c indicates the % removal of chlorpyrifos by graphene, GO, and rGO. Graphene exhibits the 80% adsorption with 3% photocatalysis. GO exhibits 50% adsorption with 6% photocatalysis. While in the case of rGO shows the 72% adsorption with 13% photocatalysis. Figure 3d shows the digital image of chlorpyrifos solution after photocatalytic treatment with graphene, GO, and rGO after 90 min.

The kinetics studies for the adsorption and degradation of chlorpyrifos were monitored at regular time intervals, and the obtained data was fitted for first- and second-order kinetic models which are presented in Fig. 4a, b. Figure 4a shows the dark and

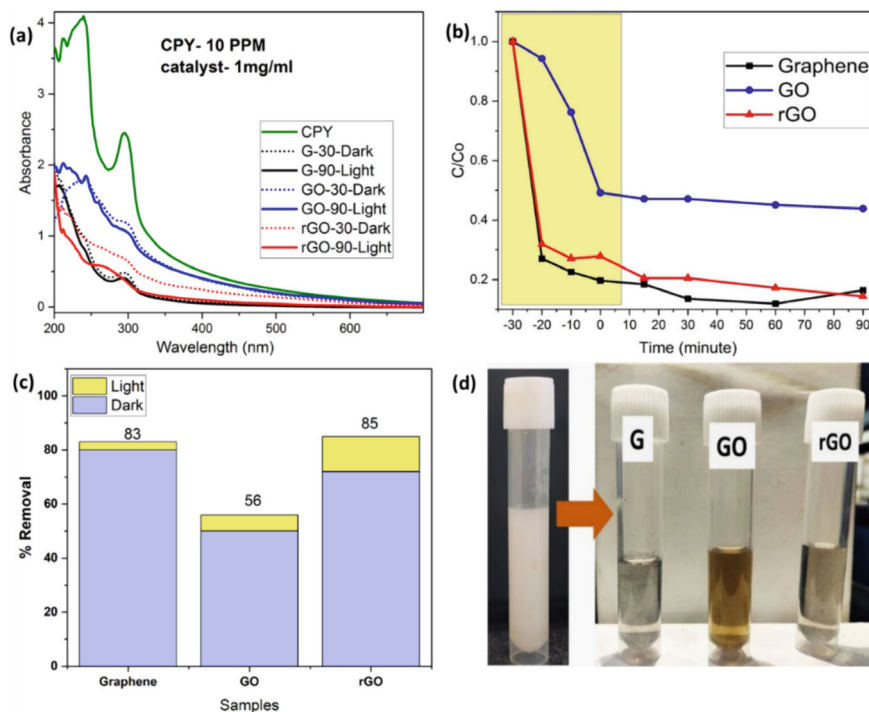


**Fig. 3** **a** Adsorption and degradation study, **b**  $C/C_0$  versus time graph, **c** % removal of chlorpyrifos and **d** images of chlorpyrifos after degradation with graphene, GO, and rGO

light environments for first order and Fig. 4b shows the dark and light environments for second-order kinetic model for graphene, GO, and rGO.

The rate constants for adsorption ( $K_{ads}$ ) and photocatalysis ( $K_{cat}$ ) are shown in Table 2 along with  $R^2$  values. The higher  $R^2$  values for the second-order kinetics for adsorption, with maximum rate constant of  $70.42 \text{ M}^{-1} \text{ s}^{-1}$  for graphene, confirm that adsorption follows second-order kinetics. The higher  $R^2$  values for the second-order kinetics for photocatalytic, with a maximum rate constant of  $12.8 \text{ M}^{-1} \text{ s}^{-1}$  for rGO, demonstrate that photocatalytic degradation follows the second-order kinetics.

In the rGO structure, the C/O ratio increases, and its properties become more similar to pristine graphene. The electrical conductivity of rGO is much higher than that of semiconducting GO. During photocatalysis experiments, rGO serves as an electron-acceptor and electron-transport material, accelerating the transfer of photo-generated electrons and preventing the recombination of electron-hole pairs, hence increasing the photocatalytic efficiency [16].

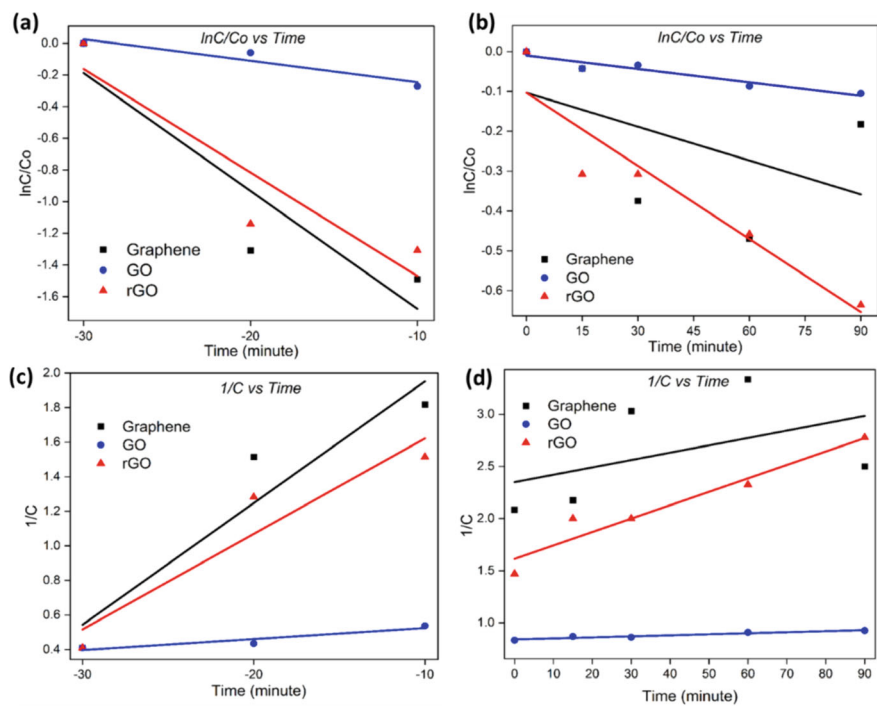


**Fig. 4** Kinetic model first-order under **a** dark and **b** light condition, kinetic model second-order under **c** dark and **d** light condition

**Table 2** Rate constant and  $R^2$  values for first- and second-order kinetic model in adsorption and photocatalysis

Sample	1st		2nd		1st		2nd	
	Adsorption				Photocatalysis			
	$K_{\text{ads}} \times 10^{-3} \text{ (s}^{-1}\text{)}$	$(R^2)$	$K_{\text{ads}} \times 10^{-3} \text{ (M}^{-1} \text{s}^{-1}\text{)}$	$(R^2)$	$K_{\text{cat}} \times 10^{-3} \text{ (s}^{-1}\text{)}$	$(R^2)$	$K_{\text{cat}} \times 10^{-3} \text{ (M}^{-1} \text{s}^{-1}\text{)}$	$(R^2)$
Graphene	74.4	0.8402	70.42	0.9023	2.83	0.2495	7.05	0.2205
GO	13.5	0.9039	6.39	0.8897	1.13	0.9208	0.99	0.9256
rGO	65.3	0.8440	55.2	0.8997	6.11	0.8896	12.8	0.9335

## 6 Conclusion

In summary, the photo-assisted degradation of chlorpyrifos was done using graphene and their derivatives. It can be concluded that graphene and its derivatives were well synthesized by modified Hummer's method and chemical reduction method. Graphene and their derivatives were characterized using XRD, FT-IR, and RAMAN spectroscopy. Graphene, GO, and rGO removed 82, 53, and 83% of chlorpyrifos in 90 min. This study shows that rGO showed better photocatalytic properties and enhanced the efficiency than pristine graphene and GO. The photo-assisted degradation of chlorpyrifos follows the second-order kinetics. The development of a photoactive catalyst like rGO and its implementation in agrochemical degradation is a cost-effective and environment-friendly approach for the treatment of wastewater. rGO can be future explored in combination with photosensitizer for enhanced catalytic response and degrade into simple products..

**Acknowledgements** The authors would like to thank the Department of Chemistry, SRDC (Solar Research and Development Centre), PDEU for support in characterization and analytical facilities. The authors would like to acknowledge the Government of Gujarat for the award of a research fellowship (KCG/SHODH/2022-23/202101585) under the Scheme for Developing-High-Quality-Research.

## References

1. Singh D et al (2020) Impacts of agrochemicals on soil microbiology and food quality. Agrochemicals detection, treatment and remediation. Elsevier, pp 101–116
2. Sebastian A, Nangia A, Prasad MNV (2020) Advances in agrochemical remediation using nanoparticles. Agrochemicals detection, treatment and remediation. Elsevier, pp 465–485
3. Morin-Crini N et al (2022) Removal of emerging contaminants from wastewater using advanced treatments: a review. *Environ Chem Lett* 1–43
4. Saravanan A et al (2022) Degradation of toxic agrochemicals and pharmaceutical pollutants: effective and alternative approaches toward photocatalysis. *Environ. Pollut* 118844
5. Smith AT et al (2019) Synthesis, properties, and applications of graphene oxide/reduced graphene oxide and their nanocomposites. *Nano Mater Sci* 1(1): 31–47 %@ 2589–9651
6. Gotoh K et al (2011) Exfoliated graphene sheets decorated with metal/metal oxide nanoparticles: simple preparation from cation exchanged graphite oxide. *Carbon* 49(4):1118–1125 %@ 0008–6223
7. Abid et al (2018) Reduced graphene oxide (rGO) based wideband optical sensor and the role of temperature, defect states and quantum efficiency. *Sci Rep* 8(1):3537 %@ 2045–2322
8. Hidayah NMS et al (2017) Comparison on graphite, graphene oxide and reduced graphene oxide: synthesis and characterization. AIP Publishing
9. Karim MR, Hayami S (2017) Chemical, thermal, and light-driven reduction of graphene oxide: approach to obtain graphene and its functional hybrids. In: *Graphene materials—advanced applications*, p 89
10. Habte AT, Ayele DW (2019) Synthesis and characterization of reduced graphene oxide (rGO) started from graphene oxide (GO) using the tour method with different parameters. *Adv Mater Sci Eng* 2019:1687–8434

11. Bera M, Gupta P, Maji PK (2018) Facile one-pot synthesis of graphene oxide by sonication assisted mechanochemical approach and its surface chemistry. *J Nanosci Nanotechnol* 18(2):902–912 % @ 1533–4880
12. Kanta U-A et al (2017) Preparations, characterizations, and a comparative study on photo-voltaic performance of two different types of graphene/TiO<sub>2</sub> nanocomposites photoelectrodes. *J Nanomater* 2017:1687–4110
13. Johra FT, Lee J-W, Jung W-G (2014) Facile and safe graphene preparation on solution based platform. *J Ind Eng Chem* 20(5):2883–2887 % @ 1226–086X
14. Perumbilavil S et al (2015) White light Z-scan measurements of ultrafast optical nonlinearity in reduced graphene oxide nanosheets in the 400–700 nm region. *Appl Phys Lett* 107(5 % @ 0003–6951)
15. Lockridge O, Veudier L, Schopfer LM (2019) Half-life of chlorpyrifos oxon and other organophosphorus esters in aqueous solution. *Chem-Biol Interact* 311:108788 % @ 0009–2797
16. Zangiabadi M et al (2019) Evaluating the efficiency of the GO-Fe<sub>3</sub>O<sub>4</sub>/TiO<sub>2</sub> mesoporous photocatalyst for degradation of chlorpyrifos pesticide under visible light irradiation. *Appl Organomet Chem* 33(5):e4813 % @ 0268–2605

# Air Quality Index Management of Medium-Sized Community Space in Gurugram, Haryana



Vivek Jaiswal , Shubham Singh, and Sanjay Maurya

## 1 Introduction and Background

Air pollution is a real issue and a ticking time bomb. Not only developed but even developing countries with considerable populations need help in front of this challenge. As per the World Health Organization report in 2022 [1], India has a  $53.3 \mu\text{g}/\text{m}^3$  concentration of PM<sub>2.5</sub> [Particulate matter of size less than  $2.5 \times 10^{-6}$  m (micron)] against the recommendable limit of  $15 \mu\text{g}/\text{m}^3$ . Although it is slightly lower than 2021 ( $58.1 \mu\text{g}/\text{m}^3$ ), it is still four-fold higher than what makes air breathable. All this hazardous rise in PM concentrations and air pollution leads to many catastrophic consequences. These particulate matter and other unwanted gases in polluted air cause respiratory diseases, heart, and pulmonary obstructive infections, strokes, and chronic issues such as lung cancer and asthma. The Government of India and its policymakers focus on this through the National Clean Air Programme, Pradhan Mantri Ujjwala Yojana, and others. However, a long road is still ahead to travel for safer air. Generally, air quality is not directly referred to through concentration but through air quality index (AQI). AQI is better and more holistic than citing the concentration of only one-sized particulate matter. AQI is an index that summarizes the status of air quality daily [2]. It could be local, outdoor, and indoor in the environment in which it is evaluated. Generally, outdoor AQI is considered the most affected and polluted due to the many deterrents present. Table 1 with the value of AQI represents the quality of air:

The factors affecting AQI values are ozone concentration, particle pollution, carbon monoxide, and sulfur dioxide [3]. Thus, the different purification techniques have other target species to purify the air. The choices of purification depend on

---

V. Jaiswal (✉)

Pandit Deendayal Energy University, Gujarat 382007, India

e-mail: [vivek.jaiswal@sot.pdpu.ac.in](mailto:vivek.jaiswal@sot.pdpu.ac.in)

S. Singh · S. Maurya

Urban Air Labs, Gurugram, Haryana 122002, India

**Table 1** AQI range with the corresponding level of health concern

Air quality index (AQI)	Level of health concern
0–50	Healthy
50–100	Moderate
101–150	Breathable
151–200	Unhealthy
201–300	Extremely unhealthy
301–500	Hazardous

the environment, design, economic factors, and after-effects of the process. Existing techniques to purify the air quality are categorized into two sections: Particulate matter and gaseous purification techniques. Many characteristics must be examined for selecting a particulate matter purification technique, including temperature, humidity, exhaust gas flow pattern, particle size, and chemical nature. Hence, there are different scrubbers, filters, and separators under the particulate matter purification technique. However, there are four phenomena through which gaseous pollutants can be removed from the air: absorption, adsorption, condensation, and combustion. The first three phenomena are recovery techniques and combustion phenomena that generate flares and destroy the pollutant. All the above discussion elucidates that the task of purification of air from its pollutants is time, energy, and economically challenging.

High-efficiency particulate air filter, abbreviated as HEPA filter, is used for the removal of tiny (micron/sub-micron) and harmful particles such as pollen, pet furs, smoke, dust, and air-borne viruses with an efficiency of 99.95% (or 99.97%) [2, 4]. It is the most utilized and referred filter for clinical to industrial usage. Activated carbon filters mainly capture volatile organic compound (VOC), which may diffuse the collected gases after a few days of use and spread a fouling smell [5]. They pose a significant drawback to the non-filtration of particles; hence, they are less used. Unlike activated carbon filters, ionizers remove smaller particles and odor by throwing negatively charged ions into the air. Still, they are ineffective against large particles such as pollens. The above discussion states that air purification (or technically filtration) is a largely mechanized industry; hence, different types of filters are only used to date. In the present article, we prove that UBreathe devices are effective by following nature-based solutions with a 65% reduction of AQI in a single pass for their UBreathe Life stacked with their patent filed ‘Breathing Roots Technology’ and ‘Urban Munnar Effect.’ Also, it is reported that there is a 77% hourly decrease in AQI levels for a room size of 300 sq. ft., as per the laboratory test reports from the National Aerosol Laboratory, IIT Kanpur. This will support the claim of better nature-based solutions for real-life problems, especially environment-related issues.

## 2 Test Area and Pre-treatment

The test area includes three spaces: (a) core-team room (CTR), (b) assembly room (AR), and (c) air-crew room (ACR) with the area as given in Table 2.

Initially, the core-team room and air-crew room were used as usual seating, discussion points, and product development activities, which included soldering and prototyping activities without specific attention to ventilation, infiltration, and air quality (see Fig. 1). The assembly room was dedicated to the manufacturing and assembly activities of products. The processes usually included cutting, grinding, soldering, bonding, scrubbing, buffing, etc. The assembly area acted as a significant source of pollution for other spaces. Therefore, AQI was very drastic (ranging from 160 to 200), and the concentration of PM<sub>2.5</sub> particles varies from 85 to 125  $\mu\text{g}/\text{m}^3$ .

Before employing the proposed technique/solution for air quality improvement, a few pre-treatment steps were taken. Identification of the source of various pollutants, area segmentation, proper air ventilation, pollutant cut-off, and inter-mixing prevention mechanisms are deployed before the UBreathe solution. This was initiated to practice checking on air quality at regular intervals and adapt to day-to-day life. The source of pollutant generation identification is crucial as a significant chunk of it can be easily avoided. Infiltration, renovation, manufacturing, and cooking activities are

**Table 2** Investigated spaces with the respective area

Space	Core-team room (sq. ft.)	Assembly room (sq. ft.)	Air-crew room (sq. ft.)
Area	200	600	200

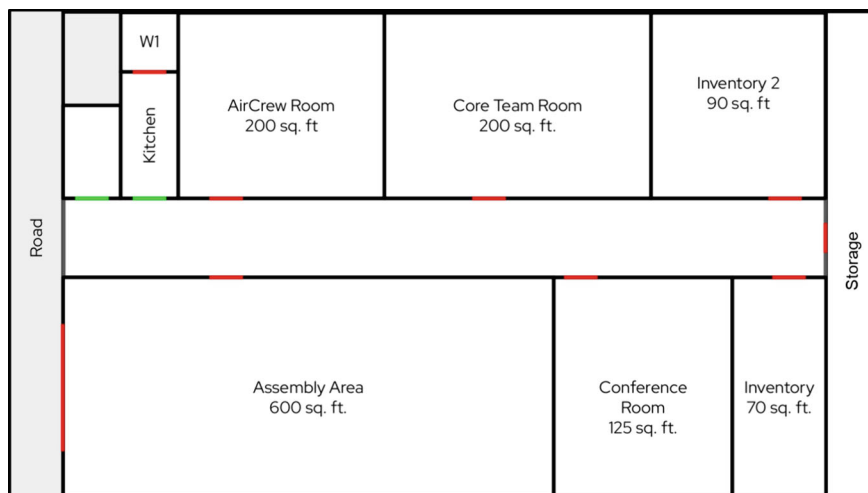


**Fig. 1** 2D layout of the site (red marked boundaries are doors and green marked boundaries are open areas)

the leading causes of pollutant generation. Infiltration can be minimized by applying specific closure and air-masking arrangements for doors and windows. Renovation activities such as painting, glass cleaning, and others generate gaseous fumigants, lead to air pollution. Segmentation of spaces is also essential, as there are many spots with breathable concentrations of PM<sub>2.5</sub>. Still, due to the presence of sites with very high concentrations of PM<sub>2.5</sub>, the whole dynamics change to polluted. So, if balanced area segmentation is done, purification will be done in a targeted manner. Last but not least, there are three mechanisms of pollutant removal, namely: (1) purification through an air conditioner, (2) purification through an air purifier, and (3) phytoremediation [6, 7] for the given space. A standard operating procedure (SOP) is designed based on the general routine of the targeted space. Following are the steps of the SOP:

- The exhaust fan must be turned on continuously. Create a little amount of negative pressure.
- While the office is still open, the cabins 8 Ub Mini and 4 Ub Life units must be turned on. (Kept preferably in the middle of the area to prevent wall blockers).
- In the assembly room, two Ub Life units must be turned on and maintained close to the work area while conducting any machining.
- All of the cabins' doors should be kept closed, and the corners of the doors and windows should be adequately sealed with tape.
- The front door should always be locked. As per customary standards, infrequent door openings provide fresh air ventilation.
- The main entry door should always be slightly ajar when painting and spraying are done. In this situation, there ought to be two purifiers operating close to the activity.
- For appropriate sunshine and fresh air, all plants must be kept in an open environment every 15 days.
- The plant's dead leaves must be routinely removed.
- All plants must receive the necessary amount of water.
- To dissolve the particles accumulating on the leaves cuticles and increase surface adsorption capacity, plants' leaves must be sprayed with moisture every two days.
- The workplace has to be cleaned often to prevent the accumulation of contaminants. Turn off the fan and purifiers while cleaning to prevent mixing up the contaminants and circulation of pollutants in the air.

### 3 Test Area and Pre-treatment

Ub Mini and Ub Life (Fig. 2) are two novel products from Urban Air Labs that are nature-based solutions to curb air pollution. It is backed by the UNDP Accelerator Lab, Biotechnology Industry Research Assistance Council (BIRAC), and other research agencies working on air quality improvement. UBreathe's technology works on the patent filed "Urban Munnar and Breathing Roots" technology and harnesses air purification coupled with 5-layer filtration techniques. The filtration technique

includes UV, charcoal, HEPA, and a stack of pre-filters with specially selected plants to remove particulate matter, volatile organic compounds, and gaseous and biological contaminants. The size of Ub Mini and Ub Life are 0.34 and 2.82 sq. ft. Hence, the installation area requirement is much less than a nominal office space. It is cost-efficient, low on maintenance, and increases available oxygen. Three essential parameters for air purification are the penetration, efficiency, and permeability of the process or technique. The efficiency is the easiest of the three as it is the ratio of the volume of clean air delivered to the total air filtered ( $\eta = V_{\text{clean}}/V_{\text{total}}$ ). Penetration refers to the particle size that passes through the filter tested; it is a vital factor in deciding which filter is suitable. Permeability measures the extent of air passage through the given material. All three elements are taken care of in UBreathe technology (see Table 3).

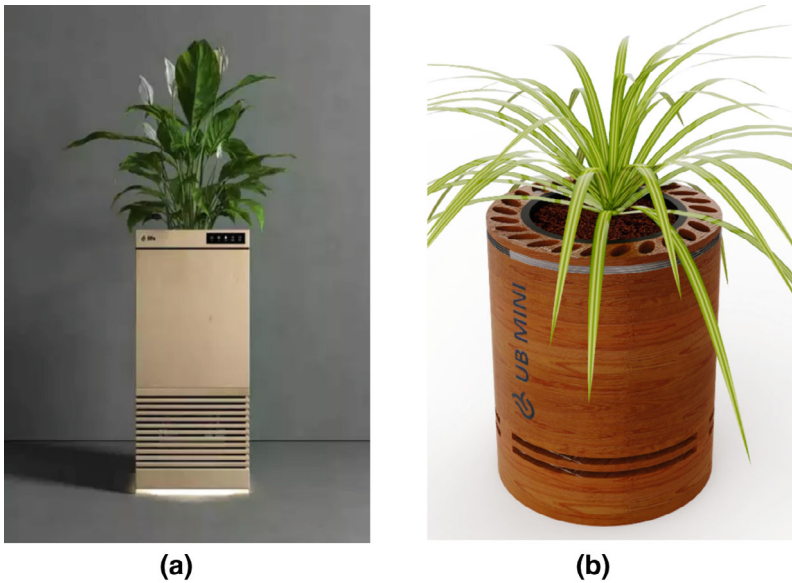


**Fig. 2** a Ub Life and b Ub Mini

**Table 3** Parameters of UBreathe products

Parameters	Ub life	Ub mini
Single-pass efficiency (%)	65	15
Penetration ( $\mu$ )	0.3	0.3
Permeability (m/s)	1.39	1.44

## 4 Result and Discussion

### 4.1 Month and Hour-Wise Variation of AQI with UBreathe

As reported in Fig. 3, the monthly AQI of the investigated areas (with the devices) is much lesser (at least by 50%) as compared to the outdoors (without the devices). The data shown is a monthly average to negate the effort of sudden surges or shortfalls. The AQI of air-crew space has the most significant change (60%<) due to the nearby placement of the UBreathe device and other precautionary measures. This result signifies the deployment of UBreathe technology for air quality improvement in the long run. The machines needed to be more capable to provide satisfactory air purification from mid-May to mid-August. The reason behind this outlier is construction activity in the vicinity of the test space for the given duration. Although a surge is noticed, AQI remains within breathable limits (< 100). For shorter or hourly exposure, Fig. 3b explains the status of AQI from 10 AM to 7 PM (practical working hours). The spaces of the assembly room only cross the regime of safe limit, and that too after lunch hours due to more gathering, higher manufacturing activities, and infiltration at the latter half of the day. Despite this, AQI is still very close to the safe limit, hence breathable (AQI safe limit is 50).

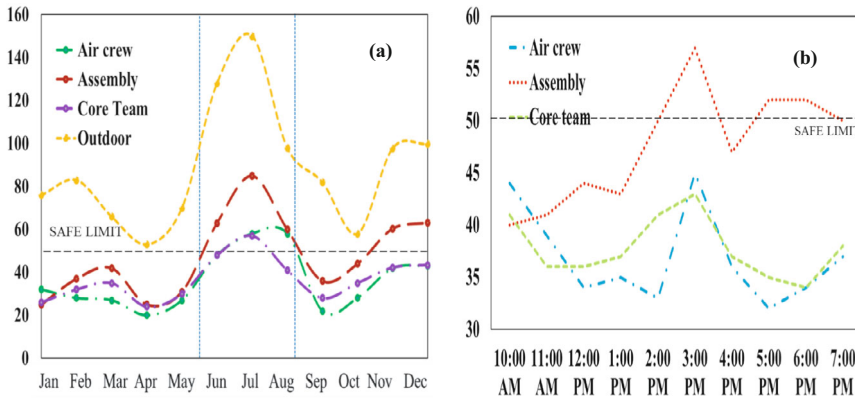
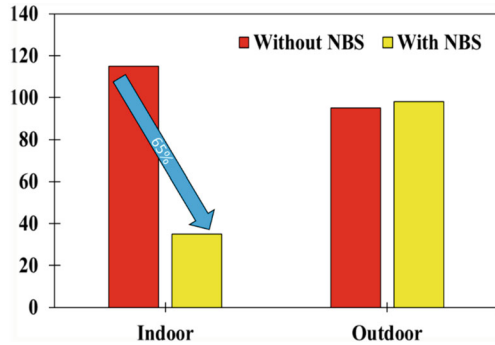


**Fig. 3** **a** Month-wise variation of AQI with (investigated spaces) and without (outdoor) UBreathe and **b** hourly variation of AQI of the investigated spaces with UBreathe

**Fig. 4** Concentration of PM2.5 particle with and without nature-based solution (NBS-UBreathe) for indoor (investigated space) and outdoor



#### 4.2 *PM2.5 Concentration Indoor Versus Outdoor with UBreathe*

The second important parameter in air quality is the level (concentration) of PM2.5 particles. Figure 4 showcases the concentration of PM2.5 particles with and without UBreathe (NBS). A 65% reduction is reported for indoor cases, from ~ 120 to ~ 35  $\mu\text{g}/\text{m}^3$ . There were no changes in PM2.5 concentration for outdoor cases.

Combining the observations of Figs. 3 and 4, it is evident that using the UBreathe solution brings down the AQI and PM2.5 concentration to at least a breathable limit, if not less. Therefore, Ub Life and Ub Mini are highly recommended for offices, assembly, closed wall structures, and gathering places for better air quality.

### 5 Conclusion

The air quality index (AQI) and concentration of particulate matter PM2.5 were targeted in the investigated spaces of different areas. Ub Life and Ub Mini were the products deployed to improve the task. The result shows that AQI is reduced by ~ 50% monthly and ~ 54% hourly with UBreathe nature-based solution. For PM2.5 concentration, the investigated spaces generally report a ~ 65% reduction. These observations were made to make the truthful claim of UBreathe for better air purification compared to existing filter-based purification.

### References

1. WHO ambient air quality database, 2022 update: status report. ISBN: 978-92-4-004769-3
2. Dubey S, Rohra H, Taneja A (2021) Assessing the effectiveness of air purifiers (HEPA) for controlling indoor particulate pollution. Heliyon 7(9)

3. Bągoszewska E, Biedroń I (2021) Efficiency of air purifiers at removing air pollutants in educational facilities: a preliminary study. *Front Environ Sci* 9:709718
4. Szabadi J, Meyer J, Lehmann M, Dittler A (2022) Simultaneous temporal, spatial, and size-resolved measurements of aerosol particles in closed indoor environments applying mobile filters in various use cases. *J Aerosol Sci* 160:105906
5. Leung DY (2015) Outdoor-indoor air pollution in an urban environment: challenges and opportunity. *Front Environ Sci* 2:69
6. Agarwal P, Sarkar M, Chakraborty B, Banerjee T (2019) Phytoremediation of air pollutants: prospects and challenges. *Phytomanage Pollut Sites*: 221–241
7. Gawrońska H, Bakera B (2015) Phytoremediation of particulate matter from indoor air by *Chlorophytum comosum* L. plants. *Air Qual Atmos Health* 8:265–272

# Application of MOFs in Membrane Modification for Treatment of Wastewater: A Review



Sapna Ajay Gawali, Sunskrati Pandey, Het Tilala, Kashyap Tailor, Swapnil Dharaskar, Nagarjuna Reddy Paluvai, Swapna P. Reddy, Manish Kumar Sinha, and Surendra Sasi Kumar Jampa

## 1 Introduction

According to the World Health Organization, a staggering 700 million individuals are deprived of access to clean water. This figure is further compounded by an additional 500 million people at risk of encountering the same issue. Regrettably, the situation is anticipated to worsen even more by the year 2025 [1]. The latest developments in separation technology have expected a green and sustainable future that advocates power protection and wastewater minimization. The concept of a smooth future emphasizes retrieval and reutilization of precious products from waste streams to improve the water finely. Releasing untreated sewage is a grossly irresponsible act that poses a serious threat to the environment and the health of human beings. It is crucial to note that heavy metal ions severely threaten one's health and are not biodegradable, unlike natural impurities. Their impact should not be underestimated threat once sewage and heavy metals into the human food chain. Effective and sustainable treatment of contamination is crucial for the reuse of wastewater, as natural water sources are scarce and not easily accessible. This need must be addressed immediately. Various wastewater treatment methods, such as adsorption, coagulation, biological treatment, and other technological advancements, can effectively address water

---

S. A. Gawali · S. Pandey · H. Tilala · K. Tailor · S. Dharaskar · N. R. Paluvai · M. K. Sinha (✉) · S. S. K. Jampa (✉)

Department of Chemical Engineering, School of Energy Technology, Pandit Deendayal Energy University, Gandhinagar 382426, India

e-mail: [manish.sinha@sot.pdpu.ac.in](mailto:manish.sinha@sot.pdpu.ac.in)

S. S. K. Jampa

e-mail: [surendra.sasikumar@sot.pdpu.ac.in](mailto:surendra.sasikumar@sot.pdpu.ac.in)

S. P. Reddy

Department of Chemical Engineering, National Institute of Technology Calicut, Kerala 673 601, India

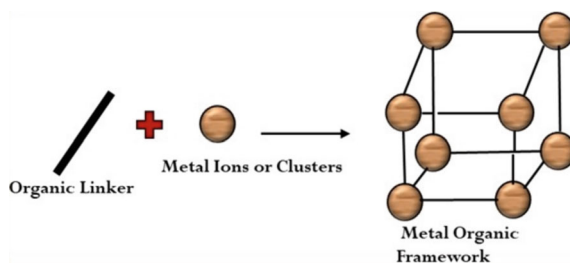
scarcity issues [2–4]. Activated carbon adsorption and other traditional water filtration methods are becoming obsolete due to their high operational costs and limited efficiency [5]. Coagulation is essential to removing trace organic matter in water and activated sludge. However, it is a time-consuming and space-intensive process that cannot be avoided [6]. Membrane technology has become a modern concept due to advancements in biology and physics. The primary objective of this technology is to precisely emulate the permeability characteristics of active cell membranes. It is imperative to note that the membrane can selectively permit certain materials to pass through on both sides [7]. Using membrane technology can provide a more environmentally friendly and efficient water and wastewater treatment. This innovative approach can effectively remove color, odor, and organic matter from water, surpassing the capabilities of traditional wastewater treatment methods [8]. When there are various components in a solution, a membrane serves as a selective barrier that blocks certain substances from passing through when there are specific driving forces such as concentration gradient, pressure gradient, or electric field. Membrane modules typically feature a single inlet for feed to traverse and dual outlets for permeate and retentate flow [9]. There are two types of membranes: symmetric and asymmetric. Symmetric membranes have a uniform pore arrangement, while asymmetric membranes are anisotropic, which means their chemical or physical properties vary depending on their location [10]. A three-layered structure typically makes up an asymmetric membrane, including the skin layer, the middle layer, and the support layer. Improving the functionality of separation processes is crucial, and the top layer plays a significant role in achieving this. By incorporating catalysts or other materials, the membrane's performance can be enhanced [11]. Membrane fouling remains one of the most significant challenges regarding membrane technology. This happens when specific materials, including organic and inorganic components, stick to the membrane's surface or interior and cause significant damage [12]. Addressing membrane fouling is crucial since it can lead to reduced productivity and quality. This, in turn, means that higher operating pressures, frequent cleanings, and a shorter membrane lifespan are needed. Furthermore, maintenance expenses tend to increase. Knowing the three types of fouling (inorganic, biological, and organic) is essential [13]. Membrane fouling, which can be detrimental to membrane applications, is primarily influenced by the characteristics of the membrane. Factors like pH, salt concentration, and membrane structure can all contribute to membrane fouling and ultimately impact the overall efficiency of membrane technology [14]. It is important to enhance the separation efficiency and broaden the application range of the membrane matrix in order to improve membrane performance. In order to prevent fouling, it is crucial to incorporate antifouling properties into membranes. There are various ways to achieve this, such as altering surface hydrophilicity, decreasing surface roughness, applying structured polymer coatings, or adding new surface functionalities [15]. Many researchers are currently striving to address the environmental disaster using economically efficient and eco-friendly methods such as metal–organic frameworks (MOFs). Membrane-based separations are presently explored as an auspicious substitution over conventional separation techniques. Metal–organic

frameworks are a highly exceptional and complex form of porous crystalline material, formed through the linkage of organic linkers and metal ions. They own an excessive handy internal surface vicinity (generally 500–7000 m<sup>2</sup> g<sup>-1</sup>) [16]. The performance of membrane separation utilizing MOF technology exceedingly relies upon at the microstructure and crystal structure of the selective layer, even as the inter-crystalline defect formation in MOFs can have both fine or poor effects at the separation overall performance. Water recycling by using membrane technology may additionally offer promising price financial savings. MOF substances have attracted good-sized interest in the subject of membrane separation, in which water–solid MOF membranes stand out specifically in the subject of wastewater remedy and water regeneration. Generally, to produce MOF membranes through conventional means, it is imperative to undergo numerous stages and operate under high-pressure circumstances [17]. Considering Zeolitic imidazolate, framework-eight (ZIF-8) is a form of typical MOF substances. The precise work of ZIF-8 due to its superior adsorption capacity and right host capability for photo catalytic substances, which makes it be an excessive-profile material inside the treatment of wastewater although it would possibly involve some troubles. ZIF-8 particles tend to aggregate, resulting in a decrease in specific surface area. Furthermore, they are difficult to recycle as they pose a challenge when it comes to separating them from water after eliminating pollutants. The assessment will center on the utilization of Zeolitic Imidazolate Framework (ZIF-8), a MOF purposely crafted to eliminate heavy metals, dyes, and oily waste refuse from aqueous solutions [18]. This article presents a comprehensive overview of the significant strides made in utilizing ZIF-8 composites as potent adsorbents and photocatalysts in eliminating wastewater pollution, the usage of ZIF-8 in contaminant elimination, mainly heavy metals, dyes, organic pollutants, and oily waste from wastewater, is a growing discipline of studies. The primary objective of this overview is to highlight the exceptional performance of ZIF-8 in eliminating heavy metals, dyes, organic pollutants, and oily waste from wastewater. Nevertheless ZIF-8 has the potential to enhance various top-notch organic methods already deemed effective for sewage effluent purification, albeit with insignificant disadvantages. For instance, the effectiveness of bio-electrochemical systems (BES) in removing heavy metals is limited due to the non-biodegradable nature of these metals. Although BES is considered a sustainable technology with minimal environmental impact, it falls short in handling such pollutants [19].

## 2 Methods for MOF Synthesis

Many ways were evolved over the years to eliminate pollutants from wastewater, consisting of biological remedies, electrochemical approaches, adsorption techniques, ion change methods, membrane separation, oxidation strategies, and so forth. The synthesis of these materials has generally been achieved specifically via solvothermal approaches. However, because of the hassle of using some solvents (particularly at some point of the synthesis but additionally in the following washing

**Fig. 1** Metal–organic framework



and activation methods), greater respectful methods with surroundings and health have arisen. Some such methods are discussed in this report. Figure 1 represents the general synthesis process of MOF in which organic linker and metal cluster are mixed in a solvent.

## 2.1 Growth from Seeds or Secondary Growth

In contrast to the *in situ* boom method, the secondary or seeded increase strategy involves planting ZIF-eight seeds on the support. Said that his approach was the best since each piece could be adjusted separately, creating a membrane that was thinner and less defective. However, compared to the *in situ* growing process previously described, this approach is more challenging. Some seeding tactics, such as dip-coating rubbing, reactive seeding, and immersion, were mentioned in earlier literature. It was reported that a ZIF-eight membrane was grown utilizing a hydrothermal seeded growth technique on a fiber made of yttria-stabilized zirconium (YSZ). A 2.5-m membrane was produced by submerging an yttria-stabilized zirconium aid in the solution of ZIF-8 for 10 s. However, ZIF-growth eight's is not even and can't completely cover the substrate's surface. ZIF-eight particle insurance is restricted as a result of the seeds clogging the help's pores. It was also proposed to look at the outcomes of several manufacturing approach to the development of ZIF-8 membrane, including secondary seeded growth, rubbing, and *in situ* crystallization. The seeding method was prepared using the hydrothermal approach. The support was then calcined for 30 min at 900 °C before the dry ZIF-eight layer was rubbed onto it [5].

## 2.2 Microwave-Assisted Growth

Due to its tremendous advantages, microwave technology has piqued the curiosity of researchers. The microwave generation is unequivocally a young generation, as it is completely devoid of any harmful compounds, does not emit gas, and requires

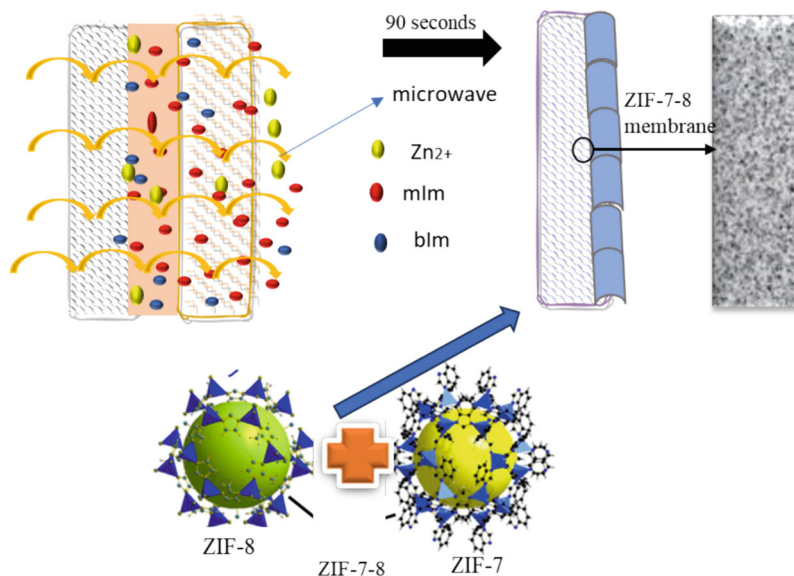


**Fig. 2** Schematic demonstrates the rapid production of mixed linker ZIF-7-8 membranes through the use of microwave-assisted in situ synthesis [20]

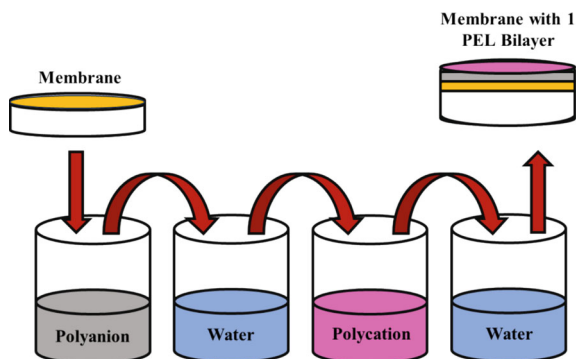
no membranes through the use of microwave-assisted in situ synthesis as shown in Fig. 2 [20].

Kwon et al. devised an efficient and uncomplicated method of producing a cohesive ZIF-8 layer through the use of microwave-assisted seeding. The process entails a number of phases, including first saturating the substrate layer with steel source solution, then exposing trigger rapid crystal growth. To maximize the heterogeneous crystallization before at maintaining a high awareness of the solution is absolutely crucial when offering support [20].

### 2.3 Layer by Layer

The precursor solution of ZIF-8 has been applied to the support layer through the layer by layer (LBL) technique and is now fully soaked. After each deposition cycle, the substrate is wiped down with solvents to remove any unreacted precursors and ensure a consistent coating of ZIF-8 on the substrate. To carry out the LBL technique, it is imperative to follow a series of steps with utmost precision. The foremost step is to employ the in situ growth method, which entails using a boom to deposit ZIF-8 nanoparticles onto the porous substrate. The creation of an ultrathin PA layer on the ZIF-8 layer and its subsequent application of IP and curing constitute the second method. The compatibility shared by polymers and ZIF-eight is remarkably high, which permits the bridging of gaps between ZIF-eight nanoparticles. Moreover, this

**Fig. 3** The layer-by-layer procedure is schematically [21]



technique can effectively overcome the clumping of nanoparticles without requiring their dispersion in a polymer matrix. The creation of ZIF-eight on the polymer support material initiated the process.

The next step involved creating a ZIF-eight/PA layer on the PSF guide, utilizing the highly effective layer-by-layer (LBL) approach. After each cycle, the washing process is completed using suitable solvents to eliminate any unused starting materials. After careful examination of the AFM image, it is clear that the PA film has successfully formed on the ZIF-8 layer. The evenly distributed PA film production increased the bonding among the zif-8 and PA layer which is shown in Fig. 3 [21].

### 3 Synthesis of MOF Membrane

Bare MOF membranes are pure MOF membranes that exhibit near-optimal selectivity, as the pore size of MOF determines their selective permeation. However, the practical applications of MOF membranes currently need to be improved due to low mechanical strength, structural defects, and instability of MOF. Therefore, it is crucial to priorities improving MOF stability and increasing the lifetime of MOF functionality to overcome these limitations [22].

#### 3.1 Blending

Blending is the most widely used method for constructing highly efficient mixed matrix membranes (MMMs) based on MOFs [23]. As shown in Fig. 4a, a blended membrane created by combining inorganic or organic hybrid material in the form of micro- or nanoparticles with a polymer matrix is known as a mixed matrix membrane. Although MOF-based MMM is stable, its construction could be more efficient and easier. Blending is typically the preferred method for preparing MOF-based MMM.

Blending can be categorized into two types—substrate-based blending and substrate-free blending. The substrate blending process comprises three essential steps. First, MOF ink is made by carefully combining MOF with polymer. Second, the mixture is expertly placed on the porous substrate via flat membrane casting, spin coating, or dip coating. Ultimately, drying totally removes the casting solution is completely eliminated throughout desiccation or drying, ensuring the highest level of quality and performance [22]. When combining PVDF with ZIF-90 particles, Flygagina et al. created a fantastic MMM by using a blending without a substrate approach [24]. Furthermore, the investigation of the compatibility between PPA and SAN mixture can be effectively utilized to enhance the efficiency and endurance of membrane combined with MOF [25]. The optimal polymeric substrate for a given MOF and solvent combination depends on understanding how various polymer blends and MOFs interact. A recent study suggests that PPA would be a more suitable polymer than PVBZ for mixing with SAN in creating MOF membranes. The compatibility of blends of poly(vinyl esters) and polyacrylates may be better understood by analogue calorimetric tests, which facilitate the creation of a homogenous and stable MOF-polymer nanocomposite membrane [26].

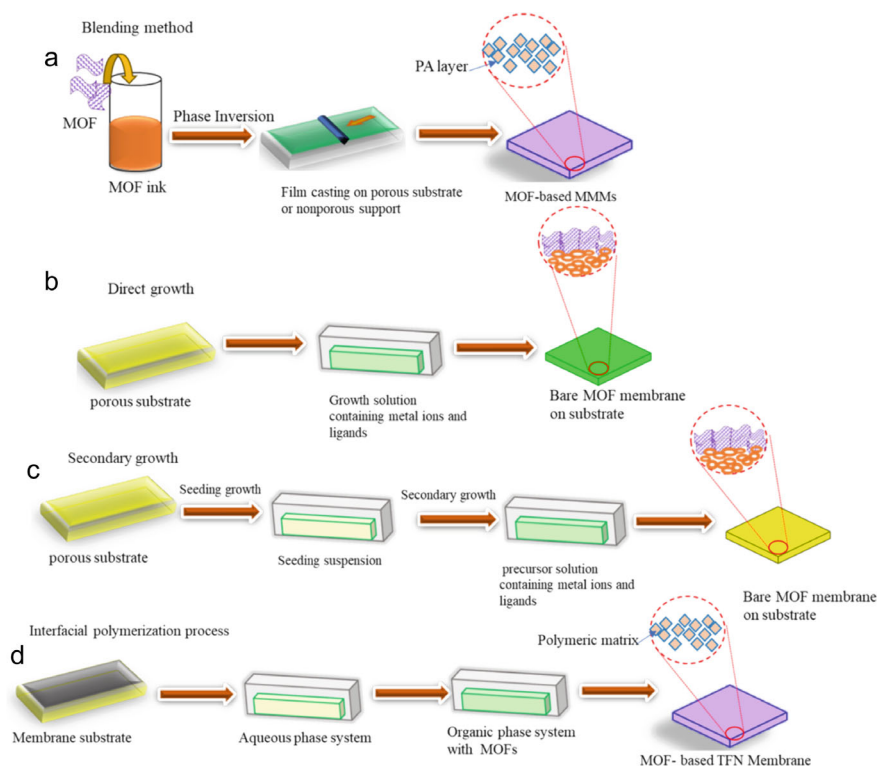


**Fig. 4** Schematic illustration of fabrication of MOF-based membrane by using **a** blending, **b** direct growth, **c** secondary growth, and **d** interfacial polymerization, methods [23, 30]

### 3.2 *Direct Growth*

In the direct growth method, the substrate is immersed in the growth solution while no crystals are attached to the surface. During the preparation stage, crystal nucleation, growth, and co-growth on the substrate occur simultaneously, as shown in the Fig. 4b. There are two distinct categories of direct growth techniques, namely direct growth on unmodified support and direct growth on modified support. One of these techniques, namely direct growth on unmodified support, was utilized by Kang et al. to create a chiral MOF membrane on a nickel net, and they have achieved great success through this method. They placed a nickel mesh substrate horizontally in an autoclave and reacted it with organic ligands at the optimal solution strength [27]. The nickel mesh was firmly surrounded by MOF crystals which progressively merged with each other. The MOF membrane efficiently separated the Diol isomers mixture with great precision. To eliminate the issue of poor bonding and enhance heterogeneous nucleation, the substrate is chemically modified as an effective solution instead of direct growth on a modified support.

### 3.3 *Secondary Growth*

During secondary growth, the membrane already affixed to a MOF crystal is efficiently employed for the in situ production of the MOF membrane, as shown in the Fig. 4c that goes with it. The formation of a thick, intergranular gap-free, and crack-free membrane is one of the primary benefits of the secondary growth approach, which is marginally more complex than the direct growth method. By managing the morphology/structure, one can achieve this. Pan et al. utilized a highly effective.

Zeolitic imidazolate framework (ZIF) membrane for the purification of organic compounds using a secondary growing technique [28]. By utilizing ZIF-8 nanoparticle as a seed layer and grafting them onto a porous  $\alpha$ - $\text{Al}_2\text{O}_3$  substrate, a dense ZIF-8 membrane was created via secondary growth. After that, the seeded surface was submerged in a ZIF-8 preliminary solution and subjected to precise reaction conditions to create a highly reproducible, solvent-stable, and thermally stable ZIF-8 membrane. The superiority of this novel membrane was demonstrated by its exceptional performance in the separation of organic mixtures.

### 3.4 *Interfacial Polymerization Process*

Interfacial polymerization is a process where two different monomers, which cannot mix, are reacted at the interface of two solutions, and it is initiated from the organic side. This technique is frequently utilized in the production of thin-film composite

membranes, which consist of a polymer layer and a substrate [29]. The polymerization that takes place at the liquid/liquid barrier is the main focus of the interfacial polymerization (IP) process. It is an extremely reliable and user-friendly approach for constructing a polyamide (PA) layer on a robust substrate, such as ceramics. Additionally, by interfacially polymerizing metal–organic frameworks (MOFs) with the thin-film nanocomposite (TFN) membrane, the performance of the membrane can be significantly improved. It is worth noting that Jeong et al. were the first to develop TFN membranes using interfacial polymerization, and this can be seen in Fig. 4d. Sorribas et al. deliberately chose to mix MOF with TFN membrane as a filler because it is an undisputed fact that MOF nanoparticles possess unique characteristics that make them stand out from other nanoparticles. These characteristics include nano-scale size, identical pore sizes, and frame-like porous morphology, which have been proven to assimilate better with polymer chains [22]. Li and his team successfully developed a high-performance thin film nanofiltration (TFN) membrane using hydrophilic hollow nano-cubes (HHNs) as the building blocks. The HHNs were obtained by etching solid ZIF-8 with tannic acid, resulting in a rich hydroxyl surface. The team then grafted the HHNs onto a polyamide (PA) layer via interfacial polymerization, which significantly improved the membrane's performance. This approach demonstrated a remarkable increase in the affinity between the metal–organic framework (MOF) and polymer. The method has immense potential for water filtration applications and can be considered a breakthrough in this field [30]. TFN membrane demonstrated superior characteristics in comparison with the bare membrane. It demonstrated a 2.0% boost in rejection and a 190% rise in permeability. Due to HHN's negative charge, hydrophilicity, and hollow structure, TFN exhibits increased antifouling characteristics. However, *N,N*-dimethylformamide (DMF), which is not regarded as a “green” membrane because of its corrosivity, low melting point, and hazardous byproduct dimethyl sulfide, was utilized, Interfacial polymerization as a solvent and activator during the manufacturing of the TFN membrane [30].

#### **4 Membrane with MOF Utilized for Treatment of Wastewater**

MOF-containing membranes are an excellent solution for water pollution control. They are highly effective in separating pollutants from water, containing oil water emulsion and organic pollutants, heavy metal ions and organic dyes. Its adjustable components and controllable arrangements make them a reliable choice for water treatment. This chapter exhaustively discusses the representative applications of MOF-containing membranes in water treatment and highlights them in Tables 1, 2, 3 and 4.

**Table 1** For oil/water separation following MOF membranes used

Pollutants	Membranes	Key performance			References
		Permeability ( $L m^{-2} h^{-1} bar^{-1}$ )	Rejection (%)	Flux ( $kg m^{-2} h^{-1}$ )	
Oil/water	UiO-66	–	100	$12.7 \times 104$	[49]
Oil/water	Wood/MIL-100 (Fe)	–	99.9	1257	[50]
Oil/water	TMU-5/PES	–	> 98	182	[51]
Oil/water	PEI/PVP/MOF-71	–	85.4	$147.20 \pm 1.05$	[52]
BPA	LacPAN-MIL-101-L	708	92	–	[53]
BPA	C-MIL-125-NH <sub>2</sub> -HM	–	100	–	[54]

**Table 2** For pesticide removal following MOF membranes used

Adsorbent	BET surface area ( $m^2 g^{-1}$ )	Adsorbate	Conditions			References
			Conc ( $mg L^{-1}$ )	Time (min)	pH	
MIL-53(Cr)	1438	2, 4-dichlorophenoxyacetic acid	100	720	2.8	[55]
MIL-101 (Cr)	2510	Diazinon	150	3	–	[56]
Cu-BTC	–	14C-ethion	75	150	7	[57]
ZIF-8(Zn)	–	Prothiofos	50	480	–	[58]
ZIF-67(Zr)	–	Ethion	150	720	4.5	[59]

**Table 3** For dye removal following MOF membranes used

Targets	Membranes	Key performance		References
		Permeability ( $L m^{-2} h^{-1} bar^{-1}$ )	Rejection (%)	
MB	ZIF-300	> 25.0	99.6	[54]
MB	ZIF-8/PEI	33.0	99.6	[60]
MB	UiO-66-(COOH) <sub>2</sub> /prGO	14.7–12.5	95.1	[61]
MB	MOF-808	4.37	> 99.8	[62]
MB	UiO-66-rGO-1	–	98.7	[63]

### 4.1 Oil and Micro-pollutants Removal

The issue of wastewater between routine of human existence and industrial effluent is an undeniable and urgent problem for the environment. It is a direct result of the growing population and rapid industrialization and demands immediate attention for

**Table 4** For heavy metal separation following MOF membranes used

Targets	Membranes	Key performance			References
		Adsorption (mg g <sup>-1</sup> )	Rejection (%)	Permeability (L m <sup>-2</sup> h <sup>-1</sup> bar <sup>-1</sup> )	
Pb(II)	MOF-74/ Nafion	18	–	–	[64]
Pb(II)	PA 300	151	–	–	[64]
Pb(II)	PA 808	119.9	–	–	[65]
Pb(II)	A-12/Zn	–	78	105	[66]

effective solutions [31]. Clean water is essential for maintaining a healthy lifestyle, and to satisfy our regular water needs, water must be filtered and treated. Today, the most common oils and soluble organic compounds like antibiotics are examples of the two categories of organic substances resulting in contaminated water. It is imperative to take action towards water filtration and treatment to ensure that our water is safe and healthy for consumption [31]. Antibiotics are frequently administered to humans and animals to combat bacterial infections, but it is crucial to remember that these pharmaceuticals harm water supplies and create organic waste, which is then susceptible to the growth of drug-resistant bacteria and a worrying rise in human diseases and illnesses affecting aquatic life. It is crucial to take action and address this issue before it worsens [32]. The elimination of antibiotics such as ciprofloxacin from water has become a crucial area of research. Researchers are looking for effective and efficient ways to remove these pollutants. Furthermore, the presence of Bisphenol A (BPA) which occurs in the category of endocrine-disrupting compounds (EDCs) in water sources is a growing concern as these compounds pose a significant threat to human health. However, removing these compounds is a challenging task and requires specialized methods. While the advanced Oxidation process has been used to eliminate micropollutants, it is not widely used due to its high cost and difficulty in recovering nanoparticles [33]. The composite membrane developed by Dai et al. is a breakthrough in the elimination of Endocrine Disrupting Chemicals (EDCs) like methylparaben, propylparaben, benzyl paraben, and bisphenol A. The MOF0.20 membrane is made up of a chromium plate and a polyamide layer, which provides selective channels that significantly increase the rejection rate of EDCs compared to Nanofiltration (NF) membranes. The rejection rate for methylparaben rises from 27.7 to 47.4%; increases from 25.2 to 45.9% for propylparaben; increases from 31.3 to 51.1% for butylparaben; and improvements from 64.9 to 79.8% for bisphenol A. These results demonstrate that the MOF0.20 membrane is highly effective in removing EDCs. A particularly often employed enzyme for catalyzing oxidative coupling reactions of phenolic chemicals, such as BPA, is, without a doubt, horseradish peroxidase. The entire procedure generates radicals like phenoxy that go through polymerization, resulting in insoluble precipitates that can be effectively eliminated by simply filtering water [34]. Furthermore, many of the enzyme-combined membranes are manufactured using microfiltration membranes

and are typically working within the incubation mode in batch to batch, making them a highly efficient solution.

Even after being exposed to proteolysis, the membrane combined with MOF has shown remarkable resilience, making it a highly efficient and reliable option for wastewater treatment. It is also a cost-effective and environmentally friendly solution for the removal of oily wastewater. On the other hand, most of the conventional techniques employed for wastewater treatment such as skimming, dispersion, photocatalysis, adsorption, and in situ combustion are not only expensive and complicated but also have adverse impacts on the environment and consume a significant amount of energy resources. Therefore, the MOF membrane is a more practical and sustainable option for treating oily wastewater, as confirmed by Table 1. Gu et al. have successfully developed a highly efficient ZIF-8@rGO@sponge membrane by use of self-assembly of high temperature reduction, which has embedded MOF inside GO nanosheets, as shown in Fig. 5a. This membrane offers an ultrahigh adsorption selectivity and a separation efficiency of over 98% for oily wastewater due to a synergistic effect. Notably, the membrane demonstrates remarkable recyclability, as it can be applied 100 times with the same outcomes each time. These findings provide valuable insights for researchers who wish to develop novel membranes for water treatment purposes. By carefully controlling MOF nanoparticles' size and surface area, the oil wettability of the membrane can be enhanced [35].

Xiu and his team of researchers have successfully developed a composite electrospun membrane for oil–water separation. They accomplished this by embedding ZIF-8 nanoparticles into polylactide (PLA) to create membrane with PLA/ZIF-8. By enhanced the amount of ZIF-8 nanoparticle, they were able to significantly improve the roughness of the membrane, which led to a reduction in the diameter of the blended fiber. The finding is that when ZIF-8 nanomaterials were added, the diffusion time of saxoline droplets on the membrane reduced, suggesting a significant improvement in

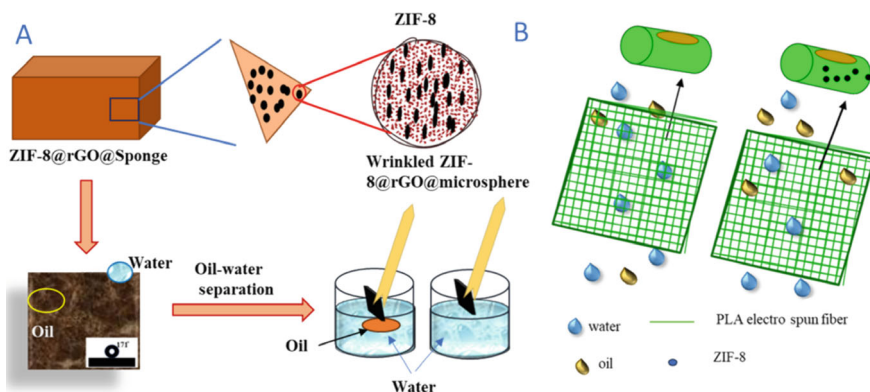


**Fig. 5** a schematic demonstration shows the assemble of wrinkled ZIF-8@rGO@sponge and how it can be used to separate oil and water [35]. b Method of purifying oil and water is by using membrane with PLA/ZIF-8 [36]

oil wettability. The membrane permits water molecules to flow across in the purification of oil and water, while effectively separating oil globules from the membrane through absorption or blocking. This resulted in a remarkable increase in the efficiency of separation, particularly for the purification of diesel and water. Figure 5b clearly illustrates the efficacy of this process [36]. The MOF membranes are highly effective in eliminating micropollutants over hydrophobic, hydrogen bonding, and pi-pi interactions, making them a promising solution for decontamination. Although most research in this field focuses on separating one of these components and is typically conducted in laboratory scale, it is imperative to develop MOF membranes that are capable of realistically and effectively removing these impurities from actual wastewater in sewage disposal facilities. It is an urgent challenge that requires immediate attention and dedicated efforts from researchers to design and manufacture MOF membranes that can efficiently remove micro contaminants from wastewater.

## 4.2 Pesticide Removal

The current state of the world population growth is alarming, and it has resulted in a widespread food crisis. To meet the increasing demand for food, farmers have no other choice but to rely heavily on agricultural chemicals to boost crop yields. Pesticides and Organic impurities can have properties like dangerous and carcinogenic properties, which can adversely affect both the ecosystem and human health. The use of agricultural pesticides need to keep herbs and plants free from pests is growing alarmingly. These herbicides tend to build up in the ground and may even infiltrate subterranean water sources. Additionally, they are carried away by agricultural effluent and eventually find their way into human body's situation that can be fatal for the consumer. It is imperative that we take action to address this issue and find alternative methods of pest control that are safer for both the environment and human health [37]. Agricultural effluents and natural water environments are frequently contaminated with a various of pesticides and antibiotics, including atrazine, malathion, tetracycline, and sulfamethazine [37]. Dimethoate is an extremely toxic pesticide that can cause serious health problems if it persists in the environment or is used in large quantities. Its presence has proven detected in various food products, including cow's milk. In mammals, including humans, it is absorbed through the skin or inhalation, leading to the restriction of the enzyme like acetylcholinesterase and disrupting regular conduction of impulses from nerves. Therefore, the removal of organophosphate residues from the nature is of utmost importance, and research in this area is highly promising for environmental scientists. Several methods have been developed for removing pesticides from water, including degradation, photocatalytic degradation, bioremediation, nanofiltration, and adsorption. Photocatalysis is a cost-effective method that uses light as the primary energy source to break down organic pollutants by generating reactive oxygen species (ROS) [38]. Several MOF composites have been published for the adsorption of glyphosate and dimethoate, such as GO@Zr-MOF and functionalized with Al-MOF. However, because these materials are only

offered in form of powder, their potential uses are restricted. On the other side, MOF membranes are porous in structure and exhibit superior rejection of pesticides due to their regrowth and recycling properties. Abdelhameed et al. used in-situ growing methods to create a Cu-BTC@CA MOF membrane to remove pesticides such as dimethoate from effluent. This membrane included several fractures as a flaw despite its great absorption capability. Furthermore, researchers have reported exceptional rejection rates for various pollutants using different MOF-based membranes. For instance, the MOF-2/g-C<sub>3</sub>N<sub>4</sub> membrane demonstrated rejection rates of Atrazine 98%, Tetracycline 95%, Sulfamethazine 89%, and Sulfamethazine 92%. Another membrane, the membrane with MOF NH<sub>2</sub>-MIL-125 (Ti), show excellent rejection for Fenitrothion 17.8, Imidan 96.2, and Fenthion 66. Additionally, a membrane with BWO@MIL-100 (Fe) MOF, produced outstanding rejection rates 84% for Pirimicarb after 240 min and at a 5 pH. Another noteworthy example is the PVDF/ZIF-8 membrane, which showed great rejection of microorganisms and contaminants from dairy milk, generated by mixing ZIF-8 on the PVDF polymer membrane, operating at a normal pH of 6.89–7 [39, 40].

### 4.3 Organic Dye Waste

Numerous studies have conclusively proven that effective solutions are imperative for reducing the amount of dye-containing industrial waste that is released into the surroundings. Dyes discharged through the surroundings via flowing water can cause severe damage to the environment because of the existence of highly toxic and non-decomposable compounds in massive amounts, which damage the life of plants and cause an adverse effect on species. It is high time that textile wastewater is addressed as a major issue that needs to be resolved at the earliest. Residual discharges from dyeing aids, which usually consist of inorganic minerals, are a major environmental hazard because they combine dye molecules with minerals, including NaCl and Na<sub>2</sub>SO<sub>4</sub>. These salts have made it more difficult for textile waste to biodegrade. Therefore, for resource recovery and environment protection, it is crucial to prioritize the purification and removal of salts [40]. MOF structures with outstanding adsorption and catalytic qualities, as NH<sub>2</sub>-MIL125 (Ti), are a great option for treating sewage and water in the field of ecology [41]. Its exceptional porosity and definite area, this MOF can do beyond only filtering out impurities; Reactive dyes are among the substances that are incredibly successful at dissolving due to their extraordinary photocatalytic capabilities [42]. The use of PMR is a promising method for treating textile industrial waste, but it faces a major challenge in the form of fouling, which can cause pressure loss, reduce flux, and lower the effectiveness of the membrane process. This ultimately affects the costly regeneration of the membrane is adversely impacting the economy. To overcome this issue, it is essential to prevent flux reduction. Pre- or post-treatment photocatalysis phases for membrane separation represent a potential solution. Although the use of photocatalytic processes increases the retention time of the entire treatment process, it

can reduce membrane fouling by degrading macromolecules. Another approach is to manufacture an active membrane, which has a longer lifetime than compared to the traditional one and doesn't need to be renewed as frequently [43]. Ahmadi et al. have successfully developed a highly effective photocatalytic membrane for the treatment of textile wastewater. The membrane, modified with MOF  $\text{NH}_2\text{-MIL125}$  (Ti) nanoparticles through PMR method, is automatic cleaning and results in recovery of water flux through photodegradation of layer of foulant on the membrane's. This is a significant breakthrough in wastewater treatment technology and holds great promise for industrial and environmental applications [44]. MOF polycrystalline membranes are currently at the forefront of dye decontamination research due to their simple pore dimension adjustments, the dye molecules are prevented from pouring out while still allowing water molecules to flow through. A superior ZIF-8 membrane was expertly prepared on PES using a phase transformation interfacial growth strategy. With an impressive 99% rejection rate for Congo red, and the ability to effectively decontaminate Rhodamine B, Coomassie brilliant blue, and Congo red, this membrane is a powerful solution for dye decontamination. The effectiveness of these membranes in decontaminating dyes is undeniable [45].

#### **4.4 Heavy Metal Removal**

The world's population is increasing at an alarming rate, and industries are developing and evolving rapidly. However, the inevitable consequences of industrialization have led to severe water pollution. Various studies have reported that many heavy metals, like copper, lead, mercury, silver, nickel are the direct result of activities like chemical manufacturing, coal extraction, fertilizer and other chemical usage, solid waste disposal, and sewage outflow. It is imperative that we take immediate action to address this problem and find solutions to prevent further damage to our planet [46]. The accumulation of pollutants in organisms due to contaminated water can pose significant possible dangers to people, animals, and the environment as a whole. Maximum allowable levels for heavy metals were published by WHO. Such metals are Cd, Pb, Hg, Lead, arsenic, cadmium, and Cr(VI) are harmful to human organs and cause serious diseases. Adsorption stands out as the ultimate and most economical solution for the removal of heavy metal pollutants from water, given the fact that disposing of such water is not a recommended approach. Although alternative methods like coagulation, ion exchange, membrane filtration, electrochemical techniques and chemical precipitation exist, none of them can match the efficiency and cost-effectiveness of adsorption [47]. ZIF membranes exhibit superior stability of both. Yuan and their team have successfully produced pure ZIF-300 membranes on alumina ( $\text{Al}_2\text{O}_3$ ) using the secondary growth method [48]. In addition to its remarkable size selectivity and water equilibrium, the ZIF-300 membrane has a desired water permeance of  $39.2 \text{ L m}^{-2} \text{ h bar}$  and an amazing 99.21% rejection rate for Cu(II) ions. These are the desired outcomes. Li and their team have developed a revolutionary PAA/ZIF-8/PVD membrane that exhibits remarkable properties, including

excellent Ni(II) ZIF-8 is an exceptional material that can effectively decontaminate water systems containing high concentrations of salts. It has a remarkable adsorption capacity of  $76.5 \text{ mg g}^{-1}$  at low equilibrium for heavy metals such as As (V). Additionally, Wu et al. have demonstrated that a modified version of ZIF-8 with dual mesoporosity has an even higher adsorption capacity than the unmodified ZIF-8 prepared in  $\text{H}_2\text{O}$  and  $\text{CH}_3\text{OH}$ , and can be easily fabricated in aqueous solution at room temperature [45]. A novel nanofibrous MOF membrane has been developed for efficient water purification. The membrane can remove Pb(II) ions with a moderate permeance and its permeate purity meets drinking water standards. The efficiency and selectivity of MOF membranes in terms of separation are not only judged by stability and functional group, but also by other parameters such as MOF size, membrane thickness, and hydrophilicity of polymer. The highly negative surface charge of the MOFs facilitates the removal of metal ions. This membrane is highly versatile and can be utilized both as a stand-alone filter for water purification or as an essential component in wastewater treatment systems [43]. Membranes with MOF are the ideal solution for separating heavy metal ions due to their rapid rate of equilibrium, large capacity for rejection, and extremely selective reaction. The two main processes behind MOF membrane separations are pore-filling action and electrostatic interaction and there is no doubt about their effectiveness. While researchers have been focusing on removing single ion of metal at once, it is imperative to conduct widespread research on the simultaneous purifying of various contaminants by membranes since the water environment is complex and constantly changing. This research is crucial for wastewater decontamination and purification.

## 5 Another MOF Applications

Figure 6 represents the different application of MOFs. MOFs, or metal–organic frameworks, are a family of materials with a large surface area, significant porosity, and great crystallinity that make them perfect for gas adsorption and storage. They have a wide range of uses, including drug delivery, biosensing, energy storage and conversion, catalysis, and gas sensing. MOFs have demonstrated tremendous promise in photoelectronic, energy, and the environment, spurring advancements in both theoretical and applied research. The energy, environmental protection, and healthcare domains have all benefited from MOFs' adaptability and tunability.

### 5.1 MOF in the Field of Gas Storage and Separation

There are various methods for storing gas properly, but they all require a high-pressure tank and a multistage compressor. However, such methods can be quite expensive, so there is a need for a more simple and cost-effective approach. Numerous materials, such as zeolite and modified porous carbons, were created to address these issues and

**Fig. 6** Application of MOF

produce better gas storage techniques. MOFs are favored for their easy preparation, high surface area, versatile functionalization, and adjustable pore structure [63]. When coal-fired power plants produce exhaust gas, it contains pollutants such as  $\text{SO}_x$ ,  $\text{NO}_x$ , and trace elements. The gas mixture also contains 15–16%  $\text{CO}_2$ , 73–77%  $\text{N}_2$ , 5–7%  $\text{H}_2\text{O}$ , and 3–4%  $\text{O}_2$ . In most actual ways, separation, there are harsh environments, often with water or moisture, which make the process more difficult [67]. Removing trace  $\text{CO}_2$  from air is essential for both human health and the ecosystem. Fortunately, MOFs are an effective solution for lowering the level of  $\text{CO}_2$  in the atmosphere. In particular, SIFSIX-3-Cu, a specialized MOF, has demonstrated a remarkable ability to selectively adsorb trace  $\text{CO}_2$  with high stability and strong affinity, even at high humidity levels. This makes it a highly valuable tool in the fight against  $\text{CO}_2$  pollution [68]. It's important to note that several well-known MOFs, such as NU-100, Mg-MOF-74, MOF-5, and HKUST-1, have been proven to absorb significant amounts of  $\text{CO}_2$ . NU-100 can absorb 69.8% of  $\text{CO}_2$  at 298 K and 40 bar, while Mg-MOF-74 can absorb 68.9% at 278 K and 36 bar. MOF-5 can absorb 58 wt.% of  $\text{CO}_2$  at 273 K and 10 bar, and HKUST-1 can absorb 19.8% of  $\text{CO}_2$  at 298 K and 1 bar. It's clear that these MOFs, among others, can effectively and significantly absorb  $\text{CO}_2$  [69]. Significant evolution has been created in storage of gas and purification due to the structure and pore functionality of MOFs (Metal–Organic Frameworks). MOFs' unique properties, such as their breathing occurrence and massive surface area, make them assuring contender for different separation process. Currently, MOFs are mostly used as adsorbents or additives for membrane. However, investigation should focus on controlling access to the empty space and functionalities inside MOFs, and addressing some issues like adsorption and desorption in MOF-packed tanks, improving packing efficiency, and increasing MOFs' reusability. It is necessary to investigate high-affinity binding sites inside MOFs for the adsorption of highly corrosive hazardous gases. A better understanding of the relationship between MOFs' porosity, structure, and functionalization can lead to the rational design of smart MOF materials for gas storage and separation applications.

## 5.2 MOFs in the Field of Catalysis

The persistent porosity of MOFs due to strong metal–ligand interactions allows for the complete removal of molecules of solvent that do not collapse structurally, establishing their tremendous potential as heterogeneous catalysts. The efficacy of MOFs as catalysts is attributed to the elimination of ligands, usually solvent, which ultimately results in a free coordination site on the metal [63]. This occurs because unsaturated, or unstable, ligands found in MOFs, do not entirely surround the metal centers. Simms et al. provide a detailed discussion of MOFs, a class of porous materials, and their critical significance in producing synthetic enzymes that function in biological processes. A highly efficient bifunctional photocatalyst MOF has been developed, called Zr-OT-EY (EY stands for Eosin Y dye). This catalyst features EY acting as a Lewis acid on the Nodes in the MOF metal cluster metal cluster nodes in the MOF, resulting in a high TON (turn over number) of 1980. This catalyst has been proven to be highly effective in cross-coupling catalytic reactions of C–H compounds with electron-deficient alkenes or azodicarboxylates, producing C–C and C–N products [23]. Photoactive metal–organic frameworks (MOFs) are the most promising candidates for catalyzing the degradation of volatile organic compounds (VOCs). The GC-N-TiO<sub>2</sub> catalyst, produced by encapsulating photocatalyst TiO<sub>2</sub> into ZIF-8 and modifying it with N-doped graphite carbon GC-N through synthesis by using hydrothermal process, outperforms Pt catalysts in the photocatalytic degradation of toluene with significant durability even after 20 recycling cycles. Moreover, GC-N-TiO<sub>2</sub> generates highly reactive oxygen species (ROS) by transferring photogenerated electrons to oxygen in the pyridinic N in GC-N. This makes it the most efficient and durable catalyst for photocatalytic degradation of VOCs [70]. MOFs play a vital role in catalysis owing to their highly customizable architecture and controlled pore functionality. By incorporating catalytic sites into their pores, their efficiency can be significantly enhanced. Moreover, their crystalline nature enables the analysis of active site distribution and the influence of the structural framework on catalytic activity. MOFs have the potential to bridge the gap between micro- and mesoporous materials, making them a highly promising choice for commercial application in heterogeneous catalysis. Metal–organic frameworks (MOFs) are highly stable in different temperature and pH conditions, and play a crucial role in catalytic reactions for converting and selecting desirable products. Despite their effectiveness, MOFs can sometimes exhibit conflicting performance due to the presence of different metal active sites. However, by modifying MOFs to absorb visible light, they can become efficient photocatalysts under solar irradiation. This makes them an excellent option for removing pollutants from the environment. It is essential to understand the structural characteristics and reaction mechanisms of MOF catalysts to develop efficient catalysts for specific catalytic processes. Nevertheless, it is crucial to acknowledge that MOFs have practical limitations due to severe reaction conditions for organic reactions, difficult-to-expose Lewis sites, and incompatible pore surroundings. Furthermore, MOFs have encountered significant challenges in reactions such as enantioselective processes, C–H activation, and olefin

metathesis. The structure of MOFs is highly sensitive to the acidity and alkalinity of solvents, excess impurities, and reaction temperatures during synthesis, which can affect their morphology or crystal. Future research should focus on creating MOFs with improved capabilities across various catalytic applications.

### ***5.3 MOFs in the Field of Nanomedical***

MOFs have garnered significant interest in the field of nanomedicine due to their unique properties and potential applications. As a type of metal–organic self-assembly material, nano-MOFs offer the benefits of both bulk MOFs and nanomaterials, making them a significant concern in medical research. With their tunable pore structure, controlled molecular arrangement, and easy chemical functionalization, MOFs are excellent nanocarriers that provide new opportunities in the nanomedical field. Moreover, MOFs have several advantages over traditional nanocarriers, including adjustable structure and composition, high porosity for drug loading, and weak coordination bonds for easy degradation in biological environments. These characteristics make MOFs a highly promising nanomedicine platform that could revolutionize drug delivery and medical treatment. It's important to note that MOFs have a highly porous structure that allows them to achieve outstanding drug loading and prolonged release capabilities. When compared to mesoporous silica materials, MOFs exhibit a remarkable four-fold increase in drug loading capacity, with the ability to adsorb up to 1.4 g of ibuprofen for up to 21 days [63]. Non-toxic MOFs, which are metal–organic frameworks, have become increasingly popular in biological and medical applications due to their flexible pore sizes, high surface area, and diverse physical and chemical properties. MOFs are widely used in biological sensing, drug release, biological catalysis, and other applications. It is crucial that MOFs possess excellent chemical stability in physiological conditions, such as stomach acidity, intestinal alkalinity, and peristalsis in the esophagus, stomach, and intestines. As such, MOFs must have exceptional resistance to hydrolysis and collapse [71]. MOFs are increasingly being utilized in various biomedical applications, especially for drug loading and delivery systems targeting antiviral and cancer compounds. However, the significant challenges of solubility, long-term stability, toxicity, biocompatibility, and biodegradability cannot be ignored. The potential of MOFs is limited by strong interactions through pore encapsulation and surface adsorption. Therefore, it is imperative to design MOF-drug conjugates with enhanced biostability, biocompatibility, and therapeutic efficiency to develop smart delivery systems that can overcome these challenges.

## 6 ZIF-8 Based Mixed Matrix Membranes

Metal–organic frameworks, such as zeolite imidazolate frameworks (ZIFs), are formed by the combination of organic linkers with metal ions. These frameworks possess similar properties to zeolites, including porosity, thermal and chemical stability, and a bond angle of  $145^\circ$ . The bonds formed in ZIFs are the M-Im-M bond, which has a tetrahedral structure linking each metal to a nitrogen atom to form a shape with 4, 6, and 12 of  $ZnN_4$ ,  $CuN_4$ , and  $CoN_4$ , respectively. It is worth noting that ZIF-8 is widely used in the production of thin polyamide membranes due to its small pore size and large surface area [55]. Table 5 represent the Different membrane fabrication technique with ZIF-8 modified for removal of waste from waste water. The MMMs investigated the 98.6% rejection of methyl blue with the help of an in-situ technique by using ZIF-8 as filler for modification of the membrane [27]. Lee et al. reported ZIF-8 modified with TFN polymer, then the result becomes high permeability of water and a 99.2% rejection of salt [36, 72]. Kebria et al. reported the ZIF-8 chitosan incorporated with PVDF polymer then the result shows 99.5 percent salt rejection. It was increased as compared to plain PVDF (41%) [73].

## 7 Future Prospects and Conclusion

Despite the development of over 20,000 ZIFs in the last decade, only a minuscule percentage has been utilized to create ZIF-based multilayer membrane (MMM). The primary reasons for this are diffusivity, selectivity, pore size, stability, and interfacial defects in the ZIF-polymer interaction. The challenges faced by ZIFs MMMs to achieve required separation performance and membrane properties include choosing the appropriate ZIFs/polymer combination, lower water stability than conventional fillers, poor distribution in the polymer matrix, poor interfacial contact, and poor adhesion between ZIFs and the polymer matrix. Additionally, the stability of ZIFs in the used fluid, such as water/salt solution, significantly impacts the stability and performance of ZIFs-MMMs. The ZIF-8 membrane proves to be highly efficient in its ability to separate waste water. This is due to its impressive porosity, large surface area, and adjustable structure as a MOF. Researchers have enhanced the capabilities of ZIF-8 by preparing its membranes in two ways: as a pure membrane or as part of a blended matrix membrane. These methods were used to improve its decorative potential. Numerous techniques have been formulated to direct the ZIF-8 membrane. The MMMs have multiple effective strategies available, including the blending method, in situ growth approach, and layer-by-layer method. To effectively utilize ZIF-8 for nanofiltration, it is imperative that future studies on ZIF-8 membranes prioritize the following areas of interest. To create simple and adaptable methods for producing ZIF-8 membranes. Instructions for creating ZIF-8 membranes that exhibit exceptional stability and versatility in both aqueous and organic media.

**Table 5** Different membrane fabrication techniques with ZIF-8 modified for removal of waste from wastewater

Polymer matrix	Filler	Fabrication technique	Permeation flux	Rejection factor	References
PA	ZIF-8	Zif-8 nanoparticles were unequivocally dispersed in the TMC hexane solution during the phase inversion process	$29.7 \text{ L m}^{-2} \text{ h}^{-1}$	99.6%	[74]
PDMS	ZIF-8	The creation of MOF takes place within the composite polymer matrix	$1778 \text{ g m}^{-2} \text{ h}^{-1}$	Appropriate separation factor. 12.1	[75]
PVDF	ZIF-8	PVDF membrane synthesized with DMF solvent, chitosan, acetic acid, and ZIF-8 using phase inversion method	$4.3 \text{ kg m}^{-2} \text{ h}^{-1}$	Salt rejection 99.3%	[76]
PAN	ZIF-8	ZIF-8 membrane hybrid created via self-assembly on PAN substrate surface	$265\text{--}53 \text{ L m}^{-2} \text{ h}^{-1} \text{ M Pa}^{-1}$	99.8%	[77]
PVP	ZIF-8	Non solvent phase inversion method by using PVP, DMAc and PES		98.56% dye removal at 1% filler loading	[78]
PTFE	ZIF-8	Modified membrane with up to 20% particle weight loadings by evaporating the solvent	$5.48 \times 10^4 \text{ L m}^{-2} \text{ h}^{-1} \text{ bar}^{-1}$	Adsorption capacity increases	[79]

(continued)

**Table 5** (continued)

Polymer matrix	Filler	Fabrication technique	Permeation flux	Rejection factor	References
PES	ZIF-8	Nanocomposite membranes made from PES/ZIF-L using non-solvent induced phase separation can be created at room temperature	265 L m <sup>-2</sup> h <sup>-1</sup>		[80]

ZIFs are a revolutionary hybrid composite with unparalleled properties that combine organic ligands and metallic complexes. They offer a practical solution to membrane limitations, such as the challenging trade-off between selectivity and permeability in polymeric membranes. The incorporation of organic ligands in ZIFs significantly improves the MOF interaction with polymeric matrices, leading to better filler dispersion. By increasing ZIFs loading by more than 10%, clusters are formed, which have a substantial impact on the membrane's efficiency. ZIF clusters increase pore widths, resulting in nonselective voids that significantly enhance water and salt permeability while rejecting salt. The properties and structure of ZIFs and the injection of fillers into the polymeric matrix have a significant effect on the quality and efficiency of ZIFs-MMMs. The rapid expansion of research and resources has made it possible to learn a lot about the rapid proliferation of ZIF-8 membranes. However, ZIF-8's use and advancement in other fields are still not well-established. This is related to a variety of factors, including the stability, selectivity, and overall performance of the generated membrane, as well as factors like pore size and stability. Aside from the aforementioned matter, other significant concerns must be addressed regarding ZIF-8. These include its suitability with the support or polymer matrix and the difficulties in achieving proper dispersion. Additionally, defects, including cracking, continuous growth, pore blocking, polymer chain stiffening, and interfacial void creation, may arise in the ZIF-eight membrane. These defects are a result of insufficient interfacial interaction between MOF and the polymer device or substrates in the MMM membrane. It is imperative to enhance the potential scale of the ZIF-8 membrane as one of the objectives. To ensure the stability of the ZIF-8 MMM membrane, it is crucial to reinforce the weak adhesion of ZIF-8 to the polymer matrix. It is paramount to acknowledge the inferior balance of ZIF-8 in comparison to other fillers, particularly zeolites. The difference in water balance and stability is especially important when it comes to organic media. The majority of ZIF-8 MMMs and pure ZIF-8 membranes require the help layer throughout preparation. The membrane's inability to perform separation tasks is caused by the ZIF-eight nanoparticles' weak adherence to the membrane guide, which causes the layers to rip off. Utilizing a surface modification is an absolute must to prevent any delamination from occurring between the substrate and the ZIF-eight layer. The instability

of the membrane is directly attributed to the flexibility of the ZIF-8 framework. The scaling up of the ZIF-8 membrane for commercial and industrial applications is an imperative consideration that demands attention. Membrane using Zeolite-8 can be synthesized through a highly efficient process that significantly reduces both time and cost. Moreover, the synthetic conditions are so minimal that polymer supports can be utilized. Notably, this process can be carried out at room temperature. The ZIF-8 membrane's water balance is important, but the software for extending the filtration period will be the major obstacle for commercial implementation.

**Acknowledgements** I am thankful to the Department of Chemical Engineering, Chemistry, Physics and Solar Energy of Pandit Deendayal Energy University (India) for supporting the central instrumental facilities for materials characterization.

**Conflict of Interest** The author(s) has no competing interests to declare that are relevant to the content of this manuscript.

## References

1. Goals MD (2005) International decade for action water for life, 2005–2015 = Décennie internationale d'action sur le thème «L'eau, source de vie», 2005–2015. *Wkly Epidemiol Rec* 80(22):2005–2015
2. Qu W, Yuan T, Yin G, Xu S, Zhang Q, Su H (2019) Effect of properties of activated carbon on malachite green adsorption. *Fuel* 249(February):45–53. <https://doi.org/10.1016/j.fuel.2019.03.058>
3. Ma B, Xue W, Hu C, Liu H, Qu J, Li L (2019) Characteristics of microplastic removal via coagulation and ultrafiltration during drinking water treatment. *Chem Eng J* 359:159–167. <https://doi.org/10.1016/j.cej.2018.11.155>
4. Li N, Liu Q, Zhou GQ, Dai MX, Kong Q (2019) Contaminant removal and microorganism response of activated sludge in sulfamethazine wastewater treatment. *Int Biodeterior Biodegrad* 143(November 2018). <https://doi.org/10.1016/j.ibiod.2019.05.022>
5. Yuan Q, Zhu G (2021) A review on metal organic frameworks (Mofs) modified membrane for remediation of water pollution. *Environ. Eng. Res.* 26(3):2. <https://doi.org/10.4491/eer.2019.435>
6. Laine JM, Vial D, Moulart P (2000) Status after 10 years of operation—overview of UF technology today. *Desalination* 131(1–3):17–25. [https://doi.org/10.1016/S0011-9164\(00\)90002-X](https://doi.org/10.1016/S0011-9164(00)90002-X)
7. Issaoui M, Limousy L (2019) Low-cost ceramic membranes: synthesis, classifications, and applications. *Comptes Rendus Chim* 22(2–3):175–187. <https://doi.org/10.1016/j.crci.2018.09.014>
8. Thakur VK, Voicu SI (2016) Recent advances in cellulose and chitosan based membranes for water purification: a concise review. *Carbohydr Polym* 146:148–165. <https://doi.org/10.1016/j.carbpol.2016.03.030>
9. Zhang R, Ji S, Wang N, Wang L, Zhang G, Li J-R (2014) Coordination-driven in situ self-assembly strategy for the preparation of metal-organic framework hybrid membranes. *Angew Chem* 126(37):9933–9937. <https://doi.org/10.1002/ange.201403978>
10. Goei R, Lim TT (2014) Asymmetric TiO<sub>2</sub> hybrid photocatalytic ceramic membrane with porosity gradient: Effect of structure directing agent on the resulting membranes architecture and performances. *Ceram Int* 40(5):6747–6757. <https://doi.org/10.1016/j.ceramint.2013.11.137>

11. Ihsanullah et al (2016) Fabrication and antifouling behaviour of a carbon nanotube membrane. *Mater Des* 89:549–558. <https://doi.org/10.1016/j.matdes.2015.10.018>
12. Mikhaylin S, Bazinet L (2016) Fouling on ion-exchange membranes: classification, characterization and strategies of prevention and control. *Adv Colloid Interface Sci* 229:34–56. <https://doi.org/10.1016/j.cis.2015.12.006>
13. Liao Y, Bokhary A, Maleki E, Liao B (2018) A review of membrane fouling and its control in algal-related membrane processes. *Bioresour Technol* 264:343–358. <https://doi.org/10.1016/j.biortech.2018.06.102>
14. Goh PS, Lau WJ, Othman MHD, Ismail AF (2018) Membrane fouling in desalination and its mitigation strategies. *Desalination* 425(August 2017):130–155. <https://doi.org/10.1016/j.desal.2017.10.018>
15. Jeong BH et al (2007) Interfacial polymerization of thin film nanocomposites: a new concept for reverse osmosis membranes. *J Memb Sci* 294(1–2):1–7. <https://doi.org/10.1016/j.memsci.2007.02.025>
16. Jun BM et al (2020) Applications of metal-organic framework based membranes in water purification: a review 247
17. Qadir D, Mukhtar H, Keong LK (2017) Mixed matrix membranes for water purification applications. *Sep Purif Rev* 46(1):62–80. <https://doi.org/10.1080/15422119.2016.1196460>
18. Modi A, Jiang Z, Kasher R (2022) Hydrostable ZIF-8 layer on polyacrylonitrile membrane for efficient treatment of oilfield produced water. *Chem Eng J* 434:133513. <https://doi.org/10.1016/j.cej.2021.133513>
19. Zhou H CJ, Kitagawa S (2014) Metal-organic frameworks (MOFs). *Chem Soc Rev* 43(16):5415–5418. <https://doi.org/10.1039/c4cs90059f>
20. Hillman F, Brito J, Jeong HK (2018) Rapid one-pot microwave synthesis of mixed-linker hybrid zeolitic-imidazolate framework membranes for tunable gas separations. *ACS Appl Mater Interfaces* 10(6):5586–5593. <https://doi.org/10.1021/acsami.7b18506>
21. Dmitrenko M, Ljamin V, Kuzminova A, Lahderanta E, Solovyev N, Penkova A (2021) Modification approaches to enhance dehydration properties of sodium alginate-based pervaporation membranes. *Membranes* 11(4). <https://doi.org/10.3390/membranes11040255>
22. Li X, Liu Y, Wang J, Gascon J, Li J, der Bruggen B (2017) Metal-organic frameworks based membranes for liquid separation. *Chem Soc Rev* 46(23):7124–7144. <https://doi.org/10.1039/C7CS00575J>
23. Dechnik AJ, Gascon J, Doonan C, Sumbly CJ *Chemie*. <https://doi.org/10.1002/anie.201701109>
24. Li Q et al (2017) Improved ethanol recovery through mixed-matrix membrane with hydrophobic MAF-6 as filler. *Sep Purif Technol* 178:105–112. <https://doi.org/10.1016/j.seppur.2017.01.024>
25. Rana D, Mandal BM, Bhattacharyya SN (1993) Miscibility and phase diagrams of poly(phenyl acrylate) and poly(styrene-co-acrylonitrile) blends. *Polymer* 34(7):1454–1459. [https://doi.org/10.1016/0032-3861\(93\)90861-4](https://doi.org/10.1016/0032-3861(93)90861-4)
26. Rana D, Mandal BM, Bhattacharyya SN (1996) Analogue calorimetry of polymer blends: poly(styrene-co-acrylonitrile) and poly(phenyl acrylate) or poly(vinyl benzoate). *Polymer* 37(12):2439–2443. [https://doi.org/10.1016/0032-3861\(96\)85356-0](https://doi.org/10.1016/0032-3861(96)85356-0)
27. Kang Z et al (2013) ‘Single nickel source’ in situ fabrication of a stable homochiral MOF membrane with chiral resolution properties. *Chem Commun* 49(90):10569–10571. <https://doi.org/10.1039/C3CC42376J>
28. Hu Y et al (2011) Metal-organic framework membranes fabricated via reactive seeding. *Chem Commun* 47(2):737–739. <https://doi.org/10.1039/c0cc03927f>
29. Devic T, Serre C (2014) High valence 3p and transition metal based MOFs. *Chem Soc Rev* 43(16):6097–6115. <https://doi.org/10.1039/C4CS00081A>
30. Liao Z et al (2019) Hydrophilic hollow nanocube-functionalized thin film nanocomposite membrane with enhanced nanofiltration performance. *ACS Appl Mater Interfaces* 11(5):5344–5352. <https://doi.org/10.1021/acsami.8b19121>
31. Ahmed S (2023) CTAB-assisted fabrication of hierarchical flower-like magnesium oxide adsorbent for enhanced removal performance towards phosphate. *J Magnes Alloy* 11(9):3231–3240. <https://doi.org/10.1016/j.jma.2022.02.007>

32. Gai S et al (2021) Fabrication of highly stable metal–organic frameworks and corresponding hydrophobic foam through a reticular chemistry strategy for simultaneous organic micropollutant and insoluble oil removal from wastewater. *J Mater Chem A* 9(6):3369–3378. <https://doi.org/10.1039/D0TA09624E>
33. Vickers NJ (2017) Animal communication: when i'm calling you, will you answer too? *Curr Biol* 27(14):R713–R715. <https://doi.org/10.1016/j.cub.2017.05.064>
34. Escalona I, de Grooth J, Font J, Nijmeijer K (2014) Removal of BPA by enzyme polymerization using NF membranes. *J Memb Sci* 468:192–201. <https://doi.org/10.1016/j.memsci.2014.06.011>
35. Artikel A *Angewandte Chemie*. <https://doi.org/10.1002/ange.201814487>
36. Dai X, Cao Y, Shi X, Wang X (2016) The PLA/ZIF-8 nanocomposite membranes: the diameter and surface roughness adjustment by ZIF-8 nanoparticles, high wettability, improved mechanical property, and efficient oil/water separation. *Adv Mater Interfaces* 3(24). <https://doi.org/10.1002/admi.201600725>
37. Du J-J, Gao R-X, Yu H, Li X-J, Mu H (2015) Selective extraction of dimethoate from cucumber samples by use of molecularly imprinted microspheres. *J Pharm Anal* 5(3):200–206. <https://doi.org/10.1016/j.jpha.2014.10.004>
38. Hu Y, Bai Y, Li X, Chen J (2013) Application of dielectric barrier discharge plasma for degradation and pathways of dimethoate in aqueous solution. *Sep Purif Technol* 120:191–197. <https://doi.org/10.1016/j.seppur.2013.10.005>
39. Zhu J et al (2016) Surface zwitterionic functionalized graphene oxide for a novel loose nanofiltration membrane. *J Mater Chem A* 4(5):1980–1990. <https://doi.org/10.1039/C5TA08024J>
40. Wang L, Wang N, Zhang G, Ji S (2013) Covalent crosslinked assembly of tubular ceramic-based multilayer nanofiltration membranes for dye desalination 1–9. <https://doi.org/10.1002/aic>
41. Huang Q, Hu Y, Pei Y, Zhang J, Fu M (2019) In situ synthesis of TiO<sub>2</sub>@NH<sub>2</sub>-MIL-125 composites for use in combined adsorption and photocatalytic degradation of formaldehyde. *Appl Catal B Environ* 259:118106. <https://doi.org/10.1016/j.apcatb.2019.118106>
42. Gokulakrishnan SA, Arthanareeswaran G, László Z, Veréb G, Kertész S, Kweon J (2021) Recent development of photocatalytic nanomaterials in mixed matrix membrane for emerging pollutants and fouling control, membrane cleaning process. *Chemosphere* 281:130891. <https://doi.org/10.1016/j.chemosphere.2021.130891>
43. Molinari R, Lavorato C, Argurio P (2017) Recent progress of photocatalytic membrane reactors in water treatment and in synthesis of organic compounds. A review. *Catal Today* 281:144–164. <https://doi.org/10.1016/j.cattod.2016.06.047>
44. Ahmadi A, Sarrafzadeh M-H, Hosseini A, Ghaffari S-B (2022) Foulant layer degradation of dye in photocatalytic membrane reactor (PMR) containing immobilized and suspended NH<sub>2</sub>-MIL125(Ti) MOF led to water flux recovery. *J Environ Chem Eng* 10(1):106999. <https://doi.org/10.1016/j.jece.2021.106999>
45. Li Z et al (2019) A new ZIF molecular-sieving membrane for high-efficiency dye removal. *Chem Commun* 55(24):3505–3508. <https://doi.org/10.1039/C9CC00902G>
46. Vu TA et al (2015) Arsenic removal from aqueous solutions by adsorption using novel MIL-53(Fe) as a highly efficient adsorbent. *RSC Adv* 5(7):5261–5268. <https://doi.org/10.1039/C4RA12326C>
47. Hu J, Zhao L, Luo J, Gong H, Zhu N (2022) A sustainable reuse strategy of converting waste activated sludge into biochar for contaminants removal from water: modifications, applications and perspectives. *J Hazard Mater* 438:129437. <https://doi.org/10.1016/j.jhazmat.2022.129437>
48. Yuan J et al (2019) Fabrication of ZIF-300 membrane and its application for efficient removal of heavy metal ions from wastewater. *J Memb Sci* 572:20–27. <https://doi.org/10.1016/j.memsci.2018.10.080>
49. Zhao X et al (2018) AC SC. *ECSN*. <https://doi.org/10.1016/j.chemosphere.2018.04.023>
50. Yu Y et al (2023) A wood-based MOF membrane with high flux and efficiency for oil-in-water emulsions separation. *Colloids Surf A Physicochem Eng Asp* 674:131852. <https://doi.org/10.1016/j.colsurfa.2023.131852>

51. Gholami F, Zinadini S, Zinatizadeh AA, Abbasi AR (2017) TMU-5 metal-organic frameworks (MOFs) as a novel nanofiller for flux increment and fouling mitigation in PES ultrafiltration membrane. *Sep Purif Technol.* <https://doi.org/10.1016/j.seppur.2017.11.054>
52. Shen S, Li H, Shen Y, Bai R, Zhang G (2023) Modification of PVDF membrane by post-modified NH<sub>2</sub>-MIL-88B(Fe) showing improved permeability and oil/water separation performance. *J Environ Chem Eng* 11(3):109621. <https://doi.org/10.1016/j.jece.2023.109621>
53. Ren Z, Luo J, Wan Y (2018) Highly permeable biocatalytic membrane prepared by 3D modification: metal-organic frameworks ameliorate its stability for micropollutants removal. *Chem Eng J.* <https://doi.org/10.1016/j.cej.2018.04.203>
54. Luis J, Turnes G, Palomino C (2019) Chemosphere carbon composite membrane derived from MIL-125-NH<sub>2</sub> MOF for the enhanced extraction of emerging pollutants 231:510–517. <https://doi.org/10.1016/j.chemosphere.2019.05.173>
55. Jung BK, Hasan Z, Jung SH (2013) From water with a metal-organic framework. *Chem Eng J* 234:99–105. <https://doi.org/10.1016/j.cej.2013.08.110>
56. Mirsoleimani-azizi SM, Setoodeh P, Samimi F, Shadmehr J, Hamed N, Rahimpour MR (2018) Diazinon removal from aqueous media by mesoporous MIL-101(Cr) in a continuous fixed-bed system. *Biochem Pharmacol* 101. <https://doi.org/10.1016/j.jece.2018.06.067>
57. Abdelhameed RM, Abdel-Gawad H, Silva CM, Rocha J, Hegazi B, Silva AM (2017) Kinetic and equilibrium studies on the removal of 14 C-ethion residues from wastewater by copper-based metal-organic framework. *Int J Environ Sci Technol.* <https://doi.org/10.1007/s13762-017-1624-4>
58. Abdelhameed RM, Taha M, Abdel-gawad H, Mahdy F (2019) Zeolitic imidazolate frameworks: experimental and molecular simulation studies for efficient capture of pesticides from wastewater. *J Environ Chem Eng* (October):103499. <https://doi.org/10.1016/j.jece.2019.103499>
59. Seo YS, Khan NA, Jung SH (2015) Adsorptive removal of methylchlorophenoxypropionic acid from water with a metal-organic framework. *Chem Eng J.* <https://doi.org/10.1016/j.cej.2015.02.007>
60. Yang L, Wang Z, Zhang J (2017) Zeolite imidazolate framework hybrid nano filtration (NF) membranes with enhanced permselectivity for dye removal. *J Memb Sci* 532(February):76–86. <https://doi.org/10.1016/j.memsci.2017.03.014>
61. Zhang P, Gong J, Zeng G, Song B, Liu H (2018) AC SC. *ECSN.* <https://doi.org/10.1016/j.chemosphere.2018.04.064>
62. Wu M et al (2023) Fabrication of water-stable MOF-808 membrane for efficient salt/dye separation. *J Memb Sci* 686:122023. <https://doi.org/10.1016/j.memsci.2023.122023>
63. Guan K et al (2017) 3D nanoporous crystals enabled 2D channels in graphene membrane with enhanced water purification performance. *J Memb Sci* 542(June):41–51. <https://doi.org/10.1016/j.memsci.2017.07.055>
64. Albuquerque GH, Herman GS (2016) Membranes for removal of metal ions from aqueous media chemically modulated microwave-assisted synthesis of MOF-74 (Ni) and preparation of MOF-matrix based membranes for removal of metal ions from 74. <https://doi.org/10.1021/acs.cgd.6b01398>
65. Efome JE, Rana D, Matsuura T, Lan CQ (2018) Metal-organic frameworks supported on nanofibers to remove heavy metals. *J Mater Chem A* 6(10):4550–4555. <https://doi.org/10.1039/c7ta10428f>
66. Samanta A, Das S, Jana S (2018) Exploring b-FeOOH nanorods as an efficient adsorbent for arsenic and organic dyes, pp 2467–2473. <https://doi.org/10.1002/slct.201703022>
67. Liang L et al Carbon dioxide capture and conversion by an acid-base resistant metal-organic framework. *Nat Commun.* <https://doi.org/10.1038/s41467-017-01166-3>
68. Wong-foy AG, Matzger AJ, Yaghi OM (2010) Exceptional H<sub>2</sub> saturation uptake in microporous metal-organic frameworks, pp 3494–3495
69. Ghanbari T, Abnisa F, Wan Daud WMA (2020) A review on production of metal organic frameworks (MOF) for CO<sub>2</sub> adsorption. *Sci Total Environ* 707:135090. <https://doi.org/10.1016/j.scitotenv.2019.135090>

70. Li D, Yadav A, Zhou H, Roy K, Thanasekaran P, Lee C (2023) Advances and applications of metal-organic frameworks (MOFs) in emerging technologies: a comprehensive review 2300244:1–32. <https://doi.org/10.1002/gch2.202300244>
71. Horcajada P, Serre C, Vallet-regí M, Sebbañ M, Taulelle F, Førey G (2006) *Zuschriften*, pp 6120–6124. <https://doi.org/10.1002/ange.200601878>
72. Wang Y et al (2014) Synthesis of ZIF-8 in a deep eutectic solvent using cooling-induced crystallisation. *Micropor Mesopor Mater* 195:50–59. <https://doi.org/10.1016/j.micromeso.2014.04.016>
73. Kebria MRS, Rahimpour A, Bakeri G, Abedini R (2019) Experimental and theoretical investigation of thin ZIF-8/chitosan coated layer on air gap membrane distillation performance of PVDF membrane. *Desalination* 450:21–32. <https://doi.org/10.1016/j.desal.2018.10.023>
74. Aljundi IH (2017) Desalination characteristics of TFN-RO membrane incorporated with ZIF-8 nanoparticles. *Desalination* 420(June):12–20. <https://doi.org/10.1016/j.desal.2017.06.020>
75. Mao H, Zhen HG, Ahmad A, Zhang AS, Zhao ZP (2019) In situ fabrication of MOF nanoparticles in PDMS membrane via interfacial synthesis for enhanced ethanol permselective pervaporation. *J Memb Sci* 573:344–358. <https://doi.org/10.1016/j.memsci.2018.12.017>
76. Ibrahim NA, Wirzal MDH, Nordin NAH, Abd Halim NS (2018) Development of polyvinylidene fluoride (PVDF)-ZIF-8 membrane for wastewater treatment. *IOP Conf Ser Earth Environ Sci* 140:1. <https://doi.org/10.1088/1755-1315/140/1/012021>
77. Wang C et al (2018) In situ growth of ZIF-8 on PAN fibrous filters for highly efficient U(VI) removal. *ACS Appl Mater Interfaces* 10(28):24164–24171. <https://doi.org/10.1021/acsami.8b07826>
78. Wanie Hazmo NH, Naim R, Jye LW, Ismail AF (2020) Effect of composite multi-walled carbon nanotube and zeolitic imidazolate framework-8 on the performance and fouling of PVDF membranes. *J Membr Sci Res* 6(4):424–432. <https://doi.org/10.22079/JMSR.2020.128313.1390>
79. Ragab D, Gomaa HG, Sabouni R, Salem M, Ren M, Zhu J (2016) Micropollutants removal from water using microfiltration membrane modified with ZIF-8 metal organic frameworks (MOFs). *Chem Eng J* 300:273–279. <https://doi.org/10.1016/j.cej.2016.04.033>
80. Maroofi SM, Mahmoodi NM (2019) Zeolitic imidazolate framework-polyvinylpyrrolidone-polyethersulfone composites membranes: From synthesis to the detailed pollutant removal from wastewater using cross flow system. *Colloids Surf A Physicochem Eng Asp* 572:211–220. <https://doi.org/10.1016/j.colsurfa.2019.03.093>

# Identification of Sensitive Region by Short Term Shoreline Change Analysis Over Gulf of Khambhat, Gujarat



Keval H. Jodhani , Dhruvesh Patel , and N. Madhavan 

## 1 Introduction

Shoreline change is intricate phenomenon that stems from the complex interplay of geological, hydrological, and meteorological factors. Natural processes like wave action, tidal currents, and wind-driven erosion contribute to the continual reshaping of coastlines around the world. Additionally, geological characteristics such as the type of sediment, rock formations, and coastal landforms significantly influence how shorelines evolve [1]. Over longer timescales, factors like sea-level fluctuations and climate change exert considerable influence on shoreline dynamics, leading to shifts in land–water boundaries. Human activities, including urban development, construction of coastal defenses, and alteration of river courses, further amplify the extent and rate of shoreline change. This intricate interplay of natural processes and human interventions underscores the need for a holistic understanding of the basic background of shoreline change, as it serves as a foundation for informed management and conservation strategies in coastal regions [2].

Shoreline change, a dynamic and essential facet of coastal geography, refers to the continuous alteration of the interface between land and water along coastlines. It encompasses the intricate processes of erosion, deposition, and sediment movement driven by natural forces such as waves, tides, currents, and wind, as well as human

---

K. H. Jodhani (✉) · D. Patel  
Department of Civil Engineering, School of Technology, Pandit Deendayal Energy University,  
Gandhinagar, Gujarat 382007, India  
e-mail: [jodhanikeval@gmail.com](mailto:jodhanikeval@gmail.com)

K. H. Jodhani  
Department of Civil Engineering, Institute of Technology, Nirma University, Ahmedabad,  
Gujarat 382481, India

N. Madhavan  
Petroleum Engineering, School of Petroleum Technology, Pandit Deendayal Energy University,  
Gandhinagar, Gujarat 382007, India

activities. As shorelines respond to these influences, they undergo shifts in shape, position, and composition over time. The study of shoreline change is vital for understanding the vulnerability of coastal environments to environmental shifts and for designing effective strategies to mitigate the impacts of erosion and sea-level rise [2, 3]. Whether assessing the effects of climate change and the impact of climatic variables in term of extremes (Flood or drought) [4–7] or evaluating the consequences of human development near coastlines, a comprehensive grasp of shoreline change is indispensable for ensuring the sustainable management of these critical and dynamic zones. The study of shoreline change is of paramount importance due to its critical implications for both natural ecosystems and human communities. Understanding the dynamics of shorelines is essential for predicting and mitigating the impacts of erosion, flooding, and sea-level rise. This knowledge informs coastal management decisions, allowing for the development of effective strategies to safeguard infrastructure, habitats, and valuable coastal resources. Furthermore, as coastal areas continue to face the pressures of urbanization and climate change, a comprehensive understanding of shoreline change is crucial for sustainable development [8, 9]. By analyzing historical trends and projecting future scenarios, researchers and policy-makers can collaboratively design solutions that balance ecological preservation with socioeconomic needs. In essence, the need for shoreline change study arises from the urgency to foster resilient coastal environments that can adapt to dynamic natural processes and human influences while ensuring the well-being of both ecosystems and societies [1, 10, 11].

Coastal regions across the globe are inherently dynamic and undergo continuous transformations due to the intricate interplay of natural processes and human activities. The Gulf of Khambhat, located in the western part of India's coastline, presents a compelling case study in understanding these complex dynamics. This region holds immense ecological significance as a habitat for diverse marine life, including various species of fish, crustaceans, and migratory birds. Moreover, the Gulf has been a historical and cultural center, witnessing centuries of maritime trade and cultural exchange. However, the Gulf of Khambhat, like many coastal areas, faces mounting challenges due to the intensified impacts of climate change, urbanization, and industrialization. Rising sea levels, changing weather patterns, and growing human settlements along its shores have heightened the vulnerability of this coastal zone to shoreline changes such as erosion and accretion. These alterations not only impact the local environment but also pose a threat to infrastructure, agriculture, and the livelihoods of communities that depend on the coastal resources [12–14].

In this context, a rigorous examination of short-term shoreline changes within the Gulf of Khambhat becomes imperative. The aim of this research is to delve into the patterns, causes, and consequences of these changes in order to identify regions that are particularly sensitive to such shifts [15, 16]. By pinpointing areas with high rates of shoreline erosion or accretion, this study seeks to provide actionable insights for informed decision-making in coastal management and sustainable development planning. The Gulf's complex geography, characterized by its diverse coastal landforms, sedimentary dynamics, and proximity to urban centers, presents a unique setting for such an analysis [17, 18]. Understanding the underlying factors



## 2 Study Area

The Gulf of Khambhat, alternatively known as the Gulf of Cambay, is situated within the Arabian Sea and possesses a distinctive trumpet-like shape. Positioned between the mainland of Gujarat and the Saurashtra peninsula, its geographical coordinates are approximately between latitudes  $20^{\circ}30'$  and  $22^{\circ}20'$  and longitudes  $71^{\circ}45'$  and  $72^{\circ}53'$  E. Encompassing an expanse of approximately 3120 km, the Gulf of Khambhat measures around 70 km in width and 130 km in length, featuring an average depth of 30 m [21]. This gulf experiences potent tidal currents that play a significant role in both the pronounced deposition and erosion characteristics of the region. Bordered by the districts of Navsari, Valsad, and Surat, the Gulf of Khambhat is enclosed by these administrative divisions. Figure 2 shows the study area map with sensitive regions (A: Mahadevpur region, B: Vishwamitri river estuary, C: Gogha region near Bhavnagar).

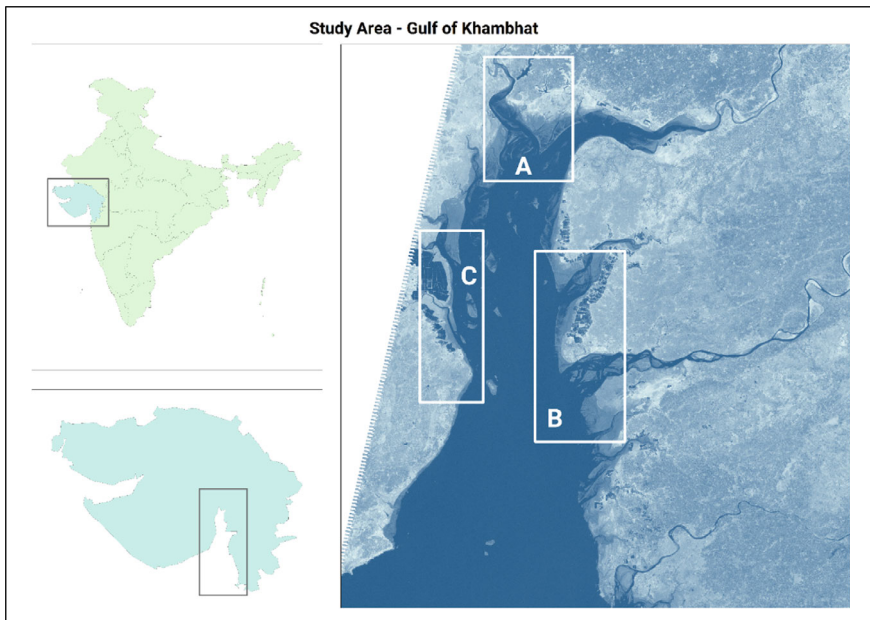


**Fig. 2** Study area map

### **3 Methodology**

The methodology employed in this research involves a synergistic combination of advanced remote sensing techniques and sophisticated geographical information systems (GIS) analysis. This integrated approach is designed to provide a comprehensive and accurate assessment of the short-term shoreline changes occurring within the Gulf of Khambhat.

#### ***3.1 Data Acquisition and Preprocessing***

The foundation of this study lies in the acquisition of high-resolution satellite imagery covering a specific time frame. These images are chosen based on their temporal proximity and spatial resolution to ensure a detailed view of the Gulf's coastline. Acquired satellite data may include optical imagery capturing visible and infrared wavelengths, data with negligible cloud cover and providing accurate shoreline mapping.

#### ***3.2 Shoreline Extraction and Change Detection***

The acquired satellite imagery is processed using sophisticated image processing algorithms to extract the shoreline positions for the selected time periods. Georeferencing and image rectification techniques are employed to ensure spatial accuracy. A change detection analysis is then carried out, wherein the extracted shorelines from different time steps are compared to quantify the extent and direction of shoreline changes. This process yields valuable information about erosion-prone and accretion-prone regions.

#### ***3.3 Geographic Information Systems (GIS) Analysis***

The extracted shoreline data is integrated into a GIS platform, allowing for spatial analysis and visualization of the identified changes. Geographic information systems facilitate the overlay of various layers, such as meteorological data, coastal geomorphology, and land use patterns. This integration aids in understanding the potential influencing factors behind the observed shoreline changes, thereby contributing to a more comprehensive interpretation of the data.

By integrating these methodologies, this research endeavors to provide an in-depth examination of short-term shoreline changes in the Gulf of Khambhat. The synergistic use of advanced technologies, field data, and historical context offers a holistic view of the complex dynamics at play, thereby contributing to informed

decision-making for effective coastal management and sustainable development practices.

## 4 Results and Discussion

The discussion segment of this research paper engages in a thorough examination and interpretation of the results obtained from the short-term shoreline change analysis within the Gulf of Khambhat. By delving into the implications, underlying factors, and broader significance of the findings, this section aims to provide a comprehensive understanding of the observed shoreline changes. As demonstrated in Fig. 3, shoreline change and deposition and erosion in part A during 2008–2009 and Fig. 4, shoreline change and deposition and erosion in part A during 2009–2010. Table 1 describes the erosion and deposition area in part A during 2008–2010. The erosion in the part A is very extensive. The cumulative erosion observed over a period of three years were 207.73 km<sup>2</sup>, 167.85 km<sup>2</sup>, and 48.94 km<sup>2</sup> whereas deposition 91.03 km<sup>2</sup>, 20.9 km<sup>2</sup>, and 11.81 km<sup>2</sup>, over the region A, B, and C, respectively. The main reason for erosion were strong tidal currents accompanied by wave action. Situation of erosion is magnified by degradation of mangrove cover over mudflats whereas accretion is the result of the sediment load transportation and deposition from the various rivers, i.e., Mahi, Narmada, Sabarmati, Vishwamitri, Tapi rivers.

### 4.1 Factors Driving Shoreline Changes

One of the key focal points of the discussion revolves around the factors driving the identified shoreline changes. The integration of remote sensing, GIS analysis, and field surveys reveals that a combination of natural processes and anthropogenic activities play a pivotal role. The interactions between sediment supply, wave energy, coastal geomorphology, and human interventions contribute to the spatial distribution of erosion and accretion hotspots.

### 4.2 Anthropogenic Influences

Human activities, such as urban development, coastal infrastructure construction, and alteration of natural sediment transport, are identified as major contributors to the observed shoreline changes. The concentration of human settlements along certain stretches of the Gulf's coastline has led to altered sediment dynamics, disrupting the natural equilibrium and exacerbating erosion. This underscores the need for sustainable land use practices and appropriate coastal development regulations.

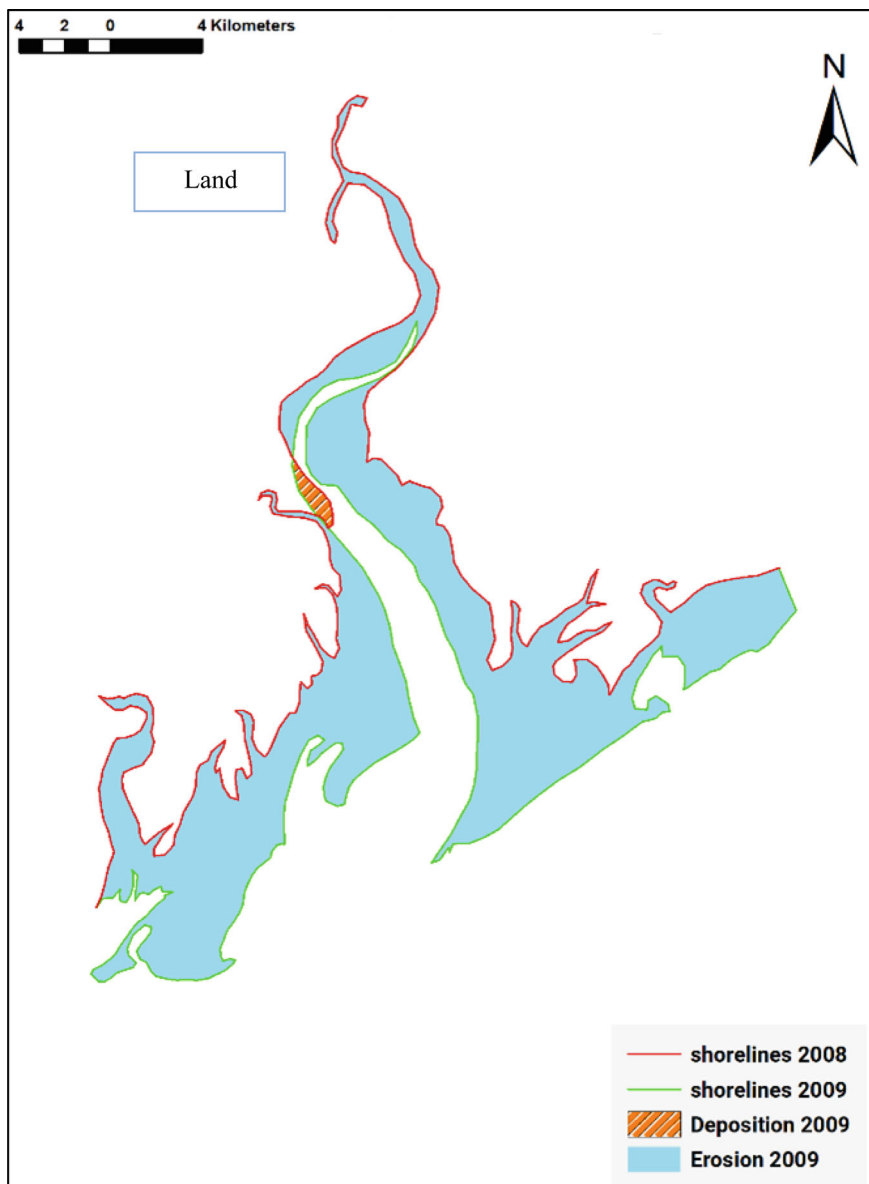


**Fig. 3** Shoreline change and deposition and erosion in region A from 2008 to 2009

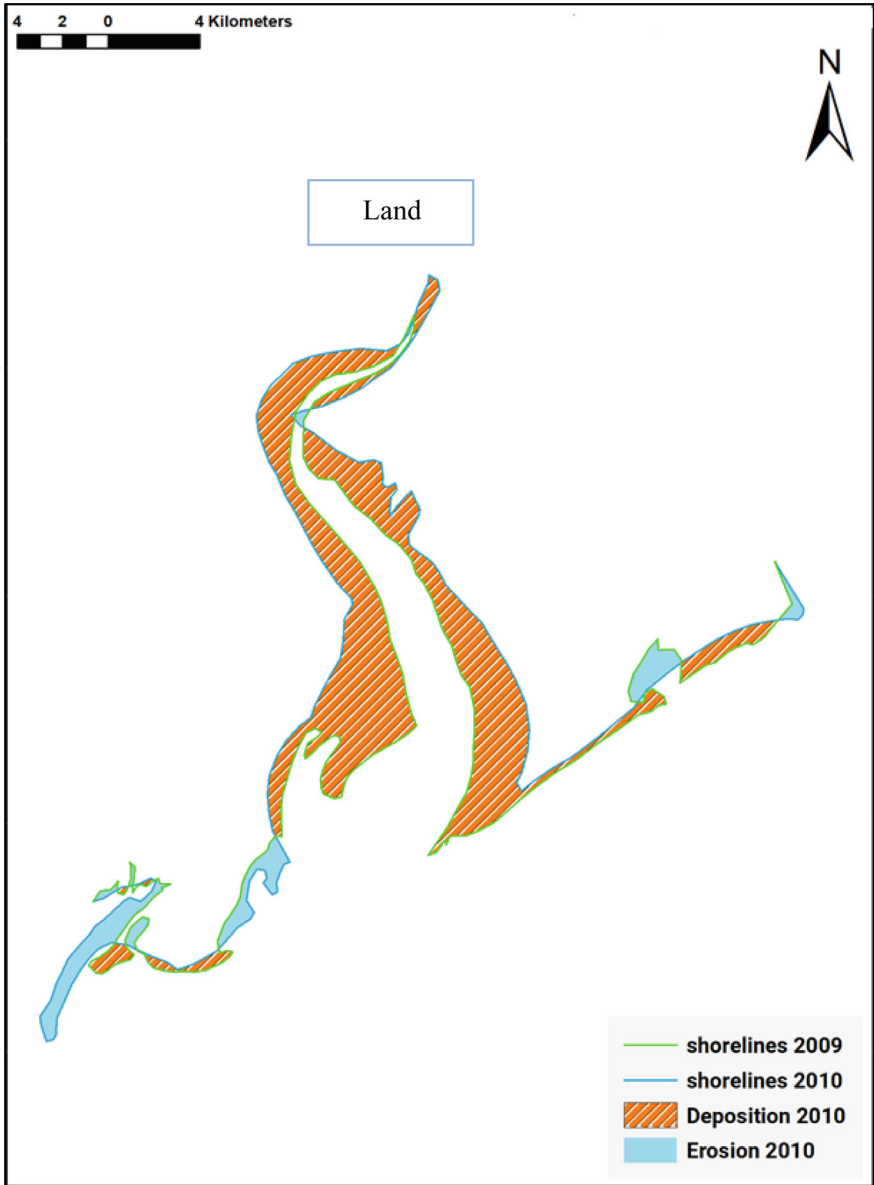


**Fig. 4** Shoreline change and deposition and erosion in region A from 2009 to 2010

**Table 1** The area of erosion and deposition in study region A from 2008 to 2010

Year	Area of erosion (km <sup>2</sup> )	Area of deposition (km <sup>2</sup> )
2008–2009	192.25	2.56
2009–2010	15.48	88.47

### ***4.3 Climate Change and Variability***

The discussion also delves into the implications of climate change and variability on shoreline dynamics. Rising sea levels, intensified storm events, and altered wave patterns are shown to impact erosion and accretion patterns. The correlation between meteorological events and shoreline changes highlights the increasing vulnerability of coastal areas to changing climatic conditions.

### ***4.4 Adaptation Strategies***

The research findings have direct implications for the formulation of adaptive coastal management strategies. By identifying sensitive regions prone to rapid shoreline changes, decision-makers can prioritize erosion control measures, beach nourishment initiatives, and the establishment of setback regulations. Additionally, the data supports the integration of climate resilience considerations into coastal planning, emphasizing the importance of a proactive approach to address future challenges.

### ***4.5 Importance of Historical Context***

The historical context provided by the analysis of past storm events, sea-level fluctuations, and long-term coastal evolution trends enriches the discussion. It helps differentiate between short-term fluctuations and enduring trends, enhancing the understanding of the Gulf's dynamic nature. This historical perspective is crucial for discerning patterns and projecting future scenarios.

### ***4.6 Interdisciplinary Approach***

The discussion underscores the significance of the interdisciplinary approach adopted in this study. By integrating remote sensing, GIS analysis, field surveys, meteorological data, and historical context, the research provides a holistic understanding of shoreline changes. This approach demonstrates the need to bridge scientific insights with practical applications for effective coastal management and resilience-building. The discussion segment of this research paper contextualizes and interprets the results of the short-term shoreline change analysis within the Gulf of Khambhat. By exploring the driving factors, anthropogenic influences, climate change implications, and adaptation strategies, the discussion aims to provide a comprehensive framework for understanding the observed alterations. Through this multifaceted analysis, the study contributes not only to scientific knowledge but also to the formulation of

strategies that safeguard the ecological integrity and socioeconomic sustainability of the Gulf's coastal regions.

Shoreline changes were digitized and visually interpreted for the assessing the deposition and erosion for the study region A, B, and C. The erosion and deposition were observed and the eroded area was 192.25 km<sup>2</sup>, and deposited area was 2.56 km<sup>2</sup>, for the period of 2008–2009 over the study region demonstrated in Fig. 3. The main reason for erosion were strong tidal currents accompanied by wave action. Similarly, the eroded area was 15.48 km<sup>2</sup>, and deposited area was 88.47 km<sup>2</sup>, for the period of 2009–2010 over the study region A demonstrated in Fig. 4. The area of erosion and deposition in study region A from 2008 to 2010 is illustrated in Table 1. For 2008 to 2009 significant erosion is observed due to human activities, including urbanization, deforestation, and unsustainable agricultural practices, playing role in destabilizing the soil. Changes in sediment transport dynamics, possibly influenced by alterations in river discharge or coastal currents, could have additionally worsened the process of erosion, furthermore this process are responsible for deposition in 2009 to 2010.

The erosion and deposition were observed from shoreline change and the eroded area was 91.36 km<sup>2</sup>, and deposited area was 4.16 km<sup>2</sup>, for the period of 2008–2009 over the study region B demonstrated in Fig. 5. Similarly, the eroded area was 76.49 km<sup>2</sup>, and deposited area was 16.74 km<sup>2</sup>, for the period of 2009–2010 over the study region B demonstrated in Fig. 6. The area of erosion and deposition in study region B from 2008 to 2010 is illustrated in Table 2.

The erosion and deposition were observed from shoreline change and the eroded area was 27.48 km<sup>2</sup>, and deposited area was 3.12 km<sup>2</sup>, for the period of 2008–2009 over the study region C demonstrated in Fig. 7. Similarly, the eroded area was 21.46 km<sup>2</sup>, and deposited area was 8.69 km<sup>2</sup>, for the period of 2009–2010 over the study region C demonstrated in Fig. 8. The area of erosion and deposition in study region C from 2008 to 2010 is illustrated in Table 3. It can be observed in part C less amount of accretion is happening during 2008–2010 and moderate amount of erosion is observed.

## 5 Conclusion

The implications and recommendations derived from the results of the short-term shoreline change analysis within the Gulf of Khambhat are vital for guiding future coastal management strategies and sustainable development practices. This section of the research paper explores the actionable insights that arise from the study and offers a roadmap for informed decision-making. The identification of erosion-prone and accretion-prone regions within the Gulf of Khambhat has direct implications for coastal management. Erosion-control measures, such as constructing protective structures or implementing beach nourishment projects, can be strategically implemented in vulnerable areas. At the same time, the findings emphasize the need for adaptive strategies that can adjust to changing natural processes and evolving climatic conditions. The cumulative erosion observed over a period of three years

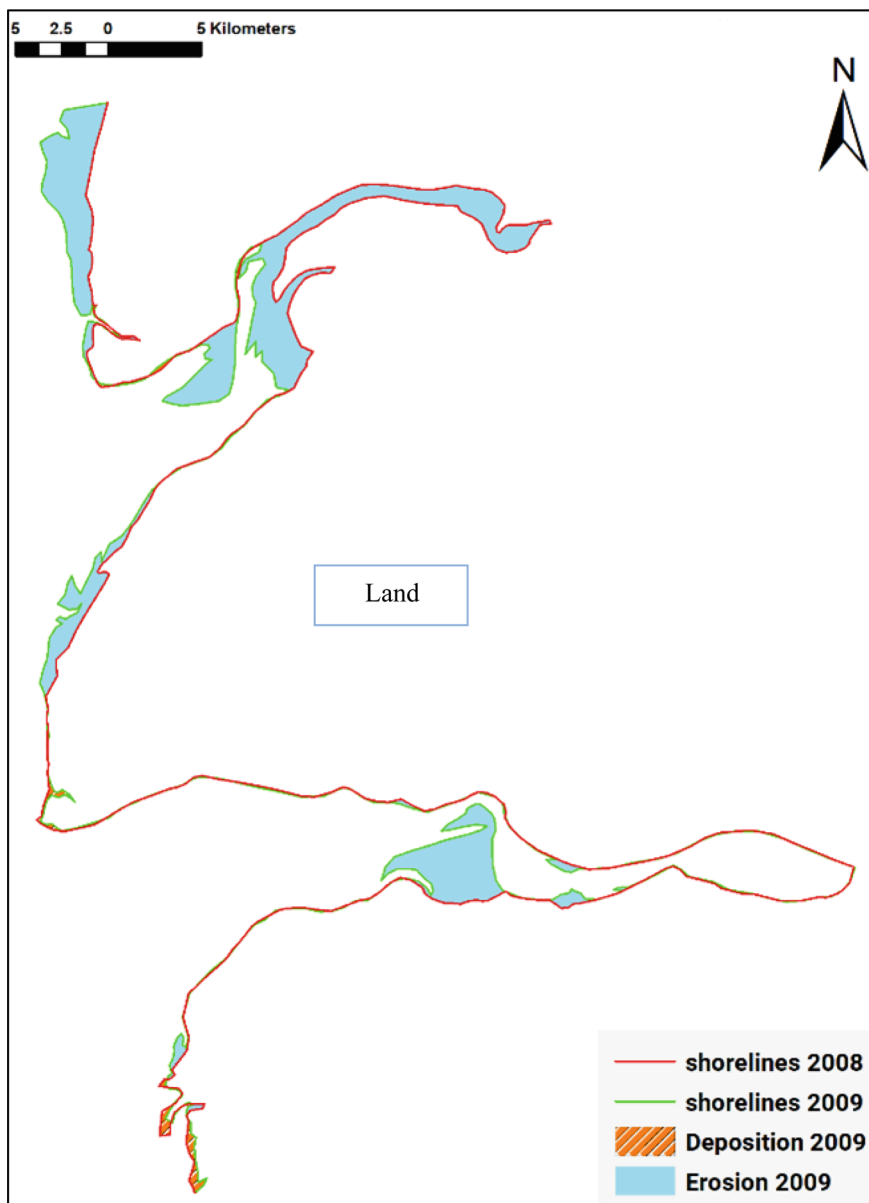
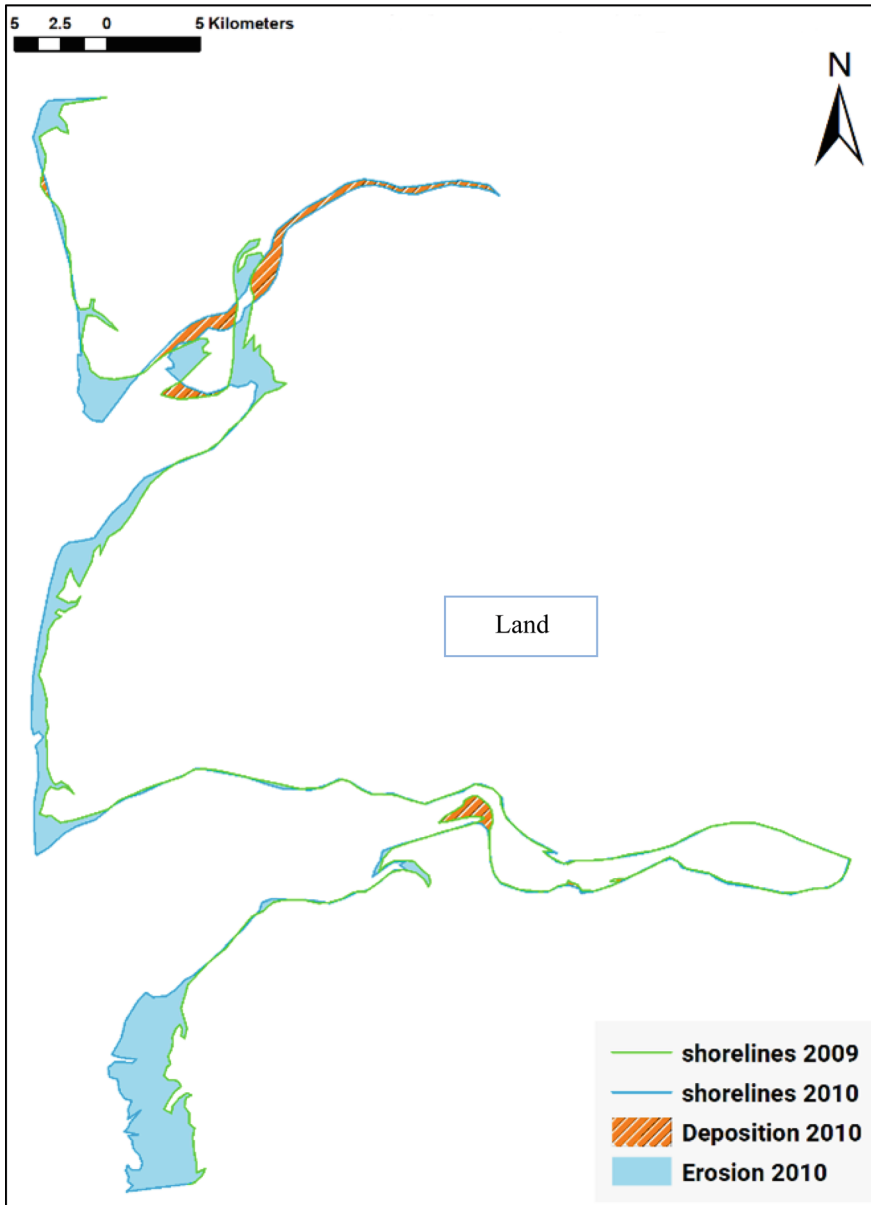


Fig. 5 Shoreline change and deposition and erosion in region B from 2008 to 2009



**Fig. 6** Shoreline change and deposition and erosion in region B from 2009 to 2010

**Table 2** The area of erosion and deposition in study region B from 2008 to 2010

Year	Area of erosion (km <sup>2</sup> )	Area of deposition (km <sup>2</sup> )
2008–2009	91.36	4.16
2009–2010	76.49	16.74



Fig. 7 Shoreline change and deposition and erosion in region C from 2008 to 2009



**Fig. 8** Shoreline change and deposition and erosion in region C from 2009 to 2010

**Table 3** The area of erosion and deposition in study region C from 2008 to 2010

Year	Area of erosion (km <sup>2</sup> )	Area of deposition (km <sup>2</sup> )
2008–2009	27.48	3.12
2009–2010	21.46	8.69

were 207.73 km<sup>2</sup>, 167.85 km<sup>2</sup> and 48.94 km<sup>2</sup> whereas deposition 91.03 km<sup>2</sup>, 20.9 km<sup>2</sup>, and 11.81 km<sup>2</sup>, over the region A, B, and C, respectively. The research findings highlight the importance of incorporating shoreline dynamics into urban planning and development practices. By designating setback zones that restrict construction near erosion-prone areas, policymakers can minimize the risk to infrastructure and property. Integrating ecological considerations and preserving natural buffers can contribute to resilient and sustainable development that respects both human needs and the environment. The correlation between meteorological events and shoreline changes underscores the significance of integrating climate resilience strategies into coastal planning. Designing infrastructure that can withstand extreme weather events and sea-level rise is crucial to minimize the impact of future changes. Implementing nature-based solutions, such as mangrove restoration and dune protection, can enhance the resilience of coastal ecosystems. The research outcomes can serve as a foundation for public awareness and education campaigns. Communicating the findings to local communities and stakeholders can foster a greater understanding of the dynamic nature of coastlines and the importance of responsible coastal management. Encouraging community engagement and participation can lead to more effective implementation of conservation efforts.

The implications and recommendations drawn from the research not only inform strategic decisions but also underscore the need for a proactive, integrated, and adaptive approach to coastal management and development. By incorporating the findings into policy frameworks and action plans, stakeholders can work together to protect the Gulf of Khambhat's coastal ecosystems, cultural heritage, and economic vitality, while fostering resilience against the challenges of an ever-changing coastline. By uncovering patterns, establishing correlations, and offering actionable recommendations, this study contributes to the broader discourse on sustainable coastal management, climate resilience, and informed decision-making. The Gulf of Khambhat serves as a microcosm of global coastal challenges, making the insights gained from this research relevant not only to the local context but also to coastal zones worldwide facing similar dynamics.

**Acknowledgements** Authors acknowledge the support of Pandit Deendayal Energy University and Nirma University.

## References

1. Natarajan L, Sivagnanam N, Usha T, Chokkalingam L, Sundar S, Gowrappan M, Roy PD (2021) Shoreline changes over last five decades and predictions for 2030 and 2040: a case study from Cuddalore, southeast coast of India. *Earth Sci Inform* 14:1315–1325. <https://doi.org/10.1007/s12145-021-00668-5>
2. Bamunawala J, Ranasinghe R, Dastgheib A, Nicholls RJ, Murray AB, Barnard PL, Sirisena TAJG, Duong TM, Hulscher SJMH, van der Spek A (2021) Twenty-first-century projections of shoreline change along inlet-interrupted coastlines. *Sci Rep* 11:14038. <https://doi.org/10.1038/s41598-021-93221-9>

3. Basheer Ahammed KK, Pandey AC (2022) Assessment and prediction of shoreline change using multi-temporal satellite data and geostatistics: a case study on the eastern coast of India. *J Water Clim Change* 13:1477–1493. <https://doi.org/10.2166/wcc.2022.270>
4. Gupta N, Banerjee A, Gupta SK (2021) Spatio-temporal trend analysis of climatic variables over Jharkhand, India. *Earth Syst Environ* 5:71–86. <https://doi.org/10.1007/s41748-021-00204-x>
5. Gupta SK, Gupta N, Singh VP (2021) Variable-sized cluster analysis for 3D pattern characterization of trends in precipitation and change-point detection. *J Hydrol Eng* 26:04020056. [https://doi.org/10.1061/\(ASCE\)HE.1943-5584.0002010](https://doi.org/10.1061/(ASCE)HE.1943-5584.0002010)
6. Gond S, Gupta N, Patel J, Dikshit PKS (2023) Spatiotemporal evaluation of drought characteristics based on standard drought indices at various timescales over Uttar Pradesh, India. *Environ Monit Assess* 195:439. <https://doi.org/10.1007/s10661-023-10988-2>
7. Gond S, Gupta N, Dikshit PKS, Patel J (2023) Assessment of drought variability using SPEI under observed and projected climate scenarios over Uttar Pradesh, India. *Phys Chemis Earth Parts A/B/C* 131:103440. <https://doi.org/10.1016/j.pce.2023.103440>
8. Kankara RS, Selvan SC, Markose VJ, Rajan B, Arockiaraj S (2015) Estimation of long and short term shoreline changes along Andhra Pradesh coast using remote sensing and GIS techniques. *Proc Eng* 116:855–862. <https://doi.org/10.1016/j.proeng.2015.08.374>
9. Abd-Elhamid HF, Zelenáková M, Barańczuk J, Gergelova MB, Mahdy M (2023) Historical trend analysis and forecasting of shoreline change at the Nile Delta Using RS data and GIS with the DSAS tool. *Remote Sens (Basel)* 15:1737. <https://doi.org/10.3390/rs15071737>
10. Alharbi OA, Hasan SS, Fahil AS, Mannaa A, Rangel-Buitrago N, Alqurashi AF (2023) Shoreline change rate detection applying the DSAS technique on low and medium resolution data: case study along Ash Shu'aybah-Al Mujayrimah coastal Area of the Eastern Red Sea, Saudi Arabia. *Reg Stud Mar Sci* 66:103118. <https://doi.org/10.1016/j.risma.2023.103118>
11. Zambrano-Medina YG, Plata-Rocha W, Monjardin-Armenta SA, Franco-Ochoa C (2023) Assessment and forecast of shoreline change using geo-spatial techniques in the Gulf of California. *Land (Basel)* 12:782. <https://doi.org/10.3390/land12040782>
12. Ghanavati M, Young I, Kirezci E, Ranasinghe R, Duong TM, Luijendijk AP (2023) An assessment of whether long-term global changes in waves and storm surges have impacted global coastlines. *Sci Rep* 13:11549. <https://doi.org/10.1038/s41598-023-38729-y>
13. Fernández-Mora A, Criado-Sudau FF, Gómez-Pujol L, Tintoré J, Orfila A (2023) Ten years of morphodynamic data at a micro-tidal urban beach: Cala Millor (Western Mediterranean Sea). *Sci Data* 10:301. <https://doi.org/10.1038/s41597-023-02210-2>
14. Triana K, Solihuddin T, Husrin S, Risandi J, Mustikasari E, Kepel TL, Salim HL, Sudirman N, Prasetyo AT, Helmi M (2023) An integrated satellite characterization and hydrodynamic study in assessing coastal dynamics in Cirebon, West Java. *Reg Stud Mar Sci* 65:103107. <https://doi.org/10.1016/j.risma.2023.103107>
15. Jodhani KH, Jodhani KH, Patel D, Madhavan N (2023) Land use land cover classification for REL river using machine learning techniques. In: 2023 International Conference on IoT, Communication and Automation Technology (ICICAT). IEEE, pp 1–3
16. Jodhani KH, Patel D, Madhavan N, Singh SK (2023) Soil erosion assessment by RUSLE, Google Earth engine, and geospatial techniques over Rel River Watershed, Gujarat, India. *Water Conserv Sci Eng* 8:49. <https://doi.org/10.1007/s41101-023-00223-x>
17. Adams KD (2023) Wind, waves, sediment transport, and potential for shoreline development on Earth and on Mars. *Icarus* 405:115695. <https://doi.org/10.1016/j.icarus.2023.115695>
18. McLean R, Thom B, Shen J, Oliver T (2023) 50 years of beach–foredune change on the southeastern coast of Australia: Bengello Beach, Moruya, NSW, 1972–2022. *Geomorphology* 439:108850. <https://doi.org/10.1016/j.geomorph.2023.108850>
19. Jodhani KH, Patel D, Madhavan N (2023) A review on analysis of flood modelling using different numerical models. *Mater Today Proc* 80:3867–3876. <https://doi.org/10.1016/j.matpr.2021.07.405>

20. Hoque A, Rahman M, Paul GC (2023) 1D–2D mathematical modeling of wave refraction and wave attenuation by mangrove forests. *Ocean Eng* 286:115619. <https://doi.org/10.1016/j.oceaneng.2023.115619>
21. Jodhani K, Bansal P, Jain P (2021) Shoreline change and rate analysis of Gulf of Khambhat using satellite images. Springer, Singapore, pp 151–170

# Water Consciousness and Indian Cinema: A Critical Discourse Analysis of Select Hindi Language Movies



Amrita Chakraborty  and Sunayan Bhattacharjee 

## 1 Introduction

Cinema is a complete art form—not so much because it encompasses all the other art forms but mostly because it wields the largest impact [2]. As much as it has often been bracketed as a platform for entertainment, it has also been extensively used for spreading information and sensitizing people on myriad issues [3]. The celebrated French auteur Jean-Luc Godard once famously said, “Cinema is the most beautiful fraud in the world.” [4]. While Godard’s conjecture cannot be logically or structurally contested for obvious reasons, the fact remains that cinema has historically played an instrumental role in creating awareness about multiple social, political, cultural, and economic concerns [5].

If one closely looks at cinematic history from across the globe, one will find that there are innumerable instances when cinema played the role of an activist. Cinema had its tryst with such intricate global issues as climate change, gender equality, racial harmony, equitable distribution of resources, queer identity, nationalism, and decolonization [6]. In the identical vein, many filmmakers have experimented with cinema that specifically deals with awareness about the proper utilization of water. Some such movies include the likes of Stan Phillips’ *Water Follies* (1976), Irena Salina’s *Flow: For Love of Water* (2008), Sam Bozzo’s *Blue Gold: World Water Wars* (2008), and Tim Neeves’ *Brave Blue World* (2020).

However, there is one movie that needs to be specifically mentioned here for its deep ecocentrism around water conservation. James Cameron’s epic science fiction movie *Avatar: The Way of Water* (2022) takes the discourse around water to the

---

A. Chakraborty

School of Liberal Studies, Pandit Deendayal Energy University, Gandhinagar, Gujarat, India

S. Bhattacharjee (✉)

Department of Liberal Arts, Humanities and Social Sciences, Manipal Academy of Higher Education, Manipal, India

e-mail: [sunayan.bhattacharjee@manipal.edu](mailto:sunayan.bhattacharjee@manipal.edu)

next logical level. It adopts a philosophical route in creating water consciousness [7]. It equates the way of life with the way of water to craft a near spiritual message on the sheer importance of water in people's lives. While the movie does its bit in engendering the much-needed discussion around water and its conservation, the discussions that emanate from viewings of the movie constitute the most important bit [8]. After the release of the movie, movie-goers from across the globe created a sort of a frenzy on the social media platform. While all of it did not contribute to the creation of water awareness, there were informed discourses that grew around the central theme of the movie. The fact that nearly three-quarters of the earth's surface is water and most of it cannot be used for people's daily needs received quite a bit of traction in the weeks following the release of the movie. *Avatar: The Way of Water* clearly points to the power of cinema in crafting an alternative discourse around water—a discourse that is polarly different from the profit-centric approach adopted by non-sustainable ventures from almost all the corners of the world.

While movies from the West had their impact on water conservation efforts, Indian movies have seldom joined the bandwagon in creating consciousness around water. Movies dealing with water have been too few and far between. However, some Indian projects here and there have tried creating consciousness around a sustainable water future [9]. It is important that such attempts are acknowledged and discussed to create a meaningful and popular discourse on water—primarily through the usage of the audiovisual medium.

In the given pursuit, the researchers examine five Indian films that focus on creating water consciousness—either directly or subtly. These are Ashutosh Gowariker's *Lagaan* (2001), Shyam Benegal's *Well Done Abba* (2010), Girish Malik's *Jal* (2013), Nila Madhab Panda's *Kaun Kitney Paani Mein* (2015), and *Kadvi Hawa* (2017), also by Nila Madhab Panda. While *Lagaan* has specific water references, the other films primarily revolve around water.

The reasons for selecting the movies are three-fold—(i) the fact that all the movies are in Hindi and the language has somewhat been able to transcend regional barriers in India; (ii) all the films are spaced over a period of 16 years thereby representing the evolution of thoughts on the cinematic representation of water; and (iii) both mainstream and parallel movies have been included in the study, so that one can clearly understand both the popular and the nuanced discourses on water.

## 2 Relevance of the Study

- (i) The researchers expect that the study would significantly add to the understanding of the role played by visual media in general and cinema in particular in creating consciousness about water.
- (ii) The study is expected to show a future trajectory of creating consciousness about water through the usage of visual media.

### 3 Objectives

- (i) To analyze the role of Hindi language movies in creating water consciousness among the audience using distinctive case studies.
- (ii) To decode the specific elements that attempt to create water consciousness among the audience.

### 4 Methodology

The researchers conducted a critical discourse analysis (CDA) of all the five selected movies to decode the cinematic texts used. This is done to showcase the power of cinema in creating consciousness around proper water conservation. Before going any further, it is important that one understands the meaning of CDA.

CDA is a specific interdisciplinary research technique that makes a distinct attempt at understanding the usage of languages [10]. Despite the wide variety of methodological approaches that CDA entails, scholars look at the usage of languages as being representative of the existing social norms and practices [11]. Languages also embody the subtle and not so subtle power hierarchies and ideologies that are hidden in discourses.

For the current paper, the researchers describe the structure of the cinematic text at the surface level—both aural and visual. For doing so, the researchers apply the laws of linguistic analysis. Furthermore, the researchers correlate the cinematic text with the social context, thereby decoding the water elements used in the movies.

The researchers have chosen CDA as it helps in establishing the relationship between cinematic text and ingrained water debates with the social context being the background.

For the study, the researchers selected five scenes each from all the five movies that concern the narrative around water consciousness. The specific scenes were selected based on their capacities to contribute to the composite meanings of the five movies. Eventually, the visual and linguistic analyses of these scenes were contrasted against the social understandings of water vis-à-vis the authenticity of those portrayals and their departures from the social constructs [12]. The fundamental intent of conducting this study was to reaffirm the power of popular media in general and cinema in particular in creating a discourse around water conservation.

The researchers would like to give a disclaimer here. Discourse analysis can be a subjective affair given the fact that the interpretation of a given text depends on the perspective adopted by the analyst(s). However, the attempt would be to reduce the impact of personal biases or feelings in the analytical process. Also, the current study is specific to the context that it is setting itself in. Therefore, generalizability might be a bit of an issue while using the results in any future study. Most importantly, the current study is set in the Indian cultural and social context, and therefore, the same considerations might not be applicable for similar studies being conducted for any other culture.

## 5 First Section

### 5.1 Analysis of Lagaan

**Description and Analysis of the First Selected Scene:** In the first selected scene, the villagers of Champaner village talk about the continuing drought condition in the village and the consequent shortage of water. Some of them express their doubts about the possible arrival of rainfall. The conversation happens while the camera focuses on an extremely arid landscape bereft of any semblance of green. The sky is also shown to be clear and bright thereby indicating a continuance of the existing condition. While the discussion among the villagers is indicative of a lurking economic and human disaster, the landscape creates a strange feeling of fear and imbalance resulting from a shortage of water. In unambiguous terms, the scene is a commentary on the obvious consequences of water shortage on any human settlement. It also hints at the political, sociological, cultural, and economic repercussions of drought that has the potential to lead to a famine. Most importantly, both the visual and the aural elements of the scene serve as a warning for agriculturalists and farmers about the imminent danger of water shortage across the globe.

**Description and Analysis of the Second Selected Scene:** In the second selected scene, a lady from the village refers to water from under the soil playing an important role in mitigating the impending disaster caused by the drought. She points toward a well while making the comment. However, the well stands on a barren land thereby establishing an uncanny dichotomy of hope and despair. While the deliberation seems soothing, the visual and aural elements of the scene make a concerted attempt at establishing the importance of groundwater. Since *Lagaan* is typically representative of the Indian scenario, the concerned scene sensitizes viewers about the potential that the protection of groundwater holds for the country's residents. However, the scene also points at the wide misconception about groundwater. It reminds viewers that a continued shortage of rainwater would also result in the exhaustion of groundwater.

**Description and Analysis of the Third Selected Scene:** The third selected scene is rich—both visually and aurally. It marks the jubilation of the villagers when they see clouds hovering over the village and their subsequent disappointment when the clouds move away. When some of the villagers see clouds approaching the village, they indulge in a group song that harps on the importance of rainfall and water. The clouds hide the sun and there seems to be an element of softness engulfing the entire arid landscape. Eventually, the clouds move away, and the village is again exposed to the harshness of the sun. This is when the villagers understand that they celebrated a tad too soon and disperse in silent grief. This scene is pregnant with so many overt and covert meanings. For one, it emphasizes the value that rain holds for a predominantly agricultural settlement. Secondly, it makes a subtle commentary on the transient nature of monsoon. Most importantly, it makes the viewers aware of the relationship between the sufficient availability of water and food production.

**Description and Analysis of the Fourth Selected Scene:** In the fourth selected scene, viewers see a woman from the village pulling up water from a well. However, from her expressions, one can say that the water level is receding and there is an imminent threat of the water getting exhausted. The woman looks extremely tired, and there is a clear indication of gloom and doom everywhere. The visual and aural elements in the scene point toward the obvious relationship between the availability of water and prosperity—both individual and group. In this case, the context is important to deconstruct the scene. This scene is projected while the entire village is trying to come to terms with a system of double taxation that has been levied by the local royalty driven by an upsurge in British power. Therefore, a shortage of groundwater adds to the villagers' woes. Here, the auteur raises the stake using the shortage of water as a metaphor.

**Description and Analysis of the Fifth Selected Scene:** The fifth selected scene is the last scene of the movie. It captures a moment when the proverbial good has vanquished the proverbial evil. While the villagers celebrate a victory over their colonial masters in a cricket match, the rain also starts pouring down simultaneously. In a way, the rain shown here is a heavenly vindication of the cause that the villagers were fighting for. In India, the advent of the rainy season has always been considered very auspicious. The visual and aural elements in the scene are in line with that tradition. In a largely agrarian economy, prosperity has always been equated with sufficient rainfall and hence sufficient availability of water. The scene also points toward the primordially of water in the sustenance of civilizations and consequently humanity itself.

## 5.2 *Analysis of Well Done Abba*

**Description and Analysis of the First Selected Scene:** In the first selected scene, the protagonist's daughter declines to provide water to a rickshaw driver even after the protagonist requests her to do so following his rickshaw trip. The daughter mentions the significant shortage of water in the village as a reason for her refusal. Subsequently, the protagonist gives some money to the rickshaw driver and tells him to buy and drink water at any hotel. While the visual and aural elements in the scene reek of humor, its fundamental thesis is quite grim. The viewers are made aware of how water has become more valuable than money. In fact, the scene establishes water as a distinct currency. Most importantly, the scene justifies the name of the movie, which has two meanings—one that is obvious and the other that is subtle. Since the characters in the movie speak a certain variation of Urdu, the auteur also tries his bit to showcase the shortage of water in the concerned region of Telangana (erstwhile Hyderabad).

**Description and Analysis of the Second Selected Scene:** In the second selected scene, the protagonist of the movie decides that he would utilize a government scheme to construct a well inside his house premises. The viewers see him dreaming about

how the construction of the well would significantly assist him in getting his daughter married and having a better life. In very simple terms, the availability of water is being equated with a resultant better quality of life. In water-starved areas, life revolves around the struggles to find water and the visual and aural elements of the scene point toward that. The trajectory of the rest of the movie concerns the struggle to get the water source constructed, and this scene sets the tone of that struggle.

**Description and Analysis of the Third Selected Scene:** In the third selected scene, the protagonist's brother and sister-in-law are shown to indulge in theft of water. This represents one of the most common problems in areas where there is a scarcity of water. Water is a valued proposition and as such there is widescale theft. The state of Telangana has always been one of the country's drought-prone areas. It perennially grapples with water shortage. Through the visual and aural elements in the scene, the auteur draws the viewers' attention to the fact that other areas can also become drought-prone if thoughtful usage of water is not ensured. This scene is also indicative of the non-judicious usage of water by people at large. Again, humor is subtly used to depict a very grave problem. The scene shows an arid and dry landscape where the available water is not enough to meet the needs of the population.

**Description of the Fourth Selected Scene:** In the fourth selected scene, the viewers witness large-scale systemic corruption around the construction of water wells. Right from the municipal administration to the construction workers, graft seems almost systematized. This scene makes a restrained commentary on how water is a deeply political issue. Also, the visual and aural elements follow a comic tonality while making viewers aware about the ingrained and universalized economic corruption that happens every day revolving around water. Through the usage of Hyderabad Dakhini (a variant of Urdu that is spoken in the southern states of India), the auteur paints a picture of corruption, casteism, and gender discrimination. In fact, there is an attempt to showcase the relationship between corruption and retrograde social practices. The scene also shows that while a section of the population has access to water and they tend to waste it at the drop of a hat, another section suffers from the eternal shortage of water.

**Description of the Fifth Selected Scene:** The fifth selected scene is perched toward the end of the movie. Here, the protagonist is shown to have finally managed a water well inside his residential complex. Therefore, he along with his daughter and would-be son-in-law draw water from the well and drink it with great satisfaction. Simultaneously, they say that the water is indeed sweet. There is an attempt here to distinguish between fresh water and saline water. While saline water is abundantly available, it is not fit for drinking. From the visual and aural elements that are part of the scene, it becomes clear that getting access to water is one of the greatest achievements in the life of the protagonist. While the scene is a part of the movie's larger diegesis, it also makes the viewers abundantly aware about the value of water. The scene also makes a poignant point for people with sufficient supply of water not to waste their precious natural resource.

### 5.3 *Analysis of Jal*

**Description and Analysis of the First Selected Scene:** In the first selected scene, Gujarat's Rann of Kutch is geographically, visually, and aurally introduced. There is a clear indication that it would be the setting for the film. In what might seem unnerving, the frighteningly dry and arid landscape of the region is revealed in a very systematic way. It becomes clear from the word go that the movie would end up as a tragedy—a human tragedy stemming from a natural one. Even the waterbodies are menacing, and the viewers are sensitized about the non-drinking nature of those. The scene perfectly justifies the name of the movie and is largely indicative of the fundamental enigma that would pretty much consume the entire movie's diegesis. The viewers are also made aware of flamingos flying over the waterbodies. However, even the birds do not seem reassuring in the larger backdrop that the scene paints.

**Description and Analysis of the Second Selected Scene:** In the second selected scene, the protagonist assures the villagers that there is enough water under the desert. While some believe it, there are many others who ridicule him for such an outlandish claim. In this scene, viewers see the protagonist, who calls himself the God of Water, prospecting for water across the desert land. In this case, the viewers can comprehend the importance of groundwater and its discovery in the middle of a desert. Rann of Kutch has been facing a severe water crisis for a long time subject to several natural and manmade reasons. While very few settlements in the region have access to sufficient fresh water, most of the settlements do not have enough water for survival. The visual and aural elements in the scene are indicative of the existential crisis that the region finds itself in.

**Description and Analysis of the Third Selected Scene:** The third selected scene seems to be a promiscuous one on the surface. However, it does not fail to elicit multiple meanings. In the concerned scene, the viewers see the protagonist travel to the nearby enemy village. He finds that his love interest is bathing. Subsequently, he seduces his love interest, and both have sex inside the bathroom. While this seems like an obvious scene, it is not so. For one, it is a luxury to bathe in a desert. Secondly, this comes amid the water crisis that the protagonist's village is facing on a recurrent basis. Thirdly, a subtle analogy is drawn between water and sex. While one helps sowing new crops, the second helps sowing new human beings. The visual and aural elements in the scene help establish the equivalence between the continuance of life and water thereby firmly establishing the importance of aqua.

**Description and Analysis of the Fourth Selected Scene:** In the fourth selected scene, jewelry is traded for constructing a water well in the protagonist's village. This scene is indicative of the importance that the villagers attach to a stable supply of water. Water is indeed a currency in areas that are prone to droughts. In the scene, the viewers see that the women of the village seamlessly give away their precious gold jewelry to trade it for a well. While it might seem like an unreal proposition, it is not so. Across the water-starved regions in India, marriage happens only when the groom has access to sufficient water. Thus, it is not wealth but a supply of water

that becomes the determinant for social prosperity. Visually and aurally, the village women are shown to take the most natural decision in deciding to part away with their seemingly valuable jewelries.

**Description and Analysis of the Fifth Selected Scene:** The fifth scene could be construed to have multiple meanings. The scene shows the protagonist fighting with one of the leaders of the enemy village in one of the waterbodies. The viewers see both hitting each other while they gather dust and mud on their bodies. Eventually, both become unidentifiable due to the collection of wet dirt and mud on their bodies. The visual and aural elements of the scene are designed in a way to represent the conflict that water creates. While they fight for their common love interest, it is also a metaphor for water conflicts. Across many water-starved regions of India, people have fought and died for getting hold of water sources. As the sheer amount of available water decreases across the nation, such fights might take the form of riots. In a way, the scene is a warning for people to buck up and conserve water for the larger interests of the nation and humanity.

#### **5.4 Analysis of Kaun Kitney Paani Mein**

**Description and Analysis of the First Selected Scene:** In the first selected scene, viewers see the intertwining of feudal, caste, and gender complications with the supply of water. While it rains during the scene, the princess and her lower caste lover are shot dead by the King. This incident sparks a physical, social, and psychological barrier between the higher caste people staying in the highlands and the lower caste people staying in the lowlands. In India, the access to water has always been determined by social hierarchies. While the powerful lot has managed to maintain their stranglehold over water resources, the socially powerless have always struggled. It is a commentary on how social equations determine access to important resources—the primary being water. Visually and aurally, the scene is morbidly dark as it plays out in the night while people scream for justice and their inalienable right to live.

**Description and Analysis of the Second Selected Scene:** The second selected scene focuses on the contemporary royal descendant and his struggle to have access to family-owned resources including water. The scene stands in stark contrast with the opening scene where the King is shown to be all-powerful. This scene exposes the reversal of the power dichotomy. Now, people living in the lowlands have access to sufficient water. However, people from the highlands must practically scamp for even the minimum access to water. This scene is indicative of the intrinsically political nature of the movie as it makes caste and social commentaries with water being the context. The scene is designed in a comical way though. However, the complexities remain. The visual and aural elements of the scene make a clear case for the equal distribution of water and not making it a commodity for sale in the open market.

**Description and Analysis of the Third Selected Scene:** In the third selected scene, the King strives to sell off his landed property. However, he repeatedly fails because his plots lack proper sources of water. It is extremely interesting looking at how the scene portrays the futility of having landed properties without water. The visual and aural elements of the scene point toward the virtual decapitation of royalty subject to a shortage of water resources. Over a period, there has been a shift of power—from the lazy upper caste people to the efficient lower caste workers. The scene also shows how agriculture eventually suffers when there is a continuous shortage of water. In an agrarian country like India, agricultural potential holds the key to the value that is attached to a piece of land. In the absence of proper irrigation facilities that demand a steady supply of water, a piece of land is rendered valueless.

**Description and Analysis of the Fourth Selected Scene:** In the fourth selected scene, the viewers see that the King's son is sitting quietly near a pond in the lowlands. It seems he is overwhelmed with the sheer amount of water—something that he has not experienced until now. He touches the water and evidently gets lost in a stream of thoughts. This scene is metaphorically indicative of the importance that water holds in the life of an individual. Water is often equated to life, and it cannot be any truer. The softness of the water also leads to a change in his plans. Now, he seeks to unite the two villages and make water accessible to all instead of stealing it from the lowlands. Visually and aurally, the scene points to a subtle celebration of humanity over undue rivalry. In a way, the scene portrays a triumph of basic human values and establishes the primordially of goodness in men.

**Description and Analysis of the Fifth Selected Scene:** The fifth selected scene is a typical Indian song-and-dance scene involving the King's son and the daughter of the political head of the lowlands. While the scene follows the usual trajectory of Indian cinematic romance, it becomes meaningful because of the usage of rain. Rain metaphorically represents all that is romantic and soft. In India, water is used for all functions and is almost a divine presence. This scene is indicative of the conciliation between the highland dwellers and the lowland residents. While tensions exist, a compromise seems to be in the air. The visual and aural elements in the scene are intentionally kept soft so that a feel-good factor is created. Most importantly, it is apparent from the scene that the new generation is more into collaboration than competition. It would not be an exaggeration to note that the scene emits an optimistic vibe.

## 5.5 *Analysis of Kadvi Hawa*

**Description and Analysis of the First Selected Scene:** In the first selected scene, the viewers get a sense of the harsh and visually arid Bundelkhand region in Central India through the depiction of a humble village. The camera specifically focuses on the soil, burning sun, and the topography of the village. There seems to be a scarcity of water everywhere one looks. The visual and aural elements of the scene paint

a very grim picture that links climate change with the shortage of water in many parts of the country. It points toward the shortage of water that has been troubling the villagers for a while now. This shortage of water has resulted in the reduction of agricultural output, thereby leading to a spurt in farmers' suicides, which has been a recurring problem in the country for a while. The scene serves as a warning to people who are playing with nature on different pretexts.

**Description and Analysis of the Second Selected Scene:** In the second selected scene, viewers see the protagonist using water for the purpose of excretion. The scene makes it amply clear that not enough water is there. Therefore, he must use discretion while using it. While the drinking aspect of water is usually put into focus, the other usages of water are put into the backburner. This scene makes a distinct attempt at addressing that. The scene subtly warns the viewers that the world is looking at a bleak future wherein even if water is available for drinking, it will not be available for other activities. If the viewers look a little carefully at the visual and aural elements of the scene, they would be able to figure out that the protagonist can be seen extremely awkward about the fact that he is using the water for any other purpose other than drinking.

**Description and Analysis of the Third Selected Scene:** The third selected scene focuses on bank loans. In India, farmers take loans but eventually cannot pay it back subject to agricultural setbacks. This phenomenon has led to the eternal debt trap for farmers from multiple regions in India and has led to their suicides. The scene shows a recovery agent going from door to door asking for the repayment of bank loans. While the recovery agent seems like an antagonist, he is not so as he is also working under professional and livelihood compulsions. The attempt of many debtors to run away from paying back the loans seems comical. However, the attempt points at something more ominous—the fact that most of the farmers have not been able to earn as much as they should have. While the visual and aural elements do not say anything about water directly, it does talk about the repercussions of water shortage.

**Description and Analysis of the Fourth Selected Scene:** The fourth selected scene features an interesting discussion between the protagonist and the loan recovery agent. When the agent says that he hails from the coastal state of Odisha, the protagonist retorts that the agent is very lucky as Odisha does not have a dearth of water or rainfall. What is even more interesting is how the loan agent dismisses the protagonist's statement and says that even excess rainfall can be disastrous. This scene exposes the other side of the story—the fact that cyclones and floods can also destroy agriculture. In the scene, the viewers see the protagonist and the loan agent meeting at an undisclosed location in the middle of an arid hill. While there seems to be no visual and aural indication of water anywhere, they discuss what happens when there is more water than is required.

**Description and Analysis of the Fifth Selected Scene:** The fifth selected scene is where the protagonist talks about the change in wind and how this transformation has led to the distinct change in weather. While his statement seems a little on the cryptic side, one can understand the intensity. Climate change is a reality that much of the

global leadership has already acknowledged. A humble villager also seems to be saying the same, albeit in a different tone and mode. The visual and specifically the aural elements point toward something very worrying—a catastrophic modification of the global climatic conditions. It is also a subtle way of warning the viewers of the obvious pitfalls of tinkering with the natural system. While an old and seemingly uneducated villager can understand it, it remains a mystery as to why educated developmental activists cannot. One cannot overlook the repercussions of climate change or do they!

## 6 Conclusions

After a detailed and careful analysis of all the five movies, it becomes clear that all the movies propagate the message of water conservation—albeit in ways that are essentially different. Some of the stand-out findings of the study stands thus:

- (i) The importance of time and seasonal rainfall is emphasized.
- (ii) A relationship is drawn between the sufficient supply of water and successful agricultural practices.
- (iii) The economic importance of water is highlighted.
- (iv) A close relationship is drawn between the adverse effects of climate change and dwindling water resources.
- (v) A deliberate attempt is made to sensitize people about the significance of groundwater.
- (vi) A relationship is drawn between the unfortunate practice of farmers' suicides and shortage of water.
- (vii) Water is shown to be not just an economic capital but also a social, political, and cultural capital.
- (viii) A definite commentary is also made on the havoc created by an overdose of water.
- (ix) The viewers' attention is drawn toward some of the drought-affected regions of India.
- (x) A case is made to ensure equitable distribution of water and not commodifying it.

While India is home to 18% of the global population, it only has about 4% of the planet's total freshwater resources [13]. Thus, India is one of the most water-stressed nations in the world. A 30 major Indian cities including Delhi, Mumbai, Kolkata, Bengaluru, Pune, and the likes are staring at an acute water scarcity by 2050 [14]. This impending water disaster can be averted through the execution of swift and efficient human actions that focus on a sustainable future. It is still not too late, and the current grim situation can be mended if tended to. A massive public sensitization campaign, therefore, is the need of the hour.

Cinema—a powerful entity that has hitherto been underutilizing its potential—can make a marked difference in creating a dominant social and cultural narrative around

water conservation. Individual attempts by filmmakers like the movies that have been studied in the current paper, thus, will not suffice. To make water conservation a powerful social theme and implementable idea, socially aware auteurs have to come forward and craft a concerted and time-bound cinematic initiative that will focus on multiple aspects of water conservation like: (i) individual efforts at homes, (ii) group efforts at the community level including formal and informal creation of awareness among both children and adults, (iii) strategic efforts at the bureaucratic level, and (iv) legislative efforts at the government level (both Center and States). In addition to fiction films, educational documentary films, Public Service Advertisements (PSAs), and short sensitization films can do a world of good in getting the message across to people who matter the most.

At the policy level, both Central and State Governments should come forward in sponsoring and promoting movies that spread the message of water conservation. There is an urgent requirement for a national policy framework in which new-age filmmakers are encouraged to touch upon the varied aspects of water conservation through innovative and contemporary filmmaking tools. Technological aids such as *Virtual Reality* (VR), *Augmented Reality* (AR), and *Mixed Reality* (MR) can be effectively used to create immersive experiences through films that harp on and advocate water conservation. As they say, human beings can do wonders and a strategized cinematic policy on creating water consciousness will do the wonder of going the distance in mitigating the impending water disaster in India.

## References

1. Taylor Coleridge S (2016) *The rime of the ancient mariner and other poems*, 1st edn. William Collins, Glasgow
2. nofilmschool. <https://nofilmschool.com/what-makes-cinema-great>. Accessed 30 Aug 2023
3. San Francisco Film School. <https://www.sanfranciscofilmschool.edu/using-cinema-as-a-powerful-means-of-communication-for-social-issues/>. Accessed 30 Aug 2023
4. The Economic Times. <https://economictimes.indiatimes.com/news/new-updates/cinema-is-the-most-beautiful-fraud-10-profound-sayings-of-jean-luc-godard/articleshow/94181711.cms?from=mdr>. Accessed 30 Aug 2023
5. The Indian Express. <https://indianexpress.com/article/entertainment/bollywood/udne-doctor-revathy-cinema-social-issues-5452232/>. Accessed 30 Aug 2023
6. BreakoutoftheBox. [https://www.breakoutofthebox.com/the-power-of-film-how-films-create-awareness-about-important-issues/#google\\_vignette](https://www.breakoutofthebox.com/the-power-of-film-how-films-create-awareness-about-important-issues/#google_vignette). Accessed 30 Aug 2023
7. An Darach. <https://silvotherapy.co.uk/articles/environmental-messages-in-avatar>
8. National Geographic. <https://www.nationalgeographic.com/science/article/avatar-the-way-of-water-james-cameron-science-oceans>
9. Outlook. <https://www.outlookindia.com/art-entertainment/five-films-that-flawlessly-illustrate-the-wrath-of-climate-change-news-196796>. Accessed 30 Aug 2023
10. Library and Information Management Academic Blog. <https://lmbd.org/approaches-to-discourse-analysis-how-to-do-discourse-analysis-strengths-and-weaknesses-of-discourse-analysis-when-to-use-discourse-analysis/#:~:text=Subjectivity%3A%20Discourse%20analysis%20can%20be,assumptions%20when%20conducting%20disc>. Accessed 30 Aug 2023
11. Leeuwen Tv (2006) Critical discourse analysis. *Encyclopedia of language & linguistics*, pp 290–294

12. Little W, McGivern R (2016) Gender, sex, and sexuality. Introduction to sociology
13. The World Bank. <https://www.worldbank.org/en/country/india/brief/world-water-day-2022-how-india-is-addressing-its-water-needs>
14. Mint. <https://www.livemint.com/news/india/30-indian-cities-likely-to-face-acute-water-risks-by-2050-wwf-11604371789053.html>

# Characteristic Analysis of Oil-Field-Produced Water



Om Patel , Arth Padaria , Akshay Gupta ,  
Balasubramanian Ragnathan , and S. Vinod Kumar 

## 1 Introduction

The energy sector encompasses energy generation, distribution, and consumption industries. The oil and gas industry is an energy sector, providing a considerable share of the world's energy needs [1]. Because of its significance in modern society, the oil and gas sector is a significant manufacturing process. Crude oil accounts for about 29% of India's energy consumption [2]. Petroleum is regarded as a critical energy source, and its demand is increasing due to its contribution to various applications and fields. Exploration and production efforts have been intensified to serve the expanding market for petroleum. Contaminated wastewater is a byproduct of underground oil and gas extraction. This effluent water is known as "produced water" (PW). Oil and gas wells produce a variable amount of this water that increases over time. The most prevalent byproduct of oil and gas extraction processes is produced water, a complex mixture of inorganic and organic substances. Throughout a standard oil or gas well's life, the water-to-oil ratio increases [3]. PW volume often increases with reservoir age and may account for up to 98% of total fluid volume in some circumstances. However, for the majority of oil wells, a 1:3 ratio of oil to water is commonly accepted [4].

Consequently, there has been a surge in the requirement for contaminated water to be treated. The global wastewater generated from oil and gas operations is around 250 million barrels daily, with a predicted increase of 605 million barrels per day [5]. With a refining capacity of roughly 250 million tons per year (MTPA), India

---

O. Patel · A. Padaria · A. Gupta · B. Ragnathan (✉)

Department of Petroleum Engineering, School of Energy Technology, Pandit Deendayal Energy University, Gandhinagar 382426, India

e-mail: [balaschem@gmail.com](mailto:balaschem@gmail.com)

S. Vinod Kumar

Department of Chemical Engineering, St. Joseph's College of Engineering, Chennai 600119, India

is the world's third largest user of crude oil. However, over the years, India's oil demand is projected to reach 450 MTPA [6]. According to the International Energy Agency report, India's oil consumption might increase to 6.7 million barrels per day (bpd) by 2030; and 7.4 million bpd by 2040. The final disposal of PW without sufficient treatment can damage surfaces, groundwater, and soil. A wide variety of pollutants, including petroleum hydrocarbons, oil and grease, phenol, ammonia, sulfides, and other organic composites, are present in the wastewater produced by the petroleum sector. These substances are all present in the discharged water from the petroleum industry in a very complex form that is hazardous to the environment [7]. The constituents of produced water can be classified as inorganic and organic compounds, dissolved and scattered oils, grease, heavy metals, treated chemicals, building solids, salts, dissolved gases, scale products, waxes, microorganisms, and dissolved oxygen are examples of these, pH, suspended solids (SS), and biochemical oxygen demand (BOD).

Oily wastewater contains four forms of petroleum hydrocarbons: aliphatic, aromatic, asphaltenes, and compounds containing oxygen, nitrogen, and sulfur [8]. Therefore, the amounts of these components must be removed before releasing the appropriate effluent to the receiving water body during the treatment procedures. Inorganic and organic compounds in PW are more hazardous than those in crude oil. Using PW and disposing of unprocessed produced water constituting several toxic chemicals might jeopardize environmental sustainability. The properties of the produced water must be understood to propose an effective method for reducing the level of hazardous compounds in the water before disposal. Adequate handling and administration is necessary to dispose of the produced water safely and effectively without interfering with environmental sustainability [9]. The use of PW and the dumping of untreated PW containing several toxic chemicals could jeopardize ecological stability. The PW's properties must be understood to propose an effective technique for reducing the concentration of toxic compounds in the water ahead of disposal. Appropriate handling and supervision are required, so that the PW may be disposed of safely and used effectively without interfering with the environment [10].

## ***1.1 Produced Water***

Produced water is acquired from the oil and gas industry during the drilling process that is considered wastewater. Specific amounts of water will continue to flow back to the surface during well drilling and conclusion, which is known as fracturing flowback [11]. The content and properties of chemical compounds occurring naturally in PW are inextricably linked to the geographical properties associated with every reservoir. The makeup of PW is complicated, with thousands of chemicals varying in concentration across wells and during the life of a well [12]. It combines injected water, formation fluid, petroleum products, and treatment substances. Based

on the point of origin, oil field, gas field, and coal bed methane (CBM) field produced water are the three types [13].

### ***1.2 Produced Water from Oil Field***

Groundwater or saltwater injected to maintain reservoir pressure, and solid particles and microbes may be present in the oil processing water. The majority of PW includes greater amounts of salt water than ocean water. Furthermore, the PW contains chemical substances utilized in the drilling, producing, and separating water and oil processes [14]. Though varies greatly between pumps and fields, most forms of produced water have many constituent groupings. Examples include salt concentration, salinity, total dissolved solids, and electrical conductivity. Oil, grease, and different natural inorganic and organic chemicals are the principal elements of importance in PW. Sulfate-reducing bacteria may be found in this water as well.

### ***1.3 Produced Water from Gas Field***

Condensed water and formation water are combined in the generated fluids since gas fields do not employ water injection. The chloride concentrations of this water range from very pure water to salty formation water, which has a chloride content 14 times that of seawater. It has a higher acidity than generated water from oil fields [15]. The total amount of water caused by gas fields is smaller than that of oil sources. Various gas chemical treatment agents such as ethyl glycol, methanol, and triethylene glycol are employed in gas fields. These mentioned chemicals constitute one-third of pollutant that are being released into PW. Volatile component concentrations in produced water from gas fields are higher than in oil fields [9].

### ***1.4 Factors affecting Volume of Produced Water***

Produced water constitutes most of the waste stream during the exploration and production of oil and gas operations. Water produced from oil or natural gas extraction does not have a uniform quantity because it fluctuates based on location and extraction process [16]. In comparison, offshore produced water production comes to around 90 million barrels per day. In contrast, worldwide oil output was around 78 million barrels per day, resulting in an average water-to-oil ratio (WOR) of 3.0 [9]. Drilling type is regarded as a crucial variable; for instance, for the same decline, the horizontal well produces water at a higher rate than the vertical well. The well's location, or whether it is situated inside homogenous or heterogeneous reservoirs, is another crucial consideration. An earlier-than-anticipated water output might be

caused by a well that has been improperly dug or improperly placed inside the reservoir construction. Additionally, the type of reservoirs impacts the vertical and horizontal wells. For example, when homogenous reservoirs use horizontal wells, water production decreases and the volume of water injected in the oil recovery increases [17]. The amount of produced water that is ultimately controlled over the life cycle of a well and a project might be influenced by all of the elements above to a greater or lesser extent. The economic viability of a venture is impacted by increased produced water volumes because of the cost of disposing of water, the increased size and cost of treatment facilities for water, as well as the expense of associated treatment chemical substances, the higher cost of lifting water compared to hydrocarbons, and the loss of recoverable hydrocarbons.

### ***1.5 Environmental Impacts***

One of the biggest concerns about produced water is the possibility of contaminating aquatic habitats. It typically contains hydrocarbons, heavy metals, salts, and other toxic chemicals that can affect aquatic life. These toxins, when released into rivers, streams, or marine ecosystems, have the potential to damage the habitats and general health of fish, invertebrates, and other aquatic animals. This circumstance poses a severe danger to the ecosystem's fragile equilibrium. Aquatic species are subjected to hazardous substances in the water, which can lead to decreased reproduction rates, stunted development, and increased death. Furthermore, some pollutants can accumulate in the tissues of these creatures, potentially leading to bioaccumulation in the food chain. As a result, predatory animals at the top of the food chain may be exposed to higher levels of pollution, causing threats to both wildlife and human health if people ingest infected creatures [17]. Aromatic hydrocarbons, certain alkyl phenols, and a few metals are the compounds of most environmental concern in generated water because their concentrations may be high enough to induce bioaccumulation and toxicity. Highly alkylated phenols are renowned disruptors of endocrine function; however, they are rarely found with such concentrations to impact water column animals after first dilution [18]. Produced water discharge can also lead to sediment pollution. Pollutants in the water may settle in sediments, possibly damaging benthic creatures and disturbing sediment populations. This process has the potential to progressively change the structure and function of the benthic ecosystem, adding to the overall deterioration of the environment over time. When this water is dumped into freshwater bodies, it can increase salinity, making the water unsuitable for many freshwater species and upsetting the delicate balance of the entire ecosystem. Furthermore, increased salinity might degrade water quality. Most PW has sodium as a main dissolved element, and it causes considerable soil damage by changing mineral clays and textures of the soil and triggering eventual erosion [17]. Extra sodium competes for absorption by plant roots with calcium, magnesium, and potassium; as a result, excess sodium can induce shortages in other cations. High salt

**Fig. 1** Produced water

levels can also cause poor soil structure and impede water penetration. Water salts appear to have the greatest impact on soils, water quality, and ecosystems [10].

## 2 Materials and Methods

Produced water sample was collected from gas gathering station, Gandhinagar, and stored in polyethylene container at 7 °C (Fig. 1). Chemicals used in the research were of analytical grade purchased from Sisco Research Laboratories, Mumbai, India.

## 3 Characteristics of Produced Water

The qualities of produced waters are governed by the type of either producing or storage formation used, the operating conditions, and the chemicals used in process facilities. The chemical breakdown of water produced from various sources can differ by an order of degree. In gas sectors, a variety of gas chemical treatments such as methanol, ethylene glycol, and triethylene glycol are utilized. A third of these toxins end up in water. The concentrations of these volatile components in PW from gas reserves are greater compared to that in produced water from oil wells. However, the composition of PW is very similar to that of oil and/or gas production. Some factors, including as the field's geographical location and formation, reservoir lifespan, and kind of hydrocarbon commodity produced, influence both the chemical and physical qualities of produced water [11]. BTEX (benzene, toluene, ethyl benzene, xylenes) are monocyclic aromatic hydrocarbons that constitute the majority of PW [13]. Nevertheless, considering that they evaporate quickly from saltwater, they are rarely considered when assessing the consequences of PW. However, for creatures in close proximity to emission scores, it is impossible to rule out the possibility of minor biological consequences produced by chronic exposure to BTEX over time. PAHs are polycyclic aromatic hydrocarbons. Phenol and alkyl phenol, which are

present in PW, are both dangerous and poisonous and can induce a variety of biological impacts; they are regarded to be the most concerning due to their established hormone-disrupting properties. Metals discovered in PW include arsenic, cadmium, copper, chromium, lead, mercury, nickel, and zinc [12].

### 3.1 pH

The pH meter and its accompanying electrodes were meticulously standardized by employing two reference buffer solutions, ensuring they fell within the expected pH range of the sample to be analyzed. The sample measurements were conducted under rigorously controlled conditions, employing prescribed techniques for utmost precision. The calibrated electrodes were carefully submerged into the sample, and once the electrode output attained stability, the stability indicator promptly revealed the pH and temperature readings [19].

### 3.2 Total Dissolved Solid

The water sample is evaporated until it completely dries out, leaving behind the dissolved solids as a residue. The weight of this residue is then measured, and the TDS content is calculated by considering the weight of the residue and the initial volume of the sample.

$$\text{TDS Concentration (mg/L)} = ((B-A)/C) \times (1000 \text{ mg/g}) \times (1000 \text{ mL/L})$$

$A$  = Weight of clean dry container (g).

$B$  = Weight of container and residue (g).

$C$  = Volume of sample (mL).

### 3.3 Total Suspended Solid

Suspended solids, also known as total suspended solids (TSS), are found in smaller sizes inside reservoir rocks such as quartz and clays. Furthermore, produced water (PW) contains a variety of particles and dissolved contaminants that cannot be removed by filtering. TSS composition varies depending on particle size; for example, proppant size in hydraulic fracturing ranges from 1.0 mm to bigger particles, whereas iron sulfide particles are smaller, ranging approximately 0.1 m or less. TSS is generally denser than both PW and oil, making it to settle to the bottom of containers, tanks, or pipelines, posing a number of operating issues [20].

$$\text{TSS} = ((W_f - W_i)/V) \times (1000 \text{ mg/g}) \times (1000 \text{ mL/L})$$

$W_f$  = Final weight (Filter + Solid) (g).

$W_i$  = Initial weight (Filter) (g).

$V$  = Volume of sample (L).

### 3.4 Chemical Oxygen Demand

A representative water sample is collected and combined with a potent oxidizing agent, usually potassium dichromate, and a strong acid such as sulfuric acid. The mixture is then heated through reflux at elevated temperature for a specific duration, causing the oxidation of organic compound. Once cooled, the remaining oxidizing agent is titrated using a reducing agent, leading to a color change proportional to the COD level. This color change is subsequently measured with a spectrophotometer, and the COD value is determined by referencing a calibration curve using standard solutions. COD analysis serves to evaluate the degree of organic pollution in water, proving particularly valuable for assessing the environmental impact of produced water [16].

$$\text{COD} = 8 \times 1000 \times \text{DF} \times M \times (V_B - V_S) / \text{Volume of sample}$$

DF = Factor of dilution.

$M$  = Molarity of standard solution of ferrous ammonium sulfate.

$V_B$  = Volume consumed during titration with blank solution.

$V_S$  = Volume utilized during titration sample preparation.

### 3.5 Biochemical Oxygen Demand

A produced water sample is gathered and placed in a controlled environment, kept in darkness and maintained at a specific temperature for approximately 5 days. Throughout this incubation period, microorganism in the water consume the organic substances as a food source, resulting in a reduction of dissolved oxygen. Following incubation, the remaining dissolved oxygen is measured, and the BOD is calculated by comparing the initial and final dissolved oxygen concentration. The BOD analysis is crucial for assessing the extent of organic pollution and the potential impact of the produced water on aquatic ecosystem, offering valuable insights for effective wastewater treatment and environmental conservation measures [21].

$$\text{BOD} = (\text{DO}_1 - \text{DO}_2) \times (D/V)$$

- DO<sub>1</sub> = Initial dissolved oxygen concentration in the water sample (mgmL<sup>-1</sup>).  
 DO<sub>2</sub> = Final dissolved oxygen concentration in water sample after incubation period (mgmL<sup>-1</sup>).  
 D = Dilution factor.  
 V = Volume of the water sample (mL).

### 3.6 Heavy Metals

The concentration of heavy metals in produced water (PW) is influenced by geological formations and well age. PW typically contains varying levels of lead (Pb), iron (Fe), zinc (Zn), barium (Ba), selenium (Se), strontium (Sr), and manganese (Mn) in significant quantities. Additionally, there are trace amounts of other heavy metal pollutants such as chromium (Cr), vanadium (V), copper (Cu), cadmium (Cd), mercury (Hg), and nickel (Ni) in PW. The metal concentrations are determined by the surrounding environment, with higher levels leading to toxicity and bioaccumulation [16, 22].

$$\text{Heavy metals(\%)} = \frac{C_i - C_f}{C_i} \times 100$$

where  $C_i$ —initial concentration and  $C_f$  is final concentration of heavy metals in produced water.

### 3.7 Total Nitrogen

Total nitrogen in produced water (PW) refers to the combined amount of all compounds of nitrogen, including ammonia, nitrates, and nitrites. This encompasses organically bonded nitrogen, nitrate-nitrogen (NO<sub>3</sub>-N), ammonia-nitrogen (NH<sub>3</sub>-N), and nitrite-nitrogen (NO<sub>2</sub>-N). To calculate the total nitrogen content, distinct quantities of free ammonia, nitrate-nitrite, and organic nitrogen compounds must be measured and added together.

### 3.8 Conductivity

The capacity of water to conduct electrical current is referred to as conductivity, and it is controlled by the concentration of ions in the water. This property is directly associated with factors like temperature, pH, and the level of dissolved carbon dioxide, which contribute to ion formation. Conductivity can be categorized into two types: intrinsic conductivity, which arises from the mentioned factors, and

extraneous conductivity, resulting from the presence of specific ions such as chloride, calcium, sodium, magnesium, and others in the sample [23].

$$\sigma = L/(A \times R)$$

$L$  = Length of conductor (cm or m).

$A$  = Area of cross section (cm<sup>2</sup> or m<sup>2</sup>).

$R$  = Resistance ( $\Omega$ ).

### 3.9 Sulfur Content

The total sulfur content of produced water denotes the amount of sulfur compounds contained in the water. To ascertain the total sulfur content, titration method can be employed, wherein a reagent is introduced that reacts with sulfur compounds, leading to a color change or the formation of a precipitate. The quantity of reagent utilized in the process enables the determination of the sulfur content.

## 4 Comparison of Produced Water and Drinking Water

Comparative research is conducted between produced water and conventional water used for consumption in order to evaluate the adverse effects of produced water and its hazardous constituents. Typical PW chemical parameters measured include some specifications. Metal, metalloid, and nonmetal concentrations are examples. Total suspended solids, total dissolved solids, and turbidity are examples of physical parameters. Table 1 highlights an assortment of parameters range for produced water and drinking water. The statistics reveal the high ranges of contaminants and elements found in produced water.

## 5 Conclusion

The majority of the waste fluid from oil and gas extraction activities is produced water. The environment may be contaminated by the water's toxic substances. Therefore, it is necessary to confirm that the water complies with the criteria and requirements established by the WHO before releasing it into the environment. Heavy metals, sulfur, and high TDS and TSS values make up the majority of the substances in untreated oil and gas industrial water. These descriptions demonstrate its destructive nature when put side by side with those of drinking water. It may be safely discarded or used for typical household purposes after being processed.

**Table 1** Comparison of drinking water and produced water reported value

S. No	Parameters	Standard value		Reported values	Reference
		Drinking water	Produced water		
1	pH	6.5–8.5	4.3–10	8.3	[5]
2	Total dissolved solids (mgL <sup>-1</sup> )	250–300	100–40,000	25,500	[24, 25]
3	Total suspended solids (mgL <sup>-1</sup> )	100	1.2–1000	683	[24, 26]
4	Chemical oxygen demand (mgL <sup>-1</sup> )	250–500	1220–2600	2150	[27, 28]
5	Biological oxygen demand 3 days at 27 °C (mgL <sup>-1</sup> )	25–30	75–2850	1220	[16, 28]
6	Heavy metals (mgL <sup>-1</sup> )	5–15	25–60	47.5	[16, 22, 29]
7	Total nitrogen (mgL <sup>-1</sup> )	2–6	23–26	24.6	[24]
8	Conductivity (µScm <sup>-1</sup> )	1500	4200–180,000	165,000	[10]
9	Sulfur content (mgL <sup>-1</sup> )	250	510–900	775	[30]
10	BTEX (mgL <sup>-1</sup> )	–	0.73–24.1	3.55	[16, 27]

## References

- Alley B, Beebe A, Rodgers J, Castle JW (2011) Chemical and physical characterization of produced waters from conventional and unconventional fossil fuel resources. *Chemosphere* 85:74–82. <https://doi.org/10.1016/j.chemosphere.2011.05.043>
- Agrawal P (2015) India's petroleum demand: estimations and projections. *Appl Econ* 47:1199–1212. <https://doi.org/10.1080/00036846.2014.993131>
- Olajire AA (2020) Recent advances on the treatment technology of oil and gas produced water for sustainable energy industry-mechanistic aspects and process chemistry perspectives. *Chem Eng J Adv* 4:100049. <https://doi.org/10.1016/j.cej.2020.100049>
- Munirasu S, Haija MA, Banat F (2016) Use of membrane technology for oil field and refinery produced water treatment—a review. *Process Saf Environ Prot* 100:183–202. <https://doi.org/10.1016/j.psep.2016.01.010>
- Patni H, Ragunathan B (2023) Recycling and re-usage of oilfield produced water—a review. *Mater Today Proc* 77:307–313. <https://doi.org/10.1016/j.matpr.2022.11.372>
- Amakiri KT, Canon AR, Molinari M, Angelis-Dimakis A (2022) Review of oilfield produced water treatment technologies. *Chemosphere* 298:134064. <https://doi.org/10.1016/j.chemosphere.2022.134064>
- Elmobarak WF, Hameed BH, Almomani F, Abdullah AZ (2021) A Review on the treatment of petroleum refinery wastewater using advanced oxidation processes. *Catalysts* 11:782. <https://doi.org/10.3390/catal11070782>
- Reddy MV, Devi MP, Chandrasekhar K, Goud RK, Mohan SV (2011) Aerobic remediation of petroleum sludge through soil supplementation: microbial community analysis. *J Hazard Mater* 197:80–87. <https://doi.org/10.1016/j.jhazmat.2011.09.061>

9. Liang Y, Ning Y, Liao L, Yuan B (2018) Special focus on produced water in Oil and Gas fields: origin, management, and reinjection practice. Elsevier Inc. <https://doi.org/10.1016/B978-0-12-813782-6.00014-2>
10. Hedar Y, Budiyo (2018) Pollution impact and alternative treatment for produced water. E3S Web Conf 31:1–12. <https://doi.org/10.1051/e3sconf/20183103004>
11. Liu N, Liu M, Zhang S (2015) Flowback patterns of fractured shale gas wells. *Nat Gas Ind B* 2:247–251. <https://doi.org/10.1016/j.ngib.2015.07.017>
12. Bakke T, Klungsøyr J, Sanni S (2013) Environmental impacts of produced water and drilling waste discharges from the Norwegian offshore petroleum industry. *Mar Environ Res* 92:154–169. <https://doi.org/10.1016/j.marenvres.2013.09.012>
13. Igunnu ET, Chen GZ (2014) Produced water treatment technologies. *Int J Low-Carbon Technol* 9:157–177. <https://doi.org/10.1093/ijlct/cts049>
14. Akstinat M (2019) Chemical and physicochemical properties of formation waters of the oil and gas industry. *J Hydrol* 578:124011. <https://doi.org/10.1016/j.jhydrol.2019.124011>
15. Fakhru'l-Razi A, Pendashteh A, Abdullah LC, Biak DRA, Madaeni SS, Abidin ZZ (2009) Review of technologies for oil and gas produced water treatment. *J Hazard Mater* 170:530–551. <https://doi.org/10.1016/j.jhazmat.2009.05.044>
16. Al-Ghouti MA, Al-Kaabi MA, Ashfaq MY, Da'na DA (2019) Produced water characteristics, treatment and reuse: a review. *J Water Process Eng* 28:222–239. <https://doi.org/10.1016/j.jwpe.2019.02.001>
17. Dawoud HD, Saleem H, Alnuaimi NA, Zaidi SJ (2021) Characterization and treatment technologies applied for produced water in Qatar. *Water (Switzerland)* 13:3573. <https://doi.org/10.3390/w13243573>
18. Neff J, Lee K, DeBlois EM (2011) Produced water: overview of composition, fates, and effects. [https://doi.org/10.1007/978-1-4614-0046-2\\_1](https://doi.org/10.1007/978-1-4614-0046-2_1)
19. Nirgude NT, Shukla S, Venkatachalam A (2013) Physico-chemical analysis of some industrial effluents from Vapi industrial area, Gujarat, India. *Rasayan J Chem* 6:68–72
20. Rodriguez AZ, Wang H, Hu L, Zhang Y, Xu P (2020) Treatment of produced water in the Permian basin for hydraulic fracturing: comparison of different. *Water* 12:770. <https://doi.org/10.3390/w12030770>
21. Jouanneau S, Recoules L, Durand MJ, Boukabache A, Picot V, Primault Y, Lakel A, Sengelin M, Barillon B, Thouand G (2014) Methods for assessing biochemical oxygen demand (BOD): a review. *Water Res* 49:62–82. <https://doi.org/10.1016/j.watres.2013.10.066>
22. Hardi M, Siregar YI, Anita S, Ilza M (2019) Determination of heavy metals concentration in produced water of oil field exploration in siak regency. *J Phys Conf Ser* 1156:012009. <https://doi.org/10.1088/1742-6596/1156/1/012009>
23. Kumar N, Hirschey J, LaClair TJ, Gluesenkamp KR, Graham S (2019) Review of stability and thermal conductivity enhancements for salt hydrates. *J Energy Storage* 24:100794. <https://doi.org/10.1016/j.est.2019.100794>
24. Ahmad NA, Goh PS, Yogarathinam LT, Zulhairun AK, Ismail AF (2020) Current advances in membrane technologies for produced water desalination. *Desalination* 493:114643. <https://doi.org/10.1016/j.desal.2020.114643>
25. Hussain I, Shakeel M, Faisal M, Soomro ZA, Hussain M, Hussain T (2014) Distribution of total dissolved solids in drinking water by means of Bayesian Kriging and Gaussian spatial predictive process. *Water Qual Expo Heal* 6:177–185. <https://doi.org/10.1007/s12403-014-0123-9>
26. Rahmanian N, Hajar S, Ali B, Homayoonfard M, Ali NJ, Rehan M, Sadef Y, Nizami AS (2015) Analysis of physicochemical parameters to evaluate the drinking water quality in the State of Perak. *Malaysia J Chem* 2015:10
27. Abbas AJ, Gzar HA, Rahi MN (2021) Oilfield-produced water characteristics and treatment technologies: a mini review. *IOP Conf Ser Mater Sci Eng* 1058:012063. <https://doi.org/10.1088/1757-899x/1058/1/012063>
28. Verma AK, Singh TN (2013) Prediction of water quality from simple field parameters. *Environ Earth Sci* 69:821–829. <https://doi.org/10.1007/s12665-012-1967-6>

29. Zhou Y, Lei J, Zhang Y, Zhu J, Lu Y, Wu X, Fang H (2018) Determining discharge characteristics and limits of heavy metals and metalloids for wastewater treatment plants (WWTPs) in China based on statistical methods. *Water (Switzerland)* 10:1–17. <https://doi.org/10.3390/w10091248>
30. Liu H, Fu C, Gu T, Zhang G, Lv Y, Wang H, Liu H (2015) Corrosion behavior of carbon steel in the presence of sulfate reducing bacteria and iron oxidizing bacteria cultured in oilfield produced water. *Corros Sci* 100:484–495. <https://doi.org/10.1016/j.corsci.2015.08.023>

# Treatment of Wastewater Using Conducting Polymer/Magnetite ( $\text{Fe}_3\text{O}_4$ ) Based Magnetic Adsorbent Materials



Krunal Baria, Krunal Parekh , and Syed Shahabuddin 

## 1 Introduction

Dyeing industries such as textiles, paper and pulp, tannery, and paint industries annually produce 700,000 tons of 10,000 different types of dyes and use them in various processes. A notable amount of dyes and other inorganic effluents is discharged in the natural water reservoirs at such high production rate [1]. The amount of dye effluents released into the environment by various industries is shown in Fig. 2. Market Research Future (MRFR) predicted that the textiles dye market is growing at 6% CAGR with a market revenue around 10.9 billion dollars over the forecast period of 2022–2030 [2]. The market growth also drags the concerns for environmental pollution caused by these organic dyes that needs to be addressed properly. Every industry should follow a safe and systematic application procedures to reduce the exposure of organic and inorganic effluents to the natural biotas.

Plants are depended on nutrients such as nitrogen, phosphorous, potassium, magnesium, calcium, and sulfur for their healthy growth, but the excessive concentration of nitrates, phosphates and nitrites leads to the eutrophication of the biota. Water algae and other aquatic plants show excessive growth due to the easy availability of nutrients in the water. These aquatic plants cover the surface of the water and restrict the penetration of sunlight to some extent. Such phenomenon is also observed in the case of dye effluents where it forms a reflective layer on the surface of water and restrict the sunlight penetration by reflecting the rays. Photosynthesis efficiency of aquatic plants present on the waterbed of aquatic biota gets affected by the reduced availability of sunlight. Photosynthesis processes that take place under water plays a major role to keep the aquatic life alive by maintaining the levels of chemical oxygen demand (COD) and biological oxygen demand (BOD). Increasing amount of BOD and COD can causes adverse effects to the aquatic fauna and flora.

---

K. Baria · K. Parekh · S. Shahabuddin (✉)  
Department of Chemistry, Pandit Deendayal Energy University, Gujrat 382007, India  
e-mail: [Syed.shahabuddin@sot.pdpu.ac.in](mailto:Syed.shahabuddin@sot.pdpu.ac.in)



**Fig. 1** a Magnetic adsorbent, b magnetic adsorbent in dye solution, c easy separation of adsorbent material after the application part

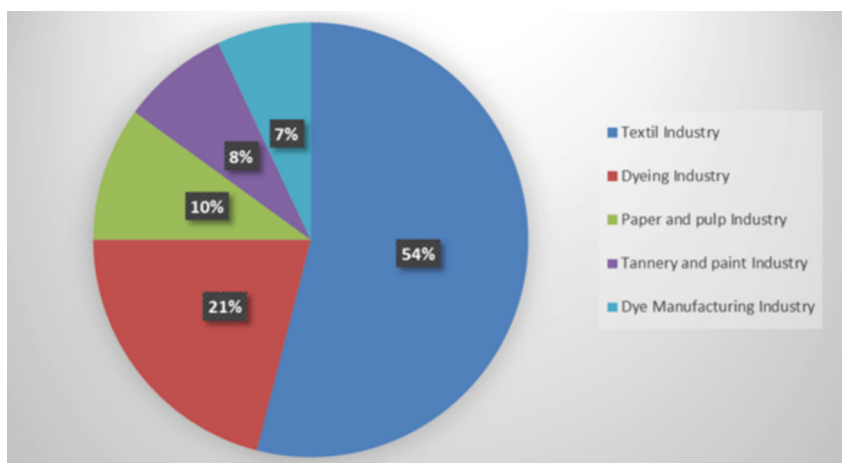


**Fig. 2** Dye effluents released into the environment by various industries [2]

A study was conducted to observe the effects of dissolved oxygen (DO) on the health of fishes near Haridwar, India. They noted that the fishes from the site of low amount of DO were suffering from an oxygen deficiency disease called asphyxiation. Lack of swim bladders in adult fishes and reduced feeding capacity led to the increased rate of mortality [3].

Vivid shade options, ease of synthesis, and various modes of application made synthetic dyes very popular worldwide. Around 70% of the produced synthetic dyes is organic azo dyes [4]. Azo the name suggests the bonding between the two nitrogen atoms in the molecule. Some of the common azo dyes are shown in Fig. 3. Azo dyes are considered highly toxic due to their carcinogenic and mutagenic capabilities. Lima et al. noted the first biomarkers for the carcinogenesis by azo dyes when they exposed the laboratory rats to the textile effluents. They observed increase in the incidence of aberrant crypts in the colon of the laboratory rats [5]. Bae and Freeman conducted a study to check the toxicity of azo dye CI Direct Blue. They noted 48-h LC<sub>50</sub> between 1.0 and 10.0 mg/L for daphnids. Any substance that is toxic toward

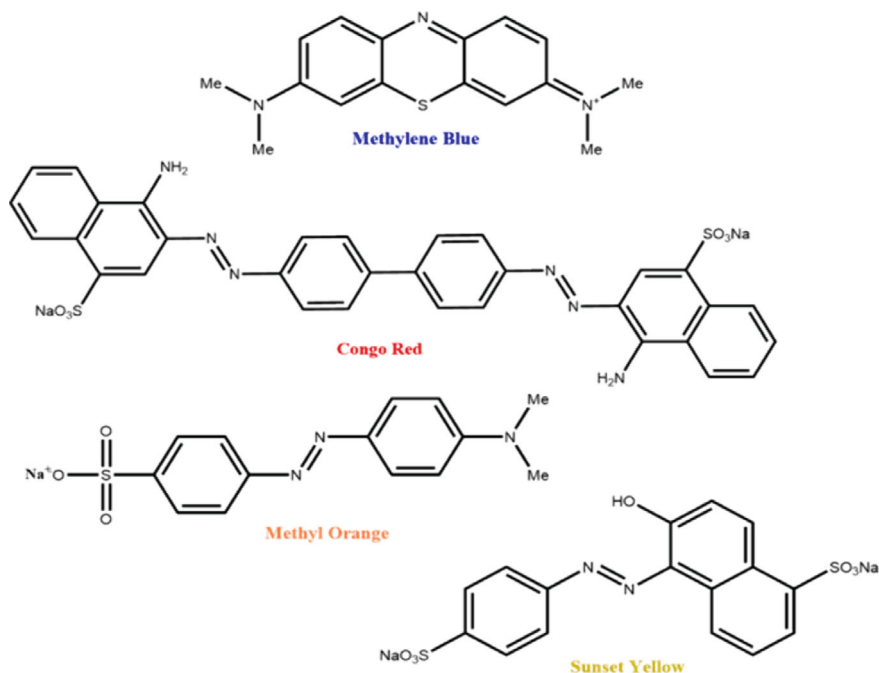


**Fig. 3** Some common azo dyes

daphnids suggest potential risk for every receptor system [6]. Tsuboy conducted a study to observe the toxic effect of CI Disperse Blue 291 azo dye. The study suggests the dose-dependent effects, DNA fragmentation, induced formation of micronuclei (MNs), and increased apoptotic index in human hepatoma cells (HepG<sub>2</sub>) [7].

The carcinogenic and mutagenic capabilities of azo dyes is relied on the nature and the position of the aromatic rings and amino groups in dye molecule. Studies on azo dye disperse Red 1 and disperse Orange 1 conducted by Chequer suggested that the frequency of micronuclei is increased in human lymphocytes and hepatoma cells in dose-dependent manner [8]. The toxicity of azo dyes is determined by the ability of dye molecules to reductively cleave to form aromatic amines under the contact of sweat, saliva, and gastric juices [9]. Thus, the reductive cleavage of azo bonds is the most important part in the activation of toxic effects of azo dyes. Some microorganism cleaves azo bonds to form nitroaniline under anaerobic conditions. Highly lipid-soluble dyes such as azo dyes containing alkylamino or acetylamino groups are biotransformed via oxidative reactions catalyzed by mono-oxygen system represented by cytochrome P-450 [10]. The oxidative metabolic process initiated by an electron transfer chain that first transfers an electron from the P-450-Fe<sup>+3</sup> complex. These complex on further reduction receives an oxygen that later on forms oxidized product in the organism. N-hydroxylation of the amino and acetylamino group takes place in the liver followed by the esterification in the presence of glucuronate or

sulfate. These formed water-soluble esters either gets excreted or it may split to form nitrenium compound ( $-\text{NH}^+$ ) that can easily bind to the nucleophilic groups of the DNA. Benzidine formed upon the reduction of some of azo dyes causes bladder cancer in humans and tumors in some animals [11].

A variety of methods have been developed over the years for removal of toxic effluents from the water such as adsorption [12], membrane filtration [13], coagulation [14], photocatalysis [15], solvent extraction [16], biological treatment [17], and chemical oxidation [18] to ensure safe and sustainable management of water. Adsorption-based materials has been widely considered due to their fast adsorption kinetics, high adsorption area, shape selectivity, cheap cost, and reusability of the materials. Adsorbents like activated carbon [19], zeolites [20], conducting polymers [21], graphene [22], MXene [23], and MOFs [24] are explored widely for the adsorption of vast variety of dyes, heavy metals, and other water pollutants.

## 1.1 Conducting Polymers

The concept of conducting polymers came into the existence in 1977, when Alan Hegger, Alan MacDiarmid, and Hideki Shirakawa examined that conductivity of polyacetylene upon oxidation with iodine increased 10-million folds. Hegger, MacDiarmid, and Shirakawa get awarded with Nobel prize in 2000 “for the discovery and development of electronically conductive polymers.” [25]. There are main two reasons that induced the interest for the study, characterization and applications of electrochemically active and conductive polymeric materials. The first reason is curiosity toward the charge transfer pathway that takes place upon redox reaction of conducting polymers. The second reason is wide field of applications of these polymeric materials such as erosion protection, energy storage, photoelectrochemistry, sensors, and adsorbents. Conducting polymers are large organic macromolecules that imitates metals by conducting electricity, but they do not possess conventional polymer properties such as strength, elasticity, or thermoplasticity. The electrical property of any material is direction depended—anisotropic [26]. Conducting polymers are non-conductive in their undoped state and act as metallic conductor upon doping. The electrical, optical, magnetic, and structural properties of these conducting polymers can be significantly enhanced by doping them with a small amount of dopant ( $\approx 10\%$ ). The process of doping is totally reversible, and during the process of doping, nature of the polymeric backbone does not change. Transformation from insulator/semi-conductor form of polymer to conductor form of polymer can be easily controlled by varying the concentration of doping materials. Properties of conducting polymers change drastically upon doping as dopant material alters the number of electrons associated to the polymeric backbone.

The electrical conductivity of any material is the measure of the energy required to promote an electron from the ground state highest occupied molecular orbital (HOMO) to excited state lowest unoccupied molecular orbital (LUMO). The energy

required is called bandgap that is measured in electron volt (eV). Conventional polymers have either completely filled or empty energy bands, and so they have a wide bandgap. Doping alters the number of electrons in the polymeric backbone that leads to the formation of new soliton, polaron, and bipolaron bands in between the HOMO and LUMO. Formation of soliton, polaron, and bipolaron bands is visualized in Fig. 4. The number of solitons, polarons, and bipolarons formed in a doped material is directly proportional to the amount of dopant molecules. New bands with overlapped valance and conduction bands are formed at a high level of doping as the localized soliton, polarons, and bipolarons start to overlap near the dopant ions. These provide enhanced electric conductivity within the conducting polymer [27, 28].

Ease of synthesis, cost effectiveness, environmental stability, and post-synthesis modification drew a lot of attention toward polyaniline (PANI) and its composite materials. PANI is a polymer of aniline monomers which upon doping exhibits good electrical conductivity. PANI has a positively charged backbone that is suitable for the adsorption of wide range of molecules, and it can also be modified for the adsorption of heavy metals from the water. Various polyaniline-based composites has been registered over the years for the adsorption of dye molecules, heavy metals, and other toxic effluents from water such as PANI/PPy/HMS composite for Cd(II) [30], PANI/PPy copolymer for Co(II) [31], PANI/Sb<sub>2</sub>O<sub>3</sub> composite for Pb(II) [32], and PANI/rGO for Hg(II) [33].

Conducting polymers has been emerged as a prominent adsorbent for the adsorption of organic dye molecules from the wastewater due to their high adsorption

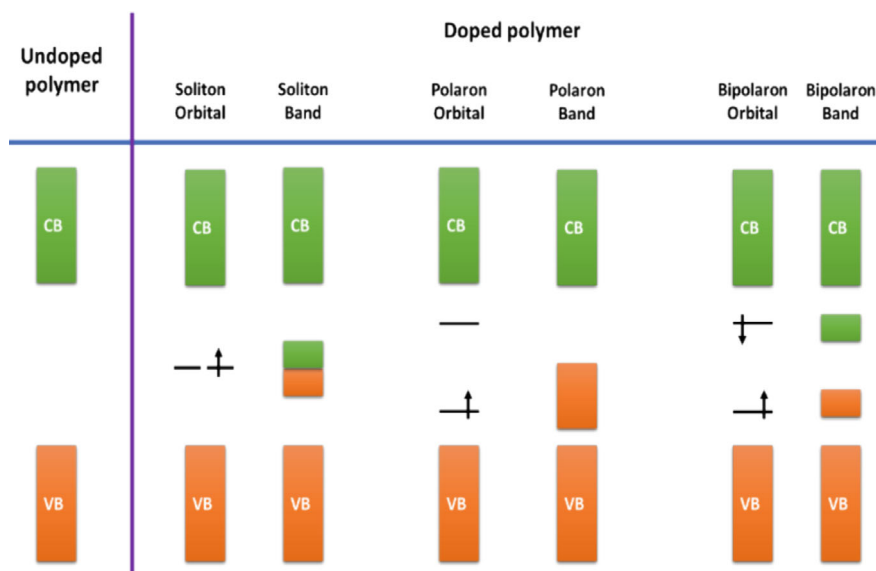
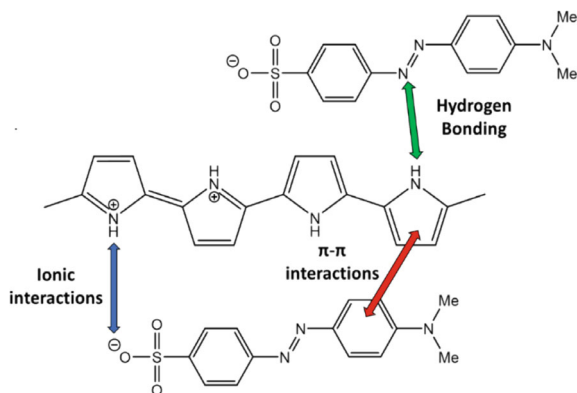


Fig. 4 Formation of soliton, polaron, and bipolaron bands in conducting polymers [29]

**Fig. 5** Various molecular interaction that leads to the adsorption of methyl orange (MO) dye on conducting polymer polypyrrole [34]



capacity and fast adsorption kinetics. There are several molecular interactions that lead to the adsorption of foreign molecule on the conducting polymers. Various kind of molecular interactions are illustrated in Fig. 5. The first interaction is the  $\pi$ - $\pi$  interaction of  $\pi$ -electron clouds on aromatic rings of dyes molecules and polymer backbone. These sharing of electrons between the  $\pi$ -electron clouds is also favorable from the energy point of view. The second type of interaction is the ionic interaction that takes place between polycation conducting polymer and anionic groups of the dye molecules or vice-versa.

The third type of interaction is hydrogen bonding between the hydrogen atoms of nitrogen on conducting polymer with the nitrogen or oxygen group present on the dye molecules. The insolubility of conducting polymer in aqueous medium is the result of intermolecular hydrogen bonding between the amino  $-\text{NH}-$  and imine  $-\text{N}=\text{N}-$  nitrogen atoms [35]. The other kind of interaction is hydrophobic interaction as conducting polymers imitate surfactant that has a hydrophilic and a hydrophobic part. The hydrophobic part of the dye molecules is stiff and favors the formation of self-assembled aggregates. Other weak interactions such as dipole-dipole interactions, dispersion force, and weak interactions like van der Waals also promote the adsorption of dye molecule on the conducting polymer.

Various composites of polyaniline such as PANI/ZnO for methylene blue and malachite green [36], PANI/SrTiO<sub>3</sub> for methylene blue [37], MnFe<sub>2</sub>O<sub>4</sub>/PANI for rhodamine B [38], ZnO/rGO/PANI for methyl orange [39], and PANI/TiO<sub>2</sub> for reactive red-45 [40] has been studied for the photocatalytic degradation of dyes. The photocatalytic degradation process of dye molecules is illustrated in Fig. 7. This photocatalytic degradation proceeds via several phases. The first phase is the adsorption phase in which various molecular interactions leads to the adsorption of dye molecules on the surface of the conducting polymer. The second phase is the photo-oxidation phase in which the conducting polymer is irradiated with UV-Vis light that promotes an electron ( $e^-$ ) from the valance band (HOMO) to conduction band (LUMO) and leaves a hole ( $h^+$ ) behind on HOMO. These photogenerated charge

carriers are highly reactive and tend to react with surrounding oxygen and water molecules.

The third phase is the ionization of water and oxygen ionsorption in which the photogenerated holes ( $h^+$ ) reacts with the surrounding water and form hydroxyl radicals ( $\cdot OH$ ). These hydroxyl radicals are very strong oxidizing agents that react with the adsorbed dye molecules and mineralize them depending on their structure and stability. At the same time, photogenerated electrons ( $e^-$ ) react with surrounding oxygen and form superoxide radicals ( $\cdot O_2^-$ ). This superoxide gets protonated to form hydroperoxyl ( $\cdot O_2H$ ) that gets further converted into hydrogen peroxide ( $H_2O_2$ ) that cleaves to form more hydroxyl radicals ( $\cdot OH$ ). The main factor restricting the photocatalytic activity of any photocatalyst is the recombination of hole-electron pair. This recombination of electron-hole can be drastically reduced by making composite materials of photocatalyst. The photoluminescence (PL) spectra of  $TiO_2$ ,  $TiO_2/0.5Pd$  and  $TiO_2/0.5Pd/0.6PPy$  suggested lowest PL intensity for the  $TiO_2/0.5Pd/0.6PPy$  [42]. This indicates a better inhibition of electron-hole pair recombination and better photocatalytic activity for the ternary photocatalyst. The synergetic effects of the various constituents of composite material enhance the photocatalytic activity of the photocatalyst. The main problem with the conducting-polymer-based photocatalyst is the separation of catalyst from water after its application part. One way to recover the catalyst from water is the process of sedimentation and filtration which is time consuming and expensive. The separation of photocatalyst from water can also be achieved with the help of external magnetic force in the case of magnetic materials. Iron-oxide-based magnetic nanoparticles such as magnetite ( $Fe_3O_4$ ), maghemite ( $\gamma-Fe_2O_3$ ), and hematite ( $\alpha-Fe_2O_3$ ) have been widely explored for their various applications. The presence of iron oxide magnetic nanoparticles (MNPs) ensures the easy separation of photocatalyst from water after the application part.

The present study is focused on the removal of methylene blue (MB) dye using PANI/ $Fe_3O_4$  nanocomposite.  $Fe_3O_4$  magnetic nanoparticles were synthesized via co-precipitation method while PANI conducting polymer was synthesized via oxidative polymerization method. Figure 8 shows the synthetic approach for composite material of PANI/ $Fe_3O_4$ . The composite material was prepared via in-situ oxidative polymerization process at a weight ratio of 1:0.25 for PANI to  $Fe_3O_4$ .

The introduction of iron oxide to PANI not only ensures the easy recovery of the photocatalyst from the water but also enhances the photocatalytic activity of PANI conducting polymer by separating the charge carriers and thus restricting the recombination of electron-hole pairs. Figure 6 depicts the charge transfer mechanism that takes place between polyaniline and magnetite in a composite system. The photocatalytic activity of catalyst on degradation of methylene blue dye has been studied under the influence of visible light. Facile synthesis, cost effectiveness, ease of recovery, and high photocatalytic activity make this PANI/ $Fe_3O_4$  nanocomposite a potential photocatalyst for the removal of azo dye methylene blue.

**Fig. 6** Charge transfer mechanism of composite photocatalyst

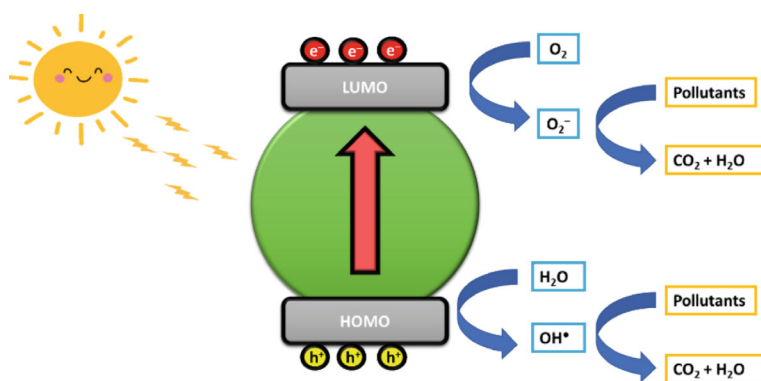
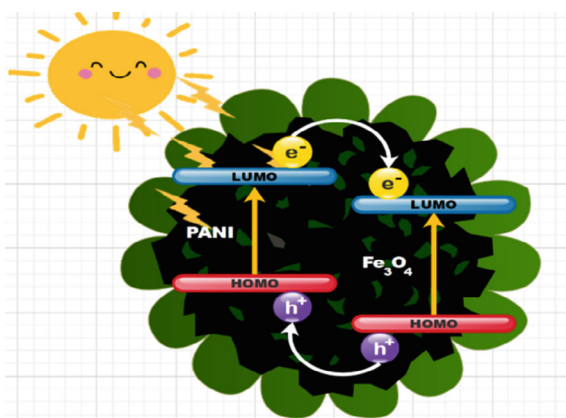


**Fig. 7** Process of photocatalytic degradation [41]

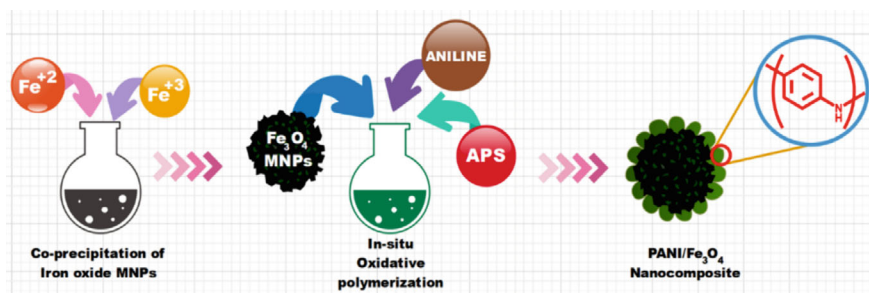


**Fig. 8** Synthesis approach to PANI/Fe<sub>3</sub>O<sub>4</sub> nanocomposite

## 2 Experimental Section

### 2.1 Chemicals

Distilled aniline (Sigma-Aldrich), ammonium peroxydisulfate (Sigma-Aldrich), iron (III) chloride hexahydrate (reagent grade > 98%, chunks, Sigma-Aldrich), iron (II) chloride tetrahydrate (reagent plus 98%, Sigma-Aldrich), ammonia solution 0.91 d (extra pure, Finar), hydrochloric acid solution.

### 2.2 Synthesis of Polyaniline Conducting Polymer

Polyaniline is generally present in three forms named emeraldine, leucoemeraldine, and pernigraniline. The leucoemeraldine and pernigraniline are fully reduced and fully oxidized forms of polyaniline, respectively. Emeraldine form has partially oxidized and partially reduced structure. Electric conductivity is implemented in these non-conductive polymers by protonation process. Non-conducting and unprotonated form of conducting polymer is referred as emeraldin base that can be converted to protonated conducting form called emeraldin salt which is half oxidized and fully protonated form. Polyaniline emeraldin salt was synthesized via oxidative polymerization method using ammonium peroxydisulfate (APS) as an oxidant. There are several other oxidants that can be used for oxidative polymerization of aniline like  $\text{FeCl}_3$ ,  $\text{H}_2\text{O}_2$ ,  $\text{K}_2\text{Cr}_2\text{O}_7$ , and  $\text{KIO}_3$ . However, studies suggest that polyaniline prepared using APS oxidant exhibits the highest conductivity. The polymerization process is more dependent on the degradation process and less dependent on the oxidative potential of the particular oxidant [43]. Generally, the ratio of aniline to APS used for oxidative polymerization is around 1:1.2 as each of the  $\text{S}_2\text{O}_8^{2-}$  ion is a  $2e^-$  acceptor (oxidizer) which means two electrons are removed from each aniline monomer during polymerization. In this method, first 1 gm of aniline was dispersed in 1N hydrochloric acid. The nature and concentration of dopant acid has a great influence on the physiochemical properties and molecular weight of resulting emeraldin salt product. Acidic medium ( $\text{pH} \leq 3$ ) helps in the solubilization of aniline in water and restricts the formation of undesired side branches. The reaction mixture allowed to stir at 500 rpm in ice bath until 0–4 °C reaction temperature was obtained. Acidic solution of APS was added to the aniline at this point and the reaction mixture allowed to stir at 0–4 °C for 2 h. Low temperature is preferred for this reaction to obtain relatively high molecular weight polymers with less defects. Defects in polymers are due to the undesirable branching caused by ortho-coupling of polyaniline rings rather than normal para-coupling [44, 45]. MacDiarmid suggested that the oxidative polymerization of aniline around 1–5 °C yields PANI polymers with molecular weights of 30,000–60,000 gm/mol [46]. Polyaniline of low polydispersity ( $\text{PD} < 2.0$ ) and high molecular weight ( $M_w > 100,000$ ) are desired for the industrial application which can be synthesized at temperatures below – 30 °C. After 2 h, the

synthesized particles were collected via vacuum filtration and washed with distilled water until the filtrate turns colorless. After that the particles were washed with 0.5 N hydrochloric acid several times and obtained green polyaniline emeraldine salt was oven dried at 80 °C overnight.

### 2.3 Synthesis of Magnetite ( $Fe_3O_4$ ) MNPs

$Fe_3O_4$  MNPs were synthesized via co-precipitation of  $Fe^{+2}$  and  $Fe^{+3}$  ions in the presence of base. Magnetite  $Fe_3O_4$  has cubic inverse spinel crystal structure consisting of  $Fe^{+3}$  and  $Fe^{+2}$  ions.  $Fe^{+2}$  ions occupy 25% of interstitial octahedral sites, and  $Fe^{+3}$  ions occupy 25% of octahedral sites and 12.5% tetrahedral sites. Magnetic moments of  $Fe^{+2}$  and  $Fe^{+3}$  ions present in octahedral voids are ferromagnetically coupled, but magnetic dipoles of  $Fe^{+3}$  present in octahedral voids and  $Fe^{+3}$  present in tetrahedral void are opposite to each other and thus magnetite is ferrimagnetic in nature with low coercivity ( $H_C$ ) and high saturation ( $M_S$ ) of magnetization [47, 48]. The general elemental formula of magnetite is  $(Fe^{+2}_{octahedral})(Fe^{+3}_{octahedral})(Fe^{+3}_{tetrahedral})O_4$ . Generally preferred molar ratio of  $Fe^{+2}$ – $Fe^{+3}$  is 1:2 in nitrogen inert atmosphere as it prevents the oxidation of  $Fe^{+2}$  ions to  $Fe^{+3}$  ions. However,  $Fe^{+2}$ – $Fe^{+3}$  ratio has a great influence on the final product when the reaction is performed in oxidizing atmosphere. In the presence of oxygen,  $Fe^{+2}$  ions are oxidized to  $Fe^{+3}$  resulting in the formation of maghemite ( $\gamma$ - $Fe_2O_3$ ). The presence of maghemite phase decreases the saturation magnetization of main magnetite phase. To form a pure magnetic phase of magnetite and to compensate the oxidation of  $Fe^{+2}$ , an excessive amount of  $Fe^{+2}$  is used for the synthesis [49]. In this method, first we dissolved  $Fe^{+2}$  and  $Fe^{+3}$  ions in distilled water at 1:1.75 molar ratio. The reaction vessel was purged with nitrogen to provide an inert atmosphere. First, the reaction mixture was stirred at 80 °C and 300 rpm for an hour. After an hour, ammonia solution was added to the reaction mixture until the pH reaches to 10, and the reaction mixture was allowed to stir at 300 rpm for another hour at 80 °C under nitrogen inert atmosphere. Studies suggest that the average particle size of synthesized  $Fe_3O_4$  nanoparticles increased and bandgap energy decreased with increasing reaction temperature [50]. After the reaction, the synthesized MNPs were collected via centrifugation of reaction mixture at 4000 rpm for 5 min. Collected particles were washed with distilled water several times. Obtained magnetite  $Fe_3O_4$  MNPs were oven dried at 80 °C overnight.

### 2.4 Synthesis of PANI/ $Fe_3O_4$ Composite

Composite material of polyaniline and magnetite was synthesized via in-situ oxidative polymerization method suggested by MacDiarmid and Epstein [27]. In this method, first, the MNPs were dispersed into 1 N hydrochloric acid and then distilled aniline was added to the solution. The reaction mixture was allowed to stir in ice

bath until 0–4 °C temperature was obtained. Acidic solution of APS was added to the reaction mixture, and the mixture was stirred at 0–4 °C for 2 h. After the reaction, the synthesized particles were washed via distilled water and then with 0.5 N hydrochloric acid. Prepared PANI/Fe<sub>3</sub>O<sub>4</sub> composite was oven dried at 80 °C overnight.

## 2.5 Dark Adsorption and Photocatalytic Studies

Dark adsorption and photocatalytic studies of the synthesized materials had been conducted using 450-W high pressure mercury vapor visible light lamp in photocatalytic reactor. Freshly prepared 10 ppm solution of MB dye had been filled into the reactor vessel, and synthesized photocatalyst was dispersed into the reactor vessel at a loading ratio of 0.3 mg/ml. Dye solution was continuously stirred into the dark environment, and samples of solution were collected at every 15 min. The visible lamp was turned on as soon as the adsorption equilibrium was achieved, and samples of dye solution were collected at specific time interval. All collected dye samples were examined via UV-Vis spectrophotometer, and a graph of wavelength vs. absorbance was plotted to evaluate the percentage removal of dye.

## 3 Results and Discussion

### 3.1 FT-IR Spectroscopy

Infrared spectrogram of all three material is depicted in Fig. 9. The characteristic peaks of 1567 cm<sup>-1</sup> is attributed to the C–C stretching of benzenoid and 1491 cm<sup>-1</sup> is attributed to the C–C stretching of quinoid form of chains in PANI backbone. The peak at 1289 cm<sup>-1</sup> is due to the C–N and C=N stretching, whereas the peaks of 1139 cm<sup>-1</sup> and 796 cm<sup>-1</sup> are the result of in-plane and out of plane C–H bending, respectively.

Magnetite has a single sharp peak at 540 cm<sup>-1</sup> which can be attributed to the Fe–O bonds present in the matrix. A broad peak at 3450 cm<sup>-1</sup> suggests the formation of Fe–OH bonds on the surface of magnetite MNPs. FT-IR spectrum of composite material consists all the peaks from PANI and Fe<sub>3</sub>O<sub>4</sub> suggesting the formation of composite material.

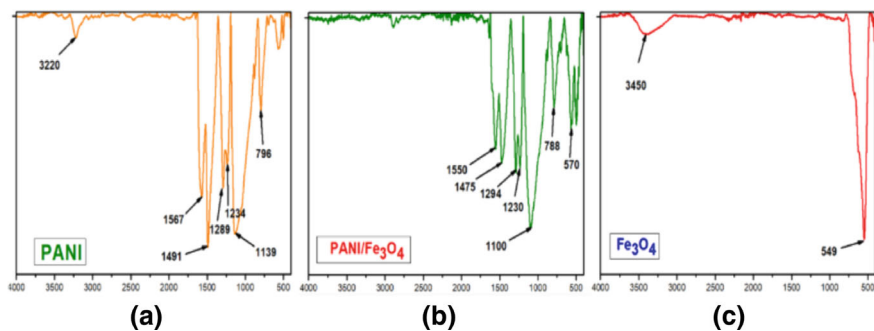


**Fig. 9** FT-IR spectrogram of **a** PANI, **b** PANI/Fe<sub>3</sub>O<sub>4</sub>, **c** Fe<sub>3</sub>O<sub>4</sub>

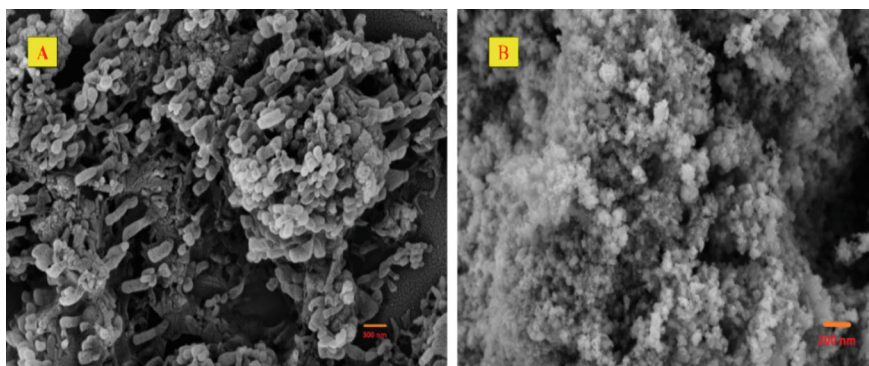


**Fig. 10** FE-SEM images of **a** PANI, **b** Fe<sub>3</sub>O<sub>4</sub>

### 3.2 FE-SEM Analysis

FE-SEM imaging of the samples was performed using Ultra-55 Zeiss OXFORD-INCA to evaluate the morphological and structural parameters of the synthesized materials. Results of SEM imaging are depicted in Fig. 10. The images of polyaniline suggest formation of polymer with nanotube like morphology with length ranging from 50 to 200 nm. SEM images of Fe<sub>3</sub>O<sub>4</sub> MNPs show formation of very fine magnetic nanoparticles ranging from 10 to 20 nm in diameter.

### 3.3 XRD Analysis

Figure 11 illustrates the X-ray diffractogram of all three materials. X-ray diffraction spectroscopy was performed using PANalytical XRD instrument. The X-ray diffractogram of PANI homopolymer shows characteristic peaks  $2\theta = 20.25^\circ$  and

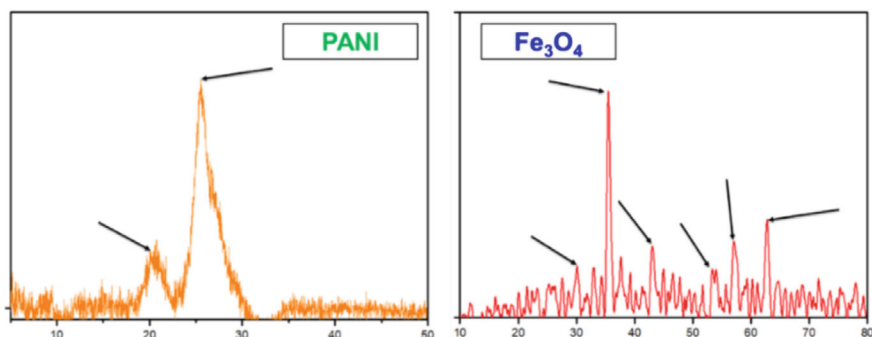


**Fig. 11** X-ray diffractogram of PANI and  $\text{Fe}_3\text{O}_4$

$25.35^\circ$  that suggest the formation of polycrystalline PANI structure [51]. The peaks at  $20.25^\circ$  and  $25.35^\circ$  is assigned to benzenoid and quinoid structures in PANI [52].

X-ray diffractogram of  $\text{Fe}_3\text{O}_4$  includes characteristic peaks at  $2\theta = 30.1^\circ, 35.5^\circ, 43^\circ, 53.95^\circ, 57^\circ,$  and  $62.77^\circ$  with the indices (2 2 0), (3 1 1), (4 0 0), (4 2 2), (5 1 1), and (4 4 0), respectively. X-ray diffractogram data suggests the formation of inverse spinel  $\text{Fe}_3\text{O}_4$  MNPs. (PCPDFWIN v2.02, PDF No. 890691) [53].

### 3.4 Dark Adsorption Studies

The removal efficiency of all the synthesized materials was evaluated using the UV-Vis adsorption spectroscopy. A graph of wavelength vs. absorbance was plotted in order to observe the change in dye concentration over time. UV-Vis spectrograms of polyaniline and polyaniline/magnetite composite which is depicted in Fig. 12a, b. The UV-Vis spectrogram of polyaniline suggested a very low amount of MB dye adsorption, whereas a small increase in the adsorption of MB was noted in the case of composite material of PANI and  $\text{Fe}_3\text{O}_4$  due to the increased surface area.

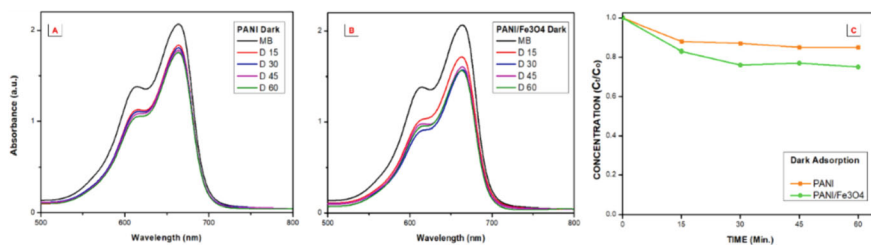


**Fig. 12** Dark adsorption UV-Vis spectrogram of **a** PANI, **b** PANI/ $\text{Fe}_3\text{O}_4$ , **c** adsorption rate of PANI and PANI/ $\text{Fe}_3\text{O}_4$

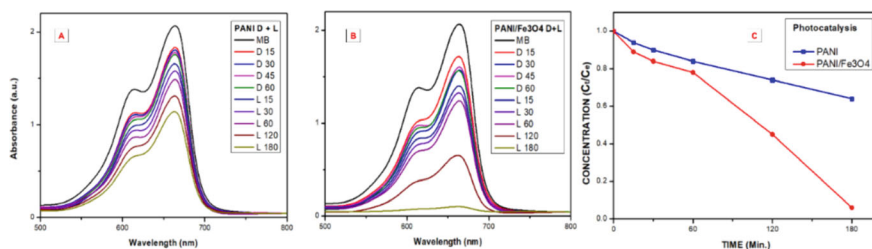


**Fig. 13** Photocatalytic UV-Vis spectrogram of **a** PANI, **b** PANI/Fe<sub>3</sub>O<sub>4</sub>, **c** photocatalytic degradation rate

Figure 12c is the plot of time vs. concentration ( $C_0$  = Initial concentration and  $C_t$  = Concentration at particular time interval) for PANI and PANI/Fe<sub>3</sub>O<sub>4</sub>; there was no significant change in adsorption observed after an hour suggesting that the adsorption equilibrium was achieved. The low adsorption of MB dye is due to the repulsion between cationic methylene blue dye and polycation polyaniline polymer. Adsorption equilibrium was achieved under 60 min for both of the materials. The adsorption percentage were 15% and 24% for PANI and PANI/Fe<sub>3</sub>O<sub>4</sub> composite, respectively.

### 3.5 Photocatalytic Studies

The UV-Vis spectrogram of PANI and PANI/Fe<sub>3</sub>O<sub>4</sub> is illustrated in Fig. 13a, b, respectively. The UV-Vis spectrogram of PANI suggested 45% removal of MB dye under 3 h of visible light exposure. The low removal efficiency of PANI is due to the recombination of the electron–hole pairs that reduce the efficiency of photocatalyst.

The composite material PANI/Fe<sub>3</sub>O<sub>4</sub> exhibits excellent photocatalytic activity as predicted. The increased photocatalytic activity of composite material by the synergetic effects of parent materials was evident of the charge transfer mechanism taking place between PANI and Fe<sub>3</sub>O<sub>4</sub>. Figure 13c depicts the plot of time versus concentration ( $C_e$  = Concentration at adsorption equilibrium and  $C_t$  = Concentration at specific time interval) for PANI and PANI/Fe<sub>3</sub>O<sub>4</sub> that throws light on the charge transfer mechanism that takes place in composite material where photogenerated charges are transferred from one material to another. A rapid change in degradation rate after an hour intimate that the process of charge separation requires time. The photocatalyst was recovered from the water with the help of external magnetic force. A 95% removal of MB dye was observed for PANI/Fe<sub>3</sub>O<sub>4</sub> composite after 3 h of photocatalytic treatment.

## 4 Conclusion

PANI conducting polymer and PANI/Fe<sub>3</sub>O<sub>4</sub> composite have been synthesized as mentioned above, and their adsorption capacities have been evaluated using MB dye as a reference. Increased adsorption capacity for composite material is due to the increased surface area of the composite material. Both materials obtain adsorption equilibrium within 60 min at constant stirring of solution. Amount of methylene blue MB dye adsorbed by PANI and PANI/Fe<sub>3</sub>O<sub>4</sub> is 15% and 24%, respectively. This poor adsorption is attributed to cationic-cationic repulsions between the PANI polycation polymer and cationic MB dye that restricts the adsorption of dye molecules on polymer. PANI/Fe<sub>3</sub>O<sub>4</sub> composite have larger surface area than bare PANI because during the in-situ polymerization process, Fe<sub>3</sub>O<sub>4</sub> magnetic nanoparticles tend to agglomerate in the solution and the formation of polymer takes place on these agglomerated particles. Photocatalytic studies have been conducted to find the dye removal efficiency of synthesized materials under visible light source. PANI and PANI/Fe<sub>3</sub>O<sub>4</sub> have removed 45% and 95% MB dye, respectively. Graphs obtained from the photocatalytic studies of PANI show a linear curve suggesting that no significant change in the rate of degradation over the period of time. Low removal efficiency of PANI suggests that the electron-hole pair recombination suppresses the photocatalytic activity of bare conducting polymer PANI. On the other hand, the graph obtained from the photocatalytic studies of PANI/Fe<sub>3</sub>O<sub>4</sub> shows a nonlinear curve over the first 60-min time period. The nonlinear slope changes into a high gradient slope after the first 60-min as the rate of degradation rapidly increases. This rapid increase in the rate of degradation of dye is due to the charge transfer mechanism that takes place between the PANI and Fe<sub>3</sub>O<sub>4</sub> molecules present inside the composite material. The transfer of photogenerated charges inhibits the recombination of electron-hole pairs and therefore increases the photocatalytic activity of conducting polymer. Rapid degradation takes place after first 60-min suggesting that the separation of charge is a time-consuming process.

## References

1. Moussavi G, Mahmoudi M (2009) Removal of azo and anthraquinone reactive dyes from industrial wastewaters using MgO nanoparticles. *J Hazard Mater* 168(2–3):806–812
2. Textile dyes market by type, size, share and global forecast—2030 (2023). Available from <https://www.marketresearchfuture.com/reports/textile-dyes-market-3111>
3. Sharma P, Gupta S (2014) Study of amount of oxygen (BOD, OD, COD) in water and their effect on fishes. *Am Int J Res Formal Appl Nat Sci* 7(1):53–58
4. Cotillas S et al (2018) Removal of Procion red MX-5B dye from wastewater by conductive-diamond electrochemical oxidation. *Electrochim Acta* 263:1–7
5. de Lima ROA et al (2007) Mutagenic and carcinogenic potential of a textile azo dye processing plant effluent that impacts a drinking water source. *Mutation Res/Genetic Toxicol Environ Mutagenesis* 626(1–2):53–60
6. Bae J-S, Freeman HS (2007) Aquatic toxicity evaluation of new direct dyes to the *Daphnia magna*. *Dyes Pigment* 73(1):81–85

7. Tsuboy M et al (2007) Genotoxic, mutagenic and cytotoxic effects of the commercial dye CI disperse blue 291 in the human hepatic cell line HepG2. *Toxicol Vitro* 21(8):1650–1655
8. Chequer FMD et al (2009) The azo dyes disperse red 1 and disperse orange 1 increase the micronuclei frequencies in human lymphocytes and in HepG2 cells. *Mutation Res/Genetic Toxicol Environ Mutagenesis* 676(1–2):83–86
9. Pielesz A et al (2002) Detection and determination of aromatic amines as products of reductive splitting from selected azo dyes. *Ecotoxicol Environ Saf* 53(1):42–47
10. Hunger K (1994) On the toxicology and metabolism of azo dyes. *Chimia* 48(11):520–520
11. Combes R, Haveland-Smith R (1982) A review of the genotoxicity of food, drug and cosmetic colours and other azo, triphenylmethane and xanthene dyes. *Mutation Res/Rev Genetic Toxicol* 98(2):101–243
12. Burakov AE et al (2018) Adsorption of heavy metals on conventional and nanostructured materials for wastewater treatment purposes: a review. *Ecotoxicol Environ Saf* 148:702–712
13. Hube S et al (2020) Direct membrane filtration for wastewater treatment and resource recovery: a review. *Sci Total Environ* 710:136375
14. Teh CY et al (2016) Recent advancement of coagulation-flocculation and its application in wastewater treatment. *Ind Eng Chem Res* 55(16):4363–4389
15. Shahabuddin S et al (2015) Synthesis of chitosan grafted-polyaniline/ $\text{Co}_3\text{O}_4$  nanocube nanocomposites and their photocatalytic activity toward methylene blue dye degradation. *RSC Adv* 5(102):83857–83867
16. Chang SH (2020) Utilization of green organic solvents in solvent extraction and liquid membrane for sustainable wastewater treatment and resource recovery—a review. *Environ Sci Pollut Res* 27(26):32371–32388
17. Grandclément C et al (2017) From the conventional biological wastewater treatment to hybrid processes, the evaluation of organic micropollutant removal: a review. *Water Res* 111:297–317
18. Miklos DB et al (2018) Evaluation of advanced oxidation processes for water and wastewater treatment—a critical review. *Water Res* 139:118–131
19. Mariana M et al (2021) Recent advances in activated carbon modification techniques for enhanced heavy metal adsorption. *J Water Process Eng* 43:102221
20. Sodha V et al (2022) Comprehensive review on zeolite-based nanocomposites for treatment of effluents from wastewater. *Nanomaterials* 12(18):3199
21. Syed S (2016) Polyaniline based nanocomposites as adsorbents and photocatalysts in the removal of organic dyes. University of Malaya
22. Xu L, Wang J (2017) The application of graphene-based materials for the removal of heavy metals and radionuclides from water and wastewater. *Crit Rev Environ Sci Technol* 47(12):1042–1105
23. Assad H et al (2022) An overview of MXene-Based nanomaterials and their potential applications towards hazardous pollutant adsorption. *Chemosphere*: 134221
24. Rani L et al (2020) A critical review on recent developments in MOF adsorbents for the elimination of toxic heavy metals from aqueous solutions. *Environ Sci Pollut Res* 27:44771–44796
25. Shirakawa H et al (1977) Synthesis of electrically conducting organic polymers: halogen derivatives of polyacetylene,  $(\text{CH})_x$ . *J Chem Soc Chem Commun* 16:578–580
26. McGehee MD, Heeger AJ (2000) Semiconducting (conjugated) polymers as materials for solid state lasers. *Adv Mater* 12(22):1655–1668
27. MacDiarmid AG, Epstein AJ (1989) Polyanilines: a novel class of conducting polymers. *Faraday Discuss Chem Soc* 88:317–332
28. Bredas JL, Street GB (1985) Polarons, bipolarons, and solitons in conducting polymers. *Acc Chem Res* 18(10):309–315
29. Le T-H, Kim Y, Yoon H (2017) Electrical and electrochemical properties of conducting polymers. *Polymers* 9(4):150
30. Javadian H, Sorkhrodi FZ, Koutenaei BB (2014) Experimental investigation on enhancing aqueous cadmium removal via nanostructure composite of modified hexagonal type mesoporous silica with polyaniline/polypyrrole nanoparticles. *J Ind Eng Chem* 20(5):3678–3688

31. Javadian H (2014) Application of kinetic, isotherm and thermodynamic models for the adsorption of Co (II) ions on polyaniline/polypyrrole copolymer nanofibers from aqueous solution. *J Ind Eng Chem* 20(6):4233–4241
32. Khalili R (2014) Preparation and characterization of polyaniline/sb2o3 nanocomposite and its application to removal of pb ( ) from aqueous media. *Int J Eng* 27(2):239–246
33. Li R, Liu L, Yang F (2013) Preparation of polyaniline/reduced graphene oxide nanocomposite and its application in adsorption of aqueous Hg (II). *Chem Eng J* 229:460–468
34. Stejskal J (2020) Interaction of conducting polymers, polyaniline and polypyrrole, with organic dyes: polymer morphology control, dye adsorption and photocatalytic decomposition. *Chem Pap* 74(1):1–54
35. Trchová M, Stejskal J (2011) Polyaniline: the infrared spectroscopy of conducting polymer nanotubes (IUPAC technical report). *Pure Appl Chem* 83(10):1803–1817
36. Eskizeybek V et al (2012) Preparation of the new polyaniline/ZnO nanocomposite and its photocatalytic activity for degradation of methylene blue and malachite green dyes under UV and natural sun lights irradiations. *Appl Catal B* 119:197–206
37. Shahabuddin S et al (2016) SrTiO<sub>3</sub> nanocube-doped polyaniline nanocomposites with enhanced photocatalytic degradation of methylene blue under visible light. *Polymers* 8(2):27
38. Zeng S et al (2016) Magnetically recyclable MnFe<sub>2</sub>O<sub>4</sub>/polyaniline composite with enhanced visible light photocatalytic activity for rhodamine B degradation. *J Ceram Soc Jpn* 124(10):1152–1156
39. Wu H et al (2016) A new ZnO/rGO/polyaniline ternary nanocomposite as photocatalyst with improved photocatalytic activity. *Mater Res Bull* 83:434–441
40. Gilja V et al (2017) Stability and synergistic effect of polyaniline/TiO<sub>2</sub> photocatalysts in degradation of azo dye in wastewater. *Nanomaterials* 7(12):412
41. Namsheer K, Rout CS (2021) Conducting polymers: a comprehensive review on recent advances in synthesis, properties and applications. *RSC Adv* 11(10):5659–5697
42. Li X et al (2017) Precisely locate Pd-polypyrrole on TiO<sub>2</sub> for enhanced hydrogen production. *Int J Hydrogen Energy* 42(40):25195–25202
43. Pron A et al (1988) The effect of the oxidation conditions on the chemical polymerization of polyaniline. *Synth Met* 24(3):193–201
44. Adams P, Apperley D, Monkman A (1993) A comparison of the molecular weights of polyaniline samples obtained from gel permeation chromatography and solid state <sup>15</sup>N nmr spectroscopy. *Polymer* 34(2):328–332
45. Kenwright A et al (1992) Solution-state carbon-13 nuclear magnetic resonance studies of polyaniline. *Polymer* 33(20):4292–4298
46. MacDiarmid A et al (1987) Polyaniline: synthesis and characterization of the emeraldine oxidation state by elemental analysis. In: *Conducting polymers: special applications proceedings of the workshop held at Sintra, Portugal, 28–31 July 1986*. Springer
47. Klotz S et al (2008) Magnetism and the Verwey transition in Fe<sub>3</sub>O<sub>4</sub> under pressure. *Phys Rev B* 77(1):012411
48. Cornell RM, Schwertmann U (2003) *The iron oxides: structure, properties, reactions, occurrences, and uses*, vol 664. Wiley-VCH Weinheim
49. Jiang W et al (2011) The effect of [Fe<sup>3+</sup>]/[Fe<sup>2+</sup>] molar ratio and iron salts concentration on the properties of superparamagnetic iron oxide nanoparticles in the water/ethanol/toluene system. *J Nanopart Res* 13:5135–5145
50. Saragi T et al (2018) The impact of synthesis temperature on magnetite nanoparticles size synthesized by co-precipitation method. *J Phys Conf Ser*
51. Rahy A, Yang DJ (2008) Synthesis of highly conductive polyaniline nanofibers. *Mater Lett* 62(28):4311–4314
52. Shi L et al (2009) Preparation of TiO<sub>2</sub>/polyaniline nanocomposite from a lyotropic liquid crystalline solution. *Synth Met* 159(23–24):2525–2529
53. Shagholani H, Ghoreishi SM, Mousazadeh M (2015) Improvement of interaction between PVA and chitosan via magnetite nanoparticles for drug delivery application. *Int J Biol Macromole* 78

# Potential Impacts of Landfill Leachate on the Quality of Groundwater Bodies



Jagriti Patel, Sanskriti Mujumdar, and Vijay Kumar Srivastava

## 1 Introduction

The generation of solid waste is exhibiting a sustained upward trajectory because of population growth and increased economic activity. Over an extended period, the predominant approach to handling household solid waste commonly entailed its placement in exposed locations. These locations were ultimately abandoned without taking into account the adverse effects they had on surface water resources, groundwater, atmospheric conditions, and soil composition [1]. The most common and straightforward method of dealing with the massive volumes of garbage produced every day is to landfill it in designated areas. However, dumping waste in open landfills is one of the riskiest waste management strategies [2]. Landfills give rise to numerous significant concerns, primarily stemming from the buildup of solid waste. This accumulation results in the creation of a highly concentrated liquid known as leachate, which is expelled from the waste due to water infiltration. Consequently, leachate contaminates both nearby groundwater tables and surface water bodies. Despite the implementation of an engineered sanitary landfill with a lining system, there remains a significant likelihood of infiltration of hazardous leachate [3].

This fluid that is derived from the lower regions of solid waste treatment plants consists of soluble organic and inorganic compounds, along with suspended particles. The composition of landfill leachate can vary greatly depending on factors such as the

---

J. Patel (✉)

Department of Environmental Studies, Faculty of Science, The Maharaja Sayajirao University of Baroda, Vadodara, Gujarat 390002, India

e-mail: [jagriti.p-envphd@msubaroda.ac.in](mailto:jagriti.p-envphd@msubaroda.ac.in)

S. Mujumdar

Department of Civil Engineering, Faculty of Technology and Engineering, The Maharaja Sayajirao University of Baroda, Vadodara, Gujarat 390002, India

V. K. Srivastava

The Maharaja Sayajirao University of Baroda, Vadodara, Gujarat 390002, India

type of solid waste being buried, the chemical and biochemical processes involved in waste decomposition, and the overall moisture content of the waste. The primary constituents found in the leachate consist of dissolved organic compounds, inorganic macro-compounds, and various heavy metals including copper, lead, cadmium, chromium, and nickel, among others. Additionally, leachate contains a multitude of detrimental chemicals such as heavy metals and salts. Numerous hazardous substances were also identified in landfill leachate, including halogen-containing compounds, phenols, aromatic compounds, new emerging contaminants, and pesticides [2]. These toxic chemicals make their way toward the nearby groundwater bodies and surface water bodies and start to deteriorate it.

The major issue related to leachate pollution is the contamination of groundwater bodies. The poisoning of groundwater sources by leachate pollution is the primary concern. Groundwater, an indispensable asset for every nation, stands as one of the utmost crucial resources. The potential for groundwater contamination in the proximity of landfills is heightened due to the presence of waste leachate, which possesses the capacity to function as a deleterious agent. When groundwater becomes tainted in such a manner, it presents a grave threat to not only the well-being of mankind but also the ecological balance of our surroundings [4]. There are numerous studies that have been conducted on the topic of groundwater contamination caused by leachate leakage, and several methods have been developed to detect and mitigate the problem. In the context of sustainable water resources management, a study was conducted to assess the potential contamination and environmental consequences of leachate originating from a landfill. This study aimed to gain valuable knowledge regarding the potential environmental impacts associated with landfill leachate in the specific region. Additionally, the study offers recommendations for effectively managing and mitigating these impacts in order to promote sustainable water resources management practices [5].

Evaluation of groundwater and soil samples taken near the municipal solid waste disposal to determine the extent of pollution was done. Heavy metal concentrations, organic contaminants, and other indications of pollution were likely among the parameters evaluated. Specific toxins that have made their way into the groundwater were named, and the dangers they pose to water quality and availability were explained [6].

Numerous studies have been conducted using the water quality index to demonstrate the harmful effects of leachate on aquatic environments. To evaluate the landfill's impact on groundwater quality, this study uses both traditional water quality index (WQI) and analytical hierarchy process (AHP)-based WQI approaches [7]. Index developed specifically to measure landfills' impact on water quality called the landfill water pollution index (LWPI) [8]. This index considers a wide range of water quality indicators and their relative weight in assessing pollution. The LWPI allows scientists to quantitatively assess the level of contamination in the groundwater close to landfills.

There have been many studies employing GIS and other statistical techniques to evaluate leachate's impact on groundwater contamination. The researchers engaged in a discourse regarding the spatial arrangement of groundwater contamination in the

vicinity of the landfill site, discerning regions that exhibit heightened vulnerability to pollution. The investigation should also take into account the hydrogeological and climatic variables that impact the movement and destiny of leachate in the semi-arid area of Hamedan [9]. The study utilizes statistical methodologies to analyze and interpret the data obtained from the groundwater samples. The analysis will involve the identification of correlations, trends, and patterns among different parameters, aiding in the understanding of the hydrochemical characteristics of the groundwater [10].

In the city of Vadodara, which is located in Gujarat, India, there is a municipal solid waste dump, and the purpose of this study is to investigate its consequences. This research explores the impacts that leachate has on groundwater bodies in the surrounding area by conducting a physicochemical investigation of numerous criteria to estimate concentration, and as a result, the impact that it has on groundwater.

## 2 Study Area

Located in western India at a height of 128 ft. (39 m), the city of Vadodara is found at 22.30° N 73.19° E. Vadodara's waste is collected from all areas and dumped into the main landfill, which is the city's primary landfill. Daily M.S.W. production in Vadodara amounts to 750.00 M.T. The landfill is located near the Makarpura region of Vadodara, Gujarat (latitude: 22.234098; longitude: 73.207417). The location of the city and the landfill is shown in Fig. 1. The spatial locations of the sampling sites are documented in Table 1, along with the corresponding sampling radius. The samples collected within this radius are categorized as L for leachate samples, LG for groundwater samples obtained from within the landfill, and G for groundwater samples collected from other locations.

## 3 Materials and Methods

Fourteen samples (12 ground water + 2 leachate) were taken. Random sampling was used to gather the samples. To determine the extent to which leachate has contaminated nearby groundwater sources and to track the progression of contamination as one moves away from the landfill, samples were taken at regular intervals throughout a 3 km radius. Groundwater is typically utilized for both irrigation and drinking purposes in the city of Vadodara. Samples were examined in the laboratory using the Standard Methods for the Examination of Water and Wastewater issued by the American Public Health Association (APHA).

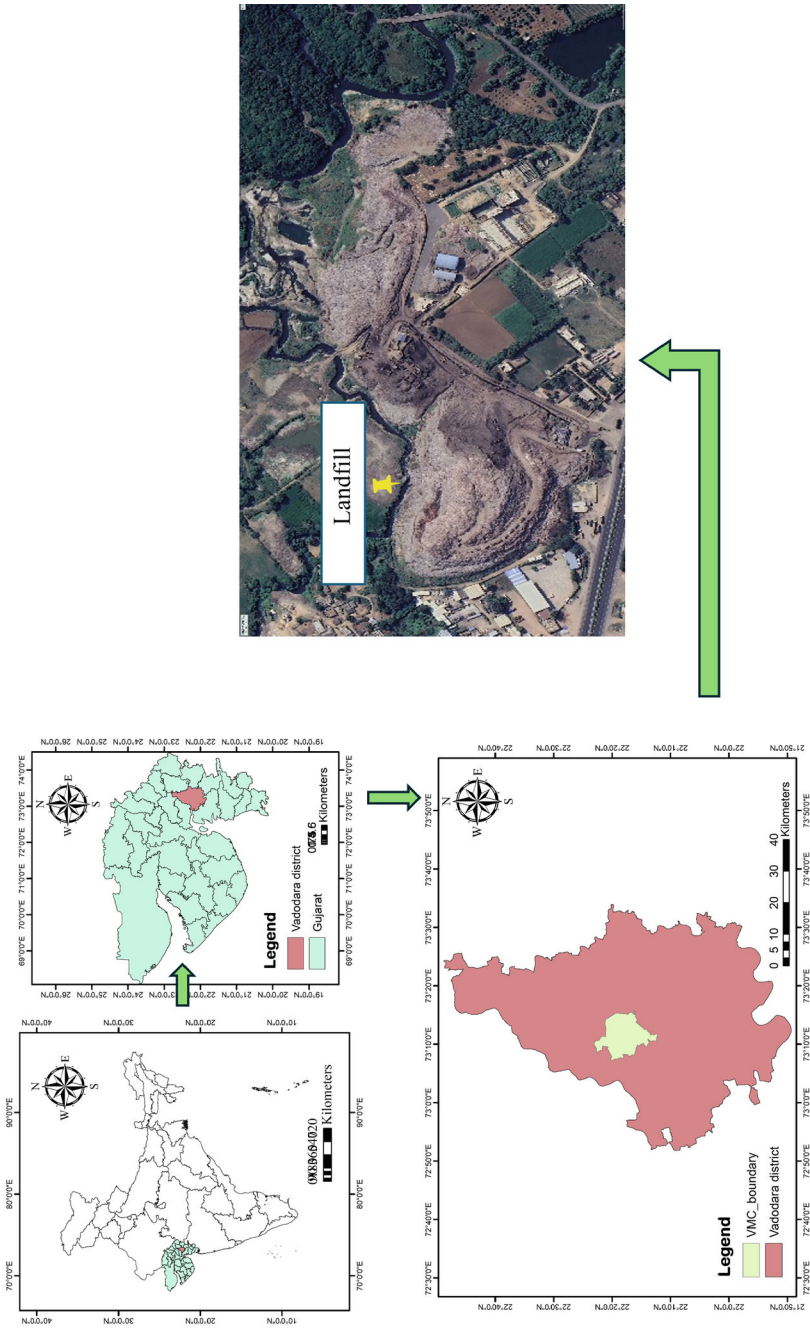


**Fig. 1** Location map of study site Iambuva landfill, Vadodra, Gujarat, India

**Table 1** Sampling coordinates

Sample	Latitude	Longitude	Radius (km)
L1	22°14'01.0" N	73°12'21.4" E	0
L2	22°14'01.7" N	22°14'01.7" N	0
LG1	22°13'59.9" N	73°12'20.5" E	1
LG2	22°13'52.3" N	73°12'21.4" E	1
G1	22°13'59.2" N	73°12'19.0" E	1
G2	22°13'51.6" N	73°12'04.0" E	1
G3	22°13'33.4" N	73°12'16.8" E	1
G4	22°13'11.4" N	22°13'11.4" N	2
G5	22°13'12.2" N	73°13'17.1" E	3
G6	22°12'50.9" N	73°13'42.7" E	3
G7	22°14'12.9" N	73°13'19.7" E	2
G8	22°14'15.7" N	73°13'00.3" E	2
G9	22°14'04.9" N	73°12'35.0" E	1
G10	22°13'30.7" N	73°11'17.3" E	3

### 3.1 Leachate Analysis

Two samples of leachate were obtained from the trenches situated beneath the waste piles exhibiting a flow pattern resembling that of a narrow stream, one from the lower part of the landfill and other from the upper part. The leachate samples were meticulously gathered and subjected to analysis for variables including temperature, pH, and electrical conductivity (EC). The samples were subsequently placed in a temperature-controlled environment of 4 °C for additional ex-situ analysis of biochemical oxygen demand (BOD), chemical oxygen demand (COD), alkalinity, total hardness, turbidity, chloride ( $\text{Cl}^-$ ), calcium (Ca), magnesium (Mg), total dissolved solids (TDS), sodium (Na), potassium (K), lithium (Li), fluoride ( $\text{F}^-$ ), ammonium ( $\text{NH}_4$ ), sulfate ( $\text{SO}_4$ ), nitrate ( $\text{NO}_3$ ), and heavy metals.

### 3.2 Groundwater Analysis

Two groundwater samples were obtained from the two boreholes situated within the landfill site. The samples from outside the landfill were collected using the grab sampling method, employing a random sampling technique. Due to the presence of numerous sources of groundwater in the vicinity of the landfill, random sampling techniques were employed. This method was chosen to ensure fair and unbiased representation of the various sources of groundwater. By using random sampling, we were able to collect a representative sample of the groundwater sources, which allowed us to obtain a more accurate understanding of the overall quality of the

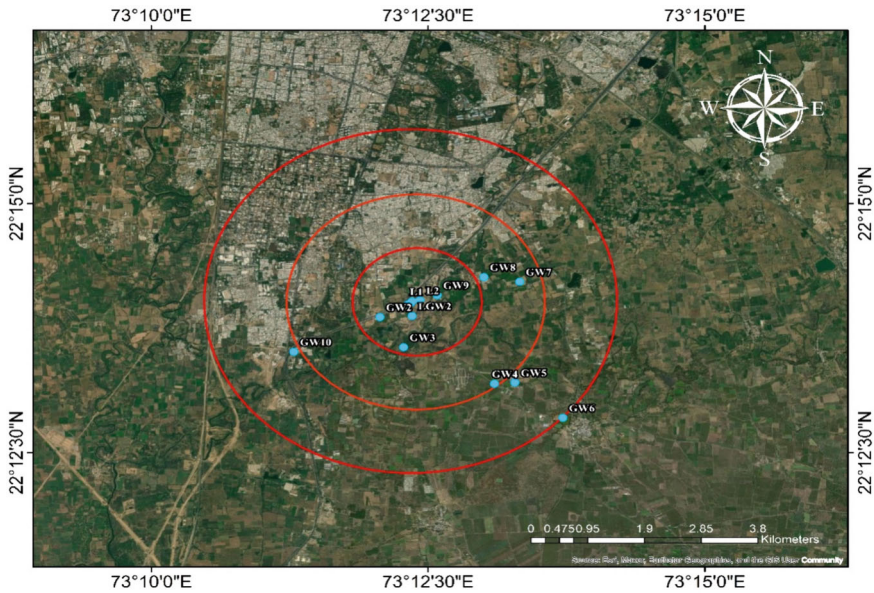


**Fig. 2** Sampling points

groundwater in the area [11]. Four samples were collected within a 1 km radius, three within a 2 km radius, and three within a 3 km radius. The samples were collected in bottles of 1 L capacity. On-site measurements of pH, temperature, and electrical conductivity (EC) were recorded, and samples were immediately transported to the laboratory and stored at 4 degrees Celsius for all other analyses, including BOD, COD, alkalinity, total hardness, turbidity,  $CL^-$ , TDS, Na, K,  $F^-$ ,  $NH_4$ ,  $SO_4$ ,  $NO_3$ , and heavy metal. The locations of the sampling sites are shown in Fig. 2.

## 4 Results and Discussion

The physicochemical properties of leachate typically exhibit variations based on the composition of the solid waste deposited and the age of the landfill [12]. The study involved a thorough examination of the physicochemical parameters. These parameters were compared against the standards set by the Bureau of Indian Standards (BIS). Additionally, any parameters that were not covered by BIS were compared against the standards established by the World Health Organization (WHO) (Table 2). To streamline the presentation of the findings, a correlation analysis is conducted to provide insights for a more sophisticated analysis and examine the interrelationships among the parameters.

**Table 2** BIS and WHO standards for drinking water

Parameters	BIS	WHO
pH	6.5–8.5	–
Turbidity	1–5 NTU	5 NTU
Alkalinity	200–600 (mg/L)	20–200 (mg/L)
TH	200–600 (mg/L)	10–500 (mg/L)
Ca	75–200 (mg/L)	–
Mg	30–100 (mg/L)	–
CL	250–1000 (mg/L)	200–300 (mg/L)
TDS	500–2000 (mg/L)	1000 (mg/L)
Na	–	200 (mg/L)
K	–	12 (mg/L)
F <sup>-</sup>	1–1.5 (mg/L)	1.5 (mg/L)
NH <sub>4</sub>	0.5 (mg/L)	0.2 (mg/L)
SO <sub>4</sub>	200–400 (mg/L)	–
NO <sub>3</sub>	45 (mg/L)	50 (mg/L)
Zn	1–5 (mg/L)	5 (mg/L)
Pb	0.01 (mg/L)	0.01 (mg/L)
Mn	0.1–0.3 (mg/L)	0.4 (mg/L)
Cd	0.003 (mg/L)	0.003 (mg/L)
Cr	0.05 (mg/L)	0.05 (mg/L)
Cu	0.05–1.5 (mg/L)	2 (mg/L)
Ni	0.02 (mg/L)	0.07 (mg/L)
Fe	0.3 (mg/L)	0.1 (mg/L)

#### 4.1 Leachate Characterization

The leachate and groundwater samples were collected and characterized in the month of January 2023. The physicochemical parameters of collected leachate are given in Table 3.

The measured values of both leachate samples exhibited a degree of similarity. The pH values of the samples were determined to be approximately 8.3 and 8.9. The observed pH indicates an alkaline characteristic, potentially resulting from a dissolution of bicarbonates [13]. The high level of pH is also an indication of old state of the landfill leachate [14]. The electrical conductivity (EC) values of the leachate samples were determined to be 21,538 and 24,615 (uS/cm), and the TDS values were 13,784 mg/L and 15,753 mg/L. These elevated EC and TDS values indicate the existence of dissolved inorganic substances within the leachate sample [5] and deposition of high amount of salts and hazardous wastes of the landfill. The organic compounds loadings present in leachate are commonly assessed by measuring biochemical oxygen demand (BOD) and chemical oxygen demand

**Table 3** Parameters of leachate

Sr. No.	Parameters	L1 (mg/L)	L2 (mg/L)
1	Temperature	24.10	23.7
2	pH	8.35	8.98
3	EC (uS/cm)	21,538	24,615.38
4	BOD	2279.20	2150.148
5	COD	3816.69	3662.333
6	Turbidity	89	30.3
7	Alkalinity	15,502.67	15,133.35
8	Total hardness	1100	2700
9	Ca hardness	842	1052.33
10	Mg hardness	260.67	1652.33
11	Cl <sup>-</sup>	4756.33	7880
12	TDS	13,784	15,753.85
13	Na	206.86	231.913
14	K	229.70	274.66
15	Li	1.78	1.28
16	F <sup>-</sup>	0.68	0.98
17	NH <sub>4</sub>	1568.69	2501
18	SO <sub>4</sub>	1768.83	3156
19	NO <sub>3</sub>	4954.20	4341.68
20	Zn	3.50	2.05
21	Pb	0.6	0.51
22	Mn	2.6	3.81
23	Cd	0.15	0.12
24	Cr	4.4	5.3
25	Cu	0.97	1
26	Ni	3.8	2.5
27	Fe	26.6	43
28	Co	0.91	0.5

(COD). The leachate samples L1 and L2 exhibited values of BOD of 2279, 2150 and COD of 3816, 3662 (mg/L). Discussing the turbidity measurements, which indicate sediment accumulation resulting from pollution, it is observed that the values differ between the two samples. Specifically, sample L1 exhibits a turbidity value of 89 NTU, while sample L2 demonstrates a turbidity value of 30.3 NTU.

The leachate samples exhibited a significant level of hardness, primarily attributed to the elevated concentrations of calcium (Ca) and magnesium (Mg). Both samples exhibited a significant concentration of chlorides, with levels ranging from 4756.33 to 7880 mg/L. This phenomenon may be attributed to the existence of industrial waste or fertilizers within the landfill. Leachate typically exhibits a substantial abundance

of primary constituents, including ammonia, sulfates, nitrates, and trace metals. In the current investigation, it has been observed that the concentrations of sulfates, nitrates, and ammonia are significantly elevated. The concentrations of major cations such as sodium (Na) and potassium (K) were determined using flame photometry. The concentration of lithium (Li) was also assessed in samples of leachate. However, there is limited research conducted on this particular cation in leachate or water, and there is currently no established standard acceptable range for its concentration.

The heavy metal concentration in a landfill tends to be higher during the initial stages due to increased metal dissolved caused by pH levels that are low resulting from the generation of organic acids. In this study, the most prevalent heavy metals are found to be Fe, Cr, Cd, Pb, Mn, and Ni. The observed phenomenon could potentially be attributed to the existence of batteries, paint products, leather, metallic products, wood preservatives, metal scrap, or plastics that have been discarded at the solid waste disposal site [15].

## 4.2 *Groundwater Characteristics*

The water surrounding the waste disposal site is utilized for a variety of domestic and potable applications. Hence, it is imperative to conduct an analysis of the quality of groundwater. Groundwater samples were systematically gathered within a 3 km radius encompassing the dumping sites. To investigate the impact of leachate on groundwater, a total of 12 samples were randomly collected from locations within a 3-km radius surrounding the landfill site. Two samples were obtained from the interior of the landfill, while the remaining samples were collected predominantly from boreholes located outside the landfill. Figure 3 depicts the graphical representation of various parameters observed in the samples along with acceptable ranges.

The data suggests that the majority of the parameters exceed the acceptable range as defined by the standards provided by Bureau of Indian Standards (BIS) and World Health Organization (WHO). The concentration of pollutants exhibits a significant decrease as the distance from the landfill site increases. The measured parameters, including total dissolved solids (TDS), total hardness, chloride, fluoride, sodium, and ammonia, exhibited values that exceeded the acceptable thresholds. However, certain parameters such as turbidity, potassium, and sulfate exhibit values that fall below the acceptable range. Based on the aforementioned data, it is evident that the samples in close proximity to the landfill or within a 1 km radius exhibit the highest levels of pollution. This evidence demonstrates that leachate has the potential to serve as a viable source of groundwater contamination. The primary factor contributing to an elevated concentration of anions, such as ammonia, nitrate, chloride, and fluoride, can be attributed to the substantial presence of household kitchen waste and fertilizer waste.

Atomic absorption spectroscopy (AAS) was employed for the purpose of detecting heavy metals. The highest concentrations were observed for Pb (lead), Cd (cadmium), Cr (chromium), and Ni (nickel) in mg/L. These elements were found to exceed

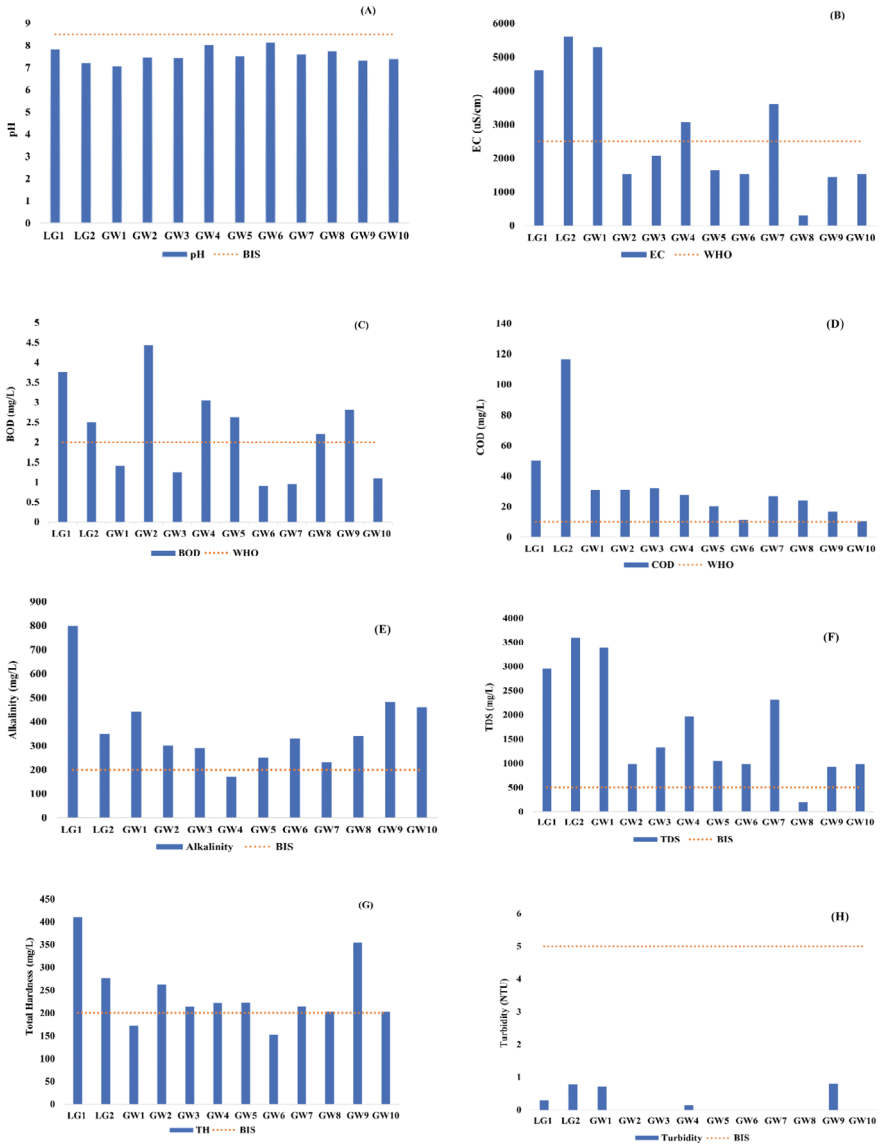


**Fig. 3** Concentration of different parameters in groundwater samples as compared to the standard values. *Note* BIS standards for pH, alkalinity, TDS, total hardness, turbidity, fluoride, chloride, ammonia (NH<sub>4</sub>), nitrate (NO<sub>3</sub>), and sulfate (SO<sub>4</sub>); WHO standards for EC (electrical conductivity), BOD (biochemical oxygen demand), COD (chemical oxygen demand), Na (sodium), and K (potassium)

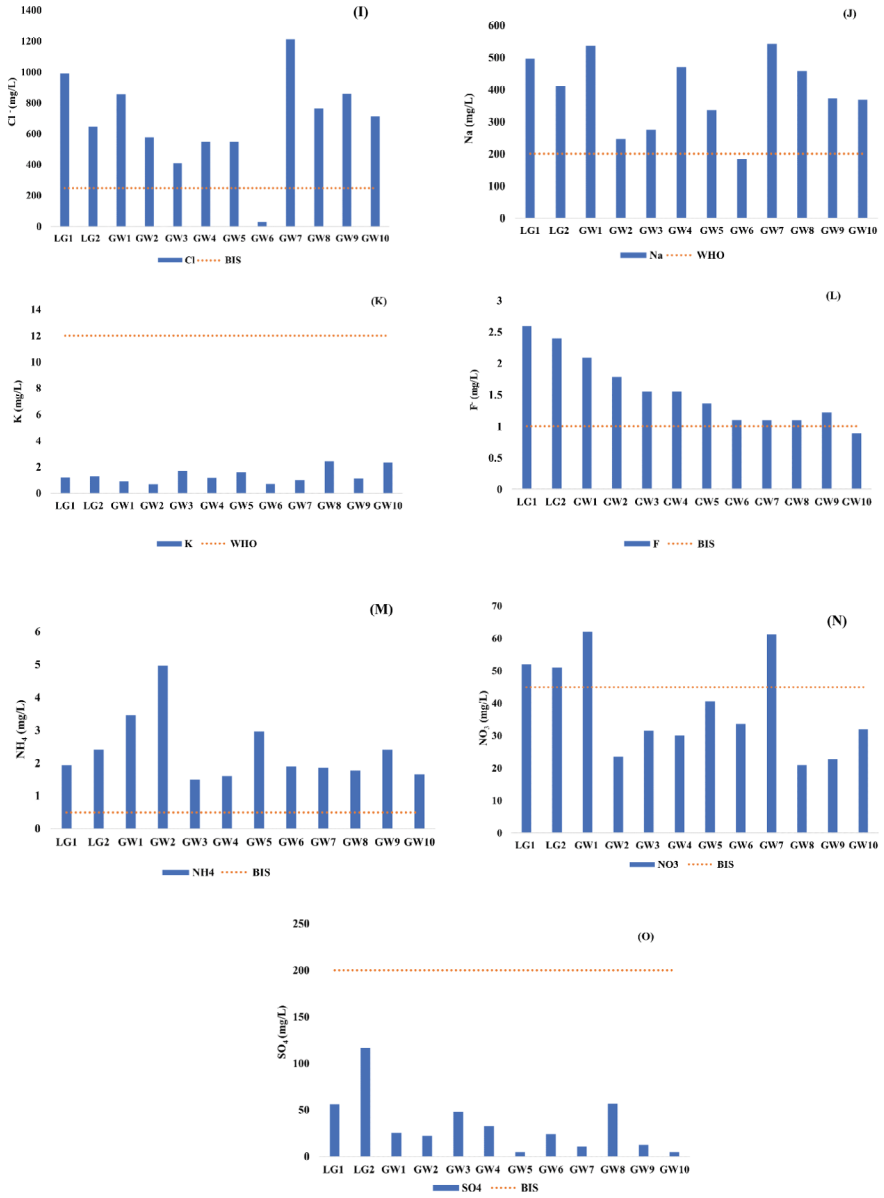


Fig. 3 (continued)

the allowable limits as well (Fig. 4). Landfilling of solid waste in a disorganized manner has a negative impact on the surrounding environment. There exist numerous factors contributing to the presence of heavy metals in the leachate. Sources such as electronics, metal plating waste, painting waste, and old batteries, when co-disposed with municipal solid waste, contribute to the elevated levels of heavy metals in landfill sites [16].

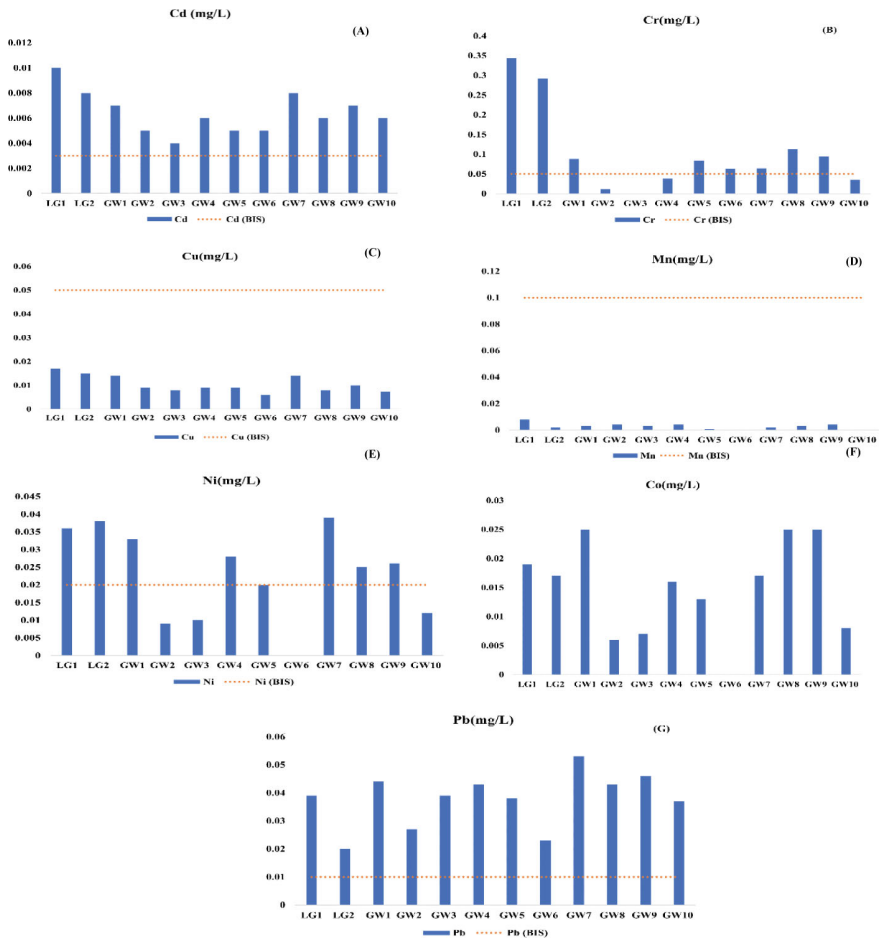
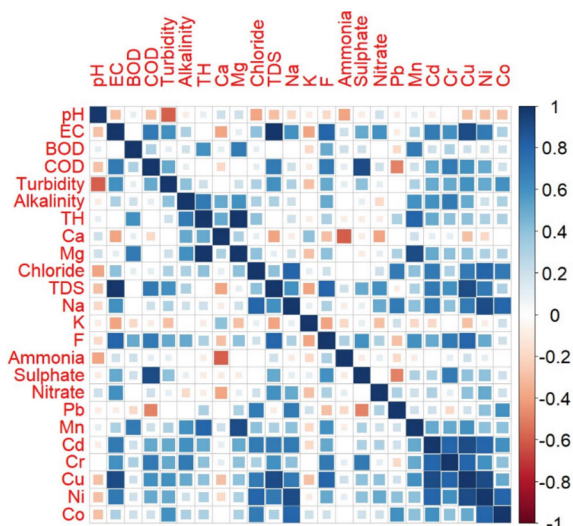


Fig. 4 Heavy metal analysis of groundwater

**Fig. 5** Correlation matrix of various parameters in groundwater



### 4.3 Correlation Analysis

Correlation analysis was done to find the relation between various parameters using Pearson's correlation matrix (Fig. 5). The correlation matrix reveals a significant correlation between EC and TDS, indicating a strong relationship between these two variables. The electrical conductivity (EC) exhibits a notable correlation with pH, fluoride ion concentration ( $F^-$ ), and copper ion concentration (Cu). The observed positive correlation between certain heavy metals and other parameters such as Cl, TDS, and Mg could potentially be attributed to the infiltration of elements found in leachate, which may have infiltrated into the soil beds and subsequently reached the table of groundwater. The observed correlation between sulfate and COD levels could potentially be attributed to microbial processes occurring in the system, as suggested by [17]. There exists a robust correlation between total dissolved solids (TDS) and heavy metals, suggesting that the presence of dissolved heavy metals has a substantial impact on the TDS levels in groundwater [18]. Hence, it can be hypothesized that the majority of the highly correlated pairs are associated with anthropogenic inputs rather than natural processes.

## 5 Conclusion

Groundwater plays a crucial role in providing water resources for towns as well as villages in emerging nations. The study on the effects of the disposal of municipal solid waste sites has demonstrated the fact that groundwater in the vicinity of these sites is found to be extensively polluted as a result of leachate infiltration.

The results suggested that leachate was high in almost all the measured parameters like BOD, COD, hardness, alkalinity, chloride, ammonia, sulfate, and nitrate. Also a higher concentrations of heavy metals were found in the leachate samples which had major effect on the groundwater samples nearby the landfill. Overall quality of the groundwater samples in the vicinity of the landfill was not satisfactory as major parameters like TDS, hardness, chloride, fluoride, and ammonia were above the acceptable limits. The water resources may have been affected by landfill leachate, which contains harmful substances like heavy metals, organic compounds, and other toxic substances. The data collected revealed elevated levels of heavy metals such as cadmium (Cd), chromium (Cr), nickel (Ni), and lead (Pb), which exceeded the acceptable limits set by the Bureau of Indian Standards (BIS). Correlation studies have revealed a significant correlation between the presence of heavy metals and various parameters, suggesting a strong influence of heavy metals on the contamination of groundwater caused by leachate. Due to this reason, it is advisable to promptly implement corrective actions to safeguard the groundwater.

**Declaration of Competing Interest** The author states that they have no conflicts of interest.

## References

1. Asouam S et al (2021) Physicochemical characterization of the leachate of the Tamelast landfill site, Grand Agadir (Morocco). *Ecol Eng Environ Technol* 22
2. Ahmed A, Alluqmani A, Shafiquzzaman M (2019) Impacts of landfill leachate on groundwater quality in desert climate regions. *Int J Environ Sci Technol* 16:6753–6762
3. Smith C, Hopmans P, Cook F (1996) Accumulation of Cr, Pb, Cu, Ni, Zn and Cd in soil following irrigation with treated urban effluent in Australia. *Environ Pollut* 94(3):317–323
4. Nagarajan R, Thirumalaisamy S, Lakshumanan E (2012) Impact of leachate on groundwater pollution due to non-engineered municipal solid waste landfill sites of erode city, Tamil Nadu, India. *Iranian J Environ Health Sci Eng* 9:1–12
5. Alemayehu T et al (2019) Assessment of the impact of landfill leachate on groundwater and surrounding surface water: a case study of Mekelle city, Northern Ethiopia. *Sustain Water Resour Manag* 5:1641–1649
6. Alghamdi AG, Aly AA, Ibrahim HM (2021) Assessing the environmental impacts of municipal solid waste landfill leachate on groundwater and soil contamination in western Saudi Arabia. *Arab J Geosci* 14:1–12
7. Chakraborty S, Kumar RN (2016) Assessment of groundwater quality at a MSW landfill site using standard and AHP based water quality index: a case study from Ranchi, Jharkhand, India. *Environ Monit Assess* 188:1–18
8. Talalaj IA, Biedka P (2016) Use of the landfill water pollution index (LWPI) for groundwater quality assessment near the landfill sites. *Environ Sci Pollut Res* 23:24601–24613
9. Vahabian M, Hassanzadeh Y, Marofi S (2019) Assessment of landfill leachate in semi-arid climate and its impact on the groundwater quality case study: Hamedan, Iran. *Environ Monit Assess* 191:1–19
10. Gaikwad SK et al (2020) Assessment of the groundwater geochemistry from a part of west coast of India using statistical methods and water quality index. *HydroResearch* 3:48–60
11. Gibbons RD, Bhaumik DK, Aryal S () *Statistical methods for groundwater monitoring*. Wiley

12. Tričys V (2002) Research of leachate, surface and ground water pollution near Šiauliai landfill. *Aplinkos tyrimai, inžinerija ir vadyba* 19(1):30–33
13. Maqbool F et al (2011) Effect of landfill leachate on the stream water quality
14. Jorstad L, Jankowski J, Acworth R (2004) Analysis of the distribution of inorganic constituents in a landfill leachate-contaminated aquifer: Astrolabe Park, Sydney, Australia. *Environ Geol* 46:263–272
15. Singh S et al (2016) Assessment of pollution potential of leachate from the municipal solid waste disposal site and its impact on groundwater quality, Varanasi environs, India. *Arabian J Geosci* 9:1–12
16. Kanmani S, Gandhimathi R (2013) Assessment of heavy metal contamination in soil due to leachate migration from an open dumping site. *Appl Water Sci* 3:193–205
17. Samarathunga I et al (2016) Effect of chemical oxygen demand (COD) to sulfate ( $\text{SO}_4^{2-}$ ) ratio on sulfate reduction in anaerobic digestion of sulfate rich wastewater
18. Alansi RQ et al (2021) Determination of heavy metals in groundwater around Al-Buraihi sewage station in Taiz City, Yemen. *J Health Pollut* 11(30):210604

# Batch Reverse Osmosis: Evolution from the Concept to the Technology



Dhaval Patel , Dipak Ankoliya , Milan Raninga , Anurag Mudgal , Vivek Patel , Jatin Patel , Varsha Mudgal , and Himanshu Choksi 

## 1 Introduction

Water-scare regions worldwide raise anxiety about finding an alternative; seawater and brackish water desalination have become excellent alternatives to the problem [1]. Membrane-based technologies like reverse osmosis (RO) have become very mature in the field of desalination. RO is a technology that is easy to install and energy efficient with lower operating costs compared to thermal-based technology [2]. The significant energy consumption in RO is the pumping energy of the process. Specific energy consumption for seawater RO (SWRO) and brackish water RO (BWRO) is  $3.5 \text{ kWh/m}^3$  and  $0.5 \text{ kWh/m}^3$ , respectively [3]. However, the energy consumption of water treatment using RO technology has decreased in past few decades from 15 to  $2 \text{ kWh/m}^3$  [4]. The improvement in energy efficiency is mainly because of development of membrane with higher permeability and selectivity, pumps with improved efficiency, and implementation of energy recovery devices; additional improvement in the energy consumption can be done by optimizing plant design and operating parameter [5]. For the reduction of energy consumption, a novel design of the RO is proposed by various researchers like multi-stage RO, semi-batch RO, close-circuit RO (CCRO), semi-close RO, hybrid RO systems, etc. [1, 6–9]. Although, the energy consumption of SWRO and BWRO largely depends on the total dissolved solids (TDS) of the water, and it is usually lower for the BWRO as its TDS range varies

---

D. Patel (✉) · D. Ankoliya · M. Raninga · A. Mudgal · V. Patel · J. Patel · V. Mudgal  
Mechanical Engineering Department, School of Technology, Pandit Deendayal Energy University,  
Gandhinagar 382426, India  
e-mail: [dhaval.20patel@gmail.com](mailto:dhaval.20patel@gmail.com)

A. Mudgal  
e-mail: [anurag.mudgal@sot.pdpu.ac.in](mailto:anurag.mudgal@sot.pdpu.ac.in)

H. Choksi  
Chemical Engineering Department, School of Technology, Pandit Deendayal Energy University,  
Gandhinagar 382426, India

from 1000 to 10,000 ppm as compared to more than 35,000 ppm in SWRO [2]. The specific energy requirement for surface water is 0.2–0.4 kWh/m<sup>3</sup>, while for seawater is 2.5–4.0 kWh/m<sup>3</sup> and which can be elevated to 3.5–4.5 kWh/m<sup>3</sup>, including pretreatment and post-treatment processes [10–12]. The energy intensiveness of these processes makes the technology less attractive. However, upgradation in technology like semi-batch RO, CCRO, and batch RO (BRO) leads towards energy efficiency.

Technological development and increased attention towards BRO in recent years have led to new configurations, simple designs, and enhanced output [13, 14]. BRO process is a scalable industrial process is gaining attention recently. BRO is a cyclic process that uses time average feed pressure to obtain the required pressure with minimum energy consumption [15]. BRO operates cyclically with the pressurization, purge, and refill phase [16]. The BRO process recirculates the brine coming out from the RO membrane to the feed side; however, it does not mix with the fresh feed [13]. The BRO process requires the pressure to overcome the osmotic pressure of the feed water (mixed with the recirculated brine) over the cycle operation without loss of energy and mixing with fresh feed water [13, 17, 18]. In the continuous RO process, the pressure at the beginning of the cycle reaches the maximum. It remains constant throughout the process, leading to higher energy consumption than the BRO [9, 13]. Analytically the recovery and efficiency of the BRO process is higher compared to conventional RO; but it produces permeate during only the pressurization phase (also known as permeate production phase), while during the purge and refill phase (flush and recharge), there is no permeate production. This is why, while comparing with continuous RO based on the output per meter square area of membrane, permeate water flux is higher in batch processes which also reflects in energy consumption and energy penalty of BRO process discourage compared to conventional RO [19].

An improved model of BRO gives fouling resistance and batter output and provides information regarding osmotic backflow [16, 20, 21]. A pilot-scale implementation using an industrial-scale membrane is carried out [15, 16]; still, the technology is at the level of TRL5 [22]. Although there is an advancement in technology, BRO and RO are technologies that can elevate the system recovery up to a certain level because of their maximum operating pressure or membrane bursting pressure. So, there is a need for brine discharge in this technology [23, 24]. However, treatment of the groundwater and wastewater in the context of zero liquid discharge requires high pressure, so high-pressure recovery of minerals will be possible. In applications like electroplating wastewater treatment, steel industry wastewater treatment requires higher pressure [25].

In contrast, many reverse osmosis systems are built and operated for clean water production and wastewater treatment with various configurations like CCRO, multi-stage RO, semi-close RO, semi-batch RO, BRO, and hybrid batch semi-batch RO. However, BRO shows the potential to take technology from TRL 5 to TRL 9. This technology shows uniqueness towards the high recovery and low specific energy consumption. High recovery of the system leads to a smaller brine volume which can be treated quickly, and the process can become a minimal/zero liquid discharge process. However, for minimal liquid discharge, the subsequent technology also requires less energy, and it is easy to handle the brine. Ultimately, the system becomes

cost-effective. This article aims to summarize the available design of BRO technologies and their states of commercialization. The hurdles the technology faces are also essential to discuss to overcome. The commercialization of the technology is in its early phase.

## 2 Batch RO System

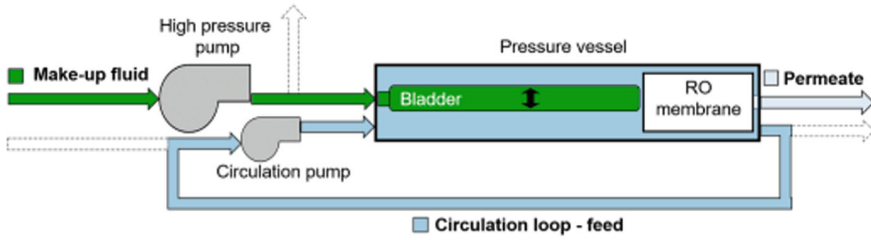
To achieve ZLD and MLD, membrane- and thermal-based technologies are used. However, thermal-based technologies are energy intensive. Similarly, ZLD techniques are energy intensive as they separate all impurities from the wastewater stream [1, 26]. That is why MLD utilizes various applications like groundwater desalination and wastewater treatment [27]. High recovery membrane-based processes with good energy efficiency would have potential in MLD/ZLD by reducing the size of the thermal-based treatment. Also, MLD/ZLD systems operate on the membrane bursting pressure, and fouling is one of the primary concerns in this type of application; thus, the RO is the most potential membrane-based technology for the application of MLD/ZLD [1, 28]. The significant challenges with reverse osmosis technology are brine discharge and higher energy consumption.

In the last two decades, several studies have provided a solution for desalination using research on BRO. This technology aims to resolve the two major problems of the RO: energy consumption and high saline brine discharge [29]. The BRO technology offers high recovery with minimum energy consumption.

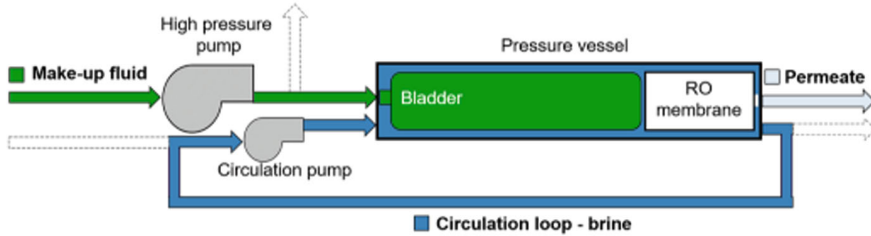
The most common BRO design typically uses bladder and piston arrangements [16]. These two types of systems are constructed and tested in a laboratory environment. Quantum J. Wei et al. discussed a bladder-type BRO system [20]. The operation stage of the bladder-type BRO is shown in Fig. 1. This system operates in four phases, as shown in Fig. 1. During phases A1 and A2, the permeate is produced. At the beginning of the cycle, the feed is circulating in the circulation loop at its maximum volume while bladder is at its minimum. The permeate production stage will be over once targeted recovery is achieved. The total amount of water is fixed in the bladder and circulation loop. The high-pressure pump introduces the makeup fluid to the bladder, and it expands. The permeate production is also started and produced at a similar rate as makeup fluid [20].

After completion of the permeate production phase, flush and recharge started. At the end of the permeate production phase, the circulation loop is full of the concentrated liquid, which must be replaced with the feed water. The system valve arrangement is made in the manner that during the flush phase, the fresh feed water replaces the brine, and during the recharge phase, the new feed is introduced in the system, and water from the bladder is removed. After completion of this phase system is ready for operation (permeate production phase), the study exhibits the comparison between the continuous RO, BRO, double-acting BRO, and previous work done on BRO. It shows that if we work with the higher flux with BRO will not have too much energy penalty and will still be better than continuous RO [20].

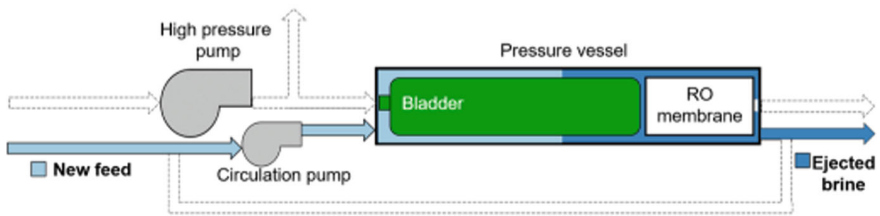
**A1. Beginning of permeate production phase**



**A2. End of permeate production phase**



**B. Flush phase**



**C. Recharge phase**

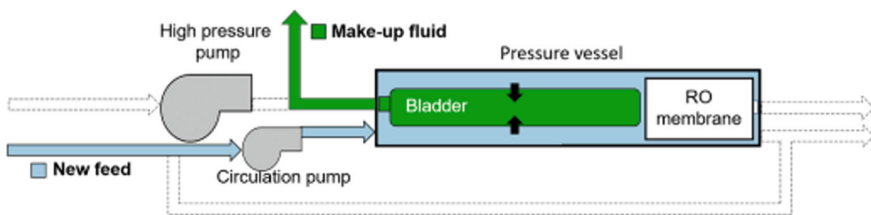


**Fig. 1** Bladder-type BRO cycle's operation stages [20]<sup>1</sup>

Sandra Cordoba et al. utilised a similar double-acting BRO configuration for better efficiency and less downtime [13]. A system is designed in such a way that feed/brine

<sup>1</sup> “Reprinted from Desalination 479 (2020), Quantum J. Wei, Carson I. Tucker, Priscilla J. Wu, Ali M. Truworthly, Emily W. Tow, John H. Lienhard V: *Impact of salt retention on true batch reverse osmosis energy consumption: Experiments and model validation*, 114177, Copyright (2019), with permission from Elsevier.”

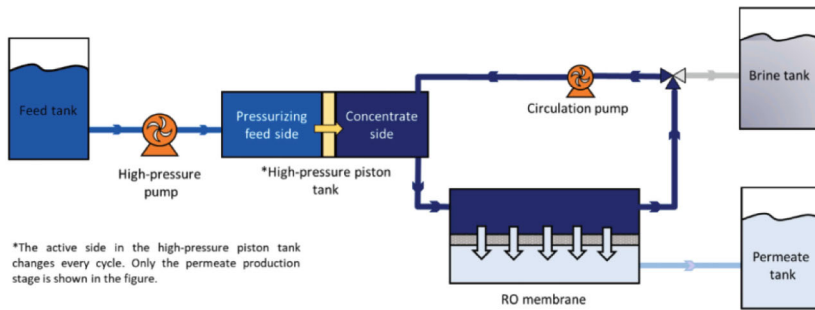
on both sides instead of displacing the recirculating brine with permeate as a fresh feed/working fluid. The system initially starts the high-pressure pump and fills the feed water on side 1 in the high-pressure tank. Also, the pipe and RO membrane are fed with water for the priming. Priming is done initially when the system is started (shown in Fig. 2B(a)). After that high-pressure pump supplies the water on side 2 in the high-pressure tank. Pressurized water thrusts the piston and displaces water from side 1 of the high-pressure tank into the RO membrane. This phase creates permeate water collected on the tank, and produced brine is recirculated back to side 1 in a high-pressure tank, as shown in Fig. 2B(b). Water from side 1 is used as a working fluid in this phase. The flushing stage is initiated when the piston reaches the end of the high-pressure tank, in which high-pressure pump supplies the feed and replaces the brine in the pipes and RO module, as shown in Fig. 2B(c). During flushing stage, permeate output is blocked, which does not allow the air in membrane element, which also prevents the entering of the airborne contaminants to enter in membrane permeate side [13, 17].

After that, the system is ready to enter the permeate production phase again as shown in Fig. 2B(d). Figure 2B(e) shows the earlier BRO configuration proposed by Warsinger et al. This configuration used only one side of the fluid as a working fluid. The downtime/reset time is also higher for this configuration. The new configuration developed by the Sandra Cordoba et al. has certain advantages over the previous one. The new configuration offers a lower reset time as this configuration consisting of a double-acting cylinder and proper sealing will ensure no mixing with the permeate. The system has a non-zero start-up time; initially, priming is required to remove air from the pipes and membrane [13]. The study also reveals that BRO can achieve higher efficiency with low specific energy consumption over various conditions. Past studies show poor performance at higher salinity and recovery [17]. However, the requirement of higher permeate flux leads to a higher-pressure requirement and specific energy consumption [13].

T. Y. Qiu et al. discussed the cyclic operation of the BRO illustrated in Fig. 3. They achieved this operation in three stages, namely pressurization, purging, and refill: initially cylinder, pumps, and RO module filled with the water [30]. During the first stage, valve 3 is open, and valve 1 and valve 2 are closed. The piston applied pressure on the water, causing the pressurized water in the RO module, which caused the water to pass from the RO membrane. Permeate water is produced during this phase. The water concentration increases at the end of the membrane, which is adjusted with the recirculation pump by supplying freshwater and keeping the concentration nearly the same at the inlet and outlet of the RO membrane. As the piston reaches the cylinder's end, only brine is left in the RO module. So, during the purging operation, valve 3 closes, and valves 1 and 2 open. The brine is replaced with the freshwater from pumps; the last stage is refill, so valves 1 and 3 remain open, and valve 2 becomes closed. The pumps supply the water into the cylinder and refill the whole system. The system is once again ready to operate from the initial stage. Figure 3 shows a solid line as a flow path and a dashed line as a no flow path [30, 31].

T. Y. Qiu et al. initially tested the system using a material testing machine to check the feasibility of the mechanically driven BRO system. Figure 4 shows the test rig initially used to test the mechanically driven brackish water reverse osmosis

(A)



(B)

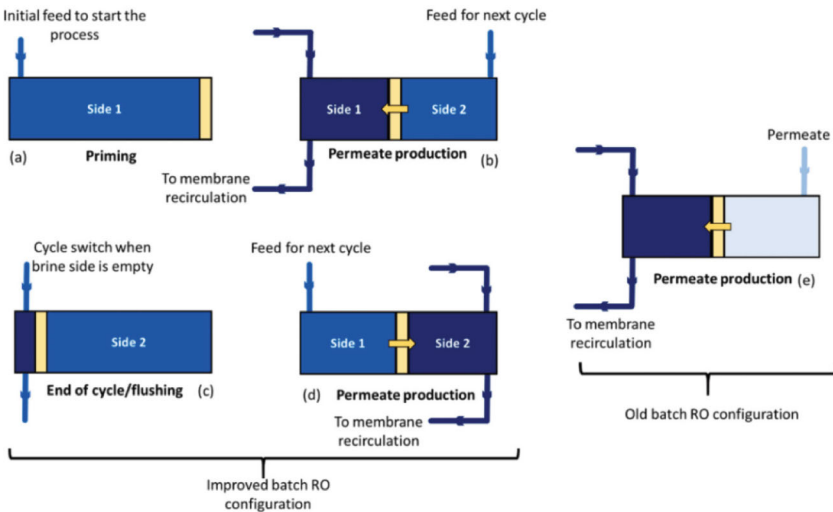


**Fig. 2** A BRO configuration utilised by Sandra Cordoba et al. and **B** steps of the operations of the BRO compared to the proposed by Warsinger et al. [13]<sup>2</sup>

(BWRO) system [30]. The primary use of the material testing machine is to provide desired varying pressure to maintain the constant displacement. Due to the laboratory environment’s limitation, they tested only the pressurization mode using that material testing machine. They turned off the material testing machine as the piston reached the end of the cylinder. The feed water has a 3500 ppm NaCl solution. Initially, they used piston movement to 50 mm/min. They initially achieved a 66% recovery ratio. The permeate water quality is achieved below 500 ppm [31].

<sup>2</sup> “Reprinted from Desalination 506 (2021), Sandra Cordoba, Abhimanyu Das, Jorge Leon, Jose M Garcia, David M Warsinger: *Double-acting batch reverse osmosis configuration for best-in-class efficiency and low downtime*, 114959, Copyright (2021), with permission from Elsevier.”

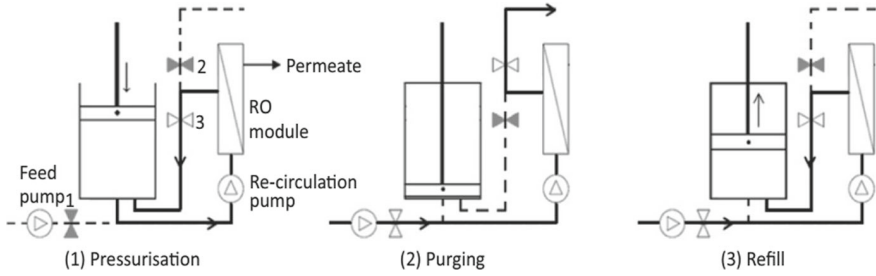


**Fig. 3** Piston-type BRO's working phases [30]<sup>3</sup>



**Fig. 4** Material testing machine coupled with BRO system, (1) material testing machine, (2) pump cylinder, (3) pressure gauge, (4) recirculating pump (3 m<sup>3</sup>/h maximum flow rate—wilo), and (5) RO membrane module (Dow FILMTEC BW30-2540) [31]

<sup>3</sup> “Reprinted from Desalination 368 (2015), T.Y. Qiu, P.A. Davies: *Concentration polarization model of spiral-wound membrane modules with application to batch-mode RO desalination of brackish water*, 36–47, Copyright (2015), with permission from Elsevier.”

To address the energy consumption issue, the system's recovery, and brine management, T.Y. Qiu et al. introduce the DesaLink-powered BRO system. It is the approach in which the solar Rankine cycle is coupled with BRO to gain mechanical advantage. The motivation towards developing the DesaLink, solar steam Rankine cycle-based reverse osmosis is the limitation of the solar photovoltaic RO for brackish groundwater desalination like high cost and low efficiency. However, the steam Rankine cycle also has its drawbacks, like the small scale is unsuitable for low power outputs because of the leakage losses in turbine blades and blade friction losses. This is why the steam power piston is utilized instead of the steam turbine, which uses a linkage mechanism to transfer the mechanical power instead of the rotary mechanism. The DesaLink mechanism concept is shown in Fig. 4 [31].

The DesaLink is the concept of connecting two pistons using a crank and linkage to increase mechanical advantage by transferring mechanical power to another piston. The crank mechanism can transfer the power 55–94% efficiently based on the expansion ratio of the steam, recovery ratio, etc. They fixed the system's recovery (70%) by fixing the volume of the cylinder. The RO membrane element is Dow Filmtec type BW30-2540 used. Figure 5 shows the actual prototype of the DesaLink. The system achieved 75% recovery by using 200 °C and 10 bar pressure in the steam cylinder. The feed water quality is 4000 ppm. The authors used the Kimura-Sourirajan mass transfer model to validate the spiral wound RO membrane. A genetic algorithm method is developed to calculate the Sherwood correlation parameter [31].

A. Mudgal et al. developed a steam Rankine cycle-based RO plant with a linkage mechanism. The linkage mechanism is designed to gain mechanical advantage and minimize energy penalty [32]. A steam-jacketed arrangement is used to achieve isothermal expansion for the better thermodynamic efficiency. Steam is generated using a biomass boiler. The pressure is developed using the mechanism shown in Fig. 6 and which is used to produce permeate from the RO membrane [32].

The authors demonstrate the feasibility of the thermal energy-based steam Rankine cycle for BRO systems. They achieved a 70–76% recovery ratio with feed water salinity of 4000 ppm. They demonstrate to deliver 7 m<sup>3</sup>/day freshwater production at 71 INR/m<sup>3</sup> [32].

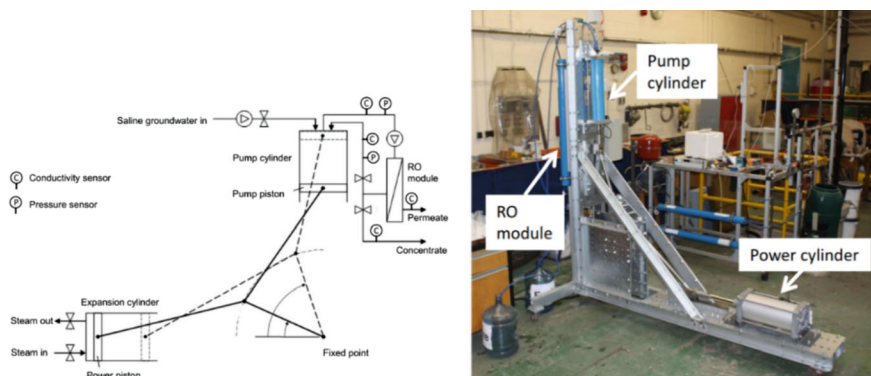


**Fig. 5** DesaLink schematic and prototype [31]

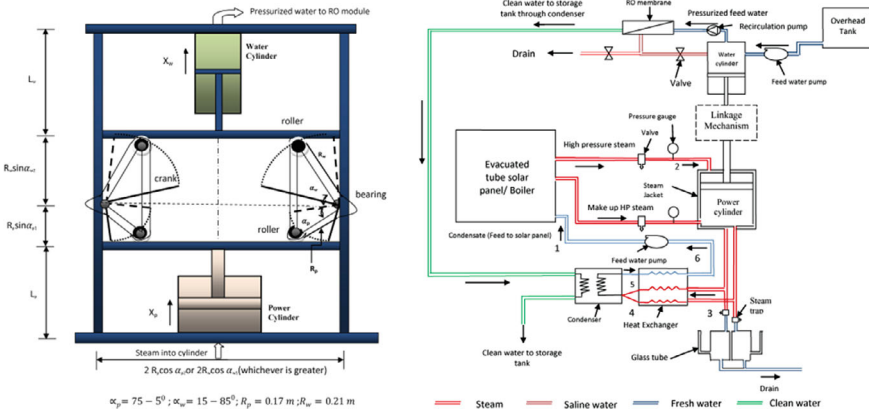


**Fig. 6** Linkage mechanism with power piston and water piston and schematic diagram of the Rankine cycle-based steam-operated RO desalination plant [32]<sup>4</sup>

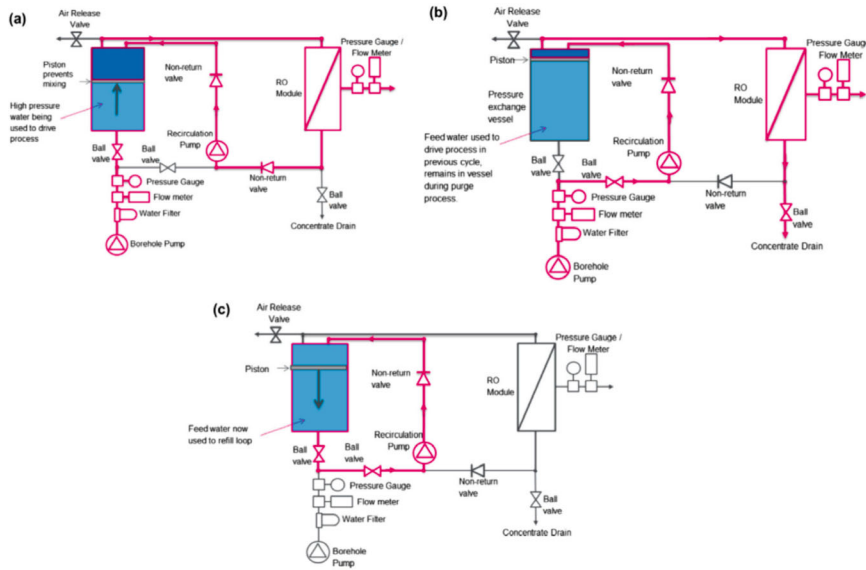
Davies et al. modified their DesaLink mechanism and shifted to the pumping power to develop pressure from the thermal (steam)-based power production [33]. The system’s working is similar to the one explained in Fig. 3. However, this system contains a cylinder with the free piston and works in the same three phases as shown in Fig. 7. The piston used in the cylinder is made of high-density polyethylene material as it has low water absorption, corrosion, chemical resistance, and good impact properties. Piston is provided with the O-ring seal to provide seal and separate the water from both sides of the cylinder. Also, it ensures the movement of the piston inside the cylinder. A DC helical rotor pump (Grundfos SQF 0.6–2) is used as a high-pressure (borehole pump) pump. The system consisting of two identical polyamide thin film composite membranes (Filmtec BW30—2.5 in. diameter × 40 in. long module capable of withstanding 41 bar pressure) was connected in parallel [33].

Feed water salinity utilized in the system is 2000, 3000, and 5000 ppm. The system’s hydraulic SEC varies from 0.135 to 0.337 kWh/m<sup>3</sup>. The water flux of the system varied from 6.9 to 24.2 LMH. They observed that SEC decreases as the pressure and flux reduce. However, low pressure and flux lead to a higher permeate salinity. The system obtained a 70% recovery ratio with 0.6 kWh/m<sup>3</sup> electrical SEC. This system utilizes 33% less energy than close-circuit desalination [33].

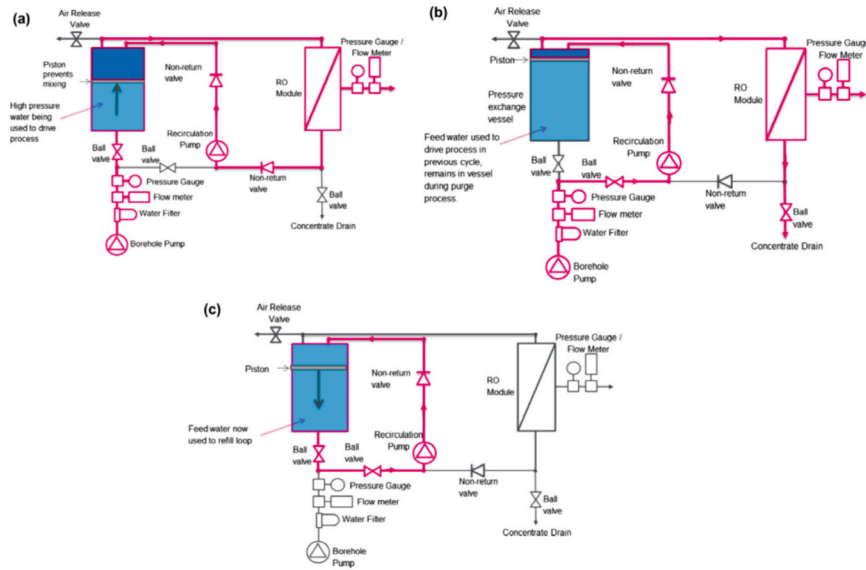
After the successful trial of the prototype of BRO with free piston arrangement at Aston University, P A Davies and his team developed a lab-scale experimental setup of different configurations, as shown in Figs. 8, 9, 10 and 11. The prototype shown in the figure uses the manual control valve without measuring the electric energy consumption.

Figure 9 consists of the double-acting system with the four stages of the operation. (1) pressurization—refill, (2) purge, (3) pressurization—refill, and (4) purge. The

<sup>4</sup> “Reprinted from Desalination 385 (2016), A. Mudgal, P.A. Davies: A cost-effective steam-driven RO plant for brackish groundwater, 167–177, Copyright (2016), with permission from Elsevier.”



**Fig. 7** Schematic diagram for the operation of BRO system **a** pressurization phase, **b** purge phase, and **c** refill phase [33]



**Fig. 8** Prototype of the free piston-operated BRO system—Version 1 [33]

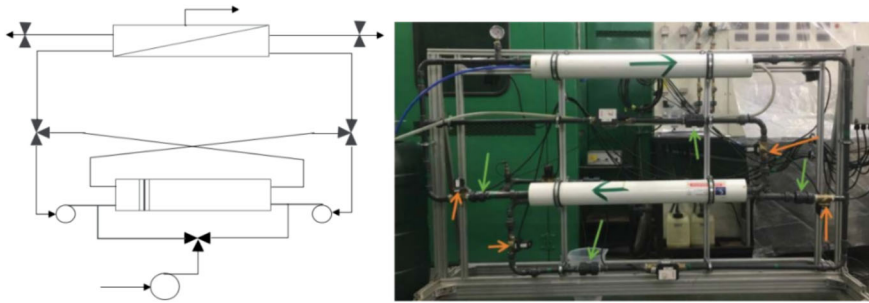


**Fig. 9** BRO configuration Version 2—double-acting BRO system developed at Aston University, UK; here, the yellow arrow shows solenoid valves, and the green arrow shows the non-return valve [14]

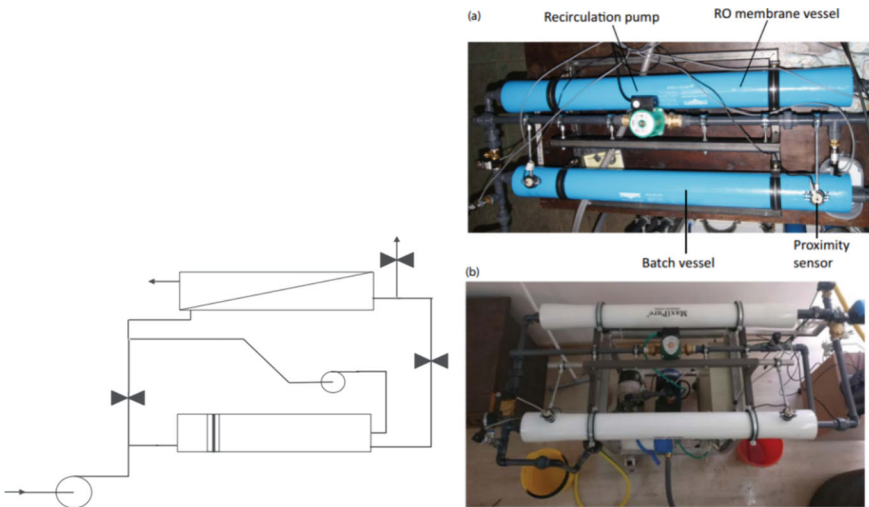


**Fig. 10** BRO configuration Version 3—single-acting BRO system developed at **a** Aston University, UK, and **b** Arava Institute of Environmental Studies, Israel [14]

significant advantage of this system is the less tendency of fouling due to its double-acting configuration as flow occurs from both sides of the membrane module. The construction of this test rig uses RO housing as a pressure/work exchanger assembly (batch vessel) to avoid the extra cost of standard parts. This pressure/work exchange assembly (batch vessel) contains polyethylene or acetal pistons and RO housing.

Figure 10 shows the third version of the prototype of their system; the system consists of automatic control and proximity sensors for the detection of the position of the piston at the end of the travel. However, the earlier version of the system consists of flow and pressure sensors to detect the same. Similarly, they developed the system with three pressure/work exchanger assemblies and three RO membranes.

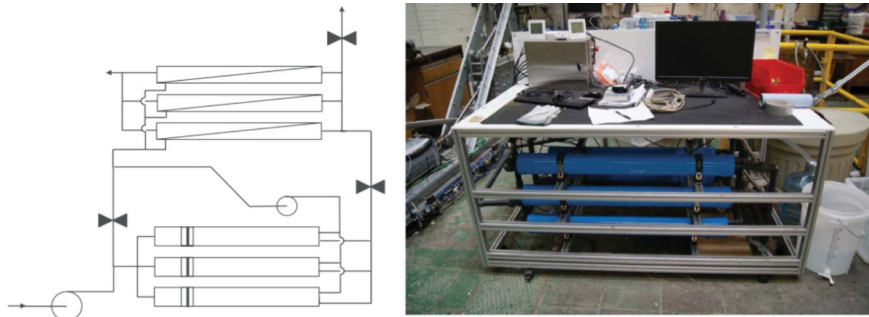


**Fig. 11** BRO configuration Version 4—single-acting double-stage BRO system with multiple vessels developed at Aston University [14]. Key: ► non-return valve; ⚡ 2-port valve; ⚡ 3-port valve; ○ feed pump; ○ recirculation pump; RO pressure vessel ; batch vessel 

This experiment is performed to observe the effect of upscaling on the capacity of the system.

As shown in Figs. 8, 9, 10 and 11, all the BRO configurations developed by P A Davies and his team at Aston University were tested under similar conditions. They used 2000 ppm water as a feed to BRO system. This solution is made from tap water and culinary-grade NaCl. They added sodium meta-bisulfite to neutralize the present chlorine in tap water.

Table 1 gives the results obtained with a different configuration of the BRO system. The different configurations were developed as improvements in the predecessor. All configurations were tested with a feed salinity of 2000 ppm. The systems show a recovery ratio greater than 70%. The specific energy consumption of the system is also improved with the latest configuration as the implementation of the good performing membrane, efficient pump, and efficient system design. The system also achieved the target output of the per day production of the permeate water.

K. Park et al. investigated and gave the first design of a free BRO for ground brackish water treatment. The study includes designing, modelling, and optimization of the system [15]. The system consists of two pumps, three valves, two RO pressure vessels—one consisting of a membrane and the other consisting free piston (pressure/work exchange assembly), and a control panel as shown in Fig. 12. The system works in two phases, namely (1) Pressurization and (2) Purge and refill valve. Clean water is produced during only the pressurization stage. The systems have three valves: recirculation, bypass, and brine. During the pressurization phase, recirculation valve is open, and the other two valves are closed; the supply pump is forwarding water with pressure to the pressure/work exchange vessel, which generates the force on the piston and displaces the water on the other side of the pressure/work exchange vessel and forward to RO membrane. Due to pressure, the RO membrane permeates water and recirculates brine through a recirculation pump to pressure/work exchange vessel till the piston reaches the other end of the vessel [15, 16].

**Table 1** Results obtained by various BRO configuration

Parameter	Version 1	Version 2	Version 3	Version 4
	Single-acting three-stage operation	Double-acting	Single-acting two-stage operation	Single-acting two-stage operation—multi-vessel
Control	Manual	Automatic	Automatic	Automatic
Piston detection method	Flow and pressure sensors	Flow and pressure sensors	Proximity sensors	Proximity sensors
Feed salinity (ppm)	2000	2000	2000	2000
Recovery (%)	70	76	73	72
SEC ideal minimum (kWh/m <sup>3</sup> )	0.074	0.080	0.077	0.076
SEC hydraulic (kWh/m <sup>3</sup> )	0.27	0.19	0.36	0.2
SEC electrical (kWh/m <sup>3</sup> )	Not measured	2.62	2.31	1.26
Rejection (%)	88	80.5	95	90
Output (m <sup>3</sup> /day)	Not measured	1.32	2.86	3.76
References	[33, 34]	[35]	[36]	[14]

In the purge and refill phase, the recirculation valve is closed, and bypass valve and brine valve are open. The water from the supply pump replaced the brine in the RO membrane and refill the pressure/work exchange vessel with the help of a recirculation pump. This cycle completes in very few seconds and produces brine [15, 16].

The system can achieve 80% recovery with less than 0.5 kWh/m<sup>3</sup> specific energy consumption. They suggested that BRO needs 3–4 cycles to become a steady state. Also, they concluded that once it reaches a steady state, salt retention between cycles tends to increase during the start of the cycle, each by 16%, which leads to an increase in the system's pressure and energy consumption. For a short time, it will give concentrated water, and then, it will produce permeated water with good quality. The SEC of the supply pump significantly contributes about 75–85% of that total energy consumption. While the recirculation pump only carries 10–20% of the energy consumption. At 17.3 LMH water flux, with the range of salinity 1–5 g/L, they observed 0.48–0.83 kWh/m<sup>3</sup> SEC. Over the cycle's operation, with feed salinity of 1 g/L with recovery of 80% and water flux of 18.1 LMH, they observed that the

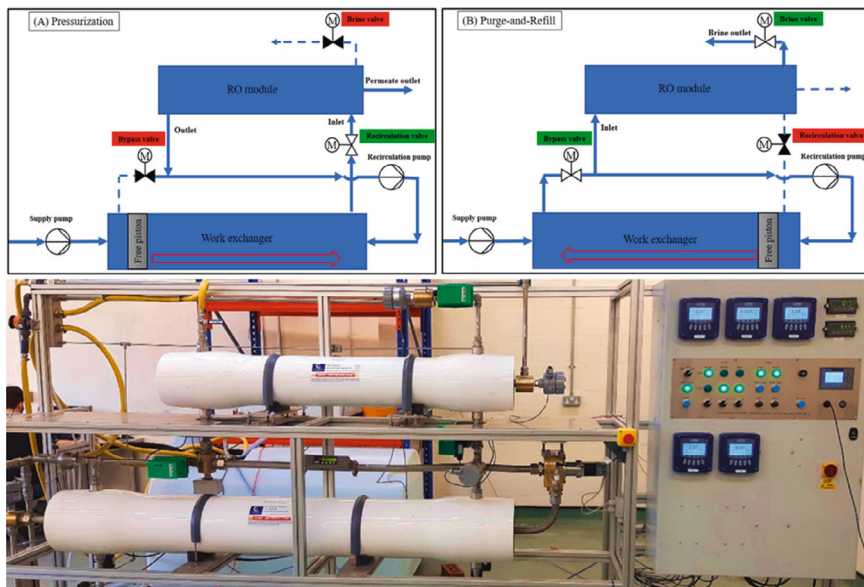


**Fig. 12** BRO: **a** pressurization phase of operation **b** purge and refill phase of the operation and actual image of the BRO system [16]

permeate salinity increases in first 30 s and then drops and increases slowly with time. They also carried the sensitivity of recirculation flow over the SEC and found that it weakly depends on each other. Recirculation flow ratio 1.5–3 gives minimum SEC [16].

Ebrahim Hosseinipour et al. and K. Park et al. gave the concept of the hybrid batch/semi-BRO (HSBRO) system and successfully tested the concept with their pilot-scale experimental setup [25, 37]. The system operates similarly to the BRO as described above, but it has one additional phase of semi-batch pressurization. So the system works over three consecutive steps; (1) semi-batch pressurization, (2) batch Pressurization, and (3) purge and refill [25].

The process starts with regular purge and refill mode to replace any existing brine from the system left during the last operation. This process prepares the system for the pressurization stage. As the pressurization phase starts, it is a semi-batch pressurization phase in which the bypass valve and recirculation valve are open; while the brine valve is closed. As the bypass valve is open, the piston remains at the left side of the pressure/work exchange vessel with no force to drive it. The supply pump provides sufficient pressure to overcome the osmotic pressure, and permeate will start to produce. Brine is recirculated in pressure/work exchange vessel and mixed with the fresh feed during the process. This mixed feed will pass into the RO module. The shift from the semi-batch pressurization is either fixed time, fixed volume, or according to the threshold pressure. After that, in the next phase, the bypass valve is closed, and the other valve remains in the same position. The operation is now

converted into batch pressurization. The piston starts to move from left to right and permeate production is continuous until the piston reaches the end of the pressure/work exchanger. However, there is no mixing of fresh feed coming and brine produce. The piston transfers the water, which is on the right side of it, to the RO membrane. The concentrated brine stream is recirculated, which causes concentration to rise inside the vessel and demands a higher-pressure requirement. At last purge and refill stage is same as in BRO system [25].

HSBRO is the process that can attain higher recovery with a similar BRO exponential setup. It is observed that with HSBRO operation with feed salinity of 500–1500 ppm, the system can achieve 94% recovery with 18.9 LMH permeate water flux. 93–94% salt rejection is achieved during the system's operation. The hydraulic SEC and electrical SEC vary in the 0.2–0.31 and 0.42–0.54 kWh/m<sup>3</sup>. It is also observed that there is a salt diffusion during purge and refill mode, and due to this, initial peak was observed in permeate quality, which resulted in the 0.6–0.9% reduction in the salt passage. Based on the model, authors also predicted that a solution with 10,000 mg/L can be treated with a higher recovery of 90%, hydraulic SEC less than 1.4 kWh/m<sup>3</sup>, and 23.7% second law efficiency [25].

### 3 Comparison Between BRO and Continuous RO

Chougradi et al. compared the conventional reverse osmosis with the BRO. They used both seawater and brackish water with salinity 35 g/L and 5 g/L, respectively. Fourteen membrane elements with 37 m<sup>2</sup> area of each were selected for the study. In continuous RO configuration, seven elements were placed in RO membrane housing while in the case of batch reverse osmosis there were only one element per RO membrane housing. The pressure drop per membrane module is considered 0.2 bar. Membrane water permeability for brackish water is 5 LMH/bar and for seawater is 3 LMH/bar while operating flux is 25 LMH for brackish water and 15 LMH for seawater. The high-pressure pump's efficiency is considered 80% while energy recovery device's efficiency is considered 97% and concentration polarization factor is considered as 1 [5].

The specific energy consumption for continuous RO and BRO with energy recovery device over the range of the recovery is shown in Fig. 13 for brackish water and seawater. It is evident from the graph that the brackish water BRO is energy efficient after the 50% recovery ratio, and for seawater, it is energy efficient for the whole range of recovery. They concluded that brackish water batch process takes 9%, 19%, and 34% less energies at 60, 70, and 80% recovery ratio; while for seawater BRO takes 17%, 23%, and 31% less energy for 40%, 50%, and 60% recovery ratio compared to the continuous RO [5].

BRO process utilizes the variable pressure as per the requirement of the osmotic pressure with time. A linear pressure profile is compared with pressure profile which gives 15 LMH constant flux. Figure 14a and b shows that BRO performs well under linear profile where its specific energy consumption is very similar to the BRO with

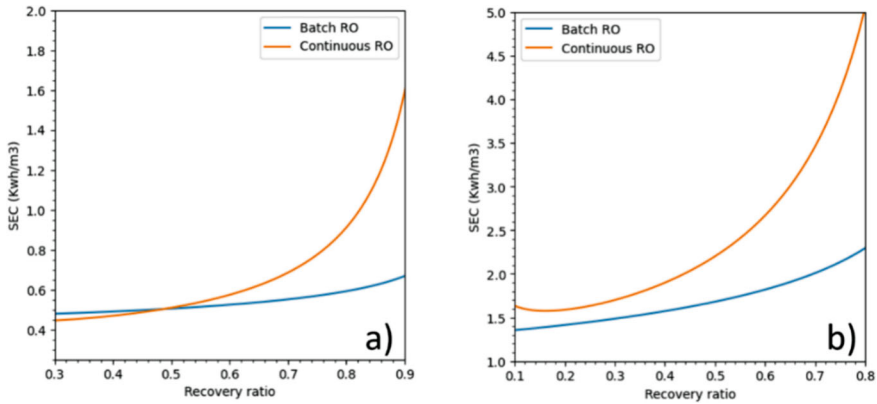


**Fig. 13** Recovery ratio versus specific energy consumption of continuous RO and BRO for **a** brackish water and **b** seawater [5]

constant flux, especially when recovery is below 50% [5]. The results suggest that BRO energy consumption is variable depends upon the flux and pressure profile; this is the indication that BRO needs the improvement in terms of the minimization of the SEC.

Cordoba et al. compared the energy consumption of the batch reverse osmosis with continuous RO and continuous RO with pressure exchanger as shown in Fig. 15. It has been observed by them that BRO configuration requires least energy for the treatment of the water with various salinity at different recovery ratio. While continuous RO requires more energy at higher recovery ratio (> 70%) and at higher salinity and continuous RO with pressure exchanger requires higher energy at higher recovery ratio (> 80%) [17].

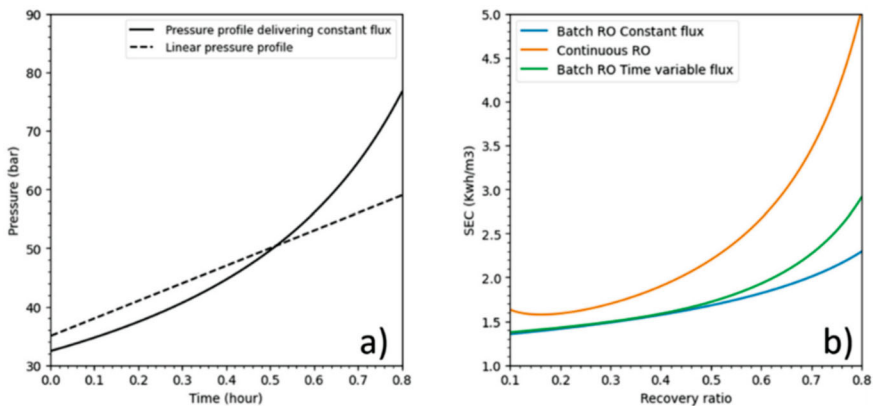


**Fig. 14** **a** Pressure profile of BRO for seawater (salinity 35 g/L) and **b** specific energy consumption of BRO with constant, time variable flux, and SEC of continuous RO [5]

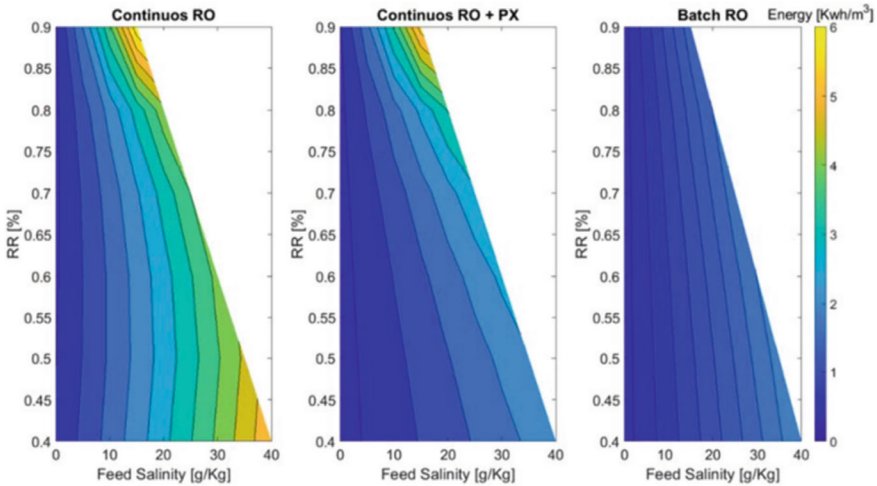


**Fig. 15** Energy consumption of various configuration of reverse osmosis at various recoveries and feed salinity [17]

At initial salinity, continuous RO and continuous RO with pressure exchanger have lower specific energy consumption. Down time of the system is also remarkably decrease with the BRO configuration proposed by Cordoba et al. Reduction in downtime is done due to the reduction in flushing time [17].

#### 4 Discussion on the Summary

BRO is an innovative technology that uses time-varying pressure to reduce thermodynamic losses, resulting in less energy consumption. The BRO treats fixed volume during its stage of operation. It takes a fixed quantity during its stage of operation, treat it, and discharges it. BRO process tackles issues like energy consumption, membrane fouling and scaling, system recovery, higher downtime, high investment cost, etc. The BRO process can achieve a high recovery ratio with lower energy consumption. It can cope with membrane fouling by its process design and avoiding high concentration on membrane surface, increasing the membrane life, and reducing the need for chemical cleaning. BRO system design is simple; it avoids the complex energy recovery device installation and a number of circulation pumps. The system’s simple design makes operating easy and lower maintenance costs. The design of the BRO consists of either a bladder or a double-acting piston–cylinder arrangement. This arrangement helps to attain a time-varying minimum average feed pressure. The earlier design of the BRO has lower productivity with higher downtime; however, with evaluation in BRO design, the productivity is increased, and downtime is decreased. It is also evident that RO has higher capital and maintenance costs. Unlike RO, BRO is a

technology that overcomes the capital and maintenance costs issue with the design evaluation.

BRO has some drawbacks; it requires piston–tank/bladder arrangement to attain the minimum average feed pressure, which may require knowledge to design and manufacture. Also, the start-up time, system depressurization, osmotic backwash during the refill/reset phase, and lower permeate quality are the issues the BRO process encountered. It is also observed with reverse osmosis processes when handling high salinity waters (> 70,000 ppm); it requires osmotic pressure more than the burst pressure of the membrane. In this scenario, an osmotic-assisted or multi-staging process can be utilized.

A methodology part consists of various configurations of BRO by researchers. The significance of reviewing these configurations is to see the potential of the technology towards brine management, energy consumption, and recovery. The various configurations were designed with either a free piston–vessel assembly or a bladder-type arrangement. However, literature and implementation of the free piston-operated BRO system are to a large extent. An earlier design of the BRO configuration uses the thermal energy-driven linkage mechanism to produce the pressure and drive the RO systems. Those configurations have a major problem of steam leakages and system maintenance as it consists of more moving parts. The corrosion in the steam cylinder is also a problem encountered by the researchers. Evaluation in the system design shows the shift from the thermal energy-based driving force to the pump produced driving force. New configurations adopted the free piston containing pressure exchanger assembly to drive the BRO processes. The main advantage of batch processes is that it is a time-varying desalination system that uses minimum average feed pressure for desalination. The pressure gradually increases throughout the cycle, and the peak pressure reaches the end of the cycle. This gives the advantage in terms of energy consumption of the system.

It is evident that very few studies and experiments were conducted on the true batch process listed in Table 2. However, it shows potential to treat brackish water and seawater. It shows an advantage compared to the conventional RO technology in terms of concentration polarization as recirculation happens in the BRO process.

Table 1 consists of various configurations and details of BRO configuration. The highest recovery of 94% is observed with the hybrid batch/semi-batch RO system (HSBRO). Specific energy consumption is one more aspect that has been assessed during this study. This application is the most potential towards minimal/zero liquid discharge. As recovery of this system is higher, so the energy and cost for post-treatment are very low.

The BRO systems experienced higher SEC values like 0.4–0.84 kWh/m<sup>3</sup> at 1000–5000 ppm feed water salinity compared to the theoretically predicted 0.39 kWh/m<sup>3</sup>. This discrepancy occurs due to the assumption of pump efficiency taken as 70% of the high-pressure pump and 50% of the recirculation pump. In actual practice, the pump efficiency lies between 10 and 65%. Another assumption is made for membrane permeability. The assumed permeability of membrane  $A_w$  is 8.32 LMH/bar compared to the experimentally determined 4.4 LMH/bar. It is observed by various researchers that an increase in permeability results in a decrease in SEC.

**Table 2** Summary of various BRO configurations developed by the various researchers

Sr. No.	BRO type	Feed salinity tested (ppm)	Permeate quality (ppm)	Permeate flux (LMH)	Specific energy consumption (kWh/m <sup>3</sup> )	Recovery (%)	Membrane used	References
1	Bladder-type BRO system	35,000 (2000)	– (80)	19.2 (–)	1.97 (–)	50 (52)	Hydranautics ESPA-2514—spiral wound element	[20]
2	DesaLink-based BRO system	4000	320	–	–	70	Dow FILMTEC type BW30-2540	[31]
3	BRO with pressure exchange assembly—free piston type	2000–5000	248–1002	6.9–22.8	0.135–0.337 (hydraulic SEC)	30–70	FilmTec BW30	[33]
4	Power cylinder-operated BRO system	4000	–	–	4–6 (thermal energy used as motive force)	70–76	XLE-2540 (Filmtec)	[32]
5	Free piston-operated BRO system	1000–5000	–	11–22	0.48–0.83	80	FilmTec, Eco Pro-440	[16]
6	Free piston-operated BRO system—hybrid batch/semi-batch operation	500–1500	–	18.9	0.42–0.54	94	Eco Pro-440 membrane element (Dupont) with 41 m <sup>2</sup> active area	[25]

(continued)

Table 2 (continued)

Sr. No.	BRO type	Feed salinity tested (ppm)	Permeate quality (ppm)	Permeate flux (LMH)	Specific energy consumption (kWh/m <sup>3</sup> )	Recovery (%)	Membrane used	References
7	Piston tank configuration double-acting BRO system <sup>a</sup>	35,000	–	15	1.8	50	Membrane with 7.4 m <sup>2</sup> area, Membrane permeability 2 L/(m <sup>2</sup> × h × bar)	[13]
8	Free piston-operated BRO <sup>a</sup>	1000–8000 (30,000–44,000)	–	–	0.395–0.884 (1.923–2.509)	94.1–96.9 (64.0–65.3)	XLE-440 LG-BW440R LG-SW440R	[22]

<sup>a</sup> Indicates the theoretical study carried out by the author

Hosseinipour et al. carried out the various experiments using different salinity, recirculation flow ratio, and at different water flux. They observe the effect of this parameters in hydraulic SEC and electrical SEC. They experimented with 2, 3, 4 and 5000 ppm solution salinity, 1.55, 2.13, 2.73 3.35, and 3.92 recirculation flow ratio and 11, 13.1, 15.1 17.3, 19.3, and 21.2 LMH water fluxes. Observation from the experiment concludes that hydraulic SEC increase with the feed salinity and water fluxes (at 4000 ppm feed water salinity). However, in the case of recirculation flow ratio, there is a minor difference in hydraulic SEC at 4000 ppm feed water salinity. As shown in Fig. 16a, the electrical SEC is higher as salinity increases, and it also indicates that after 2 recirculation flow ratio there is an increment in electrical SEC. Also, authors compared the electrical SEC and hydraulic SEC as shown in Fig. 16b; it indicates that at higher salinity the difference between electrical SEC and hydraulic SEC is smaller. Similar trend also observed that both electrical and hydraulic SEC in increasing with feed salinity and water flux (at 4000 ppm feed water salinity) and smaller increment in SEC were observed with increment in recirculation flow ratio. However, the major contribution in SEC was done by the supply/high-pressure pump during pressurization phase [16]. Hosseinipour et al. also observed that at higher flux the output of the system is also higher. It is a trade-off between electrical SEC and output of the system, e.g. doubling the water flux resulted into 28% higher electrical SEC while the output of the system increases by 74%. Additionally lower flux results into the poor quality of the permeate [16].

It is also observed that the efficiency of the high-pressure pump drops ~ 10% from 60% during the purge and refill phase. Usually, the pump used as high-pressure pumps is positive displacement pumps, which are not optimized to run at lower pressure. However, a combination of a positive displacement pump (for the pressurization phase) and a centrifugal pump (for the purge and refill phase) will be beneficial in terms of energy efficiency. This may increase the capital cost of the system.

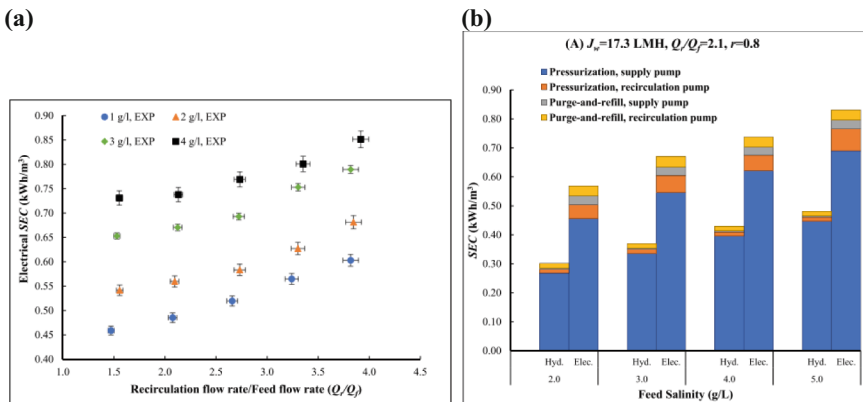


**Fig. 16** a Electrical specific energy consumption at various recirculation flow ratio and b effect of feed salinity on electrical specific energy consumption [16]

For ZLD/MLD applications Hosseinipour et al. showed the hybrid semi-batch/batch reverse osmosis process. They measured the 0.20–0.31 kWh/m<sup>3</sup> and 0.42–0.54 kWh/m<sup>3</sup> hydraulic and electrical SEC at 94% recovery for 500–1500 ppm feed salinity and also obtain 18.9 LMH flux with 17.5 m<sup>3</sup>/day output. They also use feed salinity of 6000 ppm and reaches to the 95% recovery with greater than 120 bar pressure. This data shows that this application has greater potential towards the ZLD/MLD applications [25].

Figure 17 shows the energy consumption of the supply/high-pressure pump and recirculation pump during different stage of the hybrid semi-batch/BRO operation. They compared the electrical SEC for three different salinities of 500, 1000, and 1500 mg/L at recovery of 94% and water flux 23.6 LMH. The significant energy is consumed by the supply pump during the semi-batch pressurization. While the contribution of the recirculation pump is about 10–12% in total electrical SEC [25].

Figure 18a shows the variation of permeate salinity with the time with semi-batch pressurization and batch pressurization at 94% recovery and 21.3 LMH. It depicts that initially permeate quality rises sharply, and after 30 s, it quickly dropped and then rises slowly. The initial peak was observed due to the salt diffusion after the purge and refill mode. During this phase, brine is continuously passes from the membrane, and when pressurization phase starts again, then salty water leaves first before permeate and leads to the initial peak. This initial peak is higher in comparison with the batch reverse osmosis. This initial peak can cause detrimental effect on the overall permeate TDS and rejection of the membrane. The graph (Fig. 18a) shows that permeate conductivity tends to increase in batch pressurization mode. Figure 18b shows the contribution of supply/high-pressure pump and recirculation pump during operation of the system for  $r = 94%$  and  $r = 97.9%$  at 500 mg/L feed salinity. The supply pump contributes 77% and 59% in semi-batch pressurization mode at  $r = 97.9%$  and  $r = 94%$ , respectively. The concentration inside the system

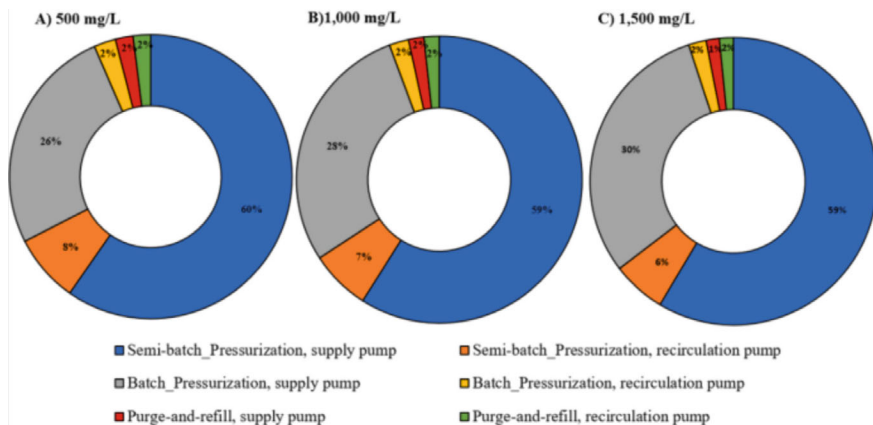
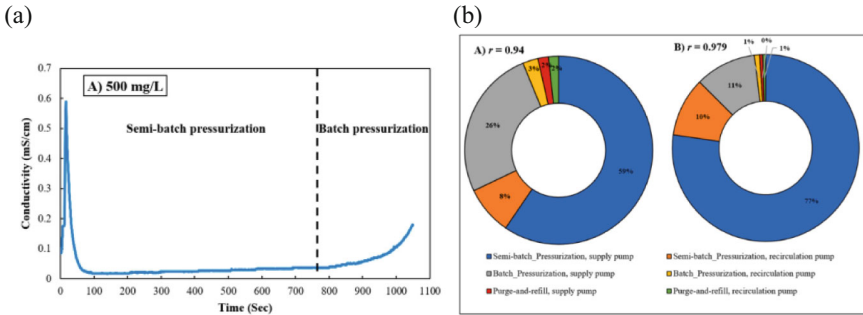


Fig. 17 Breakdown of electrical energy consumption by pump during different phase of operation [25]



**Fig. 18** **a** Permeate conductivity profile over the time for 500 mg/L feed salinity for recovery 90%, and 21.3 LMH water flux and **b** break down of electrical SEC at  $r = 94\%$  and  $r = 97.9\%$  for 500 mg/L and 23.4 LMH water flux [25]

becomes higher at higher recovery, which leads to the higher-pressure requirements and ultimately higher energy contribution from high-pressure pump [25].

**Challenges associated with Batch Reverse Osmosis technology**

To compete with established reverse osmosis (RO) technologies, BRO is a relatively new and difficult technology that has to be developed and optimized. BRO faces various technical challenges to commercialization. The following are the significant reasons why this technology is facing hurdles to reach at TRL 9.

1. Development of the bladder or high-pressure double-acting piston–cylinder arrangement to achieve batch configuration is quite complex in terms of the system’s operation.
2. Improvement on the membrane materials to achieve good performance and durability at higher pressure and salinity.
3. Reduction of the membrane fouling and scaling for the system’s improved performance.
4. Optimization of the system design to achieve a better trade-off between energy consumption, recovery ratio, permeate quality, and production of the system.
5. Scale up the system to a large scale from the pilot-scale prototype and operate this with the integration of the exiting RO plant.

BRO technology gives high recovery in the 70–94% range with energy efficiency with compact and straightforward design arrangements. It consists of fewer components for the simplicity of the design. Despite numerous advantages compared to conventional continuous reverse osmosis systems, it faces several challenges. The studies are carried out on a pilot prototype scale, and future work should focus on the bigger systems with output on the commercial scale. Also, the work should be carried out on the high-pressure test rig for the MLD/ZLD applications. However, higher recovery processes generate a lower amount of brine. It is easy for any consecutive technology to treat the lower volume of brine and utilization the brine as a resource to approach zero liquid discharge. The membrane with high permeability will be the

future focuses in BRO and RO systems. A pump with high efficiency and a combination of a positive displacement pump and centrifugal pump as a supply pump with cost-effectiveness will be the research focal point in the field of BRO. For the BRO systems, reduction of dead volume can be done by minimizing pipe volume, dead volume in RO vessels, and pressure exchange vessel. It is essential to reduce dead volume to attain the desired/designed recovery of the system. Also, refining the valve operations in the BRO system is essential to future research. Fouling on the membrane is not extensively studied for BRO applications. Investigation of the fouling and concentration polarization, optimization of the batch process, detailed cost analysis, and cost optimization will be the future researches in BRO process.

**Acknowledgements** The authors are thankful to the INDIA-H<sub>2</sub>O project by the Department of Biotechnology, Government of India (Project No. BT/IN/EU-WR/40/AM/2018) and the European Union's Horizon 2020 research and innovation programme under grant agreement No. 820906 for funding this research and also thankful to Pandit Deendayal Energy University for providing good environment and necessary infrastructure for the research.

## References

1. Werber JR, Deshmukh A, Elimelech M (2017) Can batch or semi-batch processes save energy in reverse-osmosis desalination? *Desalination* 402:109–122. <https://doi.org/10.1016/j.desal.2016.09.028>
2. Greenlee LF, Lawler DF, Freeman BD, Marrot B, Moulin P (2009) Reverse osmosis desalination: water sources, technology, and today's challenges. *Water Res* 43(9):2317–2348. <https://doi.org/10.1016/j.watres.2009.03.010>
3. Li M (2020) Effects of finite flux and flushing efficacy on specific energy consumption in semi-batch and batch reverse osmosis processes. *Desalination* 496:114646. <https://doi.org/10.1016/j.desal.2020.114646>
4. Elimelech M, Phillip WA (2011) The future of seawater desalination: energy, technology, and the environment. *Science* (80-) 333(6043):712–717. <https://doi.org/10.1126/science.1200488>
5. Chougradi A, Zaviska F, Abed A, Harmand J, Jellal JE, Heran M (2021) Batch reverse osmosis desalination modeling under a time-dependent pressure profile. *Membranes (Basel)* 11(3):1–20. <https://doi.org/10.3390/membranes11030173>
6. Qiu T, Davies PA (2012) Comparison of configurations for high-recovery inland desalination systems. *Water (Switzerland)* 4(3):690–706. <https://doi.org/10.3390/w4030690>
7. Warsinger DM, Tow EW, Nayar KG, Maswadeh LA, Lienhard VJH (2016) Energy efficiency of batch and semi-batch (CCRO) reverse osmosis desalination. *Water Res* 106:272–282. <https://doi.org/10.1016/j.watres.2016.09.029>
8. Mo Z, Li D, She Q (2022) Semi-closed reverse osmosis (SCRO): a concise, flexible, and energy-efficient desalination process. *Desalination* 544. <https://doi.org/10.1016/j.desal.2022.116147>
9. Patel D, Mudgal A, Patel V, Patel J (2021) Water desalination and wastewater reuse using integrated reverse osmosis and forward osmosis system. *IOP Conf Ser Mater Sci Eng* 1146(1):012029. <https://doi.org/10.1088/1757-899x/1146/1/012029>
10. Voutchkov N (2018) Energy use for membrane seawater desalination—current status and trends. *Desalination* 431:2–14. <https://doi.org/10.1016/j.desal.2017.10.033>
11. Wakeel M, Chen B, Hayat T, Alsaedi A, Ahmad B (2016) Energy consumption for water use cycles in different countries: a review. *Appl Energy* 178:868–885. <https://doi.org/10.1016/J.APENERGY.2016.06.114>

12. Kim J, Park K, Yang DR, Hong S (2019) A comprehensive review of energy consumption of seawater reverse osmosis desalination plants. *Appl Energy* 254:113652. <https://doi.org/10.1016/j.apenergy.2019.113652>
13. Cordoba S, Das A, Leon J, Garcia JM, Warsinger DM (2021) Double-acting batch reverse osmosis configuration for best-in-class efficiency and low downtime. *Desalination* 506:114959. <https://doi.org/10.1016/j.desal.2021.114959>
14. Abu H et al (2019) Off-grid desalination for irrigation in the Jordan Valley. *Desalination Water Treat* 168:143–154. <https://doi.org/10.5004/dwt.2019.24567>
15. Park K, Burlace L, Dhakal N, Mudgal A, Stewart NA, Davies PA (2020) Design, modelling and optimisation of a batch reverse osmosis (RO) desalination system using a free piston for brackish water treatment. *Desalination* 494:114625. <https://doi.org/10.1016/j.desal.2020.114625>
16. Hosseini pour E, Park K, Burlace L, Naughton T, Davies PA (2021) A free-piston batch reverse osmosis (RO) system for brackish water desalination: experimental study and model validation. *Desalination* 527:115524. <https://doi.org/10.1016/j.desal.2021.115524>
17. Warsinger DM, Córdoba SP, Das A (2019) Improved batch reverse osmosis configuration for better energy efficiency. In: *IDA 2019 world congress on water reuse and desalination*, Dubai, UAE, 20–24 Oct 2019
18. Das A, Warsinger DM (2021) Batch counterflow reverse osmosis. *Desalination* 507:115008. <https://doi.org/10.1016/j.desal.2021.115008>
19. Swaminathan J, Tow EW, Stover RL, Lienhard JH (2019) Practical aspects of batch RO design for energy-efficient seawater desalination. *Desalination* 470. <https://doi.org/10.1016/j.desal.2019.114097>
20. Wei QJ, Tucker CI, Wu PJ, Trueworthy AM, Tow EW, Lienhard VJH (2020) Impact of salt retention on true batch reverse osmosis energy consumption: experiments and model validation. *Desalination* 479:114177. <https://doi.org/10.1016/j.desal.2019.114177>
21. Burlace L, Davies PA (2022) Fouling and fouling mitigation in batch reverse osmosis: review and outlook. *Desalination Water Treat* 249:1–22. <https://doi.org/10.5004/dwt.2022.28103>
22. Park K et al (2022) Batch reverse osmosis (BRO)-adsorption desalination (AD) hybrid system for multipurpose desalination and minimal liquid discharge. *Desalination* 539:115945. <https://doi.org/10.1016/j.desal.2022.115945>
23. Davenport DM, Wang L, Shalusky E, Elimelech M (2021) Design principles and challenges of bench-scale high-pressure reverse osmosis up to 150 bar. *Desalination* 517:115237. <https://doi.org/10.1016/j.desal.2021.115237>
24. Wang Z, Deshmukh A, Du Y, Elimelech M (2019) Conventional RO stage feed fresh water RO stages hypersaline brine for ZLD / MLD. *Water Res* 115317. <https://doi.org/10.1016/j.watres.2019.115317>
25. Hosseini pour E, Karimi S, Barbe S, Park K, Davies PA (2022) Hybrid semi-batch/batch reverse osmosis (HSBRO) for use in zero liquid discharge (ZLD) applications. *Desalination* 544. <https://doi.org/10.1016/j.desal.2022.116126>
26. Tong T, Elimelech M (2016) The global rise of zero liquid discharge for wastewater management: drivers, technologies, and future directions. *Environ Sci Technol* 50(13):6846–6855. <https://doi.org/10.1021/acs.est.6b01000>
27. Wang Z, Deshmukh A, Du Y, Elimelech M (2020) Minimal and zero liquid discharge with reverse osmosis using low-salt-rejection membranes. *Water Res* 170(203):1–24. <https://doi.org/10.1016/j.watres.2019.115317>
28. Schwantes R, Chavan K, Winter D, Felsmann C, Pfaffert J (2018) Techno-economic comparison of membrane distillation and MVC in a zero liquid discharge application. *Desalination* 428:50–68. <https://doi.org/10.1016/j.desal.2017.11.026>
29. Yusuf A et al (2020) A review of emerging trends in membrane science and technology for sustainable water treatment. *J Clean Prod* 266:121867. <https://doi.org/10.1016/j.jclepro.2020.121867>
30. Qiu TY, Davies PA (2015) Concentration polarization model of spiral-wound membrane modules with application to batch-mode RO desalination of brackish water. *Desalination* 368:36–47. <https://doi.org/10.1016/j.desal.2014.12.048>

31. Qiu TY, Igobo ON, Davies PA (2013) DesaLink: solar powered desalination of brackish ground-water giving high output and high recovery. *Desalin Water Treat* 51(4–6):1279–1289. <https://doi.org/10.1080/19443994.2012.714604>
32. Mudgal A, Davies PA (2016) A cost-effective steam-driven RO plant for brackish groundwater. *Desalination* 385:167–177. <https://doi.org/10.1016/j.desal.2016.02.022>
33. Davies PA, Wayman J, Alatta C, Nguyen K, Orfi J (2016) A desalination system with efficiency approaching the theoretical limits. *Desalin Water Treat* 57(48–49):23206–23216. <https://doi.org/10.1080/19443994.2016.1180482>
34. Wayman J, Davies P (2015) Brackish ground water desalination using solar reverse osmosis. MEng Diss. <https://doi.org/10.13140/RG.2.1.1256.6881>
35. Davies PA, Khatoon F (2016) Double-acting batch-RO system for desalination of brackish water with high efficiency and high recovery Double-acting batch-RO system for desalination of brackish water with high efficiency and high recovery
36. Valley J, Davies PA (2018) Performance analysis and optimisation of a saline groundwater batch reverse osmosis desalination system for irrigation and education in the Jordan Valley. Academic Advisor. <https://doi.org/10.13140/RG.2.2.31624.16643>
37. Park K, Davies PA (2021) A compact hybrid batch/semi-batch reverse osmosis (HBSRO) system for high-recovery, low-energy desalination. *Desalination* 504:114976. <https://doi.org/10.1016/j.desal.2021.114976>

# Breaking of Butyric Acid–Water Azeotrope: Experimental Analysis on Air Gap Membrane Distillation



Rajeshwar Kholapure, Kailash Singh, Sushant Upadhyaya, and Divya Gaur

## 1 Introduction

Air gap membrane distillation (AGMD) is a thermally driven separation process. In AGMD, a vapour pressure gradient (driving force) is established across the membrane due to the temperature difference between the two sides of the hydrophobic microporous membrane. The hydrophobic property of the membrane prevents liquid while allowing vapour to travel through [1]. In the present work, the applicability of the AGMD technique has been experimentally researched for the breaking of the butyric acid–water azeotrope (18.4 wt% of butyric acid). Several methods, such as azeotropic distillation [2], extractive distillation [3], capillary distillation [4], pervaporation [5], and diffusion distillation [6], were used for the breaking of azeotrope. The disadvantages of these technologies include high energy consumption and the recovery of essential components. The AGMD methodology has significant advantages over the conventional approach to azeotrope breaking [7–10]. The theory behind the AGMD process is that the diffusivity of different components in the air plays an essential role in breaking azeotropes. To break the butyric acid/water azeotrope, an AGMD element with a 0.22 m pore size and 175 m thickness of polytetrafluoroethylene (PTFE) flat sheet membrane was used in this experimental study. It was observed that the butyric acid selectivity in the permeate was less than one, indicating a higher butyric acid concentration in the retentate relative to the permeate. The AGMD method is utilized in a variety of commercial applications, including desalination [11, 12], volatile organic component (VOC) separation [13], food industries [14], and azeotropic separation [8]. The butyric acid forms an azeotrope with water at 18.4 wt% of butyric acid. Butyric acid has a boiling temperature of 165.5 °C, while an azeotropic mixture of butyric acid and water has a boiling point of 99.94 °C.

---

R. Kholapure (✉) · K. Singh · S. Upadhyaya · D. Gaur  
Department of Chemical Engineering, Malaviya National Institute of Technology, Jaipur 302017, India  
e-mail: [rajesh31gp@gmail.com](mailto:rajesh31gp@gmail.com)

**Table 1** Operating parameters used for the experimental study

Process parameter	Value
Temperature of feed solution	60 °C
Flow rate of feed solution	1–5 L/min
Temperature of cooling water	10 °C
Flow rate of cooling water	2–5 L/min
Air gap width	3–7 mm

Butyric acid/water mixtures form the minimum boiling azeotrope. Butyric acid is an important chemical that is used in a variety of sectors, including chemical, food, beverage, pharmaceutical, polymer, paint, cosmetics, and perfume. The operating parameters used for the experimental study are shown in Table 1.

Based on existing research work, very few experimental studies have been completed in the field of azeotropes separation by using the AGMD process. The separation of propionic acid–water [7], hydrochloric acid–water [7, 8], and formic acid–water [9] azeotropic mixture by using the AGMD process has been studied in the literature. However, no research has been seen in the literature for breaking the azeotropic mixture of butyric acid/water by using AGMD so far to the best of my knowledge.

## 2 Experimental

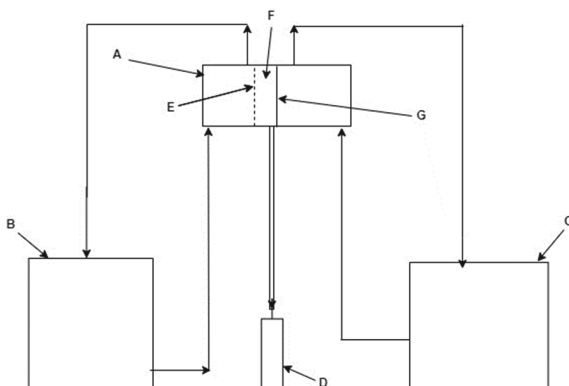
### 2.1 Membrane and Feed Solution Used for the Experimental Study

For the experimental work, an AGMD element with 0.22  $\mu\text{m}$  pore size, 150  $\mu\text{m}$  thickness, 85% porosity, and a 55 mm diameter of microporous hydrophobic polytetrafluoroethylene (PTFE) flat sheet membrane was used. The thermal conductivity of the membrane used for the study is 0.28 W/m K. Butyric acid and distilled water were used to prepare an azeotropic feed solution with a butyric acid concentration of 18.4 wt%. The acid–base titration method was used to estimate the concentration of butyric acid in permeate and retentate. Sodium hydroxide solution and phenolphthalein indicator were the titrant and indicator used for the acid–base titration.

### 2.2 AGMD Experimental System

The AGMD configuration used for the investigation is depicted in Fig. 1. The setup consists of the feed portion, the air gap/permeate section, and the cooling section.

**Fig. 1** Schematic diagram of AGMD experimental setup. A—AGMD module, B—Feed tank, C—Water chiller, D—Permeate receiver, E—Membrane, F—Air gap, G—Cooling plate



The feed section and air gap section, and the air gap section and cooling section, are separated by the hydrophobic membrane and condensing plate, respectively. The desired temperature of the feed solution was continuously circulated to the feed section by a pump. Similarly, the cooling water was constantly recirculated to the cooling section. Butyric acid and water vapours condensed on the condensing plate after passing through the membrane and air gap. The glass receiver was used to catch the permeate.

### 3 Results and Discussion

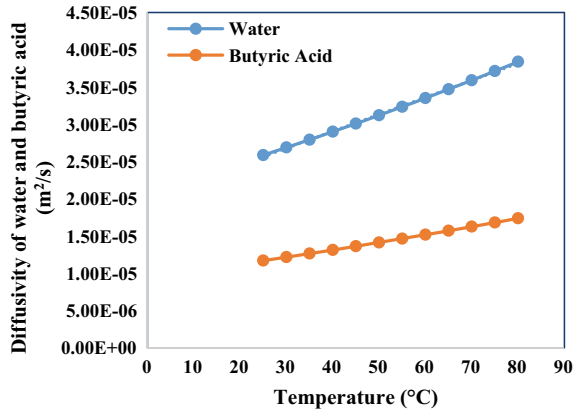
#### 3.1 Diffusivity of Butyric Acid and Water in Air with Temperature

Figure 2 demonstrates that as feed bulk temperature increased from 25 to 80 °C, the diffusivity of butyric acid and water air increased linearly. Figure 2 shows that the diffusivity of water in the air is greater than the diffusivity of butyric acid in the air. The following equation has been developed from a combination of kinetic theory and corresponding state arguments for predicting the diffusivity of water and butyric acid in air at low pressure [15].

$$\frac{PD_{AB}}{(P_{CA}P_{CB})^{\frac{1}{3}}(T_{CA}T_{CB})^{\frac{5}{12}}\left(\frac{1}{M_A} + \frac{1}{M_B}\right)^{\frac{1}{2}}} = a\left(\frac{T}{\sqrt{(T_{CA}T_{CB})}}\right)^b$$

For pair consisting of water and non-polar gas ( $a = 3.640 \times (10)^{-4}$ ,  $b = 2.334$ ).

**Fig. 2** Effect of bulk feed temperature on diffusivity of water and butyric acid



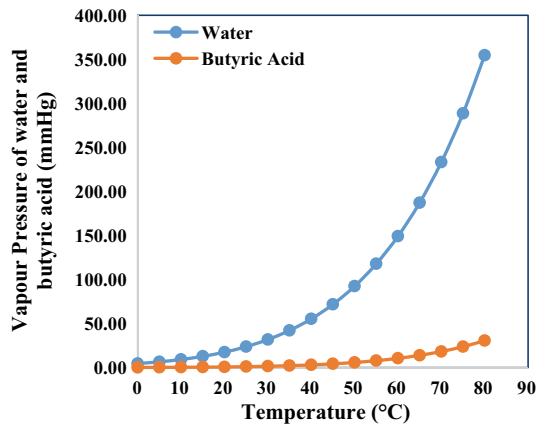
### 3.2 Vapour Pressure of Water and Butyric Acid with Temperature

Figure 3 shows that when the temperature increases from 0 to 80 °C, the vapour pressure of water and butyric acid increases exponentially. Figure 3 shows that the vapour pressure of water is greater than that of butyric acid. This is mainly due to the fact that butyric acid has a lower boiling point than water. The vapour pressure of water and butyric acid was determined using the Antoine equation, which is shown below.

$$\log_{10}(P) = A - \frac{B}{C + T}$$

Here,  $P$  is the vapour pressure in mmHg, and  $T$  is the temperature in °K

**Fig. 3** Effect of bulk feed temperature on vapour pressures of water and butyric acid



### 3.3 *Effect of Process Parameters*

Several experiments were carried out to separate butyric acid–water azeotropic feed mixtures. The effect of operating variables such as feed flow rate and cooling water flow rate on combined permeate flux, butyric acid selectivity, and permeate and retentate butyric acid concentration was experimentally examined.

In my research, I utilized a fabricated setup for air gap membrane distillation. This method utilized air gap rings with dimensions of 3, 5, 7, 9, and 11 mm. Out of the available options, I have selected air gap rings with measurements of 3, 7, and 11 mm. The influence of feed flow rate on flux is significant when the air gap width is small. However, when the air gap increases, the impact of flow rate on permeate flux becomes negligible. As the width of the air gap increases, both the permeate flux and the selectivity in the permeate decrease. This is primarily due to the fact that mass transfer resistance increases as the air gap width increases. The presence of an air gap leads to a decrease in heat loss through conduction, as air is considered to be stagnant and functions as an insulator.

#### 3.3.1 **Effect of Feed Flow Rate**

Figures 4 and 5 show the effect of feed flow rate on total permeate flux and selectivity for different air gap widths while keeping all other parameters constant, such as feed temperature at 60 °C, cooling water temperature at 10 °C, and cooling water flow rate at 1 L/min. It can be noted that at azeotrope feed concentration, the total permeate flux and selectivity of butyric acid in permeate increased with increasing feed flow rate from 1 to 5 L/min. The phenomenon is mostly due to thermal boundary layer shrinkage, which results in a rise in Reynolds number at small air gap widths. The high Reynolds number causes turbulence, which lowers the butyric acid diffusional resistance through the membrane by lowering the interfacial butyric acid concentration. It can be shown that at the smallest air gap, the influence of feed flow rate on permeate flux predominates; however, as air gap width increases, the influence of feed flow rate decreases. Additionally, as the feed flow rate is increased, butyric acid's selectivity increases. As a result, the concentration of butyric acid increases in the permeate while it is nearly constant in the retentate, as illustrated in Figs. 6 and 7.

#### 3.3.2 **Effect of Cooling Water Flow Rate**

By changing cooling water flow rate from 2 to 6 L/min, feed temperature to 60 °C, feed flow rate 1 L/min, and cooling water temperature to 10 °C, the effect of cooling water flow rate on permeate flux and selectivity was investigated. As illustrated in Figs. 8 and 9, the total permeate flux and selectivity were not significantly affected by increasing the cooling water flow rate from 2 to 6 L/min. This is because the air gap

**Fig. 4** Effect of feed flow rate on total permeate flux at different air gap width (bulk feed temperature = 60 °C, cooling water temperature = 10 °C, and cooling water flow rate = 1 L/min)

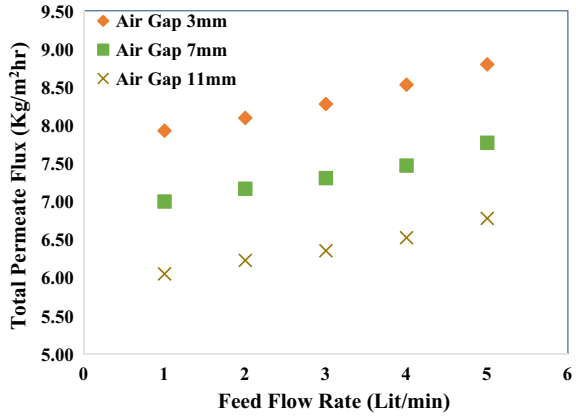


**Fig. 5** Effect of feed flow rate on selectivity of butyric acid at different air gap width (bulk feed temperature = 60 °C, cooling water temperature = 10 °C, and cooling water flow rate = 1 L/min)

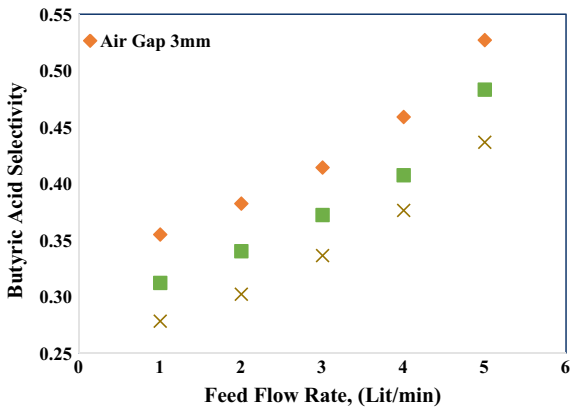


**Fig. 6** Effect of feed flow rate on concentration of butyric acid in permeate at different air gap width (feed temperature = 60 °C, coolant temperature = 10 °C, and coolant flow rate = 1 L/min)

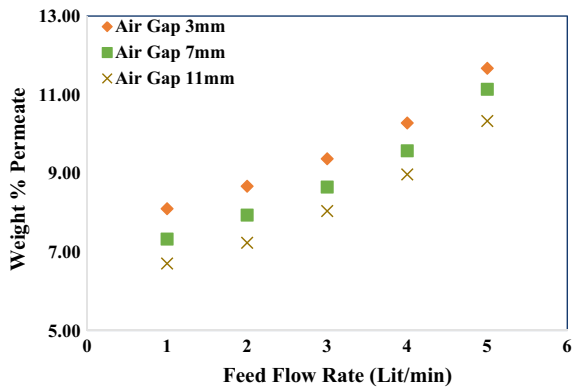
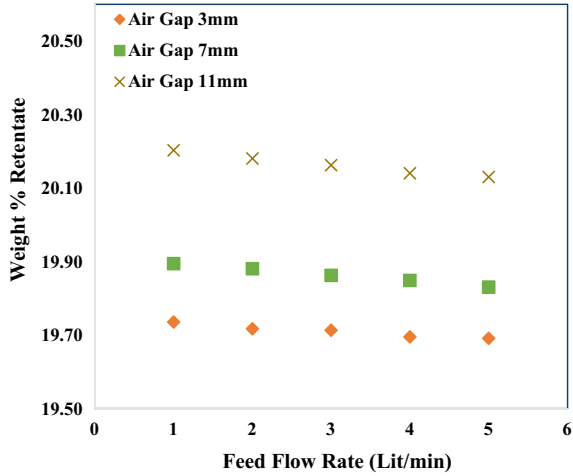


**Fig. 7** Effect of feed flow rate on concentration of butyric acid in retentate at different air gap width (bulk feed temperature = 60 °C, cooling water temperature = 10 °C, and cooling water flow rate = 1 L/min)



heat transfer coefficient, which is much smaller than the heat transfer coefficient on the hot side and the heat transfer coefficient on the cold side, dominates the overall heat transfer coefficient. A second reason is the small length of the AGMD module, which keeps inlet and outlet temperatures of the cooling water almost equal. As depicted in Figs. 10 and 11, there was a negligible change in permeate concentration and no change in retentate concentration when the cooling water flow rate was increased from 2 to 6 L/min. Due to the minimal effect of cooling water flow rate on permeate flux and selectivity, relatively few experimental studies have been carried out in this area.

**Fig. 8** Effect of cooling water flow rate on total permeate flux at different air gap width (bulk feed temperature = 60 °C, cooling water temperature = 10 °C, and feed flow rate = 1 L/min)

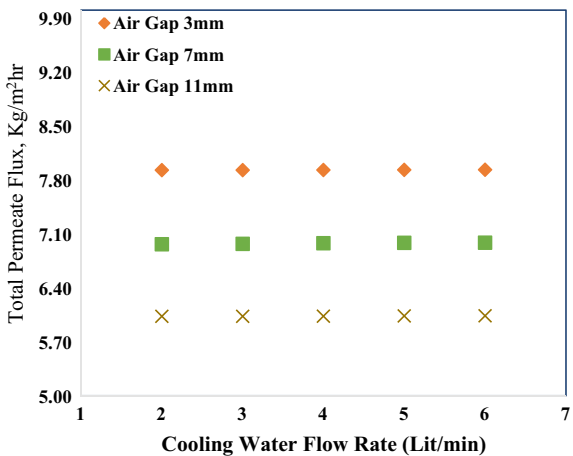


**Fig. 9** Effect of cooling water temperature on butyric acid selectivity for different air gap widths (bulk feed temperature = 60 °C, cooling water temperature = 10 °C, and feed flow rate = 1 L/min)

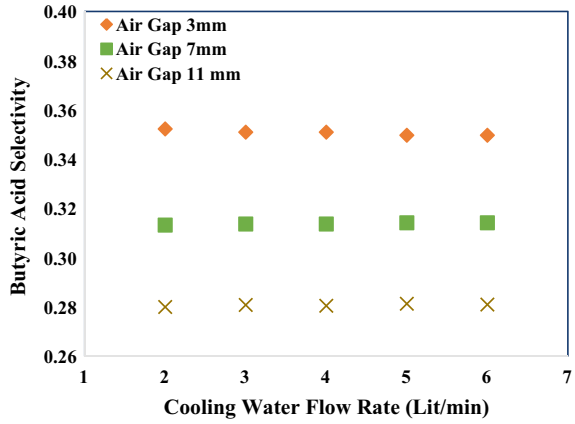


**Fig. 10** Effect of cooling water flow rate on concentration of butyric acid in permeate at different air gap width (feed temperature = 60 °C, cooling water temperature = 10 °C, and feed flow rate = 1 L/min)

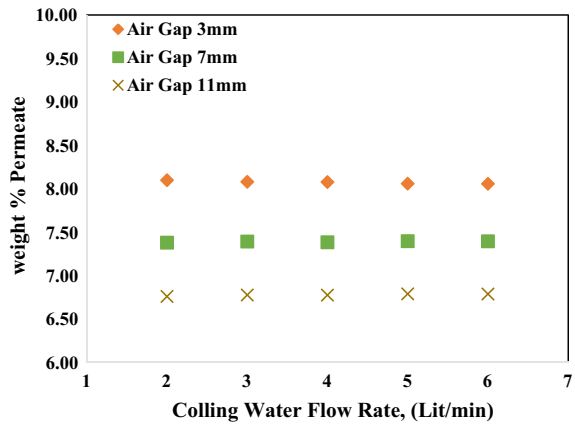
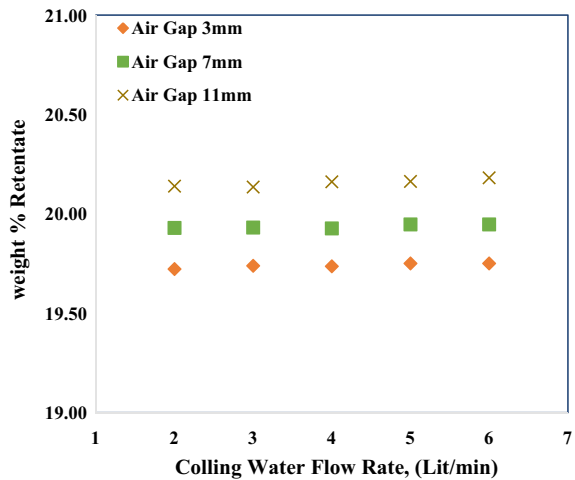


**Fig. 11** Effect of cooling water flow rate on concentration of butyric acid in retentate at different air gap width (bulk feed temperature = 60 °C, cooling water temperature = 10 °C, and feed flow rate = 1 L/min)



## 4 Conclusions

The effect of operating parameters such as feed flow rate and cooling water flow rate on flux, selectivity, and concentration of butyric acid in the retentate and permeate was determined. The following conclusions can be drawn from experimental results:

- The experimental results demonstrate that the total permeate flux increases from 7.93 to 8.80 kg/m<sup>2</sup>h and the butyric acid selectivity increases from 0.35 to 0.53 as the feed flow rate increases from 1 to 5 L/min at a 3 mm air gap thickness. In addition, as the feed flow rate increases from 1 to 5 L/min at a 3 mm air gap thickness, the concentration of butyric acid in permeate increases from 8.09 to 11.67 wt%, while the concentration of butyric acid in retentate declines from 19.74 to 19.69. The concentration of butyric acid in the permeate and retentate was determined by acid–base titration.
- The experimental results demonstrate that the total permeate flux was slightly increased from 7.92 to 7.93 kg/m<sup>2</sup>h and the butyric acid selectivity was constant at 0.35 as the cooling water flow rate increased from 2 to 6 L/min at a 3 mm air gap thickness. In addition, as the cooling water flow rate increases from 2 to 6 L/min at a 3 mm air gap thickness, the concentration of butyric acid in permeate is sharply decreased from 8.10 to 8.05 wt%, while the concentration of butyric acid in retentate is slightly increased from 19.72 to 19.75. From these experimental results, it was concluded that the total permeate flux, selectivity, and concentration of butyric acid in permeate and retentate were not significantly affected by increasing the cooling water flow rate from 2 to 6 L/min.
- The membrane selectivity of butyric acid in permeate was observed to be less than one, indicating that a lower concentration of butyric acid was achieved in permeate than in retentate.
- The results of the experiment indicate that the butyric acid–water azeotrope breaks in both the permeate and the retentate. Thus, it is concluded that there is a strong possibility of employing the AGMD technique for azeotropic mixture separation.

## 5 Scope for Future Work

An intriguing prospect lies in assessing the viability and effectiveness of the AGMD process for separating various aqueous azeotropic mixtures, such as benzyl alcohol/water, and phenol/water. Additionally, it is essential to analyse the impact of various operational factors, including bulk feed temperature, cooling water flow rate, air gap thickness, as well as membrane parameters like membrane thickness, membrane porosity, pore size, and thermal conductivity, on the azeotrope breaking point and selectivity.

## References

1. Kimura S, Nakao SI, Shimatani SI (1987) Transport phenomena in membrane distillation. *J Memb Sci* 33:285–298. [https://doi.org/10.1016/S0376-7388\(00\)80286-0](https://doi.org/10.1016/S0376-7388(00)80286-0)
2. Shan B, Niu C, Meng D, Zhao Q, Ma Y, Wang Y, Zhang F, Zhu Z (2021) Control of the azeotropic distillation process for separation of acetonitrile and water with and without heat integration. *Chem Eng Process Process Intensif* 165:108451. <https://doi.org/10.1016/j.cep.2021.108451>
3. Li R, Meng X, Liu X, Gao J, Xu D, Wang Y (2019) Separation of azeotropic mixture (2, 2, 3, 3-tetrafluoro-1-propanol + water) by extractive distillation: entrainers selection and vapour-liquid equilibrium measurements. *J Chem Thermodyn* 138:205–210. <https://doi.org/10.1016/j.jct.2019.06.026>
4. Yeh GC, Yeh BV, Ratigan BJ, Correnti SJ, Yeh MS, Pitakowski DW, Fleming W, Ritz DB, Lariviere JA (1991) Separation of liquid mixtures by capillary distillation. *Desalination* 81(1–3):129–160
5. Kanse NG, Dawande SD (2017) Separation of ethanol/water (azeotropic mixture) by pervaporation using PVA membrane. [www.sciencedirect.com/www.materialstoday.com/proceedings214-7853](http://www.sciencedirect.com/www.materialstoday.com/proceedings214-7853)
6. Fullarton D, Schlünder EU (1986) Diffusion distillation—a new separation process for azeotropic mixtures part II: dehydration of isopropanol by diffusion distillation. *Chem Eng Process Process Intensif* 20(5):265–270
7. Udriot H, Araque A, Von Stockar U (1994) Azeotropic mixtures may be broken by membrane distillation. *Chem Eng J Biochem Eng J* 54(2):87–93
8. Kalla S, Upadhyaya S, Singh K, Baghel R (2019) Experimental and mathematical study of air gap membrane distillation for aqueous HCl azeotropic separation. *J Chem Technol Biotechnol* 94:63–78. <https://doi.org/10.1002/jctb.5766>
9. Banat FA, Al-Rub FA, Jumah R, Shannag M (1999) Theoretical investigation of membrane distillation role in breaking the formic acid-water azeotropic point: comparison between Fickian and Stefan-Maxwell-based models. *Int Commun Heat Mass Transf* 26:879–888. [https://doi.org/10.1016/S0735-1933\(99\)00076-7](https://doi.org/10.1016/S0735-1933(99)00076-7)
10. Banat FA, Abu Al-Rub F, Jumah R, Shannag M (1999) On the effect of inert gases in breaking the formic acid-water azeotrope by gas-gap membrane distillation. *Chem Eng J* 73:37–42. [https://doi.org/10.1016/S1385-8947\(99\)00014-5](https://doi.org/10.1016/S1385-8947(99)00014-5)
11. Baig U, Azeem MA, Lawal DU, Al Abdulgader H, Baroud TN (2022) Facile and scalable fabrication of superhydrophobic PVDF membrane for the desalination of highly saline water using air-gap membrane distillation system. *J Environ Chem Eng* 10:109025. <https://doi.org/10.1016/j.jece.2022.109025>
12. Rosalam S, Chiam CK, Widyaparamitha S, Chang YW, Lee CA (2016) Water desalination by air-gap membrane distillation using meltblown polypropylene nanofiber membrane. *IOP Conf Ser Earth Environ Sci* 36:012032. <https://doi.org/10.1088/1755-1315/36/1/012032>
13. Loulergue P, Balannec B, Fouchard-Le Graët L, Cabrol A, Sayed W, Djelal H, Amrane A, Szymczyk A (2019) Air-gap membrane distillation for the separation of bioethanol from algal-based fermentation broth. *Sep Purif Technol* 213:255–263. <https://doi.org/10.1016/j.seppur.2018.12.047>
14. Izquierdo-Gil MA, García-Payo MC, Fernández-Pineda C (1999) Air gap membrane distillation of sucrose aqueous solutions. *J Membr Sci* 155(2):291–307
15. Byron Bird LLR, Stewart WE (2001) *Transport phenomena*, 2nd edn. Wiley, New York

# Life Cycle Assessment of Electrocoagulation Pilot Unit for Dairy Wastewater Treatment



Dipak Ankoliya , Milan Raninga , Dhaval Patel , Varsha Mudgal ,  
Prashanthi Vallamsetty, Anurag Mudgal , Manish Kumar Sinha ,  
Vivek K. Patel , Jatin Patel, Himanshu Choksi, and Prasanta Dey

## 1 Introduction

The dairy industry is water-intensive and generates large volume of wastewater. From our previous study of many Indian dairy wastewater characterization shows that wastewater from dairy has highly organic content, suspended solid, and wide pH variation [1]. Serious environment impact can occur if these wastewaters are discharged without proper treatment or without being treated. The consequences like rapid reduction of oxygen level dissolved in the water bodies where the wastewater would have discharged and lead to the destruction of aquatic life and in turn damage the environment [2].

The dairy industry normally used the conventional biological treatment plant (effluent treatment plant) to reduce the contamination of water under the discharge norms, and treated effluent is discharged in open water bodies after conventional treatment. There are two methods for biological treatment process which are aerobic and anaerobic. In aerobic treatment, the aeration is provided to add oxygen in water while anaerobic treatment occurs in absence of oxygen. Aerobic biological processes are high energy intensive, whereas anaerobic treatment of dairy wastewater reflects very poor nutrient removal, and effluents treated by anaerobic biological processes

---

D. Ankoliya (✉) · M. Raninga · D. Patel · V. Mudgal · A. Mudgal · M. K. Sinha · V. K. Patel ·  
J. Patel · H. Choksi  
Pandit Deendayal Energy University, Gandhinagar, Gujarat, India  
e-mail: [dipak.aphd20@sot.pdpu.ac.in](mailto:dipak.aphd20@sot.pdpu.ac.in)

A. Mudgal  
e-mail: [anurag.mudgal@sot.pdpu.ac.in](mailto:anurag.mudgal@sot.pdpu.ac.in)

P. Vallamsetty  
GITAM Deemed To Be University, Visakhapatnam, Andhra Pradesh, India

P. Dey  
Aston Business School, Aston University, Birmingham, UK

need additional treatment [3]. Aerobic process is used for low chemical oxygen demand (COD) value lower than 1000 mg/L while anaerobic process is suitable for higher COD value more than 4000 mg/L [4].

The life cycle assessment (LCA) is the tool which can provide how the wastewater treatment system is affected to environment in different impact categories [5]. This tool is widely used to assess the wastewater treatment [6, 7] and to improve its operation by comparing different alternative systems, designing new technologies or applying nutrient recovery methods [8].

In dairy industry, the conventional biological wastewater treatment plant is commonly running to treat wastewater. These plants have bacterial degradation process to decompose the wastewater contaminants. Some researchers have studied the EI of this conventional process for dairy industry. Stanchev et al. [9] studied the anaerobic reactor dairy wastewater treatment (aimed for circular economy) and found that it can reduce 13% of carbon footprint via energy generation compared to baseline method of directly discharging wastewater into the environment. Paulu et al. [10] studied the conventional WWTP and two modifications for LCA and found that global warming potential (GWP), eutrophication potential (EP), and marine aquatic ecotoxicity potential (MAETP) were the main impact categories.

There are some studies of alternative methods to the conventional dairy wastewater treatment to show improvement of environmental impact benefit; for example, Behjat et al. [11] showed that phosphorous recovery technologies have lower GWP and cumulative energy demand than conventional wastewater treatment. Elginöz et al. [12] studied LCA of volatile fatty acid production in anaerobic reactor of dairy wastewater treatment.

The electrocoagulation (EC) is becoming alternative to the wastewater treatment solution having high organic load, and its application in dairy wastewater is widely studied [13]. EC process has design benefit of small footprint, flexible operation, less treatment time, and odorless operation [14]. In addition, EC requires less chemicals and produces less sludge with less toxicity than the chemical coagulation process [15]. Safwat et al. [16] studied the operation phase LCA of EC system having Ti electrode for the Mn removal from the wastewater. They used ReCiPe 2016 midpoint (H) method in openLCA 1.11 software and Environmental Footprints (EF) and European Reference Life Cycle (ELCD) databases. They observed that global warming, human non-carcinogenic toxicity, and terrestrial ecotoxicity were the major environmental impact categories.

Pushpraj Patel et al. studied the adsorption and EC process to treat the greywater and found that EC process has eight times less environmental impact than the adsorption process [17]. They used CML 2001 and TRACI 2.1 methods in GaBi software for application phase of EC process in greywater treatment. Alvarez, Maria-Dolores, et al. studied the operation phase of EC-UV process in dyeing textile water to provide alternative to the existing highly environment impactful tertiary treatment [18]. They used ReCiPe (H) v1.06 midpoint and endpoint method in Simapro 7.3.3 and Ecoinvent database v3.1. Ahangarnokolaei, Mohammad Ali, et al. used Simapro 9.1.0.8 and Ecoinvent v3.3 for LCA study of the construction, operation, and destruction phase of EC and ozonation processes [19]. They showed that standalone EC process using iron or aluminum electrode is comparatively more environment friendly in textile

wastewater treatment. They considered only reactor and polymer for the construction phase analysis of EC process.

In this study, the LCA of EC pilot unit is carried out for the construction phase of system in openLCA software using Ecoinvent database. The size of EC system is of pilot scale which is capable of treating dairy wastewater at 500 L per hour. The CML 2001 and ReCiPe Midpoint (H) method is used to analyze the environmental impact of the equipment, and processes are used to develop the pilot scale EC unit. The land occupation is not considered in this study. Major previous study is focused for the operation stage of EC process in various wastewater, and only few studies cover the construction phase but only consider reactor or electrode. In this study, equipments of tank, stirrer, reactor, pump, motor, piping, electrical wiring, control panel, and structural steel are included for detailed analysis of EC unit construction phase. Also, the upstream processes are included in the inventory of analysis.

## **2 LCA Methodology for Electrocoagulation Process**

### ***2.1 Goal, Scope, and System Boundaries***

The goal of this study is to do life cycle assessment (LCA) of the manufacturing of electrocoagulation pilot setup having 500 L per hour of dairy wastewater treatment capacity. The scope of this study includes the construction phase of EC process including manufacturing and installation of setup having equipments like various tank, electric motor, pump, stirrer, support structure, wiring, and piping. Here, the manufacturing process of each equipment is considered from the starting of raw material production like steel, copper, or plastic production. The dataset is taken from the manufacturer of EC unit which is installed under center of excellence in water in university. The system boundary also includes the all equipment purchased, fabricated, and assembled at vendor's site, and then, whole setup is transported and installed at university. Figure 1 shows the scope and system boundary of the product system considered in this study.

### ***2.2 Functional Unit (FU) and Allocation Method***

The functional unit for this study would remain as the treatment of 1 m<sup>3</sup> of dairy wastewater from an initial COD value of 5600 mg/L to a final COD value of 100 mg/L using the electrocoagulation process with aluminum electrodes. The allocation method used in this study would be mass-based allocation. The mass-based allocation method would be used to allocate the environmental impacts of all inputs and outputs based on their mass proportion. In addition, the equipment inventory would be allocated based on their lifetime, with an assumption that the equipment would

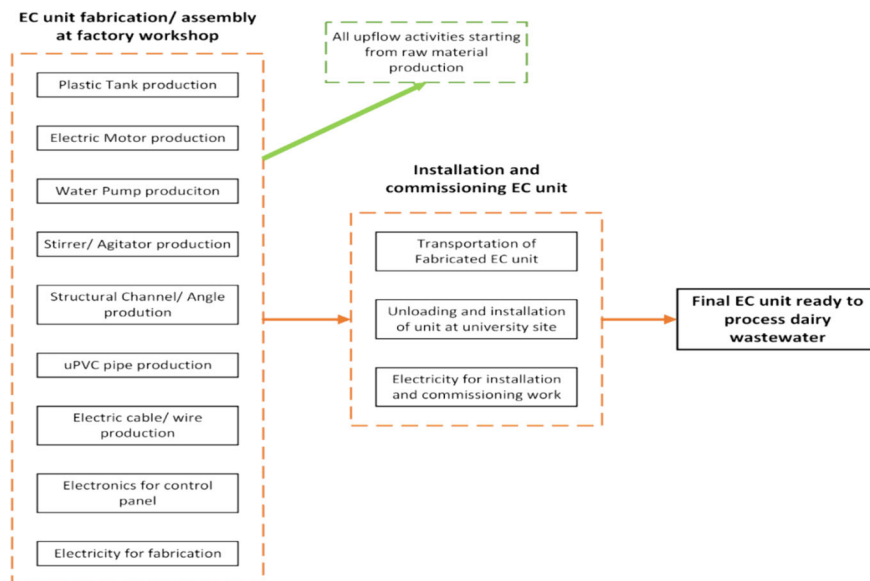


**Fig. 1** Schematic representation of the system boundary for electrocoagulation system

last for 20 years. The allocation would be based on a time-averaged allocation, which assigns the environmental impacts of equipment based on their lifespan.

Overall, the LCA study would provide a comprehensive analysis of the environmental impacts associated with the electrocoagulation process for COD removal from dairy wastewater, taking into account all relevant inputs and outputs and the inventory of the equipments used.

### 2.3 Life Cycle Inventory of EC Process Manufacturing

In this study, the inventory involved in manufacturing and installation of EC system is gathered, and accordingly, processes are created in LCA software. Here, the openLCA 1.11 software and Ecoinvent v3.7.1 database were used to assess the environmental impact assessment. The fabrication and assembly data are gathered from the supplier of this EC system. The main components of the EC system include the mixing tank, stirrer with motor, EC reactor tank, clarifier tank, and water pump with motor. These components are required at the fabrication workshop to fabricate and develop complete EC pilot plant along with the raw material for fabrication of supporting structure, piping, and electric wiring work. The main components of the EC unit and its production, fabrication, or assembly sequence along with the energy input and transportation required for installation of unit are shown in Fig. 2.

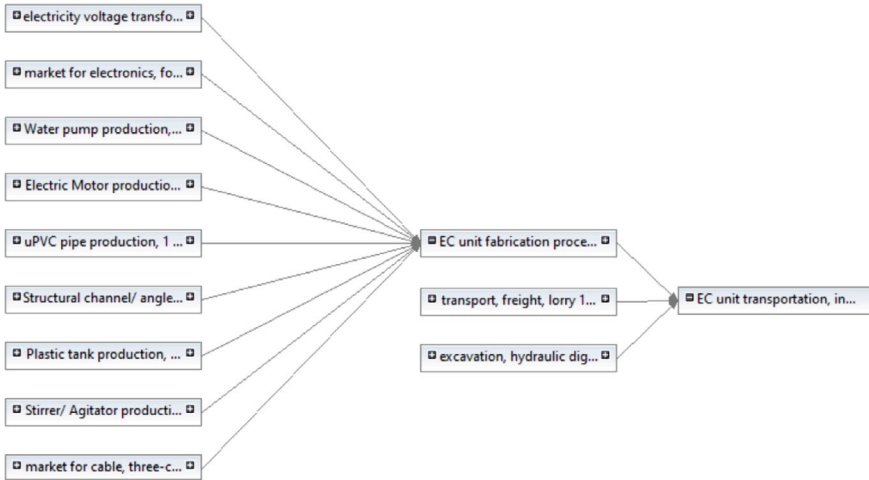


**Fig. 2** Model graph of the EC system manufacturing

Here some components are directly purchased from the local market by the supplier to assemble whole EC plant, so to get the environmental impact of the up-flow processes of these readymade components, the new processes are created for these components in openLCA based on the data available in software. The input and output (inventory) of these components are shown in Table 1.

All the product manufacturing process requires basic inputs of energy (in terms of electricity) and transportation (to reach market of product). The basic metal material of steel and copper are required in motor, pump, and stirrer product manufacturing while tank and pipe manufacturing require plastic as a basic raw material. Structural steel channel requires only steel and its working process as input. The input quantity is adapted from the existing similar product manufacturing process available in openLCA software and scaled data as per the required capacity. Also, the capacity for the process development in openLCA for all the equipment is taken standard of 1 kW for motor and pump, the 1000 L volume for tank and stirrer, 1 m for PVC pipe, and 1 kg for structural channel production. The required capacity or quantity of equipment is taken for the EC system manufacturing process as per the requirement as shown in the case study and operating principle description.

### 2.4 Case Study Description

Figure 3 illustrates the flow of the electrocoagulation process to treat the wastewater which includes the main components of mixing tank with stirrer, reactor chamber with electrode and settling tank. The wastewater first will be introduced inside the mixing tank where the pH and conductivity are adjusted to the desire value for the

**Table 1** Treated dairy wastewater characterization from some Indian dairy industry

Process created in LCA for component production	Quantity	Unit	Ecoinvent flow and provider	
<b>Plastic tank production</b>				
Input	Polymer	130	kg	HDPE, granulate/Market/APOS, U-GLO
	Additive	1	kg	Carbon black/Market/APOS, U-GLO
	Stabilizer and antioxidant	2	kg	Tris(2,4-ditert-butylphenyl) phosphite/Market/APOS, U-GLO
	Lubricant	1	kg	Lubricating oil/Market/APOS, U-RoW
	Energy	150	kWh	Electricity, low voltage/transformation from medium to low voltage/APOS, U-IN-Western grid
	Transport	126*500	kg*km	Freight, lorry 16–32 t, EURO4/Transport/APOS, U-RoW
Output	Plastic tank	1	m <sup>3</sup>	
	Waste plastic, mixture	8	kg	Market/APOS, U-IN
<b>Electric motor production, 1 kW</b>				
Input	Copper	3	kg	Copper, cathode
	Wire drawing	3	kg	Wire drawing, copper
	Steel	12	kg	Steel, low-alloyed, hot rolled
	Magnet	0.8	kg	Permanent magnet, for electric motor
	Plastic	2	kg	Polyphenylene sulfide
	Lubricant	0.7	kg	Lubricating oil
	Insulation	0.5	kg	Cellulose fiber
	Energy	120	kWh	Electricity, medium voltage
	Transport	15.7*500	kg*km	Transport, freight, lorry 16–32 metric ton, EURO4
Output	Electric motor	1	Item(s)	Electric motor, 1 kW
	Copper scrap	0.1	kg	Copper scrap, sorted, pressed
	Steel scrap	0.6	kg	Scrap steel
	Plastic waste	0.4	kg	Waste plastic, industrial electronics
	Lubricant waste	0.1	kg	Waste mineral oil
	Insulation waste	0.1	kg	Fiber and fabric waste, polyester
<b>Water pump production, centrifugal, 1 kW</b>				
Input	Steel	20	kg	Steel, low-alloyed, hot rolled

(continued)

**Table 1** (continued)

Process created in LCA for component production		Quantity	Unit	Ecoinvent flow and provider
	Copper	1.5	kg	Copper, cathode
	Wire drawing	1.5	kg	Wire drawing, copper
	Cast iron	3	kg	Cast iron
	Plastic	1	kg	Polyvinylchloride, bulk polymerized
	Bronze	0.2	kg	Bronze
	Lubricant	0.5	kg	Lubricating oil
	Energy	90	kWh	Electricity, medium voltage
	Transport	24.5*500	kg*km	Transport, freight, lorry 16–32 metric ton, EURO4
Output	Water pump	1	Item(s)	Water pump, centrifugal, 1 kW
	Scrap	1	kg	Scrap steel
	Scrap	0.1	kg	Copper scrap, sorted, pressed
	Scrap	0.3	kg	Iron scrap, sorted, pressed
	Scrap	0.2	kg	Waste plastic, industrial electronics
	Scrap	0.03	kg	Bronze scrap, post-consumer
	Waste	0.1	kg	Waste mineral oil
<b>Stirrer/Agitator production for 1000 L capacity</b>				
Input	Steel	60	kg	Steel, low-alloyed, hot rolled
	Copper	0.7	kg	Copper, cathode
	Wire drawing	0.7	kg	Wire drawing, copper
	Bronze	0.3	kg	Bronze
	Lubricant	0.3	kg	Lubricating oil
	Electricity	35	kWh	Electricity, medium voltage
	Transport	56*500	kg*km	Transport, freight, lorry 16–32 metric ton, EURO4
Output	Stirrer/Agitator	1	Item(s)	Stirrer/Agitator for 1000 L capacity
	Scrap	6	kg	Scrap steel
	Scrap	0.06	kg	Copper scrap, sorted, pressed
	Scrap	0.015	kg	Bronze scrap, post-consumer
	Waste	0.03	kg	Waste mineral oil
<b>uPVC pipe production, 1 inch dia, 1 m</b>				
Input	Plastic	0.6	kg	Polyvinylchloride, bulk polymerized
	Extrusion process	0.6	kg	Extrusion, plastic pipes

(continued)

**Table 1** (continued)

Process created in LCA for component production		Quantity	Unit	Ecoinvent flow and provider
	Stabilizer	0.018	kg	Tris(2,4-ditert-butylphenyl) phosphite
	Pigment	0.011	kg	Titanium dioxide
Output	uPVC pipe	1	m	uPVC pipe, 1-inch dia, 1 m
	Scrap	0.129	kg	Waste plastic, mixture
<b>Structural channel/angle production, steel metal</b>				
Input	Steel	1	kg	Steel, low-alloyed, hot rolled
	Metal working process	1	kg	Metal working, average for steel product manufacturing
	Transport	1*500	kg*km	Transport, freight, lorry 16–32 metric ton, EURO4
Output	Structural steel channel/ angle	1	kg	Structural channel/angle, steel metal

optimum running of EC. The stirrer provided will ensure the homogeneous mixing of the reagents with wastewater. Secondly, the wastewater then transferred to main reactor from the bottom, the DC electrical power is supplied to the electrode, and reaction of contaminants with the coagulants takes place during the upward flow of wastewater. The flow value is adjusted through the speed of the pump as per the required retention time. The bubbles generated at the cathode rise in the solution between electrodes and help in floating the flocs created by EC process to reach at the top of the reactor. At the last, the wastewater will go to clarifier tank where the coagulated contaminants will settle down and treated water will be collected from the top of the clarifier tank.

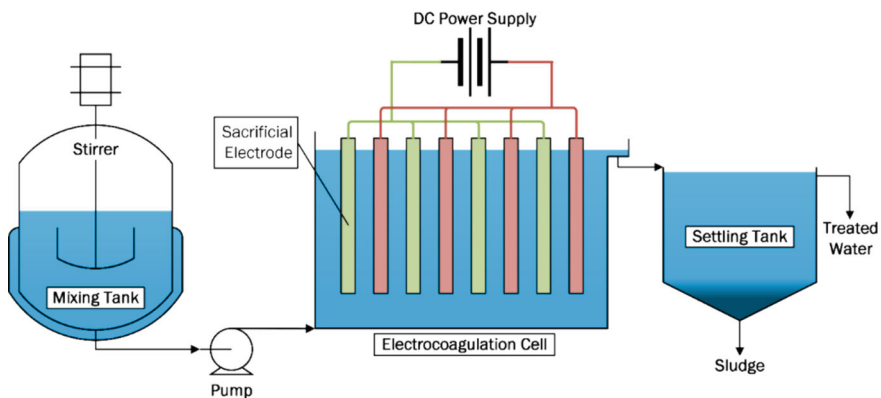


**Fig. 3** Schematic representation of the electrocoagulation system

## 2.5 Impact Assessment

For impact assessment analysis, different life cycle assessment methods can produce varying results in effect categories, values, and units. In this study, CML 2001 and ReCiPe Midpoint (H) was used for the impact assessment. These methods have used the midpoint-oriented approach to find the consequences which is obtained directly by the individual processes used in construction of whole system. The CML 2001 method is most commonly used method in LCA study of wastewater treatment processes [10].

## 3 Results and Discussion

### 3.1 Environmental Impact (EI) Assessment

Characteristic values of each impact category are interpreted by CML2001 method arising from electrocoagulation process is shown in Table 2. The impact categories having large numbers include malodorous air, marine ecotoxicity, freshwater ecotoxicity, human toxicity, climate change, land use, resource depletion, and acidification potential. The other categories having less effect are eutrophication potential, ionizing radiation, stratospheric ozone depletion, and terrestrial ecotoxicity.

**Table 2** Electrocoagulation process impact calculated by the CML 2001 method

Impact category	Result	Reference unit
Acidification potential—average European	25.79	kg SO <sub>2</sub> -Eq
Climate change—GWP 100a	6.24E + 03	kg CO <sub>2</sub> -Eq
Eutrophication potential—average European	20.36	kg NO <sub>x</sub> -Eq
Freshwater aquatic ecotoxicity—FAETP 100a	1.33E + 04	kg 1,4-DCB-Eq
Freshwater sediment ecotoxicity—FSETP 100a	3.06E + 03	kg 1,4-DCB-Eq
Human toxicity—HTP 100a	9.61E + 03	kg 1,4-DCB-Eq
Ionizing radiation—ionizing radiation	9.94E - 06	DALYs
Land use—competition	3.82E + 02	m <sup>2</sup> a
Malodorous air—malodorous air	2.05E + 08	m <sup>3</sup> air
Marine aquatic ecotoxicity—MAETP 100a	4.52E + 04	kg 1,4-DCB-Eq
Marine sediment ecotoxicity—MSETP 100a	5.30E + 04	kg 1,4-DCB-Eq
Resources—depletion of abiotic resources	48.98	kg antimony-Eq
Stratospheric ozone depletion—ODP 10a	4.75E - 04	kg CFC-11-Eq
Terrestrial ecotoxicity—TAETP 100a	3.35	kg 1,4-DCB-Eq
Photochemical oxidation (summer smog)—EBIR	1.34	kg formed ozone

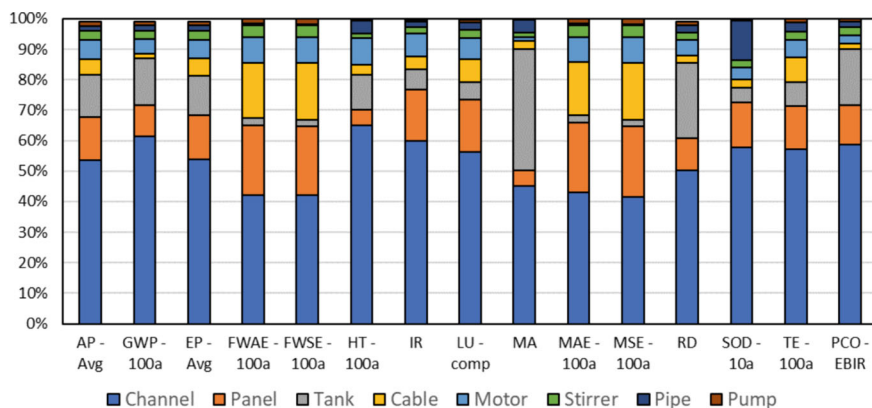


**Fig. 4** Contribution analysis of CML 2001 analysis method for the investigated EC system

The contribution analysis shows that structural steel channel process has major contribution (41.4–64.9%) in all the impact categories as shown in Fig. 4. The control panel process has the second largest contribution in each impact category except the climate change, human toxicity, malodorous air, resource depletion, and photochemical oxidation. The control panel process has contribution from 14.2 to 23.2%. The plastic tank process has second highest value (11.4–39.8%) in impact categories of climate change, human toxicity, malodorous air, resource depletion, and photochemical oxidation. The cable process has the third largest contribution in freshwater and marine ecotoxicity impact categories from 17.5 to 18.6%. So, the structural steel channel, control panel, plastic tank, and electric cable are the major contributing processes in all the impact categories of CML 2001 environmental impact assessment analysis.

Characteristic values of each impact categories are interpreted by ReCiPe Midpoint (H) method arising from electrocoagulation production is shown in Table 3. Top ten impact categories are climate change, human toxicity, metal depletion, fossil depletion, freshwater ecotoxicity, marine ecotoxicity, urban land occupation, ionizing radiation agricultural land occupation, and water depletion. These categories are contributing majorly in overall environmental impact of EC system production.

To find the impact by process in each category, the percentage of each process is calculated for each impact category. The processes involved in EC system manufacturing at supplier workshop include motor, pump, tank, structural steel channel, electric cable, control unit, pipe, stirrer, and electricity consumption. Stacked column chart is prepared to observe the comparative percentage contribution of individual process for each impact category as shown in Fig. 5. In all categories, the highest contribution is from the structural steel channel manufacturing process except in the FETPinf and METPinf impact categories where the control unit process has highest contribution. The second highest contribution is from the control unit process except in the impact categories of GWP100, FDP, PMFP, and POFP where plastic tank process; FETPinf, METPinf and ULOP where electric cable process; MEP where

**Table 3** Impact calculated by the ReCiPe Midpoint (H) method for electrocoagulation unit production

Impact category	Impact result	Unit
Climate change—GWP100	6210.06	kg CO <sub>2</sub> -Eq
Human toxicity—HTPinf	4315.43	kg 1,4-DCB-Eq
Metal depletion—MDP	3476.91	kg Fe-Eq
Fossil depletion—FDP	2033.62	kg oil-Eq
Freshwater ecotoxicity—FETPinf	716.52	kg 1,4-DCB-Eq
Marine ecotoxicity—METPinf	636.82	kg 1,4-DCB-Eq
Urban land occupation—ULOP	512.73	m <sup>2</sup> a
Ionizing radiation—IRP_HE	475.16	kg U235-Eq
Agricultural land occupation—ALOP	235.43	m <sup>2</sup> a
Water depletion—WDP	51.27	m <sup>3</sup>
Terrestrial acidification—TAP100	24.25	kg SO <sub>2</sub> -Eq
Photochemical oxidant formation—POFP	22.32	kg NMVOC
Particulate matter formation—PMFP	15.46	kg PM10-Eq
Marine eutrophication—MEP	8.28	kg N-Eq
Freshwater eutrophication—FEP	3.61	kg P-Eq
Terrestrial ecotoxicity—TETPinf	1.44023	kg 1,4-DCB-Eq
Natural land transformation—NLTP	1.21587	m <sup>2</sup>
Ozone depletion—ODPinf	0.0004	kg CFC-11-Eq

electric motor process has the second major contribution. So, control unit, plastic tank, electric cable, and electric motor production processes are also contributing along with structural steel channel. 23.5% to 68.8% of total impact is only from the steel channel process.

The results from both the methods are compared for each impact category, and it is shown in Table 4. The impact category of acidification, climate change, and ozone depletion results found very similar in both methods. Human toxicity has nearly double the value in CML 2001 method while the land use has similar trend in ReCiPe Midpoint (H) method. Ecotoxicity values are high in CML 2001 method. The terrestrial ecotoxicity has less values while freshwater and marine ecotoxicity values are very high.

The remaining categories of eutrophication potential, ionizing radiation, and photochemical oxidation have not compared due to difference in the unit of measurement. The categories like malodorous air, particulate matter formation, depletion of abiotic resources, fossil, metal and water depletion do not have similar category in both methods.

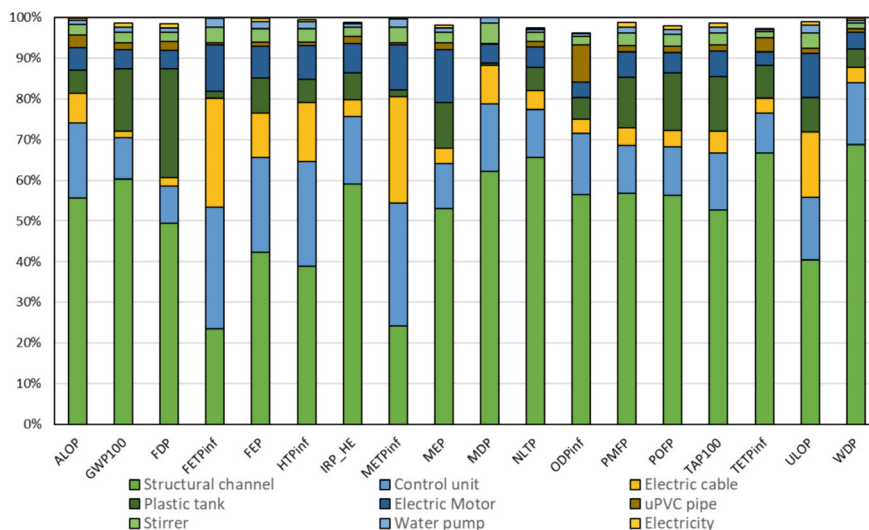


**Fig. 5** Contribution analysis for impact categories of ReCiPe Midpoint (H) analysis method for the investigated EC system

**Table 4** Comparison of result from both CML 2001 and ReCiPe Midpoint (H) method

Impact category	Impact result		Unit
	CML 2001 method	ReCiPe midpoint method	
Acidification	25.79	24.26	kg SO <sub>2</sub> -Eq
Climate change	6244.69	6210.07	kg CO <sub>2</sub> -Eq
Human toxicity	9617.88	4315.43	kg 1,4-DCB-Eq
Land use	382.24	749.39	m <sup>2</sup> a
Ozone depletion	0.000475	0.00040	kg CFC-11-Eq
Terrestrial ecotoxicity	3.35	1.44	kg 1,4-DCB-Eq
Freshwater ecotoxicity	44,079	716.53	kg 1,4-DCB-Eq
Marine ecotoxicity	98,297	636.82	kg 1,4-DCB-Eq

## 4 Conclusion

From both the environmental impact assessment methods of CML 2001 and ReCiPe Midpoint (H), it is observed that structural steel channel production has highest contribution in almost all impact categories which is ranging from 25 to 70%. This steel channel production requires major heat and energy to process the steel during the raw ingot production and during shaping in desired shape. This heat or energy is generally produced in the plant itself by different fossil fuel burning including gas, coal, and wood. Utilization of renewable energy source in this process heat application at least partially will reduce the total environmental impact of EC unit.

Secondly, the structural steel quantity required in pilot-scale plant is on higher side to make EC unit more portable than the one installed permanently at the industry user side. This can also lead to the higher contribution of this steel production process in overall analysis. The second highest contributing (10–40%) process is control panel. Here also the pilot setup is equipped with more sensors and control valves to make system more flexible for varying input and process conditions. The full scale and specific application-based setup will reduce this contribution. The other processes of plastic tank and electric cable process are third and fourth contributor having 2–40% contribution, and these equipments are necessary part of EC system. The tanks are required to give hydraulic retention time and sedimentation time to the wastewater in continuous operation of EC unit.

**Acknowledgements** Authors are thankful to the openLCA software and GreenDeLTa for providing open source database for LCA analysis. This work has partially supported by funding from (i) the Going Global Partnerships-Collaborative Grant-877775303 funded by British Council, (ii) INDIA H<sub>2</sub>O Project no: BT/IN/EU-WR/40/AM/2018 under the European Union's Horizon 2020 research and innovation program funded by Department of Biotechnology, Government of India, and (iii) LC-RED Project no: DST/TM/WTI/WIC/2K17/124 under WTI call funded by Department of Science and Technology, Government of India. We are thankful to the Pandit Deendayal Energy University, Gandhinagar, India, for providing necessary infrastructure and facilities to work.

## References

1. Ankoliya D, Mudgal A, Sinha MK, Patel V, Patel J (2021) Brackish ground water and dairy wastewater treatment using electrodialysis system. *IOP Conf Ser Mater Sci Eng* 1146(1):012006. <https://doi.org/10.1088/1757-899X/1146/1/012006>
2. Kolev Slavov A (2017) Dairy wastewaters—general characteristics and treatment possibilities—a review. *Food Technol Biotechnol* 55(1):14. <https://doi.org/10.17113/ftb.55.01.17.4520>
3. Valente GFS, Mendonça RCS, Pereira JAM (2015) The efficiency of electrocoagulation using aluminum electrodes in treating wastewater from a dairy industry. *Ciência Rural* 45(9):1713–1719. <https://doi.org/10.1590/0103-8478cr20141172>
4. Goli A, Shamiri A, Khosroyar S, Talaiekhosani A, Sanaye R, Azizi K (2019) A review on different aerobic and anaerobic treatment methods in dairy industry wastewater. *J Environ Treatm Tech* 7(1):113–141
5. Adamovici Costea DC, Ghinea C (2021) Life cycle assessment of wastewater from dairy industry. *Food Environ Saf J* 20(1). <https://doi.org/10.4316/fens.2021.007>
6. Corominas L et al (2013) Life cycle assessment applied to wastewater treatment: state of the art. *Water Res* 47(15):5480–5492. <https://doi.org/10.1016/j.watres.2013.06.049>
7. Corominas L et al (2020) The application of life cycle assessment (LCA) to wastewater treatment: a best practice guide and critical review. *Water Res* 184:116058. <https://doi.org/10.1016/j.watres.2020.116058>
8. Lam KL, Zlatanović L, van der Hoek JP (2020) Life cycle assessment of nutrient recycling from wastewater: a critical review. *Water Res* 173:115519. <https://doi.org/10.1016/j.watres.2020.115519>
9. Stanchev P, Vasilaki V, Egas D, Colon J, Ponsá S, Katsou E (2020) Multilevel environmental assessment of the anaerobic treatment of dairy processing effluents in the context of circular economy. *J Clean Prod* 261:121139. <https://doi.org/10.1016/j.jclepro.2020.121139>

10. Paulu A, Bartáček J, Šerešová M, Kočí V (2021) Combining process modelling and LCA to assess the environmental impacts of wastewater treatment innovations. *Water* 13(9):1246. <https://doi.org/10.3390/w13091246>
11. Behjat M, Svanström M, Peters G (2022) A meta-analysis of LCAs for environmental assessment of a conceptual system: phosphorus recovery from dairy wastewater. *J Clean Prod* 369:133307. <https://doi.org/10.1016/j.jclepro.2022.133307>
12. Elginöz N, Atasoy M, Finnveden G, Cetecioglu Z (2020) Ex-ante life cycle assessment of volatile fatty acid production from dairy wastewater. *J Clean Prod* 269:122267. <https://doi.org/10.1016/j.jclepro.2020.122267>
13. Ankoliya D, Mudgal A, Sinha MK, Patel V, Patel J (2023) Application of electrocoagulation process for the treatment of dairy wastewater: a mini review. *Mater Today Proc* 77:117–124. <https://doi.org/10.1016/j.matpr.2022.10.254>
14. Abd Al-Hamza SM, Abd Al-Hamed HM (2022) Using of different electrocoagulation cell configuration parameters for treating of Abu-Ghraib dairy products wastewater. *IOP Conf Ser Earth Environ Sci* 961(1):12059. <https://doi.org/10.1088/1755-1315/961/1/012059>
15. Hakizimana JN et al (2017) Electrocoagulation process in water treatment: a review of electrocoagulation modeling approaches. *Desalination* 404:1–21. <https://doi.org/10.1016/j.desal.2016.10.011>
16. Safwat SM, Mohamed NY, El-Seddik MM (2023) Performance evaluation and life cycle assessment of electrocoagulation process for manganese removal from wastewater using titanium electrodes. *J Environ Manage* 328:116967. <https://doi.org/10.1016/j.jenvman.2022.116967>
17. Patel P, Gupta S, Mondal P (2023) Life cycle assessment (LCA) of greywater treatment using ZnCl<sub>2</sub> impregnated activated carbon and electrocoagulation processes: a comparative study. *Ind Eng Chem Res*. <https://doi.org/10.1021/acs.iecr.2c03353>
18. Álvarez M-D, Buscio V, López-Grimau V, Gutiérrez-Bouzán C (2020) LCA study of a new electrochemical and ultraviolet (EC-UV) combined system to decolourise and reuse textile saline effluents: environmental evaluation and proposal to improve the production process. *Chem Eng J* 392:123696. <https://doi.org/10.1016/j.cej.2019.123696>
19. Ahangarnokolaei MA, Attarian P, Ayati B, Ganjidoust H, Rizzo L (2021) Life cycle assessment of sequential and simultaneous combination of electrocoagulation and ozonation for textile wastewater treatment. *J Environ Chem Eng* 9(5):106251. <https://doi.org/10.1016/j.jece.2021.106251>

# Presence of Endocrine-Disrupting Chemicals (EDCs) in Water, Health Impacts, and Its Treatability—A Review



Dipti Christian, M. A. Shabiimam, Hetvi Dani, and Jesic Patadiya

## 1 Introduction

Safe drinking water is a decisive factor in determining economic prosperity, the health of the general public, and environmental sustainability. Industrialization has led to an increase in the production of various chemicals that can enter drinking water sources resulting in potential exposure to various pollutants [1]. The studies on water and wastewater have been primarily focused on the natural contaminants that can be released into the environment due to various anthropogenic activities. Pure water sources like rivers, lakes, and underground sources like groundwater are often contaminated due to the discharge of untreated industrial effluents into surface and sub-surface water sources [1]. However, in recent times, the occurrence of new anthropogenic compounds in the environment called “emerging pollutants” has become a crucial concern in water and wastewater studies [2]. These emerging pollutants are generally organic in nature and have been detected using advanced analytical techniques. These trace organic pollutants can be generated from industries, sewage, agriculture, hospital, or laboratory wastewater [2].

Endocrine-disrupting chemicals (EDCs) are micro-pollutants that are exogenous in nature and primarily exist in chemicals [3, 4]. The WHO identifies EDCs as “An endocrine disruptor is an exogenous substance or mixture that alters function(s) of the endocrine system and consequently impacts health in an intact organism, or its progeny, or (sub) populations adversely” [3, 5]. These chemicals are present in a wide variety of structurally diverse forms of different sources and can get into the human body through different consumer products, personal care products, food contaminants, and waste effluents [3]. Mostly, the research gap that is encountered for treatment of endocrine-disrupting chemicals is the impact of emerging pollutants, source

---

D. Christian · M. A. Shabiimam (✉) · H. Dani · J. Patadiya  
Department of Civil Engineering, School of Technology, Pandit Deendayal Energy University,  
Gandhinagar, Gujarat 382421, India  
e-mail: [shabiimam.ma@sot.pdpu.ac.in](mailto:shabiimam.ma@sot.pdpu.ac.in)

identification, detection techniques, treatment methods, long-term health effects, and the policy and regulations.

The subject of a scientific and legal dispute is endocrine disruptors, often known as endocrine-disrupting chemicals (EDCs). Most chemicals that have been shown to affect hormones are synthetic. Their primary purpose when they were first designed was to help business and agriculture, homes and consumers, as well as personal and medical health care. However, there is a connection between these commonly used drugs and endocrine (hormonal) system diseases. For instance, it is believed that EDCs contribute to the development of chronic illnesses such as diabetes, obesity, infertility, malignancies related to hormones, and cardiovascular disease. Furthermore, EDCs have the potential to seriously impair people's health since they are present in a wide range of goods that they use or consume on a regular basis, such as paint, food packaging, toys, clothes, cosmetics, and medications [5].

Studies focussing on the health impacts of EDCs have also associated the increase in many diseases and illnesses with the rise in human exposure to these chemicals [6]. This review paper focuses on the toxic effects of EDCs on human health, the various detection techniques used, and some efficient treatment methods that can be implemented to reduce the harmfulness of EDCs in pure water streams.

## 2 Impacts of EDCs

Pesticides, solvents, plasticizers, and pharmaceutical items are only a few examples of the many products that include the synthetic chemicals that make up EDCs. When absorbed into the human body, these compounds are discovered to have a variety of negative impacts by imitating or obstructing the body's hormonal functions [7]. EDCs can interfere with a human body as natural hormonal balance, hinder or imitate the synthesis and metabolism of hormones, or change the route that hormones take through the body to influence how they operate [7]. Since hormones have different effects at different times of the life cycle, the timing and duration of EDC exposure are critical variables in determining how endocrine systems are affected by hormones. The EDCs can interact with hormonal processes through a variety of methods, and these compounds can have agonist, antagonist, direct, or indirect effects depending on how they bind to hormone receptors. Even at extremely low concentrations, these chemicals can have unexpected consequences [8]. It is crucial to evaluate substances for EDC activity within the context of fundamental endocrinology, which was developed through decades of painstaking study into the mechanisms and consequences of hormone action in both healthy and pathological conditions [8].

Initially, it was thought that only nuclear hormone receptors—including oestrogen receptors, retinoid receptors, progesterone receptors, thyroid receptors, and androgen receptors—were capable of mediating the actions of EDCs (ERs). Recent studies suggest that EDCs use a far wider range of tactics than was previously believed [7, 8], nevertheless. Table 1 lists the most frequent health effects linked to prevalent EDC substances.

**Table 1** Health impacts of EDCs

Health impact	Cause	Effect on human body	References
Reproductive effects	Bisphenol-A (BPA) Phthalates	Impaired fertility levels, altered sex hormonal levels, reproductive organ abnormalities, effect on sperm quality	[9–13]
Developmental effects	Organophosphate Pesticides Flame retardants	Neurodevelopmental disorders, cognitive impairments, congenital malformations	[9–11, 14–17]
Metabolic effects	Perfluorooctanoic acid (PFOA) Tributyltin (TBT)	Obesity, increased insulin resistance, diabetes, energy homeostasis	[18–22]
Neurological effects	Polychlorinated biphenyls (PCBs) Organophosphate Pesticides	Cognitive defects, attention deficits, neurodevelopmental disorders	[17, 19, 23–25]
Cancer	Diethylstilboestrol (DES) Dioxins	Increased risk of hormone-dependent cancer like breast, prostate, and testicular cancer	[9, 26–29]

### 3 Detection Techniques

Endocrine-disrupting chemical (EDC) detection is essential for determining their presence in various environmental matrices and assessing possible threats to the ecosystem and human health. Chemical analysis method of Gas Chromatography (GC) can be used to determine the presence of these chemicals in water [30]. These analytical methods are very sensitive to detecting the presence of these chemicals in water. However, the detection procedure is very complicated and labour-intensive and time-consuming. Hence, biosensors can be used as an effective alternative to these analytical methods. This method is rapid, cost-effective, and sensitive to detect a wide range of disrupting chemicals [31]. The most common detection techniques along with its principle are listed below in Table 2.

EDCs are also found in large quantities in various Indian water sources due to point pollution along the rivers. The Ganga River Basin is the largest in India that supports 43% of the Indian population. River Ganga is the third most polluted river among the top-ten most polluted rivers in the world with the presence of 90% plastic waste. It also receives about 501 million litres per day (MLD) of industrial effluents from 764 pollution industries. Intermediates like polyvinyl chloride (PVC), bisphenol-A (BPA), and phthalic acid esters (PAEs) are added to man-made plastic or polymers manufactured using epoxy resins and polycarbonate. The purpose of these chemicals is to increase the products' flexibility, toughness, and adhesive capabilities. However, these plasticizers are endocrine-disrupting chemicals (EDCs) that enter the river Ganga from different point sources of industrial pollution [50]. Similarly, Kumar et al. [48] studied the presence of EDC in six water bodies, i.e. four ponds and two lakes along the city of Hyderabad. Water samples were collected and oestrogens'

**Table 2** Detection techniques of EDCs

Detection technique	Principle	Target chemicals	References
Gas Chromatography (GC)–Mass Spectrometry (MS)	Depending on the mass-to-charge ratios of the compounds, separate and quantify them	Used for volatile and semi-volatile EDCs such as PCBs, pesticides, and phthalates	[12, 32–36]
Liquid chromatography (LC)–Mass Spectrometry (MS)	Separate and quantify compounds dissolved in a liquid solvent based on mass-to-charge ratios	Used for a wide scope of EDCs including hormones, bisphenols, and pharmaceuticals	[8, 37–40]
Enzyme-linked immunosorbent assay (ELISA)	Utilise antigen–antibody interactions to detect and quantify EDCs	Used for hormones, pesticides, and other EDCs in water, soil, and biological samples	[41–45]
Biosensors	Utilise biological components to interact with EDCs and produce a measurable signal. Provide rapid and sensitive detection in real-time	Phytoestrogens (e.g. Genistein), organochlorine pesticides, nonylphenol	[46–49]

concentration was determined using enzymatic-immunoassay (EIA) kits. The presence of EDCs in these water bodies was ascribed to the release of untreated sewage (animal or human) into the water bodies [51].

A similar investigation, focusing on PAEs and BPA, was also carried out in Jabalpur to ascertain the prevalence of EDCs [52]. In this study, public water delivery systems, rivers, reservoirs, and dams were evaluated as sources of community water. For the detection and quantification of EDCs in the water bodies, Gas Chromatography (GC)–Mass Spectrometry (MS) was used. The presence of bisphenol-A (BPA) and phthalate esters (PAEs) in these water bodies can be due to their wide use as plasticizers and in industries like construction, food packaging, and pharmaceuticals [52]. In addition, Tiwari et al. [53], studied the increasing pollution levels in Thane Creek of Mumbai. The creek separates Mumbai and Navi Mumbai with the presence of a large industrial estate of Thane–Belapur along its east side. This industrial estate has 1136 industries disposing of its effluents and solid waste along the creek thereby causing an increase in the pollution levels. In addition, the industrial estate houses many chemicals, textiles, and drug manufacturing industries. In this study, phthalate esters (PAEs) were detected using Gas Chromatography (GC)–Mass Spectrometry (MS), and bisphenol-A (BPA) was detected using Photodiode Array (PDA) detectors [53].

## 4 Treatment Techniques

The processes used to lower endocrine disruptor levels in water and wastewater are chemical coagulation, flocculation, precipitation, activated sludge treatments, adsorption, and membrane. Because endocrine disruptors have a variety of physical and chemical characteristics, different procedures can be applied as treatment methods to achieve various removal efficiencies [54]. Several techniques, including oxidation, membrane filtration, advanced oxidation, biosorption, adsorption, and biodegradation, have been investigated for the removal of EDCs [55–58].

Adsorption process is one of the most often used techniques for eliminating EDC from water because of its remarkable qualities, including high efficiency, low operating, and maintenance costs, and the absence of any significant by-product formation. To increase the sustainability of the endocrine disruptor's treatment procedure by adsorption, Clays [59], zeolites [60], charcoal [61], metal–organic frameworks [62], graphene oxide [63], and carbon nanotubes [63–66] are generally used for adsorption process. Due to their availability and abundance in nature, bioadsorbents can be viewed in this perspective as environmentally friendly and cost-effective substitutes for routinely employed carbon-based adsorbents. As a result, industrial wastewater and drinking water both often employed biosorption techniques for water purification [67, 68] because it is simple to use, cheap, uses little energy, and produces harmless by-products [69].

The most often used biosorbents are wood, chitosan, algae, fungus, yeast, bacteria, and agricultural waste. Compared to traditional adsorbents, these materials are typically more selective [70, 71]; the literature has discussed the potential use of a sulfonated derivative of coffee waste (CW-SO<sub>3</sub>H) as a practical and efficient biosorbent for the removal of BPA from an aqueous solution [72]. This biosorbent might be used to clean polluted water and reduce coffee waste at the same time. CW-SO<sub>3</sub>H has a stated estimated biosorption capacity of 270,000 mg/l for the elimination of BPA, which is almost five times more than the inexpensive activated carbon. The process involves creating of activated carbon from recently discarded bean (*Phaseolus vulgaris*) husk biomass at a pH of 4.80, with a maximum monolayer adsorptive capacity of 50,000 mg/l at 122°F [73].

As an alternative, a variety of endocrine disruptors can be successfully filtered out using membrane filtering techniques because they benefit from the distinct physicochemical characteristics of the membrane's manufacturing material [74–77]. The rate of removal of pollutants like bisphenol-A, alkylphenols, and carbamazepine is improved by using a membrane bioreactor in conjunction with reverse osmosis or nanofiltration for the same reasons [5, 78].

Numerous research have been done on advanced oxidation processes (AOPs), typically in combination to provide superior outcomes. These studies have been done on ozonation, UV/peroxide, Fenton, and photocatalysis. For instance, the combined UV-ozone procedure [79] is more effective than ozone alone at removing EDCs from water such bisphenol-A, 17- $\beta$ -estradiol, and estriol, whereas chlorine oxidant

creates a number of by-products without reducing EDCs [80, 81] Firstly, EE2 elimination using the Fenton technique in combination with A 99 per cent biological treatment efficiency employing UASB reactor was demonstrated. They introduced about 1000 g/L of these chemicals into the samples daily, resulting 73 to 30 percent reduction in toxicity. The complexity and variety of EDC chemical concentrations determine the usage of EDC treatments, which calls for techniques for extraction, quantification, storage, and preservation that are precise and suitable.

EDC features may be taken into account when determining a suitable removal method; in certain circumstances, each EDC contaminant may need a separate course of action. In actuality, the membrane filtering procedure is an effective way to remove EDC. Nevertheless, similar to membrane filtrations, further EDC treatment techniques cannot entirely eliminate developing pollutants. In addition, there are sustainable methods employing waste materials, even if the procedure asks for sorbent regeneration or disposal. Adsorption might be a very reliable method with low costs and minimum waste. Additionally, the photo-Fenton method demonstrated removal efficiencies for medicinal substances, many hormone types, and chemicals ranging from 95 to 100% [82, 83]. However, the difficulties of iron ion regeneration and the ultimate treatment of wastewater to meet the discharge constraints for iron concentrations dictated these approaches' limitations. Table 3 emphasises the merits and demerits of each treatment option to provide a future perspective of EDC treatment techniques in water and wastewater treatment systems.

With regard to process engineering, economic, social, and environmental components of EDC, a number of variables, including advanced oxidation procedures for the removal of heavy metals, were compared. The findings were quantitatively scored (from 1 to 5 corresponding to descriptive variables of "very low" to "very high") to outline the different performances. The results of the investigation showed that perozonation  $H_2O_2/O_3$  received the highest average rating (3.50). Other procedures performed similar level due to benefits associated with an established technology, regulation, and widespread acceptability [15]. However, because to its technological features and more effective removal of several chemicals, including hormones, phenolic compounds, and pesticides, the photo-Fenton method might be regarded as the best treatment for endocrine-disrupting substances.

Given that many EDCs are sufficiently decomposed as existing microorganisms, to boost removal percentages, degradation must be coupled with additional methods like membrane filtering and complex oxidation processes. Integrated solutions are recommended for better using the available water treatment technology in order to lower the level of EDCs.

## 5 Conclusion

An overview of the significance of endocrine-disrupting chemicals is given in this paper (EDCs), and its detection techniques and the treatment methods are available. The detection and monitoring of EDCs in water bodies are of paramount importance

**Table 3** Methods used to remove and treat chemicals that disturb the endocrine system in water and wastewater systems are compared

Methods	Merits	Demerits
Advanced oxidation process	<ul style="list-style-type: none"> <li>• Various levels of effectiveness</li> <li>• Elimination of up to 80% of EDC compounds</li> <li>• Exceptional sensitivity</li> </ul>	<ul style="list-style-type: none"> <li>• Costly</li> <li>• Substance regenerating into an active state</li> <li>• Post-processing water</li> <li>• By-product</li> </ul>
Biological process	<ul style="list-style-type: none"> <li>• High biodegradation rate of up to 90%</li> <li>• No waste products</li> <li>• Low prices</li> </ul>	<ul style="list-style-type: none"> <li>• Effectiveness connected to many enzymatic pathways</li> <li>• Period of incubation</li> <li>• Sample pretreatment as initial pollutant concentration</li> </ul>
Filtrations by membrane	<ul style="list-style-type: none"> <li>• Wide range of activities</li> <li>• Ultrafiltration is a technique that can effectively remove all endocrine disruptors</li> </ul>	<ul style="list-style-type: none"> <li>• High price</li> <li>• Hazardous waste by-product</li> <li>• Concentrates (brine) are mostly released into surface water</li> <li>• The difficulties in treating and releasing the pollutants that collected during the process</li> </ul>
Adsorption	<ul style="list-style-type: none"> <li>• Excellent efficiency minimal operating and maintenance expenses</li> <li>• No waste products</li> <li>• Simple to use</li> <li>• Low electricity usage</li> </ul>	<ul style="list-style-type: none"> <li>• Regeneration or disposal of sorbent</li> <li>• Use of unconventional adsorbents improves performance when used with adequate contact duration and dose</li> <li>• Low elimination of propranolol and carbamazepine</li> </ul>

for safeguarding both human and environmental health. The pervasive presence of these compounds, stemming from various sources, poses a significant threat to aquatic ecosystems and the organisms that rely on them. By identifying and quantifying EDCs, targeted mitigation strategies can be implemented, stricter regulations enacted, and effective treatment methods can be determined to minimise their adverse effects. The choice of detection techniques depends upon different factors like sensitivity, targeted compounds, ease of use, cost, and accessibility. Similarly, to detect hormones and estrogenic compounds, ELISA can be used effectively. EDCs have also been detected in various water bodies within India thereby increasing the need for accurate detection and quantification of these chemicals.

Effective treatment methods must be created to counteract the prevalence of EDCs in sources. This contamination can potentially be reduced by using removal methods such membrane filtering, improved oxidation processes, biosorption, and adsorption. In order to remove or degrade EDCs, these techniques rely on physical, chemical, and biological principles, which helps to improve the quality of water sources. While

each approach has advantages and disadvantages, the general objective is to reduce the amount of EDCs in water sources and the resulting health hazards.

In conclusion, the growing worry over EDC pollution of water sources emphasises the necessity of concentrated efforts in study, legislation, and technological development. The undetectable yet powerful impacts of EDCs highlight the significance of attentive monitoring, accurate detection, and effective removal methods. We can cooperate to protect water quality, public health, and the delicate balance of ecosystems from the subtle but significant effects of endocrine-disrupting chemicals by combining scientific knowledge, regulatory frameworks, and new technology.

## 6 Disclosure of Interests

The authors have no competing interests to declare that are relevant to the content of this article.

## References

1. Wee SY, Aris AZ (2019) Occurrence and public-perceived risk of endocrine disrupting compounds in drinking water. *npj Clean Water* 2(1):4. <https://doi.org/10.1038/s41545-018-0029-3>
2. Gogoi A, Mazumder P, Tyagi VK, Chaminda GT, An AK, Kumar M (2018) Occurrence and fate of emerging contaminants in water environment: a review. *Groundw Sustain Dev* 6:169–180. <https://doi.org/10.1016/j.gsd.2017.12.009>
3. Robitaille J, Denslow ND, Escher BI, Kurita-Oyamada HG, Marlatt V, Martyniuk CJ et al (2022) Towards regulation of endocrine disrupting chemicals (EDCs) in water resources using bioassays—a guide to developing a testing strategy. *Environ Res* 205:112483. <https://doi.org/10.1016/j.envres.2021.112483>
4. Zhu L, Qiu L, Zhang L, Wang J, Xie K (2016) Harmfulness, detection and treatment of EDCs in water environment. In 2015 4th international conference on sustainable energy and environmental engineering. Atlantis Press, pp 468–472. <https://doi.org/10.2991/icseee-15.2016.75>
5. Basha AT, Gebreyohannes AY, Tufa RA, Bekele DN, Curcio E, Giorno L (2017) Removal of emerging micropollutants by activated sludge process and membrane bioreactors and the effects of micropollutants on membrane fouling: a review. *J Environ Chem Eng* 5(3):2395–2414. <https://doi.org/10.1016/j.jece.2017.04.027>
6. Swedenborg E, Rüegg J, Mäkelä S, Pongratz I (2009) Endocrine disruptive chemicals: mechanisms of action and involvement in metabolic disorders. *J Mol Endocrinol* 43(1):1–10. <https://doi.org/10.1677/jme-08-0132>
7. Schug TT, Janesick A, Blumberg B, Heindel JJ (2011) Endocrine disrupting chemicals and disease susceptibility. *J Steroid Biochem Mol Biol* 127(3–5):204–215. <https://doi.org/10.1016/j.jsbmb.2011.08.007>
8. Zoeller RT, Brown TR, Doan LL, Gore AC, Skakkebaek NE, Soto AM, Vom Saal FS (2012) Endocrine-disrupting chemicals and public health protection: a statement of principles from the endocrine society. *Endocrinology* 153(9):4097–4110. <https://doi.org/10.1210/en.2012-1422>

9. Diamanti-Kandarakis E, Bourguignon JP, Giudice LC, Hauser R, Prins GS, Soto AM, Gore AC (2009) Endocrine-disrupting chemicals: an endocrine society scientific statement. *Endocr Rev* 30(4):293–342. <https://doi.org/10.1210/er.2009-0002>
10. Skakkebaek NE, Rajpert-De Meyts E, Buck Louis GM, Toppari J, Andersson AM, Eisenberg ML, Juul A (2016) Male reproductive disorders and fertility trends: influences of environment and genetic susceptibility. *Physiol Rev* 96(1):55–97. <https://doi.org/10.1152/physrev.00017.2015>
11. Mínguez-Alarcón L, Messerlian C, Bellavia A, Gaskins AJ, Chiu YH, Ford JB, Earth Study Team (2019) Urinary concentrations of bisphenol A, parabens and phthalate metabolite mixtures in relation to reproductive success among women undergoing in vitro fertilization. *Environ Int* 126:355–362. <https://doi.org/10.1016/j.envint.2019.02.025>
12. Johns LE, Ferguson KK, Meecker JD (2016) Relationships between urinary phthalate metabolite and bisphenol A concentrations and vitamin D levels in US adults: national health and nutrition examination survey (NHANES), 2005–2010. *J Clin Endocrinol Metab* 101(11):4062–4069. <https://doi.org/10.1210/jc.2016-2134>
13. Liu X, Miao M, Zhou Z, Gao E, Chen J, Wang J, Li DK (2015) Exposure to bisphenol-A and reproductive hormones among male adults. *Environ Toxicol Pharmacol* 39(2):934–941. <https://doi.org/10.1016/j.etap.2015.03.007>
14. Braun JM (2017) Early-life exposure to EDCs: role in childhood obesity and neurodevelopment. *Nat Rev Endocrinol* 13(3):161–173. <https://doi.org/10.1038/nrendo.2016.186>
15. Fast SA, Gude VG, Truax DD, Martin J, Magbanua BS (2017) A critical evaluation of advanced oxidation processes for emerging contaminants removal. *Environ Process* 4:283–302. <https://doi.org/10.1007/s40710-017-0207-1>
16. Shelton JF, Geraghty EM, Tancredi DJ, Delwiche LD, Schmidt RJ, Ritz B, Hertz-Picciotto I (2014) Neurodevelopmental disorders and prenatal residential proximity to agricultural pesticides: the CHARGE study. *Environ Health Perspect* 122(10):1103–1109. <https://doi.org/10.1289/ehp.1307044>
17. Braun JM, Kalkbrenner AE, Just AC, Yolton K, Calafat AM, Sjödin A, Lanphear BP (2014) Gestational exposure to endocrine-disrupting chemicals and reciprocal social, repetitive, and stereotypic behaviors in 4- and 5-year-old children: the HOME study. *Environ Health Perspect* 122(5):513–520. <https://doi.org/10.1289/ehp.1307261>
18. Grün F, Blumberg B (2009) Endocrine disruptors as obesogens. *Mol Cell Endocrinol* 304(1–2):19–29. <https://doi.org/10.1016/j.mce.2009.02.018>
19. Heindel JJ, Blumberg B, Cave M, Machtiger R, Mantovani A, Mendez MA, Vom Saal F (2017) Metabolism disrupting chemicals and metabolic disorders. *Reprod Toxicol* 68:3–33. <https://doi.org/10.1016/j.reprotox.2016.10.001>
20. Kuo CC, Moon K, Thayer KA et al (2013) Environmental chemicals and type 2 diabetes: an updated systematic review of the epidemiologic evidence. *Curr Diab Rep* 13:831–849. <https://doi.org/10.1007/s11892-013-0432-6>
21. Rancière F, Lyons JG, Loh VH, Botton J, Galloway T, Wang T, Magliano DJ (2015) Bisphenol A and the risk of cardiometabolic disorders: a systematic review with meta-analysis of the epidemiological evidence. *Environ Health* 14:1–23. <https://doi.org/10.1186/s12940-015-0036-5>
22. Tang-Péronard JL, Andersen HR, Jensen TK, Heitmann BL (2011) Endocrine-disrupting chemicals and obesity development in humans: a review. *Obes Rev* 12(8):622–636. <https://doi.org/10.1111/j.1467-789X.2011.00871>
23. Kim K-H et al (2014) Effects of endocrine-disrupting chemicals on the brain. *Dev Med Child Neurol* 56(3):312–317. <https://doi.org/10.3389/fendo.2014.00146>
24. Richardson JR, Taylor MM, Shalat SL, Guillot TS III, Caudle WM, Hossain MM et al (2015) Developmental pesticide exposure reproduces features of attention deficit hyperactivity disorder. *FASEB J* 29(5):1960. <https://doi.org/10.1096/fj.14-260901>
25. Chevrier J, Gunier RB, Bradman A, Holland NT, Calafat AM, Eskenazi B, Harley KG (2013) Maternal urinary bisphenol a during pregnancy and maternal and neonatal thyroid function in the CHAMACOS study. *Environ Health Perspect* 121(1):138–144. <https://doi.org/10.1289/ehp.1205092>

26. Zoeller RT et al (2012) Endocrine-disrupting chemicals and public health protection: a statement of principles from the endocrine society. *Endocrinology* 153(9):4097–4110. <https://doi.org/10.1210/en.2012-1422>
27. Forti GC et al (2019) Endocrine disrupting chemicals and human health in breast cancer. *Horm Cancer* 10(1):21–35. <https://doi.org/10.1016/j.pharmthera.2019.107398>
28. Soto AM, Sonnenschein C (2010) Environmental causes of cancer: endocrine disruptors as carcinogens. *Nat Rev Endocrinol* 6(7):363–370. <https://doi.org/10.1038/nrendo.2010.87>
29. Weijs L, Roach AC, Yang RS, McDougall R, Lyons M, Housand C, Blust R (2013) 6.2 Paper XI. Introduction 7:257
30. Snyder S, Vanderford B, Pearson R, Quinones O, Yoon Y (2003) Analytical methods used to measure endocrine disrupting compounds in water. *Pract Period Hazard Toxic Radioact Waste Manag* 7(4):224–234. [https://doi.org/10.1061/\(ASCE\)1090-025X\(2003\)7:4\(224\)](https://doi.org/10.1061/(ASCE)1090-025X(2003)7:4(224))
31. Yildirim N, Long F, Gao C, He M, Shi HC, Gu AZ (2012) Aptamer-based optical biosensor for rapid and sensitive detection of 17 $\beta$ -estradiol in water samples. *Environ Sci Technol* 46(6):3288–3294. <https://doi.org/10.1021/es203624w>
32. Blumberg B et al (2006) Hormone receptors: new targets for endocrine disruptors. *Pediatr Res* 60(3):340–347. [https://doi.org/10.1007/398\\_2018\\_20](https://doi.org/10.1007/398_2018_20)
33. Johns LE, Ferguson KK, McElrath TF, Cantonwine DE, Meeker JD (2016) Urinary phthalate metabolite and bisphenol-A concentrations in association with serum vitamin D levels: results from pregnant and non-pregnant women in two US populations. *ISEE Conf Abstr* 28(1):3–156. <https://doi.org/10.1289/isee.2016.3372>
34. de Faria HD, de Carvalho Abr ao LC, Santos MG, Barbosa AF, Figueiredo EC (2017) New advances in restricted access materials for sample preparation: a review. *Anal Chim Acta* 959:43–65. <https://doi.org/10.1016/j.aca.2016.12.047>
35. Talley TS, Venuti N, Whelan R (2020) Natural history matters: plastics in estuarine fish and sediments at the mouth of an urban watershed. *PLoS One*, 1–19. <https://doi.org/10.1371/journal.pone.0229777>
36. Rocha MJ, Cruzeiro C, Rocha E (2013) Development and validation of a GC–MS method for the evaluation of 17 endocrine disruptor compounds, including phytoestrogens and sitosterol, in coastal waters—their spatial and seasonal levels in Porto coastal region (Portugal). *J Water Health* 11(2):281–296. <https://doi.org/10.2166/wh.2013.021>
37. Fox GA (2001) Effects of endocrine disrupting chemicals on wildlife in Canada: past, present and future. *Water Qual Res J* 36(2):233–251. <https://doi.org/10.2166/wqrj.2001.014>
38. Afonso-Olivares C, Montesdeoca-Esponda S, Sosa-Ferrera Z, Santana-Rodr guez JJ (2016) Analytical tools employed to determine pharmaceutical compounds in wastewaters after application of advanced oxidation processes. *Environ Sci Pollut Res* 23:24476–24494. <https://doi.org/10.1007/s11356-016-7325-6>
39. Silloniz IZ (2017) Analytical method development for the occurrence, distribution and transformation assessment of fluorinated compounds in biota and packaging materials (Doctoral dissertation, Universidad del Pa s Vasco-Euskal Herriko Unibertsitatea)
40. Zhao Y et al (2019) Screening and confirmation of endocrine-disrupting chemicals in baby diapers using liquid chromatography tandem mass spectrometry and gas chromatography mass spectrometry. *J Chromatogr A* 1600:76–85. <https://doi.org/10.1096/fj.14-260901>
41. Sherry J (1997) Environmental immunoassays and other bioanalytical methods: overview and update. *Chemosphere* 34(5–7):1011–1025. [https://doi.org/10.1016/s0045-6535\(97\)00403-7](https://doi.org/10.1016/s0045-6535(97)00403-7)
42. Hu C, Huang D, Zeng G, Cheng M, Gong X, Wang R, Liu Y (2018) The combination of Fenton process and phanerochaete chrysosporium for the removal of bisphenol A in river sediments: mechanism related to extracellular enzyme, organic acid and iron. *Chem Eng J* 338:432–439. <https://doi.org/10.1016/j.cej.2018.01.068>
43. Prabhaskar P, Manohar RS (2002) Development of enzyme-linked immunosorbent assay for evaluation of chapati-making quality of wheat varieties. *J Agric Food Chem* 50(25):7455–7460. <https://doi.org/10.1021/jf0258151>
44. Justino CI, Freitas AC, Pereira R, Duarte AC, Santos TAR (2015) Recent developments in recognition elements for chemical sensors and biosensors. *TrAC Trends Anal Chem* 68:2–17. <https://doi.org/10.1016/j.trac.2015.03.006>

45. Zeravik J, Skryjová K, Nevoranková Z, Fránek M (2004) Development of direct ELISA for the determination of 4-nonylphenol and octylphenol. *Anal Chem* 76(4):1021–1027. <https://doi.org/10.1021/ac030217m>
46. Wang W, Wang X, Cheng N, Luo Y, Lin Y, Xu W, Du D (2020) Recent advances in nanomaterials-based electrochemical (bio) sensors for pesticides detection. *TrAC Trends Anal Chem* 132:116041. <https://doi.org/10.1016/j.trac.2020.116041>
47. Örenli D, Selvi CK, Öztürk F, Erden PE, Kılıç E (2023) Electrochemical (bio) sensors based on carbon quantum dots, ionic liquid and gold nanoparticles for bisphenol A. *Anal Biochem* 662:115002. <https://doi.org/10.1016/j.ab.2022.115002>
48. Kumar A et al (2017) Label-free impedimetric aptasensor for ultrasensitive detection of bisphenol A. *J Electroanal Chem* 798:52–59. <https://doi.org/10.1016/B978-0-12-813855-7.00009-X>
49. Kanchi S, Sabela MI, Bisetty K (2018) Analytical applications of nanoscale materials for water treatment: a review. *Nanotechnol Environ Sci*, 71–124. <https://doi.org/10.1002/9783527808854.ch4>
50. Chakraborty P, Shappell NW, Mukhopadhyay M, Onanong S, Ronnie Rex K, Snow D (2020) Surveillance of plasticizers, bisphenol A, steroids and caffeine in surface water of River Ganga and Sunderban wetland along the Bay of Bengal: occurrence, sources, estrogenicity screening and ecotoxicological risk assessment. <https://doi.org/10.1016/j.watres.2020.116668>
51. Kiran Kumar A, Sarma PN, Mohan SRV (2016) Incidence of selected endocrine disrupting estrogens in water bodies of hyderabad and its relation to water quality parameters. <https://doi.org/10.30638/eemj.2016.032>
52. Kumawat M, Sharma P, Pal N, James MM, Verma V, Tiwari RR, Shubham S, Sarma DK, Kumar M (2022) Occurrence and seasonal disparity of emerging endocrine disrupting chemicals in a drinking water supply system and associated health risk. <https://doi.org/10.1038/s41598-022-13489-3>
53. Tiwari M, Sahu SK, Pandit GG (2016) Distribution and estrogenic potential of endocrine disrupting chemicals (EDCs) in estuarine sediments from Mumbai, India. <https://doi.org/10.1007/s11356-016-7070-x>
54. Gadupudi CK, Rice L, Xiao L, Kantamaneni K (2021) Endocrine disrupting compounds removal methods from wastewater in the United Kingdom: a review. *Sci* 3(1):11. <https://doi.org/10.3390/sci3010011>
55. Okonkwo JO, Sibali LL, McCrindle R, Senwo ZN (2007) An improved activated carbon method to quantify dichlorodiphenyltrichloroethane (DDT) in surface water. *Environ Chem Lett* 5:121–123. <https://doi.org/10.1007/s10311-006-0089-3>
56. Artham T, Doble M (2012) Bisphenol A and metabolites released by biodegradation of polycarbonate in seawater. *Environ Chem Lett* 10:29–34. <https://doi.org/10.1007/s10311-011-0324-4>
57. Li G, Zhang X, Sun J, Zhang A, Liao C (2020) Effective removal of bisphenols from aqueous solution with magnetic hierarchical rattle-like Co/Ni-based LDH. *J Hazard Mater* 381:120985. <https://doi.org/10.1016/j.jhazmat.2019.120985>
58. Vieira WT, de Farias MB, Spaolonzi MP, da Silva MGC, Vieira MGA (2020) Removal of endocrine disruptors in waters by adsorption, membrane filtration and biodegradation A review. *Environ Chem Lett* 18(4):1113–1143. <https://doi.org/10.1007/s10311-020-01000-1>
59. Djebri N, Boutahala M, Chelali NE, Boukhalfa N, Larbi Z (2017) Adsorption of bisphenol A and 2, 4, 5-trichlorophenol onto organo-acid-activated bentonite from aqueous solutions in single and binary systems. *Desalin Water Treat* 66:383–393. <https://doi.org/10.5004/dwt.2017.20220>
60. Goyal N, Barman S, Bulasara VK (2016) Quaternary ammonium salt assisted removal of genistein and bisphenol S from aqueous solution by nanozeolite NaY: equilibrium, kinetic and thermodynamic studies. *J Mol Liq* 224:1154–1162. <https://doi.org/10.1016/j.molliq.2016.10.088>
61. Jun BM, Hwang HS, Heo J, Han J, Jang M, Sohn J, Yoon Y (2019) Removal of selected endocrine-disrupting compounds using Al-based metal organic framework: performance and

- mechanism of competitive adsorption. *J Ind Eng Chem* 79:345–352. <https://doi.org/10.1016/j.jiec.2019.07.009>
62. Pironti C, Ricciardi M, Proto A, Bianco PM, Montano L, Motta O (2021) Endocrine-disrupting compounds: an overview on their occurrence in the aquatic environment and human exposure. *Water* 13(10):1347. <https://doi.org/10.3390/w13101347>
  63. Zhang L, Lv J, Xu T, Yang L, Jiang X, Li Q (2013) High efficiency removal and recovery of an endocrine disrupting compound–bisphenol AF from wastewaters. *Sep Purif Technol* 116:145–153. <https://doi.org/10.1016/j.seppur.2013.05.036>
  64. de Andrade JR, Oliveira MF, da Silva MG, Vieira MG (2018) Adsorption of pharmaceuticals from water and wastewater using nonconventional low-cost materials: a review. *Ind Eng Chem Res* 57(9):3103–3127. <https://doi.org/10.1021/acs.iecr.7b05137>
  65. Maia GS, de Andrade JR, da Silva MG, Vieira MG (2019) Adsorption of diclofenac sodium onto commercial organoclay: kinetic, equilibrium and thermodynamic study. *Powder Technol* 345:140–150. <https://doi.org/10.1016/j.powtec.2018.12.097>
  66. de Souza FM, Lazarin AM, Vieira MGA, dos Santos OAA (2018) Kinetic, equilibrium, and thermodynamic study on atrazine adsorption in organophilic clay. *Desalin Water Treat* 123:240–252. <https://doi.org/10.5004/dwt.2018.22767>
  67. Coelho CM, de Andrade JR, da Silva MGC, Vieira MGA (2020) Removal of propranolol hydrochloride by batch biosorption using remaining biomass of alginate extraction from *Sargassum filipendula* algae. *Environ Sci Pollut Res* 27:16599–16611. <https://doi.org/10.1007/s11356-020-08109-4>
  68. Sahu O, Singh N (2019) Significance of bioadsorption process on textile industry wastewater. In: *The impact and prospects of green chemistry for textile technology*. Woodhead Publishing, pp 367–416. <https://doi.org/10.1016/B978-0-08-102491-1.00013-7>
  69. Kyzas GZ, Kostoglou M, Lazaridis NK, Lambropoulou DA, Bikiaris DN (2013) Environmental friendly technology for the removal of pharmaceutical contaminants from wastewaters using modified chitosan adsorbents. *Chem Eng J* 222:248–258. <https://doi.org/10.1016/j.cej.2013.02.048>
  70. Crini G, Lichtfouse E, Wilson LD, Morin-Crini N (2019) Conventional and non-conventional adsorbents for wastewater treatment. *Environ Chem Lett* 17:195–213. <https://doi.org/10.1007/s10311-018-0786-8>
  71. Escudero LB, Quintas PY, Wuilloud RG, Dotto GL (2019) Recent advances on elemental biosorption. *Environ Chem Lett* 17:409–427. <https://doi.org/10.1007/s10311-018-0816-6>
  72. Ahsan MA, Islam MT, Imam MA, Hyder AG, Jabbari V, Dominguez N, Noveron JC (2018) Biosorption of bisphenol A and sulfamethoxazole from water using sulfonated coffee waste: isotherm, kinetic and thermodynamic studies. *J Environ Chem Eng* 6(5):6602–6611. <https://doi.org/10.1016/j.jece.2018.10.004>
  73. Bello OS, Alao OC, Alagbada TC, Olatunde AM (2019) Biosorption of ibuprofen using functionalized bean husks. *Sustain Chem Pharm* 13:100151. <https://doi.org/10.1016/j.jece.2018.10.004>
  74. Rodriguez-Narvaez OM, Peralta-Hernandez JM, Goonetilleke A, Bandala ER (2017) Treatment technologies for emerging contaminants in water: a review. *Chem Eng J* 323:361–380. <https://doi.org/10.1016/j.cej.2017.04.106>
  75. Bodzek M, Konieczny K (2018) Membranes in organic micropollutants removal. *Curr Org Chem* 22(11):1070–1102. <https://doi.org/10.3390/app10082969>
  76. Zielińska M, Cydzik-Kwiatkowska A, Bułkowska K, Bernat K, Wojnowska-Baryła I (2017) Treatment of bisphenol A-containing effluents from aerobic granular sludge reactors with the use of microfiltration and ultrafiltration ceramic membranes. *Water Air Soil Pollut* 228:1–9. <https://doi.org/10.1007/s11270-017-3450-1>
  77. Si X, Hu Z, Huang S (2018) Combined process of ozone oxidation and ultrafiltration as an effective treatment technology for the removal of endocrine-disrupting chemicals. *Appl Sci* 8(8):1240. <https://doi.org/10.3390/app8081240>
  78. Kamaz M, Wickramasinghe SR, Eswaranandam S, Zhang W, Jones SM, Watts MJ, Qian X (2019) Investigation into micropollutant removal from wastewaters by a membrane bioreactor. *Int J Environ Res Public Health* 16(8):1363. <https://doi.org/10.3390/ijerph13090917>

79. Irmak S, Erbatur O, Akgerman A (2005) Degradation of 17 $\beta$ -estradiol and bisphenol A in aqueous medium by using ozone and ozone/UV techniques. *J Hazard Mater* 126(1–3):54–62. <https://doi.org/10.1016/j.jhazmat.2005.05.045>
80. Hu JY, Aizawa T, Ookubo S (2002) Products of aqueous chlorination of bisphenol A and their estrogenic activity. *Environ Sci Technol* 36(9):1980–1987. <https://doi.org/10.1021/es011177b>
81. Frontistis Z, Xekoukoulotakis NP, Hapeshi E, Venieri D, Fatta-Kassinos D, Mantzavinos D (2011) Fast degradation of estrogen hormones in environmental matrices by photo-Fenton oxidation under simulated solar radiation. *Chem Eng J* 178:175–182. <https://doi.org/10.1016/j.cej.2011.10.041>
82. Sun M, Xu D, Ji Y, Liu J, Ling W, Li S, Chen M (2016) Using Fenton oxidation to simultaneously remove different estrogens from cow manure. *Int J Environ Res Public Health* 13(9):917. <https://doi.org/10.3390/ijerph13090917>
83. Raji M, Mirbagheri SA, Ye F, Dutta J (2021) Nano zero-valent iron on activated carbon cloth support as Fenton-like catalyst for efficient color and COD removal from melanoidin wastewater. *Chemosphere* 263:127945. <https://doi.org/10.1016/j.chemosphere.2020.127945>

# Electrochemical Coagulation of Wastewater Using Aerial Roots of Banyan Tree as Adsorbent



Sachin Mane and Pratiksha P. Patil

## 1 Introduction

The consequences of human interference with nature have been consistently borne by the environment. Industrial effluents discharged into ecosystems result in cacophony of impurities, their variations quantifiable through metrics like biological oxygen demand, chemical oxygen demand, total suspended solids, as well as attributes such as organic and non-organic constituents, color, odor, and more [1–3]. In the realm of contemporary solutions, electrochemical coagulation emerges as an appealing avenue for wastewater treatment through the incorporation of natural coagulants. Its appeal lies in its eco-friendly nature and operational simplicity. Originally designed to eliminate heavy cations and microbial populations from wastewater, this method evolved haphazardly due to its remarkable benefits and the vast potential it demonstrated across diverse water treatment applications [4, 5]. The efficacy of electrochemical coagulation hinges upon factors like pH levels, current density, applied voltage, stirring rate, and interelectrode distance [6–10]. This approach offers superior efficacy, cost-efficiency, and safety when juxtaposed with conventional methodologies. Its prowess in eliminating even the minutest colloidal particles surpasses conventional activated sludge procedures and other techniques. Moreover, its adaptability allows it to tailor treatment intensity according to the impurity load, achieved by adjusting influencing parameters [11–14]. Electrochemical coagulation stands as a revolutionary force in wastewater treatment, vouched for as a worthy alternative to entrenched technologies across industrial and domestic sectors. Its environmental friendliness is undeniable, leaving no detrimental impact on the surroundings [6, 15, 16]. This process operates by neutralizing residual charges via applied voltage, catalyzing coagulation through adsorption. It effectively reduces the need for excessive synthetic coagulants that otherwise neutralize surplus non-organic coagulants,

---

S. Mane · P. P. Patil (✉)  
D. Y. Patil College of Engineering, Akurdi, Pune, India  
e-mail: [pratikshapatil8098@gmail.com](mailto:pratikshapatil8098@gmail.com)

minimizing the potential for secondary chemical contamination [8, 12, 17]. The method extends its prowess to tackling heavy metals, both organic and non-organic impurities, emulsifiers, color, body, COD, and more. The selection of electrode materials significantly influences the percentages of COD, BOD, turbidity, and ammonia removal. Among these, copper electrodes yield optimal outcomes, yet their cost impedes widespread application [7, 14, 18, 19]. For practical electrode use, Al and Cu electrodes shine, liberating three electrons each under high voltage and current density [15, 20]. This study's prime objective is to dissect the electrochemical coagulation process bolstered by a natural adsorbent—an aqueous solution derived from the aerial roots of the banyan tree. This novel approach enriches the coagulant bed, enhancing impurity sedimentation during the electrochemical coagulation process.

### 1.1 Process of Electrocoagulation

When an electric current courses through wastewater via electrodes in an electrocoagulation tank as shown in Fig. 1, it instigates the creation of metal ions at the anode and the liberation of free electrons. Simultaneously, water molecules disintegrate at the cathode, engendering hydrogen ions and OH<sup>-</sup> ions. These hydrogen ions subsequently engage in reactions, culminating in the production of hydrogen gas at the cathode. In parallel, metal ions intermingle with OH<sup>-</sup> ions, engendering the formation of floc molecules [7, 20, 21]. The introduction of a coagulant fosters the destabilization of these floc molecules, prompting their absorption into coagulant molecules. This interaction begets macro-sized, weighty floc particles that subsequently settle under the influence of gravitational force [22, 23]. Thus sedimented, these floc particles can be extracted from the lower strata. The efficacy of the electrochemical coagulation technique pivots significantly on several variables, including treatment duration, pH levels, current density, coagulant concentration, applied voltage, inter-electrode spacing, the immersed electrode's surface area, and ambient temperature [21–24].

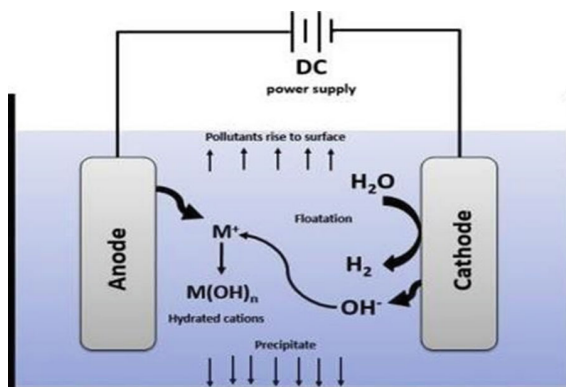
Reactions in electrocoagulation tank:

At Anode:  $M \rightarrow M^{++} + e^{-}$  (Anode sacrifices metal ions to generate free electrons).

At Cathode:  $H_2O + e^{-} \rightarrow OH^{-} + H_2$  (Generates H<sub>2</sub> gas and creates an environment for electrolysis) [8, 12, 25, 26].

- pH Levels: Electrolysis leads to a pH increase in the medium due to the release of hydrogen gas (H<sub>2</sub>) at OH<sup>-</sup> ions. This shift can detrimentally impact the efficiency of electrolysis. A pH range of 5–6 is recommended to ensure safety and optimal performance [6, 7, 10].
- pH Range:
  - 0–5: Highly acidic conditions.
  - 6–14: Unfavorable for effective electrolysis. 5–6: Ideal range for electrolytic processes.

**Fig. 1** Basic structure of electrochemical coagulation process. Source Factors influencing electrochemical Coagulation



- **Current Density:** Amplifying current density enhances ion production per second, thereby accelerating impurity removal. However, this escalation also expedites electrode decomposition. Beyond a current density of  $25 \text{ A/cm}^2$ , impurity removal rates plateau [6, 8, 10].
- **Electrolysis Time:** The duration of electrolysis correlates directly with the rate of impurity elimination [6, 27].
- **Applied Voltage:** The voltage applied during electrolysis directly influences the pace of impurity removal [4, 8].
- **Electrode Material:** Common electrode materials encompass aluminum and iron. While copper electrodes yield exceptional outcomes, their cost-effectiveness for large-scale treatment plants is questionable. Carbon electrodes are preferred due to their non-corrosive nature [14, 17, 28].
- **Coagulant Quantity:** The amount of coagulant employed directly affects the speed of impurity removal [29, 30].
- **Interelectrode Distance:** Augmenting electrode spacing curtails capital costs, albeit at the potential expense of treatment efficiency [31].

## 2 Material and Methodology

For the execution of this research, the experimental setup entailed applying a 3 V DC current through the wastewater, with a pair of electrodes submerged and spaced 10 cm apart. The establishment of electrical continuity between electrodes and the DC supply was facilitated using simple copper wires. The trio of copper, aluminum, and carbon electrodes were harnessed and linked to the power source. Of these, the copper electrode demonstrated exceptional efficacy, capitalizing on its inherent purifying attributes. In contrast, aluminum electrodes, favored for their economic viability, contributed four negative electrons to the electrolytic process. The non-metallic carbon electrode, characterized by its minimal dissolution and corrosion

rates, emerged as the economically judicious choice for wastewater treatment. Specifications encompassed a 15 cm length, 4 cm width, and 2 mm thickness for the copper electrodes. A pair of carbon electrodes, measuring 10 mm in diameter and 18 cm in length, complemented these. Additionally, a 2 mm thick aluminum sheet served as an electrode.

A coagulant solution was prepared from banyan tree aerial roots: 100 g of these roots were cut into pieces, combined with 50 ml of distilled water, and homogenized. Filtering yielded a dense, fibrous paste, which, when diluted with 1000 ml of distilled water, produced the aqueous banyan tree solution. Two experiments transpired in an electrocoagulation tank using wastewater samples containing 360 mg/L of COD, sourced from a sewage treatment plant. The treated effluent's COD was measured after 10 min of detention time in the initial experiment. Meanwhile, the second experiment employed the aqueous form of banyan tree aerial roots as a coagulant for electrocoagulation, maintaining identical operating conditions as the first experiment. To pinpoint the optimal dose of banyan tree aerial root coagulant, quantities ranging from 1 to 6 ml were tested in conjunction with the same trio of electrodes utilized in the initial experiment. The sludge generation rate during electrolysis was evaluated by dividing COD removal values by the 10 min electrolysis time per sample. These metrics provided insights into which electrode combination and parameter set yielded optimal wastewater treatment outcomes and sludge generation rates.

### 3 Result and Discussion

Analysis of Table 1 reveals a notable trend: the COD values of treated samples lacking the inclusion of aerial root coagulant exceed those of treated samples utilizing coagulant derived from banyan tree aerial roots. In the quest to determine the optimal coagulant dosage derived from an aqueous solution of banyan tree aerial roots, a systematic exploration spanning 1–6 ml of coagulant dosage was undertaken in tandem with wastewater treatment. Table 1 distinctly highlights that a coagulant dose of 3 ml yielded the most significant COD reduction across all three electrode types employed for electrolysis. In terms of COD removal efficacy, as outlined in Table 2, copper electrodes achieved a remarkable 92% efficiency in wastewater treatment, surpassing aluminum and carbon electrodes which achieved 81% and 78% COD removal efficiencies, respectively. Figure 2 visually elucidates that the electrocoagulation process, when coupled with coagulant addition, enhances COD removal in contrast to treatment without coagulant.

The implications are clear: The introduction of the banyan tree aerial root coagulant in its aqueous state accelerates sludge formation rates and accomplishes wastewater purification without necessitating elevated voltage supplies [32–34]. Significantly outperforming its aluminum and carbon counterparts, the copper electrode distinguishes itself due to its release of three charged free electrons, inherently unstable when juxtaposed with aluminum's three free electrons and the four electrons of non-metallic carbon, resulting in its sustained electricity flow. The data depicted

**Table 1** COD of treated wastewater in mg/l

Electrode coagulant added in ml							
	0	1	2	3	4	5	6
Copper	124	120	70	30	50	65	100
Aluminum	143	140	100	70	75	90	130
Carbon	155	150	125	80	100	110	170

**Table 2** COD removal efficiency in % of treated wastewater

Electrode coagulant added in ml							
	0	1	2	3	4	5	6
Copper	65.56	66.67	80.56	91.67	86.11	81.94	72.22
Aluminum	60.28	61.11	72.22	80.56	79.17	75.00	63.89
Carbon	56.94	58.33	65.28	77.78	72.22	69.44	52.78

**Fig. 2** Graph of coagulant dose versus COD removal efficiency



in Table 2 corroborates this, showcasing heightened COD removal efficiency. This effect can be attributed to the inclusion of the coagulant derived from banyan tree aerial roots in their aqueous form. This coagulant aids in impurity absorption along the carbon chain of amino acids and the sequential copper arrangement, thereby yielding consistently enhanced results. The profound cleansing properties of this coagulant further amplify its prowess [35–37]. While the increment in efficiency appears modest in Fig. 3, its impact on electrode erosion is substantial. Impurities garnishing the amino acid chains of banyan tree aerial roots, in place of metal ions with limited surface area, significantly exacerbate electrode erosion. In contrast, the coagulant fashioned from an aqueous solution of banyan tree aerial roots presents a far larger surface area than any metal ion, enhancing the likelihood of impurity adsorption along amino acid carbon chains. Consequently, this coagulant emerges as a superior option for expediting wastewater treatment processes. The inclusion of the coagulant is pivotal in boosting electrocoagulation efficiency, concurrently mitigating electrode corrosion, and consequentially reducing implementation costs. Figure 3 provides a clear insight: the introduction of the coagulant amplifies the

**Fig. 3** Graph of comparison of COD removal efficiency with and without coagulant

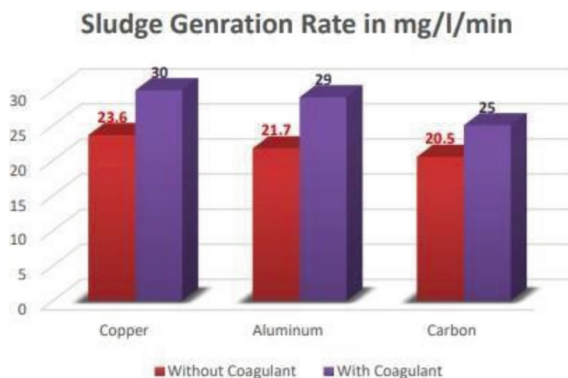


**Table 3** Sludge generation rate in mg/l/min

Electrode	Without coagulant	With coagulant
Copper	23.6	30
Aluminum	21.7	29
Carbon	20.5	25

sludge generation potential and accelerates the purification pace. This augmentation signifies that coagulant incorporation holds the potential to curtail the necessary wastewater electrolysis duration. This time compression translates to heightened cost, cost-effectiveness, curbing electricity expenses, and elongating the electrode replacement cycle. As depicted in Table 3, the rate of sludge generation surged by approximately 5–7 mg/L/min, contingent on the electrode type employed.

## 4 Conclusion

Within this study, the infusion of banyan tree aerial roots, fashioned into a coagulant, into the electrocoagulation process ushers in heightened impurity removal capabilities, surpassing the conventional aeration tank technique and standard electrocoagulation approach. The integration of aqueous aerial root solution into electrocoagulation augments treatment efficacy by bolstering sludge production, concurrently extending electrode longevity via erosion reduction. This technique operates on a diminished power supply in contrast to conventional electrocoagulation methods, thereby slashing energy consumption. The amino acid content within the coagulant forms intricate bonds with ionized organic and inorganic impurities, inducing their settling along amino acid chains to forge more effective adsorbents than metal ions. This additive accelerates both time and cost-effectiveness, curbing electrode wastewater decomposition rates. The aqueous banyan tree aerial root's protein chain serves as an adept adsorbent, facilitating the sedimentation of suspended impurities within

the tank sans the need for additional voltage. The absence of necessity for metal ions obviates the requirement for supplementary electricity to facilitate adsorption. This process could further evolve through the development of an artificially engineered adsorbent featuring elongated chains surpassing banyan tree aerial roots. Such an adsorbent would offer a more stable surface area than natural counterparts while still permitting hassle-free decomposition, all without detriment to the environment.

## References

1. Mickova I (2015) Advanced electrochemical technologies in wastewater treatment part I: electrocoagulation. *Am Sci Res J Eng Technol Sci* 14(2):273–294
2. Zaleschi L, Teodosiu C, Cretescu I, Rodrigo MA (2012) A comparative study of electrocoagulation and chemical coagulation processes applied for wastewater treatment. *Environ Eng Manag J* 11(8):1517–1525
3. Birima AH, Hammad HA, Dessa MNM, Muda Z (2013) Extraction of natural coagulant from peanut seeds for the treatment of turbid water. *Int Conf Energy Environ* 16(5):1
4. Kazi T, Virupakshi A (2013) Treatment of tannery wastewater using natural coagulants. *Int J Innov Res Sci Eng Technol* 2(8):43–47
5. Kumar V, Norzila O, Syazwani A (2017) Application of natural coagulants to treat wastewater—a review. *MATEC Website Conf* 103(9):1
6. Chopra A, Sharma AK, Kumar V (2011) Overview of electrolytic treatment: an alternative technology for purification of wastewater. *Arch Appl Sci Res* 3(5):291–306
7. Bharath M, Krishna BM, Manoj KB (2018) A review of electrocoagulation process for wastewater treatment. *Int J ChemTech Res* 11(3):289–302
8. Dehghani M, Seresht SS, Hashemi H (2013) Treatment of hospital wastewater by electrocoagulation using aluminum and iron electrodes. *Int J Environ Health Eng* 2(5):32–37
9. Abbas SH, Ali WH (2018) Electrocoagulation technique used to treat wastewater: a review. *Am J Eng Res* 7(10):74–88
10. Neerajasree VR, Ashokan V (2019) Effect of natural coagulants on the treatment of automobile service station waste water. *Int Res J Eng Technol* 6(6):161–164
11. Arora A, Kaur R, Kaur A, Singh N, Sharma S (2018) Treatment of wastewater through electrocoagulation. *Pollut Res* 37(2):394–403
12. UkiweL N, Ibeneme SI, Duru CE, Okolue BN, Onyedika GO, Nweze CA (2014) Chemical and electrocoagulation techniques in coagulation flocculation in water and wastewater treatment—a review. *Int J Recent Res Appl Stud* 18(3):285–294
13. Chaturvedi SI (2013) Electrocoagulation: a Novel wastewater treatment method. *Int J Mod Eng Res* 3(1):93–100

14. Vijayaraghavan G, Sivakumar T, Kumar AV (2011) Application of plant based coagulants for wastewater treatment. *Int J Adv Eng Res Stud* 1(1):88–92
15. Soni B, Swami M, Shah HR (2015) Electrochemical methods for wastewater treatment. *Indian J Appl Res* 5(1):70–73
16. Saravan J, Priyadarshini G, Soundaamal A, Sudha G, Suriyakala K (2017) Wastewater treatment using natural coagulant. *Int J Civil Eng* 4(3):40–42
17. Botte GG (2017) Electrochemical technologies for water treatment, management, and efficiency. *Electrochem Soc Interface* 26(2):53–61
18. Mathuram M, Meera R, Vijayaraghavan G (2018) Application of locally sourced plants as natural coagulants for dye removal from wastewater: a review. *J Mater Environ Sci* 9(7):2058–2070
19. Patil C, Hugar M (2015) Treatment of dairy wastewater by natural coagulants. *Int Res J Eng Technol* 2(4):1120–1125
20. Latha A, Partheeban P, Ganesan R (2017) Treatment of textile wastewater by electro-chemical method. *Int J Earth Sci Eng* 10(1):146–149
21. Zailani LWM, Zin NSM (2017) Application of electrocoagulation in various wastewater and leachate treatment- a review. *IOP Conf Series Earth Environ Sci* 140(1–9):1
22. Cezmierska M, Szczes A, Wilkolazka AJ (2015) Purification of wastewater by natural flocculants. *J Biotechnol Comput Biol Bionanotechnol* 96(4):272–278
23. Ashrafuzzaman Md, Fakhruddin ANM, Hossain A (2011) Reduction of turbidity of water using locally available natural coagulants. *Int Sch Res Netw ISRN Microbiol* 2011:1–6
24. Mathew A, Dubey A, Rajan R, Mahindrakar A (2014) Laboratory electrocoagulation using carbon electrodes and comparative coagulation studies. *Int J Eng Res Technol* 3(9):518–521
25. Dewa KS, Nyom S (2018) Indirect electrochemical oxidation with multi carbon electrodes for restaurant wastewater treatment. *J Ecol Eng* 19(1):200–204
26. López MM, Vereá L, Verde A, Lara B, Campos J, Najera MC, Sebastian PJ (2018) Improvement of the carbon electrode treatment to obtain bioanodes for microbial electrolysis cell (MEC). *Int J Electrochem Sci* 13:3970–3985
27. Ahmed SN, Saad AA (2013) Electrocoagulation technology in wastewater treatment: a review of methods and applications. *Civil Environ Res* 3(11):29–42
28. Sign AK, Awasthi M (2017) Treatment of hospital wastewater using electrochemical method. *Ind J Ind Electron Elect Eng* 5(7):4–9
29. Jog O (2018) Hospital wastewater treatment by the electro-coagulation process. *Int J Adv Res Ideas Innov Technol* 4(6):495–496
30. Fersi C, Gamra AB, Bozrati H, Gorgi C, Irmani A (2018) Characterizing the performance of coagulation-flocculation using natural coagulants as pretreatment of tannery wastewater. *J Mater Environ Sci* 9(8):2379–2386
31. Butler E, Yung-Tse H, Ruth YuY, Mohammed SA (2011) Electrocoagulation in wastewater treatment. *Water* 3(2):495–425
32. Khader EH, Mohammed THJ, Mirghaffari N (2018) Use of natural coagulants for removal of COD, Oil, and turbidity from production in the petroleum industry. *J Pet Environ Biotechnol* 9(3):1–7
33. Ugwa SN, Umaokoro AF, Echiegu EA, Ugwuishiwu BO, Enweremadu CC (2017) Comparative study of the use of natural and artificial coagulants for the treatment of Sulage. *Cogent Eng* 4(1):1–13

34. Benalia A, Derbal K, Panico A, Pirozzi F (2019) Use of acron leaves as a natural coagulant in a drinking water treatment plant. *Water* 11(1):1–12
35. Huimin F, Youngwen M, Jinqun W, Yan W (2020) Removal of gentian violet and rhodamine B using banyan aerial roots after modification and mechanism studies of differential adsorption behaviors. *Environ Sci Pollut Res* 27(9):9152–9166
36. Shabina AR, Anu N (2016) Comparative study of adsorption of Cr(Vi) from waste water using tapioca peel and banyan tree root. *Int J Sci Eng Res* 7(4):304–306
37. Gnanasundaram N, Thanapalan M, Rambabu K, Sathiyarayanan K, Pau L (2021) Adsorptive removal of phenol using banyan root activated carbon. *Chem Eng Commun* 208(6):831–842

# Analysis of Groundwater Quality in the Coastal Stretch of Bhavnagar, Gujarat



Nayankumar P. Soni, S. D. Dhiman, and Singh Garima Shailendra

## 1 Introduction

The quantity and quality of groundwater are essential factors in the context of modern water management. The main element affecting water quality is pollution, which comes from many different sources. Sectoral approaches divide the overall amount of available water, creating a shortage. Groundwater pollution in coastal locations is mostly caused by seawater intrusion. Overexploitation is a severe problem that affects the potability of water [1]. Hydrogeochemical processes control the chemistry of water. In many coastal towns and cities, groundwater appears to be the only source of freshwater for domestic, agricultural, and industrial purposes [2]. Groundwater is the underground liquid that exists in the saturated zone, which is below the earth's surface and has a varied thickness and depth [3].

Because many things can dissolve in water and others may float there, there is a chance of contamination with dangerous substances. They consist of petroleum, hydrocarbons (oil), pesticides, minerals, and pathogenic (disease-causing) bacteria [4]. Groundwater is often less likely to get contaminated than surface waterways like streams, rivers, and lakes due to the fact that poisons must pass through the earth in order to reach the water [5]. Even yet, contamination is still a possibility, especially if the rocks and soil above have openings that let dangerous compounds flow around

---

N. P. Soni (✉)  
Gujarat Technological University, Ahmedabad, India  
e-mail: [nayan7096@gmail.com](mailto:nayan7096@gmail.com)

S. D. Dhiman  
Civil Engineering Department, B.V.M. Engineering College, Vallabh Vidyanagar, Gujarat, India  
e-mail: [sddhiman@bvmengineering.ac.in](mailto:sddhiman@bvmengineering.ac.in)

S. Garima Shailendra  
Department of Civil Engineering, Shantilal Shah Government Engineering College, Bhavnagar, Gujarat, India

more easily [3, 6]. To ascertain the qualities of groundwater, analysis of its chemical, physical, and biological components is frequently required.

The aim of this study is to understand the hydrochemical characteristics of the study area by calculating the Water Quality Index and creating Hill–Piper Trilinear diagrams. The current study will be conducted in the coastal region near Bhavnagar for the hydrochemical examination and calculation of hydrochemical parameters [7, 8]. The Weighted Arithmetic Index Method, as described by Brown et al. in 1972, will be used to generate the Water Quality Index using MS-Excel to ascertain the main hydrochemical input parameters and evaluate the kind of groundwater in the research area [6].

## 2 Study Area

The studied area in the current paper is the Saurashtra region's Bhavnagar shoreline. At 21.76°N latitude and 72.15°E longitude, Bhavnagar, popularly known as Kathiawar, is a seaside city on Saurashtra's eastern coast as shown in Fig. 1. It is typically 24 m (78 feet) tall. The Bhavnagar district covers a total area of 108.27 km<sup>2</sup>. Bhavnagar experiences mild winters from November to February, scorching, dry summers from March to mid-June, and the rainy monsoon season from mid-June to October. Bhavnagar gets 655 mm, or 26 inches, of rain every month during the monsoon season. Temperatures in Bhavnagar typically range from 13.8 to 42.6 °C, and average temperature is 27.7 °C annually. There is a lot of medium-black soil in the Bhavnagar district. Along the Shetrunji River, which passes through portions of the Gariyadhar and Palitana talukas, alluvial soil may be seen. This region's soil is less productive due to its salinity. Alkaline soil can be found in several areas of the Gariyadhar Taluka. Their composition is made up of both productive and unproductive soils, according to the Central Ground Water Board Report 2014.

## 3 Data Collection

For the current investigation, data were acquired from the Geo-hydrologist, Groundwater Investigation Unit-3, for the years 2017–2021. Data on groundwater quality was gathered for this study from 24 well locations both close to and distant from Bhavnagar's coastline. Latitude, longitude, geology, and significant cations and anions including sodium (Na), potassium (K), calcium (Ca), magnesium (Mg), chloride (Cl), sulfate (SO<sub>4</sub>), carbonate (CO<sub>3</sub>), and bicarbonate (HCO<sub>3</sub>) are among these facts. Total dissolved solids (TDS), total hardness (TH), fluoride (F), pH, and electrical conductivity (EC) are some examples. For the present study, as shown in Fig. 2, information was acquired over a five-year period for the premonsoon and postmonsoon seasons. Every well discovered in the research area was taken to be a dug well based on the data.

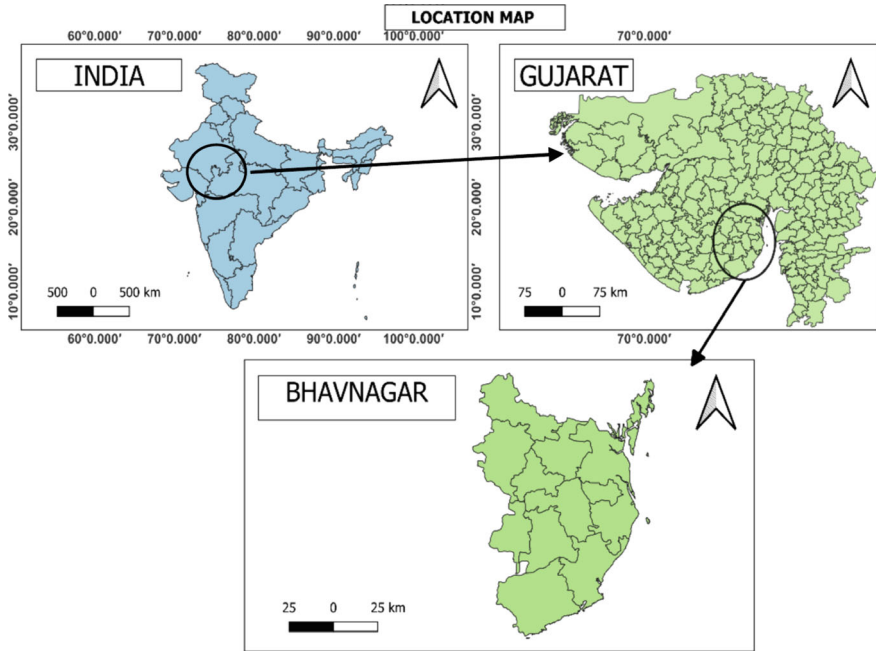


Fig. 1 Location map of study area

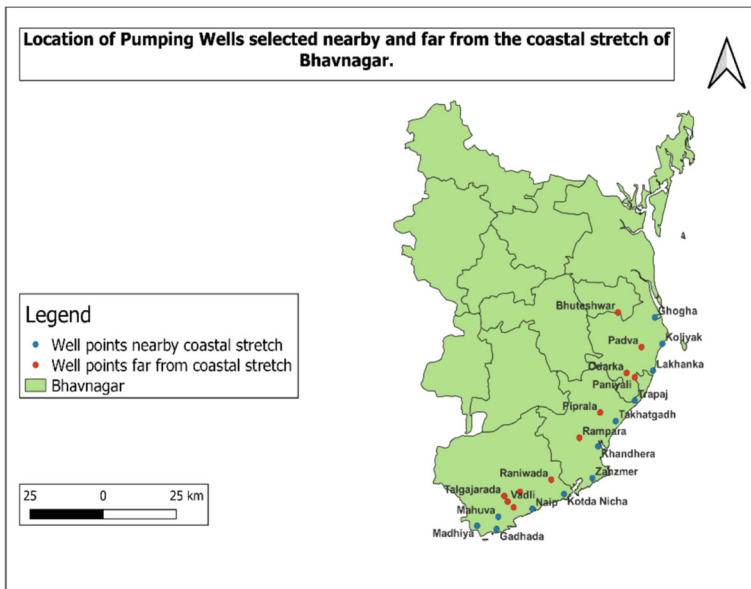


Fig. 2 Location of well points selected nearby and far from the coastal stretch of Bhavnagar (Source QGIS Desktop 3.26.3)

## 4 Research Methodology

A. Weighted Arithmetic Index Method Calculation with MS-Excel Software (by Brown et al. 1972)

**Step 1:** Using the formula, determine the unit weight ( $W_n$ ) factors for each parameter

$$W_n = \frac{K}{S_n}$$

where

$$K = \frac{1}{1/S_1 + 1/S_2 + 1/S_3 + \dots + 1/S_n}$$

$$= \frac{1}{\sum \frac{1}{S_n}}$$

$S_n$  = Standard desirable value of the  $n$ th parameters.

$W_n = 1$ (unity) when all the chosen parameters unit weight factors are added together.

**Step 2:** Using the formula, determine the sub-index ( $Q_n$ ) value

$$Q_n = \frac{[(V_n - V_o)] \times 100}{[(S_n - S_o)]}$$

where

$V_n$  = Mean concentration of  $n$ th parameters.

$S_n$  = Standard desirable value of the  $n$ th parameters.

$V_o$  = Actual values of the parameters in pure water (generally  $V_o = 0$ , for most parameters except for pH)

$$Q_{pH} = \frac{[(V_{pH} - 7)] \times 100}{[(8.5 - 7)]}$$

**Step 3:** Adding Step 1 and Step 2, WQI is determined as follows

$$\text{Overall WQI} = \frac{\sum W_n Q_n}{\sum W_n}$$

B. Using QGIS 3.28.1 Software Version, Perform Spatial IDW Interpolation

**Step 1:** Preparing a Shapefile

In order to easily obtain shape files for any type of research topic, it is required to be familiar with QGIS software because it is public domain. Since QGIS is a free program, shape files can be obtained from their official websites. To access the Indian spatial data, you must first surf the DIVA GIS website and obtain a free shapefile. Launching QGIS after creating a new project and choosing Add Layer and Add Vector Layer are the following steps. To change the style, font, label, symbology, and other settings for a vector layer that you have added to a layer group, use the layer properties option by right-clicking on the layer. Your file will now be saved as an ESRI Shapefile with the OK button clicked.

**Step 2:** Creating an Inverse Distance Weighted (IDW) Interpolation File

Make an Interpolated (IDW) Inverse Distance Weighted file by going to Layer and choosing Add delimited text layer. Text layer files with delimited fields should be saved in CSV (comma-separated values) format. Select the Grid (Inverse Distance to a Power) option under Analysis by navigating to the raster option in the QGIS software's menu bar. After selecting the appropriate ESRI Shapefile to be interpolated and the Water Quality Index (WQI) option in the advance parameters field option, run the software.

Select the Clip Raster by Mask Layer option under Extraction after choosing the Raster option from the menu bar of the QGIS software once more. Once the required Mask Layer name has been entered in the Mask Layer box in [EPSG:4326] format, run the software.

#### ***4.1 Piper Diagram Data Analysis of Hydrochemical Facies***

In 1944, Arthur M. Piper first proposed using a Piper diagram to illustrate the facts related to water chemistry. It can be used to understand the origin of the dissolved salts in water [9]. A Piper diagram provides a visual representation of the chemistry of a water sample or samples. Separate ternary graphs are used to display the cations and anions. Sodium, potassium, calcium, and magnesium are the apex cations of the cation plot [10]. At the peak of the anion plot are the hydrogen carbonate anions, sulfate, chloride, and carbonate anions.

Hydrochemical facies can be used to categorize the water samples represented on the Piper diagram. The regions of the cation and anion triangles can be determined by the dominant cation(s) or anion(s), and their combination produces the diamond-shaped section of the diagram.

## **4.2 *Piper Diagram Plotting and Data Input with GW\_Chart Software***

The GW Chart was created by the United States Geological Survey (USGS). This application generates specific graphs for use in groundwater studies. The GW Chart-Piper Graph uses a Piper diagram to graphically represent the chemistry of a water sample [4]. All of the allowed data formats for the Piper diagram include ratios, percentages, milliequivalents per liter, and milligrams per liter. The key input parameters for the GW Chart-Piper Graph are hydrochemical parameters such as calcium (Ca), magnesium (Mg), sodium (Na), potassium (K), carbonate ( $\text{CO}_3$ ), bicarbonate ( $\text{HCO}_3$ ), chlorine (Cl), sulfate ( $\text{SO}_4$ ), and total dissolved salts (TDS).

## **4.3 *The advantages of using piper diagram over other methods are as under***

The Piper diagram assists in categorizing analytical data, which is essential for determining the origins of the dissolved components in water.

The procedure's feasibility relies on the fact that natural water maintains chemical equilibrium between its anions and cations.

The primary cations found in water bodies like rivers, lakes, and groundwater are typically calcium ( $\text{Ca}^{2+}$ ), magnesium ( $\text{Mg}^{2+}$ ), and sodium ( $\text{Na}^+$ ), while the main anions include bicarbonate ( $\text{HCO}_3^-$ ), sulfate ( $\text{SO}_4^{2-}$ ), and chloride ( $\text{Cl}^-$ ).

Piper diagrams are valuable as they serve for both categorizing water quality information and detecting influences on the data, like the mixing of different types of water, ion exchange, and the formation or disappearance of minerals.

# **5 Result and Discussion**

## **5.1 *Premonsoon (May 2017) and Postmonsoon (Oct 2017) IDW Interpolation of WQI for Well Points Near the Coastal Stretch of Bhavnagar***

The Weighted Arithmetic Water Quality Index method (WAWQI) developed by Brown et al. in 1972 for the evaluation of water quality specifies that the acceptable limit and the allowable limit of the Water Quality Index value are 25 and 100, respectively. From the Premonsoon and Postmonsoon Inverse Distance Weighted (IDW) Interpolation of WQI for Well Points Near the Coastal Stretch of Bhavnagar, it can be seen that the wells area represented for the premonsoon period by light orange color has a lower concentration of WQI value, say less than 65.81, and dark

maroon color has a greater concentration of WQI value, say greater than 139.74. It is also evident that the wells region shown for the postmonsoon period by the white color has a lower WQI value concentration, say less than 50.41 and dark blue has more concentration, say greater than 151.98. This concentration exceeds the permitted level.

According to the color-coded WQI value intervals in Fig. 3, the places with the highest concentrations of WQI values for the premonsoon are Dudhala, Gadhada villages in the Mahuva Taluka, and Ghogha Village in the Ghogha taluka of Bhavnagar, respectively. WQI values in these regions are roughly 168.73, 164.59, and 160.59. The Mahuva Taluka in Bhavnagar, where the premonsoon WQI concentration of 41.05 and 53.96, respectively, has the lowest premonsoon WQI concentration.

The postmonsoon locations in Bhavnagar with the highest concentrations of WQI values are Madhiya Village in the Mahuva Taluka and Ghogha Village in the Ghogha Taluka, where the corresponding values are 185.94 and 171.37. With postmonsoon WQI values of 16.55 and 37.56, the two villages of Takhatgad and Trapaj in Talaja Taluka of Bhavnagar, respectively, had the lowest value concentration.

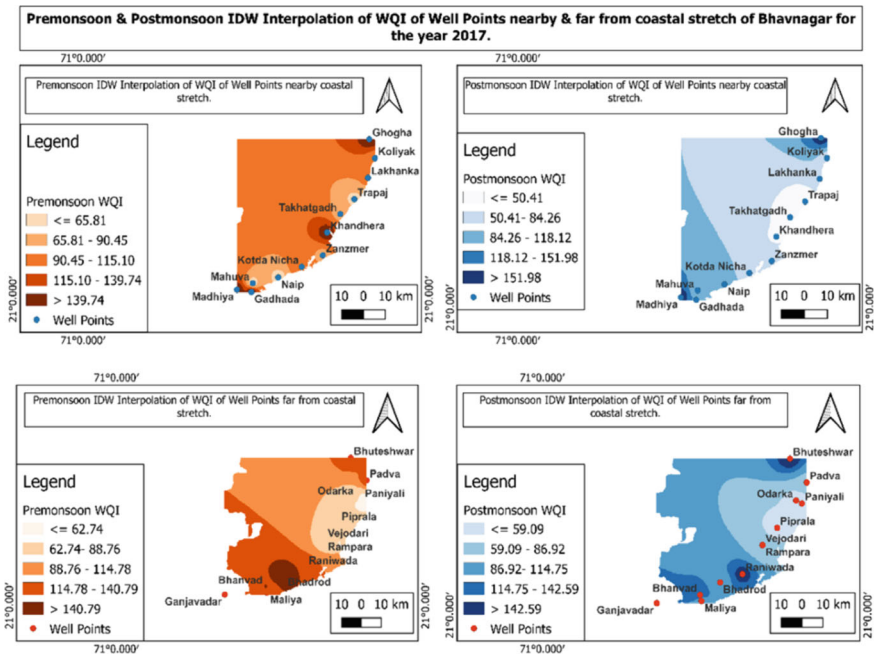


**Fig. 3** Premonsoon and postmonsoon IDW interpolation of WQI for well points nearby and far from the coastal stretch of Bhavnagar for the year 2017

**Table 1** Premonsoon and postmonsoon WQI values for well points nearby coastal stretch for the year 2017

Well No	Village	Latitude	Longitude	Premonsoon WQI	Postmonsoon WQI
1	Ghogha	21.68	72.26	160.59	171.37
2	Koliyak	21.6	72.28	99.43	68.47
3	Lakhanka	21.51	72.25	94.05	68.31
4	Trapaj	21.42	72.19	56.64	16.55
5	Takhatgadhd	21.36	72.13	80.19	37.56
6	Khandhera	21.28	72.07	160.06	44.94
7	Zanzmer	21.18	72.05	79.4	76.28
8	Kotda Nicha	21.13	71.96	113.41	81.72
9	Naip	21.09	71.85	53.96	83.98
10	Mahuva	21.06	71.74	41.05	90.35
11	Gadhada	21.03	71.74	164.59	116.14
12	Madhiya	21.04	71.67	162.73	185.94

### ***5.2 Premonsoon (May 2017) and Postmonsoon (Oct 2017) IDW Interpolation of WQI for Well Points Far from the Coastal Stretch of Bhavnagar***

The Mahuva Taluka in Bhavnagar has the greatest WQI value concentration during the premonsoon, with a value of 166.81. This is what the color caption for the WQI value intervals in the figure indicates. The premonsoon WQI values are lowest in Rampara Village in Talaja Taluka and Paniyali Village in Ghogha Taluka in Bhavnagar, with respective values of 29.74 and 36.66.

The postmonsoon location with the highest concentration of WQI value is Bhuteshwar Village in Bhavnagar, which is around 170.44 according to the color legend for the WQI value intervals in the figure. The lowest postmonsoon WQI value concentrations were found in Piprala, Talaja Taluka, and Odarka, Ghogha Taluka, both in Bhavnagar. These values were 31.25 and 44.8, respectively (Tables 1 and 2).

### ***5.3 Premonsoon (May 2021) and Postmonsoon (Oct 2021) IDW Interpolation of WQI for Well Points Near the Coastal Stretch of Bhavnagar***

It is clear from Fig. 3 that the wells region shown by the light orange color for the premonsoon era has a lower concentration of WQI value, say less than 79.32, while the dark maroon color has a bigger concentration of WQI value, say greater than 157.09. Similarly, the wells region indicated during the postmonsoon period by the

**Table 2** Premonsoon and postmonsoon WQI values for well points far from coastal stretch for the year 2017

Well No	Village	Latitude	Longitude	Premonsoon WQI	Postmonsoon WQI
1	Bhuteshwar	21.69	72.14	138.44	170.44
2	Padva	21.59	72.21	131.01	79.83
3	Odarka	21.51	72.16	70.82	44.8
4	Paniyali	21.49	72.19	36.66	46.97
5	Piprala	21.38	72.08	78.7	31.25
6	Rampara	21.31	72.01	29.74	60.64
7	Vejodari	21.31	72.01	125.77	78.1
8	Raniwada	21.18	71.92	140.13	159.9
9	Bhadrod	21.14	71.81	166.81	90.35
10	Bhanvad	21.09	71.72	141.98	144.14
11	Maliya	21.06	71.73	121.05	91.01
12	Ganjavadar	21.05	71.52	144.35	131.73

light blue color has a lower concentration of WQI value, say less than 87.04, and the dark blue color has a bigger concentration of WQI value, say greater than 160.15. This concentration is higher than what is permissible.

According to the color legend for the WQI value intervals in the figure, the premonsoon WQI value concentration is highest in Ghogha Village in Ghogha Taluka, Dudhala, and Gadhada village in Mahuva Taluka in Bhavnagar, at 201.05, 181.59, and 160.33, respectively. The premonsoon lowest WQI value concentrations in Bhadrod, Naip, and Takhatgadh villages in the Talaja Taluka of Bhavnagar are 53.3, 67.18, and 76.71, respectively.

The highest postmonsoon WQI value concentrations were found in the villages of Madhiya and Dudhala in the Mahuva Taluka and Khandhera Village in the Talaja Taluka in Bhavnagar, with values of 184.96, 162.37, and 154.76, respectively. The postmonsoon lowest WQI value concentration is roughly 62.67, 74.94, and 73.62 in Trapaj and Takhatgadh villages in Talaja Taluka, as well as in Naip Village in Mahuva Taluka in Bhavnagar.

#### **5.4 Premonsoon (May 2021) and Postmonsoon (Oct 2021) IDW Interpolation of WQI for Well Points Far from the Coastal Stretch of Bhavnagar**

While the dark maroon color in Fig. 4 has a larger concentration of WQI value, say more than 162.78, the wells region represented by the white color for the premonsoon era has a lower concentration of WQI value, say less than 84.28. In a similar vein, the white color represents the wells region for the Postmonsoon period and indicates

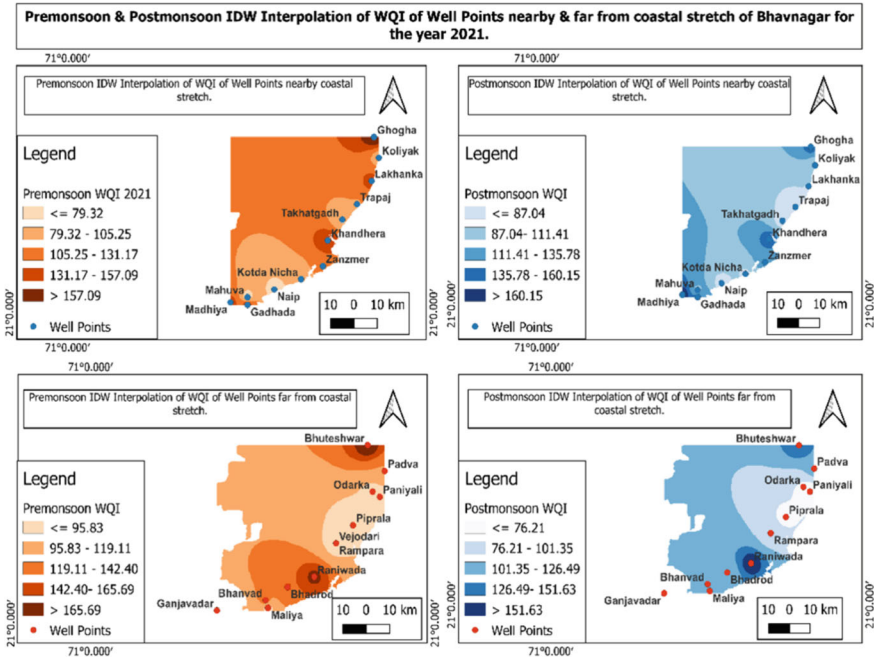


**Fig. 4** Premonsoon and postmonsoon IDW interpolation of WQI for well points nearby and far from the coastal stretch of Bhavnagar for the year 2021

a lower WQI value concentration, say less than 76.27, while the dark blue color indicates a higher WQI value concentration, say larger than 151.65.

According to the color-coded WQI value intervals in the Fig. 5, the Bhuteshwar and Raniwada villages in the Mahuva Taluka of Bhavnagar have the highest concentration of premonsoon WQI values, which are roughly 189.02 and 175.24, respectively. The lowest premonsoon WQI value concentration is found in Rampara Village in Talaja Taluka of Bhavnagar, measuring correspondingly 63.06.

The villages in Bhavnagar with the highest postmonsoon WQI value concentration are Raniwada in the Mahuva Taluka, Timbi in the Jafrabad Taluka in Amreli, and Bhuteshwar in Bhavnagar, with respective values of 176.81, 154.07, and 152.92. The lowest postmonsoon WQI value concentrations, with respective values of 51.03 and 61.15, were found in the villages of Paniyali in Ghogha Taluka and Piprala in Talaja Taluka in Bhavnagar (Tables 3, 4 and 5).

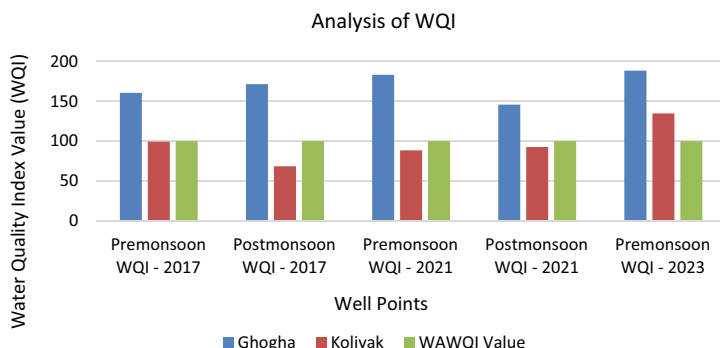


**Fig. 5** Analysis of WQI for pre— and postmonsoon of 2017, 2021, and 2023

**Table 3** Premonsoon and postmonsoon WQI values for well points nearby coastal stretch for the year 2021

Well No	Village	Latitude	Longitude	Premonsoon WQI	Postmonsoon WQI
1	Ghogha	21.68	72.26	183.05	145.72
2	Koliyak	21.6	72.28	88.41	92.57
3	Lakhanka	21.51	72.25	139.78	86.67
4	Trapaj	21.42	72.19	104.15	62.67
5	Takhatgadh	21.36	72.13	76.71	74.94
6	Khandhera	21.28	72.07	157.93	154.76
7	Zanzmer	21.18	72.05	119.52	122.61
8	Kotda Nicha	21.13	71.96	78.19	83.16
9	Naip	21.09	71.85	67.18	73.62
10	Mahuva	21.06	71.74	53.3	100.68
11	Gadhada	21.03	71.74	160.33	149
12	Madhiya	21.04	71.67	143.18	184.96

### 5.5 Piper Trilinear Diagrams for Well Locations Near Coastal Stretch of Bhavnagar (Premonsoon May 2021 and Postmonsoon Oct 2021)

Plotting major cation and anion concentration on a Piper trilinear diagram reveals that Na-Cl is the major water type dominant, whereas mixed Ca-Mg-Cl water type is least common in the well points during premonsoon season while Na-Cl is the major water type dominant (Table 6). However, minimal amounts of mixed Ca-Mg-Cl water type are visible in the well points close to the coastline stretch of Bhavnagar during postmonsoon season as shown in Fig. 6.

**Table 4** Premonsoon and postmonsoon WQI values for well points far from coastal stretch for the year 2021

Well No	Village	Latitude	Longitude	Premonsoon WQI	Postmonsoon WQI
1	Bhuteshwar	21.69	72.14	189.02	152.92
2	Padva	21.59	72.21	118.88	121.29
3	Odarka	21.51	72.16	91.15	74.78
4	Paniyali	21.49	72.19	78.36	51.03
5	Piprala	21.38	72.08	72.53	61.15
6	Rampara	21.31	72.01	63.06	63.59
7	Vejodari	21.31	72.01	114.46	118.92
8	Raniwada	21.18	71.92	175.24	176.81
9	Bhadrod	21.14	71.81	143.47	100.29
10	Bhanvad	21.09	71.72	129.29	99.94
11	Maliya	21.06	71.73	87	122.89
12	Ganjavadar	21.05	71.52	106.74	144.5

**Table 5** Analysis of WQI for well points at Ghogha and Koliyak for premonsoon (2017, 2021, and 2023)

Well points	Ghogha	Koliyak
Premonsoon WQI—2017	160.59	99.43
Postmonsoon WQI—2017	171.37	68.47
Premonsoon WQI—2021	183.06	88.41
Postmonsoon WQI—2021	145.72	92.57
Premonsoon WQI—2023	188.29	134.75

**Table 6** Data on main cations and anions for nearby coastal stretch well points for premonsoon (May 2021)

Well No	Village	Ca	Mg	Na	K	CO <sub>3</sub>	HCO <sub>3</sub>	Cl	SO <sub>4</sub>	TDS
1	Ghogha	150	246	1120	5.70	0	366	1800	910	4620
2	Koliyak	95	153	635	13.40	0	354	880	610	2770
3	Lakhanka	185	249	789	11.80	0	281	1640	570	3750
4	Trapaj	90	156	149	1.30	0	171	384	324	1330
5	Takhatgadh	50	126	297	2.30	0	305	576	109	1500
6	Khandhera	35	60	261	4.40	12	244	392	92	1110
7	Zanzmer	175	315	1300	7.80	0	244	3000	108	5150
8	Kotda Nicha	90	126	661	7.20	0	159	1320	88	2480
9	Naip	40	63	398	58.40	12	439	560	125	1700
10	Mahuva	30	42	79	5.40	0	183	192	0	530
11	Gadhada	60	102	613	22.8	24	622	920	20	2400
12	Madhiya	200	315	2150	14.3	0	207	3800	890	7590

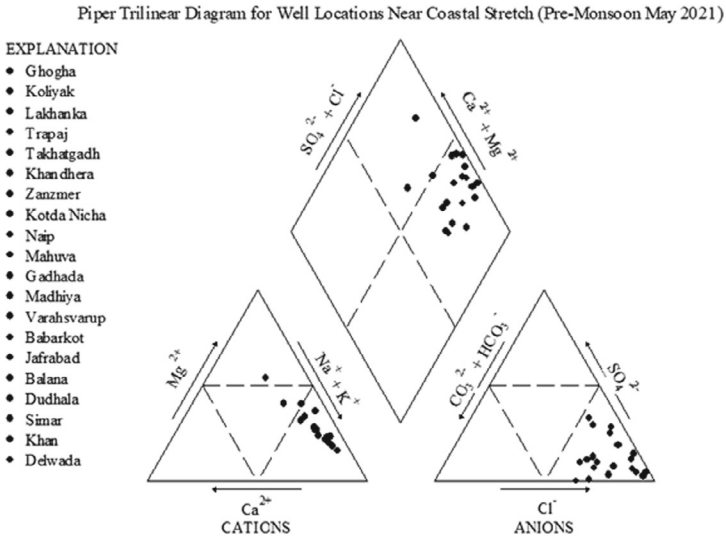


Fig. 6 Piper trilinear diagram (Premonsoon May 2021) for well points nearby coastal stretch

### 5.6 Piper Trilinear Diagrams for Well Locations Away from Coastal Stretch of Bhavnagar (Premonsoon May 2021 and Postmonsoon Oct 2021)

By plotting the major cation and anion concentration on a Piper trilinear diagram, it can be seen from Fig. 7 that Na-Cl is the major dominant water type. In contrast, mixed Ca-Mg-Cl and Ca-Na-HCO<sub>3</sub> water types are seen least in the well points during the premonsoon season (Fig. 8), while Na-Cl is the major water type dominant (Tables 7, 8 and 9).

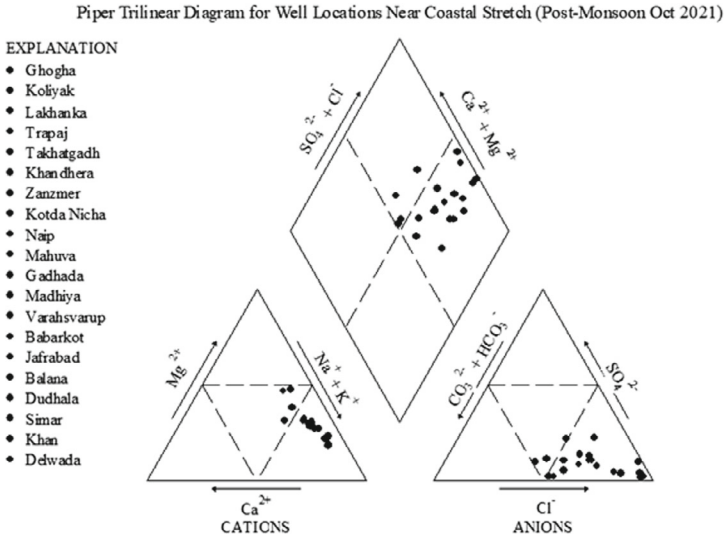


Fig. 7 Piper Trilinear diagram (Postmonsoon Oct 2021) for well points nearby coastal stretch

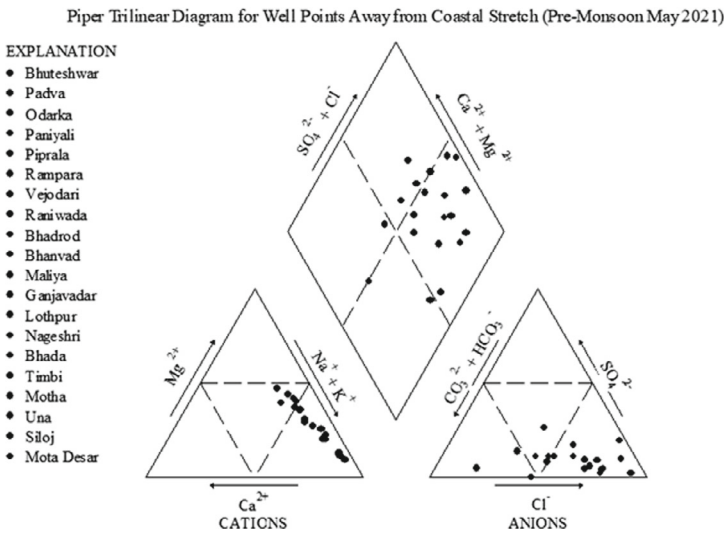


Fig. 8 Piper trilinear diagram (Premonsoon May 2021) for well points far from coastal stretch

**Table 7** Data on main cations and anions for nearby coastal stretch well points for postmonsoon (Oct 2021)

Well No	Village	Ca	Mg	Na	K	CO <sub>3</sub>	HCO <sub>3</sub>	Cl	SO <sub>4</sub>	TDS
1	Ghogha	50	45	120	13.68	35	230	190	12	700
2	Koliyak	50	105	470	13.7	0	293	680	332	1960
3	Lakhanka	60	90	364	0.8	0	451	448	266	1690
4	Trapaj	40	78	120	3.7	0	354	216	75	890
5	Takhatgadh	35	99	162	3.2	0	256	336	107	1020
6	Khandhera	40	66	144	14.7	0	415	200	64	950
7	Zanzmer	200	360	1360	5	2	281	3200	86	5550
8	Kotda Nicha	90	132	432	25.4	0	439	800	116	2070
9	Naip	35	57	319	42.4	12	281	480	108	1340
10	Mahuva	30	42	313	4.9	24	354	352	94	1220
11	Gadhada	60	90	658	14.5	24	488	1545	115	2430
12	Madhiya	150	300	1800	17.4	0	305	3600	210	6390

**Table 8** Data on main cations and anions for far by coastal stretch well points for premonsoon (May 2021)

Well No	Village	Ca	Mg	Na	K	CO <sub>3</sub>	HCO <sub>3</sub>	Cl	SO <sub>4</sub>	TDS
1	Bhuteshwar	50	90	222	16.40	24	842	128	46	1430
2	Padva	50	84	376	352	12	512	352	320	1720
3	Odarka	70	162	341	4.80	0	512	640	162	1920
4	Paniyali	30	42	83	3.60	0	256	128	0	560
5	Piprala	35	75	140	4.20	0	305	216	66	860
6	Rampara	55	99	146	1.10	0	232	304	121	990
7	Vejudari	75	165	997	6.80	0	268	1760	286	3570
8	Raniwada	150	258	906	16.60	0	122	1760	600	3880
9	Bhadrod	25	39	525	2.20	24	769	296	166	1880
10	Bhanvad	45	93	252	7.8	12	293	472	41	1240
11	Maliya	35	51	181	17.9	24	305	240	54	920
12	Ganjavadar	125	246	703	1.6	0	220	1760	58	3160

**Table 9** Data on main cations and anions for far by coastal stretch well points for postmonsoon (Oct 2021)

Well No	Village	Ca	Mg	Na	K	CO <sub>3</sub>	HCO <sub>3</sub>	Cl	SO <sub>4</sub>	TDS
1	Bhuteshwar	30	57	242	9.6	24	720	80	65	1240
2	Padva	30	51	300	136	12	769	136	41	1360
3	Odarka	30	48	62	3.2	0	281	96	0	530
4	Paniyali	25	51	78	1.1	12	195	144	0	520
5	Piprala	30	57	94	3.6	12	171	216	0	600
6	Rampara	35	54	108	4.1	0	183	240	54	680
7	Vejudari	55	96	964	3.5	0	598	1280	308	3310
8	Raniwada	140	231	655	13.3	0	305	1440	300	3130
9	Bhadrod	30	42	313	4.9	24	354	352	94	1220
10	Bhanvad	55	87	269	0.0	12	146	480	129	1220
11	Maliya	25	39	140	23.2	12	232	216	19	710
12	Ganjavadar	30	42	373	8.6	0	451	336	189	1440

## 6 Conclusion

In the north-eastern portion of the research region, more for well sites near the coastal length than for well points further from the coastal stretch, and less in the south-western section, it has been noted that groundwater quality has drastically reduced. This difference in hydrochemistry is caused by the subsequent overuse of groundwater and its contamination by seawater intrusion.

The results of WQI show that most of the well points groundwater samples of nearby coastal stretch of Bhavnagar remain harder throughout the study area as compared to the well points groundwater samples far from the coastal stretch of Bhavnagar.

Spatial interpolation maps of major ions and WQI show that groundwater quality is substantially deteriorated in north-eastern side of the coastal stretch of Bhavnagar more for nearby well points at coastal stretch than well points far from the coastal stretch.

This contrast in hydrochemistry is attributed to subsequent over-exploitation of groundwater.

In the area under investigation, total 58% (7 out of 12 wells) in premonsoon and 50% (6 out of 12 wells) in postmonsoon has been found to have WQI value of greater than 100 as per BIS standard. It indicates that the groundwater is contaminated due to seawater intrusion.

Highest value of WQI (104.15–201.05) for premonsoon and (100.68–184.96) for postmonsoon had been found in Ghogha, Lakhanka, Trapaj, Khan, Zanzmer, Gadhada, and Madhiya village and lowest value of WQI (53.30–88.41) for premonsoon and (62.67–92.57) for postmonsoon had been found in Mahuva, Naip, Kotda-Nicha, Takhatgadh, and Koliyak village nearby coastal stretch of Bhavnagar.

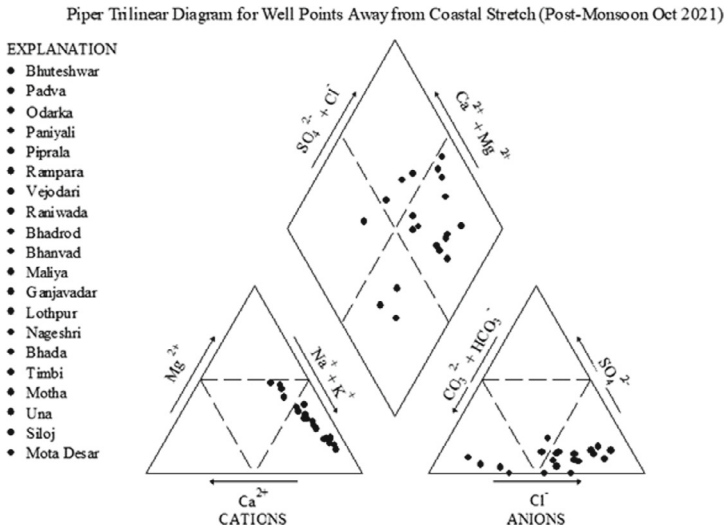


**Fig. 9** Piper trilinear diagram (Postmonsoon Oct 2021) for well points far from coastal stretch

Highest value of WQI (114.46–189.02) for premonsoon and (100.29–152.90) for postmonsoon had been found in Bhuteshwar, Padva, Vejedari, Raniwada, Bhadrod, Vagnagar and Talgajarda village and lowest value of WQI (63.06–91.15) for premonsoon and (51.03–74.78) for postmonsoon had been found in Odarka, Paniyali, Piparla, Rampara village far from coastal stretch of Bhavnagar.

By plotting major cation and anion concentration on a piper trilinear diagram, it can be observed that Na-Cl is the major water type dominant and Ca-Cl water type is seen least during premonsoon period, whereas Na-Cl is the major water type dominant in the area and slight minor content of mixed Ca-Na-Cl type is observed during postmonsoon period nearby coastal stretch of Bhavnagar.

From the piper trilinear diagram as shown in Fig. 9, it can be observed that Na-Cl, mixed Ca-Na-HCO<sub>3</sub> type are the major water type dominant during premonsoon period whereas Na-Cl, Na-HCO<sub>3</sub>, and Na-HCO<sub>3</sub>-Cl are the major water types dominant in the stretch far from coastal stretch of Bhavnagar during postmonsoon period.

This reveals that sodium, chloride, and bicarbonate dominate the ionic concentration in the groundwater due to action of weathering of minerals as well as ion exchange process.

## References

1. Sajil Kumar PJ, Elango L, James EJ (2014) Assessment of hydrochemistry and groundwater quality in the coastal area of South Chennai India. *Arab J Geosci* 7:2641–2653
2. Mao M, Wang X, Zhu X (2016) Hydrochemical characteristics and pollution source apportionment of the groundwater in the east foothill of the Taihang Mountains, Hebei Province. Springer J
3. Mohan BS, Satyanarayana G, Seethram P, Sree GS (2017) Interpretation of ground Water sample analysis around Etcherla in Srikakulam District, Andhra Pradesh. *India SSRG Int J Appl Chem* 4:4–12
4. Patel RL, Dhiman SD (2017) Groundwater quality assessment for irrigation water use in Mahi right bank command area, Gujarat, India. Kalpa Publications in Civil Engineering ICRISSET
5. Sadashivaiah C, Ramakrishnaiah CR and Ranganna G (2008) Hydrochemical analysis and evaluation of groundwater quality in Tumkur Taluka, Karnataka State, India. *Int J Environ Res Public Health*
6. Pradhan B, Pirasteh S (2011) Hydro-chemical analysis of the ground water of the basaltic catchments: upper Bhatsai region Maharashtra. *Open Hydrol J* 5(1):6
7. Jeong CH (2001) Effect of land use and urbanization on hydrochemistry and contamination of groundwater from Taejon area Korea. *J Hydrol* 253(1–4):194–210
8. Badmus GO, Akinyemi OD, Gbadebo AM, Oyedepo JA (2020) Hydrochemical analysis of groundwater quality along the coastal aquifers in part of Ogun Waterside Ogun State southwestern Nigeria. *Heliyon*. 6(12):1
9. Askri B (2015) Hydrochemical processes regulating groundwater quality in the coastal plain of Al Musanaah, Sultanate of Oman. *J Afr Earth Sci* 1(106):87–98
10. Nayak A, Matta G, Uniyal DP (2021) Hydrochemical characterization of groundwater quality using chemometric analysis and water quality indices in the foothills of Himalayas. Springer J

# Surface Water Quality Assessment of Lakhisarai Stretch of Kiul River in Bihar



Gaurav Kumar and Neeta Kumari

## 1 Introduction

Surface water deterioration in most developing countries is caused due to urbanization rather than agriculture or industrial pollutants [6]. River embankments are encroached and used as dumping ground for garbage and sewage effluent [3]. The untreated wastewater from the locality is discharged into the river basin leading to deterioration in the health of the river [25].

According to reports by WHO, BIS, CPCB, and ICMR, approximately 70% of river water in India is deemed contaminated, primarily attributed to human-induced activities [7]. Various methods and techniques are adopted to assess the physico-chemical parameters of rivers which have been reported in different literatures [20]. The water quality of the Kiul River was assessed by prescribed standard APHA methods, then using key physicochemical parameters, Water Quality Index (WQI) was determined. It gives an idea of overall water quality.

The Water Quality Index (WQI) is a numerical expression that provides a summarized assessment of the overall quality of water based on multiple water quality parameters. It offers a convenient way to communicate the composite water quality status. Water Quality Index results are derived by integrating diverse physical, chemical, and biological parameters into various mathematical equations [23]. The method reflects the holistic well-being of the river [10]. Horton [9] and Brown et al. [5] initially proposed the Water Quality Index (WQI) method. In contemporary times, various methods have been developed for calculating WQIs, and these approaches are currently employed worldwide such as [15] Weighted Arithmetic Water Quality Index (WAWQI), Canadian Council of Ministers of the Environment Water Quality Index (CCMEWQI) and US National Sanitation Foundation Water Quality Index

---

G. Kumar · N. Kumari (✉)

Department of Civil and Environmental Engineering, B.I.T., Mesra, Ranchi 835215, India  
e-mail: [neetak@bitmesra.ac.in](mailto:neetak@bitmesra.ac.in)

(NSFWQI), and many more studies were done on water quality indices reported in various literature [12].

The Weighted Arithmetic Water Quality Index (WAWQI) is a tool used to evaluate water quality by assigning importance to different parameters based on their impact. In simpler terms, it provides a single number that represents the overall health of water, considering various factors like pollutants and their concentrations. WAWQI is a valuable real-world application as it helps decision-makers, environmentalists, and authorities to quickly grasp and communicate the overall quality of water bodies. This helps in planning actions and policies for water management and conservation. To obtain the specific standard values and ideal ranges for a WAWQI calculation, it is essential to refer to the guidelines or regulations provided by the relevant environmental agencies or institutions in your specific region or country. These standards are often established based on scientific assessments, environmental goals, and considerations for human and ecological health.

The conducted research in the Lakhisarai region has predominantly focused on ground water [19] with a noticeable absence of studies specifically addressing the physicochemical parameters and heavy metal content of the Kiul River. This identified gap in the existing literature emphasizes the need for comprehensive investigations to understand the potential impact of the river on both human health and the surrounding environment. The chosen approach for computing the Water Quality Index (WQI) is the Weighted Arithmetic Water Quality Index (WAWQI). This method, known for its simplicity, proves adequate in accurately reflecting the actual health condition of the Kiul River [18].

The results indicate that turbidity is a major concern due to the river being a hotspot for sand mining activities, soil erosion, urbanization, deforestation, waste discharge, and sedimentation. Additionally, iron content exceeds permissible limits, primarily from direct sewage discharge into the water, resembling open dumping practices along with other factors. Station (1) exhibits a significant increase in Water Quality Index (WQI) due to iron content, four times higher than the permissible limit, coupled with the highest recorded turbidity in the surface water of the river. The Kundar Barrage is identified as the primary cause, altering natural river flow and inducing sediment resuspension, along with disrupting flow dynamics.

## 2 Study Area

Lakhisarai District is situated between latitudes  $25^{\circ}01' N$  and  $25^{\circ}22' N$  and longitudes  $85^{\circ}50' E$  and  $86^{\circ}17' E$ . Originating in the Giridih District [21], the Kiul River traverses through Lakhisarai, Sheikhpura, and Jamui districts. Along its course, it receives tributaries like Barnar on the right bank and the primary tributary, Harohar, on the left bank. The river eventually joins the Ganga River near Surajgarha within Lakhisarai District (Source: National Institute of Hydrology, Roorkee 1998–99). The district experiences an annual average rainfall of 1170 mm, with the majority occurring

during the Southwest monsoon, as mentioned on the Lakhisarai District website hosted by the National Informatics Centre (Fig. 1a).

The Kiul River flowing through the entire Lakhisarai District has been studied through eight sampling stations of geographical importance in the town [14]. Eight sampling stations were selected based on accessibility during both seasons. Stations S4 and S5, the closest ones, are located at the heart of the town, while the remaining six were selected based on dense human settlements along the river stretch and also due to their geographical significance (Fig. 1b). The latitude and longitude coordinates are given in Tables 1 and 2 which indicates the distances between the stations in kilometers.

### 3 Methodology

Water samples were collected from eight sampling locations (S1–S8). The sampling was done as per the established standard sampling methods (IS: 2498, 1966—Part 1). The sampling was carried out for two seasons, namely Pre-monsoon and Post-monsoon season [12]. Pre-monsoon sampling was conducted in the month of May, while post-monsoon sampling took place in September month. The analysis of physicochemical parameters, including pH, temperature, turbidity, total dissolved solids, dissolved oxygen, and B.O.D., adhered to the standard procedure outlined in APHA (2012). Each analysis underwent three trials, and the mean value was recorded, as per the approach described by Gupta et al. [7] and Khatri et al. [13].

#### 3.1 Calculation of Water Quality Index (WQI)

Methodologies used for the calculation of WQI using selected physicochemical parameters were reported in different literatures [1, 10, 15, 26]. In Weighted Arithmetic Water Quality Index (WAWQI), the standard values may be defined for individual water quality parameters and the overall WAWQI is typically categorized into different classes, such as excellent, good, fair, poor, or unsatisfactory.

The assigned quality classifications determine the ideal values for WAWQI. For instance, water quality is ideal in scenarios where the index ranges from 0 to 100 and when WAWQI values are higher. Conversely, lower values for WAWQI are considered ideal in instances where a lower score aligns with better water quality.

##### Step 1:

Initially, the unit weight ( $W_i$ ) for various parameters is computed using a formula specified below [2]. The  $W_i$  is inversely proportional to the standard score ( $S_{\text{standard}}$ ) each multiplied by the constant ( $K$ ).

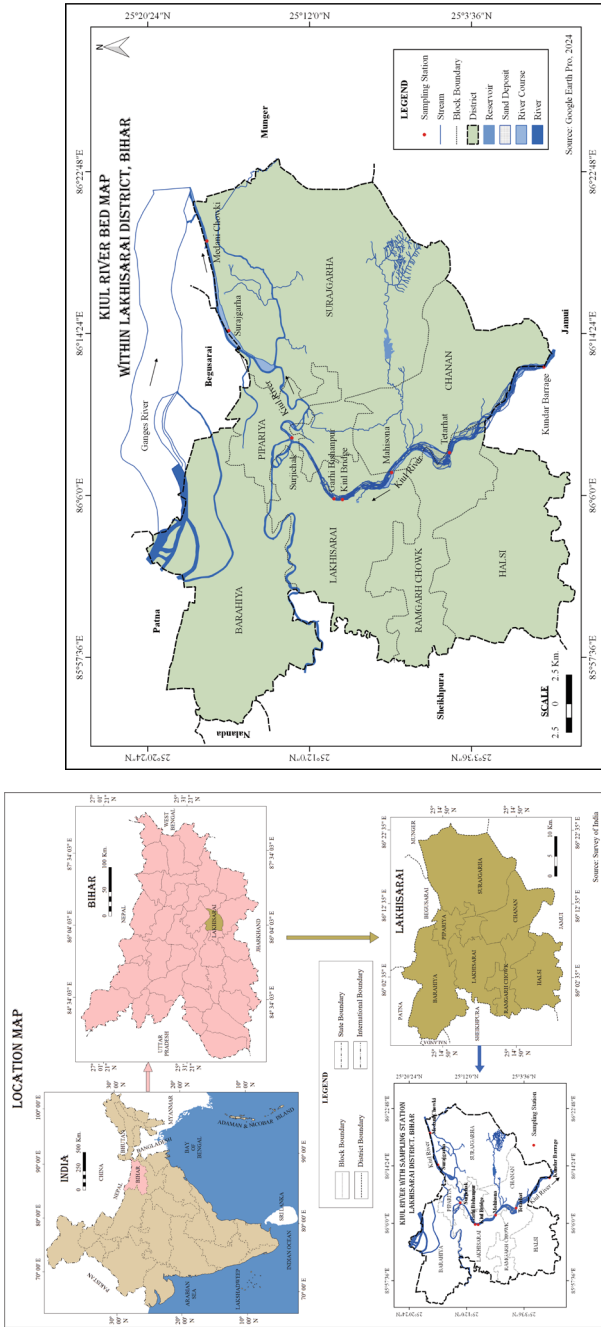


Fig. 1 a Map of the study area featuring sampling sites, b KUIL river bed map

**Table 1** Sampling stations with their latitudes and longitudes

Sampling station	Description	Latitude	Longitude
S1	Kundar Barrage	24°59'50.8"N	86°12'39.8"E
S2	Tetarhat	25°04'44.7"N	86°08'13.0"E
S3	Mahisona	25°07'44.8"N	86°07'11.1"E
S4	Kiul bridge	25°10'17.9"N	86°05'47.1"E
S5	Garhi Bishanpur	25°10'44.3"N	86°05'49.4"E
S6	Surjichak	25°12'55.4"N	86°08'59.0"E
S7	Surajgraha	25°16'22.1"N	86°14'25.4"E
S8	Medni Chowki	86°14'25.4"E	86°19'11.9"E

**Table 2** Sampling sites and their distance with their consecutive sampling site

Kiul River (within Lakhisarai)	71
S1–S2	13.553
S2–S3	8.068
S3–S4	5.891
S4–S5	0.8585
S5–S6	7.603
S6–S7	20.818
S7–S8	8.973

$$W_i = \sum \left( K \frac{1}{S_{\text{standard}}} \right) \tag{1}$$

**Step 2:**

The constant (*K*) is derived through a formula

$$K = \frac{1}{\sum \left( \frac{1}{s_1} + \frac{1}{s_2} + \frac{1}{s_3} + \dots + \frac{1}{s_n} \right)} \tag{2}$$

**Step 3:**

Assess the quality rating scale (*Q<sub>i</sub>*) for the *i*th parameter in a set of *n* samples using the provided equation

$$Q_i = \left( \frac{Q_{\text{actual}} - Q_{\text{ideal}}}{S_{\text{standard}} - Q_{\text{ideal}}} \right) \times 100 \tag{3}$$

**Step 4:**

Lastly, the value of WQI can be calculated by grouping the quality rating with unit weight linearly by the given equation

$$WAWQI = \frac{\sum_{i=1}^{i=N} Q_i W_i}{\sum W_i} \tag{4}$$

where

- $Q_i$  = Assign a quality rating to individual parameters;
- $Q_{actual}$  = Concentration of ith parameter for analyzing water;
- $Q_{ideal}$  = Optimal parameter level in pure water top of form,  $Q_{ideal} = 0$  (Except pH = 7 and DO = 4.6 mg/l);
- $S_{standard}$  = Standard value of ith parameter;
- $K$  = Proportionality constant;
- $W_i$  = Unit weight of water quality parameter;
- $N$  = Count of water quality parameters.

### 4 Results and Discussion

The seasonal variation data for various physicochemical parameters across all eight stations (S1–S8) were given in Tables 3 and 4. According to established standards for pH (6.5–8.5), by regulatory bodies such as BIS, ICMR, and WHO, the pH levels in this study fall within the acceptable range. However, a low seasonal variation is noted due to the presence of free CO<sub>2</sub> [16]. During the monsoon season, a slight acidity is observed, attributed to an increase in CO<sub>2</sub> concentration.

**Turbidity** in the study found within the range from 13.3 to 108 NTU, surpassing the permissible limits of 5.5 and 2.5 NTU recommended by CPCB, ICMR, and WHO. The highest turbidity was reported in the post-monsoon season for (S1) because barrages can affect the natural erosion and sedimentation processes in the river. Changes in sediment transport and deposition patterns influenced turbidity level both upstream and downstream of the barrage. This attributed to turbulent flow causing soil erosion and stirring up of sand and silt from the river bottom [8].

**Table 3** Water quality data of Kiul River for pre-monsoon at different stations

	B.O.D	EC	Iron	Zinc	pH	Turbidity	TDS	DO
S1: Kundar Barrage	1.9	236	0.06	0.08	7.9	29	153.4	8.4
S2: Tetarhat	2.8	250	0.08	0.06	7.8	19.8	162.5	5.2
S3: Mahisona	2.4	236	0.13	0.09	7.7	13.3	153.4	7.9
S4: Kiul Pool	3.3	280	0.37	0.08	7.6	36.7	182	8.8
S5: Garhi Bishanpur	2.7	291	0.11	0.09	7.3	33.9	189.15	6.8
S6: Surjichak	3.4	291	0.07	0.08	7.5	51.3	189.15	8.2
S7: Surajgraha	3.1	472	0.12	0.07	7.4	28.1	306.8	7.8
S8: Medni Chowki	4.3	412	0.11	0.06	7.3	30.2	267.8	8.4

**Table 4** Water quality data of Kiul River for post-monsoon at different stations

	B.O.D	EC	Iron	Zinc	pH	Turbidity	TDS	DO
S1: Kunder Barrage	1.2	176	1.243	0.218	6.51	108	114.4	6.4
S2: Tetarhat	2.2	226	1.11	0.22	6.82	74	146.9	6.8
S3: Mahisona	3.1	251	0.73	0.17	7.1	26.2	163.15	8.6
S4: Kiul Pool	2.5	294	0.46	0.1	7.2	50.9	191.1	8
S5: Garhi Bishanpur	2.9	305	0.32	0.12	7.3	42.1	198.25	7.6
S6: Surjichak	1.9	260	0.52	0.16	7.16	71.5	169	7.4
S7: Surajgraha	2	296	0.28	0.2	7.22	59	192.4	7.5
S8: Medni Chowki	1.4	292	0.82	0.24	7.24	72	189.8	6.5

**Total Dissolved Solids (TDS)** values fall within the range of 114.4 to 306.8 mg/l, well within the permissible limit of 500 mg/l according to standard values. Increased TDS value at different sampling sites were attributed to anthropogenic activities and sewage effluent discharge along the riverbank [24].

**Dissolved Oxygen (DO)** values ranged from 5.2 to 8.8 mg/l which exceeded the prescribed limit of 5 mg/l, indicating well-oxygenated conditions. This indicated that sewage effluents discharged into the area containing minimal organic matter. As the district does not have well-pronounced industrial setup, it lacks industrial effluents, resulting in higher DO levels [26].

**Biochemical Oxygen Demand (B.O.D.)** values ranged from 1.2 to 4.3 mg/l. The highest B.O.D. value was reported from S8 during the summer season, possibly due to a high rate of organic matter decomposition at elevated temperatures and low water currents [17]. For **Iron (Fe)**, the esthetic limit for iron in drinking water is 0.3 mg per liter (mg/L) to prevent taste and staining issues. Iron can react with disinfectants like chlorine, forming undesirable byproducts [11]. For **Zinc (Zn)**, a provisional guideline value of 5 mg per liter (mg/L) was suggested for zinc in drinking water. The obtained results were within permissible limits. Exposure to high concentrations of zinc in drinking water can cause nausea, vomiting, and gastrointestinal discomfort [22]. The values obtained for the aforementioned aspects are graphically represented in Fig. 2.

#### 4.1 Water Quality Index

After scrutiny of the physicochemical parameters and noted seasonal fluctuations at each sampling station, Water Quality Index (WQI) was computed, utilizing the Weighted Arithmetic Water Quality Index (WAWQI) methodology.

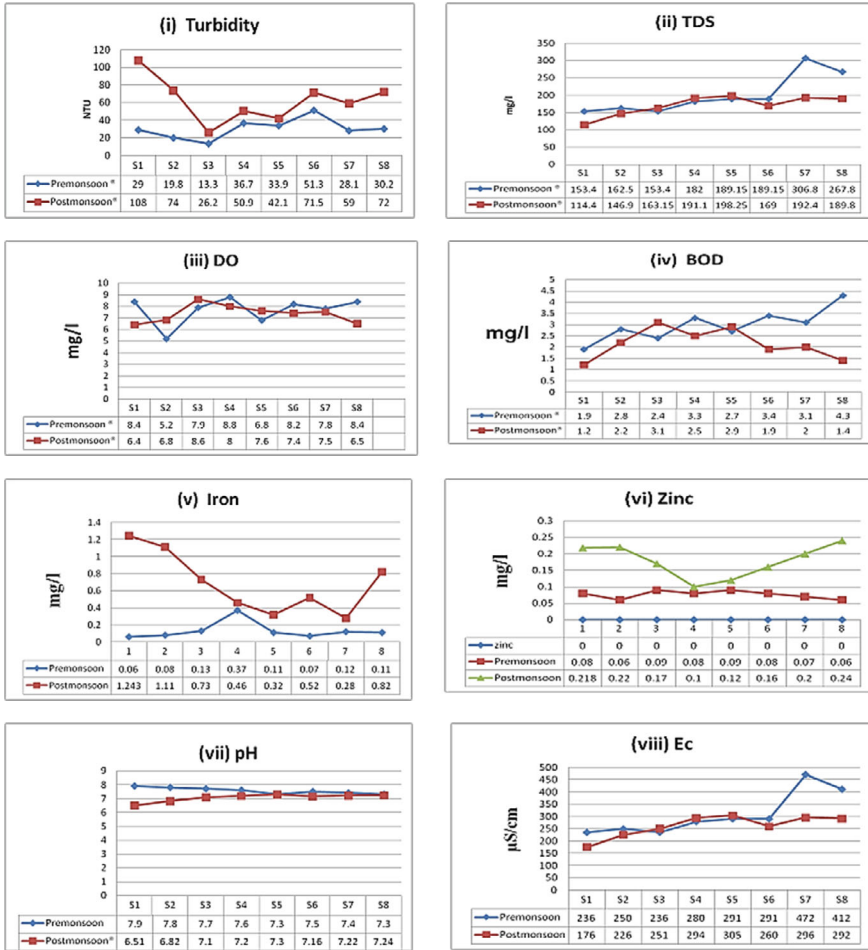


**Fig. 2** Graphical representation of obtained values (i) Turbidity, (ii) Total dissolved solids, (iii) Dissolved oxygen, (iv) Biochemical oxygen demand, (v) Iron, (vi) Zinc, (vii) pH, (viii) Electrical conductivity

The outcomes are represented in Table 5, showcasing the Water Quality Index (WQI) results for individual sampling stations. Seasonal variations are visually represented in Fig. 3, illustrating the fluctuation trends. The WQI standard values from Table 6 served the basis for analyzing the water quality of the Kiul River, culminating in a comprehensive and generalized conclusion.

**Table 5** Obtained WQI form sampling station

WQI	Pre-monsoon	Post-monsoon
S1	55.83	422.17
S2	51.67	360.43
S3	59.69	224.75
S4	144.70	176.97
S5	72.47	134.36
S6	81.59	208.84
S7	71.87	137.19
S8	74.62	283.37

**Fig. 3** Graph of WQI showing seasonal variations

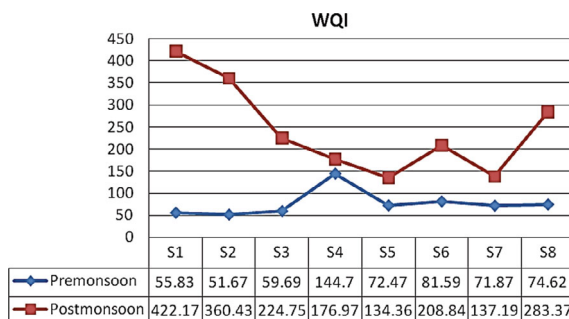


**Table 6** Standard value of WQI [4]

Water Quality Index	
0–25	Excellent
26–50	Good
51–75	Poor
76–100	Very poor
> 100	Unfit for consumption

## 5 Conclusion

The study on the Kiul River in Lakhisarai involved the assessment of various physicochemical parameters at eight different stations. Parameters included pH, turbidity, total dissolved solids (TDS), biological oxygen demand (BOD), dissolved oxygen (DO), electrical conductivity (EC), iron, and zinc as per the standard procedure. The findings highlighted concerns with turbidity, iron, and electrical conductivity in the Kiul River. These issues necessitated standard purification processes. Other parameters met the permissible limits. Pre-monsoon Water Quality Index (WQI) was relatively safe, but post-monsoon showed concerns. Sand mining, urbanization, soil

erosion, untreated sewage discharge, and open dumping were the main contributors to the observed challenge. Authorities must take decisive action to halt waste discharge into the river basin and also prohibit sand mining activities in the region. Government oversight is crucial to regulate scientific sand mining, ensuring adherence to existing rules. Rapid population growth in Lakhisarai demands urgent action, with the imperative need for a sewage treatment plant to handle waste responsibly. Public awareness against open dumping, both in cities and river bodies, is essential. Encroachment on river banks poses a major concern, urging municipal authorities to promptly address and halt illegal construction activities through enforcement.

## References

1. Adimalla N, Qian H (2019) Groundwater quality evaluation using water quality index (WQI) for drinking purposes and human health risk (HHR) assessment in an agricultural region of Nanganur, south India. *Ecotoxicol Environ Saf* 176:153–161. <https://doi.org/10.1016/j.ecoenv.2019.03.066>
2. Al-qaness MA, Dahou A, Abd Elaziz M, Helmi AM (2023) Multi-ResAtt: multilevel residual network with attention for human activity recognition using wearable sensors. *IEEE Trans Industr Inf* 19(1):144–152. <https://doi.org/10.1109/TII.2022.3165875>
3. Anzum HMN, Shaibur MR, Nahar N, Akber A, Hossain MS, Al Mamun S (2023) Changing dynamics of river ecosystem from aquatic to terrestrial: a case of Bhairab River, Jashore, Bangladesh. *Watershed Ecol Environ* 5:134–142. <https://doi.org/10.1016/j.wsee.2023.05.001>
4. Brown RM, McClelland NI, Deininger RA, O'Connor MF (1972) A water quality index—crashing the psychological barrier. In: *Indicators of Environmental Quality: Proceedings of a symposium held during the AAAS meeting in Philadelphia, Pennsylvania, 26–31 Dec 1971*. Springer US, pp 173–182. [https://doi.org/10.1007/978-1-4684-2856-8\\_15](https://doi.org/10.1007/978-1-4684-2856-8_15)
5. Brown RM, McClelland NI, Deininger RA, Tozer RG (1970) A water quality index-do we dare. *Water Sew Work* 117(10)
6. Chen SS, Kimirei IA, Yu C, Shen Q, Gao Q (2022) Assessment of urban river water pollution with urbanization in East Africa. *Environ Sci Pollut Res* 29(27):40812–40825. <https://doi.org/10.1007/s11356-021-18082-1>
7. Gupta N, Pandey P, Hussain J (2017) Effect of physicochemical and biological parameters on the quality of river water of Narmada, Madhya Pradesh, India. *Water Sci* 31(1):11–23. <https://doi.org/10.1016/j.wsj.2017.03.002>
8. Hafeez M, Yuan C, Shahzad K, Aziz B, Iqbal K, Raza S (2019) An empirical evaluation of financial development-carbon footprint nexus in One Belt and Road region. *Environ Sci Pollut Res* 26:25026–25036. <https://doi.org/10.1007/s11356-019-05757-z>
9. Horton RK (1965) An index number system for rating water quality. *J Water Pollut Control Fed* 37(3):300–306
10. Iticescu C, Georgescu LP, Murariu G, Topa C, Timofti M, Pintilie V, Arseni M (2019) Lower Danube water quality quantified through WQI and multivariate analysis. *Water* 11(6):1305. <https://doi.org/10.3390/w11061305>
11. Kachroud M, Trolard F, Kefi M, Jebari S, Bourrié G (2019) Water quality indices: challenges and application limits in the literature. *Water* 11(2):361. <https://doi.org/10.3390/w11020361>
12. Karunanidhi D, Aravinthasamy P, Subramani T, Chandrajith R, Raju NJ, Antunes IMHR (2022) Provincial and seasonal influences on heavy metals in the Noyyal River of South India and their human health hazards. *Environ Res* 204:111998. <https://doi.org/10.1016/j.envres.2021.111998>

13. Khatri N, Tyagi S, Rawtani D, Tharmavaram M, Kamboj RD (2020) Analysis and assessment of ground water quality in Satlasana Taluka, Mehsana district, Gujarat, India through application of water quality indices. *Groundw Sustain Dev* 10:100321. <https://doi.org/10.1016/j.gsd.2019.100321>
14. Kothari V, Vij S, Sharma S, Gupta N (2021) Correlation of various water quality parameters and water quality index of districts of Uttarakhand. *Environ Sustain Indic* 9:100093. <https://doi.org/10.1016/j.indic.2020.100093>
15. Lukhabi DK, Mensah PK, Asare NK, Pulumuka-Kamanga T, Ouma KO (2023) Adapted water quality indices: limitations and potential for water quality monitoring in Africa. *Water* 15(9):1736. <https://doi.org/10.3390/w15091736>
16. Mukate S, Wagh V, Panaskar D, Jacobs JA, Sawant A (2019) Development of new integrated water quality index (IWQI) model to evaluate the drinking suitability of water. *Ecol Ind* 101:348–354. <https://doi.org/10.1016/j.ecolind.2019.01.034>
17. Nong HN, Falling LJ, Bergmann A, Klingenhof M, Tran HP, Spöri C, Jones TE (2020) Key role of chemistry versus bias in electrocatalytic oxygen evolution. *Nature* 587(7834):408–413. <https://doi.org/10.1038/s41586-020-2908-2>
18. Patel DD, Mehta DJ, Azamathulla HM, Shaikh MM, Jha S, Rathnayake U (2023) Application of the weighted arithmetic water quality index in assessing groundwater quality: a case study of the South Gujarat region. *Water* 15(19):3512. <https://doi.org/10.3390/w15193512>
19. Sharma B, Pandey A (2022) Mapping of Erosion Hazard in and around Kharagpur Hills, Bihar using hydrological indices. <https://sciforum.net/manuscripts/12638/manuscript.pdf>
20. Sharma R, Kumar R, Satapathy SC, Al-Ansari N, Singh KK, Mahapatra RP, Pham BT (2020) Analysis of water pollution using different physicochemical parameters: a study of Yamuna River. *Front Environ Sci* 8:581591. <https://doi.org/10.3389/fenvs.2020.581591>
21. Singh SP, Dutta PK (2020) Influence of physico-chemical and radiological parameters in the ground water of Lakhisarai district of Bihar, India. *Poll Res* 39:64–69
22. Son C, Hegde S, Smith A, Wang X, Sasangohar F (2020) Effects of COVID-19 on college students' mental health in the United States: interview survey study. *J Med Internet Res* 22(9):e21279. <https://doi.org/10.2196/21279>
23. Syeed MM, Hossain MS, Karim MR, Uddin MF, Hasan M, Khan RH (2023) Surface water quality profiling using the water quality index, pollution index and statistical methods: a critical review. *Environ Sustain Indic* 1:100247. <https://doi.org/10.1016/j.indic.2023.100247>
24. Taloor AK, Pir RA, Adimalla N, Ali S, Manhas DS, Roy S, Singh AK (2020) Spring water quality and discharge assessment in the Basantar watershed of Jammu Himalaya using geographic information system (GIS) and water quality index (WQI). *Groundw Sustain Dev* 10:100364. <https://doi.org/10.1016/j.gsd.2020.100364>
25. Yang L, Chen W, Zeng J, Pan S, Zhong Y, Gu T (2023) Regional differences and driving forces of ecosystem health in Yangtze River Basin, China. *Environ Sci Pollut Res* 30(27):70985–71000. <https://doi.org/10.1007/s11356-023-27230-8>
26. Zotou I, Tsihrintzis VA, Gikas GD (2020) Water quality evaluation of a lacustrine water body in the Mediterranean based on different water quality index (WQI) methodologies. *J Environ Sci Health Part A* 55(5):537–548. <https://doi.org/10.1080/10934529.2019.1710956>

# Decolorization of Textile Wastewater Using the Electrocoagulation Process



M. A. Shabiimam and Tirtha Trivedi

## 1 Introduction

Globally, the growth of industrialization is increasing rapidly. It is comforting to humankind but adversely affected the environment. In environmental pollution talk, efficient, cost-effective, and eco-friendly treatment of wastewater is one of the major issues. Many industries that produce dye-containing wastewater are food, textile, cosmetics, paper and pulp, leather, and pharmaceutical industries [1]. Regarding the usage of raw materials, equipment, processes, and production; the textile industries are one of the largest revenue-generating departments worldwide [2]. This industry uses a huge amount of water as well as chemicals in a wide range of manufacturing processes like sizing, de-sizing, scouring, mercerizing, bleaching, dyeing, printing, and finishing [3, 4]. Approximately, more than 100,000 commercial dyes are available and about 700,000 to 1 million tons of dyes are produced annually in the world [5]. The usage of synthetic dyes has increased in the textile industry because it is cost-effective and highly stable to temperature, light and detergents [6]. Nearly, 10,000 synthetic dyes are manufactured, including vat, azo, direct, reactive, acidic, basic, nitro, disperse dyes, etc. [7]. Among these different synthetic dyes available, azo dye is the most used dye as it is more economical and it is the largest class (production of more than 50%) of synthetic dyes where azo bond ( $-N=N-$ ) is present in their molecular structure [6, 8]. Azo dyes and their degradation like aromatic amines are highly carcinogenic [9]. Apart from dyes, this wastewater usually contains contaminants such as dissolved solids, non-biodegradable compounds, colored compounds, acids, bases, organic compounds, high COD, and conductivity [3, 10]. Researcher has studied RY 145 dye treatment using ozonation and bio char [11, 12]. Dyeing and finishing are the most important processes in textile industries that produce color

---

M. A. Shabiimam (✉) · T. Trivedi  
Department of Civil Engineering, School of Technology, Pandit Deendayal Energy University,  
Gandhinagar, Gujarat 382421, India  
e-mail: [shabiimam.ma@sot.pdpu.ac.in](mailto:shabiimam.ma@sot.pdpu.ac.in)

and suspended solids in the environment [13]. Dye-containing effluent is a world-wide environmental issue as it contains very stable dyes because of its hydrophilic nature [14]. Textile dyes are highly toxic in nature, especially azo dyes which have toxic and complex aromatic compounds that are generally responsible for color in the wastewater [9]. Textile industries produce a large amount of wastewater. When receiving body receives this colored water, it creates an unaesthetic appearance problem, sunlight can barely pass through this water which results in undeveloped or underdeveloped aquatic plants, and disturbance to marine life, as well as these toxic compounds, which are mutagenic to animals and microbial species. Thus, textile wastewater is very dangerous in terms of volume and composition. For this reason, it is necessary to treat textile wastewater, chiefly to remove the color from the wastewater and then discharge it into the surface water bodies [3, 15].

The aim of the study is to treat the Reactive Yellow 145 using electrocoagulation technique. Reactive Yellow 145 is one of the compound widely used in textile industry. India's textile city Tiruppur, Tamil Nadu is highly polluted by textile wastewater. Residents and farmers claimed that bleaching and dyeing processes of the textile industries discharge threatening colored and chemical effluents into the surface water bodies without any treatment at midnight or when it's raining [16]. The Indian city of Kanpur serves as a key center for the textile industry, and companies located there discharge untreated textile wastewater into the Ganga River through canals and drains that eventually flow into the Bay of Bengal [17].

Various techniques are adopted to decolorize the textile wastewater, which is aerobic and anaerobic degradation, filtration, adsorption, biological oxidation, advanced oxidation process, chemical coagulation, flocculation, precipitation, physicochemical techniques, ion-exchanges, biological process, Fenton and electro-Fenton processes, photo-oxidation, etc. [1]. Among these technologies, some advanced treatment processes are highly expensive while other treatment processes are cost-effective but are less effective having higher treatment time [18, 19]. Among all these treatment techniques, the electrocoagulation (EC) process is an inexpensive, less sludge-producing, and very efficient wastewater treatment process [10]. EC has the great advantage of no need of adding chemicals in the treatment process and hence generates less sludge than other processes [20]. Some studies have shown effective removal of wide range of dyes from the wastewater [21, 22]. EC is easy to operate and maintain, has no secondary pollution, and has less reaction time [23].

In the current study, an electrocoagulation technique was employed for treating a synthetic Reactive Yellow 145 (RY145) dye solution. We investigated the effects of voltage, reaction time, pH, and concentration of the supporting electrolyte (NaCl) on the process. Design-Expert 13 employs Response Surface Methodology to optimize all these parameters for optimal removal efficiency at lowest operating costs. All of the experiments are generated using the Box-Behnken design.

### **Importance of this study**

Two separate parts form the current study. The first phase provides the ideal conditions for various parameters for maximizing dye removal efficiency from the wastewater, and the second phase provides information on running costs for the EC process.

The focus of the first portion will be on the unique interests of those who are active in researching, evaluating, and selecting technologies and business models across all sectors. While operating costs and long-term economic inflation are taken into consideration in the second half of the study, it will be of interest to environmental managers. As a result, the objective of this study is to carry out a techno-economic evaluation of EC for the removal of RY145 dye.

## 2 Literature Review

The color removal using various technologies is discussed in Table 1.

### Research Gap

From the above literature review, various treatment techniques are available for dye treatment. However, conventional coagulants create sludge and biological treatment may help to remove organic loading but the color removal efficiency is not significant. So electrocoagulation creates less sludge and more decolorization efficiency.

## 3 Materials and Methodology

### 3.1 Chemical Structure and Characteristics of Dye

The characteristics of Reactive Yellow 145 yellow is discussed in Table 2.

### 3.2 Preparing Synthetic Dye Wastewater

- **Preparation of Stock Solution**

This dye's stock solution was made by combining 0.5 g of dye with 500 ml of distilled water.

- **Preparation of Experimental Solution**

In order to make a synthetic experimental solution with a 50 ppm concentration, 950 ml of distilled water was used to dilute 50 ml of the stock solution.

- **Before the Experimental Run**

To maintain the dye solution's conductivity, sodium chloride (NaCl) was added at a concentration of 0.4 g/L. Sodium hydroxide (NaOH) and sulfuric acid (H<sub>2</sub>SO<sub>4</sub>) were used to change the pH of the solution. For each run, two iron plates from the nearby fabrication shop were used in the EC process.

**Table 1** Dye removal using different technologies and their removal efficiencies

Dye name	Removal technique used	Removal efficiency (%)	References
Reactive Red 141	Adsorption technique on modified chitin at different concentrations and temperatures	92.76	[24]
	Adsorption using new biochar derived from pecan nutshell	85	[8]
	Electrochemical degradation using a filter press with $\beta$ PbO <sub>2</sub> anode	90	[25]
	Nano-biocomposites as an adsorbent	–	[26]
	Using bacterial isolate <i>Rhizobium radiobacter</i> MTCC 8161	90	[27]
Reactive Black 5	Adsorption on cross-linked chitosan beads	–	[28]
	Adsorption using carbon nanotubes	Nearly 100	[29]
	Suspended and attach growth sequencing batch bioreactor	92	[30]
	Fenton's oxidation process	99	[31]
	Adsorption on bentonite clay in a batch	–	[32]
Reactive Yellow 84	Adsorption on nanoparticles of calcium carbonate followed by photo degradation	Up to 99	[33]
	Adsorption on Borassus Flabellifer nanocomposites	–	[34]
	Adsorption onto the animal bone meal	–	[35]
	Using nano-sorbent as zinc-aluminum layered double hydroxide	–	[36]
Reactive Yellow 145	Photocatalytic degradation	65	[37]
	Adsorption of chitosan	80	[38]
	O <sub>3</sub> and H <sub>2</sub> O <sub>2</sub> /UV-C processes	64	[39]

**Table 2** Characteristics and chemical structure of selected dye

Dye name	Molecular structure	Molecular formula	Molecular weight
Reactive Yellow 145	<p>Single Azo class</p> <p style="text-align: center;"><b>Single Azo class</b></p>	$C_{28}H_{20}ClN_9Na_4O_{16}S_5$	1026.25

- **After the Experimental Run**

Acid wash was given to the used electrodes followed by wiping with acetone to remove impurities builds up on it. Also, acetone is used to eliminate impurities built up on the surface of the reactor after each experimental run.

### 3.3 Electrocoagulation Unit

Figure 1 shows the experimental setup in the procedure. Iron plates act as electrodes in the electrochemical reactor which forms the electrocoagulation unit, which also includes, a DC power supply, and magnetic stirrer. The specification of electrochemical reactor is shown in Table 3.

### 3.4 About Software Used for the Experimental Design

In this investigation, the treatment efficiencies and operational costs of synthetic textile wastewater were optimized using RSM by Design Expert 13.0 (trial version). Three independent variables (*A*-pH, *B*-reaction time, and *C*-applied voltage) and a three-level, full-factorial Box–Behnken Design (BBD) were used. The main benefits of this research strategy are; it minimizes the number of experimental runs required to optimize the entire process while providing a comparison of the corresponding importance of the relevant factors.

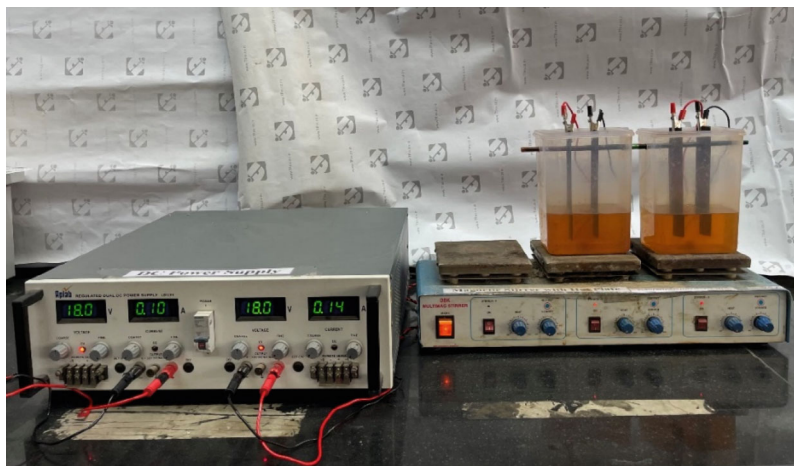


**Fig. 1** Electrocoagulation unit setup

**Table 3** Properties of the electrochemical reactor

The volume of the reactor (L)	1.2
Volume of the experimental solution to be treated (mL)	500
Material of the reactor	Plastic
Anode material	Iron
Cathode material	Iron
Electrode thickness (mm)	1
Electrode size (mm × mm)	16 × 3
Electrode arrangement	Vertically parallel
Electrode gap (cm)	2.5
Number of electrodes used in each reactor	2

### 3.5 Calibration of the Dye

From the literature survey, the maximum wavelength ( $\lambda_{\max}$ ) of this dye is found out at 419 nm [37]. The values of absorbance at different concentrations from 1 to 6 ppm is shown in a graphical representation (Fig. 2).

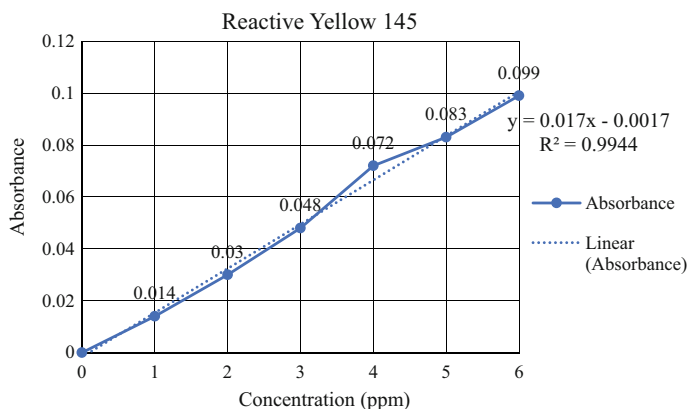


Fig. 2 Calibration curve of RY145 dye

## 4 Result and Discussion

### 4.1 Results of the Experiments Using RSM

The experiments were conducted using  $3^3$  factorial experimental designs and their input parameter ranges are shown in Table 4. The three independent numeric variables are the pH (2–10) of the solution, reaction time (10–50 min), and applied voltage (6 to 30 V). These three independent variables have an impact on two responses which are dye removal efficiency and the operating cost of the treatment (Table 4).

There was a total of seventeen experiments with 5 center points as a result of combining these factors with experimental design. All seventeen experimental runs were performed as per Table 5. During the experiments, the initial dye concentration was kept constant at 50 ppm, salt concentration for each experiment was kept at 0.4 g/l and inter-electrode distance in the reactor was kept at 2.5 cm. The out put response were color removal efficiency (%) and operating cost (Rs/m<sup>3</sup>).

- The experimental results of seventeen designed experiments are given in Table 5.

The correlation coefficient ( $R^2$ ) value for color removal efficiency and operating cost is 0.9997 and 0.9999 from the Fit Statistic (Table 6). It assesses the adequacy of a model. The degree to which the independent characteristics have an impact on the

Table 4 Levels and variables used in the experimental design of the EC process

	Name	Units	Low	High
A [Numeric]	<b>pH</b>	–	2	10
B [Numeric]	<b>Reaction time</b>	Min	10	50
C [Numeric]	<b>Voltage</b>	V	6	30

**Table 5** Response results of DOE

	Factor 1	Factor 2	Factor 3	Response 1	Response 2
Std.	A: pH	B: Reaction time	C: Voltage	Color removal efficiency	Operating cost
		Min	V	%	Rs/m <sup>3</sup>
8	10	30	30	92.91	72.88
12	6	50	30	96.91	143.72
4	10	50	18	92.46	72
17	6	30	18	91.84	30.24
2	10	10	18	4.2	9.36
9	6	10	6	2.32	1.79
13	6	30	18	88.79	29.16
16	6	30	18	90.44	29.16
6	10	30	6	1.56	6.053
14	6	30	18	91.38	28.08
1	2	10	18	12.88	44.28
5	2	30	6	23.71	30.94
10	6	50	6	23.62	6.726
3	2	50	18	93.79	241.2
7	2	30	30	95.22	284.09
11	6	10	30	89.71	23.3
15	6	30	18	89.22	31.32

response is represented by the coefficient of determination ( $R^2$ ). Both responses'  $R^2$  values are very near to 1 which indicates that the independent parameters have a high significance impact on both responses and indicating that the suggested model was extremely appropriate.

It is desired and shown for this model that  $R^2$ , adjusted  $R^2$ , and predicted  $R^2$  are in close vicinity to one another. Lower value of co-efficient of variation (CV) indicates a high level of precision in both of responses.

For purposes of prediction, second-order polynomial models were created for the RSM responses for the electrocoagulation process and the primary impacts of those three independent factor variables on it. This is suitable for forecasting color

**Table 6** Fit statistic

	Color removal efficiency (%) $R_1$	Operating cost (₹/m <sup>3</sup> ) $R_2$
$R^2$	0.9997	0.9999
Adjusted $R^2$	0.9989	0.9998
Predicted $R^2$	NA <sup>(1)</sup>	NA <sup>(1)</sup>
C. V. (%)	2.08	1.93

removal and operational cost of EC process based on the ANOVA analysis, it agrees well with a quadratic model. Fit summary suggested a quadratic model, but the reliability of the reduced cubic model was assessed using ANOVA to examine other co-relation between three variables. Below are the reduced cubic regression model in terms mathematical equations Responses for decolorization efficiency (Eq. 1) and operating cost (Eq. 2)

$$\begin{aligned} \text{Decolourisation Efficiency} &= 90.33 - 6.12A + 7.13B \\ &+ 40.17C + 1.84AB + 4.96AC - 3.52BC - 19.65A^2 \\ &- 19.86B^2 - 17.34C^2 + 35.17A^2B + 0.5450A^2C \\ &- 3.61AB^2 \end{aligned} \quad (1)$$

$$\begin{aligned} \text{Operational Cost} &= 29.59 - 59.02A + 31.34B \\ &+ 39.63C - 33.57AB - 46.58AC + 28.87BC \\ &+ 58.36A^2 + 3.76B^2 + 10.54C^2 + 33.55A^2B \\ &+ 40.37A^2C + 7.99AB^2, \end{aligned} \quad (2)$$

where  $A = \text{pH}$

$B = \text{Reaction time}$

$C = \text{Voltage.}$

Table 7 shows the actual as well as predicted values of both responses for 17 runs. Where  $R_1$  is decolorization efficiency and  $R_2$  is operational cost.

From the above table, it can be seen that the majority of the predicted values and actual values are same and other predicted values are seen to be very close to the actual values. Values are differing may be because of the probability of some result points are resting outside the predicted line.

Figure 3a, b indicated the chart of predicted versus actual values for both the responses 1 and 2, respectively.

The predicted and actual positions for both responses are in close proximity, indicating an “excellent” model fit.

- The significance of variables in the responses is validated by the ANOVA. At a 95% confidence level of the  $p$ -value, all model terms were evaluated. The ANOVA (analysis of variance) produced from the RSM for the reduced cubic model is given in Table 8.

The ideal  $p$ -value for the model or variable is 0.05.  $P$ -values less than 0.005 are regarded as extremely significant. Here, for Response 1 and Response 2, model's  $p$ -value is  $< 0.0001$ , which indicates the models are extremely significant. For the Response 1, reaction time and voltage are very significant whereas for Response 2, pH, reaction time, and voltage are very significant. In total, 746.70 and 755.06 are model's  $F$ -value for  $R_1$  and  $R_2$ , respectively. This higher  $F$ -values for model indicates the suitability of variation and the model is highly significant.

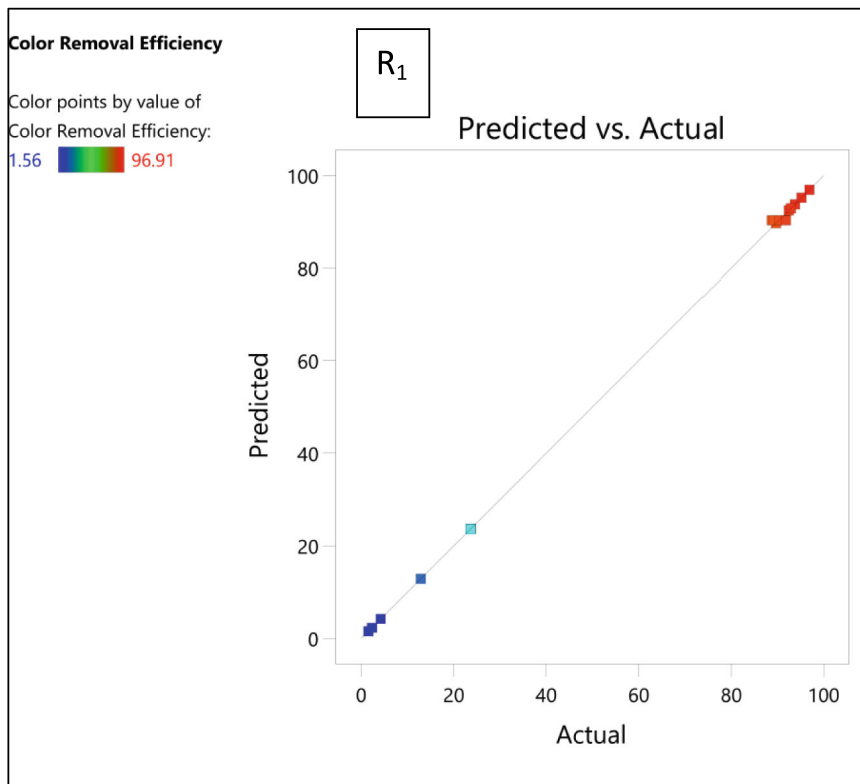
**Table 7** Predicted versus actual values of experiments

Run order	% Color removal $R_1$		Operational cost ( $\text{₹}/\text{m}^3$ ) $R_2$	
	Actual value	Predicted value	Actual value	Predicted value
1	92.91	92.91	72.88	72.88
2	96.91	96.91	143.72	143.72
3	92.46	92.46	72.00	72.00
4	91.84	90.33	30.24	29.59
5	4.20	4.20	9.36	9.36
6	2.32	2.32	1.79	1.79
7	88.79	90.33	29.16	29.59
8	90.44	90.33	29.16	29.59
9	1.56	1.56	6.05	6.05
10	91.38	90.33	28.08	29.59
11	12.88	12.88	44.28	44.28
12	23.71	23.71	30.94	30.94
13	23.62	23.62	6.73	6.73
14	93.79	93.79	241.20	241.20
15	95.22	95.22	284.09	284.09
16	89.71	89.71	23.30	23.30
17	89.22	90.33	31.32	29.59

- **Impacts of Operational parameters on the decolorization efficiency and operational cost analysis**

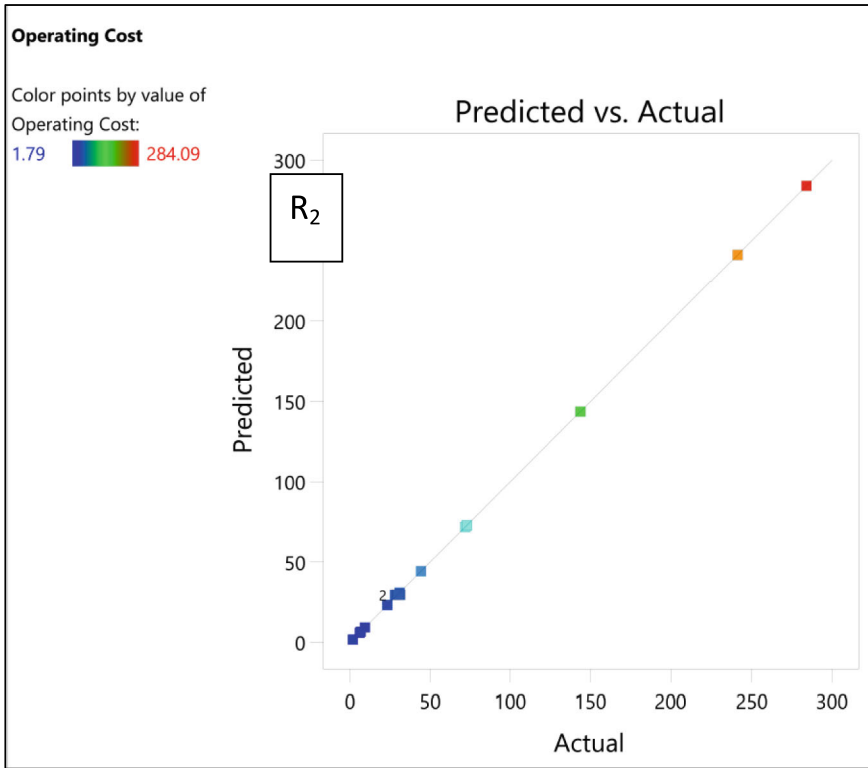
1. *Effects of Initial pH and Reaction Time*

From Fig. 4a, b for the maximum reaction time, the dye removal efficiency for both acidic and basic pH is good at a constant voltage of 18 V, but for acidic pH in these mentioned conditions, the operational cost is very high which is not acceptable in industrial application purpose. For lower reaction time, for acid and basic pH solution at constant current value, dye removal efficiency is low. Hence, reaction time for the treatment is more important. The pH of the solution combined with the effect of reaction time does not have much influence. Therefore, neutral pH is considered since there is no need to add chemicals in the treatment operation. In terms of operational cost, reaction time should be in range. More reaction time will consume more amount of current for the treatment and that will increase the cost of the operation. Figure 5a, b illustrates that initial and voltage both are influencing parameters on the decolorization efficiency.



(a)

**Fig. 3** a and b Predicted versus actual plot for % color removal efficiency ( $R_1$ ) and operating cost ( $R_2$ )



(b)

Fig. 3 (continued)

(1) Effects of initial pH and voltage

Figure 6a, b indicates that at lowest voltage and at basic pH, there is the lowest dye removal efficiency in constant 30 min of reaction time. However, for the acidic pH under above mentioned conditions, the dye removal efficiency is also low. pH has not much influence on the dye removal efficiency but it has great impact on the operational cost of the treatment process. For low value of voltage, decolorization efficiency is very low as there is not sufficient current supplied that can form metal ions in the reactor. However, for maximum voltage, removal efficiency is extremely good for every pH value. Acidic dye solution has very good removal at higher voltage, but the operation cost is drastically high. Also, as we discussed further, higher voltage leads to high operational cost. Hence, we can conclude that average pH and voltage would be the best condition for both decolorization of wastewater and its operational cost.

**Table 8** Analysis of variance

Source	% Color removal ( $R_1$ )			Operational cost ( $\text{₹}/\text{m}^3$ ) ( $R_2$ )		
	df	F-value	p-value	df	F-value	p-value
Model	12	1231.85	< 0.0001	12	5984.25	< 0.0001
A-pH	1	85.49	0.0008	1	9190.31	< 0.0001
B-reaction time	1	116.06	0.0004	1	2590.83	< 0.0001
C-voltage	1	3689.18	< 0.0001	1	4142.19	< 0.0001
AB	1	7.72	0.0499	1	2972.84	< 0.0001
AC	1	56.25	0.0017	1	5723.77	< 0.0001
BC	1	28.41	0.0060	1	2198.84	< 0.0001
A <sup>2</sup>	1	928.84	< 0.0001	1	9458.26	< 0.0001
B <sup>2</sup>	1	948.80	< 0.0001	1	39.17	0.0033
C <sup>2</sup>	1	723.46	< 0.0001	1	308.27	< 0.0001
A <sup>2</sup> B	1	1413.77	< 0.0001	1	1484.74	< 0.0001
A <sup>2</sup> C	1	0.3395	0.5914	1	2149.41	< 0.0001
AB <sup>2</sup>	1	14.92	0.0181	1	84.29	0.0008

## (2) Effects of reaction time and voltage

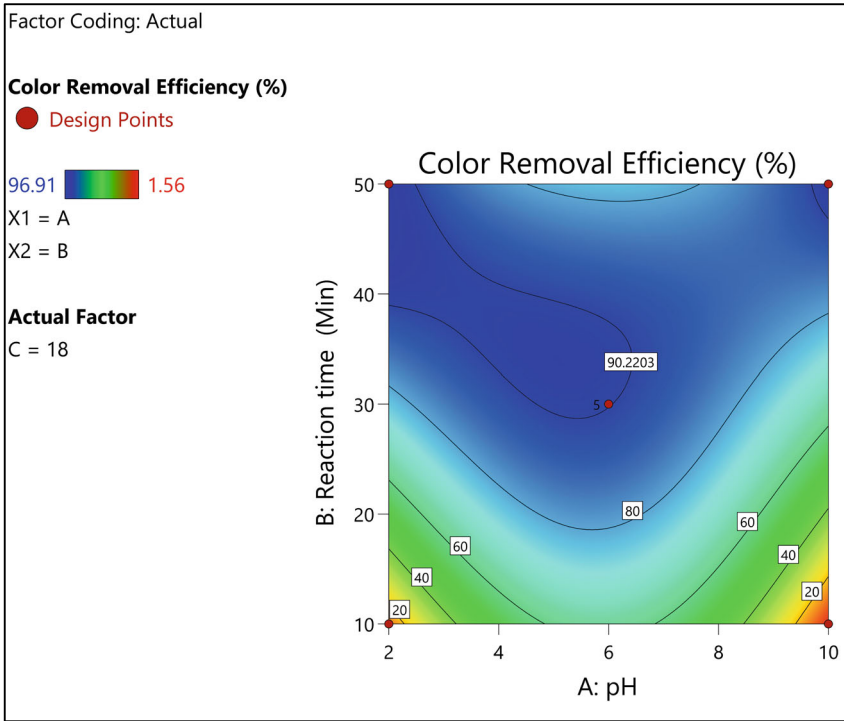
Figure 7a, b illustrates that reaction time and voltage both are influencing parameters on the decolorization efficiency. Both parameters are directly proportional in dye removal efficiency. For operational cost, both parameters are inversely proportional. When reaction time and voltage are both low, efficiency is very poor. A higher current promotes more oxidation, resulting in more precipitation in removing the color from wastewater. Although the highest reduction was achieved at 30 V, an ideal voltage of 18 V was preferred economically. For the purpose of industrial application, more reaction time is not advisable hence, 30 min of reaction time is preferred for both responses.

### • Optimization of Variable Parameters Using Ramp Function

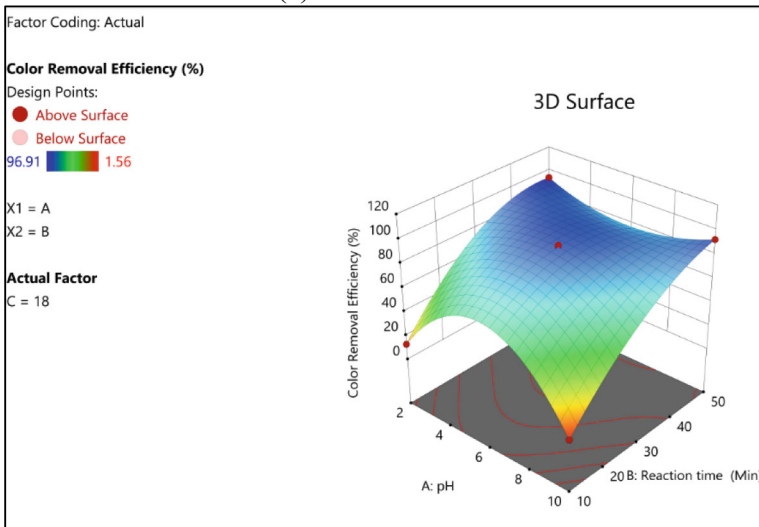
Using Design-Expert software, the experimental conditions were optimized by approximating response functions which are dye elimination with its operational cost. Figure 8 presents the optimized results from the ramp functions at its maximum desirability. Then, in order to verify the predicted performance, an individual run was carried out under these ideal circumstances. Maximum dye removal is 96.91% and its operating cost is 29.59  $\text{₹}/\text{m}^3$  of treated wastewater obtained with optimal operating parameters having 6 pH, 30 min reaction time and 18 V voltage, indicating that the model's prediction at 0.966 desirability was accurate.

### • Salt Concentration Optimization

After the optimization of three variable parameters, supporting electrolyte (NaCl) concentration is optimized. Under all those optimized conditions, salt concentration

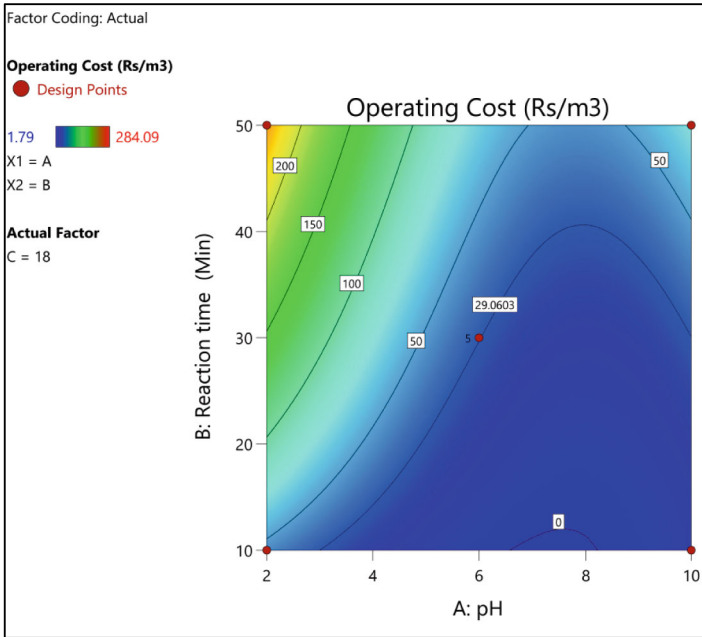


(a)

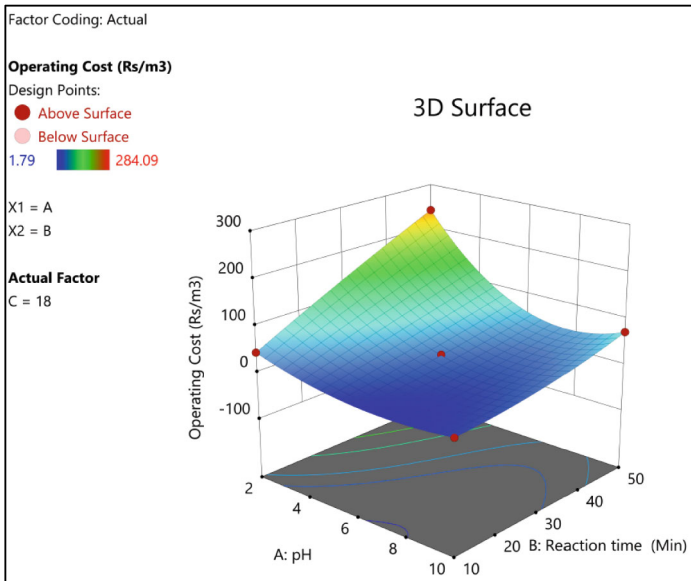


(b)

**Fig. 4** a and b 2D and 3D plot on effect of initial pH and reaction time on color removal efficiency. c and d 2D and 3D plot on effect of initial pH and reaction time on operational cost

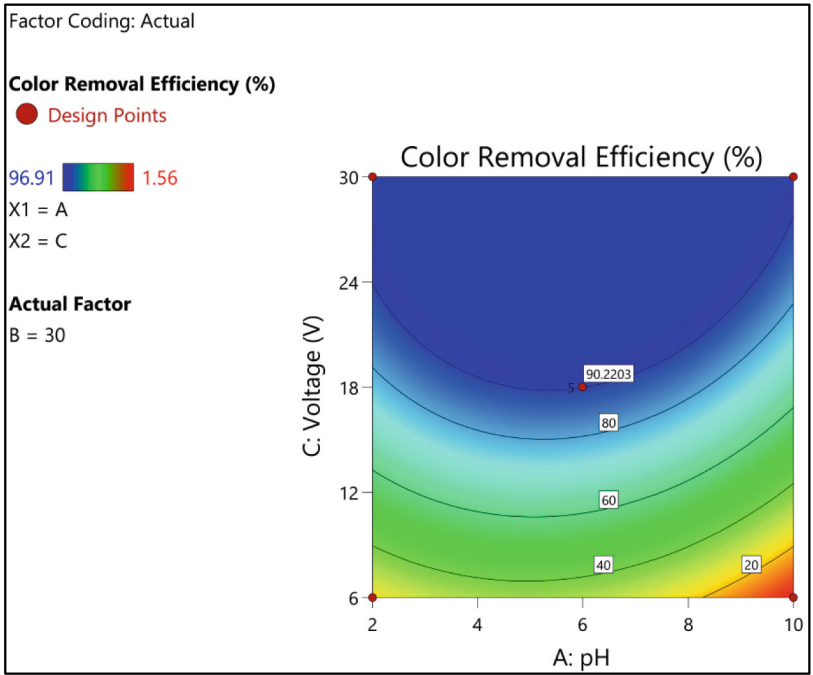


(c)

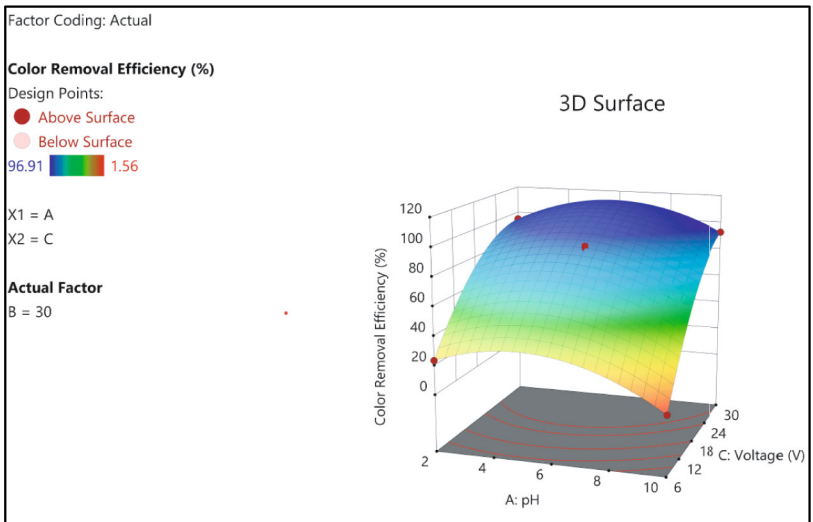


(d)

Fig. 4 (continued)

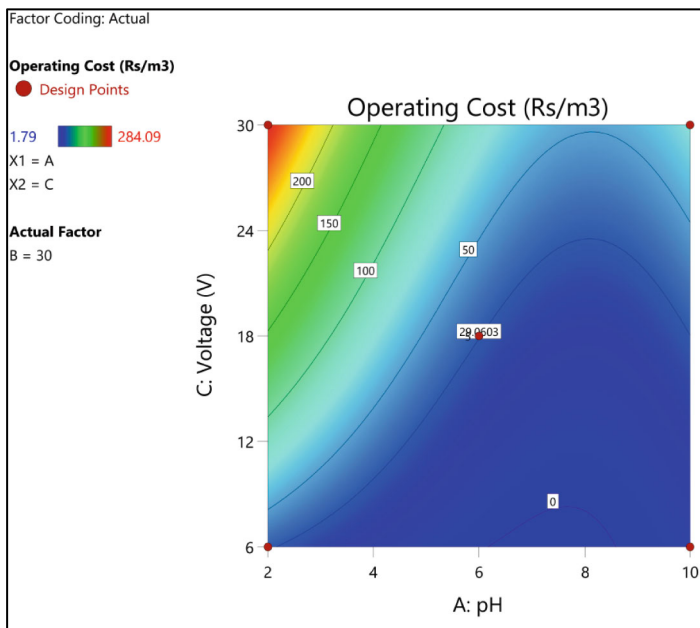


(a)

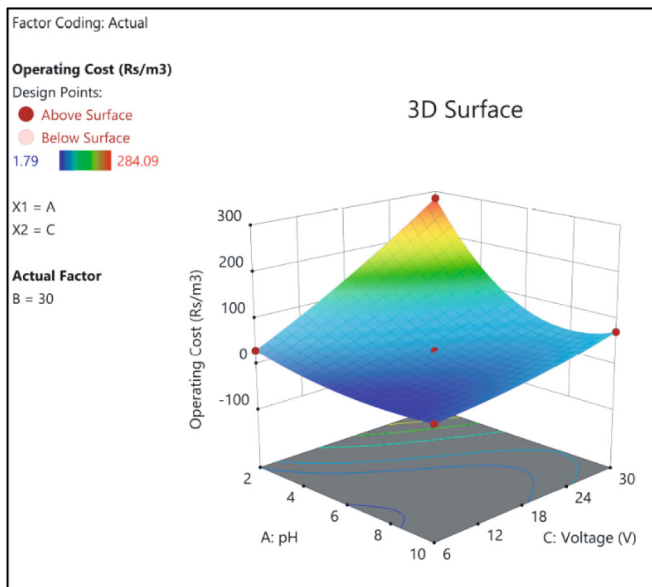


(b)

Fig. 5 a and b 2D and 3D plot on effect of initial pH and applied voltage on color removal efficiency

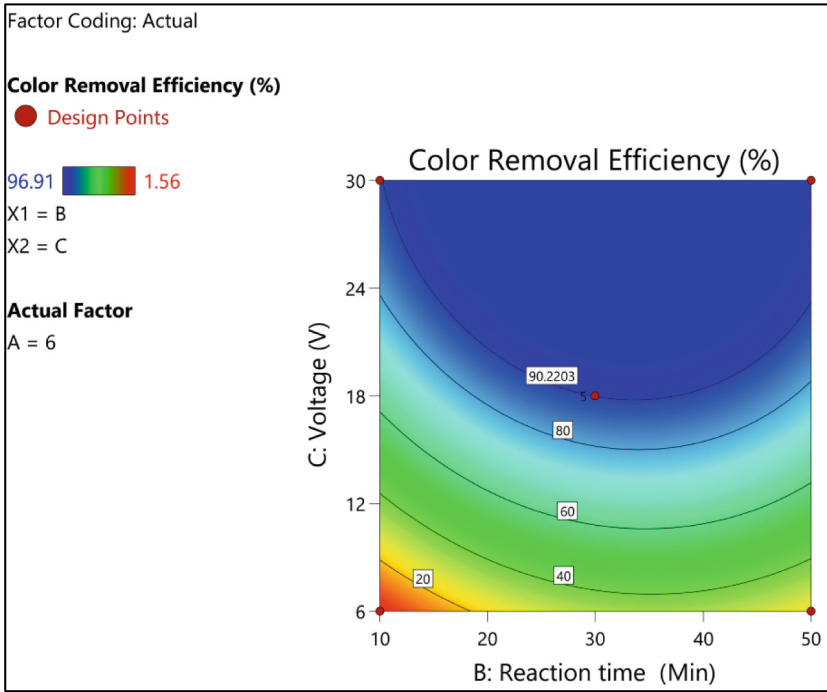


(c)

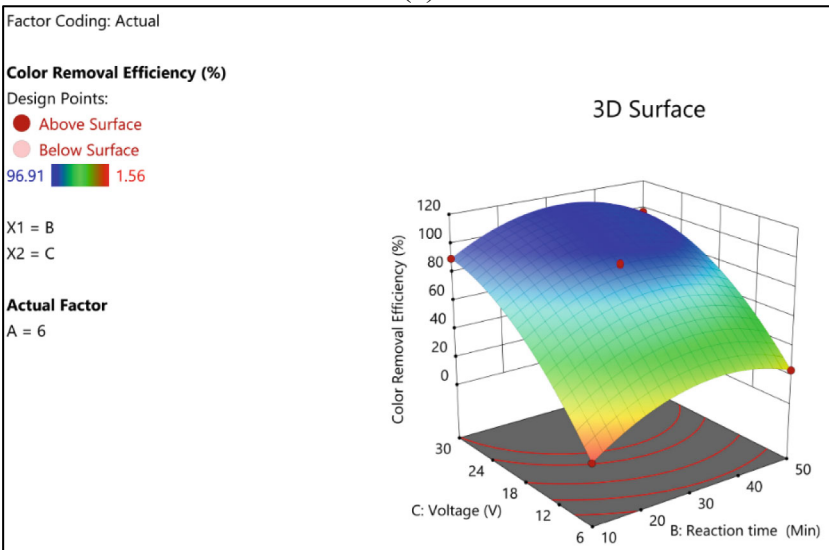


(d)

Fig. 6 a and b 2D and 3D plot on effect of initial pH and applied voltage on operational cost

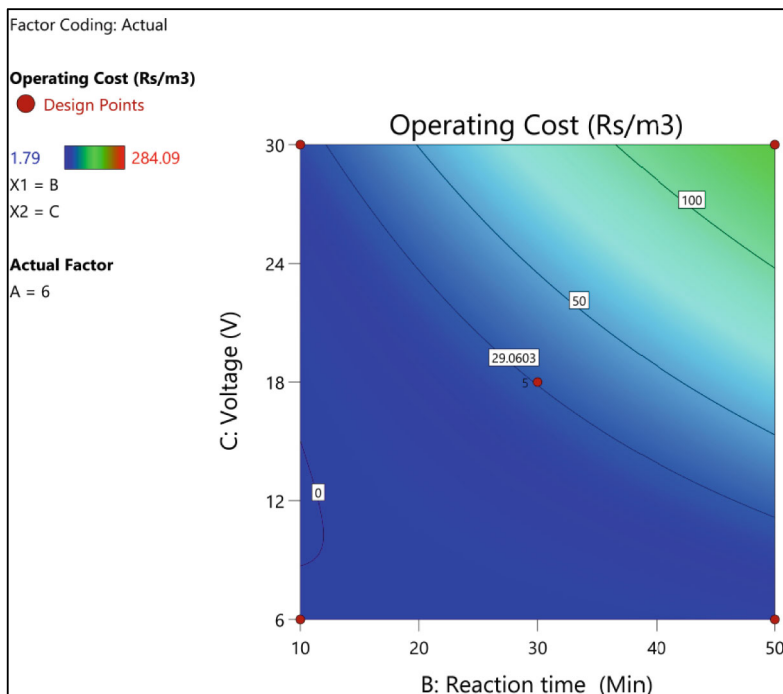


(a)

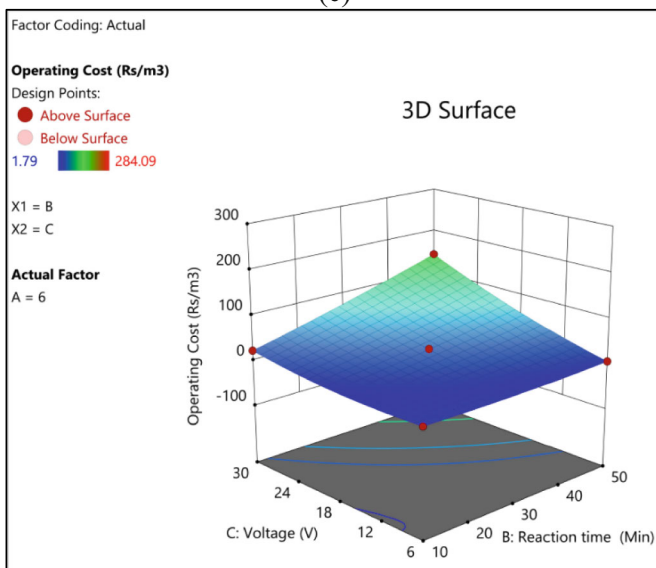


(b)

**Fig. 7** a and b 2D and 3D plot on effect of reaction time and applied voltage on color removal efficiency. c and d 2D and 3D plot on effect of reaction time and applied voltage on operational cost



(c)



(d)

Fig. 7 (continued)

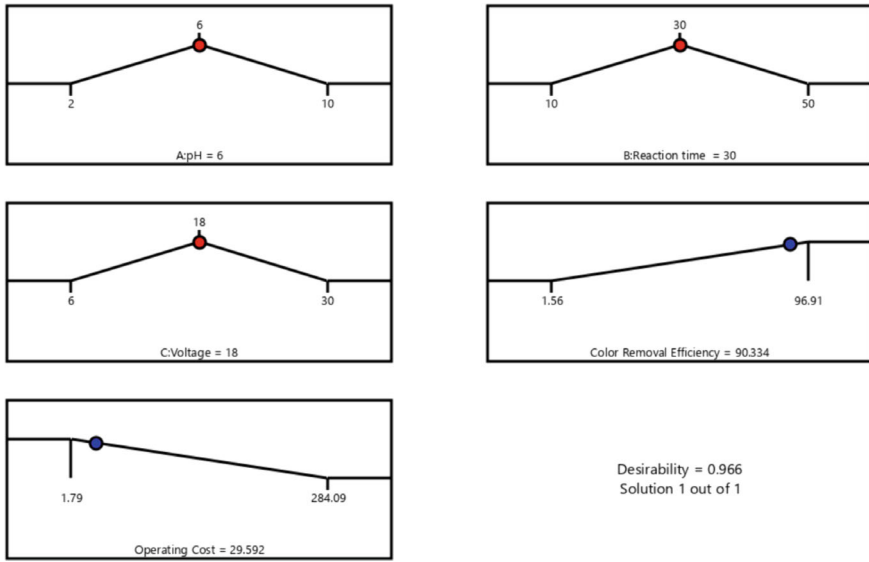
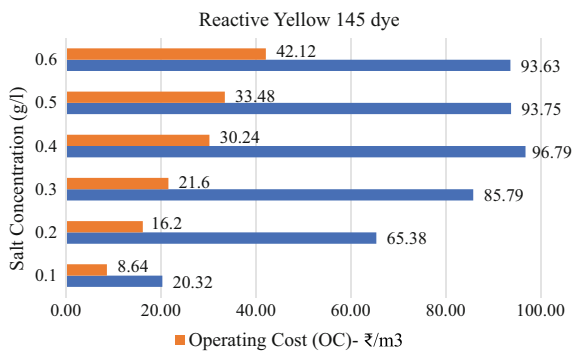


Fig. 8 Optimized results from the ramp functions

was varied from 0.1 g/l to 0.6 g/l for treating wastewater. The effect of the different salt concentrations applied on wastewater are shown below.

Figure 9 shows, there is a negative influence on dye removal efficiency after 0.4 g/l concentration as efficiency decreases with the increase in salt concentration. But with the increase in salt concentration, the operational cost keeps increasing. When the sodium chloride content was increased to > 0.4 g/l, the removal efficiency was decreased. This phenomenon could be caused by the circumstances around a constant voltage and rising electrolyte concentrations. The maximum dye removal efficiency is observed at 0.4 g/l of salt concentration with optimum operating cost (Fig. 10).

Fig. 9 Results of salt concentration variation



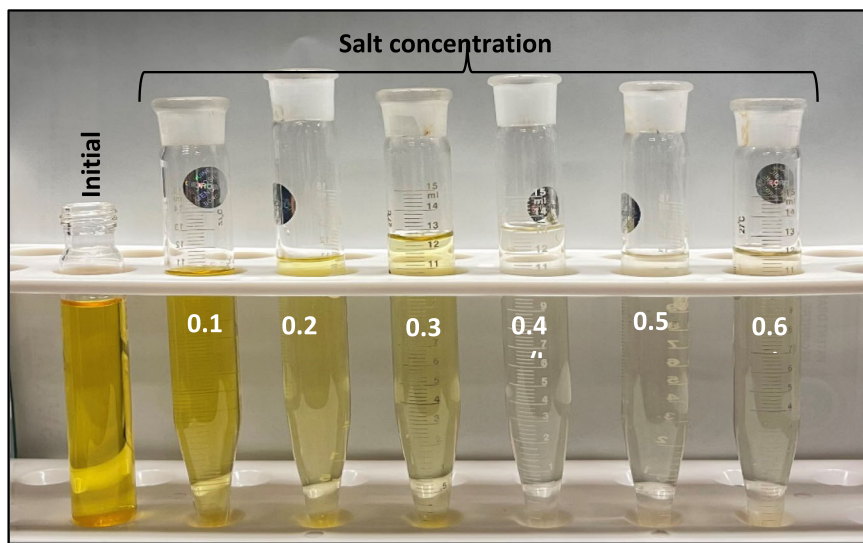


**Fig. 10** Results after salt concentration variation

## 5 Conclusion

In this work, the decolorization and cost-effectiveness of the Reactive Yellow 145 dye solution was evaluated using the electrocoagulation method. Variables such as the applied voltage, the initial pH of the solution, the reaction time, and the concentration of the electrolyte (NaCl) all had an impact on this process. The RSM strategy was used to optimize the method, which reduced the amount of time and experimental work needed. The process was successfully simulated using a second-order polynomial Box-Behnken Design (BBD), which produced prediction models for two response variables: the effectiveness of dye removal and the operating cost for the treatment process. The decolorization of Reactive Yellow 145 dye with pH 6, 30 min of reaction time, 18 V of applied voltage, and 0.4 g/l of salt concentration dye was removed with a 96.79% removal efficiency at the lowest operational cost of 30.24/m<sup>3</sup>. Overall, it was determined that the method was successful in eliminating for this dye cost-effectively.

**Disclosure of Interests** The authors have no competing interests to declare that are relevant to the content of this article.

## References

1. Zidane F et al (2008) Decolorization of dye-containing effluent using mineral coagulants produced by electrocoagulation. *J Hazard Mater* 155(1–2):153–163. <https://doi.org/10.1016/j.jhazmat.2007.11.041>
2. Gündüz Z, Atabey M (2016) Effects of operational parameters on the decolourisation of Reactive Red 195 dye from aqueous solutions by electrochemical treatment. *Int J Electrochem Sci* 14(6):5868–5885. <https://doi.org/10.20964/2019.06.37>
3. Criado SP, Gonçalves MJ, Ballod Tavares LB, Bertoli SL (2020) Optimization of electrocoagulation process for disperse and reactive dyes using the response surface method with reuse application. *J Clean Prod* 275 (2020). <https://doi.org/10.1016/j.jclepro.2020.122690>
4. Kobya M, Demirbas E, Can OT, Bayramoglu M (2006) Treatment of levafix orange textile dye solution by electrocoagulation. *J Hazard Mater* 132(2–3):183–188. <https://doi.org/10.1016/j.jhazmat.2005.07.084>
5. Mishra S, Maiti A (2018) The efficacy of bacterial species to decolourise reactive azo, anthroquinone and triphenylmethane dyes from wastewater: a review. *Environ Sci Pollut Res* 25(9):8286–8314. <https://doi.org/10.1007/s11356-018-1273-2>
6. Kumar D, Patel Z, Pandit P, Pandit R, Patel A, Joshi M (2021) Textile Industry Wastewaters From Jetpur, Gujarat, India, Are Dominated by Shewanellaceae, Bacteroidaceae, and Pseudomonadaceae Harboring Genes Encoding Catalytic Enzymes for Textile Dye Degradation, vol 9, no. Sept, pp 1–15 (2021). <https://doi.org/10.3389/fenvs.2021.720707>
7. Kishor R et al (2021) Ecotoxicological and health concerns of persistent coloring pollutants of textile industry wastewater and treatment approaches for environmental safety. *J Environ Chem Eng* 9(2):105012. <https://doi.org/10.1016/j.jece.2020.105012>
8. Zazycki MA, Godinho M, Perondi D, Foletto EL, Collazzo GC, Dotto GL (2018) New biochar from pecan nutshells as an alternative adsorbent for removing Reactive Red 141 from aqueous solutions. *J Clean Prod* 171:57–65. <https://doi.org/10.1016/j.jclepro.2017.10.007>
9. Merzouk B, Gourich B, Sekki A, Madani K, Vial C, Barkaoui M (2009) Studies on the decolorization of textile dye wastewater by continuous electrocoagulation process. *Chem Eng J* 149(1–3):207–214. <https://doi.org/10.1016/j.cej.2008.10.018>
10. Nandi BK, Patel S (2017) Effects of operational parameters on the removal of brilliant green dye from aqueous solutions by electrocoagulation. *Arab J Chem* 10:S2961–S2968. <https://doi.org/10.1016/j.arabjc.2013.11.032>
11. Tanatti PN (2021) Treatability of wastewater containing Reactive Yellow 145 dyestuff by ozonation process. *Sak Univ J Sci* 25(4):995–1002. <https://doi.org/10.16984/taufbilder.876926>
12. Krishnasamy S, SaiAtchyuth BA, Ravindiran G, Subramaniyan B, Ramalingam M, Sai Vamsi JUB, Razaack NA (2022) Effective removal of Reactive Yellow 145 (RY145) using biochar derived from groundnut shell. *Adv Mater Sci Eng* 2022. <https://doi.org/10.1155/2022/8715669>
13. Mollah MYA et al (2004) Treatment of orange II azo-dye by electrocoagulation (EC) technique in a continuous flow cell using sacrificial iron electrodes. *J Hazard Mater* 109(1–3):165–171. <https://doi.org/10.1016/j.jhazmat.2004.03.011>
14. Salmani ER, Ghorbanian A, Ahmadzadeh S, Dolatabadi M, Nemanifar N (2016) Removal of Reactive Red 141 dye from synthetic wastewater by electrocoagulation process: investigation of operational parameters. *Iran J Heal Saf Environ* 3(1):403–411 [Online]. Available: [http://www.ijhse.ir/index.php/IJHSE/article/view/135/pdf\\_52](http://www.ijhse.ir/index.php/IJHSE/article/view/135/pdf_52)
15. Atiya MA, M-Ridha MJ, Saheb MA (2020) Removal of aniline blue from textile wastewater using electrocoagulation with the application of the response surface approach. *Iraqi J Sci* 61(11):2797–2811. <https://doi.org/10.24996/ijcs.2020.61.11.4>
16. Adane T, Adugna AT, Alemayehu E (2021) Textile industry effluent treatment techniques. *J Chem* 28(2021):1–4. <https://doi.org/10.1155/2021/5314404>
17. Naresh R, Mani S, Mulla SI, Dattatraya G (2017) Ecotoxicology and environmental safety degradation and decolorization potential of an ligninolytic enzyme producing *Aeromonas*

- hydrophila* for crystal violet dye and its phytotoxicity evaluation. *Ecotoxicol Environ Saf* 156(Nov):166–175. <https://doi.org/10.1016/j.ecoenv.2018.03.012>
18. Alshamsi FA, Albadwawi AS, Alnuaimi MM, Rauf MA, Ashraf SS (2007) Comparative efficiencies of the degradation of Crystal Violet using UV/hydrogen peroxide and Fenton's reagent. *Dyes Pigments* 74:283–287. <https://doi.org/10.1016/j.dyepig.2006.02.016>
  19. Kothari MS, Vegad KG, Shah KA, Aly Hassan A (2022) An artificial neural network combined with response surface methodology approach for modelling and optimization of the electrocoagulation for cationic dye. *Heliyon* 8(1):e08749. <https://doi.org/10.1016/j.heliyon.2022.e08749>
  20. Barrera-díaz CE, Lugo-lugo V, Bilyeu B (2012) A review of chemical, electrochemical and biological methods for aqueous Cr (VI) reduction. *J Hazard Mater* 223–224:1–12. <https://doi.org/10.1016/j.jhazmat.2012.04.054>
  21. Yang CL, McGarrahan J (2005) Electrochemical coagulation for textile effluent decolorization. *J Hazard Mater* 127(1–3):40–47. <https://doi.org/10.1016/j.jhazmat.2005.05.050>
  22. Mbacké MK et al (2016) Electrocoagulation process applied on pollutants treatment—experimental optimization and fundamental investigation of the crystal violet dye removal. *J Environ Chem Eng* 4(4):4001–4011. <https://doi.org/10.1016/j.jece.2016.09.002>
  23. Mollah MYA, Schennach R, Parga JR, Cocke DL (2001) Electrocoagulation (EC)—science and applications. *J Hazard Mater* 84:29–41
  24. Dolphen R, Sakkayawong N, Thiravetyan P, Nakbanpote W (2007) Adsorption of Reactive Red 141 from wastewater onto modified chitin. *J Hazard Mater* 145(1–2):250–255. <https://doi.org/10.1016/j.jhazmat.2006.11.026>
  25. Aquino JM, Rocha-Filho RC, Rodrigo MA, Sáez C, Cañizares P (2013) Electrochemical degradation of the Reactive Red 141 dye using a boron-doped diamond anode. *Water Air Soil Pollut* 224(1). <https://doi.org/10.1007/s11270-012-1397-9>
  26. Vanaamudan A, Sudhakar PP (2015) Equilibrium, kinetics and thermodynamic study on adsorption of Reactive Blue-21 and Reactive Red-141 by chitosan-organically modified nanoclay (Cloisite 30B) nano-bio composite. *J Taiwan Inst Chem Eng* 55:145–151. <https://doi.org/10.1016/j.jtice.2015.03.025>
  27. Telke A, Kalyani D, Jadhav J, Govindwar S (2008) Kinetics and mechanism of Reactive Red 141 degradation by a bacterial isolate *Rhizobium radiobacter* MTCC 8161. *Acta Chim Slov* 55(2):320–329
  28. Kim TY, Park SS, Cho SY (2012) Adsorption characteristics of Reactive Black 5 onto chitosan beads cross-linked with epichlorohydrin. *J Ind Eng Chem* 18(4):1458–1464. <https://doi.org/10.1016/j.jiec.2012.02.006>
  29. De Luca P, Nagy JB (2020) Treatment of water contaminated with Reactive Black-5 dye by carbon nanotubes. *Materials (Basel)* 13(23):1–19. <https://doi.org/10.3390/ma13235508>
  30. Saba B, Khalid A, Nazir A, Kanwal H, Mahmood T (2013) Reactive Black-5 azo dye treatment in suspended and attach growth sequencing batch bioreactor using different co-substrates. *Int Biodeterior Biodegrad* 85:556–562. <https://doi.org/10.1016/j.ibiod.2013.05.005>
  31. Meriç S, Kaptan D, Ölmez T (2004) Color and COD removal from wastewater containing Reactive Black 5 using Fenton's oxidation process. *Chemosphere* 54(3):435–441. <https://doi.org/10.1016/j.chemosphere.2003.08.010>
  32. Amin MT, Alazba AA, Shafiq M (2015) Adsorptive removal of Reactive Black 5 from wastewater using bentonite clay: Isotherms, kinetics and thermodynamics. *Sustain* 7(11):15302–15318. <https://doi.org/10.3390/su71115302>
  33. Brinza L, Maftai AE, Tascu S, Brinza F, Neamtu M (2022) Advanced removal of Reactive Yellow 84 azo dye using functionalised amorphous calcium carbonates as adsorbent. *Sci Rep* 12(1):1–15. <https://doi.org/10.1038/s41598-022-07134-2>
  34. Indhu S, Muthukumaran K (2018) Removal and recovery of Reactive Yellow 84 dye from wastewater and regeneration of functionalised *Borassus flabellifer* activated carbon. *J Environ Chem Eng* 6(2):3111–3121. <https://doi.org/10.1016/j.jece.2018.04.027>
  35. El Haddad M et al (2012) Adsorptive removal of Reactive Yellow 84 dye from aqueous solutions onto animal bone meal. *J Mater Environ Sci* 3(6):1019–1026

36. Abdolmohammad-Zadeh H, Ghorbani E, Talleb Z (2013) Zinc-aluminum layered double hydroxide as a nano-sorbent for removal of Reactive Yellow 84 dye from textile wastewater effluents. *J Iran Chem Soc* 10(6):1103–1112. <https://doi.org/10.1007/s13738-013-0255-z>
37. Aguedach A, Brosillon S, Morvan J (2005) Photocatalytic degradation of azo-dyes Reactive Black 5 and Reactive Yellow 145 in water over a newly deposited titanium dioxide. *Appl Catal B* 57(1):55–62. <https://doi.org/10.1016/j.apcatb.2004.10.009>
38. Kalkan NA, Aksoy S, Aksoy EA, Hasirci N (2012) Adsorption of Reactive Yellow 145 onto chitosan coated magnetite nanoparticles. *J Appl Polym Sci* 124(1):576–84. <https://doi.org/10.1002/app.34986>
39. Gül Ş, Özcan-Yıldırım Ö (2009) Degradation of Reactive Red 194 and Reactive Yellow 145 azo dyes by O<sub>3</sub> and H<sub>2</sub>O<sub>2</sub>/UV-C processes. *Chem Eng J* 155(3):684–690. <https://doi.org/10.1016/j.cej.2009.08.029>

# Membrane Desalination of Wastewater for the Contaminant Removal and Reduction of Fouling



S. Vinod Kumar , Balasubramanian Raguathan , and K. Nishant 

## 1 Introduction

A worldwide problem that is becoming more and more significant is the lack of freshwater supply. Water makes up 75% of the globe's surface, making it the most plentiful resource there is, although most of water reservoirs are not immediately useful. In many places of the world, the balance of freshwater supplies does not match population density and water use [1]. The total salts in seawater are usually between 30,000 and 40,000 ppm, whereas brackish water has salinity levels of up to 10,000 ppm. As a result, both fluids are unsuitable for drinking and most of household purposes. When drinking water indicators of quality are considered, the World Health Organization (WHO) permits salinities between 400 and 900 ppm in specific circumstances [2]. The acceptable limit is reached via the desalination process, which reduces the total dissolved solids. Seawater (67%) has been desalinated the most, brackish water came in second with 20%, followed by water from streams (9%), and then wastewater (5%) [3]. Thermal, membrane, and phase-change process separation are main types of desalination procedures. Several phase-change methods include multi-stage flash, multi-effect boiling, atmospheric compression, freezing, humidification/dehumidification, and solar-powered stills. Electrodialysis (ED), distillation by membrane (MD), and reverse osmosis (RO) are membrane-based procedures [4]. Membrane distillation is a method that can be successfully used for seawater desalination or purification in commercial settings because of its potential reduced energy usage and simplicity. For the procedure of desalination, energy from sustainable sources is preferred to assist down the desalination expenses. A lab balance

---

S. Vinod Kumar · K. Nishant

Department of Chemical Engineering, St. Josheph College of Engineering, Chennai 600119, India

B. Raguathan (✉)

Department of Petroleum Engineering, School of Energy Technology, Pandit Deendayal Energy University, Gandhinagar 382426, India

e-mail: [balaschem@gmail.com](mailto:balaschem@gmail.com)

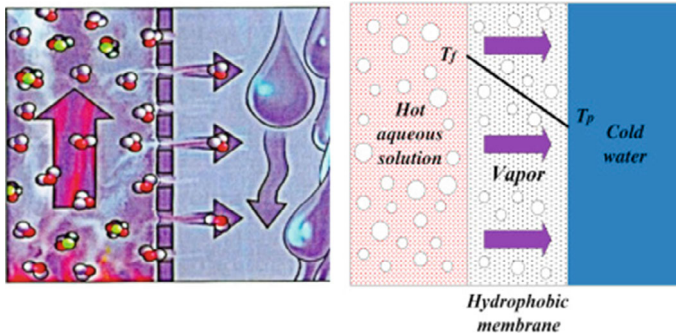


**Fig. 1** Membrane distillation process

specifications were followed when using the membrane distillation unit [5]. As the first step, a thorough analysis of the fundamental concepts and arrangements of the physical properties of membranes, the effects of operating conditions, the properties of mass and heat transport, and the water treatment process was carried out after heating the membrane unit [6]. The membranes in desalination process may become clogged with extra salt and other pollutants (Fig. 1). Due to this, the membranes' effectiveness is impacted, which is explored in more detail in the next section along with strategies for lowering fouling during desalination of saltwater [7].

### **1.1 Membrane Distillation (MD)**

MD, a thermally driven membrane process, separates cold and hot streams of water using a water-repellent micro porous membrane. Using a porous membrane that does not serve as a wet table for the solvent, mass exchange takes place [8]. The two fluids in contact with the membrane have temperatures that vary. Vapor can flow through the membrane's pores but not liquid water because of its hydrophobic nature. A partial pressure gradient is formed by the temperature differences, which allows [9]. On the low-temperature side, the steam condenses, creating a distillate. Several methods of collecting permeate, mechanisms for mass transfer across membranes, and the causes of driving force production can all be used to do MD [7]. The method has a number of benefits, such as the ability to use waste grade heat, the creation of highly water that is clean, virtually concentration-independent functioning, simplicity in comparison with traditional exothermic reactions, lower mechanical properties specifications for membranes used, etc. [10].

A concentrated brine solution can be utilized to produce freshwater and to extract crystals. Moreover, compared to other membrane extraction techniques like RO, the membrane porosity needed for MD is comparatively higher. As a result, fouling is less of an issue for MD process. It is possible to link the MD system with other

separation strategies to create a more thorough filtering system, such as ultrafiltration and a reverse osmosis unit [11].

## ***1.2 Membrane Fouling***

Fouling is generally the accumulation of unwelcome deposits inside or on the exterior of a membrane that reduces the efficacy of the substrate's rejection of salt and penetrated flux [12]. The desalination and purification processes may be severely harmed by fouling. Deposits are created when the foulants, which are frequently colloidal in nature, contact with one another or a membrane's surface. MD experiences all kinds of contaminations that happen in other membrane-separation methods. A fouled layer adds extra thermal and hydrodynamic resistances, and these limitations are influenced by the porosity and the density of the fouled layer [13]. The main factors of the variety of fouled that will form on the top of the membrane are the kind, concentration, and properties of the substances that are present in the supply water as well as the overall chemical reactions of the feed water itself [14]. Contrarily, interaction between contaminants and the membrane's interface may enhance the potential for contamination; hence, membrane properties can greatly affect fouling. The degree of fouling can also be influenced by operational factors such as feed temperature and flow rate [15].

## ***1.3 Characteristics of Membrane***

- Membrane should be porous.
- Process liquids should not be overload a membrane by passing it across.
- The holes of the membrane should not be home to any capillary condensation.
- The balance between the vapor and liquid phases of the various process.
- Liquids' constituents must not be affected by the membrane.
- The process liquid must directly touch at least one side.
- The driving force is a small pressure difference in the vapor phase.
- Behind this membrane functioning for each component.
- Permeate flow and diffusion length are negatively correlated, and membrane vacancies must have free route.
- The membrane material should have less thermal conductivity.

**Table 1** Membrane specification

Membrane specification	
Medium	0.20 $\mu\text{m}$ hydrophobic PTFE
Support medium	Polypropylene
Cage/core/end caps	Polypropylene
Gasket	Silicon
Inter support ring	Stainless steel

**Table 2** Membrane dimension

Membrane dimensions	
Normal length	25.54 cm
Outer diameter	7.01 cm
Inner diameter	3.25 cm

## 2 Materials and Methods

### 2.1 Specifications and Dimension

For membrane distillation, membranes were bought from Mumbai Trinity Technologies Ltd. The effective membrane surface of the polytetrafluoroethylene membrane filters utilized in this experiment for the DCMD arrangement is  $5.6 \text{ m}^2$ , as stated by the manufacturer. DCMD arrangement of desalination process is used in this article [16]. Specification and dimensions of membrane listed in the following Tables 1 and 2.

### 2.2 Membrane Material

Membrane distillation membranes (PVDF) are typically made of polytetrafluoroethylene (PTFE), polypropylene (PP), and polyvinylidene fluoride. The porosities, pore diameters, and thicknesses of the membranes vary from 0.6 to 0.95, 0.2 to 0.1  $\mu\text{m}$ , and 0.04 to 0.25 mm, respectively [17]. The surface energy and thermal conductivity of the above materials are listed in Table 3. PTFE is the most hydrophobic of these materials, has excellent thermal and chemical stability, and is oxidation-resistant [18]. Nevertheless, it also has the greatest conductance, which will result in increased heat transmission through PTFE membranes. PVDF offers strong heat resistance, mechanical strength, and hydrophobicity. The most recent technological advancements have produced materials with high porosity, high hydrophobicity, and strong mechanical strength, such as carbon nanotubes, chemically enhanced PES, and fluorinated copolymers. Stretched, sintered, and these components are processed via the phase conversion to produce MD membranes [19].

**Table 3** Different membrane conductivities

Membrane material	Surface energy (* $10^{-3}$ N/m)	Conductivity (W/m K)
PTFE	10–25	0.30
PP	31	0.20
PVDF	29	0.15

### 2.3 Experimental Procedure

In this experiment, water was heated by adjusting the temperature from 94 to 98 °C as well as the concentration by adding table salt (NaCl) in increments of 100 to 800 g per 20 L of water. By evaluating several variables, such as permeate flow, inlet and exit temperatures, the amount of recovered freshwater, and salt rejection, one can assess the efficiency and performance of the filtration system. The saltwater is initially fed into the steam evaporator, where it is heated up and the vapors are transferred to another chamber with the membranes. This chamber also has a temperature sensor to determine the feed liquid's initial and final temperatures, as well as a condenser to condense the feed liquid as it passes through the PTFE membranes. These membranes are hydrophobic by nature and function as a filter for polluted water where vapor pressure changes induce gaseous mass exchange. In this experiment, different concentrations of saltwater were introduced into a steam evaporator apparatus, which was heated to a constant temperature of 91–97 °C. The equipment has good insulation to heat from escaping into the surrounding area. Vapor was then allowed to pass through the membrane's pores, where it experienced a difference in vapor pressure before condensing on the other side. At the side of the distillate, the permeate temperature was 55 °C. The amount of distillate product on permeate stream was studied, together with permeate flow and thermal efficiency.

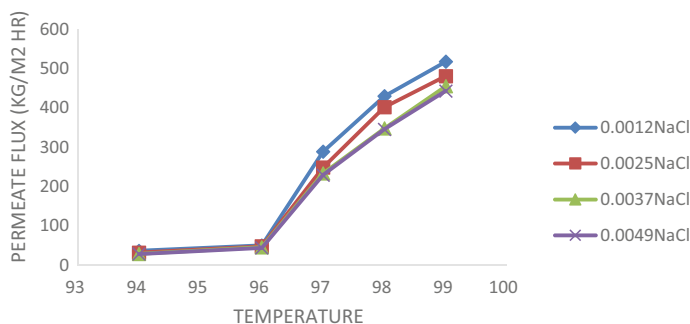
## 3 Results and Discussion

Throughout the course of the experiment, the volume of water drunk remained constant. The rate of flow of the filtrate was changed at various feed temperatures to gain an idea of how different dependent parameters, such as filtrate temperatures, condensate temperatures and rate of flow, and salts refusal, could vary for varied salt concentrations (Table 4). The sampling feed requirements for the operation for 100 g of sodium chloride in 25 L of water comprise parameters that are tested for both outflow and inflow samples obtained at different temperatures [20].

The stability of the 97 °C solution's curve steadily declines as the solution's NaCl content rises, the graph's depiction of the polarization caused by the increasing temperature, the drop in vapor pressure caused by the salt quantity, the border dosage at the membrane's terrain, and so on (Fig. 2).

**Table 4** Permeate flow influenced by temperature and concentration

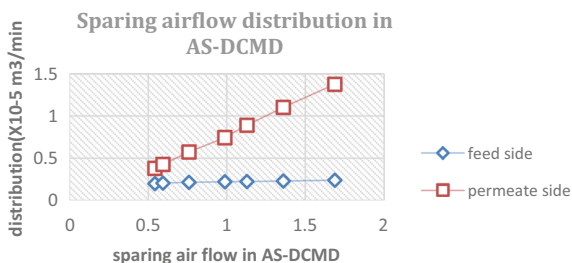
Feed temperature (°C)	Various flux concentrations of sodium chloride salts (kg/m <sup>2</sup> h)			
	0.0012	0.0025	0.0037	0.0047
94	38.01	35.89	30.76	28.76
96	52.64	50.07	45.29	45.64
97	280.35	250.67	230.56	250.55
98	445.90	409.78	350.59	350.59
99	530.92	487.65	460.07	440.53

**Fig. 2** Permeate flux versus temperature

### 3.1 Augmentation in AS-DCMD's Flux

AS-performance DCMDs were evaluated for how well they would increase flow and decrease fouling. Figure 3 investigates the effects on air sparging, and permeate flow was measured and observed in both conventional DCMD and AS-DCMD modes. The membranes permeate or feed side can be utilized to inject the sparging air in an AS-DCMD system. Additionally, it was found that some of the sparging air could get through the membrane barriers and reach the other side. As an illustration, air pumped into the feed side migrated to the permeate end [8]. The addition of atmospheric sparging on input side did not appreciably enhance performance or help reduce fouling when compared to air sparging on permeate side. Research was conducted in DCMD and AS-DCMD. It was clear that AS-DCMD was the best strategy for dealing with the flux [21]. The sparging rate of airflow was changed from  $0.20 \times 10^{-5}$  to  $3.00 \times 10^{-5}$  m<sup>3</sup>/min at flow rates of 0.20 m<sup>3</sup>/min for feed and permeate. It was found that the flux increase over DCMD was between 5 and 25% for air sparging in both feed and permeate sides. Moreover, flux as the SGMD was much less than that produced with ASDCM [22].

**Fig. 3** Sparring airflow versus distribution



### 3.2 Reduced Fouling in AS-DCMD

Using saltwater, the fouling behavior and efficient air sparring mitigation were investigated (Fig. 4). To evaluate the PTFE membranes in saltwater solutions, DCMD and AS-DCMD methods were used. Studies were conducted under feed to permeate 1:1 flow rate (0.2 m<sup>3</sup>/min) conditions. In this instance, the sparring airflow rate was maintained at an ideal rate of  $2 \times 10^{-5}$  m<sup>3</sup>/min. The percentage flux reduction caused by fouling over the surface of the membrane as compared to the starting flux was determined to be 56.7% in DCMD run of PTFE membrane. For DCMD and AS-DCMD modes, the corresponding relative flux decreases were 58.89% and 42.45%, respectively (Table 5).

The experimental circumstance:  $T$  (feed) = 96 °C,  $T$  (permeate) = 55 °C, and  $F_f$  = 0.2 m<sup>3</sup>/min.

**Fig. 4** Ordinalized flux drop as a result of the salt solution fouling the PTFE membrane and partial flux recovery after air sparring

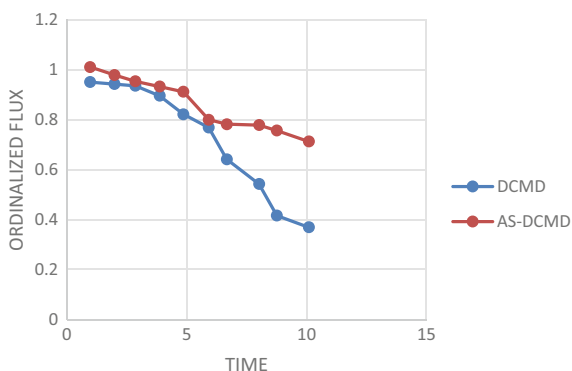


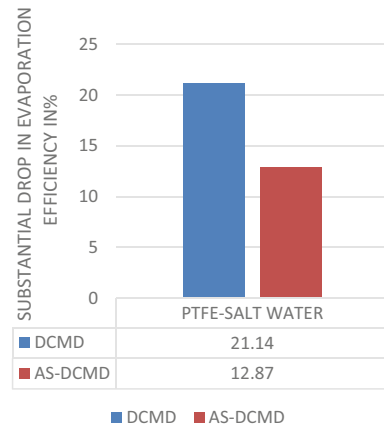
**Table 5** Membrane surface deposition and the proportion of deposition drop

System used	Reduced flux %, DCMD	Reduced flux %, AS-DCMD	Salts retained in DCMD (mg)	Reduced deposition %
PTFE-saltwater	58.89	42.45	18.76	32.67

With DCMD and AS-DCMD, additionally includes an overview of salts deposits. The table clearly shows that adding air sparring to traditional DCMD decreased for saltwater solutions, with 67 and 65 weight percentages of salt accumulation, respectively. Evaporation efficiency (EE) is the proportion of power required for evaporating water to sensible heat lost during the MD process, which is used to assess how well heat is utilized [23].

The relationship between the variations of NaCl in water concentration and the distillate’s conductivity is displayed. It has been discovered that when concentration rises, conductivity rises slowly and steadily. Considering that salt is an excellent conductor, this tendency has been adopted. Increased turbulence decreases temperature and concentration polarization in MD while increasing the rate of heat transfer. When the blocked membrane pores were cleansed and made more accessible by air sparring, less crystal were formed, which improved the MD performance. Also, crystal growth and formation were avoided on the membrane’s interface by the high shear stress caused by the flowing air. Last but not least, air sparring reduced the barrier resistance and enhanced the turbulence at the membrane’s surface. It is abundantly obvious that, despite a rise in the salt content in the feed, substantial salts elimination (95%) is achievable in membrane distillation but not in reverse osmosis. This demonstrates that membrane distillation is more efficient than reverse osmosis since the greatest percentage of salts elimination is accomplished. By using an MD in conjunction with an environmentally friendly energy source, such as solar power, development may be produced. This would end up resulting in freshwater production and lower energy use. Low flux and fouling can be crucial factors at high salt concentrations, which is where AS-DCMD excels (Fig. 5).

**Fig. 5** PTFE-saltwater versus evaporation efficiency



## 4 Conclusion

In all MD setups, the flux generally increases with feed temperature in an expanding manner. The input temperature has a significant impact on the flow since solvent levels shift dramatically with the flow temperatures power MD. Note that operation at temperatures above 100 °C may result in a loss in membrane selectivity and serious scaling issues. Nevertheless, with back-pulsing, significant improvement was attained by surface modification, particularly for low feed concentrations and quick filtering periods.

Because it does not use any chemicals, this approach is incredibly advantageous on the lab scale. The process for MD desalination could be strengthened by a membrane with anti-fouling skin layer qualities. Membrane cleaning might be done during the least expensive time of day to reduce operating expenses. Chemical cleaning requires ample time for the chemicals to interact with precipitated materials. Therefore, it is anticipated that increased cleaning duration will result in more flux recovery at the start of the cleaning process.

## References

1. Okello C, Tomasello B, Greggio N, Wambiji N, Antonellini M (2015) Impact of population growth and climate change on the freshwater resources of Lamu Island, Kenya. *Water (Switzerland)* 7:1264–1290. <https://doi.org/10.3390/w7031264>
2. Modi FM, Gadani DH, Rana VA (2020) Estimation of sea water salinity from dielectric measurements: effect of temperature. *Indian J Pure Appl Phys* 58:439–447. <https://doi.org/10.56042/ijpap.v58i6.27321>
3. Feria-Díaz JJ, Correa-Mahecha F, López-Méndez MC, Rodríguez-Miranda JP, Barrera-Rojas J (2021) Recent desalination technologies by hybridization and integration with reverse osmosis: a review. *Water (Switzerland)* 13:1–40. <https://doi.org/10.3390/w13101369>
4. Esmaeilion F (2020) Hybrid renewable energy systems for desalination. *Springer Int Publ.* <https://doi.org/10.1007/s13201-020-1168-5>
5. Najim A (2022) A review of advances in freeze desalination and future prospects. *NPJ Clean Water* 5 (2022). <https://doi.org/10.1038/s41545-022-00158-1>
6. Le NL, Nunes SP (2016) Materials and membrane technologies for water and energy sustainability, *Sustain. Mater Technol* 7:1–28. <https://doi.org/10.1016/j.susmat.2016.02.001>
7. Bin Abid M, Wahab RA, Salam MA, Gzara L, Moujдин IA (2023) Desalination technologies, membrane distillation, and electrospinning, an overview. *Heliyon* 9:e12810. <https://doi.org/10.1016/j.heliyon.2023.e12810>
8. Parani S, Oluwafemi OS (2021) Membrane distillation: recent configurations, membrane surface engineering, and applications. *Membranes (Basel)* 11. <https://doi.org/10.3390/membranes11120934>
9. Sharma AK, Juelfs A, Colling C, Sharma S, Conover SP, Puranik AA, Chau J, Rodrigues L, Sirkar KK (2021) Porous hydrophobic–hydrophilic composite hollow fiber and flat membranes prepared by plasma polymerization for direct contact membrane distillation. *Membranes (Basel)* 11:1–16. <https://doi.org/10.3390/membranes11020120>
10. Dhoke C, Zaabout A, Cloete S, Amini S (2021) Review on reactor configurations for adsorption-based CO<sub>2</sub> capture. *Ind Eng Chem Res* 60:3779–3798. <https://doi.org/10.1021/acs.iecr.0c04547>

11. Reig M, Vecino X, Cortina JL (2021) Use of membrane technologies in dairy industry: an overview. *Foods* 10:1–29. <https://doi.org/10.3390/foods10112768>
12. El Batouti M, Alharby NF, Elewa MM (2022) Review of new approaches for fouling mitigation in membrane separation processes in water treatment applications. *Separations* 9. <https://doi.org/10.3390/separations9010001>
13. Ahmed MA, Amin S, Mohamed AA (2023) Fouling in reverse osmosis membranes: monitoring, characterization, mitigation strategies and future directions. *Heliyon* 9:e14908. <https://doi.org/10.1016/j.heliyon.2023.e14908>
14. Alkhatib A, Ayari MA, Hawari AH (2021) Fouling mitigation strategies for different foulants in membrane distillation. *Chem Eng Process Process Intensif* 167:108517. <https://doi.org/10.1016/j.cep.2021.108517>
15. Siddique T, Dutta NK, Choudhury NR (2021) Mixed-matrix membrane fabrication for water treatment. *Membranes (Basel)* 11. <https://doi.org/10.3390/membranes11080557>
16. Mohammad Ameen NA, Ibrahim SS, Alsahy QF, Figoli A (2020) Highly salinewater desalination using direct contact membrane distillation (DCMD): experimental and simulation study. *Water (Switzerland)* 12. <https://doi.org/10.3390/W12061575>
17. Huang FYC, Arning A (2019) Performance comparison between polyvinylidene fluoride and polytetrafluoroethylene hollow fiber membranes for direct contact membrane distillation. *Membranes (Basel)* 9. <https://doi.org/10.3390/membranes9040052>
18. Parvate S, Dixit P, Chattopadhyay S (2020) Superhydrophobic surfaces: insights from theory and experiment. *J Phys Chem B* 124:1323–1360. <https://doi.org/10.1021/acs.jpcc.9b08567>
19. Khraisheh M, AlMomani F, Al-Ghouti M (2021) Electrospun Al<sub>2</sub>O<sub>3</sub> hydrophobic functionalized membranes for heavy metal recovery using direct contact membrane distillation. *Int J Energy Res* 45:8151–8167. <https://doi.org/10.1002/er.5710>
20. Demska-Zakęś K, Gomułka P, Rożyński M, Zakęś Z (2021) Effect of a short-term sodium chloride bath on juvenile pikeperch (*Sander lucioperca*) welfare. *Aquac. Reports* 19. <https://doi.org/10.1016/j.aqrep.2020.100569>
21. Liu Y, Xiao T, Bao C, Zhang J, Yang X (2018) Performance and fouling study of asymmetric PVDF membrane applied in the concentration of organic fertilizer by direct contact membrane distillation (DCMD). *Membranes (Basel)* 8:1–13. <https://doi.org/10.3390/membranes8010009>
22. Said IA, Chomiak T, Floyd J, Li Q (2020) Sweeping gas membrane distillation (SGMD) for wastewater treatment, concentration, and desalination: a comprehensive review. *Chem Eng Process Process Intensif* 153:1–35. <https://doi.org/10.1016/j.cep.2020.107960>
23. Jouhara H, Khordehghah N, Almahmoud S, Delpéch B, Chauhan A, Tassou SA (2018) Waste heat recovery technologies and applications. *Therm Sci Eng Prog* 6:268–289. <https://doi.org/10.1016/j.tsep.2018.04.017>

# Emerging Water Desalting Technologies: Current Status, Challenges, and Future Trends



M. A. Shabiimam, Jay Dhorawala, and Tirtha Trivedi

## 1 Introduction

In recent times, numerous regions have confronted water scarcity issues due to declining groundwater levels [1]. As the global population continues to grow, access to water has considerably diminished. Many communities worldwide speculate that the surging population and its escalating water demands surpass the capacities of conventional water resources [2]. Responding to the United Nations projection that between 2 and 7 billion individuals might encounter water scarcity [3], it's important to note that seas cover approximately 70.8% of Earth's surface and contain around 97% of its water, though less than 3% of this is freshwater suitable for consumption. This situation has prompted countries to turn to the desalination of ocean water, despite the substantial costs involved in this water supply method. Notably, several Gulf nations heavily rely on desalinated water to meet industrial and domestic needs [1]. However, a significant portion of seawater is unfit for consumption due to its high salinity [4], necessitating the conversion of saltwater into freshwater through desalination technologies.

Desalt procedures primarily fall into two categories: thermal desalination and membrane desalination. The most basic form of thermal desalination involves evaporating brine to produce freshwater and subsequently condensing the resulting steam. This method traces back centuries; even Aristotle in the past documented a thermal desalination technique based on brine vaporization and recondensation [4]. Desalination plants emerged in water-stressed cities during the nineteenth century, utilizing multi-effect distillation (MED), multi-stage flash distillation (MSF), and reverse osmosis (RO) technologies [5]. The rapid increase in demand for potable water has fueled the construction and advancement of desalination plants [6].

---

M. A. Shabiimam (✉) · J. Dhorawala · T. Trivedi  
Department of Civil Engineering, School of Technology, Pandit Deendayal Energy University,  
Gandhinagar, Gujarat 382421, India  
e-mail: [shabiimam.ma@sot.pdpu.ac.in](mailto:shabiimam.ma@sot.pdpu.ac.in)

However, the escalating demand for seawater desalination has prompted explorers to explore alternative technologies. Notably, optimum energy-intensive reverse osmosis (RO) plants have seen improvements in energy-efficient pumps, energy recovery devices [7, 8]. Another strategy to lower energy usage is leveraging the osmotic pressure of brine, exemplified by forward osmosis (FO). Despite its advantages over reverse osmosis, FO still faces commercialization challenges, and related processes like pressure-delayed osmosis (PRO) and osmosis-increase reverse osmosis remain at the laboratory stage.

A thermally driven membrane separation method called Membrane Distillation (MD) has emerged for marine and brackish water desalination [9]. MD offers benefits such as high rejection of non-volatile compounds, lower operating stress compared to RO, reduced operating temperatures, and a smaller footprint compared to traditional distillation methods like MSF and MED [10]. This review focuses on ongoing research, technological challenges in emerging desalination technologies, including those with nearby commercial viability, and novel concepts in electrochemical desalination. By highlighting material and process developments, we address factors that impede the widespread adoption of forward osmosis and membrane distillation and discuss material innovations in these methods that could drive technological upgradability in the near future.

## 2 Up-and-Coming Desalination Technologies

### 2.1 *Forward Osmosis*

Forward osmosis (FO) has undergone extensive exploration since its initial identification in the 1930s [11], encompassing a wide spectrum of potential applications for desalination. Unlike the utilization of hydraulic pressure, the FO technique leverages elevated osmotic pressure to compel water passage through a partially permeable membrane from the feeding solution [12].

Following the retrieval and recycling of extract solutes through the draw solution, water emerges as a byproduct. A commonly favored draw solution involves the amalgamation of ammonia and carbon dioxide gas [13]. By appropriately blending ammonia and carbon dioxide in specific ratios, a solution endowed with high osmotic pressure can be generated, facilitating efficient extraction of water from saline feeds. The notable advantage of this amalgamation is its suitability for reapplication within the FO process post-heating and regeneration, thereby casting FO as an amalgamation of thermodynamic and membrane processes.

FO systems operate across two distinct functional modes contingent on whether the active layer faces the feed solution (FO mode) or the draw solution (D mode) (PRO mode). Owing to its inherent nature, forward osmosis commands lower energy consumption in contrast to pressure-driven processes, with FO membranes exhibiting enhanced resistance to fouling [14]. The FO desalt approach is bifurcated into two

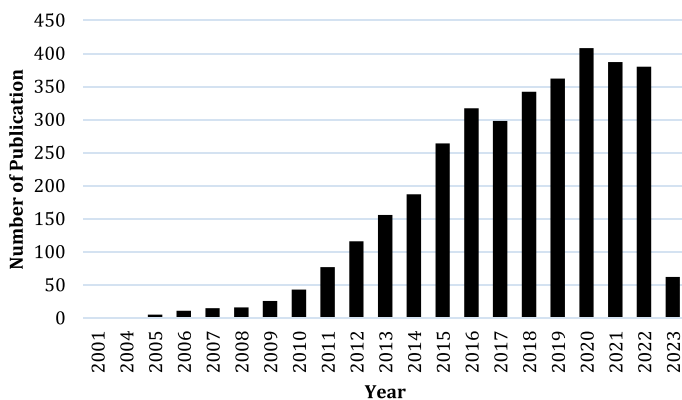


**Fig. 1** Number of articles published between 2001 and 2023 about “forward osmosis” (Scopus)

stages, necessitating the sequential occurrence of osmosis followed by the regeneration of the draw solution. Their efficiency of the FO desalination mechanism hinges upon the recovery of the draw solution alongside the osmotic movement of water molecules through the FO membrane. Despite its frequent oversight, the recovery phase holds the potential to significantly influence overall energy utilization, contingent upon the chosen technique and draw solute. In terms of draw solution recovery, debates exist regarding whether the FO-NF/RO system use more power in comparison to conventional RO. While certain investigations contravene this assertion, others identify minimal disparities [15].

The volume of publications centered around FO has experienced a marked surge since 2009, maintaining an approximate annual count of 250 articles between 2016 and 2018, as underscored by a recent citation analysis appraisal [16].

This augmentation can be partially attributed to innovations in FO membrane materials, primarily emerging from many foreign countries. The amplification in literature articles pertaining to forward osmosis spanning from 2001 to 2020 is visibly manifested in Fig. 1. Recent progress in FO desalination research has mostly been made in improving functional membrane materials, choosing the right draw solutes, and coming up with workable ways to recover the draw solutes. These endeavors are geared toward curbing energy consumption and positioning FO as a formidable contender in the realm of desalination methods. However, our scrutiny encompasses not only the strides achieved in membrane materials specific to forward osmosis but also the impediments impeding their widespread industrial integration.

### 2.1.1 Membrane Material

The search for membranes with higher flux and exceptional salt rejection has spurred comprehensive study in the field of forward osmosis (FO) [11]. FO membranes must exhibit elevated rejection rates for draw solutes, minimal fouling risk, and the

prevention of reverse salt flow. These considerations are particularly crucial when employing fine-film composite membranes. It is imperative for the active part to be sufficiently thick, and the design of each layer should prioritize efficiency. Employing a thin support layer promotes both high solute rejection and flux. Notably, a key distinction between support layers for reverse osmosis (RO) and FO lies in the fact that TFC-RO membranes, often incorporating an aiding layer, might not be optimally suited for FO application. Consequently, considerable attention has been directed toward refining the support layer. Hydrophilicity and mechanical stabilization—two factors that are critical for FO applications—are taken into consideration when building the support layer for FO desalination. Some of the challenges associated with this aspect are being effectively addressed through ongoing research on membranes employed in contemporary forward osmosis processes.

Early investigations into forward osmosis employed thin-film composite reverse osmosis (TFC-RO) membranes featuring a resilient backing layer designed to endure substantial hydraulic pressures. In spite of this, these membranes had fairly thick support layers, which created a diffusive boundary layer that caused the osmotic pressure to drop along the active layer gradient. Internal concentration polarization (ICP) was the name given to this phenomenon, which severely limited the propulsive force for mass transfer, preventing water flow and hindering FO efficiency [17]. The optimization of substrate design plays a pivotal role in diminishing S and alleviating ICP [16, 18].

Research has thus delved into developing and modifying support layers as a pivotal facet of enhancing forward osmosis membrane performance. Recent reviews that delve into the nuances of the support layer emphasize its importance [17, 19, 20]. In the subsequent sections, we explore the latest advancements in both active and supportive layers, with the aim of enhancing FO performance.

### **2.1.2 Selection of Draw Solutes**

Many people know that draw solutes (DS) play a big part in forward osmosis (FO) processes because they add a lot of the energy that is needed for FO-based water treatment methods. To choose the best DS, the first step is to carefully look at all the possible materials, taking into account their natural properties such as solubility, pH, specifications, osmotic pressure, and how well they work with the forward osmosis membrane. This step establishes the foundation for the DS selection process. Subsequently, a comprehensive evaluation of the performance of promising DS materials is conducted at the laboratory scale, which is followed by a conclusive assessment of their effectiveness in full-scale applications. It's important to note that additional criteria might need consideration based on specific application demands.

An ideal draw solute for FO procedures must possess a range of qualities to be deemed suitable. These include exhibiting high water flux while minimizing back solute flux, displaying minimal reverse draw solute flux, showcasing optimal temperature stability, chemical inertness, and neutral pH. Furthermore, properties such as lesser molecular weight, recyclability, less toxic substances, resistance to fouling,

and chemical inertness to the employed membrane are essential attributes [21, 22]. Prospective draw solutes are recommended to possess higher osmotic pressures than the corresponding feed solutions [23].

To effectively serve as a functional draw agent in FO processes, a material must produce significantly high pressure compared to the feed. Particularly in the scene of desalt procedure, the pressure of the solutions should remain well below the threshold of 7.7 atm for brackish feed solutions and remain considerably limited to 27 atm concerning seawater feed solutions [24].

## ***2.2 Draw Solutes in Forward Osmosis Processes***

In the realm of FO systems, a range of draw solutes and recovery methodologies have been proposed [25]. Over time, diverse categories of draw solutes have emerged. Notably, the study highlights major draw solutes, including polarity and unstable liquids, water-based gels, and nano-substances. These solutes exhibit remarkable versatility and responsiveness to stimuli, enabling them to modulate their interaction with water and enhance water flow. Conversely, other research has indicated that inorganic, polymeric, and organic draw solutes fall under the non-responsive category [26]. As a relatively new type of draw solute, carbonaceous compounds have only recently been added to the field of solar evaporation-based FO desalination [21].

## ***2.3 Selection of Non-responsive Draw Solutes***

Inorganic salts have emerged as prominent candidates among various draw agents employed in forward osmosis (FO) investigations, firstly due to their capacity to produce significant osmotic stress and their suitability for direct utilization without necessitating additional treatment. Achilli and colleagues [22] conducted a comprehensive study involving a variety of inorganic-based draw solutes with equal mass to discern their performance as draw solutions based on a range of performance- and cost-related parameters.

The study pinpointed several challenges encompassing return salt flow, low water flux, high viscosity, inadequate water solubility, the presence of scale precursor ions, and fouling. In a related study, Phuntsho et al. [23] looked into how FO could be used for desalination in irrigation. They also tested several other inorganic salts, which are usually thought of as fertilizers, to see if they could work as draw solutes. Among the draw solutions, KCl, NaNO<sub>3</sub>, and KNO<sub>3</sub> exhibited favorable water flow characteristics, while NH<sub>4</sub>H<sub>2</sub>PO<sub>4</sub>, (NH<sub>4</sub>)<sub>2</sub>HPO<sub>4</sub>, Ca(NO<sub>3</sub>)<sub>2</sub>, and (NH<sub>4</sub>)<sub>2</sub>SO<sub>4</sub> recorded comparatively lower scores.

Furthermore, Alnaizy et al. [27] explored the utilization of copper sulfate (CuSO<sub>4</sub>) as a draw agent in FO desalt processes, aiming to reduce the energy requirements for clean water recovery. The research showed that the FO process can be used to recover

freshwater by causing  $\text{CuSO}_4$  and  $\text{BaSO}_3$  to metathesis precipitate. However, the method's drawback stemmed from the relatively high cost associated with chemicals and raw materials.

### 2.3.1 Selection of Responsive Draw Solutes and Synthetic Materials

An alternative class of draw solutions procuring significant traction in recent times within the realm of forward osmosis (FO) research is responsive draw solutes. This category encompasses materials capable of adapting their structural properties in response to temperature variations, notably including hydrogels and nanoparticles.

Nanoparticles have emerged as promising contenders for extracting solutes in FO desalt processes, facilitated by the burgeoning field of nanomaterials research. Notably, hydrophilic magnetic nanoparticles (MNPs) have garnered attention as potential draw solutes. The concept of employing MNPs to extract draw agents was initially proposed in existing work by Warne and colleagues in early 2012 [28–30]. Ling et al. [31] did a study on magnetic nanoparticles and surface chemistry. They used MNPs that had been modified with 2-pyrrolidone, triethylene glycol, and polyacrylic acid. Among these, polyacrylic acid-capped magnetic nanoparticles (PAA-MNPs) exhibited the highest water flux, although particle aggregation led to reduced water flow. Ge et al. [32] studied how poly(ethylene-glycol) diacid-coated MNPs of various sizes could be used as draw solutes. They observed high osmotic pressures and smooth water flows. Polymer hydrogels have also been harnessed as extracting agents in FO studies.

Li et al. [33] evaluated the water-draining capability of more than three distinct polymer hydrogels through a semipermeable membrane, utilizing a heating process for dewatering.

Researchers looked at different kinds of hydrogels, such as poly(acrylamide) (PAM), poly(sodium acrylate) (PSA), and ionic polymer hydrogels poly(sodium acrylate), and poly(sodium acrylate)-co-poly(N-isopropyl acrylamide). These hydrogels exhibited varying water fluxes, with PSA and PSA-NIPAM hydrogels showcasing the highest and lowest water fluxes, respectively, which diminished over time.

Furthermore, the utilization of switchable polarity solvents (SPS) has gained prominence as a noteworthy avenue in FO research. Stone et al. [28] explored tertiary amines, water, and carbon dioxide as new SPSs for drawing solutes in the FO process. Researchers have also looked into other responsive draw solutes, such as 2-methylimidazole-based compounds with one or two electrons, nanoscale ferric oxide MNPs ( $\text{Fe}_3\text{O}_4$ ), and nanoscale dextran-coated ferric oxide MNPs. Moreover, organic extracted solutes and carbon-dependent draw solutes have been addressed in the literature. However, despite the myriad criteria decided for the selection of appropriate material and fabrication as draw solutes, it is evident from the diverse array of draw solutions discussed within FO processes that each harbors its own set of challenges.

## 2.4 *Real Time Monitoring in FO*

Each desalination system must be reliably monitored on a regular basis to determine the water quality and plant output. The permeate conductivity is being frequently measured to confirm that the end product's water meets the requirements. At the end of the procedure, it is feasible to measure the permeate conductivity, but this does not authorize the diagnosis of damaged membranes. In many of desalination facilities [34], it is standard procedure to manually sample from pipelines at each membrane element until the problem is found. Membrane dirtiness and scaling can be discovered by continuously monitoring flow and/or performing a membrane footprint analysis. While the second needs dismantling the module, the first takes a lot of time. The interest in creating non-intrusive, in-situ monitoring techniques for membrane operations has increased recently; these would help with both predictive maintenance and data-driven planning for potential membrane replacement.

A non-destructive method called ultrasonic time domain reflectometry involves passing an ultrasonic pulse through a material and recording the echoes that are created at interfaces. These echoes signify variations in acoustic impedance [35]. UTDR has already been used for fouling detection in reverse osmosis [36, 37] and microfiltration [38]. However, although the measured signal's amplitude is correlated with the layer's density, the layer's poor packing made it challenging to characterize fouling in forward osmosis using UTDR. Fouling in forward osmosis was first defined by Lai et al. [39] using UTDR. By measuring the opacity of the thick layer and monitoring hole blockage with UTDR, they showed that UTDR provides a more accurate measure of fouling than flux drop using silica as a major fouling agent.

Optical Coherence Tomography (OCT) is a useful tool for real-time monitoring because it uses interference signals to look at and identify structures and foulant layers while operations are happening. In a pioneering study, Gao et al. [40] introduced fouling detection in filtration processes through the application of OCT. Subsequently, this approach was employed by Liu et al. [41] to investigate the fouling tendencies within an aqueous solution containing bentonite particles. While it is worth noting that OCT encounters challenges in discerning disparities among fouling layers when the thickness exceeds 3 m, it remains proficient in identifying fouling behavior, particularly in scenarios involving low-pressure operations.

## 2.5 *Membrane Distillation*

In contrast to phase-change thermal desalination techniques that involve altering the state of matter, reverse osmosis (RO) has been acknowledged for its comparatively lower energy consumption. RO is still thought to be a more energy-efficient method than thermal desalination, even though the amount of feed used has gone up and the

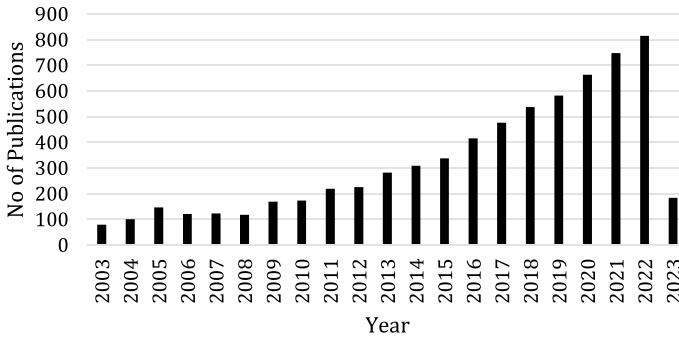


**Fig. 2** Number of articles published between 2003 and 2023 about “membrane distillation” (Scopus)

pump needs more electricity to run. This is especially true for treating solutions with a total dissolved saltiness (TDS) of more than 50,000 ppm.

Nevertheless, current commercially available RO membranes face physical limitations that hinder their effective operation under the extreme pressures required for desalinating solutions exceeding 80 bars. This limitation has paved the way for membrane distillation (MD), an innovative approach that draws insights from thermal desalination, offering a compelling alternative. Notably, MD’s energy expenditure remains independent of input salinity, offering a distinct advantage. When compared to conventional thermal procedures like multi-stage flash (MSF) and multi-effect distillation (MED), MD boasts several noteworthy benefits, including its smallness, flexibility, and remarkably low temperature requirements. This has led to a surge in scientific focus surrounding MD, resulting in a growing body of dedicated literature in this field (refer to Fig. 2).

In MD, a membrane separates the feed and permeate sides while a temperature gradient is applied to them. As the feed is heated, water vaporizes on the warmer feed side, passes through the membrane pores, and condenses on the cooler permeate side. This process enhances the vapor pressure difference across the membrane. While MD has faced challenges in terms of water flow and energy consumption, various configurations have been explored to address these issues.

Figure 2 presents the primary challenges encountered in MD and the latest strategies developed to overcome them.

## 2.6 Special Wettability of Membranes

Membranes utilized in membrane distillation applications are typically designed to be permeable and hydrophobic in order to repel moisture. Regrettably, the existing membranes’ minimal resistance to wetting has hindered the widespread adoption of MD devices [37]. Hydrophobic surfaces have been linked to diminished vapor

flow. In a study by Li et al. [42], where alkylsilane molecules were employed to modify quartz fiber membranes using a 0.5 M NaCl input, the membrane exhibiting the least wetting resistance was also observed to possess the highest steam flow in the context of DCMD. Given the trade-off between wetting resistance and vapor flow, researchers are actively exploring membranes with enhanced wettability [43]. Ensuring proper pretreatment techniques to eliminate contaminants from the feed water is crucial before conducting MD, as the presence of organics and oils can exacerbate wetting tendencies [44].

In a recent comprehensive analysis of unique wettability membranes, researchers from the Shon group categorized commercial membranes with altered surfaces, nanocomposite membranes, and a variety of additional fabrication methods aimed at achieving special wettability [43].

In pursuit of enhancing water flow, a rational avenue lies in the modification of membrane structures. The issue of limited water flow in hydrophobic membranes utilized in MD, owing to wetting concerns, necessitates remediation. Even though hydrophobicity might not be the best for vapor flow and antifouling, it is necessary in the barrier layer that is in contact with the feed solution. This paradigm has stimulated extensive investigation into the realm of hydrophilic-hydrophobic dual-layer membranes. Specifically, the integration of hydrophilic layers adjacent to hydrophobic ones has emerged as a strategic approach. This entails the incorporation of a thin hydrophobic layer proximate to the feed, complemented by a porous hydrophilic layer on the opposing side. The porous hydrophilic coating makes the material stronger, reduces heat loss through conduction, improves vapor flow, and lowers the number of fouling events [45]. On the other hand, the hydrophobic layer acts as a deterrent to the passage of saline water through the membrane.

In the trajectory of MD advancements, the concept of hydrophilic-hydrophobic composite materials for desalination purposes was initially proposed in 2005 [46]. This approach involved the utilization of dual-layer structures, comprising both hydrophilic and hydrophobic components, with the feed introduced to either the hydrophilic or hydrophobic layer.

Subsequently, the innovation of 2-layer hollow fibers was realized through spinning, a feat accomplished by Chung's research team based in Singapore [45]. Pioneering the theoretical underpinnings, the first computational model to examine the concept of dual-layer composite membranes in MD was presented by Qtaishat et al. [47], providing a framework for the methodical design of efficient MD membranes. Their groundbreaking work encompassed the optimization of membrane preparation parameters and the synthesis of a diverse array of hydrophobic and hydrophilic membrane materials [46, 48, 49].

Over the span of 2011–2021, various research groups have successfully engineered water repelling-water attracting membranes employing an assortment of materials and technologies. Recently, Zhang et al. [50] achieved a noteworthy upgrade in the flux of a commercial PTFE membrane employed in vacuum membrane distillation (VMD) for seawater, heated to 70 °C. They used a polydopamine-based hydrophilic surface layer as part of their plan, which led to an amazing 326% increase in flux.

## 2.7 Real-Time Monitoring of Membrane Distillation

In the realm of in-situ methodologies applied to membrane distillation (MD), a synergistic integration of optical and electrical techniques is employed. A significant stride in this domain is accredited to Jacob et al. [51] who pioneered an innovative in-situ approach for appraising membrane pore wetting. Their methodology capitalizes on the optical attributes and light transmission characteristics of the membrane to quantify the extent of pore wetting. Another important thing that Chen et al. [46] did was come up with a way to measure cross-membrane impedance, which lets us watch the pore wetting kinetics happen in real time. Ahmed et al. [48] have recently developed a simple electric technique for DCMD moisture sensing.

Fortunato et al. [49] have made commendable headway by harnessing in-situ monitoring through Optical Coherence Tomography (OCT), paired with membrane autopsy, to glean deeper insights into fouling mechanisms and ascertain optimal sampling intervals. The application of OCT has also been explored by Bauer et al. [52] and Lee et al. [53], both of whom leveraged it for real-time visualization and scaling assessment within an operational DCMD system, thereby facilitating timely detection and imaging. Interestingly, it was unveiled that the feed spacer didn't exclusively account for scaling.

Shin et al. [54] harnessed the potential of ohmic heating to elevate the temperature of an aqueous feed solution to 70 °C within the DCMD framework, all without necessitating external electrical input. Their innovation encompassed the integration of an electrochemical reactor through which the feed fluid traversed, both before and subsequent to its entry into the MD cell's feed channel. This electrochemical setup showcased a titanium (Ti) cathode measuring 30 cm<sup>2</sup> and a 1 cm<sup>2</sup> boron-doped diamond (BDD) anode.

Additionally, intermittent gas bubbling has been probed as a strategic maneuver for fouling management within the purview of MD. Multiple researchers, including a preliminary investigation targeting the salt concentration of traditional medicine [55], have delved into this approach. A study led by Rong Wang's team revealed that elevated feed temperatures, diminished feed and permeate velocities, and truncated porous fibers collectively optimized flow enhancement via bubbling [56].

An inventive strategy aimed at countering fouling instigated by salts, particulates, and organic entities was posited by Warsinger et al. [57], entailing the utilization of air layers atop surface-modified super hydrophobic membrane surfaces. This distinctive approach exhibits substantial promise in ameliorating the challenges associated with fouling.

### 3 Electrochemical Desalination

Electrochemical desalination systems operate by employing electromigration and electrosorption to extract salt ions from feed solutions. Among the electrochemical desalination methodologies, Electrochemical Desalination (ED) and Capacitive Deionization (CDI) stand out as the most extensively utilized techniques, boasting a history of over 50 years in practical application by contemporary companies.

Efforts by researchers have been dedicated to addressing the limitations inherent in these methods, aiming to enhance their performance, cost-effectiveness, and energy efficiency to compete more effectively with reverse osmosis desalination. Notwithstanding these challenges, a captivating trajectory of material-centric research over the past decade has yielded promising breakthroughs that hold the potential to elevate the significance of electrochemical desalination processes in the foreseeable future. As depicted in the accompanying Fig. 3, there has been a substantial 20-fold surge in the number of scholarly articles related to electrochemical desalination.

A potential paradigm shift within the realm of electrochemical desalination may have recently transpired, propelled by cutting-edge technologies underpinned by novel advanced materials and innovative system architectures. Prior to the integration of further technologies, it is imperative to meticulously assess the merits and demerits of existing electrochemical desalination techniques, such as ED and CDI.

This contextual backdrop sets the stage for an exploration of pioneering electrochemical desalination techniques, encompassing multi-stage designs, higher-capacity electrodes, and the intriguing concept of the “desalination battery.”

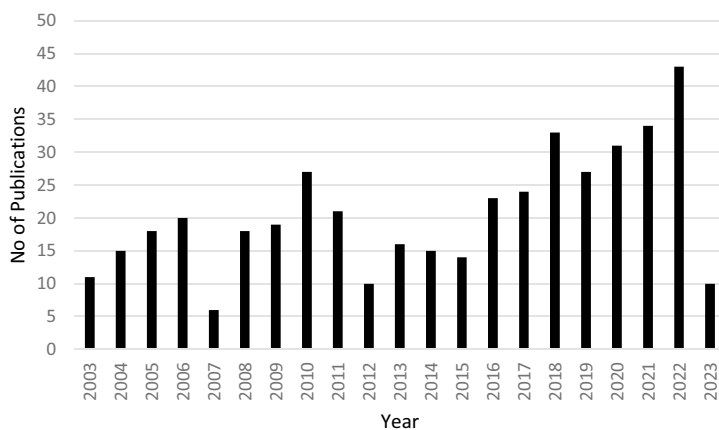


**Fig. 3** Number of articles published between 2003 and 2023 about “electrochemical desalination” (Scopus)

### 3.1 *Electrodialysis*

Electrodialysis (ED) is a process wherein ions migrate toward the positive to negative electrodes under the influence of an electric field established between these electrodes. To exclusively transport specific ions, cation exchange membranes (CEM) and anion exchange membranes (AEM) are systematically arranged in an alternating manner. This configuration results in distinct channels containing solutions with diminished ion concentrations due to ion removal, while other channels hold solutions with heightened ion concentrations stemming from the accumulation of ions bearing the same charge.

For effective implementation in ED, ion exchange membranes (IEMs) must possess exceptional permselectivity, lesser electrical resistance, and robust mechanical and thermal stabilization [57]. An essential unit in ED is the cell pair, which comprises an AEM and a CEM with vicinal flow channels [58]. In practice, a stack or module can encompass a varying number of cell pairs, ranging from a few in laboratory settings to several hundred in commercial applications [59].

The inception of ED seawater desalination dates back to 1974, when the first machine was constructed with a daily capacity of 121 m<sup>3</sup>, consuming 16.20 kWh/m<sup>3</sup> of energy [60]. Despite its recognized reliability as a desalination method, ED occupies only a minor fraction of the total industry capacity. In industrial scenarios, ED is often employed for feed solutions characterized by lower salinities, such as saline water. This was attributed to the higher fuel demand of ED when processing feed solutions with elevated ion concentrations. The comparatively elevated cost of IEMs in contrast to reverse osmosis membranes presents an additional impediment to the broader adoption of ED [59].

In recent times, there has been a resurgence of focus in electro membrane processes, driven by the aspiration to devise novel ED systems with two overarching objectives: (1) the development of a competitive seawater desalination process and (2) the reclamation of salts for brine treatment. In pursuit of enhancing ED as a viable method for seawater desalination, the European Union (EU) is actively supporting the revived water research program.

### 3.2 *Capacitive Deionization*

Capacitive Deionization (CDI), a technique dating back to the 1960s, remains relatively underutilized on a large scale for energy-efficient applications. Within CDI, an electric field is employed to direct salt ions along a specific trajectory. Employed electrodes possess differing electrical properties and are often characterized by a significant surface area and a porous nature. When exposed to an electric field, these electrodes help salt ions adhere to a double layer that develops at the interface between the electrode surface and the entire solution. The effectiveness of CDI devices in salt removal is considerably influenced by electrode material, geometry,

and various other variables. An electrode's capacity to electrostatically adsorb ions onto its inner surface is directly correlated with its surface area.

Upon modulation of the potential difference, ions are desorbed from the electrodes, allowing for their regeneration. Mechanically stable electrodes boasting robust electrical conductivity are requisite. The optimal electrode configuration must strike a balance between maximizing surface area for electrosorption and providing a rapid transit path for ions [61]. A primary challenge inhibiting the commercialization of CDI desalination is the absence of ideal electrode materials and geometries capable of facilitating rapid salt removal through elevated ion adsorption capacities. Although increasing the voltage can expedite salt removal, this approach incurs higher energy/fuel consumption and negative effects due to undesirable reactions. Traditional CDI systems prove inefficient for desalinating high saline feed solutions, including concentrated saline water and seawater.

Historically, research into capacitive deionization primarily focused on porous carbon electrodes, particularly activated carbons featuring internal areas within the range of 104 m<sup>2</sup>/g [62]. However, carbon-based materials employed as CDI electrodes extend beyond graphene and carbon nanotubes. This encompasses activated carbon fibers, graphene, and carbon aerogels. To address the limitations of certain carbon materials such as elevated production costs, limited wettability, and constrained ion adsorption capabilities, there has been an increasing focus in carbon-based materials incorporating metal oxides or polymers. Non-carbon components are introduced into these composites to enhance the ion adsorption capacity of the electrode material and provide supplementary functionalities.

## 4 Conclusion

Sustainable progress hinges on achieving energy-efficient and cost-effective desalination methods. Pioneering research is essential for unlocking the full technological potential of emerging processes, enabling them to rival established techniques like reverse osmosis and multi-stage flash. Brine treatment and zero liquid discharge have emerged as critical applications, addressing the escalating by-products from desalination and the expanding global desalination capacity. To expedite lab-scale and market-ready technology development, we present an overview of global research initiatives and national desalination projects.

Among the three processes under scrutiny—electrochemical desalination, membrane distillation, and forward osmosis—significant strides have been taken, yet substantial progress is required to surmount operational challenges for broader commercialization. While membrane distillation and forward osmosis are being explored by various pilot facilities and technology developers, breakthroughs are still needed. The third approach, useful for brackish water desalination, is hindered by material limitations and the need for innovative concepts.

Nanotechnology has revolutionized membrane comprehension and innovation. Recent advancements in desalination technology heavily leverage nanomaterials.

Incorporating nanoparticles into active and support layers of novel membrane designs for forward osmosis has improved flux, salt rejection, and antifouling properties. Electrospinning has been pivotal in crafting versatile, highly porous, interconnected electrospun membranes for TFC-FO support, presenting new topologies.

Although developing novel membranes is pivotal for new desalination techniques' commercialization, it's just one facet. The cost of draw solution replacement remains a key impediment for forward osmosis.

Efforts to curtail energy usage necessitate early and precise monitoring and management. Non-invasive, in-situ monitoring can diminish manual sample expenses, enable early detection, prolong membrane life, and reduce frequent replacements through careful regulation. Advancements in electrical and optical technologies also pave the way for real-time monitoring to integrate into medical diagnostics and therapy. While membrane development remains prominent, the last five years have witnessed growing interest in optimization strategies like intelligent monitoring, dual systems, and energy regeneration.

Capacitive deionization (CDI) is nascent because of the limited salt size of carbon-based composites. Emerging CDI variations, such as desalination batteries, utilize chemical bonding to store  $\text{Na}^+$  or  $\text{Cl}^-$  ions within the electrode material, significantly enhancing salt capacity beyond prior limitations. Recent strides in this field offer a promising avenue for research, potentially unraveling material structures and scalability. After a thorough literature review, we propose recommendations for ongoing research and development, aiming to facilitate the practical application of the aforementioned technologies in crucial commercial contexts over the coming years:

- Transitioning from pilot to full-scale facilities is contingent upon the development of cost-effective draw solution manufacturing techniques, a prerequisite even as higher flux, higher salt rejection membranes remain imperative for forward osmosis (FO) desalt procedures. The trajectory of FO research should be directed toward the innovation of hybrid FO systems, a strategic approach aimed at propelling FO desalination closer to economical feasibility.
- There is no pilot-scale research of these membranes, despite the fact that carbon nanoparticles have been included into FO membranes to enhance performance.
- The integration of specific wettability materials, such as superhydrophobic and dual-layer membranes, holds the potential to enhance two critical aspects of membrane distillation (MD): flux improvement and sustained wetting resistance. However, the performance of these membranes is significantly influenced by the composition of the feed stream and its interaction with environmental conditions. While altered wettability membranes might exhibit enhanced performance in controlled laboratory settings using simple aqueous NaCl solutions, this success is not necessarily indicative of their behavior when exposed to more complex feed solutions and real-world operational conditions. Notably, there is some indication that modified dual-layer membranes could potentially encourage the growth of scaling deposits. Consequently, a comprehensive exploration of the impact

of wettability modifications on membrane performance and stabilization under practical testing terms is imperative.

- Deeper investigations into the interplay between membranes and feed solutions, particularly within elevated temperature settings, are urgently warranted. The evaluation of practical implications resulting from wettability alterations mandates meticulous consideration of membrane design, configuration, and system dimensions. Thorough research is indispensable to comprehensively comprehending the intricate interrelationships among wetting, scale formation, fouling tendencies, and membrane behavior when exposed to authentic feed solutions. Such research endeavors are vital to providing insights into the feasibility and practical utility of wettability-driven enhancements in MD systems.
- Both membrane distillation and forward osmosis, which boast a considerable array of research-scale facilities, demand equivalent, if not heightened, attention to system design and the technological implications of scaling up, paralleling the significance accorded to membrane advancement.
- When devising new tools for real-time process monitoring and control, it is crucial to consider the efficiency of system design and its potential for scalability.
- When considering the configurations and uses of advanced technologies that are still in the process of becoming widely commercialized, there exists a significant opportunity for experimentation and customization.
- Additional research is necessary, particularly on a pilot scale, to gain a deeper insight into the economic viability and potential prospects of hybrid systems. This encompasses the advancement of desalination technologies in terms of energy efficiency, quality of produced water, water retrieval rates, and the recuperation of valuable resources.

**Disclosure of Interests** The authors have no competing interests to declare that are relevant to the content of this article.

## References

1. Mustafa J, Mourad AA-H, Al-Marzouqi AH, El-Naas MH (2020) Simultaneous treatment of reject brine and capture of carbon dioxide: a comprehensive review. *Desalination* 483:114386. <https://doi.org/10.1016/j.desal.2020.114386>
2. Bello AS, Zouari N, Da'ana DA, Hahladakis JN, Al-Ghouthi MA (2021) An overview of brine management: emerging desalination technologies, life cycle assessment, and metal recovery methodologies. *J Environ Manage* 288:112358. <https://doi.org/10.1016/j.jenvman.2021.112358>
3. Hameeteman E (2013) Future water (in) security: facts, figures, and predictions. *Glob Water Inst* 1:1–16. Available [https://img1.wsimg.com/blobby/go/27b53d18-6069-45f7-a1bd-d5a48bc80322/downloads/1c2meuvon\\_105010.pdf](https://img1.wsimg.com/blobby/go/27b53d18-6069-45f7-a1bd-d5a48bc80322/downloads/1c2meuvon_105010.pdf)
4. Subramani A, Jacangelo JG (2015) Emerging desalination technologies for water treatment: a critical review. *Water Res* 75:164–187. <https://doi.org/10.1016/j.watres.2015.02.032>

5. Eke J, Yusuf A, Giwa A, Sodiq A (2020) The global status of desalination: an assessment of current desalination technologies, plants and capacity. *Desalination* 495:114633. <https://doi.org/10.1016/j.desal.2020.114633>
6. Amma LV, Ashraf F (2020) Brine management in reverse osmosis desalination: a UAE perspective. In: 2020 advances in science and engineering technology international conferences (ASET). IEEE, pp 1–6. <https://doi.org/10.1109/ASET48392.2020.9118335>
7. Bartels CR, Andes K (2013) Consideration of energy savings in SWRO. *Desalin Water Treat* 51(4–6):717–725. <https://doi.org/10.1080/19443994.2012.700038>
8. Mayor B (2019) Growth patterns in mature desalination technologies and analogies with the energy field. *Desalination* 457:75–84. <https://doi.org/10.1016/j.desal.2019.01.029>
9. Woo YC, Kim SH, Shon HK, Tijing LD (2018) Introduction: membrane desalination today, past, and future. <https://doi.org/10.1016/B978-0-12-813551-8.00028-0>
10. Yao M, Woo YC, Tijing LD, Shim WG, Choi JS, Kim SH, Shon HK (2016) Effect of heat-press conditions on electrospun membranes for desalination by direct contact membrane distillation. *Desalination* 378:80–91. <https://doi.org/10.1016/j.desal.2015.09.025>
11. Semiat R (2008) Energy issues in desalination processes. *Environ Sci Technol* 42(22):8193–8201. <https://doi.org/10.1021/es801330u>
12. McCutcheon JR, McGinnis RL, Elimelech M (2005) A novel ammonia–carbon dioxide forward (direct) osmosis desalination process. *Desalination* 174(1):1–11. <https://doi.org/10.1016/j.desal.2004.11.002>
13. McCutcheon JR, McGinnis RL, Elimelech M (2006) Desalination by ammonia–carbon dioxide forward osmosis: influence of draw and feed solution concentrations on process performance. *J Membr Sci* 278(1–2):114–123. <https://doi.org/10.1016/j.memsci.2005.10.048>
14. Cath TY, Childress AE, Elimelech M (2006) Forward osmosis: principles, applications, and recent developments. *J Membr Sci* 281(1–2):70–87. <https://doi.org/10.1016/j.memsci.2006.05.048>
15. Awad AM, Jalab R, Minier-Matar J, Adham S, Nasser MS, Judd SJ (2019) The status of forward osmosis technology implementation. *Desalination* 461:10–21. <https://doi.org/10.1016/j.desal.2019.03.013>
16. Ang WL, Mohammad AW, Johnson D, Hilal N (2019) Forward osmosis research trends in desalination and wastewater treatment: a review of research trends over the past decade. *J Water Process Eng* 31:100886. <https://doi.org/10.1016/j.jwpe.2019.100886>
17. Du H, Thompson A, Wang X (eds) (2018) Osmotically driven membrane processes: approach, development and current status. <https://doi.org/10.5772/intechopen.68607>
18. Yip NY, Tiraferri A, Phillip WA, Schiffman JD, Elimelech M (2010) High performance thin-film composite forward osmosis membrane. *Environ Sci Technol* 44(10):3812–3818. <https://doi.org/10.1021/es1002555>
19. Alihemati Z, Hashemifard SA, Matsuura T, Ismail AF, Hilal N (2020) Current status and challenges of fabricating thin film composite forward osmosis membrane: a comprehensive roadmap. *Desalination* 491:114557. <https://doi.org/10.1016/j.desal.2020.114557>
20. Suwaileh WA, Johnson DJ, Sarp S, Hilal N (2018) Advances in forward osmosis membranes: altering the sub-layer structure via recent fabrication and chemical modification approaches. *Desalination* 436:176–201. <https://doi.org/10.1016/j.desal.2018.01.035>
21. Amjad M, Gardy J, Hassanpour A, Wen D (2018) Novel draw solution for forward osmosis based solar desalination. *Appl Energy* 230:220–231. <https://doi.org/10.1016/j.apenergy.2018.08.021>
22. Achilli A, Cath TY, Childress AE (2010) Selection of inorganic-based draw solutions for forward osmosis applications. *J Membr Sci* 364(1–2):233–241. <https://doi.org/10.1016/j.memsci.2010.08.010>
23. Phuntsho S, Shon HK, Hong S, Lee S, Vigneswaran S (2011) A novel low energy fertilizer driven forward osmosis desalination for direct fertigation: evaluating the performance of fertilizer draw solutions. *J Membr Sci* 375(1–2):172–181. <https://doi.org/10.1016/j.memsci.2011.03.038>

24. Shaffer DL, Werber JR, Jaramillo H, Lin S, Elimelech M (2015) Forward osmosis: where are we now? *Desalination* 356:271–284. <https://doi.org/10.1016/j.desal.2014.10.031>
25. Luo H, Wang Q, Zhang TC, Tao T, Zhou A, Chen L, Bie X (2014) A review on the recovery methods of draw solutes in forward osmosis. *J Water Process Eng* 4:212–223. <https://doi.org/10.1016/j.jwpe.2014.10.006>
26. Yang Y, Chen M, Zou S, Yang X, Long TE, He Z (2017) Efficient recovery of polyelectrolyte draw solutes in forward osmosis towards sustainable water treatment. *Desalination* 422:134–141. <https://doi.org/10.1016/j.desal.2017.08.024>
27. Alnaizy R, Aidan A, Qasim M (2013) Copper sulfate as draw solute in forward osmosis desalination. *J Environ Chem Eng* 1(3):424–430. <https://doi.org/10.1016/j.jece.2013.06.005>
28. Stone ML, Rae C, Stewart FF, Wilson AD (2013) Switchable polarity solvents as draw solutes for forward osmosis. *Desalination* 312:124–129. <https://doi.org/10.1016/j.desal.2012.07.034>
29. Wallace M, Cui Z, Hankins NP (2008) A thermodynamic benchmark for assessing an emergency drinking water device based on forward osmosis. *Desalination* 227(1–3):34–45. <https://doi.org/10.1016/j.desal.2007.04.097>
30. Petrotos KB, Quantick P, Petropakis H (1998) A study of the direct osmotic concentration of tomato juice in tubular membrane–module configuration. I. The effect of certain basic process parameters on the process performance. *J Membrane Sci* 150(1):99–110. [https://doi.org/10.1016/S0376-7388\(98\)00216-6](https://doi.org/10.1016/S0376-7388(98)00216-6)
31. Ling MM, Wang KY, Chung TS (2010) Highly water-soluble magnetic nanoparticles as novel draw solutes in forward osmosis for water reuse. *Ind Eng Chem Res* 49(12):5869–5876. <https://doi.org/10.1021/ie100438x>
32. Ge Q, Su J, Chung TS, Amy G (2011) Hydrophilic superparamagnetic nanoparticles: synthesis, characterization, and performance in forward osmosis processes. *Ind Eng Chem Res* 50(1):382–388. <https://doi.org/10.1021/ie101013w>
33. Li D, Zhang X, Yao J, Simon GP, Wang H (2011) Stimuli-responsive polymer hydrogels as a new class of draw agent for forward osmosis desalination. *Chem Commun* 47(6):1710–1712. <https://doi.org/10.1039/c0cc04701e>
34. Birkert (2012) Desalination: automated system monitors desalination of seawater. *Filtr Sep* 49(6):40–41. [https://doi.org/10.1016/S0015-1882\(12\)70290-2](https://doi.org/10.1016/S0015-1882(12)70290-2)
35. Krantz WB, Greenberg AR (2008) Membrane characterization by ultrasonic time-domain reflectometry. *Adv Membr Technol Appl*: 879–897. <https://doi.org/10.1002/9780470276280.ch33>
36. Eykens L, Reyns T, De Sitter K, Dotremont C, Pinoy L, Van der Bruggen B (2016) How to select a membrane distillation configuration? Process conditions and membrane influence unraveled. *Desalination* 399:105–115. <https://doi.org/10.1016/j.desal.2016.08.019>
37. Eykens L, De Sitter K, Dotremont C, De Schepper W, Pinoy L, Van Der Bruggen B (2017) Wetting resistance of commercial membrane distillation membranes in waste streams containing surfactants and oil. *Appl Sci* 7(2):118. <https://doi.org/10.3390/app7020118>
38. Taheri AH, Sim STV, Sim LN, Chong TH, Krantz WB, Fane AG (2013) Development of a new technique to predict reverse osmosis fouling. *J Membr Sci* 448:12–22. <https://doi.org/10.1016/j.memsci.2013.06.040>
39. Lai L, Sim LN, Krantz WB, Chong TH (2020) Characterization of colloidal fouling in forward osmosis via ultrasonic time-(UTDR) and frequency-domain reflectometry (UFDR). *J Membr Sci* 602:117969. <https://doi.org/10.1016/j.memsci.2020.117969>
40. Gao Y, Haavisto S, Li W, Tang CY, Salmela J, Fane AG (2014) Novel approach to characterizing the growth of a fouling layer during membrane filtration via optical coherence tomography. *Environ Sci Technol* 48(24):14273–14281. <https://doi.org/10.1021/es503326y>
41. Liu Y, Nie C, Liu X, Xu X, Sun Z, Pan L (2015) Review on carbon-based composite materials for capacitive deionization. *RSC Adv* 5(20):15205–15225. <https://doi.org/10.1039/c4ra14447c>
42. Li C, Li X, Du X, Zhang Y, Wang W, Tong T, Lee J (2020) Elucidating the trade-off between membrane wetting resistance and water vapor flux in membrane distillation. *Environ Sci Technol* 54(16):10333–10341. <https://doi.org/10.1021/acs.est.0c02547>

43. Yao M, Tijing LD, Naidu G, Kim SH, Matsuyama H, Fane AG, Shon HK (2020) A review of membrane wettability for the treatment of saline water deploying membrane distillation. *Desalination* 479:114312. <https://doi.org/10.1016/j.desal.2020.114312>
44. Chang H, Liu B, Zhang Z, Pawar R, Yan Z, Crittenden JC, Vidic RD (2020) A critical review of membrane wettability in membrane distillation from the perspective of interfacial interactions. *Environ Sci Technol* 55(3):1395–1418. <https://doi.org/10.1021/acs.est.0c05454>
45. Bonyadi S, Chung TS (2007) Flux enhancement in membrane distillation by fabrication of dual layer hydrophilic–hydrophobic hollow fiber membranes. *J Membr Sci* 306(1–2):134–146. <https://doi.org/10.1016/j.memsci.2007.08.034>
46. Chen Y, Ren R, Pu H, Chang J, Mao S, Chen J (2017) Field-effect transistor biosensors with two-dimensional black phosphorus nanosheets. *Biosens Bioelectron* 89:505–510. <https://doi.org/10.1016/j.bios.2016.03.059>
47. Qtaishat M, Khayet M, Matsuura T (2009) Novel porous composite hydrophobic/hydrophilic polysulfone membranes for desalination by direct contact membrane distillation. *J Membr Sci* 341(1–2):139–148. <https://doi.org/10.1016/j.memsci.2009.05.053>
48. Ahmed FE, Lalia BS, Hashaikheh R (2017) Membrane-based detection of wetting phenomenon in direct contact membrane distillation. *J Membr Sci* 535:89–93. <https://doi.org/10.1016/j.memsci.2017.04.035>
49. Fortunato L, Jang Y, Lee JG, Jeong S, Lee S, Leiknes T, Ghaffour N (2018) Fouling development in direct contact membrane distillation: non-invasive monitoring and destructive analysis. *Water Res* 132:34–41. <https://doi.org/10.1016/j.watres.2017.12.059>
50. Zhang Y, Shen F, Cao W, Wan Y (2020) Hydrophilic/hydrophobic Janus membranes with a dual-function surface coating for rapid and robust membrane distillation desalination. *Desalination* 491(114561):2020. <https://doi.org/10.1016/j.desal.2020.114561>
51. Jacob P, Dejean B, Laborie S, Cabassud C (2020) An optical in-situ tool for visualizing and understanding wetting dynamics in membrane distillation. *J Membr Sci* 595:117587. <https://doi.org/10.1016/j.memsci.2019.117587>
52. Bauer A, Wagner M, Saravia F, Bartl S, Hilgenfeldt V, Horn H (2019) In-situ monitoring and quantification of fouling development in membrane distillation by means of optical coherence tomography. *J Membr Sci* 577:145–152. <https://doi.org/10.1016/j.memsci.2019.02.006>
53. Lee JG, Jang Y, Fortunato L, Jeong S, Lee S, Leiknes T, Ghaffour N (2018) An advanced online monitoring approach to study the scaling behavior in direct contact membrane distillation. *J Membr Sci* 546:50–60. <https://doi.org/10.1016/j.memsci.2017.10.009>
54. Shin YU, Yun ET, Kim J, Lee H, Hong S, Lee J (2020) Electrochemical oxidation–membrane distillation hybrid process: utilizing electric resistance heating for distillation and membrane defouling through thermal activation of anodically formed persulfate. *Environ Sci Technol* 54(3):1867–1877. <https://doi.org/10.1021/acs.est.9b05141>
55. Ding Z, Liu L, Liu Z, Ma R (2011) The use of intermittent gas bubbling to control membrane fouling in concentrating TCM extract by membrane distillation. *J Membr Sci* 372(1–2):172–181. <https://doi.org/10.1016/j.memsci.2011.01.063>
56. Chen G, Yang X, Wang R, Fane AG (2013) Performance enhancement and scaling control with gas bubbling in direct contact membrane distillation. *Desalination* 308:47–55. <https://doi.org/10.1016/j.desal.2012.07.018>
57. Warsinger DM, Servi A, Van Belleghem S, Gonzalez J, Swaminathan J, Kharraz J, Gleason KK (2016) Combining air recharging and membrane superhydrophobicity for fouling prevention in membrane distillation. *J Membr Sci* 505:241–252. <https://doi.org/10.1016/j.memsci.2016.01.018>
58. Campione A, Cipollina A, Bogle IDL, Gurreri L, Tamburini A, Tedesco M, Micale G (2019) A hierarchical model for novel schemes of electrodialysis desalination. *Desalination* 465:79–93. <https://doi.org/10.1016/j.desal.2019.04.020>
59. Campione A, Gurreri L, Ciofalo M, Micale G, Tamburini A, Cipollina A (2018) Electrodialysis for water desalination: a critical assessment of recent developments on process fundamentals, models and applications. *Desalination* 434:121–160. <https://doi.org/10.1016/j.desal.2017.12.044>

60. Seto T, Ehara L, Komori R, Yamaguchi A, Miwa T (1978) Seawater desalination by electrodialysis. *Desalination* 25(1):1–7. [https://doi.org/10.1016/S0011-9164\(00\)82440-6](https://doi.org/10.1016/S0011-9164(00)82440-6)
61. Humplik T, Lee J, O'hern SC, Fellman BA, Baig MA, Hassan SF, Wang EN (2011) Nanostructured materials for water desalination. *Nanotechnology* 22(29):292001. <https://doi.org/10.1088/0957-4484/22/29/292001>
62. Biesheuvel PM, Van der Wal A (2010) Membrane capacitive deionization. *J Membr Sci* 346(2):256–262. <https://doi.org/10.1016/j.memsci.2009.09.043>

# A Conceptual Model of the Tulsishyam Hot Springs' Geothermal System, Gujarat, India



Namrata Bist , Kriti Yadav , and Anirbid Sircar 

## 1 Introduction

As coal and nuclear-generating capacity will be phased out over the next few decades, natural gas and renewable technologies will be the primary sources of additional capacity to the world power generation. As shown in Fig. 1, renewable electricity generation will outpace overall electricity demand in the near future. World renewable electricity capacity is expected to increase by more than 60% by 2026, roughly totaling the current global power capacity of fossil fuels and nuclear combined (IEA 2021). The global geothermal power market is predicted to increase at a compound annual growth rate (CAGR) of 9.6%, as illustrated in Fig. 2. Companies in the geothermal electric power generation industry are investing in new technologies to make geothermal energy more accessible for generating electricity and other heating applications [1]. Only regions with easy access to very hot water due to volcanic presence were used to collect a considerable amount of geothermal energy. In regions devoid of volcanic incursions, the companies are investing in novel techniques to make geothermal energy more accessible and extractable [2]. Low-temperature geothermal resources are small but an expanding segment of hydrothermal development in geothermal resources with temperatures below 150 °C.

Low-temperature geothermal energy is heat extracted from the ground's geothermal waters at temperatures less than 150 °C (Energygov 2022). Binary cycle power-generating technology can utilize low-temperature resources to generate electricity (Energygov 2022). The current research examined one of the geothermal hot springs, Tulsishyam, which is located in Gujarat region. The study location is in the Saurashtra basin, which is a prominent section of Peninsular India.

---

N. Bist · A. Sircar (✉)

Pandit Deendayal Energy University, Gandhinagar, Gujarat 382007, India  
e-mail: [anirbid.sircar@spt.pdpu.ac.in](mailto:anirbid.sircar@spt.pdpu.ac.in)

K. Yadav

Department of Geology, Patna University, Ashok Rajpath, Patna 800005, India

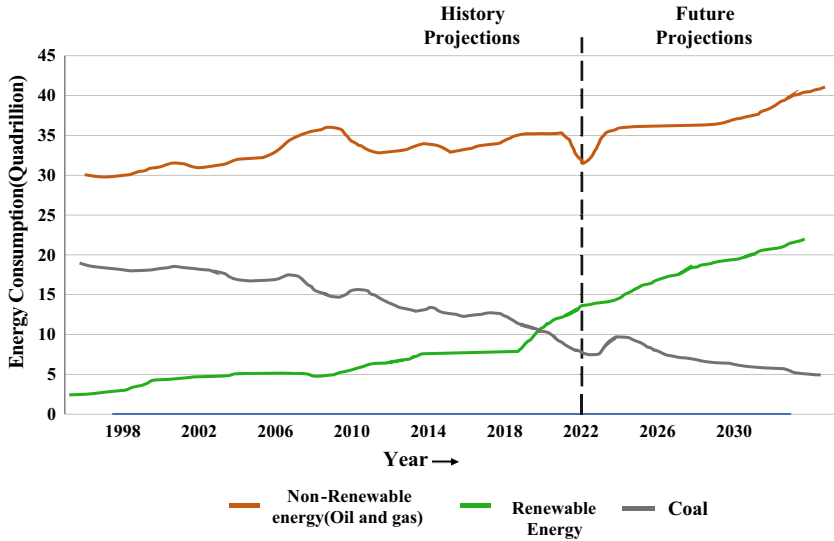


Fig. 1 Past and future projections of energy consumption by types of energy sources [2]

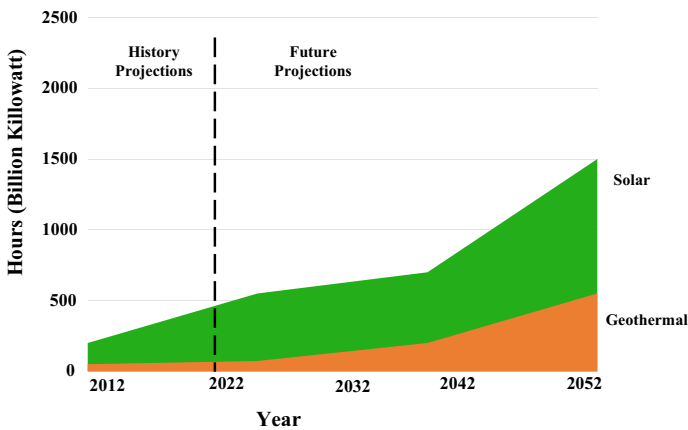
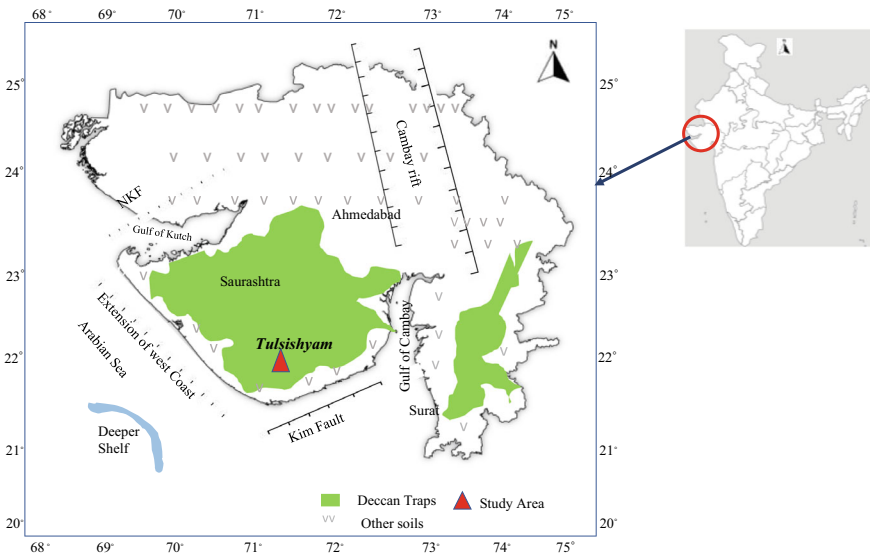


Fig. 2 Projections of renewable electricity generation by solar and geothermal energy [2]

In Gujarat, India, vast quantities of geothermal resources of low-medium enthalpy temperature ( $< 100\text{ }^{\circ}\text{C}$ ) are located (Singh et al. 2016) [3, 4]. The Deccan basalts give rise to the Tulsishyam geothermal springs. The current group has measured the surface temperature of the hot springs, which is around  $50\text{--}55\text{ }^{\circ}\text{C}$ . In this study, Gravity and Magnetic surveys were conducted, and the integrated subsurface model was prepared to understand the location of the sweet spot. The present study also aims to understand the mechanism by which the hotspot was formed.

## 2 Literature Survey of the Study Area

The Gujarat geothermal province has approximately 22 thermal springs with surface temperatures ranging from 35 to 93 °C [5]. Thermal waters near granite intrusions, such as the Godhra granite, have a high surface temperature (93 °C). According to Chandrasekhar et al. [6], Saurashtra's volcanic necks and surrounding region are igneous intrusions and alkaline complexes with a wide range of compositions, ranging from mafic/ultramafic rocks. Gravity surveys in Saurashtra have revealed many gravity highs that match to the volcanic necks and alkaline complexes of Deccan volcanism. On the other hand, their gravity anomalies suggest that their extents are almost equivalent to those discovered in western Saurashtra. The Junagadh volcanic neck-caused magnetic anomaly, on the other hand, features well-defined positive and negative magnetic centers associated with well-differentiated mafic and ultramafic circular dykes. Singh et al. [7], identified presence of several precipitated mineral phases during geothermal energy extraction, which should be considered when developing a geothermal energy application for the location. The study area Tulsishyam is situated in India's Saurashtra basin as depicted in Fig. 3. Although these basaltic rocks lack primary porosity, groundwater is abundant due to secondary porosity, which is present in worn basaltic rocks due to profound columnar cracks and vesicles at shallow depths [8].



**Fig. 3** Tectonic map of Gujarat, India. The study area is denoted by red triangle (Modified after Chopra et al. [9])

### 3 Geophysical and Geochemical Studies of the Tulsishyam Area

#### 3.1 Geophysical Prospecting via Gravity Survey of the Study Area

Gravity surveys are often used to explore particular sedimentary basins, faults, folds, and related structures based on subsurface density variations. Gravimeters are utilized as an indirect method of analyzing geothermal heat sources since they provide information about subterranean substances [10]. To further understand density fluctuations, a complete Bouguer gravity map was created. The density contrast throughout the map area determines the magnitude of gravity anomalies. The study region was subjected to a gravity survey utilizing a CG5 gravimeter to gain a better understanding of the subsurface. Figure 4a shows a complete Bouguer gravity map of Tulsishyam, indicating that our mundane surface geology conceals a fascinating geologic past. The density contrast in the subsoil influences gravity considerably.

Gravity abruptly changes by nearly 0.45 mGal on the map’s southwestern side. The broad gravity low at 21.05 latitude and 71.025 longitude is due to crustal thickening

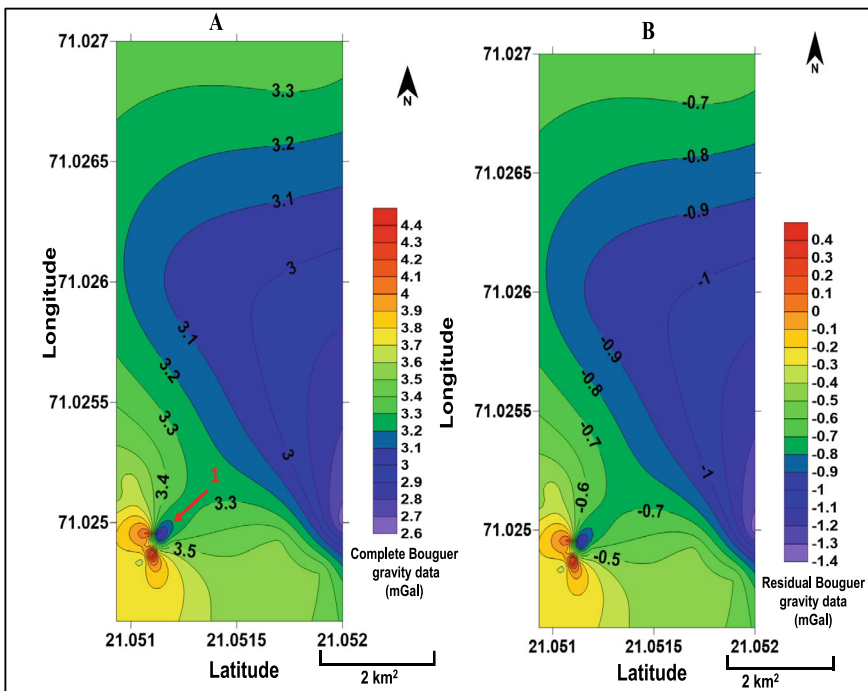


Fig. 4 a Complete Bouguer anomaly gravity map and b residual gravity map of Tulsishyam area

and flat slab subduction produced by volcanic activity. The gravity increases as we travel down to the southwest corner. It could be owing to the subduction zones fall into the mantle [11].

Gravity data are essential for modeling the geometry and depth of the subsurface. Groundwater flow models employ this geometry to confine the source of hot fluids circulating in the basin. Gravity highs can be seen throughout the entire western section of the map in the southwest portion of the map. The residual gravity map in Fig. 4b accentuates this feature. On the Bouguer analysis map, a protruding nose to the northwest can be seen, and the same can be seen more clearly on the residual gravity map.

Because the dense mantle is transported closer to the surface when the crust thins, regional gravity highs are created. The lowest gravity value can be found at position 1 in Fig. 4a. This area could be linked to land subsidence. The presence of a gravity low implies the presence of a cave system under the surface [11]. The presence of a structure that could serve as a geothermal hotspot is indicated by Point 1 on the complete Bouguer anomaly map.

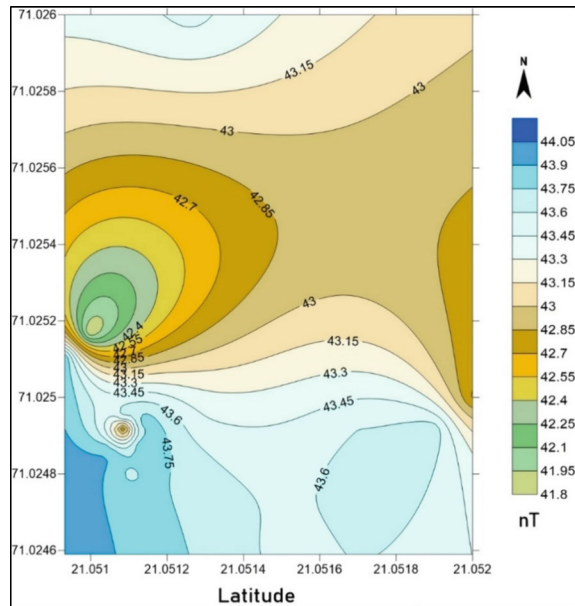
### ***3.2 Geophysical Prospecting via Magnetic Survey of the Study Area***

Gravity and Magnetic variations and geological knowledge can provide an indirect but extremely informative picture of lateral changes in rock composition and structural patterns [12]. In order to connect the gravity survey data, magnetic data were conducted in the study area. Latitude 21.0518 N and longitude 71.02586 E are the highest points on the map. The magnetic reading with the highest value is 43.15 nT. Two magnetic anomalies can be seen in Fig. 5 magnetic map, which could be caused by buried basalts in alluvium. Anomaly can be found at 71.0252° E longitude and 21.051° N latitude, according to both Gravity and Magnetic maps. The presence of various subsurface stratigraphies can be connected to a prone shift in magnetism magnitude. The structural analysis of the anomaly reveals that both maps belong to the same anomaly.

## **4 Conceptual Model of Tulsishyam Geothermal Spring: Prospect in a Cross Section**

Deccan traps are hard rocks harboring basaltic flows almost horizontally aligned across a wide area. The basaltic flows' lowest massive component has little primary porosity, but the top vesicular layer has some primary porosity due to vesicles formed by escaping gases. The big and vesicular regions have no primary permeability because the vesicles are rarely connected [6]. Groundwater can be infiltrated, stored,

**Fig. 5** Magnetic map of study area. The anomalies match at the similar location on the magnetic map as are present on the gravity map of the study area



and transferred thanks to the secondary porosity and permeability caused by fracture and jointing. The weathered zone reaches around 20 m below ground level in surface flows. Weathered flow connections have greater depths. The permeability of these zones is further increased by fracturing and jointing. Interflow zones, as well as fractured and jointed zones, have resulted in stratified aquifer systems, which account for water occurrence even at greater depths. Bore wells drilled in the district have outputs ranging from 100 to 500 m<sup>3</sup>/day. Alluvium groundwater is found in an open setting. The alluvium is only 20 m thick. Because of the clayey soil composition, rainwater percolation is poor, resulting in low yields [13]. The moderate permeability of Deccan traps allows for sufficient infiltration into the groundwater reservoir and storage of water. Various rainwater collection schemes have been built in the district based on hydrogeological characteristics [13]. Figure 6 depicts a NE–SW conceptual representation of the geological segment of the study area and postulates the methodology by which hotspot has been formed at the study area.

The general methodology for the hot spring formation is as follows. When a volcano establishes dormant stage after an eruptive cycle, magma and hot rocks may persist at relatively shallow crustal depths for hundreds or thousands of years. Groundwater seeping via faults, cracks, and porous rocks encounters and is heated by these high-temperature zones. Hot water rises, and denser, cooler water replaces it. Thus, a robust convective system may be developed and maintained. In such a hydrothermal system, rising water may reach the surface as hot springs or, if temperatures are high enough, convert low pressures to steam. Held water in some subterranean plumbing systems heats to the point where it ‘flashes’ and transforms into a stream. Cooler water in the conduits above may be aggressively blown out at the

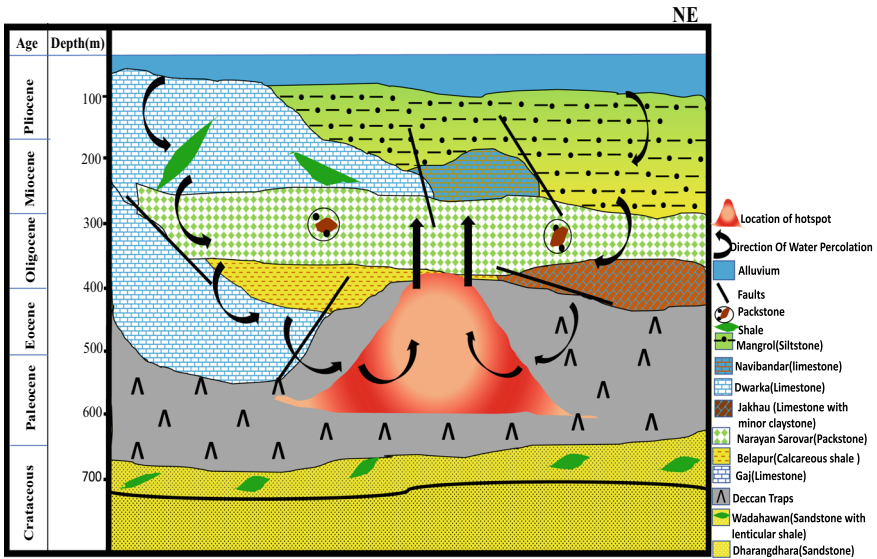


**Fig. 6** Method of transmission of heat from geothermal reservoir to the water is depicted in this conceptual subsurface model of the study region

surface due to the volume difference. Following such an incident, time passes while new water enters the system, heats up, and the cycle repeats. The current researchers attempt to explain the best model for the placement of geothermal springs in the study region. Groundwater infiltrates the subsurface by fracture and jointing, increasing the permeability of the subsurface zone. While percolating, groundwater gathers up heat from the subsurface, particularly heat from the Deccan traps. Geothermal hot springs are formed when the waters return to the surface via faults and cracks.

## 5 Conclusions

Geothermal has the potential to become a pillar of the energy transition due to its distinctive traits such as credibility, the ability to decarbonize, and the ability to induce current exploitation techniques. The geophysical examination of the Tulsishyam area in Gujarat, which is also known as one of the unrecognized geothermal potential zones, is the basis for this study. From the geophysical studies, it can be analyzed that both the Gravity and Magnetic surveys refer to the exact subsurface location where the sweet spot was found. The geothermal water in the studied region can be used for the production of electricity, farming, and industry, among other things. On a worldwide basis, geothermal has the potential to drastically reduce the amount of fossil fuels used for electricity reduction. Geothermal energy has the ability to massively impact the amount of fossil fuels that we are burning for electricity production on

a global scale. Based on its unique characteristics such as reliability, decarbonization potential, capacity to go for new exploitation techniques, geothermal has the potential to become a pillar of energy transition in the Tulsishyam area.

## References

1. OECD, D. (2020) The impact of the COVID-19 pandemic on jobs and incomes in G20 economies
2. Annual Energy Outlook (AEO2022) (2022). [https://www.eia.gov/outlooks/aeo/pdf/AEO2022\\_ReleasePresentation.pdf](https://www.eia.gov/outlooks/aeo/pdf/AEO2022_ReleasePresentation.pdf)
3. Sircar A, Yadav K, Bist N, Oza HG (2021) Geochemical characterization of geothermal spring waters occurring in South part of Gujarat and west coast geothermal province of Maharashtra, India
4. Yadav K, Sircar A (2021) Geothermal energy provinces in India: a renewable heritage. *Int J Geoh Heritage Parks* 9(1):93–107
5. Minissale A, Chandrasekharam D, Vaselli O, Magro G, Tassi F, Pansini GL, Brahamabut A (2003) Geochemistry, geothermics and relationship to active tectonics of Gujarat and Rajasthan thermal discharges, India. *J Volcanol Geoth Res* 127(1–2):19–32
6. Chandrasekhar DV, Mishra DC, Rao GVSPC, Rao JM (2002) Gravity and magnetic signatures of volcanic plugs related to Deccan volcanism in Saurashtra, India and their physical and geochemical properties. *Earth Planet Sci Lett* 201:277–292
7. Singh HK, Thankappan A, Mohite P, Sinha SK, Chandrasekharam D, Chandrasekhar T (2018) Geothermal energy potential of Tulsishyam thermal springs of Gujarat, India. *Arab J Geosci* 11(6):1–11
8. Sen S, Kundan A, Kalpande V, Kumar M (2019) The present-day state of tectonic stress in the offshore Kutch-Saurashtra Basin, India. *Mar Petrol Geol* 102:751–758
9. Chopra S, Kumar D, Rastogi BK, Choudhury P, Yadav RBS (2013) Estimation of seismic hazard in Gujarat region, India. *Nat Hazards* 65(2):1157–1178
10. Bist N, Sircar A, Yadav K (2021) Thermal zone identification by gravity data modeling using Euler deconvolution and geochemical analysis of hot springs in Saurashtra and Cambay Basins. *Indian J Sci Technol* 14(26):2189–2205
11. Gravity maps and profiles. cas.usf.edu (2017) [online]. Available [http://www.cas.usf.edu/~cconor/pot\\_fields\\_lectures/Lecture2\\_gravity\\_maps.pdf](http://www.cas.usf.edu/~cconor/pot_fields_lectures/Lecture2_gravity_maps.pdf). Accessed 08 Mar 2022
12. Magnetic maps. cas.usf.edu (2017) [online]. Available [http://www.cas.usf.edu/~cconor/pot\\_fields\\_lectures/Lecture8\\_magnetics.pdf](http://www.cas.usf.edu/~cconor/pot_fields_lectures/Lecture8_magnetics.pdf). Accessed 08 Mar 2022
13. Hydrogeology and ground water resources of Rajkot district. cgwb.gov.in (2014) [online]. Available [http://cgwb.gov.in/District\\_Profile/Gujarat/Junagadh.pdf](http://cgwb.gov.in/District_Profile/Gujarat/Junagadh.pdf). Accessed 08 Mar 2022

# Extraction of Geothermal Water Using Directed Energy Method of Millimeter-Wave Technology



Anirbid Sircar , Abhishek Nair, Namrata Bist , Kriti Yadav ,  
Vaishnavi Pandey, Neel Shah, and Bhavy Chotaliya

## 1 Introduction

The largest development potential and greatest drilling obstacles are in deep formations, which account for 30% of all oil and 60% of all gas resources and hold the majority of onshore residual resources [1]. New technical challenges arise more frequently as oil and gas exploration and development targets become more complicated, well depth increases, and high-temperature and high-pressure environments become more common, resulting in a higher time efficiency of complex accidents during drilling and a higher drilling cost. As a result, it is more difficult to drill deep and ultra-deep wells.

When high temperatures, high pressures, and acid gases are encountered at greater depths, deep drilling presents significant challenges. Typically, a combination of these factors results in considerable planning, the use of exotic materials, prolonged drilling times, and expensive costs [2]. Extremely hard rock is found at great depths, which slows drilling. According to reports, drilling costs for wells deeper than 15,000 feet are spent in the last 10% of the well since penetration rates are only about 2–3 feet per hour [3]. The majority of shale gas is produced from shallow reservoirs that are primarily located between 76 and 2439 m deep. Deep shale gas, on the other hand, is becoming more popular with time. The main difficulties encountered while drilling for shale reservoirs with high formation pressure and complex formation conditions are wellbore instability, substantial formation damage from high drilling fluid pressure, and low drilling efficiency [4].

The use of a rotating cutting tool with a downward force (wear point) to gouge or scrape the face of a rock is referred to as mechanical or conventional drilling. When

---

A. Sircar · A. Nair · N. Bist · V. Pandey · N. Shah · B. Chotaliya  
Pandit Deendayal Energy University, Gandhinagar, Gujarat 382007, India

K. Yadav (✉)  
Department of Geology, Patna University, Ashok Rajpath, Patna 800005, India  
e-mail: [kriti.yphd15@spt.pdpu.acin](mailto:kriti.yphd15@spt.pdpu.acin)

cutting, particularly hard rocks like granites, basalts, etc., as observed at considerable depths, this method has drawbacks, including wear, shortened life, and limited efficiency. Additionally, specialized piping is needed to carry that rotational torque to those high depths.

MMW has the ability to build a corrosion-resistant, hardened, sealing wellbore liner during drilling, minimizing the requirement for casing and cementing, and giving monobore capabilities for reducing bore, casing sizes, and costs in the upper interval. There may possibly be additional stimulating advantages. Lowering these up-front expenses will lower project risks for Enhanced Geothermal System (EGS) and boost EGS profitability. Less wells may be required as a result of improved EGS reservoir performance that allows for access to more rock volumes.

## **2 History of Directed Energy Drilling with Special Reference to MMW**

Since the development of the laser in 1960, research into directed energy rock drilling has been conducted. The use of directed energy as an auxiliary tool to weaken rock by heating or to create notches for simpler mechanical drilling was first limited by the availability of low-power lasers [5]. In the 1990s, demonstrations of standalone directed energy drilling were performed using megawatt StarWars lasers (the US Army MIRACL and US Air Force COIL). Rates of penetration were demonstrated to be 10 to 100 times faster than rotary drilling in shallow rock surface extraction trials [6, 7]. As a result, the notion of directed energy drilling has been proven in the lab. However, due to low efficiency, high prices, and challenges with efficient optical beam transmission, practical laser-based drilling systems have not yet been developed. A particularly difficult challenge is particle extraction without affecting the optical drilling beam [8]

All these challenges may be resolved by using millimeter-wave technology, enabling the use of directed energy drilling and fracturing devices. Moving to the MMW region of the electromagnetic spectrum was a feasible solution. Longer wavelengths can propagate more effectively through propagation routes that are loaded with small particles, and MMW sources with high power are significantly more effective, efficient, and less expensive.

Intense millimeter wave sources have higher energy, are more efficient, and have wavelengths that are more suitable for penetrating boreholes in the 30–300 GHz range compared to lasers. Several electromagnetic radiation sources are shown in Fig. 3. Gyrotrons are one of the most common sources of MMW production [9]. The gyrotron technology has been developed as part of a global effort to develop fusion energy. These MMW sources belong to the category of free electron lasers known as electron cyclotron masers. As a result of an electron beam with a high voltage inside the magnetic field, electrons spin around magnetic field lines, converting the energy of the electron beam into strong radiation via electron cyclotron resonance

[10]. Gyrotron tubes have been created at 110 and 170 GHz with continuous output levels of 1 MW, as well as electrical to millimeter-wave power conversion efficiencies greater than 50%. Gyrotrons are being used in fusion research facilities all over the world. There is a 5 MW, 6-tube 110 GHz gyrotron system in one such facility at General Atomics in San Diego. A 24 MW, 24-tube system was operating at 170 GHz at the International Thermonuclear Reactor (ITER) in Cadarache, France. The US Department of Defense built a small 2 MW, 95 GHz continuous-wave (CW) gyrotron for its active denial weapon and tested 100 kW in the field. In a Humvee or an aircraft, the entire power source for these gyrotron devices is in place. Due to their reliability and application in rural terrain, they could be easily adapted for use at remote drilling sites. It would only take a moderate development in drilling to order robust field-capable gyrotrons today [11].

### 3 Types of Deep Drilling Methods

#### 3.1 Plasma-Pulse Geo-drilling

A novel technique that could be used to supplement or replace the conventional rotary drilling approach is the application of plasma to the rock [12]. In addition to not removing rock through mechanical means, plasma-pulse geo-drilling (PPGD) uses less energy relative to the volume of rock that is removed.

This has two key benefits over traditional mechanical drilling: (i) fewer round trips are required due to the nearly wear-free drilling process, and (ii) higher rates of penetration (ROP) are possible due to the decreased volumetric energy input. By increasing the drilling economics, these two factors have significantly made it easier to access deep, hard rocks.

The electrodischarge technology (EDT), which was first invented in Russia, serves as the foundation for the mechanism of PPGD [13]. A plasma channel (streamer), which is induced by a high-voltage pulse, is started using an appropriate electrode configuration. The streamer penetrates the rock, causing it to fracture internally as depicted in Fig. 1. The drilling instrument has electrodes embedded in it, and a drilling fluid surrounds the operation (e.g., oil or water) [14].

C3controls is one such manufacturer of PPGD devices. They develop and produce standard industrial control products that comply with global industry specifications for quality and performance. Another manufacturer of PPGD equipment is Parveen Industries Private Limited. They are one of the world's leading producers and suppliers of oil and gas equipment [15].

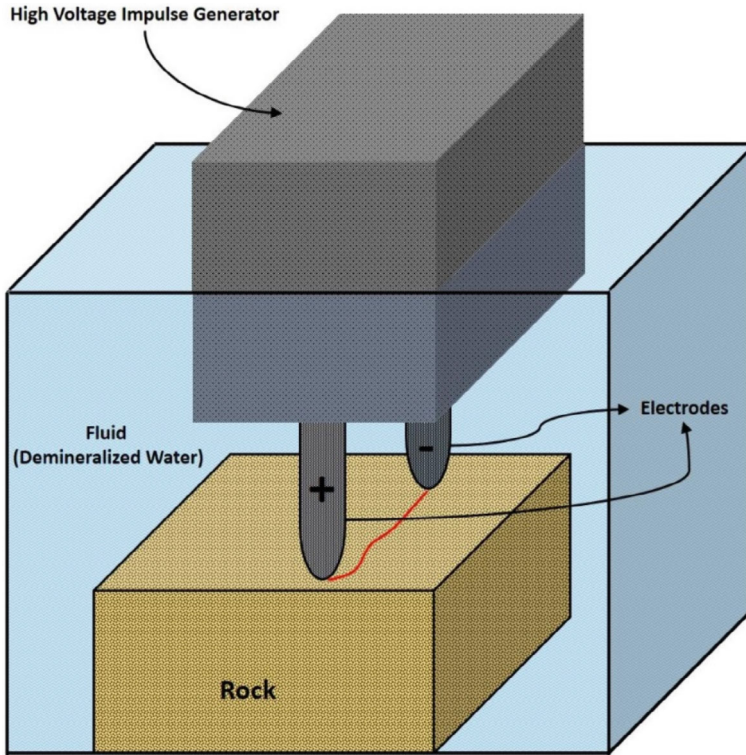


Fig. 1 Representation of working principle of plasma-pulse geo-drilling

### 3.2 Thermal Spallation Drilling

Spallation technology is based on the idea that when heated quickly by a hot fluid jet, hard, crystalline rocks break up into microscopic fragments. The benefits of spallation drilling include high penetration levels into strong rock formations, efficient energy transfer to the bit, and significantly lower wear rates. Previous studies have suggested that these advantages might result in a large reduction in drilling costs, which would therefore accelerate the development of geothermal energy generation from deep deposits.

A hot fluid jet is used in spallation technology to locally destroy the rock surface. The steep temperature gradients that the flame induces cause high local thermal stresses in the top layer of the rock surface. Cracks that are already existent will initially extend at the surface and eventually penetrate the material as depicted in Fig. 2, if the heat loads are too high. The process can continue on the newly produced surface once the cracks merge to form a so-called spall, which is ejected from the surface [16].

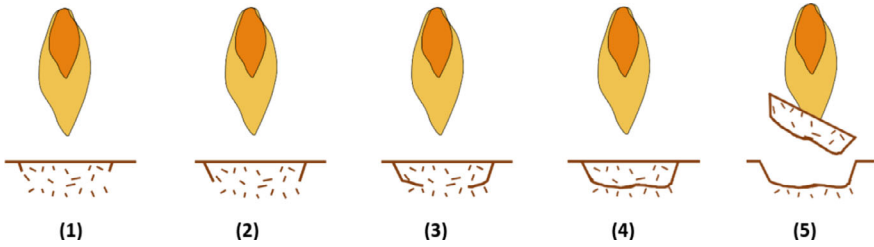


Fig. 2 Representation of working principle of thermal spallation drilling

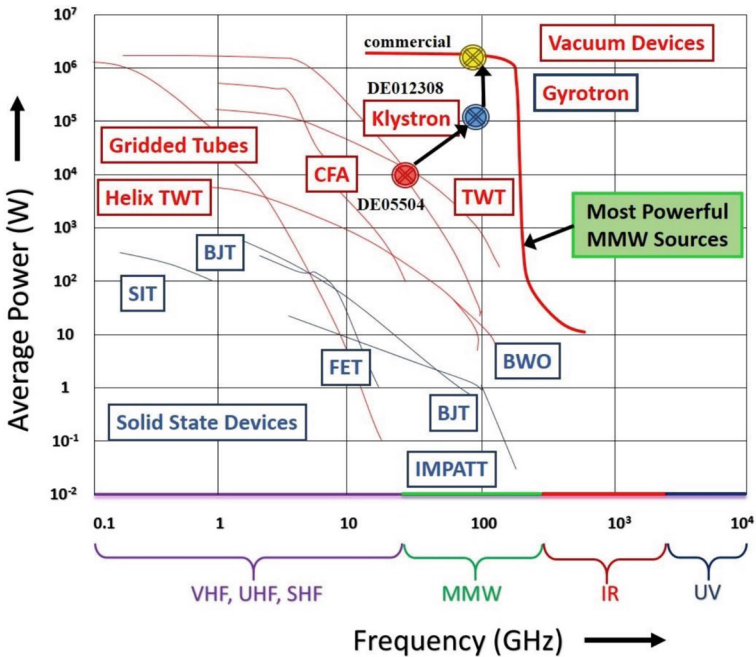


Fig. 3 Graphical representation of various electromagnetic radiation sources with its frequency range

Nearly all thermal spallation drilling rigs and channelers are produced in the USA by the Linde division of Union Carbide and Browning Engineering, Inc. The experimental rig has been developed and subjected to field testing by another company, Flame Jet Partners Ltd. These companies and their equipment are then reviewed [15].

Browning Engineering was started in 1961 by James A. Browning and is privately held. In the mid-70s, Browning developed a flame jet drilling system capable of drilling deep holes and/or chambering systems that could be used for thermal spallation purposes. It can drill holes to depths of more than 1000 feet in granite, and it is truck-equipped. Browning’s engineering has also used this technology to drill into

the Antarctic ice cap at a depth of more than 1400 feet [15]. The volume of air delivered per unit of time, together with a concurrent pressure in the atmosphere, is important to combustion and subsequently rock penetration in this type of drilling operation.

Since the end of the 1930s, Linde has been active in design, development, and field operation of jet cutting machines. Linde has also developed a line of channeling tools for cutting hard rock. Approximately 200 of these tools have been sold by the company. The concept of operation in this system is to heat the rock surface by firing a flame aimed at it and, together with the mass velocity of exhaust gases, generate an acceleration motion. When non-spallable rock or cracks are encountered, the exhaust gas temperature is high enough to fuse the rock. A combination of the mass velocity of the exhaust gases and the scrap action of the burner reamer lugs blows the molten rock away. This type of operation takes much less time than spalling [15].

### ***3.3 Flame Jet Drilling***

Flame jet drilling, one of the most often utilized thermal spallation technologies, can penetrate hard rock types at a high rate of penetration [17, 18]. Flame jet drilling has been used to remove spalls from the drill site using gas flow from the burner. When it came to the taconite industry, the technology stayed dormant until the middle of the 1970s, but during this time, it was utilized to drill geothermal wells. In the middle of the 1970s, Browning Engineering Company reported an average rate of penetration of around 52 feet per hour while drilling through granite utilizing flame jet drilling technology, which is advantageous from a deep geothermal drilling perspective. When compared to conventional methods, which have an average penetration rate of 16.2 feet per hour, jet drilling technologies substantially improve this area. It can also drill holes that are 20 times larger than the flame jet nozzle and well bores that are extremely small [19]. Due to a number of factors, including the well's need for an air-filled atmosphere for maintenance purposes and the need to remove drill site spall. Since deep drilling involves high pressures, the air-filled hole is generally unstable. Water infiltration makes this instability worse, which could impede the removal of spalls using gas [20]. The decrease in lift velocity of the exhaust gas is another obstacle to drilling big hole diameters. Therefore, efficiency of spall removal is hindered [21]. Second, high-density drilling mud, sometimes referred to as drilling mud, is necessary for deep drilling because it removes particles and balances the pressure inside the hole. This would include starting and maintaining the flame in a situation where there is liquid present.

A newly established company, Process Engineering International (PEI), Canoga Park, California, has been dedicated to patenting and developing a system of flame jet drilling using an extremely high-temperature rocket engine. Several patents were issued in the next few years, and a test facility has been set up. Different types of hard rock, such as hematite, granite, sandstone, were successfully tested on the rig [15].

### 3.4 Electropulse Boring

The concept of pulsing electrical voltage for shock wave generation and the technology developed in the 1970s. The electrode pair uses an electric pulse of between 15,000 and 200,000 V to strike the rock surface and break the front of the boulder. The underlying rock begins to shatter more when the pulse is applied again. With big rock cuttings, the method has a high rate of penetration (ROP). Innovative research was conducted in Bergen, Norway, in 2009 about digging geothermal wells using electropulse [22]. The main advantage of this method is its capacity to drill large-diameter, extremely deep holes in hard rocks.

### 3.5 Laser Drilling

The examination of drilling wells was the original application of the technology. Through the use of this technology, physical characteristics such as oil film thickness, permeability damage, and crude property detection are measured. Research on the use of laser drilling was conducted in the late 1960s and early 1970s, but the technique was abandoned due to laser inefficiency [23, 24]. But over time, advancements in fiber laser beam delivery and laser beam delivery techniques have made it possible to drill as well as send the beam to the downhole environment. The fundamental advantage of this procedure is that there is no contact between the tool and the rock face, which reduces travel time due to less wear. Laser-drilled wells need 90% less time than traditional wells due to their quick rate of penetration, resulting in less environmental damage. Furthermore, it has been discovered that laser drilling has a lower environmental impact than traditional drilling [25]. According to Bakhtbidar et al., nowadays, laser tests are carried out with a high-power laser of almost 7000 W in contrast to a low-power laser of 700 W [26].

Table 1 compares various drilling technologies and depicts their key features.

**Table 1** Various drilling technologies and their key features

Drilling technology	Key feature
Plasma pulse geo-drilling	Uses plasma rays, consumes less energy relative to the volume of the rock that is removed
Thermal spallation drilling	Hot fluid jet locally destroys the rock surface into microscopic fragments
Flame jet drilling	More effective and faster than conventional drilling in hard rock formations
Electropulse boring	Can drill huge diameter holes and extremely deep holes in hard formations
Laser drilling	Short trip time and less wear in bit parts due to no contact between tool and rock face

## 4 Millimeter-Wave Drilling

### 4.1 *About Millimeter Wave (MMW)*

The term “millimeter waves (MMW)” refers to radio waves or electromagnetic (non-ionizing) radiation of extraordinarily high frequency (EHF) (between microwave/MHz and infrared/THz categories), 30–300 GigaHertz (GHz), or 1- to 10-mm wavelengths. They are capable of effective directed transmission and are useful in applications that need a close line of sight. Gyrotrons, which are widely accessible on the market, are utilized to create MMWs with average power outputs of megawatts and efficiency levels exceeding 50%. MMWs are currently used in heating, communications, airport security, non-lethal weaponry, radar, medicine, and astronomy.

### 4.2 *Millimeter-Wave Technology*

Compared to lasers, intense millimeter-wave sources have higher energies, are more effective, and have wavelengths that are more suited for penetrating boreholes (30 to 300 GHz). Figure 3 shows a variety of electromagnetic radiation sources. One of the most popular sources for producing MMW is gyrotrons. In an international research effort to create fusion energy, gyrotron technology has been created [9]. These MMW sources belong to the category of free electron lasers known as electron cyclotron masers [10]. Electrons whirl around magnetic field lines as a result of an electron beam with high voltage inside a magnetic field, effectively converting the energy of the electron beam into strong radiation via electron cyclotron resonance [27, 28]. The gyrotron devices’ entire power source is contained within a Humvee or a plane. As a result of their reliability and usage in navigating rural terrain, they could be easily modified for use at remote drilling sites. Ordering robust field-capable gyrotron devices today would only require moderate development for drilling [11].

### 4.3 *Operation of MMW Deep Drilling System*

The only mechanically moving portion of an MMW deep drilling system is the waveguide advancement. Figure 4 depicts a cylindrical metallic waveguide that serves as a conduit for purging gas and beam energy and a cross-section of the borehole bottom. There is space for exhaust in the annular region of the well. Because an MMW beam emitted from a waveguide naturally diverges, it is less difficult to ream the borehole to a diameter greater than the core waveguide [29].

Effective MMW absorbers include rocks and glass melt [30, 31]. The rock surface temperature will quickly increase to a boiling point of over 3000 °C in a tiny borehole

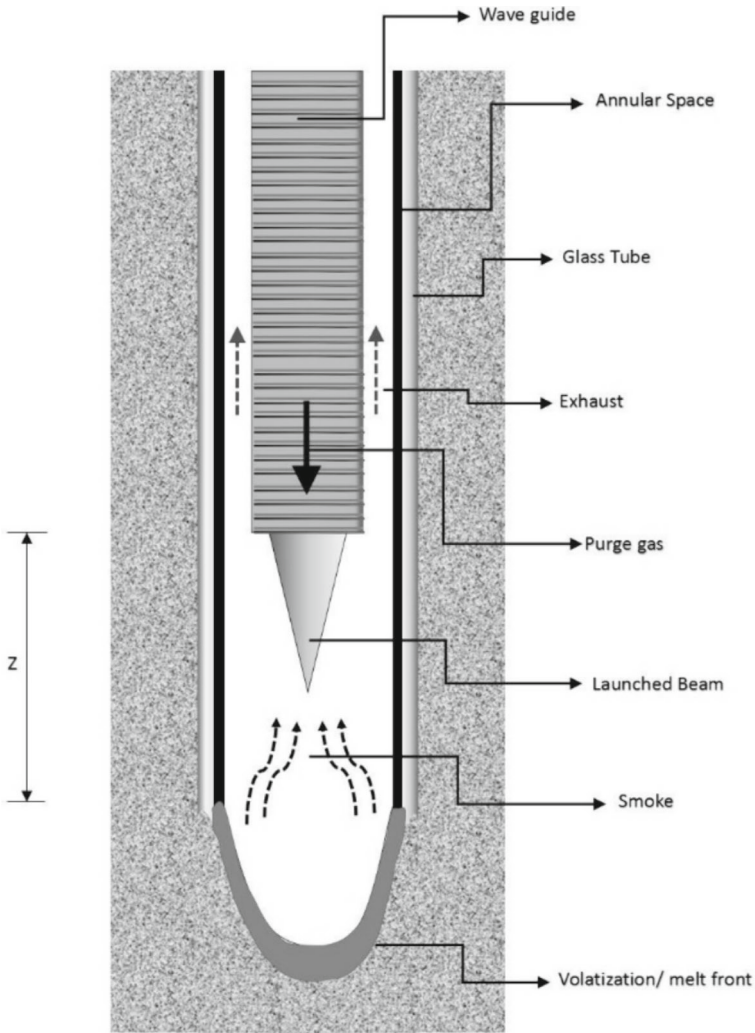


**Fig. 4** Pictorial representation of the operation of millimeter-wave-assisted drilling

with a diameter of 15 cm when a completely absorbed 1 MW beam is used. The rapidly moving ablation front would minimize heat loss to the nearby rock. The ensuing saturated pressure rock vapor will produce nanoparticle smoke, which the purge gas will blast out [32–34]. By using waveguide gaps, purge gas (for example, air) could be easily injected onto an overmoded waveguide (one that has an inner diameter that is larger than its wavelength) [35]. The purge gas would keep the waveguide clean and cool, aiding in the formation and expulsion of the rock extraction smoke. In order to boost the purge gas, subsurface water would rapidly turn into superheated steam if it were there [36]. The vitrified liner would thicken and become

more strong. As a result, penetration rates may be higher and utilize less energy than anticipated by the total rock vaporization below.

After cooling, the glass melt might solidify into a tough, high-temperature borehole wall that could later be pierced as necessary [37]. Glass materials have the ability to outlast many different types of rocks and strong concrete.

It should not be assumed that using a vitrified liner to keep the borehole open is the only choice. The ideal gas law may not hold true in this parameter space, and a supercritical rock fluid regime may occur.

#### ***4.4 Melting and Vaporizing of Rocks Using MMW-Directed Energy***

The energy required to melt and vaporize the rocks using MMW-directed energy would be based on the concept of latent heat of fusion and latent heat of vaporization. The former would be required to change the phase of rock from solid to liquid, and the latter would be useful in conversion of the liquid phase to vapor phase. In addition to these two energies, an additional variable in the form of heat capacity would be required. Heat capacity is different for different types of rocks; hence, this variable needs to be added to obtain specific solution for each type of rock. Upon adding these three variables, we will be able to obtain the energy required for melting and vaporizing any rock.

Equation (1) can be used to express the energy necessary to melt and vaporize rock:

$$H = c_p(T) \cdot \Delta T + H_f + H_v, \quad (1)$$

where  $c_p(T)$  is the heat capacity at temperature  $T$ ,  $\Delta T$  is the increase in temperature,  $H_f$  is the latent heat of fusion if  $\Delta T$  includes the melting point,  $H_v$  is the latent heat of vaporization if  $\Delta T$  includes the vaporization point.

At atmospheric pressure, basalt and granite basement rock, which are of relevance to EGS, melt at roughly 1200 °C and vaporize at little over 3000 °C [38]. Vakulenko et al. have measured the infrared emissivity of basalt melts to be between 0.2 and 0.5. In addition, Abithi et al. have shown that with increasing temperatures, basalt lava's Infrared Emissivity is decreasing to a value of 0.55 at 1050 °C. The specific energy from the vaporization of our granite sample would fall between 10 and 100 kJ/cm<sup>3</sup> if we assumed a thermal emissivity range of 0.2–0.5 [39].

#### 4.5 Calculation of Rates of Penetration for Drilling Assisted by MMW

The directed energy rate of penetration is determined by the speed at which energy may be provided in the rock using a specific displacement or extraction technique. It depends on the energy needed, the diameter of the borehole, and the beam power as expressed by Eq. (2):

$$R_p = 4/(\pi d^{(2)} E)(\epsilon_{\text{mm}} P_i - P_L), \quad (2)$$

where  $d$  is the hole diameter,  $E$  is the energy,  $\epsilon_{\text{mm}}$  is the millimeter-wave emissivity,  $P_i$  is the beam power incident on the rock surface, and  $P_L$  is the total power loss from the heated volume.

For a specific energy of vaporization of around 25 kJ/cm<sup>3</sup> and 100 kW/cm<sup>2</sup>, the ROP could be as high as 100 m/h. This would be more than 100 times faster than past experience with engineered geothermal system drilling (EGS) [39]. The removal of the rock mass would result in an electrical energy cost of approximately 7000 kWhr per cubic meter, which should remain constant at depth, regardless of the hardness or temperature of the rock. In EGS drilling technology, all the desired features are these potential ROPs, reduced costs, and linear scaling of costs [39].

Beam outputs over 1 MW will be required at rates more than 5 m/h in boreholes with a diameter of at least 20 cm (8"). A 100 m/h rate for small boreholes of 10 cm (4 inches) diameter or less may be conceivable with a 4 MW beam if pressure is sufficient to prevent plasma breakdown. Millimeter waves are suited for long-distance, high-power guided transmission in standard boreholes [40].

#### 4.6 Benefits of Millimeter Wave for Drilling and Lining Wellbores

The source to generate MMW, i.e., megawatt gyrotron is commercially available and is efficient. It is feasible to melt and evaporate specific rocks using a simple, direct, and efficient conversion of MMW energy into heat. In comparison to typical mechanical drilling, the MMW drilling system has no rotational parts; therefore, tool wear can be avoided. At greater depths, expect constant ROP. Drilling costs are predicted to rise linearly rather than exponentially as depth increases. Furthermore, rock hardness and temperature do not limit MMW drilling.

As compared with conventional drilling, MMW is a flexible system with various modes of delivery to the target. This technology is compatible with dirty environment and small particle plumes, due to Rayleigh scattering. Absorption of the beam by rock melt is more efficient in the MMW frequencies over IR. Remote real-time diagnostic (radiometry, radar, spectroscopy) and monitoring technology is available with MMW. It is an efficient long-distance, megawatt transmission technology, and wavelengths

and borehole sizes are ideally suitable for efficient beam delivery. Inherent straight borehole and diameter control up to greater depths can be achieved.

## 5 Conclusions

Traditional drilling strategies are extremely developed, yet at the same time experience issues boring through extremely hard and hot rocks for geothermal, oil, and gas applications. Actual contact between the tool bit and the stone or surface to be penetrated is a significant imperative in traditional techniques. Practical answers for drilling in hard rock formations must be created to advance the improvement of geothermal energy creation from profound assets. The drilling costs represent up to 70% of the total venture capital for a profound geothermal undertaking. Thus, a few emerging innovations are explored at present by specialists all over the planet. Millimeter waves (MMWs) are one of these innovations which conquer the impediments and diminish rock penetrating to a key interaction among energy and matter without the requirement for mechanical contact with the surface to be bored.

This study gives a brief overview of the history of directed energy drilling and describes several different deep drilling techniques, such as laser drilling, thermal spallation drilling, flame jet drilling, plasma-pulse geo-drilling, and thermal spallation drilling. The advantages of millimeter-wave technology over traditional drilling techniques are explained in length, along with its manner of operation, its utility in melting rocks at higher depths, and the rate of penetration it offers. Additionally, deep drilling with MMW from a geothermal standpoint, where piercing hard rocks are found at deeper depths, is a significant challenge. As per studies, MMW drilling is highly cost effective as compared to conventional drilling at greater depths. Hence, if implemented properly MMW drilling can be the future technology for deep drilling of wells in all the sectors like oil and gas, nuclear, and especially, in geothermal sector, where the source of energy greatly depends on the depth of wells.

## References

1. Wang H, Ge Y, Shi L (2017) Technologies in deep and ultra-deep well drilling: present status, challenges and future trend. 13th five-year plan period (2016–2020). *Natural Gas Industry B* 4(5):319–326
2. Chadwick C (2022) Challenges of deep drilling-1. Current deep-drilling technology and limitations. *Osti.gov*. <https://www.osti.gov/biblio/5394632>. Accessed 29 July 2022
3. Kelessidis VC (2009) Challenges for very deep oil and gas drilling will there ever be a depth limit. AMIREG international conference: assessing the footprint of resource utilization and hazardous waste management, pp 7–9
4. Li G, Liu H, Meng Y, Leng X, Jia H, Li H, Hu J (2012) Challenges in deep shale gas drilling: a case study in Sichuan Basin. In: IADC/SPE Asia Pacific drilling technology conference and exhibition

5. Jurewicz BR (1976) Rock excavation with laser assistance. *Int J Rock Mech Mining Sci Geomech Abstracts* 13(7):207–219
6. Umamaheshwar Rao K, Mishra B (1998) *Principles of rock drilling*. Oxford & IBH Publishing, New Delhi
7. Graves RM, O'Brien DG (1998) StarWars laser technology applied to drilling and completing gas wells. In: SPE annual technical conference and exhibition
8. Woskov P, Cohn D (2008) Drilling and fracturing with millimeter-wave directed energy. <http://www.researchgatenet/publication/2a2262554>. Accessed 14 July 2022
9. Felch KL, Danly BG, Jory HR, Kreischer KE, Lawson W, Levush B, Temkin RJ (1999) Characteristics and applications of fast-wave gyrodevices. *IEEE* 87(5):752–781
10. Nusinovich GS (2004) *Introduction to the physics of gyrotrons*. JHU Press
11. Woskov P, Cohn D (2009) Annual report 2009: millimeter wave deep drilling for geothermal energy, natural gas and oil MITEI seed fund program
12. Bazargan M, Gudmundsson A, Meredith PI (2017) Feasibility of using plasma assisted drilling in geothermal wells. *Fourth Sustain Earth Sci Conf Eur Assoc Geosci Eng* 1:1–5
13. Ushakov VY, Vajov VF, Zinoviev NT (2019) *Electro-discharge technology for drilling wells and concrete destruction*. Springer International Publishing
14. Rossi E, Adams B, Vogler D, Rudolf von Rohr P, Kammermann B, Saar MO (2020) Advanced drilling technologies to improve the economics of deep geo-resource utilization. In: 2nd applied energy symposium: MIT A + B (MITAB 2020) (virtual), vol 148
15. A Technical and Economic Evaluation of Thermal Spallation Drilling Technology (1984) Resource Technology, Incorporated 4555 South Harvard Avenue Tulsa, Oklahoma 74135
16. Kant M, Rossi E, Höser D, von Rohr PR (2017) Thermal spallation drilling, an alternative drilling technology for deep heat mining—performance analysis, cost assessment and design aspects. In: 42nd workshop on geothermal reservoir engineering, pp 13–15, 1–10
17. Augustine CR (2009) *Hydrothermal spallation drilling and advanced energy conversion technologies for engineered geothermal systems* (Doctoral dissertation, Massachusetts Institute of Technology)
18. Calaman JJ, Rolseth HC (1962) Technical advances expand use of jet-piercing process in taconite industry. *Mining Res* 473–498
19. e Silva FJR, Netto DB, da Silva LFF, Plácido JCR (2006) Analysis of the performance of a thermal spallation device for rock drilling. In: 11th Brazilian congress of thermal sciences and engineering—ENCIT, Brazil Society of Mechanical Sciences and Engineering—ABCM
20. Potter RM, Potter JM, Wideman TW (2010) Laboratory study and field demonstration of hydrothermal spallation drilling. *GRC Trans* 34:249–252
21. Williams RE (1986) The thermal spallation drilling process. *Geothermics* 15(1):17–22
22. Schiegg HO, Rødland A, Zhu G, Yuen DA (2015) Electro-pulse-boring (EPB): novel super-deep drilling technology for low-cost electricity. *J Earth Sci* 26(1):37–46
23. Qieni L, Baozhen G, Wenda Y, Yimo Z (2011) A method for measuring the thickness of transparent oil film on water surface using laser trigonometry. *Opt Lasers Eng* 49(1):13–15
24. Zekri AY, Shedid SA, Alkashfeh H (2007) A new technique for treatment of permeability damage due to asphaltene deposition using laser technology. *J Petrol Sci Eng* 59(3–4):300–308
25. Faircloth BO, Zediker MS, Rinzler CC, Koblick Y, Moxley JF (2013) Methods and apparatus for delivering high power laser energy to a surface (No. 8,424,617). *Foro Energy Inc.* (Littleton, CO)
26. Bakhtbidar M, Ghorbankhani M, Asfeh MR, Alimohammadi M, Rezaei P (2011) Application of laser technology for oil and gas wells perforation
27. Kasugai A, Sakamoto K, Takahashi K, Kajiwara K, Kobayashi N (2008) Steady-state operation of 170 GHz–1 MW gyrotron for ITER. *Nucl Fusion* 48(5):054009
28. Jacquinot J (1998) Plasma heating and current drive systems for ITER. In: 17th IEEE/NPSS symposium fusion engineering, pp 399–404
29. Rebuffi L, Crenn JP (1989) Radiation patterns of the HE11 mode and Gaussian approximations. *Int J Infrared Millimeter Waves* 10(3):291–311

30. Frasch LL, McLean SJ, Olsen RG (1998) Electromagnetic properties of dry and water saturated basalt rock, 1–110 GHz. *IEEE Trans Geosci Remote Sens* 36(3):754–766
31. Woskov PP, Sundaram SK, Daniel WE Jr, Miller D (2004) Molten salt dynamics in glass melts using millimeter-wave emissivity measurements. *J Non-Cryst Solids* 341(1–3):21–25
32. Whitlock RR, Frick GM (1994) Particle size distributions of aerosols formed by laser ablation of solids at 760 Torr. *J Mater Res* 9(11):2868–2872
33. Hunten DM, Turco RP, Toon OB (1980) Smoke and dust particles of meteoric origin in the mesosphere and stratosphere. *J Atmos Sci* 37(6):1342–1357
34. Zimmer AT (2002) The influence of metallurgy on the formation of welding aerosols. *J Environ Monit* 4(5):628–632
35. Doane JL, Moeller CP (1994) HE11 mitre bends and gaps in a circular corrugated waveguide. *Int J Electron* 77(4):489–509
36. Nikolaevskiy V, Garagash I (2003) Earth crust structure as a result of rock fracturing.... In: Stephansson O, Hudson JA, Jing L (eds) *Coupled thermo-hydro-mechanical chemical processes in geo-systems*, pp 727–732
37. Hanold RJ (1977) Rapid excavation by rock melting (LASL Subterrene Program). Status report. September 1973--June 1976 (No. LA-5979-SR). Los Alamos Scientific Lab., NM (USA)
38. Maurer WC (1976) Novel drilling techniques. In: *The cutting edge: interfacial dynamics of cutting and grinding: proceedings of a symposium sponsored by the American Association for the Advancement of Science and Supported in Part by National Institute of Dental Research and National Science Foundation*. US Department of Health, Education, and Welfare, Public Health Service, National Institutes of Health, National Institute of Dental Research
39. Woskov P, Michael P (2011) Millimeter-wave heating, radiometry, and calorimetry of granite rock to vaporization. Plasma Science and Fusion Center Massachusetts Institute of Technology Cambridge MA 02139 USA
40. Woskov P (2017) Millimeter-wave directed energy deep boreholes. In: *AIG drilling for geology II conference*. Brisbane, Australia
41. Lohr J, Cary WP, Gorelov YA, Grunloh HJ, Kajiwara K, Peavy JJ, Ponce D, Tooker J, Callis RW (2003) Practical experiences with the 6 gyrotron system on the DIII-D tokamak. In: *20th IEEE/NPSS symposium on fusion engineering*, pp 228–231

# Machine Learning-Based Predictive Models for Water Quality Index—An Analysis and Comparison



Vaishvi Shah, Ashwini Ramanuj, Krishna Patel, Shruti Jethloja, Debabrata Swain, and Manish Kumar

## 1 Introduction

Every living thing on Earth requires water to survive. Water is an invaluable resource that is fundamental to the survival and well-being of living organisms. It plays a crucial role in maintaining the balance of our planet's ecosystems and is irreplaceable for numerous human activities. Yet, in recent years, water quality has been severely threatened by a rising population, increased agricultural and industrial needs, and the growing effects of climate change.

Water is home to millions of species, from microscopic organisms to blue whales. The human body comprises approximately 60% water, and it is critical for the optimal functioning of various bodily systems. Water is also pivotal for the growth and sustenance of various plant and animal species, serving as a vital component in the process of photosynthesis, which is responsible for the generation of food and oxygen for other organisms. Furthermore, water sustains agriculture and crop growth, which is the primary source of nourishment for human life. Despite the innumerable benefits of water, human activity has led to the degradation of the natural composition of water resources.

The National Oceanic and Atmospheric Administration, defines quality of water as the state of the water as well as its physical, chemical, and biological aspects, usually in relation to how acceptable it is for a particular application. Recent activities of humans have led to the concentrations of substances in natural water resources

---

Vaishvi Shah, Krishna Patel, Ashwini Ramanuj, and Shruti Jethloja contributed equally to this work.

---

V. Shah (✉) · A. Ramanuj · K. Patel · S. Jethloja · D. Swain  
Department of Computer Science and Engineering, Pandit Deendayal Energy University,  
Knowledge Corridor, Gandhinagar 382007, Gujarat, India  
e-mail: [shah.vaishvi21@gmail.com](mailto:shah.vaishvi21@gmail.com)

M. Kumar  
Department of Electronics and Communication Engineering, Pandit Deendayal Energy  
University, Knowledge Corridor, Gandhinagar 382007, Gujarat, India

exceeding the ideal concentration values, resulting in a modification of the natural composition. For the spread of infectious diseases like polio, diarrhea, typhoid, cholera, and dysentery, water degradation is a major risk factor. This effect has led us to find an effective solution for the classification of water quality that is suitable for usage in normal, everyday life.

Classification of water quality can help alleviate major concerns about the issue. The dataset used in this work was first converted from an object datatype to a float datatype for numeric features. Later, during preprocessing, null values were replaced by the median. For removing outliers, the box plot method was used. The unit weights for each parameter were allocated using the NNMF method for an error-free and statistical calculation of the Water Quality Index (WQI). Again, filtering is applied to remove the negative values of WQI. Following this, the target variable, WQI classification feature (WQC), is added, which is divided into 4 categories according to the health guidelines and water use cases and applications. SMOTE oversampling is used to balance the data. For the classification of water quality, a comparison of the outputs from several classification models has been conducted.

## 2 Related Work

Several types of work have been done by various researchers to classify the quality of water. The various studies that were done to classify the water quality are the main subject of this section. The machine learning-based classification model, described by Radhakrishnan et al. [1], deals with the process of training based on the calculation of the weighted arithmetic water quality index (WAWQI). Three different machine learning techniques are used in this paper. When these models were tested against one another, the Decision Tree performed better [1]. The research by Abuzir et al. [2] is aimed at helping minimize and control water pollution. The dataset used in this study contains 10 features. To achieve more precision, feature extraction was done by making use of Principal Component Analysis (PCA). The models used in this study to make predictions about the classification of water quality are J48, Naive Bayes (NB), and multi-layer perceptrons (MLP). Multi-layer perceptron demonstrated the highest accuracy of all the deployed methods for WQC prediction after evaluating the results [2].

The dataset utilized by Wiryaseputra [3] was obtained through Kaggle and contains 10 parameters; after preprocessing, the null value in the dataset is replaced with the mean value. Using a boxplot, outliers were eliminated. This work incorporates machine learning methods like decision trees, XGBoost, random forests, and logistic regression to forecast the water quality. All of these algorithms were compared, and XGBoost produced the highest accurate outcomes (71.23%) [3]. Shahra et al. [4] researched and assessed the performance of two classification techniques for the classification of multiclass labels of the water quality index. The evaluation metrics used in this work is confusion matrix. Additionally, the models' overall accuracy is assessed. The results demonstrated that the ANN conducted classification more accu-

rately than the SVM, with a 94% total accuracy compared to 89% for the SVM [4]. Muhammad et al. [5] proposed a study in which they investigated and evaluated various machine learning models in order to find the critical elements that significantly influenced the categorization of the water quality of Kinta River, Perak, Malaysia. Six features were chosen for categorization out of the 53 attributes in the dataset to achieve the highest accuracy rating. The machine learning methods Bagging, Conjunctive Rule, J48, Naive Bayes and KStar are utilized in this work to categorize water quality. When the models' performance was evaluated, it was discovered that the Lazy model with the K star method had the highest accuracy of 86.67% [5].

Shamsuddin et al. conducted a study in 2022 to evaluate the efficacy of machine learning models in multiclass categorization for the purpose of evaluating the water quality of the Langat River Basin. Three models namely Decision Trees (DT), ANN, and SVM were used to classify the quality of river water. The SVM model in this study forecasts river water quality the best, according to a performance comparison of the three models. The effectiveness of the SVM model is significantly impacted by the usage of the grid search technique, the kernel function and the multiclass classification strategy in this study [6].

### 3 Methodology

#### 3.1 Proposed System

This paper presents a robust approach for classifying water quality. Figure 1 illustrates the various steps of the machine learning-based system.

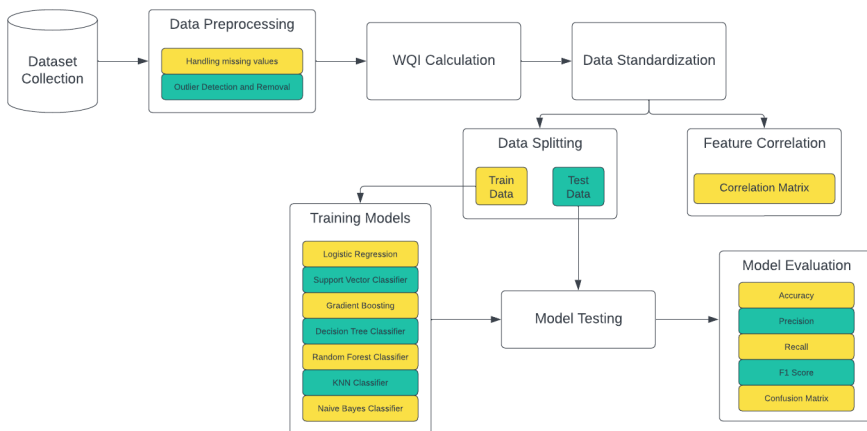


Fig. 1 Working diagram of proposed model

### 3.2 Dataset

The dataset utilized in this research is composed of 1991 records of water data in certain locations of India collected from the Indian government websites consisting of 12 features that were retrieved from the Kaggle repository [data]. The dataset used for our research is composed of 8 key characteristics: temperature, biological oxygen demand (BOD), pH, dissolved oxygen (DO), conductivity, nitrate content, fecal coliform, and total coliform.

### 3.3 Data-Preprocessing

The water dataset contained several missing values as well as the features in object data type. In the preprocessing stage, all the features in the object data type were converted to numeric form. Furthermore, central tendency values were mostly used to impute missing data. The missing values in the numerical features were imputed using the column median. The imputation of missing values for categorical variables with outliers was carried out manually using geographical station codes in accordance with the locations and states represented in the dataset. Standardization of values was done to center the values around the mean with a unit standard deviation resulting in ( $\mu = 0$  and  $\sigma = 1$ ). Standardization is given by the formula 1 below:

$$X' = \frac{(X_i - \mu)}{\sigma} \quad (1)$$

where  $\sigma$ ,  $\mu$  and  $X_i$  represent standard deviation, mean and input feature values respectively.

#### 3.3.1 Outlier Detection and Removal

The water dataset contains outliers that must be cleaned up during the preprocessing stage. An outlier is a data point that deviate significantly from the average or expected values of a dataset. Removing noise or outliers from a dataset can help improve model accuracy, reduce overfitting, improve generalization, and enhance data quality. The boxplot method has been used to detect and remove the outliers. Boxplot of all 8 numeric features is given in Fig. 2.

#### 3.3.2 WQI Calculation

A methodology based on the Weighted Arithmetic Water Quality Index Technique is applied to calculate WQI [7]. The weights are calculated using Non-Negative Matrix Multiplication Method. The typical approach to assigning weights to these water

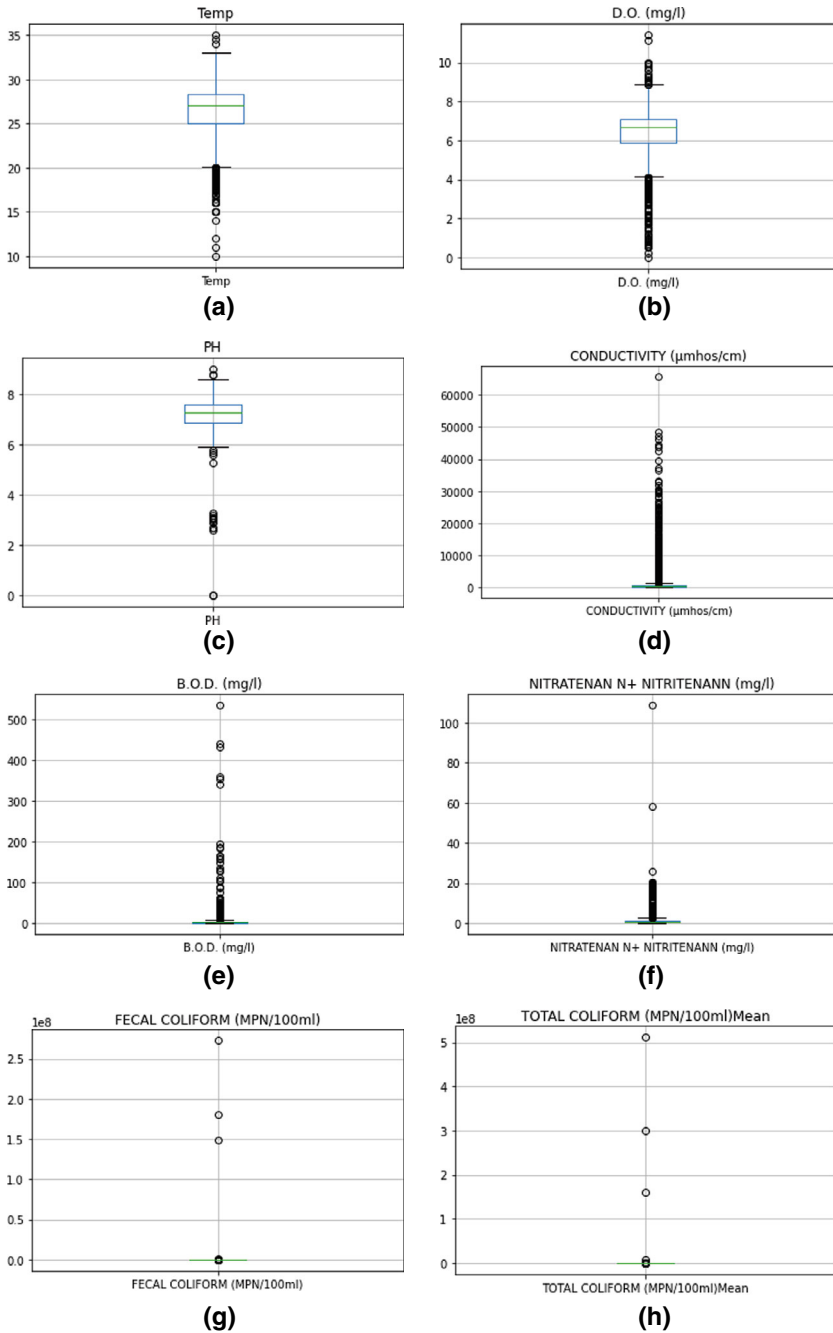


Fig. 2 Boxplot for detection and removal of outliers

**Table 1** Standard values of given parameters

Parameters	Standard values
Temperature	35 °C
B.O.D	5 mg/L
Nitrate	45 mg/L
D.O.	10 mg/L
Total coliform	1000 CFU/100 ml
pH	8.5
Conductivity	1000 $\mu$ S/cm
Fecal coliform	100 CFU/100 ml

quality factors frequently relies on expert opinion and does not accurately reflect the relative weight that each measure actually has in determining water quality. Non-Negative Matrix Multiplication Method based on statistical and mathematical principles, which can help to ensure that the weights are derived from a rigorous and scientifically sound approach. NNMF assigns weights by factorizing a non-negative matrix into two matrices, a basis matrix and a coefficient matrix. The coefficient matrix gives the weights that represent the importance of each parameter in approximating WQI.

The WQI was processed utilizing Eq. 2 below:

$$WQI = \sum_{i=1}^n q_i * w_i / \sum_{i=1}^n w_i \quad (2)$$

where  $w_i$  represents the weights assigned to each parameter by NNMF. For each parameter  $i$ ,  $q_i$  represents the quality rating scale that was generated using Eq. 3, and  $n$  stands for the total number of parameters taken into account.

$$q_i = 100 * ((v_i - v_{ideal}) / (v_{standard} - v_{ideal})) \quad (3)$$

where  $v_i$  denotes the actual value of a parameter  $i$  in the tested water samples,  $v_{standard}$  denotes the parameter's recommended standard value (as stated in Table 1) and  $v_{ideal}$  is the ideal parameter value in pure water, optimum values of all the parameters in pure water are taken as 0 excluding pH = 7.0, temp = 20 °C and D.O. = 14.6 mg/L.

### 3.3.3 Data Balancing

The dataset's imbalance causes the models that were trained on it to overfit. The imbalance in the data is addressed by oversampling. Using an SMOTE-based oversampler, the balance is accomplished. Following the use of this method, as shown in Fig. 3, the number of all sorts of classes have achieved a balanced total of 1335.

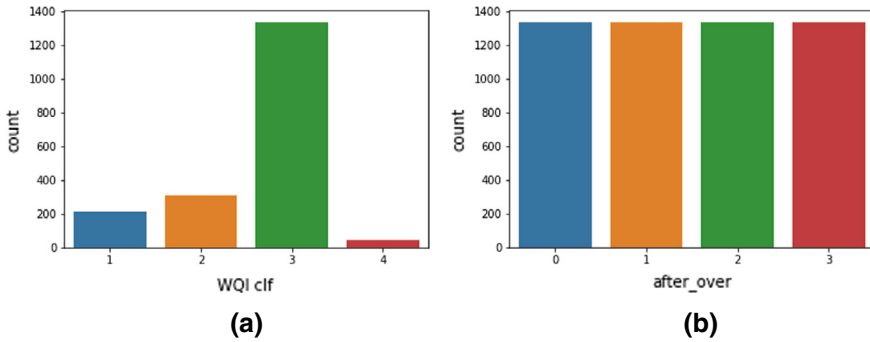


Fig. 3 SMOTE oversampling

### 3.4 Train Test Split

For the purposes of model training, the water quality dataset utilized was partitioned into two distinct subsets. 30% of the data were assigned to the testing set and the rest 70% to the training set using the train-test-split process.

### 3.5 Model Training

#### 3.5.1 Logistic Regression

The statistical technique of logistic regression models a categorical dependent variable with one or more independent variables. Specifically, it is a type of generalized linear model that assumes a binomial distribution for the dependent variable, where it takes on one of two possible outcomes. The model determines the probability that, given the values of the independent variables, the dependent variable will take on a particular value by applying a logistic function to the data as shown in Eq. 4 below.

$$\ln \left( \frac{\hat{p}}{(1 - \hat{p})} \right) = b_0 + b_1 X_1 + b_2 X_2 + \dots + b_p X_p \tag{4}$$

Here  $X$  is the independent variable(s),  $b_0, b_1, b_2, \dots, b_p$  are the coefficient(s) on the independent variable(s) and  $\hat{p}$  estimated probability of the dependent variable taking on a specific value.

### 3.5.2 K Nearest Neighbors (KNN)

KNN does not make any assumptions regarding the distribution of underlying data because it is a non-parametric technique. In contrast, KNN forecasts new data points by using the feature space's separations between the current data points. Finding the  $k$  closest neighbors to the newly classified data point is how KNN finds its neighbors;  $k$  is a user-specified hyperparameter. In classification tasks, a newly added data point's class is determined by its predominant class among the  $k$  nearest neighbors. In a regression job, the predicted value of a new data point is based on the average of the values of the  $k$  nearest neighbors. An essential component of the KNN method is the distance metric used to determine the separation between data points. The distance metric used can be either Manhattan distance or Euclidean distance as shown in Eq. 5 below.

$$D_i = \sqrt{(x_1 - x_2) + (y_1 - y_2)^2} \quad (5)$$

Here  $D_i$  represents Euclidean Distance.

### 3.5.3 Naive Bayes

The method is based on Bayes' theorem, which describes the likelihood of a hypothesis given the available information. When using Naive Bayes, the likelihood of any one feature is unaffected by the presence or absence of any other feature. In order to determine each class' likelihood in the absence of any feature information, Naive Bayes first determines each class' prior probability based on the training data.

The likelihood of an event B given an event A is different from the likelihood of an event A given an event B in a Bayesian analysis, as shown in Eq. 6 below.

$$P(A|B) \neq P(B|A) \quad (6)$$

Assuming that  $A_1, A_2, \dots, A_n$  are the feature vectors and C is the class of the water quality, respectively, the Bayes equation can be expressed as Eq. 7 below:

$$P(C|A) = \frac{P(C) \times P(A|C)}{P(A)} \quad (7)$$

where the  $P(A|C)$  is a prior probability of the class of the water quality and  $P(A)$  is the prior probability representing the feature vectors of the Water quality.

### 3.5.4 Decision Tree

This machine learning approach creates a tree-like model of decisions and outcomes, with each internal node representing a test on an attribute and each leaf node indicat-

ing a class label or numerical result. It selects the best feature to split the data at each node of the decision tree based on a measure of impurity reduction or information gain. While impurity reduction reflects a decrease in the Gini index or misclassification rate, information gain measures an increase in entropy. The program separates the dataset into subsets according to the values of each feature after it has been chosen. The method is then iteratively carried out recursively on each subset until a stopping condition is met. Decision trees can handle both continuous and categorical data, despite their propensity for overfitting.

### **3.5.5 Random Forest**

A machine learning technique from the ensemble method family that mixes numerous independent models to improve overall performance. Random Forest generates a large number of decision trees, and uses a random subset of the input features and training data to train each tree. The algorithm constructs decision trees using the same technique as the classic decision tree algorithm during the training phase. At the prediction phase, however, the algorithm aggregates all of the decision trees' predictions to make the final forecast. This can be done in two ways, by taking the majority count (in classification problems) or the average (in regression problems). This process helps to reduce the variance and increase the accuracy of the predictions.

### **3.5.6 Gradient Boosting Classifier**

This algorithm uses the ensemble method and combines various individual models to enhance performance. It is based on decision trees and is used for classifying challenges.

Gradient Boosting Classifier produces a series of decision trees, each of which attempts to correct the faults introduced by the previous tree. The method starts the training phase by constructing a single decision tree and making predictions based on the training data. Following the computation of the difference between the expected and actual values, a new decision tree is trained to predict the difference. This process is repeated several times, with each new tree adding to the overall prediction and predicting the flaws of the previous tree. The approach uses the gradient descent method to reduce the loss function.

### **3.5.7 Support Vector Machine**

SVM works by selecting the optimum hyperplane for separating data into several groups or predicting the continuous target variable. In multiclass classification, the hyperplane is in higher-dimensional space that divides the data into many classes as opposed to the binary classification hyperplane, which is a line that divides the data into two groups.

**Table 2** Bifurcation of classes

WQI value	Water quality	Usage of water	Grouping
0–25	Excellent	Consumption, watering, commercial	A
25–50	Good	Consumption, watering, commercial	B
50–75	Poor	watering, commercial	C
75–100	Very poor	watering	D

Complicated non-linear correlations between the input features and the target variable can be captured using SVM. SVM also features a regularization parameter. A large regularization parameter results in a smaller margin but more misclassifications, whereas a small regularization parameter results in a higher margin but more misclassifications. Equation 8 is shown below.

$$K(X, X') = \exp\left(\frac{-\|X - X'\|^2}{2\sigma^2}\right) \quad (8)$$

where  $X$  and  $X'$  denotes the input dataset's feature vectors and the  $\|X - X'\|^2$  denotes the squared Euclidean distance between the two feature inputs and the  $\sigma$  is a free parameter.

## 4 Classes

The generated feature—Water Quality Classification has been bifurcated into 4 categories based on the applications of water in various areas, as shown in Table 2.

## 5 Results and Discussion

The performance of the suggested approach is evaluated using a variety of measures, including:

**Accuracy:** Accuracy is defined as the number of accurate predictions the model makes divided by the total number of values in the input data. It is used to evaluate how successfully a model can forecast the labels of the input data. It is described mathematically in Eq. 9 below:

$$\text{Accuracy} = \frac{(TP + TN)}{(TP + FP + TN + FN)} \quad (9)$$

**Table 3** Accuracy scores

Model	Accuracy
Logistic regression	0.70
K nearest neighbor	0.70
Naive Bayes	0.70
Decision tree	0.94
Random forest	0.96
Gradient boosting classifier	0.96
Support vector machine	0.68

**Precision:** It ascertains which positively predicted cases fall into the positive class accurately. The ratio of true positives (TP) to the total of TP and false positives (FP) that the model predicts is known as precision. Calculations can be made using Eq. 10 below:

$$\text{Precision} = \frac{(\text{TP})}{(\text{TP} + \text{FP})} \quad (10)$$

**Recall:** It can be characterized as the proportion of correctly predicted positive events. The ratio of TP to the total of false negatives (FN) and TP in the data is known as recall. It can be quantitatively calculated using Eq. 11 below.

$$\text{Recall} = \frac{(\text{TP})}{(\text{TP} + \text{TN})} \quad (11)$$

**F1 Score:** The harmonic mean of recall and precision is known as the *F1* score. Accurate classification by the model is indicated by a high *F1* score. Equation 12 below can be utilized to compute it:

$$F1 \text{ score} = \frac{(2 \times \text{precision} \times \text{recall})}{\text{precision} + \text{recall}} \quad (12)$$

Table 3 displays the accuracy score for each of the trained models.

As indicated in Tables 4 and 5, a number of performance metrics were used to assess the two top-performing models, the Random Forest Classifier and the Gradient Boosting Classifier. Accuracy, precision, recall, confusion matrix, and F1-score were among these measurements.

The evaluation metric used is confusion matrix. Tables 6 and 7 display the confusion matrices for the two top-performing models.

These metrics are frequently employed in the field of machine learning and together they offer a thorough evaluation of the effectiveness of a classification model.

**Table 4** Classification report of random forest

Class	Precision	Recall	F1-score
1	0.97	0.85	0.90
2	0.92	0.98	0.95
3	0.93	0.95	0.94
4	0.97	1.00	0.98

**Table 5** Classification report of gradient boosting

Class	Precision	Recall	F1-score
1	0.97	0.90	0.93
2	0.94	0.98	0.96
3	0.94	0.97	0.96
4	0.99	1.00	0.99

**Table 6** Confusion matrix of random forest

	A	B	C	D
A	331	23	25	11
B	5	390	3	0
C	7	12	382	2
D	0	0	0	411

**Table 7** Confusion matrix of gradient boosting

	A	B	C	D
A	350	19	19	2
B	6	389	3	0
C	3	5	392	3
D	0	0	2	409

## 6 Comparative Analysis

The accuracy attained by several methods for classifying water quality is shown in the comparison analysis shown in Table 3. With a test accuracy score of 96.99% in our analysis, Gradient Boosting model performed brilliantly in terms of classification. The ensemble nature of the model proves particularly effective in addressing model faults, underscoring its superior performance in water quality classification. Ensemble means using a team of different models working together, which can lead to better predictions by combining their strengths. Our proposed model for water quality classification stands out from existing literature by utilizing a comprehen-

sive dataset containing 1991 records collected from diverse locations in India. This dataset incorporates 12 essential water quality parameters, providing a more encompassing perspective. Through meticulous preprocessing techniques, including data imputation, Non-Negative Matrix Factorization (NNMF), and Synthetic Minority Over-sampling Technique (SMOTE) balancing, we ensure the creation of a robust and representative training dataset. A number of research papers did not consider extensive preprocessing into account. The Water Quality Index (WQI) calculation follows a scientifically grounded Weighted Arithmetic approach, contributing to enhanced precision.

## 7 Conclusion

To classify the water quality, a number of machine learning models are developed, including Gradient Boosting Classifier, Support Vector Machine, Decision Tree, Random Forest, K Nearest Neighbors, Logistic Regression, and Naive Bayes. The effectiveness of various machine learning models was compared. The results show that the machine learning technique is appropriate for classifying water quality, with Random Forest and Gradient Boosting Classifier attending the greatest level classification accuracy of 96.05% and 96.99%, respectively. In the future, we will leverage sensor-derived real-time data to improve machine learning models' categorization performance.

## References

1. Radhakrishnan N, Pillai AS (2020) Comparison of water quality classification models using machine learning. In: 2020 5th international conference on communication and electronics systems (ICCES), pp 1183–1188. <https://doi.org/10.1109/ICCES48766.2020.9137903>
2. Abuzir SY, Abuzir YS (2022) Machine learning for water quality classification. *Water Qual Res J* 57(2):152–164. <https://doi.org/10.2166/wqrj.2022.004>. <https://iwaponline.com/wqrj/articlepdf/57/3/152/1091520/wqrjc0570152.pdf>
3. Wiryaseputra M (2022) Water quality prediction using machine learning classification algorithm. *Mach Learn* 8:4
4. Shakra EQ, Wu W, Basurra S, Rizou S (2021) Deep learning for water quality classification in water distribution networks. In: Iliadis L, Macintyre J, Jayne C, Pimenidis E (eds) *Proceedings of the 22nd engineering applications of neural networks conference*. Springer, Cham, pp 153–164
5. Muhammad S, Makhtar M, Rozaimie A, Aziz A, Jamal AA (2015) Classification model for water quality using machine learning techniques. *Int J Softw Eng Appl* 9:45–52. <https://doi.org/10.14257/ijseia.2015.9.6.05>
6. Shamsuddin IIS, Othman Z, Sani NS (2022) Water quality index classification based on machine learning: a case from the Langat river basin model. *Water* 14(19). <https://doi.org/10.3390/w14192939>
7. Tyagi S, Sharma B, Singh P, Rajendra D (2013) Water quality assessment in terms of water quality index. *Am J Water Resour* 1(2):34–38. <https://doi.org/10.12691/ajwr-1-3-3>

# Evaluation of Groundwater Quality in an Urbanized Watershed with a Special Reference to Heavy Metal Concentration



Apurva Marathe  and Prakash Samnani 

## 1 Introduction

Water stands as the paramount natural asset employed for potable consumption, agricultural irrigation, and industrial applications across diverse regions. Not solely a vital elemental component for organisms and vegetation, water also serves as a central determinant of human existence within the biosphere [1]. Throughout history, river waters have nurtured civilizations and sustained diverse life forms. Nevertheless, swift urbanization coupled with economic and industrial advancement has significantly strained this essential resource, resulting in compromised water quality and ecosystem services. Additionally, rivers serve as a receptacle for sewage, industrial discharges, and agricultural runoff [2]. Groundwater contamination by heavy metals presents a significant environmental concern. While some essential heavy metals have health benefits, surpassing permissible concentrations can lead to health issues. Introduction of heavy metals into aquifer systems can occur through both natural occurrences and anthropogenic activities. Vegetation plays a role in concentrating these metals, subsequently transferring them to surface and groundwater. Industrial activities like metal plating, alloy production, mining, and cleansing contribute substantially to heavy metal influx in aquatic environments [3]. Another route of contamination arises from excessive agrochemical use, with retained compounds infiltrating groundwater via irrigation return. Bio-toxic heavy metal buildup in crops and their subsequent transfer within the food chain pose potential threats to human health [4].

---

A. Marathe

Department of Environmental Studies, Faculty of Science, The Maharaja Sayajirao University of Baroda, Vadodara 390002, India

P. Samnani (✉)

Department of Chemistry, Faculty of Science, The Maharaja Sayajirao University of Baroda, Vadodara 390002, India

e-mail: [prakash.samnani-chem@msubaroda.ac.in](mailto:prakash.samnani-chem@msubaroda.ac.in)

Heavy metal content requires monitoring to assess the fitness of groundwater for drinking, agricultural, and industrial purposes. Interpolation in Geographic Information Systems (GISs) involves estimating values for places within a spatial dataset by considering known values at the sampled locations. In scientific applications, interpolation proves beneficial when data is localized at specific points, but a continuous and cohesive surface or map is required. The primary objective of interpolation is to fill in the gaps between data points, thereby improving the comprehensive and aesthetically pleasing portrayal of spatial phenomena. In this investigation, the method employed is inverse-distance weighting, a technique that allocates values to locations by considering their proximity and the known values of adjacent points. The closer a point is to the location being estimated, the more influence it has on the calculated value. This technique has seen widespread application in investigations of groundwater quality and pollution. Numerous research investigations are underway to examine the surface water quality of the Vishwamitri River, providing evidence of contamination in the river's surface water [5–8]. However, there are a limited number of research endeavors focused on investigating the quality of groundwater in the Vishwamitri watershed, particularly with respect to heavy metals. This study involves employing the HPI and conducting statistical analyses to examine the contamination of groundwater by heavy metals. Recognizing the significance of heavy metal presence in groundwater and its potential health effects, such a high-tech investigation holds substantial value.

## 2 Material and Methodology

### 2.1 Study Area, Topography, and Climate

The current research aims to examine the quality of groundwater in the Vishwamitri watershed, situated within the Vadodara and Panchmahal districts of Gujarat, India, Figs. 1 and 2. The study area lies between 22°10' N and 22°49' N latitudes and 73°00' E and 73°49' E longitude. Geomorphologically, the area can be classified into Hilly undulating areas and alluvial flat plains. Climatically, the study area of the district is arid to semiarid in nature. In the region, there exist three principal seasons, namely winter, summer, and monsoon. The drainage pattern identified within the Vishwamitri watershed exhibits a dendritic configuration. The aggregate geographic expanse of the watershed is 1134.15 km<sup>2</sup>. The topography within this region is predominantly characterized by a flat to gently sloping terrain, with elevations ranging from 16 to 795 m above mean sea level [9].

## Location Of Study Area- Vadodara &amp; Panchmahal

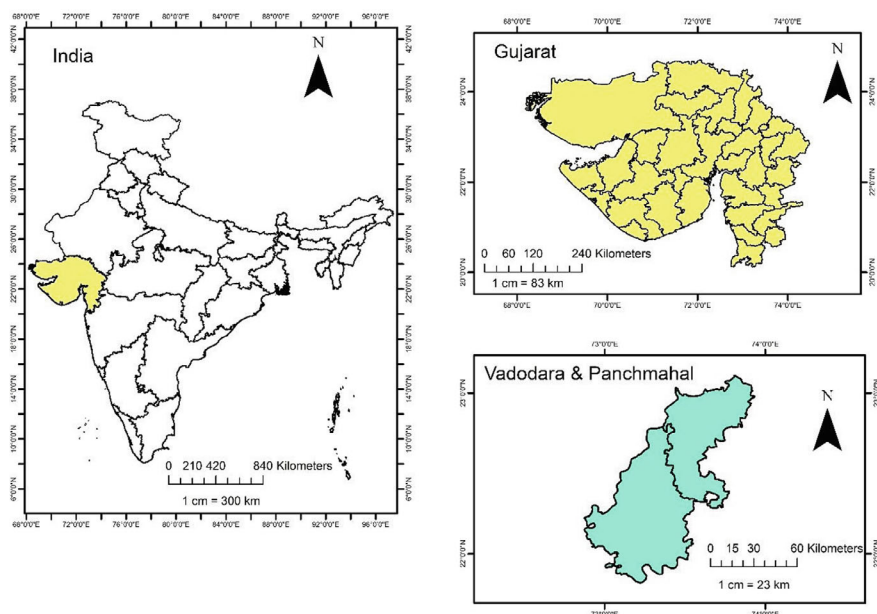


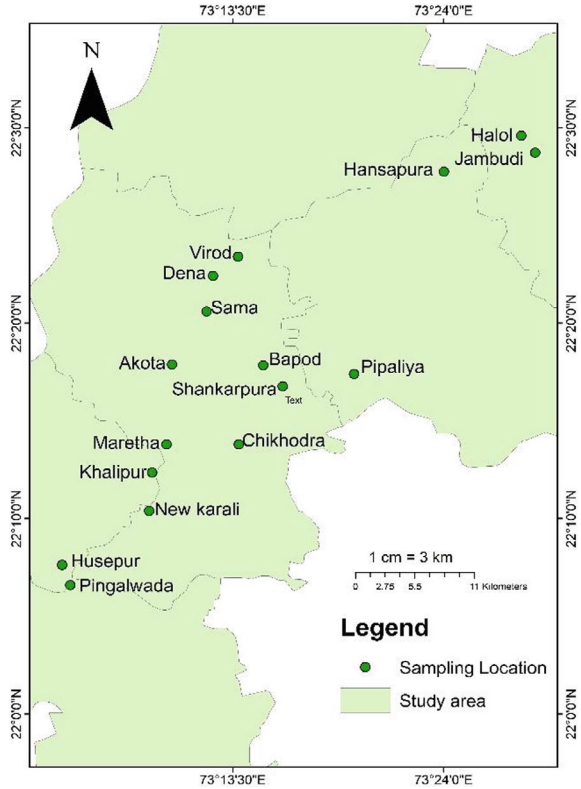
**Fig. 1** Depicting study area specifics

## 2.2 Methodology

In total, 16 groundwater samples were procured from boreholes situated at selected locations across the study area during April 2022 (pre-monsoon) and October 2022 (post-monsoon). The longitude and latitude (GPS) coordinates of each sampling location were noted down using the GPS Waypoints application. The Microsoft Excel file undergoes conversion into the Comma-Separated Values (CSV) format which is intended for mapping the geographical coordinates of sampling points in ArcGIS. The particulars of sampling sites, including their corresponding latitude and longitude coordinates, are delineated in Table 1, while the geographical positions are visually depicted in Fig. 2.

While collecting groundwater samples, the borewells were purged for approximately 5 min to remove stagnant water, to obtain a proper representative sample. Groundwater samples were acquired, and measurements of pH and temperature were performed onsite, with a portable pH meter instrument. The collected water samples were subsequently stored using high-density polyethylene (HDPE) containers. 0.5 mL of 65% AR Grade  $\text{HNO}_3$  solution (Merck) was added to acidify the samples to  $\text{pH} < 2$ , to prevent metal precipitation. The water specimens underwent filtration using Whatman filter paper specifically number 42. The filtered samples were stored

**Fig. 2** Points of sampling in the study region



in HDPE containers and stored in the refrigerator at a temperature of  $<4\text{ }^{\circ}\text{C}$ , until analysis. The water samples were further analyzed for determining the presence of heavy metals including Fe, Pb, Cr, Cu, Mn, and Cd; using an Atomic Absorption Spectrophotometer (AAS) (Perkin Elmer) instrument at the Department of Environmental Studies of University.

Throughout the analytical procedures, the standards of the American Public Health Association (APHA 2005) were followed [10]. Calibration standards provided by Merck and ultra-pure water were utilized to evaluate the precision of the analysis, with the inclusion of standards and blanks in the experimental procedure. The range of standards for Cr, Cd, Fe, Mn, Pb, and Cu are given in Table 2. ArcGIS software 10.5 was employed and inverse distance weighted (IDW) interpolation technique, to plot spatial maps.

**Table 1** Details of sampling points in study zone

Sr. No.	Location	Latitude	Longitude
1	Pingalwada	22.24075	73.22006
2	Chikhodra	22.22748	73.23041
3	Maretha	22.22585	73.17167
4	Khalipur	22.20591	73.15794
5	New Karali	22.17329	73.15553
6	Husepur	22.12724	73.08316
7	Akota	22.29805	73.17452
8	Shankarpura	22.27953	73.26641
9	Pipaliya	22.29001	73.32569
10	Bapod	22.29742	73.25022
11	Sama	22.34329	73.20317
12	Dena	22.37373	73.20861
13	Virod	22.39011	73.22936
14	Halol	22.49319	73.46461
15	Jambudi	22.47862	73.47615
16	Hansapura	22.46246	73.40038

**Table 2** Range of standards for Cr, Cd, Fe, Mn, Pb, and Cu

Sr. No.	Element	Wavelength (nm)	Min. sensitivity (mg/L)	Max. sensitivity (mg/L)	Standards (mg/L)
1	Cr	357.87	0.078	4.0	1.0, 2.0, 3.0, 4.0
2	Cd	228.80	0.010	0.5	0.1, 0.3, 0.4, 0.5
3	Fe	248.33	0.040	2.0	0.5, 1.0, 1.5, 2.0
4	Mn	279.48	0.016	1.0	0.5, 0.6, 0.8, 1.0
5	Pb	283.31	0.180	8.0	0.5, 4.0, 6.0, 8.0
6	Cu	324.75	0.025	1.3	0.1, 0.4, 0.8, 1.3

### 2.3 Heavy Metal Pollution Index

The HPI serves as a crucial instrument in the assessment of pollution related to heavy metals in water resources. Its significance lies in furnishing a quantitative assessment of pollution, highlighting regions characterized by elevated levels of pollution, prioritizing management interventions, and enabling informed decision-making to enhance water quality. The procedure for calculating the HPI involves several steps: selection of heavy metals, sampling and data collection, analysis, calculation of sub-indices, weighting, and aggregation, calculating the HPI, interpretation of HPI values, and spatial mapping and visualization. Utilizing the HPI to interpret the spatial and seasonal variations in heavy metal concentrations proves valuable in evaluating

the extent of pollution burden and the water quality trend in groundwater of river watershed [11].

The methodology of the HPI entails the allocation of a weightage ( $W_i$ ) to selected parameters, wherein the weightage is quantified as a numerical coefficient ranging within the interval of zero to one. This coefficient delineates the comparative importance of distinct quality attributes, displaying an inverse correlation with the established reference standard ( $S_i$ ) for each parameter, [12]. Within the scope of this investigation, the concentration thresholds, specifically, the uppermost acceptable value for potable water is called as standard value (denoted as  $S_i$ ) and the permissible threshold referred to as ideal value (denoted as  $I_i$ ) for each parameter, were derived from the stipulated criteria outlined in the Indian potable water regulations as documented within the Bureau of Indian Standards publication of 2012 (IS 10500). The  $S_i$  parameter signifies the utmost admissible concentration within potable water under circumstances where no viable alternative water source is accessible. Meanwhile, the  $I_i$  parameter designates the established standard boundaries for identical parameters within potable water [2]. HPI has been developed and formulated [13] as

$$\text{HPI} = \frac{\sum_{i=1}^n W_i Q_i}{\sum_{i=1}^n W_i}, \quad (1)$$

wherein the variable “ $Q_i$ ” denotes the sub-index associated with the “ $i$ th” parameter pertaining to heavy metal attributes, “ $W_i$ ” signifies the unit weight allocated to the “ $i$ th” parameter, and “ $n$ ” represents the numerical value denoting the count of parameters under consideration. The determination of the parameter’s unit weight ( $W_i$ ) is computed by,

$$W_i = k/S_i, \quad (2)$$

where  $S_i$  represents the standard numerical value for  $i$ th parameter (acceptable value, BIS 2012) and  $k$  represents the constant of proportionality (generally considered 1).

The computation of the sub-index ( $Q_i$ ) for the given parameter is conducted through a mathematical formula,

$$Q_i = \sum_{i=1}^n \frac{\{M_i - I_i\}}{S_i - I_i} \times 100. \quad (3)$$

In the given expression (3), the variable  $M_i$  represents the analyzed concentration of the heavy metal associated with the  $i$ th parameter. The variable  $I_i$  denotes the ideal or permissible concentration specified by the BIS (2012) standard for the  $i$ th parameter, while  $S_i$  signifies the standard or acceptable concentration level set by the BIS (2012) standard for the  $i$ th parameter. The quantity  $[M_i - I_i]$  signifies the difference between the two values, with no consideration for the algebraic sign, essentially indicating the absolute value.

In the framework for drinking water, it is commonly stipulated that the “critical pollution index” threshold for the HPI value is 100 [14].

### 3 Results and Discussion

#### 3.1 Heavy Metals

Tables 3 and 4 present the descriptive statistics of physical and chemical parameters and concentration of heavy metal in groundwater samples of pre-monsoon and post-monsoon season, including minimum, maximum, and mean values of each parameter, as well as their corresponding standard deviations. The acquired results were subsequently contrasted with criteria set for drinking water outlined by Bureau of Indian Standards (BIS) guidelines of 2012 given in Table 5 [12].

In the pre-monsoon period, the pH values observed in groundwater samples within the study area exhibited a range from 6.1 (at Khalipur) to 8.1 (at Sama), with a mean of  $7.09 \pm 0.48$ . In the post-monsoon period, the pH values in groundwater samples within the investigated region exhibited a range from 7.05 (Shankarpura) to 8.02 (Sama), demonstrating an average of  $7.66 \pm 0.26$ . pH influences the ionization state

**Table 3** Descriptive statistics of physical and chemical parameters and concentrations of heavy metal in pre-monsoon groundwater samples

Statistical description	pH	Temp. (°C)	Cd (ppm)	Cr (ppm)	Cu (ppm)	Fe (ppm)	Pb (ppm)	Mn (ppm)	HPI
Average	7.09	33.13	0.007	0.084	0.007	0.11	0.111	0.06	12.65
Max	8.10	36.60	0.022	0.523	0.055	0.40	0.196	0.50	81.08
Min	6.10	31.00	0.003	BDL	BDL	0.01	0.012	0.01	06.49
Std. deviation	0.48	1.90	0.006	0.119	0.014	0.12	0.038	0.12	17.75

where, BDL = Below Detection Limit

**Table 4** Descriptive statistics of physical and chemical parameters and concentrations of heavy metal in post-monsoon groundwater samples

Statistical description	pH	Temp. (°C)	Cd (ppm)	Cr (ppm)	Cu (ppm)	Fe (ppm)	Pb (ppm)	Mn (ppm)	HPI
Average	7.7	29.9	0.012	0.078	0.013	0.135	0.083	0.116	12.86
Max	8.0	32.1	0.044	0.738	0.044	0.897	0.126	0.533	81.31
Min	7.0	26.0	0.006	BDL	0.003	BDL	0.054	BDL	06.03
Std. deviation	0.2	01.5	0.009	0.189	0.012	0.224	0.018	0.146	17.79

where, BDL = Below Detection Limit

**Table 5** BIS standards for selected heavy metals

Parameter	BIS (IS 10500:2012)	
	AL	PL
pH	6.5–8.5	–
Temperature (°C)	–	–
Cd (ppm)	0.03	No relaxation
Cr (ppm)	0.05	No relaxation
Cu (ppm)	0.05	1.5
Fe (ppm)	0.3	No relaxation
Pb (ppm)	0.1	No relaxation
Mn (ppm)	0.1	0.3

where *AL*—acceptable limit, *PL*—permissible limit

of heavy metals in aqueous systems, thereby altering their affinity for binding to solid phases and influencing their transport and availability. At different pH levels, heavy metals may undergo hydrolysis reactions, forming various soluble and insoluble species. This in turn affects their mobility and potential to adsorb onto surfaces such as minerals or organic matter. Consequently, variations in pH can lead to shifts in heavy metal speciation, solubility, and subsequent concentration in environmental matrices. Tables 3 and 4 show that the concentration of iron (Fe) during the pre-monsoon season varied between 0.01 and 0.40 mg/L with a mean value of 0.11 mg/L and only two samples surpassed the specified limit samples exceeded the permissible limit (i.e., New Karali and Jamudi). For post-monsoon, the mean value of iron (Fe) is 0.14 mg/L and the concentration for selected locations ranges from 0.00 to 0.90 mg/L. Although minor quantities of iron in potable water typically pose no harm, an elevated intake of iron can lead to health complications.

Iron, under various natural environmental conditions, exhibits the ability to undergo changes in its oxidation state due to fluctuations in oxygen and pH levels in the aqueous phase. During weathering, iron is found in the form of Fe oxides. In the aqueous phase, iron exists as two species:  $\text{Fe}^{2+}$  and  $\text{Fe}^{3+}$ .  $\text{Fe}^{2+}$  shows moderate mobility, while  $\text{Fe}^{3+}$  exhibits poor mobility due to precipitation as hydrous Fe oxides when pH exceeds 3.

Iron-rich water can accelerate the corrosion of plumbing and infrastructure, leading to the release of other metals like lead and copper into the water, further compromising water quality. When used for irrigation, high iron water can reduce soil permeability and affect plant growth and yield. The upper threshold allowable value by BIS (2012) regulations of iron (Fe) is 0.3 mg/L. During the pre-monsoon period, the sampling at location 18 (Shankarpura) revealed manganese concentrations ranging from 0.01 to 0.50 mg/L. The mean concentration was determined to be 0.06 mg/L, accompanied by a standard deviation of 0.12 mg/L. In the post-monsoon period, the observed minimum concentration was 0.00 mg/L, and the maximum concentration recorded was 0.53 mg/L, yielding an average concentration of 0.12 mg/L with a standard deviation of 0.15 mg/L. Consequently, there were no substantial

alterations observed in the manganese concentration within groundwater samples between the pre-monsoon and post-monsoon periods. The maximum permissible limit of manganese (Mn) is 0.3 mg/L as specified by the BIS (2012). All groundwater samples analyzed within the study area conform to the permissible limits of manganese as defined by the BIS (2012), except for a sample from Shankarpura. The predominant cause of heightened manganese (Mn) levels observed in groundwater within particular aquifers on a regional scale is attributed to the decomposition of organic matter and the reduction of iron (hydro)oxides in the sediment occurring under conditions of reduction. Elevated levels of exposure to manganese have been correlated with neurotoxic effects, particularly in children and infants.

The concentration range of copper (Cu) at all sampling locations is within the permissible limit described by BIS (2012) standard for drinking water (i.e., 1.5 mg/L) during both seasons. The highest concentration of (Chromium) Cr at sampling locations is 0.523 mg/L (i.e., Shankarpura) and absent in the groundwater sample of Pingalwada during the pre-monsoon season, with an average concentration of 0.08 mg/L and standard deviation of 0.11 mg/L. While for post-monsoon studies, Cr concentration was detected only in groundwater samples of 4 sampling locations, where the highest concentration of Cr was found to be 0.74 mg/L (i.e., Shankarpura), and in groundwater samples of the remaining 12 sampling locations, Cr was absent, with average concentration is 0.77 mg/L, and standard deviation of 0.18 mg/L. The maximum acceptable limit of Cr is 0.05 mg/L as specified by the BIS (2012). The findings illustrated a reduction in the level of chromium concentration (Cr) at the majority of sampling sites following the monsoon season, with a few exceptions. It is important to note that chromium is recognized as a human carcinogen. Extended contact with elevated concentrations of chromium in drinking water has been linked to an elevated susceptibility to the development of lung, gastrointestinal, and various other forms of cancer.

The concentration of Cadmium (Cd) at all sampling locations exceeds the 0.003 mg/L BIS limit (2012) during both seasons. During the pre-monsoon period, the concentration range of Cd at sampling locations varied from 0.022 mg/L (i.e., Shankarpura) to the lowest concentration of 0.003 mg/L at Pingalwada and Chikhodra, with an average concentration of 0.007 mg/L and standard deviation of 0.006 mg/L, while during the post-monsoon time, the concentration range of Cd at sampling locations varied from 0.044 mg/L (i.e., Shankarpura) to the lowest concentration of 0.006 mg/L at Pingalwada and Chikhodra, with an average concentration of 0.012 and standard deviation of 0.009 mg/L. The maximum acceptable limit of Cd is 0.003 mg/L as specified by the BIS (2012). The results obtained depicted concentration levels of Cd increased in post-monsoon when compared to pre-monsoon, which concluded that there can be leaching of Cd into groundwater. Cadmium sorption is enhanced by the presence of high amounts of hydrous oxides, clay minerals, and organic matter, and its mobility is further influenced by pH, the redox state, and the ionic strength of the solution [15]. As per the classification by the International Agency for Research on Cancer (IARC) in 1993, cadmium is categorized under Group 1, indicating its carcinogenicity to humans [16]. Due to its bio-accumulative nature, cadmium has the capacity to progressively accumulate

within the organism’s system. Long-term exposure to elevated cadmium levels in drinking water can lead to various health problems in humans, including kidney damage, osteoporosis, respiratory issues, and cardiovascular problems.

Based on the acquired results, it was noted that the concentration of Lead (Pb) is exceeding the maximum acceptable limit of Pb (i.e., 0.01 mg/L) as specified by the BIS (2012) [16]. In adults, lead exposure manifests as memory deficits, abdominal pain, kidney impairment, hypertension (high blood pressure), and muscular weakness.

According to Fig. 3, the average heavy metals’ concentration follows the trend Fe (0.111 mg/L) > Pb (0.110 mg/L) > Cr (0.083 mg/L) > Mn (0.062 mg/L) > Cd (0.007 mg/L) > Cu (0.006 mg/L) for pre-monsoon samples, while for post-monsoon season, the average heavy metals’ concentration follows the trend Fe (0.135 mg/L) > Mn (0.116 mg/L) > Pb (0.083 mg/L) > Cr (0.078 mg/L) > Cu (0.013 mg/L) > Cd (0.012 mg/L) as depicted in Fig. 4.

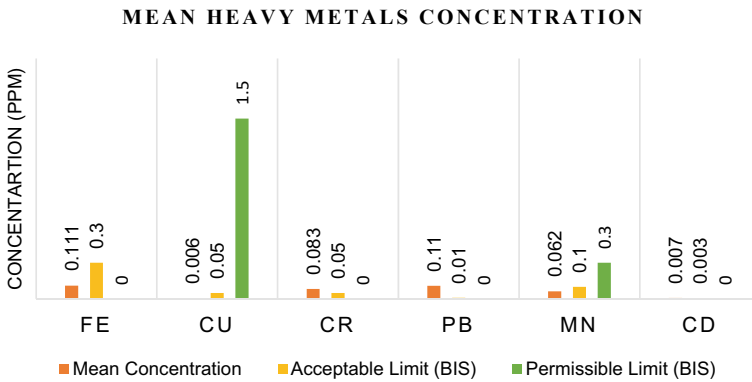


Fig. 3 Mean heavy metals’ concentration (pre-monsoon)

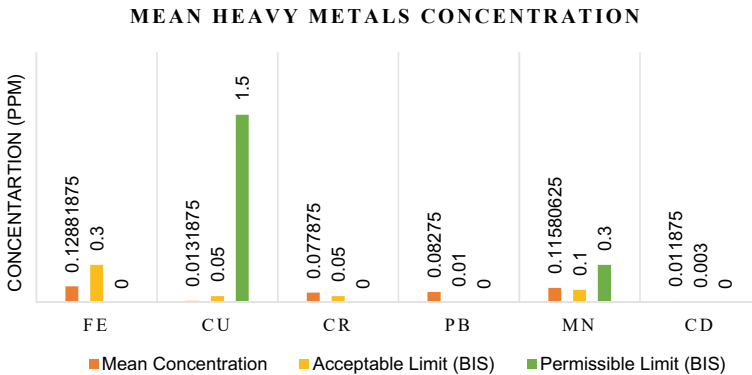


Fig. 4 Mean heavy metals’ concentration (post-monsoon)

### 3.2 Heavy Metal Pollution Index (HPI)

HPI was independently computed for each individual sampling station in the research study. The weightage ( $W_i$ ) assigned to Fe and Mn is relatively low, as these parameters have minimal impact on the whole HPI evaluation of groundwater. Conversely, heavy elements such as Pb, Cd, and Cr, which are not granted leniency in portable water standards, carry significant weightage ( $W_i$ ) in the HPI calculation. Consequently, even their lower concentrations in water samples lead to lower quality of water and result in elevated HPI values. The computation was done for percentage deviation and mean deviation, alongside the mean HPI value, for every location. During pre-monsoon, the range of the HPI varied from 6.49 (Chikhodra) to 81.08 (Pingalwada), with an average HPI value of  $12.65 \pm 17.75$ , while during post-monsoon, the range of the HPI varied from 6.03 (New Karali) to 81.31 (Pingalwada), with a mean HPI value of  $12.86 \pm 17.79$ . There is no statistically significant disparity observed in the mean values of the HPI between pre-monsoon and post-monsoon samples. The observed groundwater sample data has been employed to appraise the HPI and validate the effectiveness of the index model. The findings indicate that among the 16 sampled stations, 6.25% exhibit a HPI surpassing the mean threshold of 50. Conversely, 93.75% of the samples collected in both pre- and post-monsoon seasons demonstrate an HPI below the mean value of 50.

### 3.3 Spatial Maps

The spatial arrangements of heavy metals were cartographically depicted utilizing the inverse-distance weighted (IDW) method, which computes concentrations in close proximity to the specific geographical coordinates of the sampling locations. ArcGIS 10.6 software is used for preparation of IDW maps, incorporating longitude and latitude data. In the realm of groundwater quality assessment, factors such as pH and various heavy metal concentrations as well as HPI, ArcGIS spatial analyst modules were employed. IDW interpolation technique is applied for determining cell values based on a weighted combination of sample points, dependent on inverse distance [1]. Visual comparison of concentrations facilitated proposing of metal distributions over time and location. According to Figs. 5 and 6a–f, graphical representation illustrates spatial distribution patterns of chosen heavy metals (Cr, Fe, Pb, Mn, Cd, Cu) within the study area in the periods preceding and following the monsoon season respectively, and concentration (color pattern) ranges from low (green) to high (red) concentrations.

Overall pattern indicates poorer groundwater quality in the south compared to the north in both pre-monsoon and post-monsoon. Heavy metals and HPI hotspot are represented in the southern and central region of the study area. Figure 7a as well as Fig. 7a, b shows the difference between HPI before monsoon and after monsoon. The information can be observed in the graphical representation which depicts that the

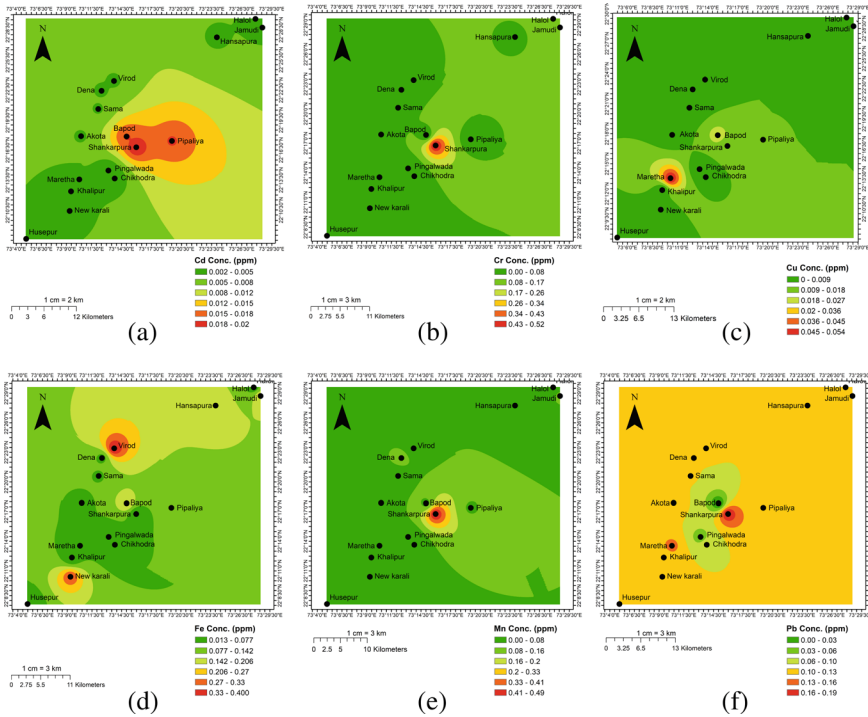


**Fig. 5** Interpolated spatial maps for heavy metals for pre-monsoon, **a** Cd, **b** Cr, **c** Cu, **d** Fe, **e** Mn, **f** Pb

highest HPI value is observed at Pingalwada. Pingalwada is the sampling point where Vishwamitri river merges into Dhadhar river. A possible reason for such a high score of HPI can be the confluence of rivers inducing alterations in flow dynamics, resulting in sediment deposition. Pollutants, including heavy metals, may accumulate at the confluence point due to the merging of waters carrying contaminants from respective upstream areas. Elevated concentrations of pollutants at the confluence are likely if upstream rivers have been contaminated through agricultural runoff, industrial discharges, or other pollution sources. This issue will be further investigated.

Among the six heavy metals examined for analysis, parameters like lead and cadmium, which are of high concern, are exceedingly even the admissible limit of portable water (BIS 2012).

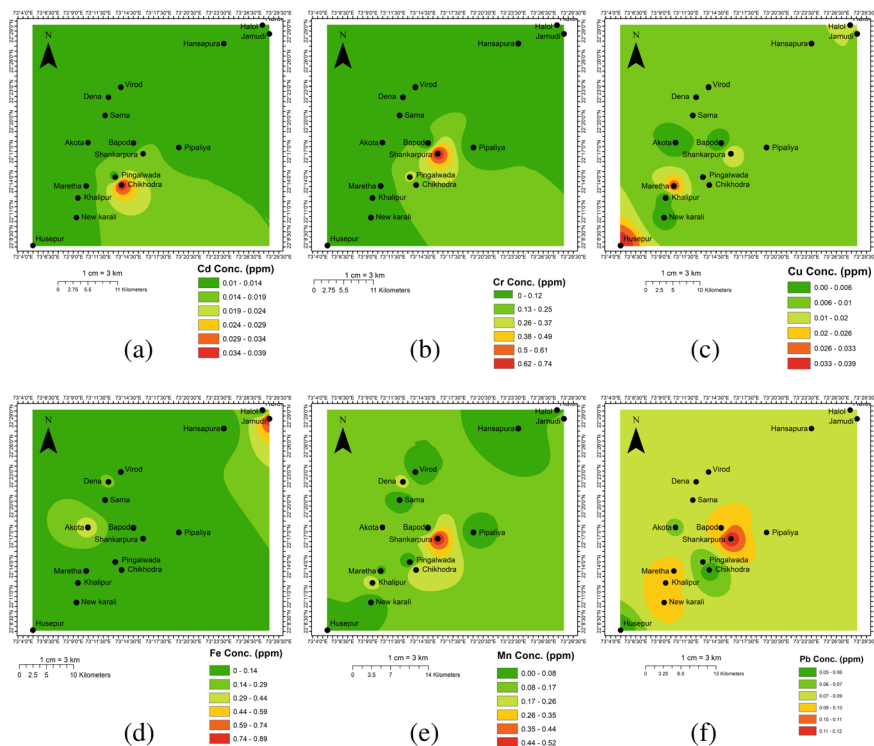


Fig. 6 Interpolated spatial maps for heavy metals for post-monsoon

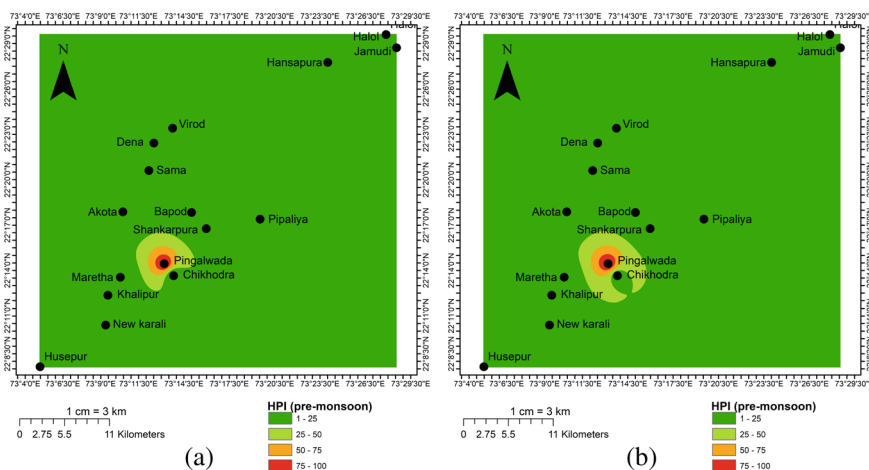


Fig. 7 Interpolated spatial maps for Heavy Metals' Pollution Index, a pre-monsoon, b post-monsoon

## 4 Conclusion

For the selected heavy metals, all the values obtained after calculation are below the critical value of 100 of HPI [17]. Thus, the groundwater quality of the Vishwamitri watershed falls below the threshold of critical pollution levels in terms of heavy metal concentration. The observed data trends indicate that the average concentrations of cadmium (Cd) and lead (Pb) during the pre-monsoon period are notably lower than the corresponding averages observed during the post-monsoon period. This discrepancy implies the operation of hydrological processes such as runoff and percolation, which contribute to an augmentation in the levels of these substantial metallic elements within the groundwater matrix. The graphic representation further substantiates this assertion. Specifically, the geographic visualization demonstrates a conspicuous pattern whereby the southern and central areas of the research area depict comparative elevated levels of heavy metal pollution the northern area. This discrepancy strongly implies the translocation of contaminants from the northern region to the southern region, primarily facilitated by the topographical gradient inherent to the study site. Consequently, the lower topographical stratum emerges as particularly susceptible to the accumulation of heavy metals within the groundwater. Despite this, local inhabitants persist in using the contaminated water, thereby exposing themselves to various health risks. It is now imperative to proactively curtail pollution by implementing precise management strategies such as effective treatment of industrial effluents and adherence to legal standards for wastewater disposal. The consumption of such water could exacerbate existing health ailments, underscoring the necessity of remediating groundwater to guarantee its portability. In the future, this study aims to identify possible heavy metal contamination sources using land use and land cover change analysis (LULCC), specifically cadmium (Cd) and lead (Pb) and undertake Health Risk Assessment (HRA) and Hazard Quotient analyses in order to determine the potential impact of being exposed to heavy metals on human health.

## References

1. Selvam S, Venkatramanan S, Singaraja C (2015) A GIS-based assessment of water quality pollution indices for heavy metal contamination in Tuticorin Corporation, Tamilnadu, India. *Arab J Geosci* 8:10611–10623
2. Bhardwaj R, Gupta A, Garg J (2017) Evaluation of heavy metal contamination using environmetrics and indexing approach for River Yamuna, Delhi stretch, India. *Water Sci* 31(1):52–66
3. Shankar BS (2019) A critical assay of heavy metal pollution index for the groundwaters of Peenya Industrial Area, Bangalore, India. *Environ Monit Assess* 191:289
4. Vetrimerugan E, Brindha K, Elango L et al (2017) Human exposure risk to heavy metals through groundwater used for drinking in an intensively irrigated river delta. *Appl Water Sci* 7:3267–3280

5. Magadum A, Patel T, Gavali D (2017) Assessment of physicochemical parameters and water quality index of Vishwamitri River, Gujarat, India. *Int J Environ Agric Biotechnol* 2(4):1505–1510
6. Bhangaonkar PD, Patel JS (2019) Assessment of heavy metals in surface water of Vishwamitri River. *Int J Hydrol Sci Technol* 9(6) (2019)
7. Siddha S, Sahu P (2022) Understanding the geochemical evolution of groundwater in Central Gujarat, India: an integrated hydrogeochemical and multivariate statistical approach. *Arab J Geosci* 15:1117
8. Mehta M (2020) Urban ecosystem changes around natural drains: case of Becharji Nala of Vishwamitri River in Vadodara City. *Int J Soc Sci* 9
9. Navadiya1 DP, Suryanarayana TMV (2016) Analysis of hydrological parameter using SWAT model: a case study of Subbasin of Vishwamitri watershed, Gujarat, India. In: National conference on water resources & flood management with special reference to flood modelling, October 14–15, SVNIT Surat
10. APHA (American Public Health Association) (2005) Standard methods for the examination of water and wastewater, 19th Edn. American Public Health Association, Washington
11. Reza R, Singh G (2010) Heavy metal contamination and its indexing approach for river water. *Int J Environ Sci Tech* 7(4):785–792
12. BIS 10500 (2003) Bureau of Indian Standards. New Delhi, India, Manak Bhavan
13. Venkata Mohan S, Nithila P, Jayarama Reddy S (1996) Estimation of heavy metals in drinking water and development of heavy metal pollution index. *J Environ Sci Health Part A Environ Sci Eng Toxicol* 31(2):283–289
14. Prasad B, Bose J (2001) Evaluation of the heavy metal pollution index for surface and spring water near a limestone mining area of the lower Himalayas. *Env Geol* 41:183–188
15. Kubier A, Wilkin RT, Pichler T (2019) Cadmium in soils and groundwater: a review. *Appl Geochem* 108:104388
16. International Agency for Research on Cancer (1993) Cadmium and cadmium compounds, vol 58. IARC, Lyon
17. Prasad B, Kumari P, Bano S et al (2014) Ground water quality evaluation near mining area and development of heavy metal pollution index. *Appl Water Sci* 4:11–17

# Identifying Climate Hotspots from Spatiotemporal Variation of Exposure Indicators for Southern Agro-Climatic Zone in Gujarat State, India



Daksh H. Soni and Geeta S. Joshi

## 1 Introduction

Climate change which can be described as long-term changes in the mean state of earth's atmospheric and land use compositions have been brought to light by numerous research works during past couple of decades. Such changes at global and/or regional level are said to be occurring due to increasing Green House Gases (GHG) eventually leading to warming of the planet [1]. Some of the observable climate change impacts such as snow-glacial melt, sea level rise, rainfall extremes, urban floods, heat/cold waves and droughts have negative socio-economic effects on humans and ecological abnormalities of biodiversity. One of the major climate change components is the exposure to climate hazards which can be analyzed through hydro-meteorological parameters such as temperature, rainfall and their long-term trends which helps in developing adaptation and mitigation policies at local level [2]. Significant research with emphasis on analyzing trends using non-parametric tests on various climate exposure indicators pointed toward the increasing or decreasing nature of trend with respective magnitude of trends [3–7].

The trends in rainfall and rainy days were analyzed in annual and seasonal time scales for Kashmir valley using MK test on IMD stations having data of varying time spans from the last century (1903–2002) explained significant decreasing in both rainfall and rainy days for monsoon and winter seasons in most stations [3]. The temperature and rainfall trends were investigated for the homogeneous zones of India utilizing MK and SEN tests on gridded monthly time series obtained from Indian Institute of Tropical Meteorology having data span 1904–2003 indicated significant

---

D. H. Soni · G. S. Joshi (✉)

Department of Civil Engineering, Faculty of Technology and Engineering, The Maharaja Sayajirao University of Baroda, Vadodara, Gujarat 390001, India

e-mail: [geeta.joshi-ced@msubaroda.ac.in](mailto:geeta.joshi-ced@msubaroda.ac.in)

positive trend for maximum temperature as well as non-significant negative trends for minimum temperature and rainfall over western region of India [4]. The long-term trends of temperature and rainfall indicators having varying time spans for upper basin of Tapi River of India were determined by applying MK, modified Mk and SEN tests highlighted negative trends in rainfall and rainy days but positive trends in rainfall intensity, hottest–coldest days and diurnal temperature range in the annual time series [5]. The spatial and temporal variations in exposure indicators were detected for the lower basin of Tapi River in India, by performing MK, SEN and Innovative Trend Analysis on stationary as well as gridded data of varying time spans noted positive trends in rainfall and minimum temperature of annual time series with high magnitudes in western parts and for maximum and mean temperature with high magnitudes in eastern parts [6]. The long-term trends in hydro-meteorological indicators of varying data spans for the lower basin of Narmada River in India were analyzed by conducting MK and SEN tests, observed positive trends in rainfall, maximum and minimum temperature in the recent years associated with anthropogenic land use changes [7].

The spatial and temporal variations in multiple exposure indicators drew attention toward identifying climate hotspots utilizing index-based approach. These hotspots can be described as the pockets that have higher probability of being exposed to climate hazards such as extreme temperatures and extreme rainfalls. The climate vulnerability of Mali is explained by de Sherbinin et al. [8], in the form of a map representing a spatial index comprised 18 different indicators of climate exposure, sensitivity and adaptive capacity aspects. The climate hazard mapping for Mali showed hotspots in the northern parts with decreasing rainfall and a very low adaptive capacity along with highlighting the use of PCA in preparation of a composite map as an alternative to overlay additive approach. The PCA in general is a dimension reduction method which identifies correlation among multiple input parameters of a particular location and returns a few uncorrelated factors giving similar representation, that of the original dataset [8]. The applicability of PCA in the field of hydrometeorology has been explored by a few researchers in the past decade [9–11].

The PCA was used to map socio-ecological susceptibility of Southern Africa considering 12 indicators of environmental, biophysical and socio-economic aspects having 10-arc minute spatial resolution with differing data spans obtained four PCs which explained 63.5% of total variation where PC4 was dominated by climatic indicators in the eastern regions [9]. The impacts of changing climate were analyzed by ten different exposure indicators of two stations located in opposite parts of Croatia having data span (1985–2016) by applying LR and MK test found positive trends for almost all the indicators in annual time series as well as PCA applied on LR coefficient and MK-Z value revealed PCs with more than 69% of total variation for both the stations [10]. The composite drought index (CDI) was prepared by employing PCA-derived weights on standardized precipitation, streamflow drought and vegetation condition indices having different time spans for Marathwada region of Maharashtra, India, obtained PC1 with highest variation of 62% and strong correlation of CDI with food grain production in comparison of other individual indices [11].

From the review of aforementioned research works, it was understood that investigation of climate hotspots is the need of the hour which has been addressed in current study as stated in the following objectives. (1) To analyze spatiotemporal trends in multiple indicators of exposure to climate hazards such as Rain, RD, LRD, NORD, Maxrain  $T_{\max}$ ,  $T_{\min}$  and HD of annual time series. (2) To assess key governing factors of aforementioned exposure indicators based on Principal Component Analysis (PCA). (3) To identify climate hotspots based on spatial distribution of composite PC map and trends magnitudes of exposure indicators.

## 2 Materials and Methods

### 2.1 Study Area and Data Collection

The southern agro-climatic zone in Gujarat state of India which is comprised of Navsari, the Dangs and Valsad districts covering about 6990 km<sup>2</sup> geographical extent located within 20.20° N to 21.10° N latitude and 72.50° E to 73.90° E longitude as shown in Fig. 1. The area elevation has a large variability with lowest of 22 m below mean sea level (msl) in the western parts which is a coastal region and 1282 m above msl in the north-east parts where Sahyadri mountain range is situated. The region observes semi-arid to dry sub-humid climate and comes under southern Gujarat heavy rainfall zone with average annual rainfall in the range of 2000 mm. The daily maximum temperature of the year ( $T_{\max}$ ) reaches up to 44 °C in summer and minimum temperature comes down to 7 °C in winter, whereas the annual mean temperature is about 27 °C. The soil profile changes drastically from loamy mixed with steep slopes in the north-east to black clayey in the central and saline soil in the south-west coastal belt with paddy, pulses and sugarcane as the major agricultural products. The study area also includes reserved and protected forest of about 1060 km<sup>2</sup> spread across eastern parts where majority of rural and tribal population resides. The major rivers of the region Purna, Ambika, Auranga, Par and Damanganga which are west flowing in the south of Tapi River lower basin. Due to high drainage density and steep slopes in the north-east parts, most of heavy rainfall quickly washes away causing less natural groundwater recharge. The rural agriculture is rain-fed in monsoon season, and during kharif and rabi seasons, it is being irrigated by surface and groundwater sources. The total population of the region is about 3.27 million and population density (person/km<sup>2</sup>) varies from 129 in the Dangs district which is totally rural area to 580 in Navsari and Valsad district which are mostly rural area with a few industries of textiles, pharmaceuticals, minerals, marine and fisheries [12]. The exposure indicators related to temperature and rainfall at 1° and 0.25° spatial resolution, respectively, have been obtained from IMD gridded data with daily frequency having time span 1951–2020 years [13, 14]. The southern agro-climatic zone including Navsari, Valsad and the Dangs districts with digital elevation and IMD temperature (6) and rainfall (21) grid points have been shown in Fig. 1.

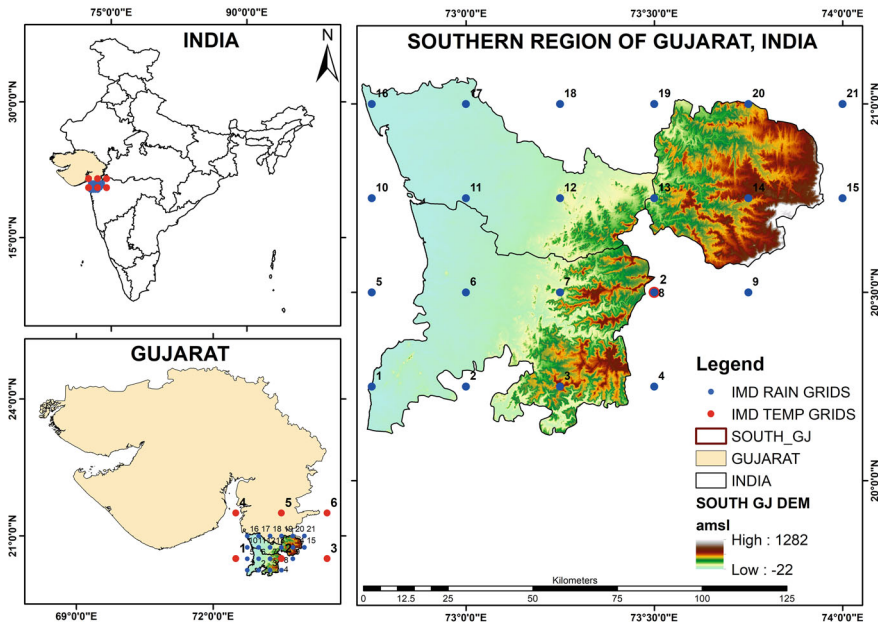


Fig. 1 Study area map of southern agro-climatic zone, Gujarat, India

## 2.2 Methodology

Present research was conducted in three steps. In the first step, necessary data were obtained and organized to perform non-parametric tests MK and SEN executed in R-studio software (version: 2023.03.0 + 386) using ‘trend’ package to determine significance and magnitude of trends of all the exposure indicators. The second step involved performing IDW interpolation [6, 7] of trend magnitudes for all the exposure indicators in GIS environment. The temperature indicators such as  $T_{\max}$ ,  $T_{\min}$  and HD were at  $1^\circ$  resolution, whereas rainfall indicators Rain, RD, LRD, NORD and Maxrain were at  $0.25^\circ$  resolution; thus, trend magnitudes of temperature indicators were extracted at rainfall (21) grid points using ‘Extract Multiple Values’ tool in ‘Extraction’ toolset from ‘Spatial Analyst’ toolbox in GIS environment. In the third and final stage, PCA was performed on trend magnitudes (SEN) of all the exposure indicators and factor scores of all PCs were obtained to prepare individual and composite PC map that helped in identifying climate hotspots.

### 3 Mann–Kendall Test (MK)

The non-parametric MK trend test by Kendall, Mann [15, 16] for analyzing trend significance is most widely used method due to its simple and robust nature in which the time series need not be normally distributed. The MK test statistics are equated below. Here,  $m_i$  and  $m_j$  are sequence-based time series data having  $n$  samples,  $t_p$  is the number of ties for  $p$ -th value,  $q$  is the number of tied values,  $\text{Var}(S)$  is the variance of ‘ $S$ ’ statistics and  $Z$  is the trend significance. If the  $Z$ -value at  $\alpha$  significance level is greater than  $Z_{1 - \alpha/2}$  taken from the normal distribution table, then the no trend null hypothesis is rejected.

$$S = \sum_{i=2}^n \sum_{j=1}^{i-1} \text{sign}(m_i - m_j), \tag{1}$$

$$\text{sign}(m_i - m_j) = \begin{cases} -1 & \text{for } (m_i - m_j) < 0 \\ 0 & \text{for } (m_i - m_j) = 0 \\ 1 & \text{for } (m_i - m_j) > 0 \end{cases}, \tag{2}$$

$$\text{Var}(S) = \frac{n(n - 1)(2n + 5) - \sum_{p=1}^q t_p(t_p - 1)(2t_p + 5)}{18}, \tag{3}$$

$$Z = \begin{cases} \frac{S-1}{\sqrt{\text{Var}(S)}} & \text{for } S > 0 \\ 0 & \text{for } S = 0 \\ \frac{S+1}{\sqrt{\text{Var}(S)}} & \text{for } S < 0 \end{cases}. \tag{4}$$

### 4 Sen’s Slope Estimation (SEN)

The trend magnitude has been determined from Sen’s slope estimator described by [17] where the slope indicates change in parameter per unit change in time. Here, all  $j < i$ ,  $P_i$  and  $P_j$  are data at  $i$  and  $j$  times. The decreasing or increasing nature of trend is indicated by negative and positive signs, respectively.

$$\beta = \text{Median} \left[ \frac{P_i - P_j}{(i - j)} \right] \tag{5}$$

## 5 Principal Component Analysis (PCA)

The PCA is basically a dimension reduction approach of multivariable statistics in which  $m$  number of input parameters are transformed into  $n$  number of PCs based on correlation, without changing the originality of underlying inputs [9]. First, the eigenvalues and eigenvectors are found based on the correlation matrix, and eigenvectors are converted to PCs in which the first PC highlights largest variation of total dataset. The relationship (positive or negative) between exposure indicators and PC containing the indicators are described as PC loadings [8]. In this research, PCA was employed on standardized trend magnitudes of exposure indicators at 21 grid points. The applicability of PCA was confirmed with Kaiser–Meyer–Olkin (KMO) where test value greater than 0.5 is desired and Bartlett where test value closed to zero is desired. The PCs were retained considering eigenvalues greater than 1 and Kaiser Normalization with varimax rotation. The PCA outcomes are in terms of correlation matrix, scree plot, table explaining total variance, rotated component matrix explaining PC loadings and factor scores of PCs which were achieved utilizing IBM SPSS Statistics software (Version 26).

## 6 Results and Discussion

Present research was attempted to identify climate hotspots in southern agro-climatic zone of Gujarat state, India, from the spatiotemporal variations of exposure indicators obtained from temperature and rainfall parameters. Trend significance and magnitudes of all the exposure indicators were determined from non-parametric tests MK and SEN, respectively, which were spatially distributed using IDW interpolation in GIS environment in the whole region for better visual interpretation. The PCA was performed on all the exposure indicators to obtain key governing factors (PCs) which also were envisioned for entire study area. Finally, aggregated composite PC map was prepared adopting ‘Raster Calculator’ tool of ‘Map Algebra’ toolset of ‘Spatial Analyst’ toolbox in GIS environment which helped in identifying climate hotspots.

### 6.1 Trends of Temperature Indicators

Figures 2 and 3 show significance and magnitude of trends for  $T_{\max}$  indicator for the southern Gujarat region. Positive trends denoted by yellow, orange and red colors are observed in the western parts which are a coastal zone and negative trends denoted by are observed in the eastern parts which are comparatively at a higher elevation with protected and reserved forest zone. The most negative magnitudes in eastern parts are in the range of ( $-0.001$  °C/year), whereas highest positive magnitudes in western parts are about  $0.0036$  °C/year, although the trends are not significant at 5%. Such

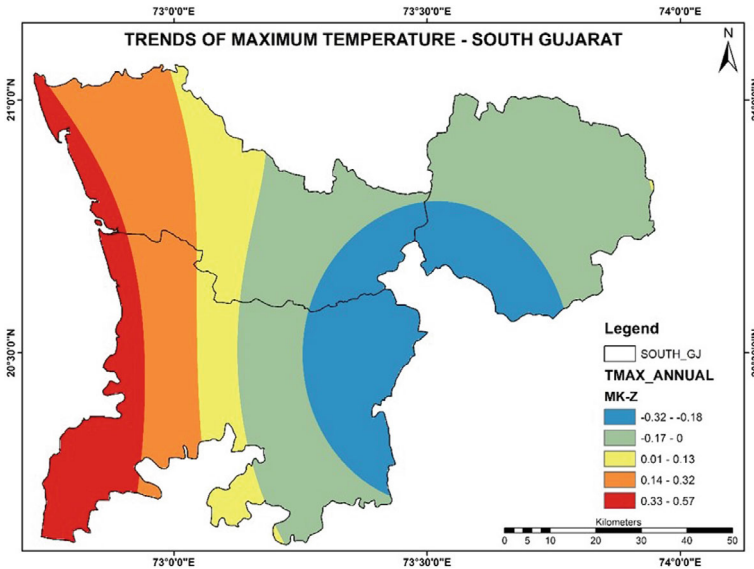


**Fig. 2** Trend significance of  $T_{max}$  by MK test

spatial variation pointed toward climate exposure due to rise in maximum temperatures is higher along the coastal belt. Figures 4 and 5 described below explain the trend significance and magnitudes of  $T_{min}$  exposure indicator in the southern agro-climatic zone of Gujarat state. Positive trends were found for the whole region in which significant (5%) trends have been represented by yellow and orange colors with red zone showing (1%) significant trends in Fig. 4. The highest positive trend magnitudes in the range of 0.03 °C/year along the coastal belt (western parts) indicated significant rising minimum temperatures causing climate exposure. The trend significance and magnitudes of HD exposure indicator is shown in Figs. 6 and 7. Positive trends indicated by orange and red zones are observed in the northern parts and negative trends denoted by blue and yellow colors are observed in the central and southern parts, but the trends are not significant at 5%. Peak positive trend magnitudes are in the range of (0.0739 days/year) observed in north-east parts which are protected and reserved forest zone, as well as in north-west parts which are saline coastal region. Such spatial distribution highlighted climate exposure due to rising hot days.

### 6.2 Trends of Rainfall Indicators

The spatial distributions of trend significance and magnitudes of Rain indicator for the southern Gujarat region have been delineated in Figs. 8 and 9, respectively. Positive trends indicated by orange zone are observed mostly in the western and

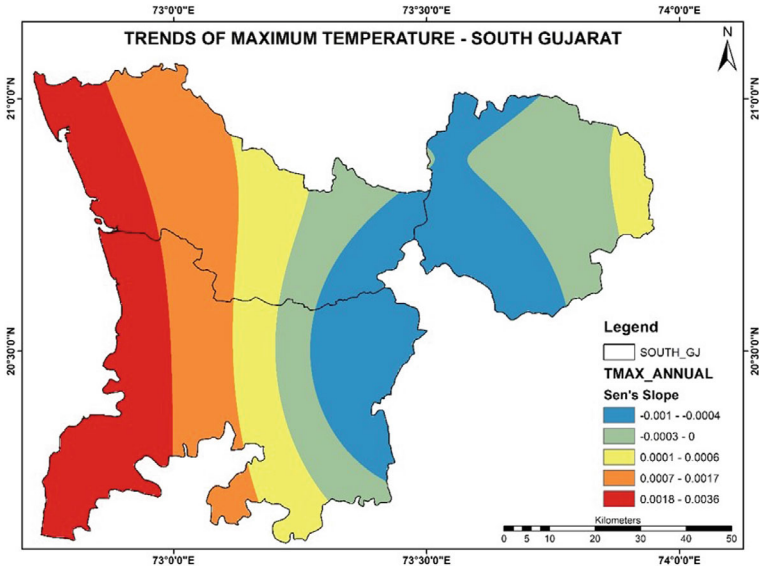


Fig. 3 Trend magnitude of  $T_{max}$  by SEN

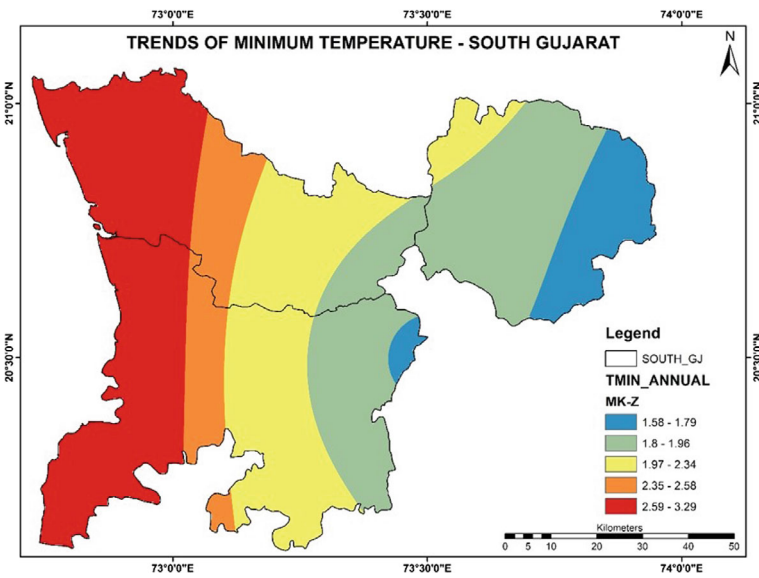


Fig. 4 Trend significance of  $T_{min}$  by MK test

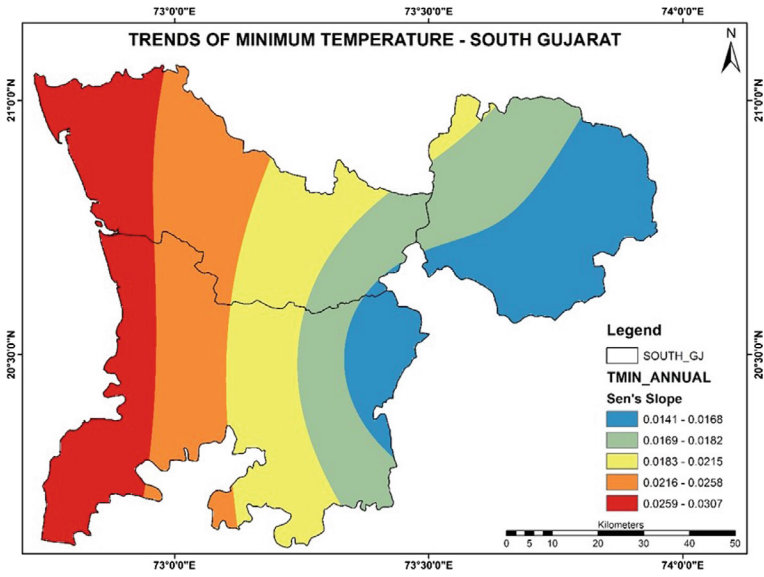


Fig. 5 Trend magnitude of  $T_{min}$  by SEN

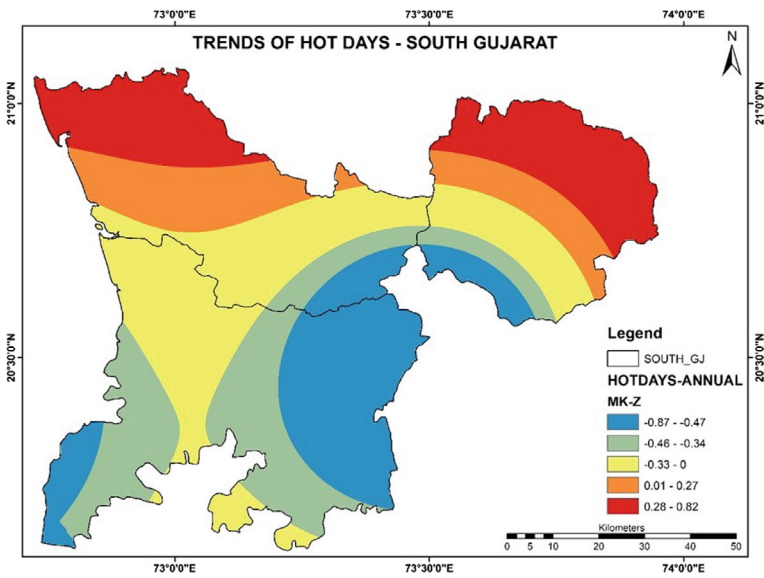
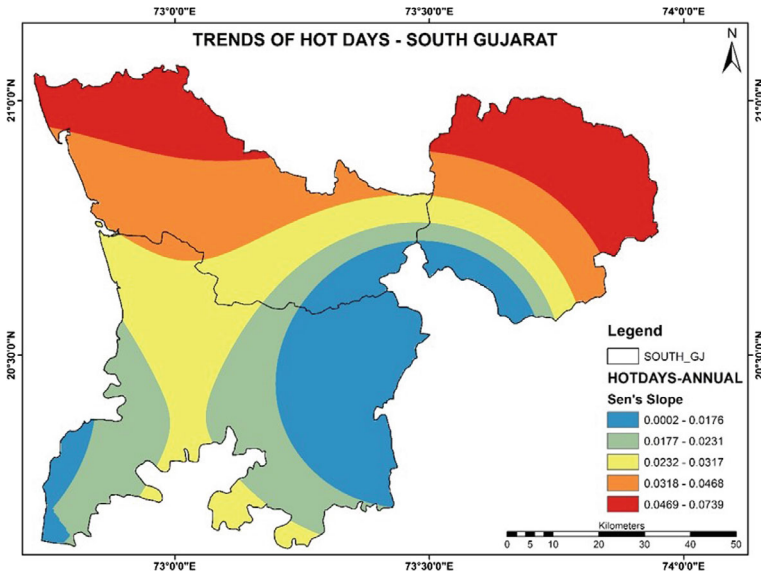
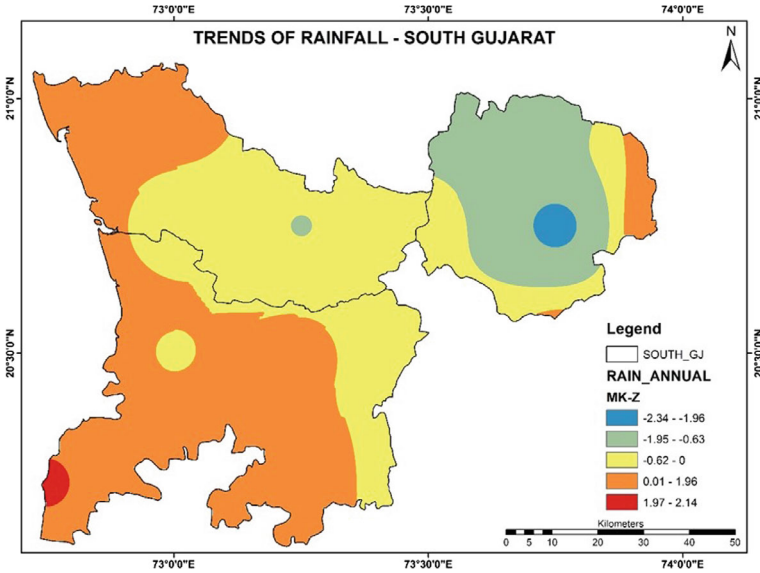


Fig. 6 Trend significance of HD by MK test



**Fig. 7** Trend magnitude of HD by SEN

southern parts, whereas negative trends indicated by yellow and light blue zone have been found in the north-east and central parts as described in Fig. 8. The significant (5%) increase denoted by red zone was observed in south-west parts along coastline, whereas significant (5%) decrease denoted by dark blue zone was found in north-east parts which is comparatively at a higher elevation with protected and reserved forests. Highest positive trend magnitudes in the south-west are about 6.72 mm/year, and most negative magnitudes are about  $-6.83$  mm/year in the north-east parts. The blue and yellow zones from Fig. 9 indicating negative magnitudes pointed toward high climate exposure due to less availability of water in near future. The orange zone showing positive magnitudes indicated low climate exposure, but the red zone showing highest positive trend magnitudes can contribute toward high climate exposure if high rainfall is found to be occurring in lesser number of rainy days and light rain days. In other words, if positive trends of Rain indicator are accompanied by negative trends of RD and LRD as well as positive trends of NORD indicators, such parts account for high climate exposure. Figures 10 and 11 explain the significance and magnitude of trends for RD exposure indicator for southern agro-climatic zone of Gujarat state. The positive trends have been found in the western parts delineated by red zone and negative trends denoted by orange, yellow and light blue zones have been found for major parts of the region except a few pockets in the north-east highlighted by dark blue zones indicated significant (5%) negative trends. The most negative trend magnitudes in the range of  $(-0.19$  days/year) found in the north-east which is the high elevation forest zone and highest positive magnitudes about  $(0.038$  days/year) have been observed in the south-west parts along the coastline. From the comparison of



**Fig. 8** Trend significance of Rain by MK test

trend magnitudes of Rain and RD indicators, similar patterns were found in majority of the region, but a few pockets in north-west and central parts highlighted increasing rainfall along with decreasing rainy days pointing toward high climate exposures in such areas due to rainfall extremity.

The trend significance and magnitudes of LRD indicator have been spatially distributed for the southern Gujarat region as described in Figs. 12 and 13, respectively. Negative trends were found for majority of the region except a few pockets in the south-east denoted by red zone in which significant (5%) negative trends were found in the north-central parts denoted by blue zone. The most negative trend magnitudes in the range of  $(-0.10 \text{ days/year})$  have been mostly observed in eastern and central parts. From the comparison of trend magnitudes of Rain and LRD indicators, high climate exposure was observed for the western and southern parts where rainfall is increasing, but light rain days are decreasing leading toward extreme rainfall and flash flood occurrences. Figures 14 and 15 show the significance and magnitude of trends of the NORD indicator for south Gujarat region. Positive trends were found for the whole region except a few pockets in the north-west parts, where negative trends have been denoted by blue zone. Significant (5%) positive trends were identified in the north-east parts denoted by orange and red zones. The highest positive trend magnitudes observed in the range of  $0.23 \text{ days/year}$  were in the north-east parts which are a forest zone at very high elevation. Based on the comparison in spatial variations of trend magnitudes of Rain, LRD and NORD indicators, the south-west parts showed increasing rainfall along with decreasing light rain days and increasing no rain days which pointed toward high climate exposure from extreme rainfalls. For

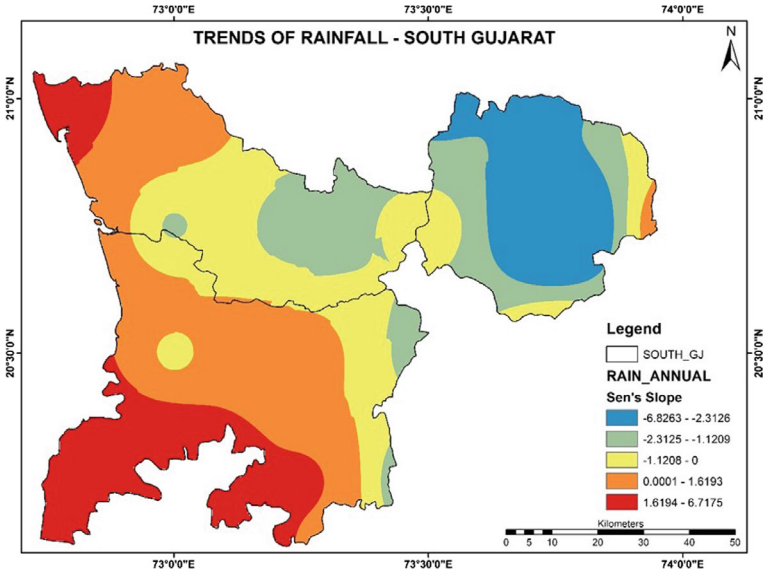


Fig. 9 Trend magnitude of Rain by SEN

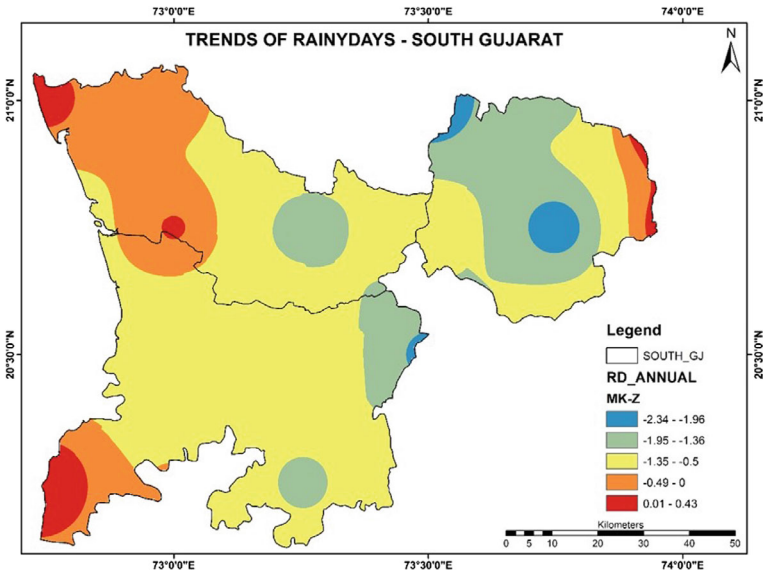
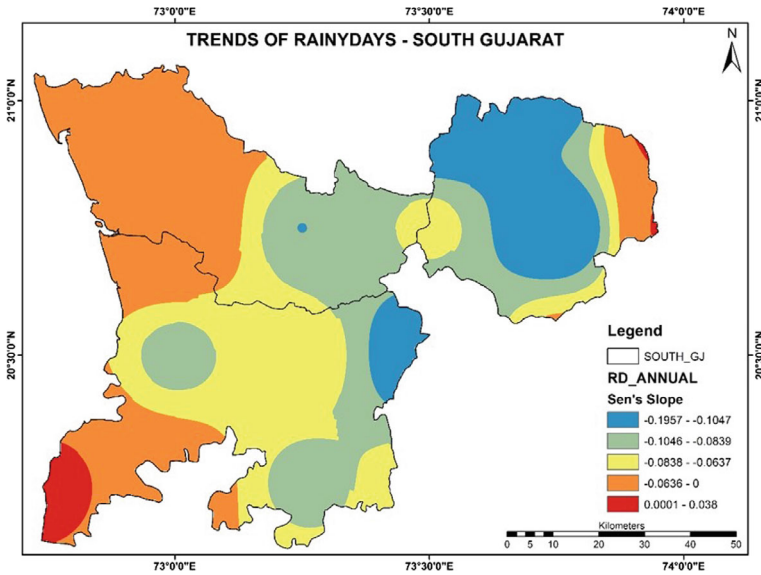


Fig. 10 Trend significance of RD by MK test



**Fig. 11** Trend magnitude of RD by SEN

the north-east parts, no rain days indicated significant rise along with significant less rainfall which account for climate exposure due to water scarcity.

The spatial variability of trend significance and magnitudes for the Maxrain indicator in the southern agro-climatic zone of Gujarat state have been described in Figs. 16 and 17, respectively. Negative trends mostly prevailed in the north-east parts, whereas the rest of the region showed positive trends in which significant (5%) trends were found in the south-west parts delineated with yellow, orange and red colors. The negative trend magnitudes are nearly about  $(-0.72 \text{ mm/day/year})$  in the north-east parts which is mountainous terrain with forest zones and highest positive magnitudes are up to  $(1.30 \text{ mm/day/year})$  in the south-west parts which is a coastal zone. The comparison of spatial distribution of trend magnitudes in Maxrain, RD, LRD and NORD indicators for south-west coastal zone, it was observed that one-day extreme rainfall significantly increased with rising no rain days but decreasing rainy days and light rain days, pointing toward high climate exposure to extreme rainfall events and flash flood scenarios.

### 6.3 Principal Component Analysis (PCA)

The PCA consisting raw data collection, standardization and organization, development of correlation matrix, checking PCA applicability, performing PCA to generate eigenvalues and eigenvectors, retention of PCs, extraction of factor scores, spatial

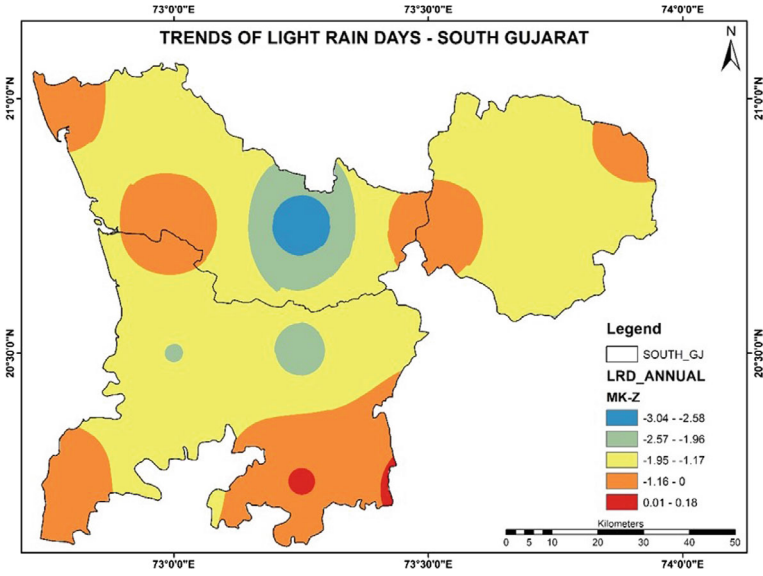


Fig. 12 Trend significance of LRD by MK test

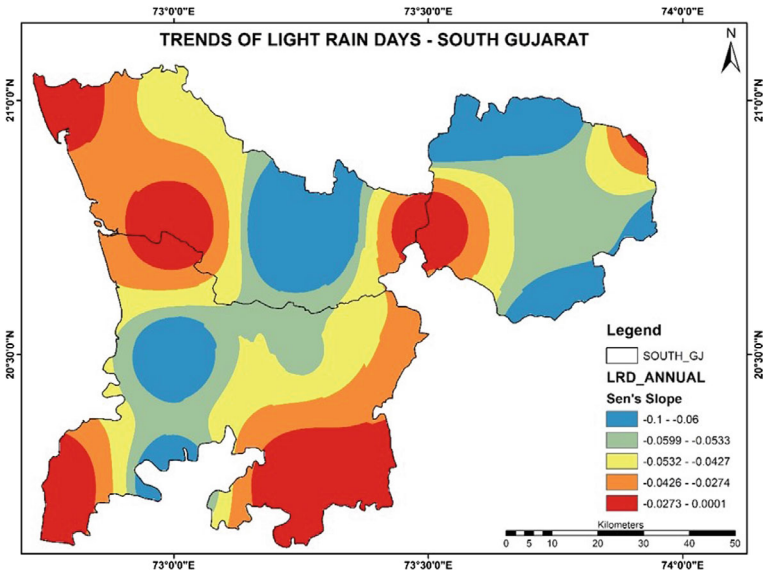


Fig. 13 Trend magnitude of LRD by SEN

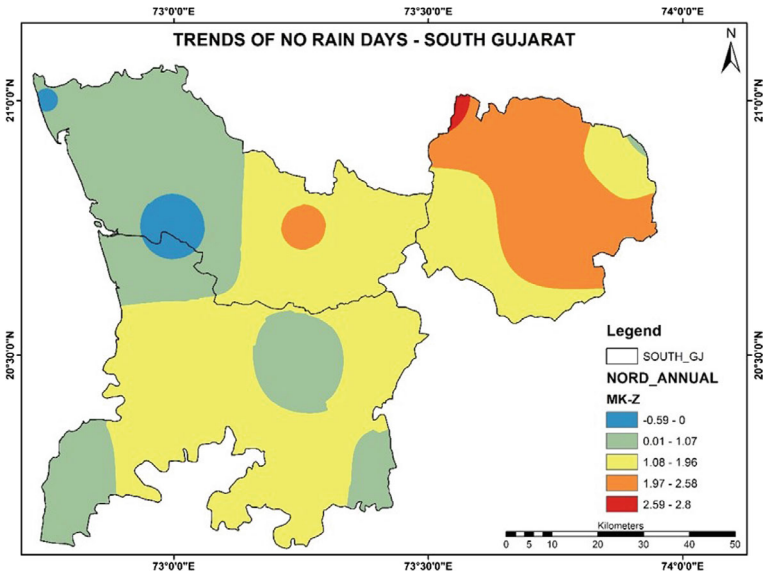


Fig. 14 Trend significance of NORD by MK test

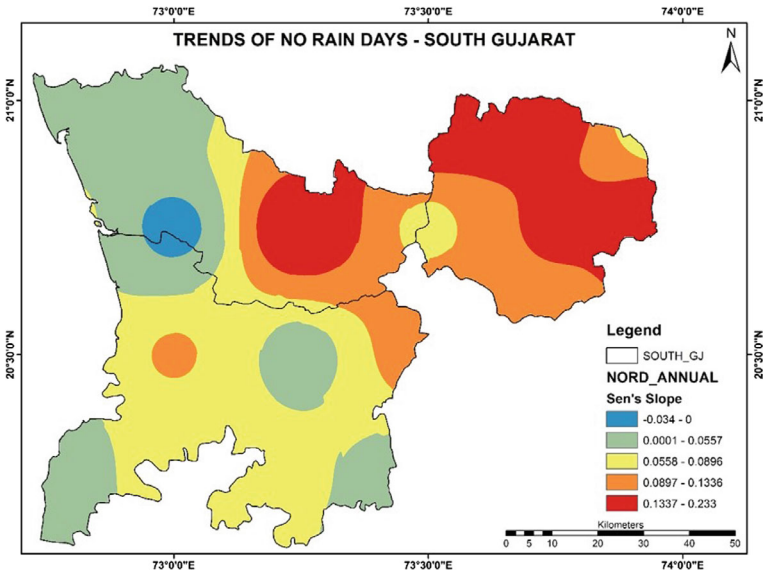


Fig. 15 Trend magnitude of NORD by SEN

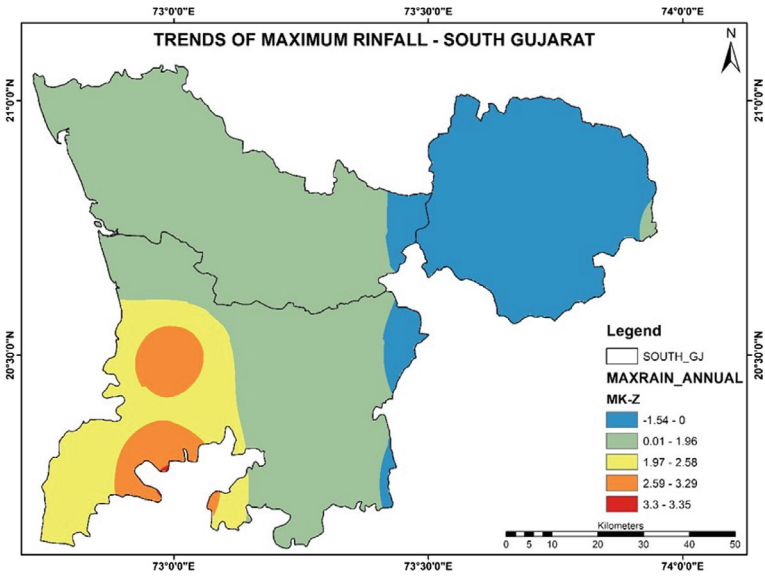


Fig. 16 Trend significance of maxrain by MK test

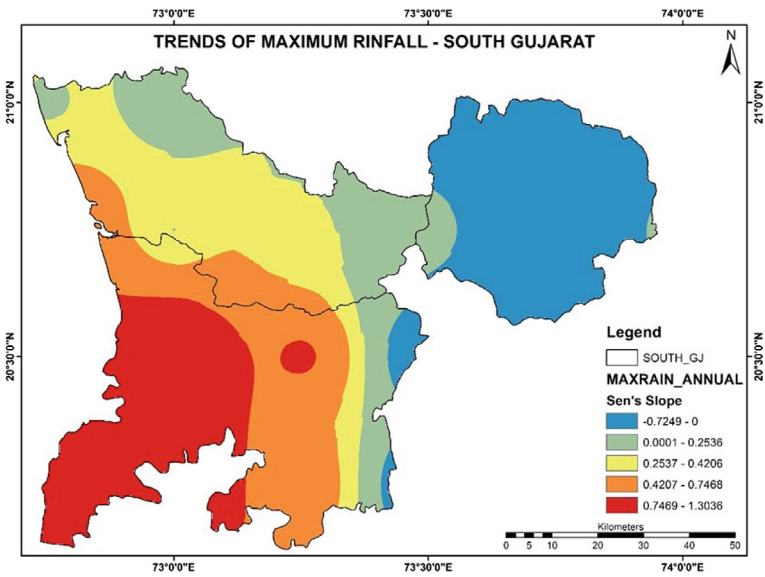


Fig. 17 Trend magnitude of maxrain by SEN

distribution of scores and identification of climate hotspots through a composite map, which were considered in present research. As the trend magnitudes of exposure indicators had different units, they were brought to the same scale by Z-score estimation and relationship among all the indicators generated by Pearson correlation is described in Table 1. The correlation coefficient less than 3 in absolute value has been assumed to show poor correlation, values between (0.3 and 0.5) show near correlation, (0.5–0.8) shows good correlation and values greater than 0.8 has been assumed to show strong correlation. From the below-mentioned correlation matrix (Table 1), strong positive correlation was found between  $T_{max}$  and  $T_{min}$  indicators, whereas strong negative correlation was discovered between LRD and NORD indicators. Rain and Maxrain showed good correlation with  $T_{max}$  and  $T_{min}$ , whereas RD and NORD showed near correlation with  $T_{max}$  indicators. RD and Maxrain showed good correlation with Rain. NORD showed negative correlation with almost all other indicators. HD is only correlated with RD and Maxrain in which positive near correlation with RD and negative near correlation with Maxrain were observed. Such inter-relationships among exposure indicators drew attention toward employing PCA.

The applicability of PCA was confirmed with KMO measure of sampling adequacy and Bartlett’s test of sphericity. The KMO test value of 0.537 which was greater than 0.5 as well as the Bartlett’s test obtained significance level of (0.000), both recommended most suitability of PCA for the exposure indicators. The PCA generated eigenvectors and eigenvalues that represented components in which eigenvalues greater than 1 were considered as principal components as described in Table 2. Three PCs (PC1, PC2 and PC3) were retained having eigenvalue >1 that showed about 85% of cumulative variation in which the first PC explained about 40% of total variation from rotation sums of squared loadings indicating, and it was able to capture majority of meaningful information. The PC loadings of rotated component matrix are described in Table 3 which refers to correlation of exposure indicators with respective PCs. Present research highlighted PC loadings greater than 6 in which all the indicators showed high positive loadings except NORD showing high negative loadings.

**Table 1** Correlation matrix of exposure indicators

Indicators	$T_{max}$	$T_{min}$	HD	Rain	RD	LRD	NORD	Maxrain
$T_{max}$	1.00							
$T_{min}$	0.92	1.00						
HD	-0.17	-0.25	1.00					
Rain	0.64	0.53	-0.14	1.00				
RD	0.36	0.14	0.30	0.61	1.00			
LRD	0.14	0.06	-0.01	0.18	0.57	1.00		
NORD	-0.30	-0.28	0.13	-0.35	0.64	-0.81	1.00	
Maxrain	0.68	0.66	-0.42	0.70	0.15	-0.15	-0.09	1.00

**Table 2** Total variance extracted from principal component analysis (PCA)

PCs	Initial eigenvalues			Extraction sums of squared loadings			Rotation sums of squared loadings		
	Total	% of variance	Cumulative %	Total	% of variance	Cumulative %	Total	% of variance	Cumulative %
1	3.61	45.114	45.114	3.61	45.114	45.114	3.208	40.106	40.106
2	2.13	26.629	71.743	2.13	26.629	71.743	2.358	29.479	69.585
3	1.09	13.662	85.405	1.09	13.662	85.405	1.266	15.820	85.405
4	0.66	8.293	93.698	–					
5	0.18	2.262	95.960						
6	0.17	2.059	98.018						
7	0.13	1.607	99.625						
8	0.03	0.375	100.000						

**Table 3** Rotated component matrix showing PC loadings

Principal components	Exposure indicators							
	$T_{\max}$	$T_{\min}$	HD	Rain	RD	LRD	NORD	Maxrain
PC1	0.911	0.861	–	0.816	–	–	–	0.877
PC2	–	–	–	–	0.693	0.945	–0.932	–
PC3	–	–	0.928	–	–	–	–	–

Present research assumed absolute values greater than 1 of factor scores in respective PCs stated high climate exposure for the southern agro-climatic zone of Gujarat state. The PC1 is consisting  $T_{\max}$ ,  $T_{\min}$ , Rain and Maxrain indicators with high positive loadings which can be interpreted as the component showing high climate exposure toward extreme temperatures and rainfalls. The spatial distribution of factors' scores of PC1 depicted in Fig. 18 highlighted two pockets, one in the north-east parts with most negative scores ( $-1.59$  to  $-1.00$ ) and the other in south-west parts with highest positive scores ( $1.01$  to  $1.77$ ). Positive factor scores dominated the western half, whereas negative scores prevailed in the eastern half of the study area which stated the combined effect of rising temperatures and rainfall has been predominantly observed in the south-west pocket. In the north-east pocket, only declining rainfall indicated high climate exposure as less availability of surface water might result in drought like scenarios, whereas falling extreme temperatures and intense rainfalls can actually be beneficial in socio-economical and biophysical aspects. Thus, it can be stated that severity of south-west pocket toward exposure to climate hazards is more than the north-east pocket.

The PC2 included high positive PC loadings of RD and LRD whereas high negative PC loading of NORD indicators and accounted for about 29% of cumulative variation. It can be understood as a component explaining climate exposure toward reduction in light rainfall leading to rise in no rainfall days. The negative factor scores

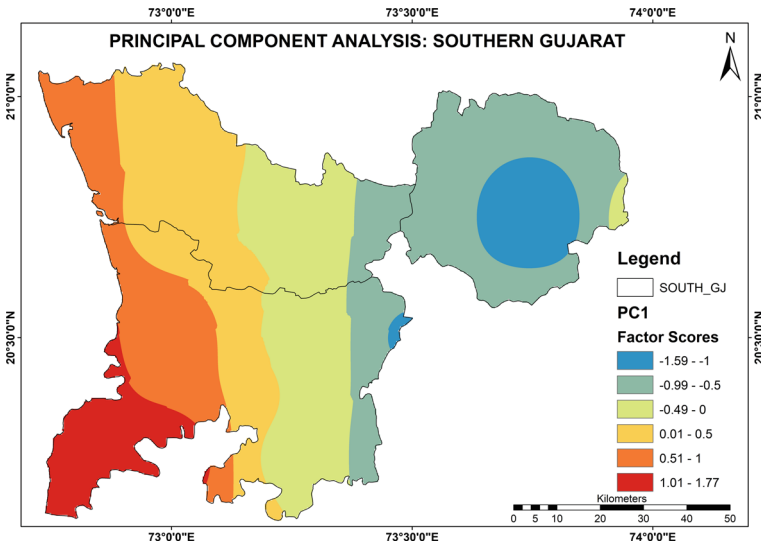


Fig. 18 Spatial distribution of PC1-factor scores

have been observed more in the eastern and central parts, whereas positive scores in the western and southern parts as described in Fig. 19. In the northern half of the region, highest positive factor scores (1.01 to 1.09) denoted by red zone were found which indicated declining light rainfall days, whereas a few pockets delineated by blue zone with most negative scores (−1.63 to −1.00) specified increasing no rainfall days along with decreasing light rainfall days making them more exposed to climate hazards. The PC3 containing high positive PC loading of HD indicator explained about 15% of cumulative variation. Positive factor scores were dominant in the northern parts, whereas in the central and southern parts, negative scores were observed as illustrated in Fig. 20. The highest positive factor scores (1.01 to 1.88) in the north-east highlighted climate exposure toward increasing hot days and occurrence of heat waves. The most negative scores (−1.55 to −1.00) in the south-east parts might be favorable in socio-economic aspects, especially in high yield of agriculture products.

The spatial distribution of composite PC map is shown in Fig. 21, which was obtained by addition of all three PCs in GIS environment using ‘Raster Calculator’ tool. The idea is to generate a single map that is able to identify climate hotspots for southern agro-climatic zone of Gujarat state based on super imposition of all the PCs as each individual PC accounted for climate exposure in various parts of the region. As the factor scores of composite map ranged from −2.70 to 2.53, it was assumed that absolute scores above 2.00 were most appropriate to highlight areas with high climate exposure. Highest positive scores (2.01 to 2.53) in north-west and south-west denoted by red zone as well as the most negative scores (−2.70 to −2.00) in north-east parts delineated by blue zone have been considered as climate hotspots. Thus,

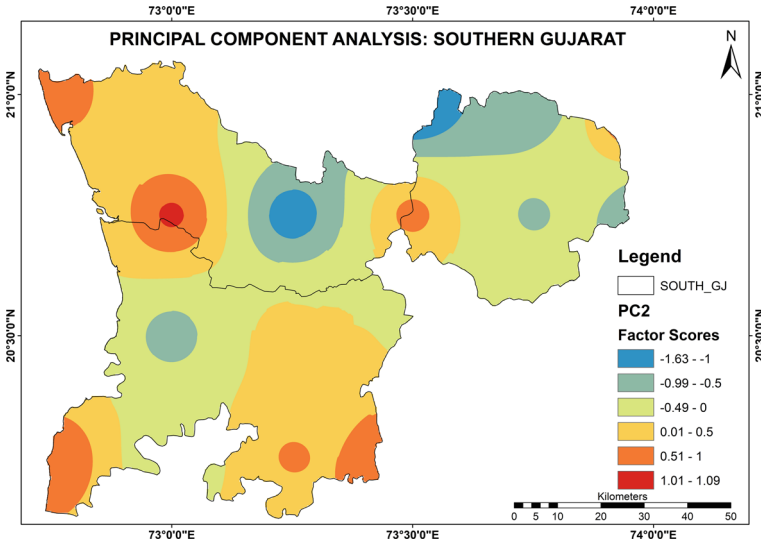


Fig. 19 Spatial distribution of PC2-factor scores

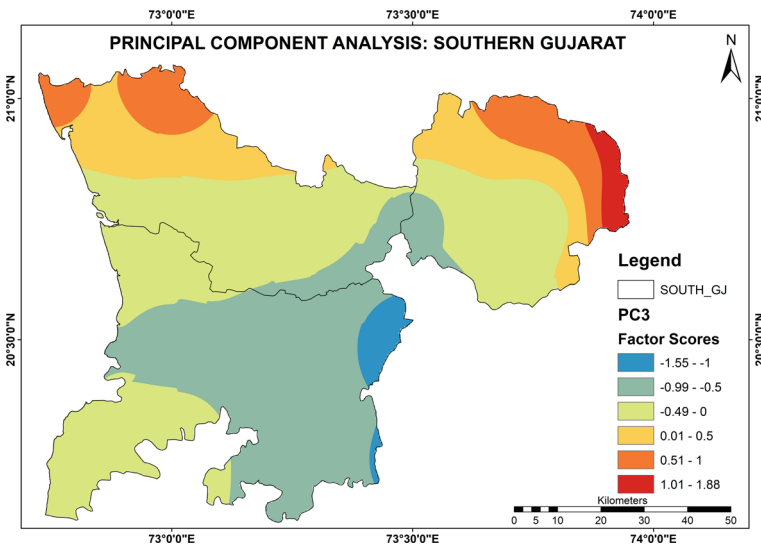


Fig. 20 Spatial distribution of PC3-factor scores

PCA-based climate hotspots were identified along the western coastal area indicating exposure to climate hazards such as extreme temperatures, intense rainfall and rapid floods as well as the eastern reserved forest zone which is located at higher elevation highlighted exposure to climate hazards such as water scarcity.

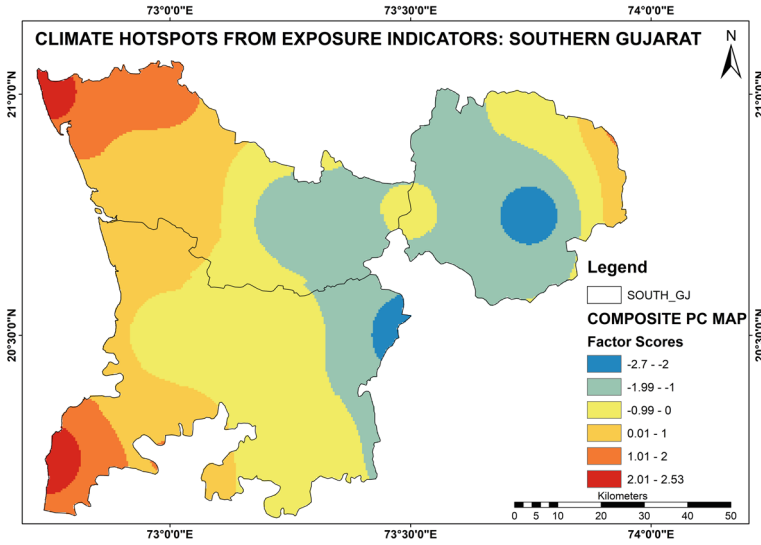


Fig. 21 Spatial distribution of composite PC map

## 7 Conclusion

Present research highlighted the importance of climate change at local level, climate variability in sub-humid coastal area and PCA utilization to identify climate hotspots for the southern agro-climatic zone of Gujarat state. The study revealed significant temporal and spatial variations in climate exposure indicators such as  $T_{max}$ ,  $T_{min}$ , HD, Rain, RD, LRD, NORD and Maxrain with the help of gridded data with very fine resolution having longer time spans. The coastal belt in the western parts of the region exhibited higher climate exposure due to rising maximum temperatures, emphasizing the need for adaptive measures to address the potential impacts of climate change along the coastline. The same area also showed increasing minimum temperatures possibly caused from urban heat island effects and anthropogenic impacts on changing atmospheric composition. Such extreme temperatures have ill impacts on elder population having heat related health issues as well as effects on crop growth, flowering and fruiting patterns, leading to potential shifts in agricultural practices reducing the productivity. Higher temperatures also accelerate evaporation rates, leading to increased water demand for irrigation putting additional pressure on water resources of the region. The research identified areas with increasing rainfall along with increasing no rain days but decreasing light rain days indicating occurrence of extreme rainfalls and potential flash floods, particularly in the western and southern parts. Certain pockets in the north-eastern parts experienced significant negative trends in rainfall and light rain days, pointing toward water scarcity issues and the potential for hydrological and agricultural droughts in such areas. The application of Principal Component Analysis (PCA) helped in identifying climate

hotspots based on the composite PC map combining multiple exposure indicators drew attention in the regions along the western coast and the reserved forest zone in the east as high-priority areas requiring targeted climate adaptation strategies. The research can further be enhanced by inclusion of other exposure indicators such as sea level rise, salinity ingress, cyclone frequency, drought prone areas, as well as assigning weights to indicators utilizing multiple criteria decision analysis methods for accurate assessment of climate hotspots.

**Acknowledgements** The authors are thankful for the financial support received from Climate Change Department of state government of Gujarat, India, under research project-CCSGS (Principal Investigator—Dr. Geeta S. Joshi).

## References

1. IPCC (2021) Climate change (2021): the physical science basis. In: Masson-Delmotte V, Zhai P, Pirani A, Connors SL, Péan C, Berger S, Caud N, Chen Y, Goldfarb L, Gomis MI, Huang M, Leitzell K, Lonnoy E, Matthews JBR, Maycock TK, Waterfield T, Yelekçi O, Yu R, Zhou B (eds) Contribution of working group I to the sixth assessment report of the intergovernmental panel on climate change. Cambridge University Press, Cambridge, UK and New York, NY, 2391 pp. <https://doi.org/10.1017/9781009157896>
2. UNDP (2010) Report on mapping climate change vulnerability and impact scenarios: a guide book for sub-national planners
3. Kumar V, Jain SK (2010) Trends in seasonal and annual rainfall and rainy days in Kashmir Valley in the last century. *Quatern Int* 212:64–69
4. Subash N, Sikka AK (2014) Trend analysis of rainfall and temperature and its relationship over India. *Theor Appl Climatol* 117:449–462. <https://doi.org/10.1007/s00704-013-1015-9>
5. Sharma PJ, Loliyana VD et al (2018) Spatiotemporal trends in extreme rainfall and temperature indices over Upper Tapi Basin, India. *Theor Appl Climatol* 134:1329–1354. <https://doi.org/10.1007/s00704-017-2343-y>
6. Chandole V, Joshi GS, Rana SC (2019) Spatio-temporal trend detection of hydro-meteorological parameters for climate change assessment in Lower Tapi river basin of Gujarat state, India. *J Atmos Solar Terr Phys* 195:105130. <https://doi.org/10.1016/j.jastp.2019.105130>
7. Joshi GS, Shah S (2022) Trend analysis of hydro-meteorological parameters and influence of anthropogenic activities in lower Narmada river basin, India. *Phys Chem Earth Parts A/B/C* 126:103148. <https://doi.org/10.1016/j.pce.2022.103148>
8. de Sherbinin A, Chai-Onn T, Giannini A, Jaiteh M, Levy M, Mara V, Pistolesi L, Trzaska S (2014) Mali climate vulnerability mapping. Technical paper for the USAID African and Latin American resilience to climate change project, Washington, DC
9. Abson DJ, Dougill AJ, Stringer LC (2012) Using principal component analysis for information-rich socio-ecological vulnerability mapping in Southern Africa. *Appl Geogr* 35(1–2):515–524. <https://doi.org/10.1016/j.apgeog.2012.08.004>
10. Tadić L, Bonacci O, Brleković T (2019) An example of principal component analysis application on climate change assessment. *Theor Appl Climatol* 138:1049–1062. <https://doi.org/10.1007/s00704-019-02887-9>
11. Prajapati VK, Khanna M, Singh M et al (2022) PCA-based composite drought index for drought assessment in Marathwada region of Maharashtra State, India. *Theor Appl Climatol* 149:207–220. <https://doi.org/10.1007/s00704-022-04044-1>
12. PMKSY (2020) District irrigation plan (2016–2020) of Navsari, Valsad and the Dangs districts. Reports of PMKSY (Predhan Mantri Krishi Sinchayee Yojana) prepared by NABCONS

13. Srivastava K, Rajeevan M, Kshirsagar SR (2009) Development of high resolution daily gridded temperature data set (1969–2005) for the Indian region. *Atmospheric science letters atmos. Sci Let.* <https://doi.org/10.1002/asl.232>
14. Pai DS, Sridhar L, Rajeevan M, Sreejith OP, Satbhai NS, Mukhopadhyay B (2014) Development of a new high spatial resolution ( $0.25 \times 0.25$ ) long period (1901–2010) daily gridded rainfall data set over India and its comparison with existing data sets over the region. *MAUSAM* 65:1
15. Kendall MG (1975) Rank correlation methods. Charles Griffin, London
16. Mann HB (1945) Nonparametric tests against trend. *Econometrica* 13:245–259
17. Sen PK (1968) Estimates of the regression coefficient based on Kendall's tau. *J Am Stat Assoc* 63

# Utilizing Agricultural Waste-Derived Activated Carbon Ash with Rapid Microwave Digestion Method to Treat Industrial Waste Water



Khushbu G. Patel, Pranav Saraswat, Nirendra M. Misra,  
and Tarun M. Patel

## 1 Introduction

Prior to discharging wastewater into water bodies, it is essential to address color removal, as color is the most noticeable contaminant in water. The wastewater generated by various industries, such as textile and dye production, often contains residual dyes, contributing to its coloration. Even a dye concentration as low as 1.0 mg in drinking water can cause significant discoloration, rendering it unsuitable for human consumption [1]. Many of the dyes in use exhibit resistance to oxidation, biodegradation, and light exposure [2]. To effectively remove colors from wastewater, the adsorption process using activated carbon (in powdered or granular form) has shown great efficiency for organic compound removal, even from diluted solutions. However, the cost of commercially available activated carbon remains a challenge due to its high expense. Commercial activated carbon is typically derived from diverse carbonaceous materials, including coal, lignite, coconut shells, wood, and peat [3]. Nonetheless, agricultural by-products present an excellent opportunity as

---

K. G. Patel (✉)

Department of Sciences, School of Technology (SOT), Pandit Deendayal Energy University,  
Ahmedabad, Gujarat 382007, India  
e-mail: [patelkhushbug09@gmail.com](mailto:patelkhushbug09@gmail.com)

K. G. Patel · N. M. Misra

Department of Sciences, School of Technology (SOT), Pandit Deendayal Energy University,  
Gandhinagar, Gujarat 382007, India

P. Saraswat

Institute of Commerce, Nirma University, Ahmedabad, Gujarat 382481, India

T. M. Patel

Department of Chemistry, Sir P. T. Science College Modasa, HNGU, Modasa, Gujarat 383315,  
India



**Fig. 1** Local farmers disposing wheat straw through open field burning

a raw material source for activated carbon production due to their abundant availability. Utilizing agricultural by-products [4] as renewable resources for activated carbon manufacturing is highly desirable to foster waste resource recycling. These by-products encompass the non-product outputs resulting from the cultivation and processing of agricultural raw materials, such as rice, corn, beans, and peanuts, and are commonly referred to as residues from agriculture and agro-industries [5]. Enormous quantities of agricultural by-products, such as rice, wheat husk, and straw, are generated during the rice and wheat milling processes. Unfortunately, these paddy wastes are often disposed of through open field burning (Fig. 1), leading to air pollution, greenhouse gas emissions, energy wastage, or left for landfilling, occupying significant space.

Researchers have explored alternative methods for dealing with agricultural waste, aiming to avoid its wasteful disposal through burning or discarding. Among these potential solutions, the conversion of agricultural waste like rice husks or wheat straws into carbon-based materials has shown promise. Countries with significant wheat production, such as India, Canada, Australia, and France, generate vast amounts of wheat straw annually, presenting an opportunity for resource utilization. One particularly promising approach involves transforming agricultural waste into ACA, which can serve as an effective adsorbent for treating industrial wastewater. ACA is renowned for its exceptional adsorption properties, making it an ideal choice for purifying water in various applications. By harnessing wheat straw and similar agricultural waste to create ACA, we can simultaneously address waste management challenges and improve industrial wastewater treatment processes. Research is ongoing to investigate the removal of different colors from aqueous solutions using various agricultural waste products under different conditions (as shown in Table 1; [1]). Among these waste products, bagasse pith-derived activated carbon emerges as a potential adsorbent for removing colors from wastewater [6–8]. Bagasse pith is a carbonaceous and fibrous solid waste produced abundantly during certain agricultural processes, often posing a disposal issue and being burnt for fuel. Consequently, the interest lies in transforming this by-product into a more valuable and useful material, such as activated carbon.

**Table 1** Studies on the removal of dyes from aqueous solutions using several agricultural wastes

S. No.	Agricultural waste	Dye name	Conditions/specifications	Refs.
1.	Banana peel	Methyl orange	pH 5, contact time: 4 h, initial dye concentration: 100 mg/L	[9]
2.	Rice husk	Congo red	pH 7, temperature: 25 °C, adsorbent particle size: 0.5–1 mm	[10]
3.	Citrus peel	Crystal violet	pH 6.5, dosage: 10 g/L, agitation speed: 150 rpm	[11]
4.	Pineapple peel	Malachite green	pH 8, agitation speed: 200 rpm, equilibrium time: 24 h	[12]
5.	Coconut shell ash	Acid red 27	pH 4.5, adsorbent dosage: 5 g, pH stability range: 4–9	[13]
6.	Corn cob	Direct blue 71	pH 7.5, contact time: 6 h, initial dye concentration: 50 mg/L	[14]
7.	Olive pomace	Basic red 46	pH 6, temperature: 30 °C, adsorbent dosage: 15 g/L	[15]
8.	Sugarcane bagasse	Reactive blue 5	pH 7, dosage: 15 g/L, adsorption kinetics: pseudo second-order	[16]
9.	Wheat straw	Acid yellow 23	pH 5, agitation speed: 150 rpm, temperature: 25 °C	[17]
10.	Coffee grounds	Disperse orange 3	pH 6.5, contact time: 3 h, initial dye concentration: 80 mg/L	[18]
11.	Soybean residue	Basic violet 14	pH 7, temperature: 35 °C, agitation speed: 180 rpm	[19]
12.	Grape pomace	Acid blue 9	pH 5.5, dosage: 20 g/L, pH stability range: 5–9	[20]
13.	Potato peel	Reactive red 120	pH 6, agitation speed: 180 rpm, adsorbent dosage: 10 g	[21]
14.	Tomato skin	Direct black 38	pH 7.5, contact time: 5 h, initial dye concentration: 120 mg/L	[22]
15.	Carrot tops	Acid green 25	pH 6, dosage: 12 g/L, temperature: 25 °C	[23]

This research endeavors to explore the potential application of ACA derived from wheat straw as an efficient adsorbent for the treatment of industrial wastewater. The study focuses on converting wheat straw into ACA, thereby addressing the environmental impact of agricultural waste while simultaneously providing a valuable

resource for wastewater treatment. The ACA exhibits unique physicochemical properties, including high surface area, porosity, and adsorption capacity, making it a promising candidate for the removal of various contaminants commonly found in industrial effluents. The investigation encompasses the synthesis process of ACA from wheat straw and aims to evaluate its efficacy in eliminating specific pollutants.

Numerous factors influencing the adsorption performance, such as contact time, pH, initial pollutant concentration, and ACA dosage, will be thoroughly assessed to understand the optimal conditions for achieving the highest adsorption efficiency. The implications of this study hold significant importance for both the agricultural and industrial sectors. By harnessing the potential of wheat straw-derived ACA, a sustainable waste management approach can be established that not only mitigates the environmental impact of agricultural residues but also offers an economically viable solution for treating industrial wastewater.

In this study, the researchers adopted a microwave-assisted acid digestion process to convert wheat straw into ACA. This novel approach enables charring at much lower temperatures compared to traditional torrefaction methods, eliminating the production of harmful smoke and airborne particulates. The acid-digested product was subsequently calcined to obtain the ACA. From the practice-oriented point of view the current study attempt to understand the cost-effectiveness and financial viability of this technique to be adopted by industry.

For the adsorption experiments, Methylene Blue was chosen as the target pollutant due to its prevalence in the effluents of various industries, including textile, leather, jute, and food production. Through the comprehensive characterization of the physical, chemical, and adsorptive properties of the generated ACA, the study aimed to evaluate its potential integration into water and wastewater treatment systems. These preliminary tests have yielded valuable insights into the product's suitability for such treatment applications. Present study aims to deliver valuable insights into economic efficiency by utilizing process costing, with the potential for large-scale implementation. The rationale for cost-effective analysis with other details are mentioned in appendix I.

## 2 Experimental

The experimental setup and analysis involved in this study are as follows:

In this investigation, wheat straw sourced from a local agricultural field served as the raw material. Solvents and reagents procured from Sigma Aldrich and Merck were employed without additional purification. The synthesized silica underwent characterization through powder X-ray diffraction analysis using a PANalytical X'Pert PRO instrument to elucidate its crystalline structure. The nanostructural morphology of the silica was examined via scanning electron microscopy (SEM) employing a Zeiss ULTRA™ 55 instrument. To facilitate SEM analysis, the product was dispersed in ethanol, affixed to carbon tape, and subsequently sputter-coated with a 10 nm layer of gold/palladium (Au/Pd) using a Leica EM ACE-200 coater. Elemental analysis of

the silica was conducted using energy-dispersive X-ray spectroscopy (EDX) with an Oxford X-MaxN detector. Fourier-transform infrared (FTIR) spectra of the synthesized product were acquired utilizing a PerkinElmer spectrometer (version 10.4.2) from KBr pellets, spanning the wavenumber range from 4400 to 400  $\text{cm}^{-1}$ . Identification of specific functional groups was achieved through the analysis of FTIR spectra. These experimental methodologies and subsequent analyses yielded valuable insights into the structural, morphological, and chemical attributes of the synthesized material, facilitating a comprehensive characterization of the investigated substance.

## **2.1 *Materials and Method***

### **2.1.1 *Materials***

Around 5 kg of wheat straw originating from the Lok-1 wheat variety was procured from a local agricultural field situated in Gujarat, India, during the winter wheat growing season. The choice of the Lok-1 wheat variety, commonly cultivated in the region during this specific season, was deliberate to ensure uniformity in the composition of the straw and the subsequent ash produced.

For the experimental procedures, concentrated hydrochloric acid (Batch No. ACOA600226, Merck-India) with a purity level of 99% was obtained from Merck chemical company and employed without any further purification.

### **2.1.2 *Method***

The size separation of the initial wheat straw sample involved a sequential process. Initially, the sample was subjected to sun-drying to eliminate moisture content. Following this, the dried sample underwent hot air oven treatment at 120 °C for a duration of 2 h using a Lab line instrument from Sun Instrument Pvt. Ltd.

This step was crucial for further removal of any residual moisture. Subsequent to the oven treatment, the dried sample was meticulously ground using a mixture-grinder and then sieved. Specifically, only particles that passed through a — 300  $\mu\text{m}$  (BS—mesh-52) sieve were retained for subsequent investigations. Microwave digestion was employed as the pre-treatment method for the wheat straw. The Microwave Accelerated Reaction System (MARS-CEM) version 194A07 was utilized for this purpose. Approximately 1 g of the dried powder sample was subjected to digestion with LR grade concentrated hydrochloric acid within a Teflon vessel named ‘Easy prep,’ designed explicitly for microwave digestion. The optimization of the digestion process, involving parameters such as temperature, time, and acid treatment, is detailed in Table 2. The resulting charred product from the microwave digestion underwent thorough washing with distilled water until the absence of chloride ions ( $\text{Cl}^-$ ) was confirmed, verified by the absence of reaction with a 0.05 N  $\text{AgNO}_3$  solution. Following extensive washing, the charred product was dried in a hot air

oven for a duration of 8 h, maintaining a temperature of 150 °C. Subsequently, the product underwent characterization, as depicted in Fig. 2, to analyze its properties and composition.

Wheat straw underwent treatment at various temperatures, with different amounts of hydrochloric acid and digestion times. The results led to the conclusion that to achieve minimum residue and maximum digestion, each gram of the sample required between 5 and 10 ml of hydrochloric acid. This was achieved by maintaining a constant temperature of 120 °C and a digestion time of 10 min (as indicated in Table 2—ACA 2). When the digestion process was conducted without the addition of acid, it resulted in the formation of hard particles. Furthermore, dilute acid (1N HCl) was found to be ineffective in producing a charred product. This lack of effectiveness could be attributed to the high moisture content present in the wheat straw sample. Based on visual estimation of the digested/charred products, it was observed that a digestion temperature of at least 120 °C was necessary to obtain desirable results. Notably, there was minimal difference between the charred products obtained at heating temperatures of 120 and 130 °C.

**Table 2** Yield of samples of raw wheat straw by microwave digester with various optimization conditions

S. No.	Power (W)	MW temperature (°C)	Time (min.)	Amount of conc. HCl (ml)	% yield (W/W %)
ACA 1	400	120	10	5	63
<b>ACA 2</b>	<b>400</b>	<b>120</b>	<b>10</b>	<b>10</b>	<b>53</b>
ACA 3	400	120	5	10	54
ACA 4	400	130	10	10	53
ACA 5	400	140	10	10	53

We used ACA 2 for water treatment

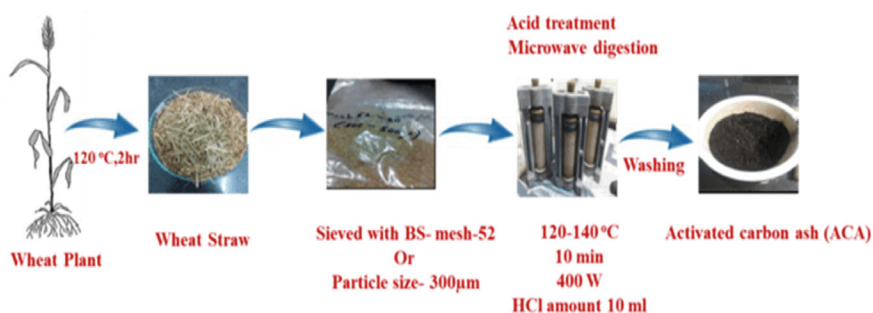


**Fig. 2** Preparation of activated carbon ash (ACA)

### 3 Characterization Study

In the analysis of the raw wheat straw (depicted in Fig. 3a), the presence of a significant quantity of  $\text{SiO}_2$  was evident, as indicated by the peaks at  $-1057$  and  $-894 \text{ cm}^{-1}$ . Peaks observed at  $1637 \text{ cm}^{-1}$  suggested the existence of non-aromatic esters ( $-\text{C}-\text{O}$ ), while those at  $3355.80 \text{ cm}^{-1}$  pointed to the presence of  $-\text{OH}$  groups. Additionally, peaks at  $1513.3 \text{ cm}^{-1}$ ,  $1423.7 \text{ cm}^{-1}$ , and  $2921.18 \text{ cm}^{-1}$  were attributed to lignin and cellulose, respectively. In a comprehensive assessment, most of the peaks in the raw wheat straw exhibited well-defined characteristics, aligning with findings from previous studies [24].

Upon characterization of the Microwave Digested Charred Material by FTIR spectroscopy in the range from  $4000$  to  $400 \text{ cm}^{-1}$  (Fig. 3b), a broad band was observed at  $3198 \text{ cm}^{-1}$  indicating the presence of  $-\text{OH}$  stretching of polymeric compounds or  $\text{N}-\text{H}$  groups. The peaks at  $2923 \text{ cm}^{-1}$  were attributed to methylene and methoxy groups. Additionally, small peaks at  $1197 \text{ cm}^{-1}$  indicated the presence of  $\text{S}=\text{O}$  groups. The band observed at  $1607 \text{ cm}^{-1}$  corresponded to carbonyl stretching vibration of amide, likely resulting from the combined effect of double-bond stretching vibration and  $-\text{NH}$  deformation band in the lead-loaded activated carbon. Notably, the functional groups  $\text{C}=\text{O}$  and  $\text{S}=\text{O}$  have a strong coordination affinity with trace metals, hence some shifts in the lead-loaded material were observed at  $1607$  and  $1197 \text{ cm}^{-1}$  [25].

The composition and physical characteristics of the activated carbon derived from wheat straw were evaluated through X-ray diffraction (XRD) analysis, as illustrated in Fig. 4a. The XRD pattern indicated a combination of amorphous and crystalline structures in the activated carbon. The scanning electron microscopy (SEM) image of the activated carbon, presented in Fig. 4b, confirmed its irregular and porous surface, characteristics considered conducive to effective Methylene Blue (MB) adsorption. Additionally, Fig. 4b revealed the absence of residual metal ions on the wheat straw-derived activated carbon, signifying its purity for potential applications. To ascertain the optimal pyrolysis temperature, the wheat straw charred product underwent analysis via thermogravimetric analysis (TGA) under air conditions, as depicted in

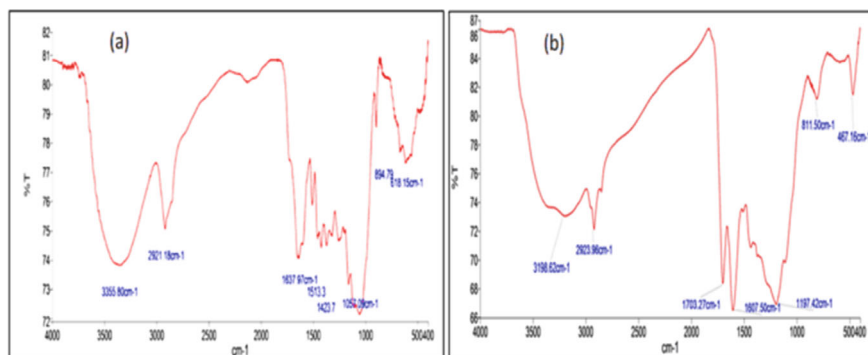


**Fig. 3** FTIR spectrum of **a** raw wheat straw and **b** microwave digested charred material (ACA)

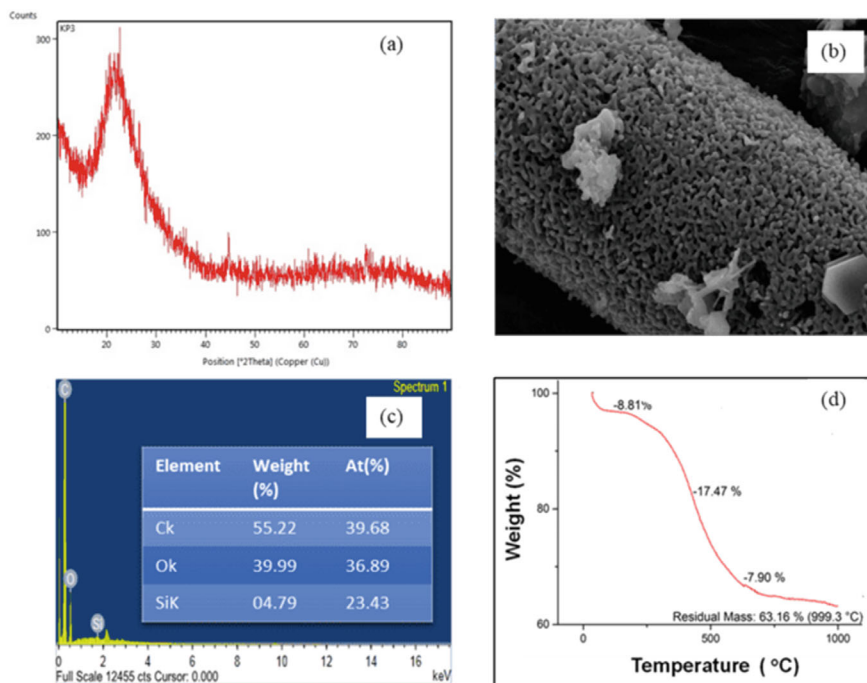


**Fig. 4** a XRD, b SEM image, c EDX analysis of activated carbon ash derived from wheat straw and d TGA of wheat straw

Fig. 4d. The TGA curve displayed a minor weight loss in the range of 70–150 °C, attributed to moisture loss. Subsequently, continuous weight loss below 200 °C indicated the decomposition of various components such as hemicelluloses, cellulose, and lignin. Notably, hemicellulose, decomposing mainly at 150–350 °C, was identified in the wheat straw. Cellulose decomposes around 350 °C, and the third stage of weight loss (approximately 26–31%) was attributed to lignin, a thermally stable aromatic polymer gradually decomposing between 370 and 600 °C. These findings facilitated the determination of the appropriate pyrolysis temperature for the production of activated carbon derived from wheat straw.

## 4 Adsorption Study

The primary objective of the present study is to produce high-quality carbon derived from wheat straw, characterized by its lightweight nature, large specific surface area, well-developed pore structure, rapid adsorption rate, single-step formation, and outstanding adsorption capacity. The resulting activated carbon exhibits an

impressive adsorptive value for methylene blue (MB) within the range of 14–16 mg/g.

In the conducted batch adsorption experiments, a 50 mL Erlenmeyer flask containing the adsorbent and 20 mL of MB solution with various initial concentrations was employed. To ensure thorough mixing, the flasks underwent agitation in a water-bath shaker at 150 rpm until equilibrium was achieved. Post-equilibration, decantation and filtration were performed, and the equilibrium concentrations of dyes in the solution were quantified at 664 nm using a UV–Visible spectrophotometer. pH adjustments were carried out using 0.10 M HCl and 0.10 M NaOH solutions. The amount of dye adsorbed and the percentage of MB removal were subsequently calculated utilizing the provided Eq. (1).

$$Q = (C_o - C_e)V/W \tag{1}$$

### 4.1 Impact of Dose of Adsorbent

To examine the impact of adsorbent dose on the adsorption process, varying amounts of adsorbent were introduced into fixed concentrations of methylene blue (MB) solutions and stirred together for 1 h. The adsorbent dose spanned from 0.05 to 0.5 g. The outcomes depicted in Fig. 5a reveal that the amount of MB absorbed per unit weight ( $Q$ ) of activated carbon diminishes with an escalating dose of adsorbent.

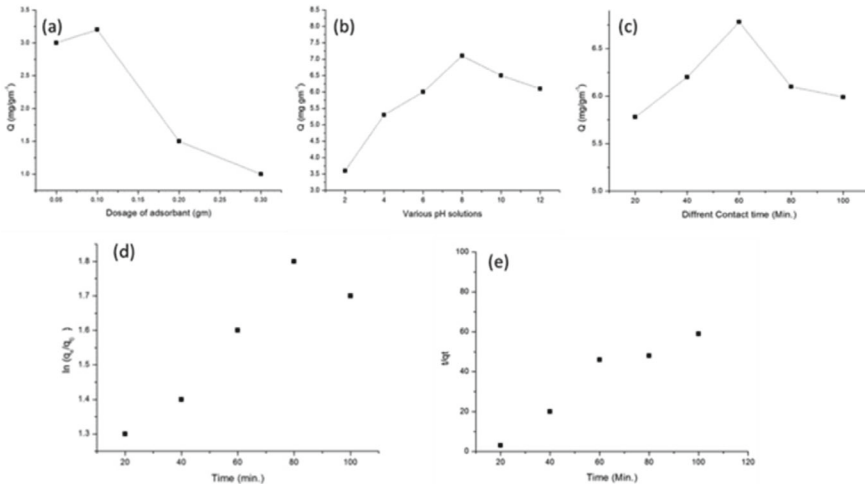


**Fig. 5** a Impact of adsorbent dosage, b pH and c contact time on MB removing process. d Pseudo first-order and e Pseudo second-order kinetic removal model parameters for adsorption of MB onto activated carbon

This decrease in  $Q$  is ascribed to the phenomenon of supercritical adsorption, which occurs rapidly on the adsorbent's surface at higher doses. This leads to a lower solute concentration in the solution compared to lower adsorbent doses. Consequently, with an increase in the adsorbent dose, the amount of dye adsorbed per unit mass of adsorbent decreases, resulting in a reduction in the  $Q$  value.

#### ***4.2 Impact of the Baseline pH Solution***

The pH of the dye solution plays a pivotal role in influencing the adsorption of methylene blue (MB) onto activated carbon, as illustrated in Fig. 5b. The observed trend reveals that the amount of MB adsorbed increases with the elevation of the solution's pH. The capacity for MB adsorption experiences a substantial increment, ranging from 3.69 to 7.10 mg/g, as the pH value escalates from 2 to 12. Notably, when the initial pH of the solution is set at 8, the MB removal capacity peaks at 7.10 mg/g for the activated carbon (AC).

In an acidic medium, the positively charged surface of the sorbent tends to impede the adsorption of the cationic adsorbate (MB). As the pH of the dye solution increases, the surface of the activated carbon acquires a negative charge. Consequently, the amount of MB removal decreases due to the repulsion between the negatively charged surface and the cationic dye. However, with a further increase in the pH of the dye solution, a stronger electrostatic attraction develops between the positively charged MB molecules and the negatively charged activated carbon surface. This heightened attraction results in an increased capacity for MB removal, and the adsorption efficiency rises as the pH value of the solution becomes more alkaline.

#### ***4.3 Impact of Duration of Contact***

The impact of contact time on the removal of methylene blue (MB) is elucidated in Fig. 5c. The graph illustrates that the adsorption process initiates at a relatively brisk pace, predominantly occurring on the outer surface of the adsorbent. This rapid initial stage is succeeded by a slower internal diffusion process, emerging as the rate-determining step. As time advances, the removal of MB diminishes, influenced by two primary factors. Firstly, as the adsorption progresses, the number of available adsorption sites on the adsorbent's surface diminishes, resulting in a decline in the adsorption rate. Secondly, the concentration of MB in the solution decreases concurrently as it is adsorbed onto the activated carbon.

The observed reduction in the adsorption rate, particularly toward the conclusion of the experiments, suggests the potential formation of a monolayer of MB on the surface of the adsorbent. At this juncture, the available surface sites become saturated with MB molecules, leading to a reduction in further adsorption [11]. This implies

that the adsorption process has reached equilibrium, and the adsorbent's surface is fully covered with MB molecules in a monolayer arrangement.

#### 4.4 Adsorption Kinetics

The rate constant of adsorption ( $k_1$ ) was determined using the pseudo first-order equation, as described in Eq. (2), where  $q_e$  and  $q_t$  represent the amounts of methylene blue (MB) adsorbed ( $\text{mg g}^{-1}$ ) at equilibrium and at time  $t$  (s), respectively.

$$\ln(q_e - q_t) = \ln q_e - k_1 t \quad (2)$$

The values of  $k_1$  were calculated from the plot of  $\ln(q_e - q_t)$  versus  $t$  (Fig. 5d) for different concentrations of MB. Despite having correlation coefficient values higher than 0.83 at high concentrations, it was observed that the experimental  $q_e$  values did not align with the calculated ones, as indicated in Table 3. Consequently, the adsorption of MB onto activated carbon was found not to adhere to a first-order kinetic model.

To address this inconsistency, a pseudo second-order equation based on equilibrium adsorption (Eq. 3) was considered, where  $k_2$  ( $\text{g/mg s}$ ) represents the rate constant of the second-order adsorption.

$$t/q_1 = 1/k_2 q_e^2 + t/q_e \quad (3)$$

The plot of  $t/q$  versus  $t$  should exhibit a linear relationship if the second-order kinetic model is applicable. This approach, not requiring prior knowledge of parameters, proved more suitable for predicting the behavior over the entire range of adsorption. The correlation coefficients for the second-order kinetic model were found to be 0.92, indicating the applicability of this kinetic equation and confirming the second-order nature of the adsorption process of MB onto activated carbon. This suggests that the adsorption of MB follows a pseudo second-order kinetic model in this specific system, rather than a first-order one.

**Table 3** Langmuir and Freundlich isotherm parameters and correlation coefficient for adsorption of MB on activated carbon

Parameters adsorption						
Absorbent	Freundlich			Langmuir		
	$Q_e$ ( $\text{mg/l}^{-1}$ )	$K_f$ ( $\text{L mol}^{-1}$ )	$R^2$	$B$ ( $\text{mg/l}^{-1}$ )	$K$ ( $\text{L mol}^{-1}$ )	$R^2$
WSA	15.78	0.93	0.99	15.23	0.26	0.85

## 5 Adsorption Isotherms

Moving on to the adsorption isotherms, these are crucial for understanding the distribution of adsorbate molecules between the liquid and solid phases at equilibrium. Two well-known isotherm models, Langmuir and Freundlich, were employed in this study. By comparing the correlation coefficients ( $R^2$ ), it was found that the Freundlich model demonstrated the best fit, surpassing the Langmuir model with  $R^2$  values equal to or higher than 0.99. This suggests that the adsorption process is heterogeneous, indicating that not all adsorbent surfaces are equally capable of experiencing adsorption. The multilayered layer formed in this adsorption model is a result of the physical interaction between the adsorbent and the adsorbate [12].

Figure 6 shows the equilibrium adsorption isotherm of MB onto activated carbon, the Langmuir adsorption isotherm, and the Freundlich adsorption isotherm. Consequently, the adsorption capacity of methylene blue (MB) cannot be precisely determined but is significantly high, with a large amount of MB being adsorbed as the equilibrium is reached, particularly at higher MB concentrations, such as when the initial concentration of MB is  $250 \text{ mg L}^{-1}$ , resulting in an adsorption capacity of approximately  $15.78 \text{ mg/g}$ .

## 6 Pricing and Cost Effectiveness of the Method

The agricultural waste can be procured from the industry at dumping price that can be utilized as the raw material for creating activated carbon ash, including rice husks, coconut shells, or sawdust. There is the reasonable cost of pre-processing agricultural waste for carbonization, including cleaning, drying, and sizing. The price of the carbonization process involves heating agricultural waste without oxygen to create activated carbon ash. This will also enhance the carbonized material's adsorption abilities, if necessary. Different activation techniques exist, including chemical activation and steam activation. The price of further processing activated carbon ash to guarantee grading and quality consistency. This is essential to activate carbon ash which can meet industry requirements for quality and effectiveness. Furthermore, there is cost associated of shipping activated carbon ash to customers or end users in packaging. In production process, we also incorporate the cost of purchasing new gear and equipment as well as their ongoing maintenance. As the product is manufactured with agriculture waste there is tiny cost for selling and distribution for the purpose, as the demand is already available in the market. Along with that we also acknowledge the costs related to following environmental laws and getting the required licenses and certifications, which is nominal and as per the state and central govt. norms.

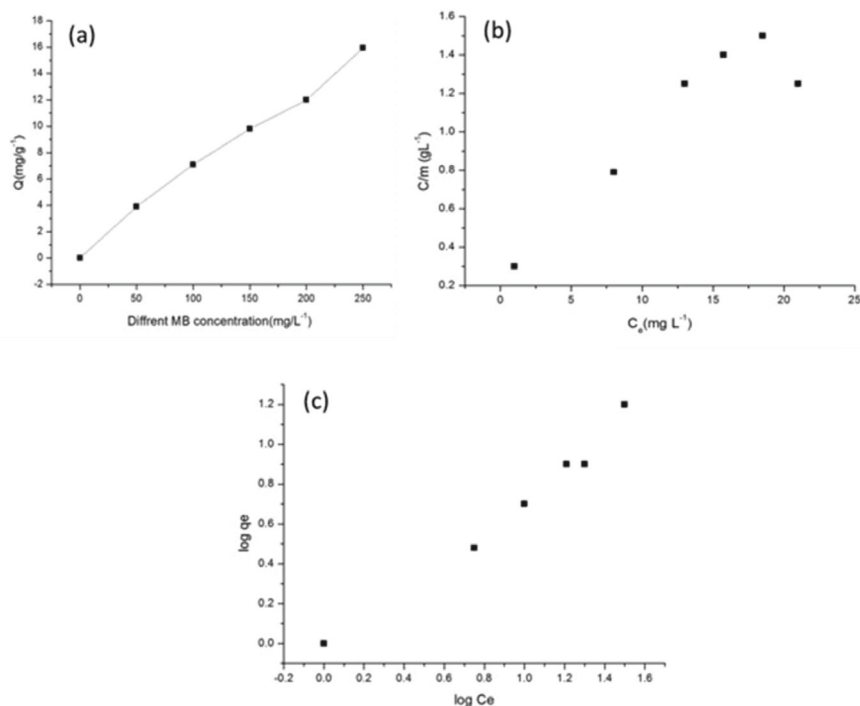


**Fig. 6** **a** Equilibrium adsorption isotherm of MB onto activated carbon, **b** Langmuir adsorption isotherm of MB onto activated carbon, **c** Freundlich adsorption isotherm of MB onto activated carbon

## 7 Conclusion

The approach used in this study offers several attractive features:

(i) The activated carbon preparation process outlined in this study is characterized by cost-effectiveness, absence of toxic gas emissions, and the utilization of agricultural waste, such as wheat straw. This approach not only mitigates environmental pollution but also proves effective in the removal of bacteria, colored matter, and other deleterious substances from the original effluent. (ii) The employment of agricultural waste, specifically wheat straw, as the primary raw material for activated carbon production exemplifies a sustainable and environmentally friendly methodology. By repurposing this readily available waste product, the study contributes to a more eco-conscious and resource-efficient approach. (iii) The adoption of a rapid microwave digestion technique stands out as a noteworthy aspect, facilitating the swift conversion of wheat straw into activated carbon within a mere 10-min duration. Importantly, this process is accomplished without the generation of airborne particulates, emphasizing its efficiency and environmental compatibility. (iv) The

activated carbon derived from wheat straw showcases significant promise as an adsorbent, particularly in the removal of methylene blue dye from aqueous solutions. Its efficacy is demonstrated across a broad spectrum of concentrations, underlining its versatility and applicability in water treatment scenarios. (v) Surface morphology analysis of the activated carbon, conducted through scanning electron microscopy (SEM), unveils a larger pore size. This characteristic contributes to an enhanced adsorption capacity, further emphasizing the material's potential utility in diverse adsorption applications. (vi) The adsorption of methylene blue dye follows a second-order kinetic model, with a specific rate constant value of 1.0497 g/mmol min for each dosage of activated carbon. (vii) The equilibrium data of adsorption aligns well with Freundlich's isotherm, indicating a multilayer adsorption process. The adsorption capacity is approximately 15.776 mg/g for each dosage of activated carbon. This approach showcases the advantages of utilizing agricultural waste, rapid digestion techniques, and the eco-friendly production of activated carbon for efficient dye removal, making it a promising and environmentally conscious solution for water treatment and waste management. (viii) This technique is financially feasible and cost savvy as the raw material is easily available at very low cost and low cost of selling and distribution because of existing demand in the market.

**Acknowledgements** The authors are grateful to the Director of the School of Technology, Pandit Deendayal Energy University, Gujarat, India, for providing necessary laboratory facilities. Author's gratitude also goes to the Institute of Commerce at Nirma University, Ahmedabad, Gujarat, India, for their academic insights and contributions to the research and the interdisciplinary exchange of ideas has enhanced the depth and scope of this study. Authors would like to acknowledge the Department of Chemistry at Sir P. T. Science College Modasa, for their valuable inputs and expertise in the chemical aspects of our research.

## References

1. Malik R, Ramteke DS, Wate SR (2007) Adsorption of malachite green on groundnut shell waste based powdered activated carbon. *Waste Manage* 27(9):1129–1138
2. Garg VK, Amita M, Kumar R, Gupta R (2004) Basic dye (methylene blue) removal from simulated wastewater by adsorption using Indian rosewood sawdust: a timber industry waste. *Dyes Pigment* 63:243–250
3. Bansode RR, Losso JN, Marshall WE, Rao RM, Portier RJ (2003) Adsorption of metal ions by pecan shell based granular activated carbons. *Biores Technol* 89:115–119
4. Ankur K, Collin G, Faujan J, Ahmad BH, Zulkarnian Z, Hussain ZM, Abdullah HA (2001) Preparation and characterization of activated carbon from Resak wood (*Vatica hulletti*). *Res J Chem Environ* 5(3):21–24
5. Tsai WT, Chang CY, Wang SY, Chang CF, Chien SF, Sun HF (2000) Cleaner production of carbon adsorbents by utilizing agricultural waste corn cob. *Resour Conserv Recycl* 32:43–53
6. McKay G, El-Guendi MS, Nassar MM (1997) Equilibrium studies for the adsorption of dyes on bagasse pith. *J Adsorp Sci Technol* 15:251–270
7. Amin NK (2008) Removal of reactive dye from aqueous solutions by adsorption onto activated carbons prepared from sugarcane bagasse pith. *Desalination* 223:152–161
8. McKay G, El Geundi M, Nassar MM (1996) Pore diffusion during the adsorption of dyes onto bagasse pith. *Process Saf Environ Prot* 74(4):277–288

9. Smith J, Johnson E, Williams D, Brown S (2019) Removal of methyl orange dye using banana peel. *J Environ Chem* 25(4):123–135
10. Johnson A, Lee J, Martinez R, Chen L (2020) Utilization of rice husk for Congo red dye removal. *Waste Manage Res* 32(6):567–578
11. Lee S, Garcia E, Wong C, Zhang Q (2018) Adsorption of crystal violet dye on citrus peel waste. *J Hazard Mater* 15(3):89–102
12. Martinez R, Kim M, Ramirez M, Patel S (2017) Malachite green removal using pineapple peel. *J Water Pollut Control* 12(2):201–214
13. Chen L, Garcia E, Wong C, Zhang Q (2019) Adsorption of acid red 27 dye on coconut shell ash. *Environ Sci Pollut Res* 28(5):4112–4124
14. Kim M, Ramirez M, Patel S, Chang W (2021) Removal of direct blue 71 using corn cob waste. *J Appl Chem* 40(7):1556–1568
15. Garcia E, Wong C, Zhang Q, Park H (2020) Application of olive pomace for basic red 46 dye removal. *Chemosphere* 18(9):789–800
16. Wong C, Zhang Q, Park H, Liu T (2018) Sugarcane bagasse as an adsorbent for reactive blue 5. *Environ Technol* 22(1):217–230
17. Zhang Q, Park H, Liu T, Ramirez M (2019) Adsorption of acid yellow 23 dye on wheat straw. *Water Res* 35(8):1123–1136
18. Park H, Liu T, Ramirez M, Patel S (2017) Disperse orange 3 dye removal using coffee grounds. *Chem Eng J* 10(6):452–465
19. Liu T, Patel S, Chang W, Khan M (2020) Removal of basic violet 14 dye using soybean residue. *J Environ Sci* 28(12):1501–1514
20. Ramirez M, Kim M, Patel S, Garcia E (2018) Adsorption of acid blue 9 dye on grape pomace. *J Chem Eng* 5(3):324–337
21. Patel S, Chang W, Khan M, Lee S (2021) Removal of reactive red 120 using potato peel waste. *Environ Sci Technol* 42(9):2019–2032
22. Chang W, Khan M, Lee J, Martinez R (2019) Tomato skin waste as an adsorbent for direct black 38 dye. *Waste and Biomass Valorization* 16(5):1245–1256
23. Khan M, Lee S, Garcia E, Wong C (2020) Application of carrot tops for acid green 25 dye removal. *J Clean Prod* 28(8):701–714
24. Smith J, Johnson AB, Brown CD (2010) Chemical composition of wheat straw and its potential as a resource for ethanol-based transport fuels. *Biores Technol*. <https://doi.org/10.1016/j.biortech.2010.01.001>
25. Zhang H, Lin S, Huang Y (2011) Surface functional groups of activated carbons and the correlation with lead adsorption. *Chem Eng J*. <https://doi.org/10.1016/j.cej.2011.01.030>

# Integrated Assessment of Groundwater of Dudhwada Village of Padra Taluka with Special Reference to Industrial Pollution



Dhruvi Rana and Sanskriti Mujumdar

## 1 Introduction

Gujarat exhibits prominent variations in topography and annual precipitation, with approximately 75% of the region being unsuitable for groundwater extraction due to its rocky terrain and coastal features [1, 2]. Irregular precipitation patterns have resulted in an inequitable dispersion of water across various geographical areas [3]. The aggregate volume of water accessible within the state is estimated to be 50 billion cubic meters, with 38 billion cubic meters constituting surface water and the remaining 12 billion cubic meters comprising groundwater [2].

A significant proportion, exceeding 80%, of the total volume of surface water, which amounts to 38 billion cubic meters, is allocated for the purpose of irrigation. This allocation is heavily reliant on groundwater resources, primarily due to the scarcity of potable water and industrial provisions [2]. Groundwater is the subsurface water found beneath the Earth's surface, infiltrating fissures within the soil and rock formations. Precipitation serves as the primary hydrological input for groundwater, as it infiltrates the soil directly and undergoes natural replenishment. Out of the world's total freshwater resources, groundwater accounts for 0.614%, rivers—0.005% and lakes—0.008% [4].

Groundwater serves as a vital source of water for both domestic and industrial purposes, as well as for irrigation on a global scale. Its availability and suitability are influenced by various factors, including the quality of recharged water, atmospheric precipitation, inland surface water, and subsurface geochemical processes

---

D. Rana

Department of Environment Studies, Faculty of Science, The Maharaja Sayajirao University of Baroda, Vadodara, India

S. Mujumdar (✉)

Civil Engineering Department, Faculty of Technology and Engineering, The Maharaja Sayajirao University of Baroda, Vadodara, India

e-mail: [ssmujumdar-ced@msubaroda.ac.in](mailto:ssmujumdar-ced@msubaroda.ac.in)

[5]. Periodic fluctuations in groundwater quality can be attributed to variations in the source and composition of recharged water, as well as hydrological and anthropogenic factors that evolve over time [6]. The rise in human-induced activities has resulted in significant impacts on the groundwater in multiple regions of Padra Taluka. The Padra Taluka in Vadodara exhibits a verdant landscape and possesses the capacity to serve as a significant source of vegetables for various regions [1]. However, it has concurrently experienced contamination as a result of industrial activities. The central objective of this study pertains to the examination of the groundwater contamination resulting from industrial effluent discharge, and its subsequent impact on the vegetation in Dudhwada and the adjacent regions of Padra Taluka. The Dudhwada region, along with its surrounding areas in Padra, is recognized as a highly developed industrial zone within the state of Gujarat. However, the majority of farmers in this region, who rely on agriculture for their livelihoods, are facing significant negative impacts as a result of the discharge of harmful chemicals. A study carried out in 2016 for assessment of groundwater quality for Vadodara district had concluded at that time that 72% of the area was fit for the purpose of drinking water [7]. However, rapid industrialization and growth of small-scale industries can play a vital role in the deterioration of groundwater quality. The same was established through a study involving screening of biological and physicochemical parameters of groundwater around Vadodara City carried out in 2019 [8] besides industrial waste, improper disposal of domestic sewage can also impact the groundwater quality which is usually the case in semi-urban or rural areas [9]. With the impact of climate change, the availability of freshwater itself becomes a big challenge and hence conservation of existing sources is of prime importance [10].

## 2 Materials and Methods

### 2.1 Study Area

Dudhwada village is situated within the Padra Taluka of the Vadodara district in the state of Gujarat, India. It is geographically positioned at the coordinates 22.189595 latitude and 72.888562 longitude. The aggregate geographic expanse of the village measures 614.48 hectares. Dudhwada exhibits a population size of 1854 individuals. Dudhwada village is estimated to contain approximately 460 residential dwellings. Padra is the closest urban settlement to Dudhwada, located at an approximate distance of 26 km [11]. Dudhwada is a highly industrialized village located in the Padra town of the Vadodara district in the state of Gujarat. Several renowned industrial conglomerates have made investments in the Padra-Jambusar state highway. Over the course of recent years, there has been a notable and abrupt surge in industrialization within Dudhwada village. This surge has resulted in the establishment of various small to medium-scale industries, including those involved in the production of dyes, pharmaceuticals, glass, and electronics. Consequently, this industrial development

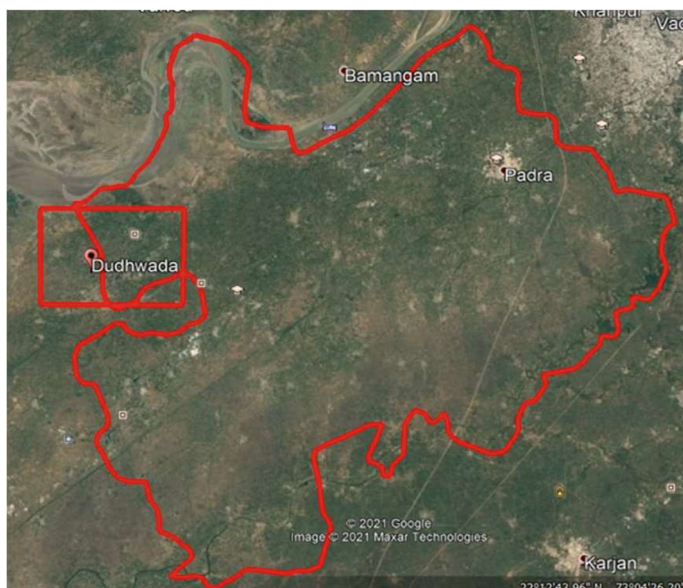


**Fig. 1.** Location of Dudhwada village. *Source* Google Earth

has directly impacted the agricultural sector and the availability of natural resources, leading to observable changes. Figure 1 shows the location of the Dudhwada site which has been selected for the study and Fig. 2 shows the locations for the sampling sites. Both the figures have been created using Google Earth.

## 2.2 Sample Collection

Dudhwada and the adjacent villages of Padra, including Piludara and Karakhdi, were selected as the primary study areas for the purpose of monitoring and identifying the sources for water sample collection. In a stochastic manner, a total of 12 samples were acquired from diverse geographical points within the Dudhwada region. The primary methods employed for sample collection included bore wells, tube wells, and hand pumps. Water samples were obtained for the purpose of analyzing various physiochemical parameters, such as pH, electrical conductivity (EC), total dissolved solids (TDS), sodium (Na), potassium (K), calcium (Ca), magnesium (Mg), chloride (Cl), fluoride (F), sulfate ( $\text{SO}_4$ ), phosphate ( $\text{PO}_4$ ), chemical oxygen demand (COD), dissolved oxygen (DO), chromium (Cr), iodine (I), manganese (Mn), nickel (Ni), cobalt (Co), lead (Pb), calcium (Ca), zinc (Zn), cadmium (Cd), and copper (Cu), as well as heavy metals. Table 1 shows the inventory of the villages from which the sampling procedure was conducted.

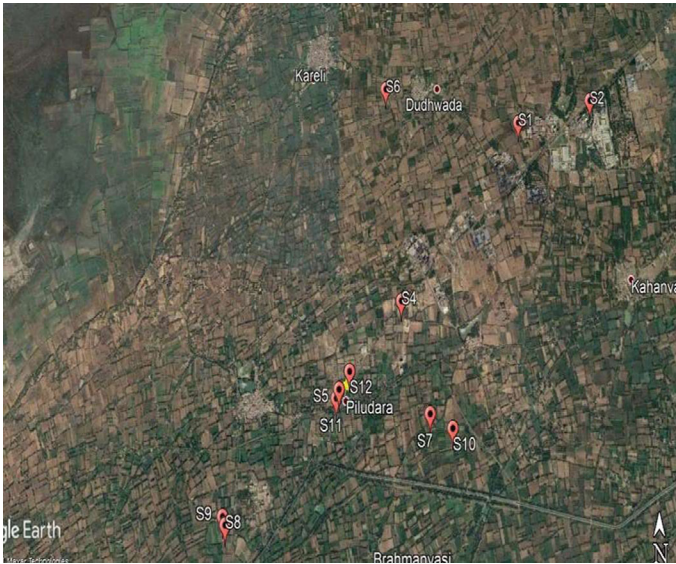


Fig. 2 Sampling sites. Source Google Earth

### 2.3 Methodology Adopted

Various researchers have emphasized on the importance of study of physicochemical and biological characteristics of groundwater sample for evaluation of water quality parameters to be carried out periodically to protect the water resources [12]. Research based on fluoride contamination and its effect on health has been carried out for different parts of the country by several researchers [13, 14]. Barodawala et al. [15] have established water quality index for Vadodara City in March 2018. Pandey et al. [16] have carried out study on the status of groundwater quality across Vadodara City. American Public Health Association has prescribed standard methods for examination of water and wastewater for assessment of its quality [17]. For this study, the samples were analyzed both for physical and chemical water quality parameters. The analysis was carried out for the major ions using the standard procedures. The pH was determined using pH meter (Model Lab India); TDS was measured by TDS meter. Electrical conductivity was measured using digital conductivity meter. Turbidity was analyzed by digital turbidity meter (Model 331 E). Cr, I, Mn, Ni, Co, Pb, Ca, Zn, Cd, and Cu heavy metals which were determined using AAS (Model Analyst 200); Na and K by flame photometer (Model Medi 382 E); total hardness (TH), calcium hardness, acidity, alkalinity, free CO<sub>2</sub>, sulfide by titrimetric method, and COD by open reflux method, DO by wrinkler's method, sulfate, fluoride, and nitrate by spectrophotometer.

12 Groundwater samples were collected. The following steps were taken in consideration during collection of samples.

**Table 1** Sampling locations

Sr. No.	Sources of collection	Area	Sampling sites	Coordinates
S1	Bore well	Agriculture field just behind industries	Dudhwada	Lat. 22.191061 Long.72.893842
S2	Bore well	Agriculture field just behind industries	Dudhwada	Lat. 22.193224 Long. 72.90416
S3	Tube well	Agriculture	Dudhwada	Lat. 22.181154 Long. 72.818897
S4	Bore well	Agriculture	Dudhwada	Lat. 22.174417 Long.72.87684
S5	Tube well	Residential	Piludara	Lat. 22.166652 Long. 72.868348
S6	Tube well	Residential	Piludara	Lat. 22.200821 Long. 72,867,127
S7	Hand pump	Agriculture	Piludara	Lat. 22.158484 Long. 72.86281
S8	Tube well	Residential	Piludara	Lat. 22.155326 Long. 72.853579
S9	Tube well	Agriculture	Piludara	Lat. 22.328484 Long. 72.756725
S10	Tube well	Agriculture cum residential	Piludara	Lat. 22.155326 Long. 72.853579
S11	Tube well	Agricultural	Piludara	Lat. 22.165891 Long. 72.867979
S12	Hand pump	Residential	Dudhwada Piludara border	Lat. 22.167813 Long 72.869087

- Selection of containers: Collection of samples was plastic carboy of 2 L each for each sample and 250 ml of BOD bottles for each. The bottles were thoroughly rinsed before collection of the samples.
- Labeling of containers: Containers were coded by name of location, date, time, and number of containers.
- Preservation of samples: The samples contained in the 250 and 150 ml sampling bottles were preserved by adding HNO<sub>3</sub> to maintain pH.
- Analytical method for study of different parameters.
- The reference that was used for the groundwater analysis is Handbook of Methods in Environmental Studies Vol. 1: Water and Wastewater Analysis by S. K. Maiti, Standard Methods for the Examination of Water and Wastewater by APHA.

A number of visual representations are depicted in Fig. 3, captured at various sampling sites, illustrating the characteristics of the water samples.

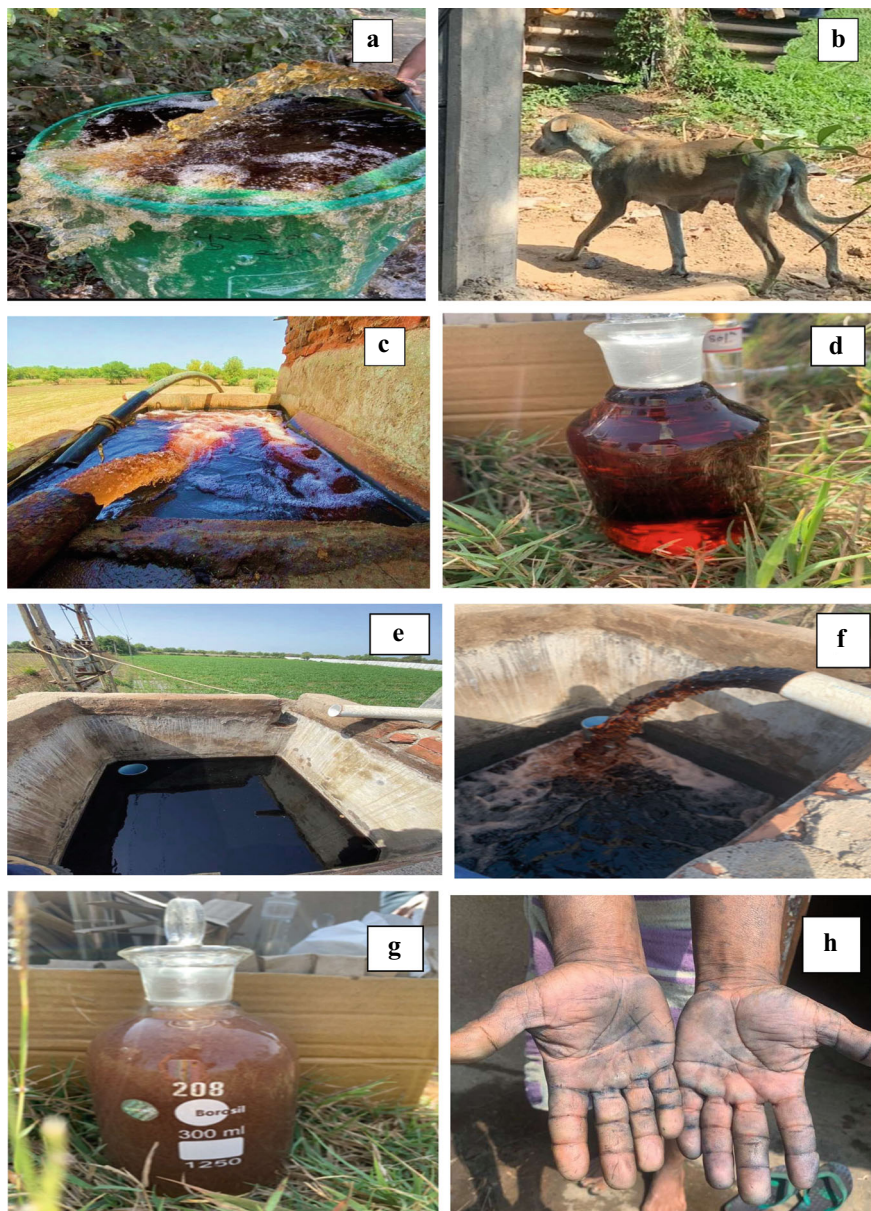


**Fig. 3** Pictures taken during Sampling. **a, c–g** Colored samples due to dye industries; **b** Effect of dye industry on stray animals; **h** Skin infections caused in worker's hand due to dye industry

### 3 Results and Discussion

A thorough examination was performed on the physicochemical characteristics of 12 groundwater samples obtained during the period of February to March 2022. The examined physical parameters include the optical properties, spectral characteristics, electrical conductivity, and concentration of solutes. The chemical parameters that were examined encompassed pH, alkalinity, total hardness (TH), calcium, magnesium, sodium, potassium, fluoride, sulfate, turbidity, and heavy metals. Based on the extensive survey conducted along the effluent channel belt, it was observed that groundwater samples obtained from the villages situated in close proximity to the disposal point of the channel displayed observable indications of groundwater contamination attributable to the presence of effluent. Table 1 displays the highest and lowest concentrations recorded for different parameters analyzed in the groundwater of the designated study region.

The recommended water quality standards for drinking purposes are provided for the purpose of conducting comparative analysis. The research results suggest that a considerable number of samples, mainly collected from Dudhwada and Piludara villages, demonstrate notably higher concentrations of pollutants that surpass the acceptable threshold for groundwater quality set by the World Health Organization (2004). The pH values of the groundwater ranged from 7.1 to 8.2, suggesting a slightly alkaline to alkaline characteristic of the groundwater. As per the World Health Organization [18], the recommended pH range for drinking water is 6.5–8.5. No groundwater samples were found to have pH values outside the acceptable range. The recorded values of EC (electrical conductivity), TDS (total dissolved solids), alkalinity, turbidity, fluoride, and hardness during the study exceeded the allowable range as shown in Table 2. The heavy metal analysis results for the samples are presented in Table 3. In the current investigation, all of the heavy metals were observed to fall within the established range.

### 4 Fixed Sensitivity of Heavy Metals (AAS)

### 5 Conclusions

Based on the GPCB July 2016 Report, it is suggested that the primary cause of groundwater contamination in this region may be attributed to unlawful practices conducted by dye intermediate facilities. This inference is supported by the observable coloration of the collected groundwater samples. The assertion made by farmers and local residents in the region suggests that numerous industries are engaging in illicit practices that result in the pollution of subterranean water sources.

Farmers are experiencing significant levels of displeasure as a result of the contamination of their bore wells caused by groundwater pollution, compounded by the perceived inadequacy of measures implemented by relevant authorities. According

**Table 2** Statistical comparison of parameters with BIS Standards (IS 10500)

Parameters	Min.	Max.	Average	SD	BIS/WHO Std. (acceptable- permissible limit)	Unit
pH	6.8	8.9	7.91	0.41	6.5–8.5	
Electrical conductivity	412	6971	2523	1433.20	1500	1500
Dissolved oxygen	0.4	15.16	4.25	3.25	8	ppm
Total dissolved solids	239	4598	1396.50	770.50	500–2000	ppm
Acidity	8.6	185	35.57	23.77	-	ppm
Alkalinity	41.7	1366.7	496.45	261.18	200–600	ppm
Sulfate	0.04	1.90	0.92	0.44	200–400	ppm
Turbidity	0.1	62.6	5.78	6.56	1–5	NTU
Fluoride	0.355	1.99	1.28	0.21	1–1.5	ppm
Hardness	138	2130	566.45	432.42	200–600	mg/l as CaCo <sub>3</sub>
Ca hardness	98	673.4	163.96	116.53	300	mg/l as CaCo <sub>3</sub>
Mg hardness	104	1843.8	405.47	405.71	100	mg/l as CaCo <sub>3</sub>
Na <sup>+</sup>	7.76	269.99	126.44	50.27		ppm
K <sup>+</sup>	1.07	76.73	3.06	11.85		ppm
Chemical Oxygen demand	4	68	23.79	11.70	250	ppm
Free CO <sub>2</sub>	0	8.8	8.72	0.86	–	ppm
Sulfide	–19.2	–2.6	–8.44	3.7	0.05-No relaxation	ppm
Nitrate	0.06	4.35	1.84	0.93	45-No relaxation	ppm
Mg	8.5	885.23	191.29	189.24		ppm
Ca	74.04	272.61	1.56	68.43		ppm

**Table 3** Sensitivity range of heavy metals

Heavy metals	Min. sensitivity	Max. sensitivity	Max range of samples
Cr	0.078	4	ND
Cd	0.01	0.5	0.286
Fe	0.04	2	1.025
Co	0.053	3	0.051
Ni	0.06	3	0.037
Cu	0.025	1.3	ND
Mn	0.016	1	ND
Pb	0.18	8	0.184
Zn	0.05	0.3	ND

to the order (dated 07.05.2004) of the Honourable Supreme Court in Written Petition 65712004, the Supreme Court Monitoring Committee (SCMC) has identified Dudhwada village in Padra Taluka of Vadodara district as being impacted by groundwater contamination. In response, the Supreme Court has directed the state government to provide clean drinking water to these affected villages. However, the villages in question lack a sufficient water supply for drinking purposes, as claimed by the villagers. The farmers expressed concerns regarding alternative applications of water, specifically for agricultural and livestock purposes. The local inhabitants and agricultural workers are utilizing water that has been compromised by pollutants for their household and farming requirements. Additionally, due to the unavailability of water of satisfactory quality, livestock are consuming this water. The bore wells in the villages of Karkhadi, Dudhwada, and Piludara exhibit clear signs of pollution, as evidenced by the observed concentrations of various parameters. Groundwater monitoring stations are strategically positioned in close proximity to dye intermediate industries for comprehensive surveillance.

### ***5.1 Recommendations***

Based on the findings of the scientific analysis, it is imperative to implement immediate measures to mitigate the significant release of chemicals into the groundwater. This is to mitigate potential adverse effects on human health. The current situation is of utmost significance owing to the elevated levels of pollution. The discharge of chemicals used in nearby industries, which were established during later stages, can be attributed to their technical responsibility.

The bore wells, hand pumps, and other small bodies of water that serve as drinking water sources for numerous animals have undergone a reddish discoloration. Approximately, 70% of agricultural practitioners employ the identical water source for the purpose of cultivating crops. Regrettably, it has led to a complete loss of their entire production. Farmers residing in the neighboring village encounter difficulties in organizing the procurement of potable water.

Multiple petitions and legal cases have been submitted regarding this matter, and ultimately, the Supreme Court has granted acceptance of the case, ruling in favor of the farmers. Regrettably, there has been a lack of intervention regarding the current circumstances, resulting in the unresolved state of the farmers' predicament.

The governing bodies should explore alternative solutions to resolve the current impasse. It is imperative to establish a reliable and accessible water supply system to facilitate agricultural sustainability for farmers. Portable reservoirs in close proximity to agricultural fields, which rely on a primary water source, should be strategically positioned to receive water from the canal or another prominent water source. This measure will ultimately mitigate the existing concerns regarding the utilization of water that has been contaminated, pending the issuance of the final ruling by the Supreme Court.

**Declaration of Competing Interest** The author states that they have no conflicts of interest.

## References

1. Nayak KM (2020) Ground water yearbook 2018–19. Central Ground Water Board (CGWB). [https://www.cgwb.gov.in/old\\_website/Regions/WCR/Reports/Gujarat\\_State\\_Year\\_Book\\_2018-19.pdf](https://www.cgwb.gov.in/old_website/Regions/WCR/Reports/Gujarat_State_Year_Book_2018-19.pdf)
2. Central Ground Water Board GWR, LTD DC (2022) Report on dynamic ground water resources of Gujarat State. [https://www.cgwb.gov.in/old\\_website/GW-Assessment/GWR-2022-Reports/State/Gujarat.pdf](https://www.cgwb.gov.in/old_website/GW-Assessment/GWR-2022-Reports/State/Gujarat.pdf)
3. Chang H, Bonnette MR (2016) Climate change and water-related ecosystem services: impacts of drought in California, USA. *Ecosyst Heal Sustain* 2(12):e01254
4. Nace RL (1975) Are we running out of water? Geological survey circular, vol 536. <http://www.tandfonline.com/doi/full/10.1179/ida.2010.2.3.1>
5. Wang W et al (2023) Water quality and interaction between groundwater and surface water impacted by agricultural activities in an oasis-desert region. *J Hydrol* 617:128937
6. WWQA (2022) World water quality alliance—work plan 2021–2022 alliance: Strategic Advisory Committee (SAC) and Technical Advisory Committee (TAC) Africa use cases a scoping different approaches for the stakeholder engagement and co-design process for the Lak
7. Agrawal S, Patel HM, Prakash IPA (2016) Ground water quality assessment of Vadodara district, Gujarat, India using GIS. *J Groundw Res* 5:495–504
8. Patel C, Ghorai Giri S (2019) Screening of biological physico-chemical parameters of ground water around Vadodara city, vol 6, pp 91–95
9. Kushwaha VB, Agrahari M (2017) Effect of anthropogenic activities on the physico-chemical quality of river Rapti effect of anthropogenic activities on the physico-chemical quality of river Rapti at Gorakhpur, India
10. Mishra RK (2015) Fresh water availability and its global challenge. *Int J Eng Sci Invent Res Dev* 2:1–3
11. Dudhwada Village. <https://villageinfo.in/gujarat/vadodara/padra/dudhwada.html>
12. Dohare D, Deshpande S, Kotiya A (2014) Analysis of ground water quality parameters: a review. *Res J Eng Sci* 3:2278–9472
13. Bhattacharya P et al (2020) Health risk assessment of co-occurrence of toxic fluoride and arsenic in groundwater of Dharmanagar region, North Tripura (India). *Groundw Sustain Dev* 11:100430
14. Dave RS (2010) Status of fluoride in ground water of several villages of Modasa Taluka, North Gujarat for drinking purpose. *Pharmacia* 2:208–220
15. Barodawala S, Parmar P, Prasad B (2018) Ground water quality index of growing smart city of Vadodara. *Int J Environ Sci Nat Resour*. 9:57–62
16. Pandey H, Thivakaran GA Study on the status of ground water quality across Vadodara city. *Int J Recent Eng Res Dev* 27–34
17. APHA (2014) Reagents and standards as per standard methods for the examination of water and wastewater
18. WHO (2004) The Global Burden of Disease Publication

# Toluene–Water Removal from Synthetic Water Using Air Gap Membrane Distillation



Divya Gaur, Sushant Upadhyaya, Kailash Singh, and Rajeshwar Kholapure

## 1 Introduction

With the progression of time and the expansion of the global population, the demand for clean water for numerous uses is rising. As can be seen, agriculture is the sector with the most water consumption [1]. The majority of the world's freshwater resources are saline. Fresh water (2.5%) is either buried underground (30% of 2.5% fresh water) or in the form of ice/snow covered mountainous regions, such as the Antarctic and Arctic (70% of 2.5% fresh water); however, only 0.3% is accessible to humans [2, 3]. Considering the limited quantity of essential clean water, the unveiling of an alternative source for freshwater production is an important subject. Aside from desalinating saline sources, exploring water reclamation from wastewater treatment stands as a promising and emerging solution to meet the projected global need for fresh water. Various sectors such as petrochemicals, fuel refineries, agriculture, food processing, textiles and leather industries, among others, have generated significant amounts of fresh water [4, 5]. Out of the multitude of methods employed for wastewater treatment, membrane-based procedures distinguish themselves by virtue of their manifold benefits. It is common practice to employ the aforementioned techniques: capacitive deionization (CDI), electrodialysis (ED), microfiltration (MF), ultrafiltration (UF), and nanofiltration (NF). The majority of these techniques function as pressure-driven mechanisms, wherein pressure differentials provide the impetus for the process of separation. Nonetheless, there are disadvantages to relying on hydraulic pressure differences. An important drawback of pressure-driven membrane processes is their vulnerability to osmotic pressure constraints, which is especially problematic when brine desalination and highly saline wastewaters are being treated with RO or NF methods. Therefore, exploring new alternatives for water and wastewater

---

D. Gaur · S. Upadhyaya (✉) · K. Singh · R. Kholapure  
Department of Chemical Engineering, Malaviya National Institute of Technology, Jaipur 302017, India  
e-mail: [supadhyay.chem@mnit.ac.in](mailto:supadhyay.chem@mnit.ac.in)

treatment is of considerable importance. Eliminating toluene from water requires the use of various membrane filtration techniques, including absorption, adsorption/co-precipitation, reverse osmosis, membrane distillation, coagulation and flocculation, absorption-ultrafiltration hybrid method, and liquid–liquid extraction. Separation by membrane distillation arises as an attractive and promising technique among the numerous approaches for treating toluene-contaminated wastewater [5, 6].

The principle underlying membrane distillation (MD) is thermal. Variations in vapor pressure difference facilitate the transport of water vapor molecules from the source water/wastewater across the hydrophobic membrane during this method [7]. By employing the MD technique, non-volatile solutes can be entirely rejected (100 percent), resulting in permeate water of high quality. In contrast to pressure-driven membrane processes such as reverse osmosis and ultrafiltration, membrane distillation is relatively unaffected by variations in salinity levels, as changes in vapor pressure have a negligible impact on the process [8]. Furthermore, in contrast to pressure-driven membrane processes such as reverse osmosis (RO) and nanofiltration (NF), MD exhibits a reduced susceptibility for contamination, which consequently leads to a reduction in flux. For instance, in RO applications,  $\text{CaSO}_4$  can induce severe scaling problems. Although pretreatment is not a prerequisite for the MD process, it might be necessary for pressure-driven processes like RO [9]. A total of four configurations comprise membrane distillation. Vacuum membrane distillation (VMD), sweeping gas membrane distillation (SGMD), air gap membrane distillation (AGMD), and direct contact membrane distillation (DCMD) are among these. Within the framework of membrane distillation, air gap membrane distillation (AGMD) is a distinct configuration. AGMD involves the integration of an air gap and a condensation layer within the membrane module. Although the presence of an air gap introduces additional resistance to mass transfer and leads to a reduction in flux, its primary function is to act as an insulator, effectively mitigating heat loss and minimizing temperature polarization [10, 11]. Few researchers had worked in the removal of volatile organic compound using vacuum membrane distillation (VMD). However, due to less difference in vapor pressure, effective separation was not obtained in VMD [12]. Therefore, another configuration of MD known as air gap membrane distillation (AGMD) is considered in this work for the removal of toluene from synthetic water.

To the authors' knowledge, there has been no work reported on the toluene separation by air gap membrane distillation till date. In this present paper, hydrophobic microporous membrane has been used for the separation of toluene-water. Effects of different operating parameters viz. feed inlet temperature and feed flow rate were investigated on the total permeate flux and selectivity at different air gap width. Fouling of membrane before and after experiments has been analyzed using field emission scanning electron microscopy.

**Table 1** Membrane characteristics

Properties	Specifications
Material	PTFE
Hydraulic diameter (mm)	55
Nominal pore size ( $\mu\text{m}$ )	0.22
Porosity %	85
Thickness ( $\mu\text{m}$ )	150
Manufacturer	Millipore

## 2 Experimental

### 2.1 Materials

Poly-tetra-fluoro-ethylene (PTFE) microporous hydrophobic membrane (purchased from Millipore, U.S.A.) was used. A Vernier Caliper was used to gage the membrane thickness, and the reading was contrasted with the figure provided by the supplier. The outline of the membrane characteristics is given in Table 1. Using a single distillation apparatus, de-ionized water (DI) was made in the laboratory. Certified ACS grade toluene (>99.0%, EMPLURA) is acquired from Savita Chemicals Co., Ltd. (India).

### 2.2 Membrane Characteristics

Scanning electron microscopy (Nova Nano FE-SEM 450) was employed to capture surface images of membrane (before and after) experiments, utilizing an acceleration voltage of 10 kV and  $10,000\times$  magnifications. For the surface images, membrane portions ( $1\times 1\times 1$  cm) were cut and mounted on the aluminum stubs using carbon tape. To ensure conductivity of the sample prior to imaging, it was coated with a layer of gold using sputtering technique.

### 2.3 Experimental Setup

The schematic representation of AGMD system is shown in Fig. 1. Using an assembled laboratory test-cell module, AGMD experiments were carried out. The feed solution present in the feed tank circulated continuously through the feed section of the AGMD module with the assistance of an acid pump. For temperature measurement of the feed solution, a Type-J thermocouple is employed. The cooling water is circulated from the chiller to the cooling section of the membrane module. Rotameters were used to determine the volumetric flow rates of the feed section and cooling

water section. AGMD studies were carried out at a range of feed temperatures (40–60 °C), with the cooling water temperature held constant at 8 °C. Therefore, as an outcome, vapor formed on the feed side flows through the membrane and condenses on the cooling plate in the air gap. The concentration of permeate was determined by collecting it and analyzing it using UV–Visible spectrophotometer (double beam) at 264 nm.

Every hour, the amount of permeate was monitored, and total permeate flux ( $J$ ) was established by Eq. 1 [13]:

$$J = \frac{V_p}{A_m \times t} \quad (1)$$

where  $V_p$ , volume of permeate (kg),  $A_m$ , membrane area ( $m^2$ ), and  $t$  (time, hr).

Toluene removal has been estimated using Eq. 2.

$$\alpha = \left( \frac{y_t/x_t}{(1 - y_t/1 - x_t)} \right) \quad (2)$$

where  $\alpha$ ,  $y_t$ , and  $x_t$  are toluene selectivity, mole fractions of toluene in permeate and retentate, respectively [14].

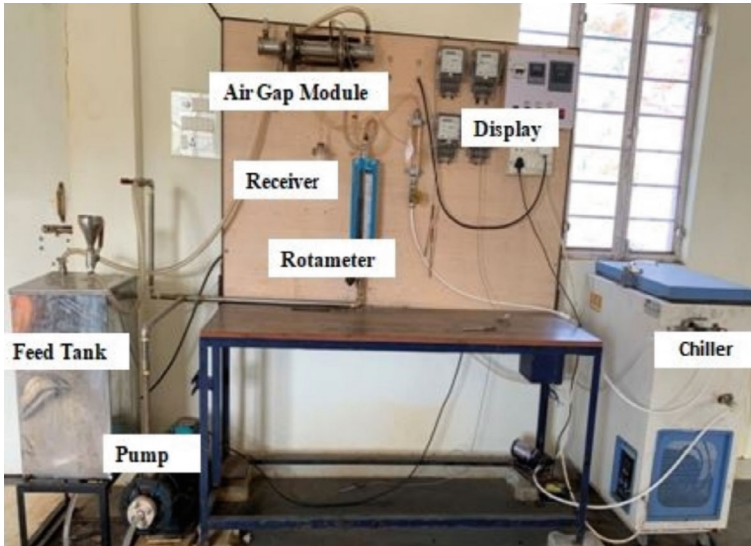


**Fig. 1** Schematic representation of air gap membrane distillation (AGMD)

### 3 Results and Discussions

#### 3.1 Effect of Feed Inlet Temperature

From Fig. 4, it is evident that when the feed inlet temperature increases from (40–60 °C) total, the total permeate flux shows a significant exponential increase at different air gap width (AGW). Specifically, at an air gap of 3 mm, total permeate flux increased from 2.88 to 4.65 kg/(m<sup>2</sup>hr). Similarly, at 7 mm of air gap width, the flux increased from 1.51 to 3.18 kg/(m<sup>2</sup>hr), and at 11 mm of air gap width, it increases from 0.28 to 0.90 kg/(m<sup>2</sup>hr). These observations were made under specific conditions, namely a feed flow rate (FFR) of 2 L/min, toluene concentration of 1000 ppm, a cooling water temperature (CWT) of 8 °C, and cooling water flow rate (CWFR) of 5 L/min. The result concludes that increasing the feed inlet temperature has a noble impact on the total permeate flux, and this effect is more pronounced with narrower gap. Evidently, owing to the exponential correlation between temperature and vapor pressure, it can be inferred that when the temperature rises, the difference in vapor pressure across the membrane also increases, as depicted in Fig. 2. When the feed temperature increased from 40 to 50 °C, the increment ratio of the total flux for 7 mm air gap width is less pronounced compared to the 3 mm air gap. This behavior can be attributed primarily to the resistance to mass transfer caused by air gap. As air gap thickness increases, mass transfer resistance increases, consequently the influence of temperature on permeate flux at narrow air gaps is more substantial than at large air gaps [15].

Vapor pressure of water and toluene is related to temperature by Antoine equation [16].

$$\log P^{\circ} = 10^{(A-B)/(T+C)} \quad (3)$$

where  $A$ ,  $B$ , and  $C$  represent the Antoine constants, and  $T$  is temperature (mmHg). The values of Antoine constants are mentioned in Table 2.

Several researchers (Biniiaz et al. 2019, Marni Sandid et al. 2021, Eryildiz et al. 2020) have identified the same trend of an exponential rise in total permeate flux. The water permeate flux demonstrates an increases from 2.77 kg/(m<sup>2</sup>.h) to 4.38 kg/(m<sup>2</sup>h), from 1.46 kg/(m<sup>2</sup>h) to 3.00 kg/(m<sup>2</sup>h), and 0.27 kg/(m<sup>2</sup>h) to 0.85 kg/(m<sup>2</sup>h), respectively. In parallel, toluene permeate flux experiences an elevation from 0.11 kg/(m<sup>2</sup>h) to 0.27 kg/(m<sup>2</sup>h), from 0.05 kg/(m<sup>2</sup>h) to 0.18 kg/(m<sup>2</sup>h), and 0.011 to 0.053 kg/(m<sup>2</sup>hr) at 40, 50 and 60 °C, can be seen from Fig. 5. In the same operating conditions, despite toluene's higher boiling point than water, permeate flux is lower than that of water. As stated in Eq. 4, the observed variations in water and toluene permeate flux at different temperatures can be attributed to the interaction between the kinetic theory of gases and the corresponding states, which influence the diffusivities of individual component as temperature changes. Using correlation, the water diffusivity in air is estimated to have increased from 0.289 to 0.335 cm<sup>2</sup>/s, while the toluene diffusivity in air increased from 0.126 to 0.146 cm<sup>2</sup>/s on increasing the temperature from 40

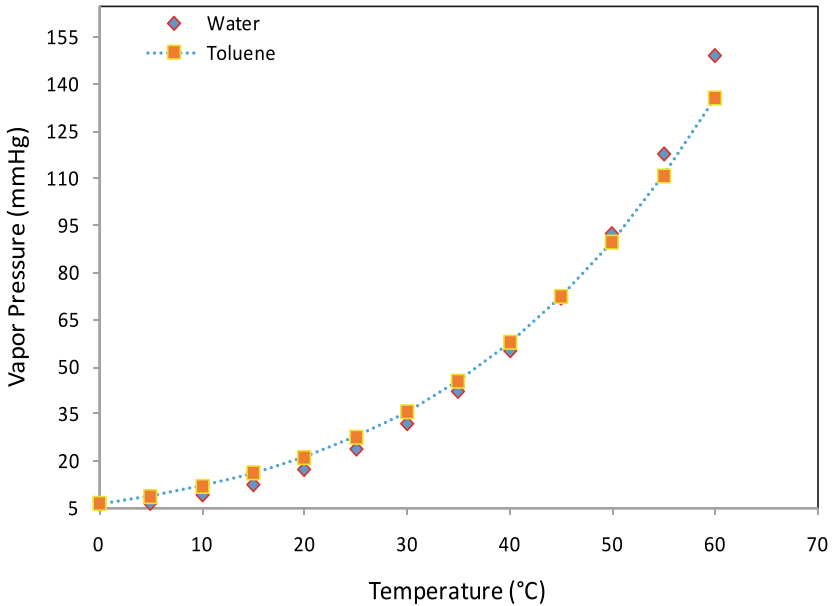


**Fig. 2** Temperature versus vapor pressure using Antoine equation

**Table 2** Antoine constants for toluene and water [17]

Components	A	B	C
Toluene	6.95	1344	219
Water	8.07131	1730.63	233.426

to 60 °C, which can be depicted from Fig. 3. [18]. At a specific temperature, the diffusivity of water is three times that of air. Therefore, the microporous hydrophobic membrane will permit greater water diffusion into the air gap.

From Fig. 6, it was found that with an increase in the feed temperature from 40 to 60 °C, toluene selectivity exhibited a notable rise from 40.02 to 62.80, 39.71 to 62.25, and 41.27 to 63.35 at air gap of 3, 7, and 11 mm, respectively. The toluene selectivity ( $\alpha$ ) is greater than one, and the water selectivity ( $1-\alpha$ ) is less than one in permeate, confirming that the AGMD method is effective for toluene separation. In addition, a greater selectivity is observed at higher temperatures, which contributes to high toluene removal efficiency.

Combining kinetic theory of gases and their corresponding states in terms of the diffusivities of individual components with temperature is described as follows [18]

$$\frac{\rho D_{AB}}{(\rho_{CA}\rho_{CB})^{\frac{1}{3}}(T_{CA}T_{CB})^{\frac{5}{12}}\left(\frac{1}{M_A} + \frac{1}{M_B}\right)^{1/2}} = a\left(\frac{T}{T_{CA}T_{CB}}\right)^b \tag{4}$$

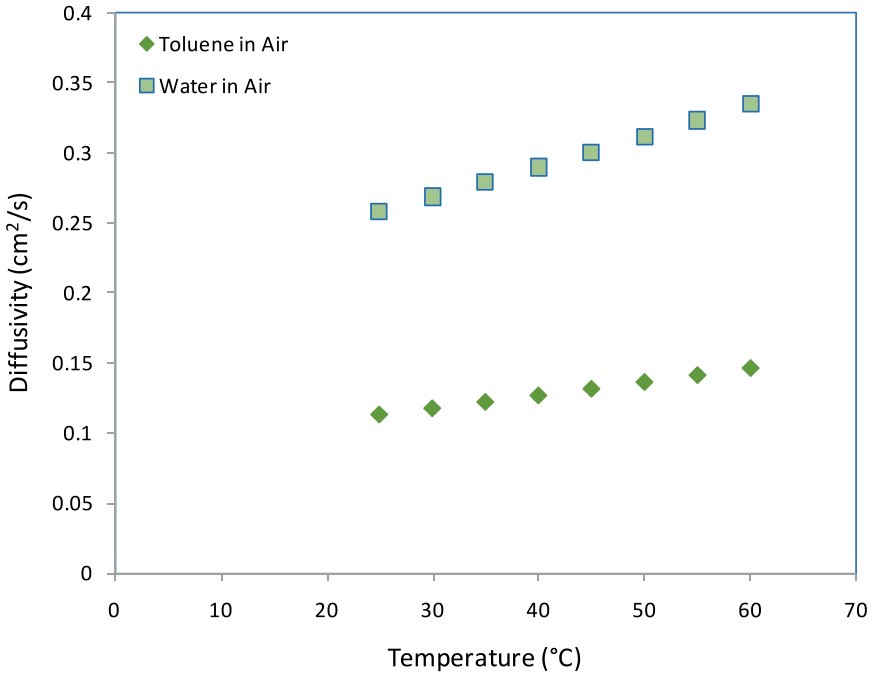


**Fig. 3** Diffusivity of toluene and water in air

where  $\rho_{DAB}$  is diffusivity,  $a$  and  $b$  are dimensionless constant,  $M_A$  and  $M_B$  are molecular weights of toluene and water,  $T_{CA}$  and  $T_{CB}$  are critical temperatures of toluene and water,  $\rho_{CA}$  and  $\rho_{CB}$  are critical pressures of toluene and water, and  $T$  is the temperature (°C).

### 3.2 Effect of Flow Rate

The effects of varying feed flow rate on the total permeate flux can be depicted from Fig. 7. The experiment was conducted at different feed temperatures ranging from 40 to 60 °C. Throughout the experiments, air gap width was kept constant at 3 mm, and coolant temperature remained fixed at 8 °C. It is clear from Fig. 7 that higher feed flow rates result in increased total permeate flux. Specifically at 40 °C

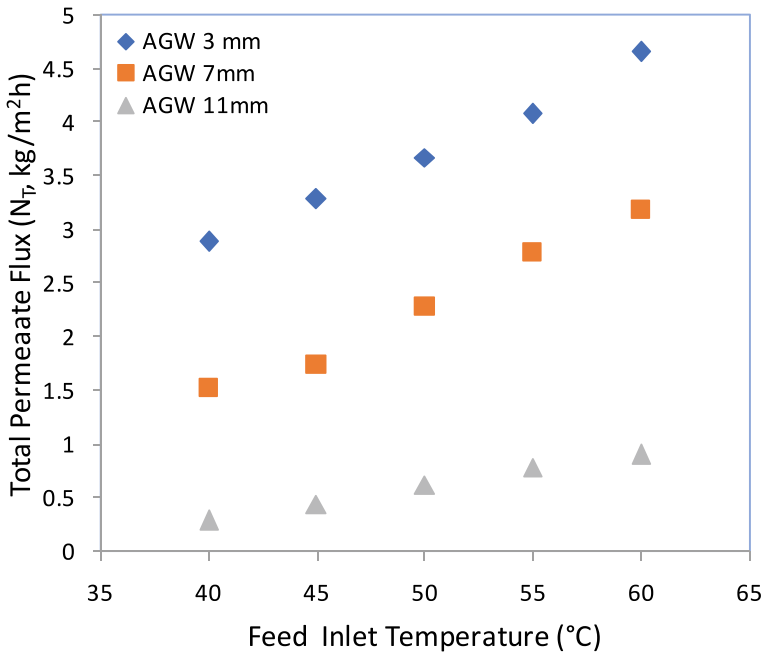


**Fig. 4** Effect of feed bulk inlet temperature on total permeate flux [Toluene concentration = 1000 ppm, Feed flow rate = 2 L/min, Chiller water temperature = 8 °C, Chiller water flow rate = 5 L/min]

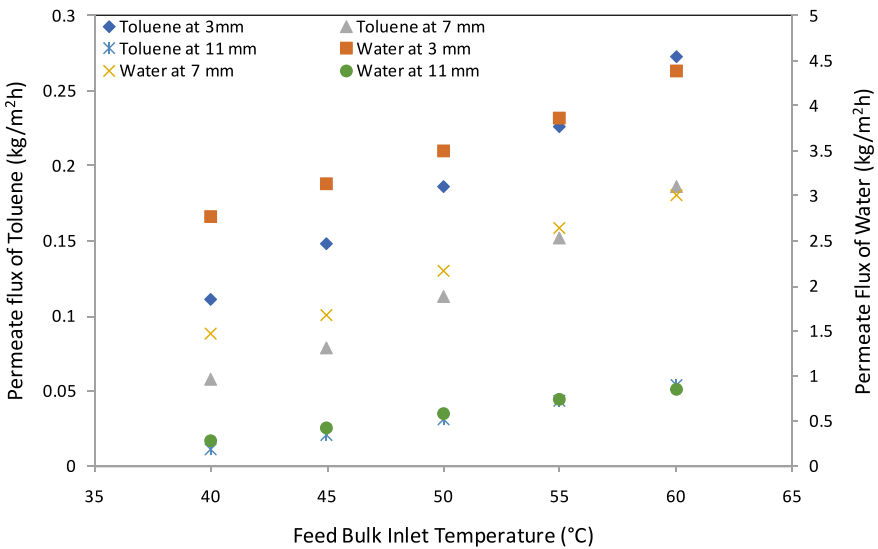


**Fig. 5** Effect of feed bulk inlet temperature on toluene and water permeate flux [Toluene concentration = 1000 ppm, Feed flow rate = 2 L/min, Chiller temperature = 8 °C, Chiller water flow rate = 5 L/min]

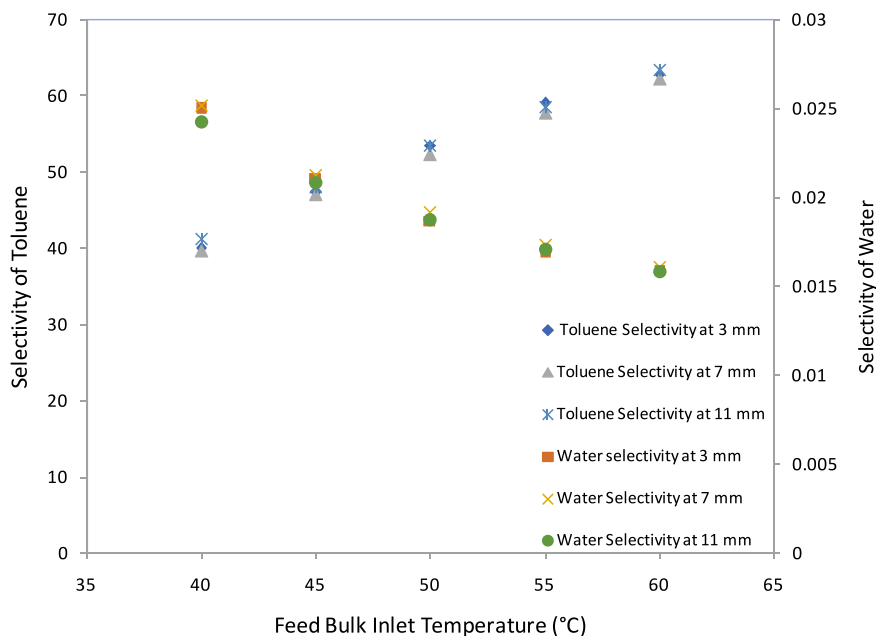


**Fig. 6** Effect of feed bulk inlet temperature on selectivity of toluene and water in permeate [Toluene concentration = 1000 ppm, Feed flow rate = 2 L/min, Chiller water temperature = 8 °C, Chiller water flow rate = 5 L/min]

the permeate flux rises from 2.69 kg/(m<sup>2</sup>h) to 3.7 kg/(m<sup>2</sup>h), at 50 °C it increases from 3.2 to 3.47 kg/(m<sup>2</sup>h), and at 60 °C it elevates from 4.34 kg/(m<sup>2</sup>h) to 5.67 kg/(m<sup>2</sup>h). This phenomenon is explicable by temperature and concentration polarization. On enhancing the mass transfer coefficient, two key factors are observed: First, it reduces the disparity between the bulk concentration and membrane surface concentration. Secondly, it also minimizes the temperature variation between the feed bulk and membrane surface, which is achieved by increasing the Reynolds number. Ultimately, this improvement in the mass transfer coefficient leads to the enhanced transport coefficients [12, 13]. Moreover, the individual permeate flux increment for toluene and water can be depicted from Fig. 8 which shows that the water permeate flux increases from 2.59 kg/(m<sup>2</sup>h) to 3.55 kg/(m<sup>2</sup>h), 3.27 kg/(m<sup>2</sup>h) to 4.20 kg/(m<sup>2</sup>h), and 4.18 kg/(m<sup>2</sup>h) to 5.43 kg/(m<sup>2</sup>h) and the toluene permeate flux from 0.098 kg/(m<sup>2</sup>h) to 0.14 kg/(m<sup>2</sup>h), 0.12 kg/(m<sup>2</sup>h) to 0.17 kg/(m<sup>2</sup>h), and 0.16 kg/(m<sup>2</sup>h) to 0.23 kg/(m<sup>2</sup>h) at 40 °C, 50 °C, and 60 °C of feed temperature, respectively, on increasing the feed flow rate from 1L/min – 5 L/min.

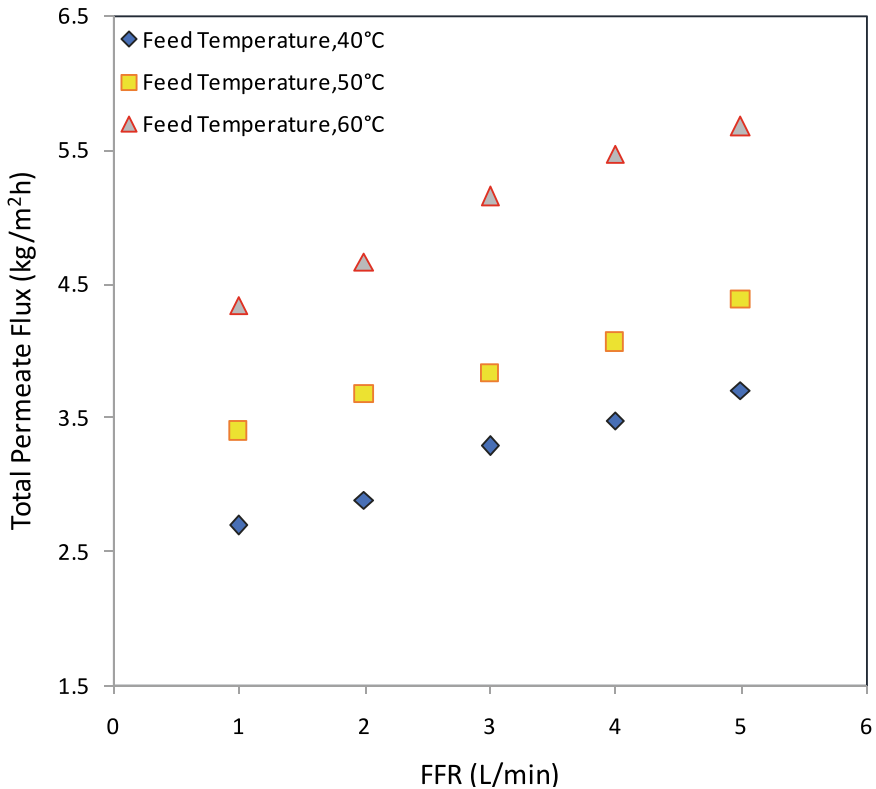


**Fig. 7** Effect of feed flow rate on total permeate flux [Toluene concentration = 1000 ppm, Air gap = 3 mm, Chiller water temperature = 8 °C, Cooling water flow rate = 5 L/min]

#### 4 Membrane Morphology

Membrane fouling was studied before and after experiments using field emission scanning electron microscopy (FE-SEM) and energy-dispersive spectroscopy (EDS) analysis after a continuous run of 250 h. In this work, poly-tetra-fluoro-ethylene (PTFE) hydrophobic porous membrane of pore size 0.22  $\mu\text{m}$  was used. The experimental setup operates continuously for the duration of 250 h with a feed flow rate of 3 L/min. The feed inlet temperature is maintained at 55 °C, and toluene feed concentration is set at 1000 ppm. The system maintains a constant air gap width of 3 mm, cooling/ chiller water at a flow rate of 5 L/min with a temperature of 8 °C. The FE-SEM and EDS micrographs for new brand membrane and used membrane

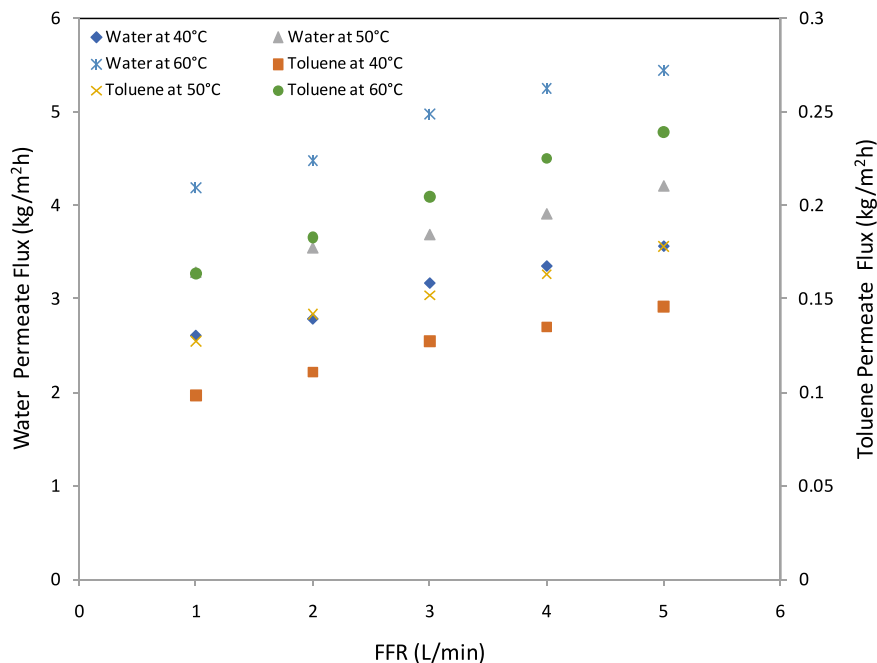
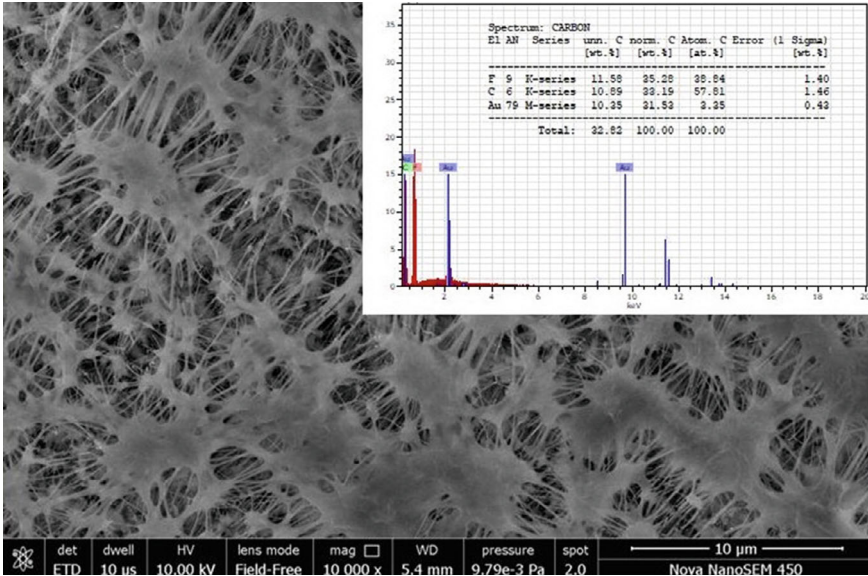
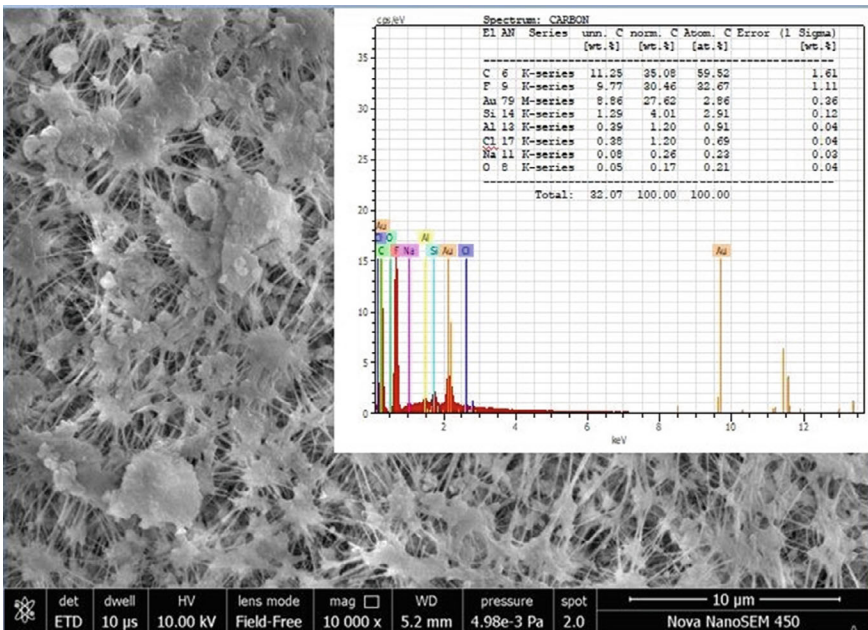


**Fig. 8** Effect of feed flow rate on individual toluene and water flux permeate flux [Toluene concentration = 1000 ppm, Air gap = 3 mm, Chiller water temperature = 8 °C, Chiller water flow rate = 5 L/min]

(after 250 h) at 10,000 × magnification and 10 kV are represented in Fig. 9a and b, respectively. On comparing FE-SEM and EDS images before and after experiment, it shows negligible organic fouling on membrane surface as both the components are volatile in nature. Based on the results mentioned below, it can be concluded that the toluene solution does not cause membrane fouling or scale formation at any feed concentration, or duration of the processes, the phenomenon remains constant.



(a)



(b)

**Fig. 9** a FE-SEM and EDS image of PTFE new brand membrane at 10,000 × magnification  
b FE-SEM and EDS image of PTFE used membrane at 10,000 × magnification

## 5 Conclusion

Experimental investigation was conducted to assess the effectiveness of air gap membrane distillation (AGMD) in separating toluene from synthetic water. A hydrophobic PTFE membrane in a flat sheet configuration was employed. The study explored the impact of operational variables viz. feed inlet temperature and feed flow rate on two key parameters—permeate flux and selectivity. The results revealed that the permeate flux exhibited an exponential rise as the feed inlet temperature was raised from 40 to 60 °C. Additionally, a notable finding was that a smaller air gap width of 3 mm led to higher permeate flux. Conversely, when feed flow rate was increased from 1 to 5 L/min, the permeate flux increased considerably, ranging from 2.69 kg/(m<sup>2</sup>h) to 3.7 kg/(m<sup>2</sup>h). For optimal outcomes, it is advisable to operate the setup at feed temperature of 60 °C and flow rate of 5 L/min to achieve a high permeate flux. The separation performance of AGMD was substantiated by the selectivity results, with toluene exhibiting a significantly higher presence in the permeate compared to the feed. This suggests effective separation of toluene through AGMD. Under specific conditions, the maximum total permeate flux was 4.65 kg/(m<sup>2</sup>h). Extended operation of 250 h revealed minimum organic fouling on membrane surface, which was notably reduced after water wash.

## Abbreviations

AGMD	Air gap membrane distillation
CWT	Cooling water temperature
CWFR	Cooling water flow rate
FFR	Feed flow rate
AGW	Air gap width
PTFE	Poly-tetra-fluoro-ethylene
FESEM	Field emission scanning electron microscopy
EDS	Energy-dispersive spectroscopy

## References

1. D'Odorico P, Chiarelli DD, Rosa L, Bini A, Zilberman D, Rulli MC (2020) The global value of water in agriculture. *Proc Natl Acad Sci USA* 117(36):21985–21993. <https://doi.org/10.1073/pnas.2005835117>
2. He C et al (2021) Future global urban water scarcity and potential solutions. *Nat Commun* 12(1):1–11. <https://doi.org/10.1038/s41467-021-25026-3>
3. Yadav GS (2020) Estimation of water scarcity in Bundelkhand region of Madhya Pradesh: an inter-district analysis. *Int J Appl Soc Sci*. <https://doi.org/10.36537/IJASS/7.11>

4. Ungureanu N, Vlăduț V, Voicu G (2020) Water scarcity and wastewater reuse in crop irrigation. *Sustain* 12(21):1–19. <https://doi.org/10.3390/su12219055>
5. van Vliet MTH et al (2021) Global water scarcity including surface water quality and expansions of clean water technologies. *Environ Res Lett* 16(2):024020. <https://doi.org/10.1088/1748-9326/abbfc3>
6. Sandid AM, Bassyouni M, Nehari D, Elhenawy Y (2021) Experimental and simulation study of multichannel air gap membrane distillation process with two types of solar collectors. *Energy Convers Manag* 1(243):114431
7. Han L, Tan YZ, Netke T, Fane AG, Chew JW (2017) Understanding oily wastewater treatment via membrane distillation. *J Memb Sci* 539:284–294. <https://doi.org/10.1016/j.memsci.2017.06.012>
8. Duong HC, Cooper P, Nelemans B, Cath TY, Nghiem LD (2016) Evaluating energy consumption of air gap membrane distillation for seawater desalination at pilot scale level. *Sep Purif Technol* 166:55–62. <https://doi.org/10.1016/j.seppur.2016.04.014>
9. Fortunato L, Elcik H, Blankert B, Ghaffour N, Vrouwenvelder J (2021) Textile dye wastewater treatment by direct contact membrane distillation: Membrane performance and detailed fouling analysis. *J Memb Sci* 636:119552. <https://doi.org/10.1016/j.memsci.2021.119552>
10. Khalifa AE, Lawal DU (2015) Performance and optimization of air gap membrane distillation system for water desalination. *Arab J Sci Eng* 40(12):3627–3639. <https://doi.org/10.1007/s13369-015-1772-0>
11. Geng H, Wu H, Li P, He Q (2014) Study on a new air-gap membrane distillation module for desalination. *Desalination* 334(1):29–38. <https://doi.org/10.1016/j.desal.2013.11.037>
12. Wu B, Tan X, Teo WK, Li K (2005) Removal of benzene/toluene from water by vacuum membrane distillation in a PVDF hollow fiber membrane module. *Sep Sci Technol* 40(13):2679–2695. <https://doi.org/10.1080/01496390500283456>
13. Banat FA, Simandl J (1999) Membrane distillation for dilute ethanol: separation from aqueous streams. *J Memb Sci* 163(2):333–348. [https://doi.org/10.1016/S0376-7388\(99\)00178-7](https://doi.org/10.1016/S0376-7388(99)00178-7)
14. Banat FA, Al-Rub FA, Shannag M (1999) Simultaneous removal of acetone and ethanol from aqueous solutions by membrane distillation: prediction using the Fick's and the exact and approximate Stefan-Maxwell relations. *Heat Mass Trans* 35(5):423–431. <https://doi.org/10.1007/s002310050344>
15. Eryildiz B, Yuksekdag A, Korkut S, Zeytuncu B, Pasaoglu ME, Koyuncu I (2020) Effect of operating parameters on removal of boron from wastewater containing high boron concentration by vacuum assisted air gap membrane distillation. *J Water Process Eng* 1(38):101579. <https://doi.org/10.1016/j.jwpe.2020.101579>
16. Banat FA, Simandl J (1994) Theoretical and experimental study in membrane distillation. *Desalination* 95(1):39–52. [https://doi.org/10.1016/0011-9164\(94\)00005-0](https://doi.org/10.1016/0011-9164(94)00005-0)
17. Smith JM, Van Ness HC, Abbott MM and Swihart MT (2018) Phase Equilibrium : Introduction
18. El-badrawi HH, Hafez ES, Fayad M, Shafeek A (1980) Ultrastructure responses of human endometrium to inert and copper IUDs as viewed by scanning electron microscopy. *Contraceptive Deliv Syst* 1(2):103–111

# Experimental Study for Removal of Pb and Cu from Industrial Wastewater by Using Low-Cost Adsorbent (Banana Peel)



Sachin Mane, Sanjana Hibare, and Pooja Kumbhare

## 1 Introduction

The presence of heavy metals in industrial wastewater has been increasing with growth in industry and human activities. Due to huge industrialization, excess amount of heavy metals accumulate in the environment that has caused tremendous problem worldwide. The existence of heavy metals in industrial wastewater has been increasing with growth of industry and human activities [1–3]. Heavy metals have five times high density compared to water, i.e., heavy metals have 5 g/cu cm and that of water is 1 g/cu cm. These heavy metals are readily soluble in aquatic environments and thus can be easily taken in by living organisms. Heavy metals have tendency to bio-accumulate. Bio-accumulate means increase in concentration of chemicals in biological organism over the time period. Nowadays, removals of heavy metals have been legally enforced since they are non-degradable in nature. Heavy metals are toxic at even low concentrations. Conventional methods such as ion exchange, chemical precipitation, adsorption, ultrafiltration, coagulation, reverse osmosis, flocculation, and membrane filtration are currently used to effectively remove heavy metals from water. But these methods generate toxic sludge, disposal of which renders expensive and non-eco-friendly in nature. Bio-adsorbent, an adsorbent material made from biomass, has received remarkable attention due to its large surface area, abundant resources, several surface groups, cost-effective process, and safeguarding the environment [4–7].

Water pollution caused by technological advancements remains a major source of concern. With an increasing discharge of heavy metals from technological activities, many aquatic ecosystems deal with metal concentrations that exceed water quality standards. Metal pollution in water, including discharge, has decreased in many

---

S. Mane (✉) · S. Hibare · P. Kumbhare

Department of Civil Engineering, D. Y. Patil College of Engineering Akurdi, Savtribai Phule Pune University, Pune, India

e-mail: [sjmane@dypcoeakurdi.ac.in](mailto:sjmane@dypcoeakurdi.ac.in)

countries as a result of stricter legislation by improved treatment or purification technology, and modified industrial activities. As a result, regulations for the disposal of waste containing heavy metals have tightened by many countries [8–11].

Banana peel shows to be an effective adsorbent and can be used to clean water from the wide range of adsorbent. Biosorbent created from banana peels has been observed to remove cadmium, copper, chromium, and lead ions from aqueous solution. Adsorption of heavy metal ions occurs as a result of physiochemical interaction, basically formation of complexes or ion exchange between metal ions and functional groups existing on the cell surface of adsorbent [2, 3, 12]. An adsorbent is material or substance which is having the capability or propensity to adsorb other substances or materials. Adsorption is a sorption process in which specific adsorbents are selectively transferred from one phase to another. Biosorbents are biologically derived materials that can absorb certain substances, particularly pollutants.

Banana peel contains organic compounds like cellulose, chlorophyll pigments that help in removal of heavy metals effectively. Banana peels are brought from local market and processed in powdered form by crushing into small pieces and added with certain chemicals like potassium hydroxide to increase the sorption capacity and remove heavy metals from industrial wastewater [13–15].

## 2 Experimental Method

### 2.1 Preparation of Banana Peel Activated Carbon (BPAC)

Banana peels were brought from local market and then washed them with distilled water to remove impurities. Then, the cleaned banana peels were chopped into small pieces of 0.5–1 cm and sun-dried for about 3–4 days. After complete drying of banana peels, they are then transferred into furnace and heated for 230 °C for about 2 h. Then, it is allowed to cool at room temperature. Then, it is crushed into powder form. After crushing of banana peels, to convert it into activated carbon, powdered form was added with HCL solution and kept for 24 h.

### 2.2 Preparation of Filter

Constructed filter is as shown in Fig. 1. There are three number of acrylic material boxes of size 30 cm × 30 cm × 30 cm which were used to construct the filter model. As acrylic material is noncorrosive, it is used to construct the filter. To maintain flows by gravity, descending order is adopted to place these boxes. Knob is used to manage the flow rate of water in the filter. The first box collects raw water; after this, knob is adjusted so that water passes through the filter with a specific period. Layer of

**Fig. 1** Filter setup for banana peel filter



banana peel ash as filter is placed in the middle box, and the water is allowed to pass through this layer. After filtration, treated water is collected in third box [16].

For every run, 2000 ml of wastewater was used to treat into the filter. To determine the flow rate, time was recorded for the sample to infiltrate.

To determine flow rate, the bucket and stopwatch method was used. The value of flow rate is calculated by the bucket volume divided by the time taken to fill up the bucket. The flow rate measured was 0.01–0.04 L/min.

### ***2.3 Treatment of Heavy Metals Using Banana Peel Activated Carbon (BPAC)***

The textile wastewater that is tested in the laboratory before treatment was added in the overhead tank of model of about 2 L, and then the activated carbon powder is placed in the model of varying thickness of 5, 10, 15, and so on. Now, slowly the wastewater is allowed to pass at a velocity by continuous method and kept in the tank for time of 20, 30, 40 min, and so on. After the mentioned time, the sample is collected and tested in the laboratory accordingly.

Various test samples are taken by the following experiments: (a) by keeping time constant with varying discharge, (b) by keeping discharge constant with varying time, (c) by varying thickness of activated carbon bed, (d) by varying initial concentration of Pb and Cu.

Then the time, thickness and discharge at which the wastewater gives maximum efficiency is noted. Graphs are prepared accordingly to note the efficiency of Pb and Cu removal from wastewater.

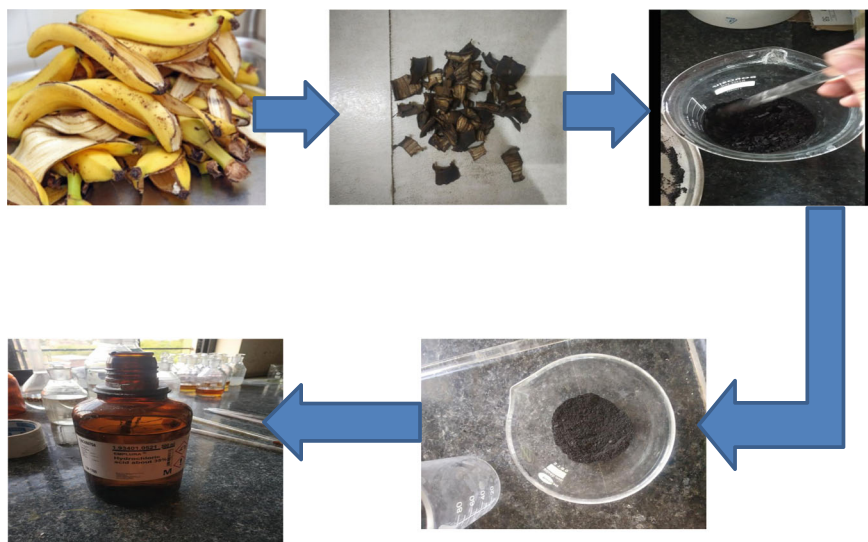


Fig. 2 Activation of banana peel carbon filter

### 3 Result and Discussions

#### 3.1 Characteristics of Banana Peel Activated Carbon

Figure 2 shows that there is a significant difference between banana peel before activation (Fig. 2) and after activation. The process of activation on banana peel is done physically through the combustion process using furnace at 230 °C for 2 h. Heating with high temperature serves to break the carbon chain of organic compounds with the help of heat, steam, and CO<sub>2</sub>. In this process, color changes from originally yellow to black.

In Figs. 3 and 4, we can see that the efficiency is at peak after 40 min contact time with wastewater. As per the basis of time, we can see that increase in the contact time gives maximum efficiency and the point at which there is no increase in efficiency is at 60 min. Pb has proved to give maximum results using activated banana peel. The maximum efficiency obtained is 92%.

Figures 5 and 6 give result of experiment in which time is kept constant at 50 min and varying discharge of about 2, 3, 4 L and so on. We can see that the optimum value is achieved at 4 L for both Pb and Cu removal.

The optimum value of time and discharge as 40 min and 4 L, respectively, were taken in next experiment. Test for various thickness of banana peel powder in activated carbon form in filter were carried out. From Figs. 7 and 8, the efficient thickness is observed 15 cm. The decrease in the value of efficiency after 15 cm thickness is due to media clogging.

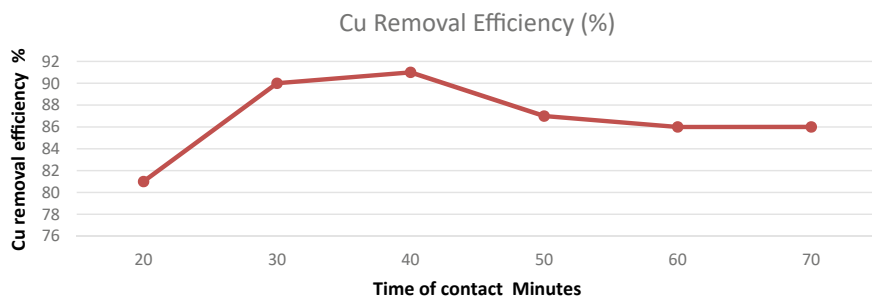


Fig. 3 Graph of Cu removal efficiency verses time of contact

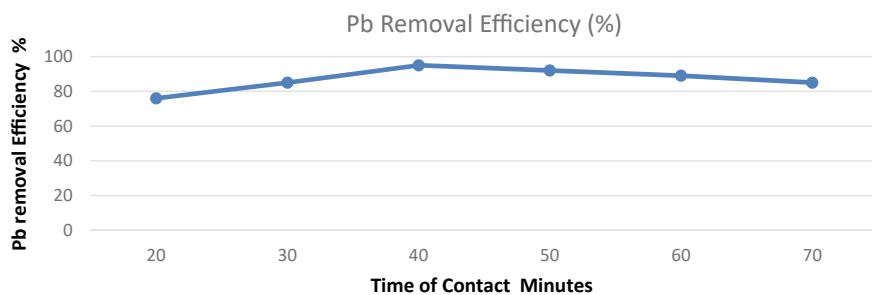


Fig. 4 Graph of Pb removal efficiency verses time of contact

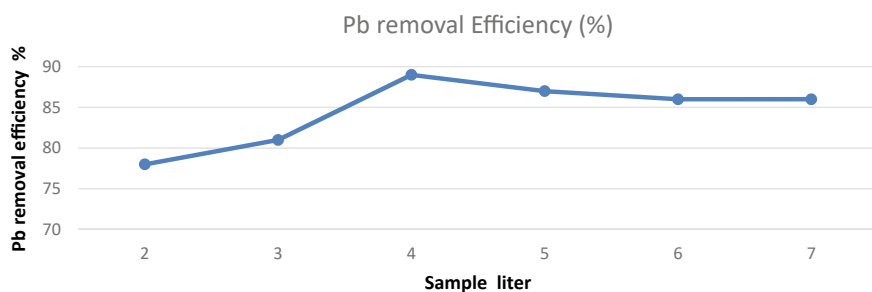


Fig. 5 Graph of Pb removal efficiency verses sample volume

From Figs. 9 and 10, it can be observed that at lowest initial concentration of Pb and Cu shows maximum removal efficiency by the prepared absorbent.

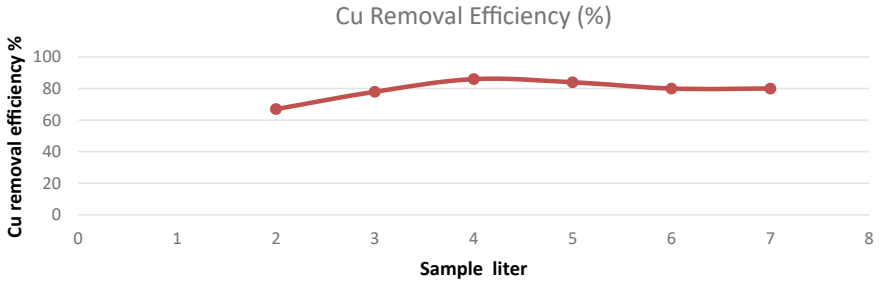


Fig. 6 Graph of Cu removal efficiency verses sample volume

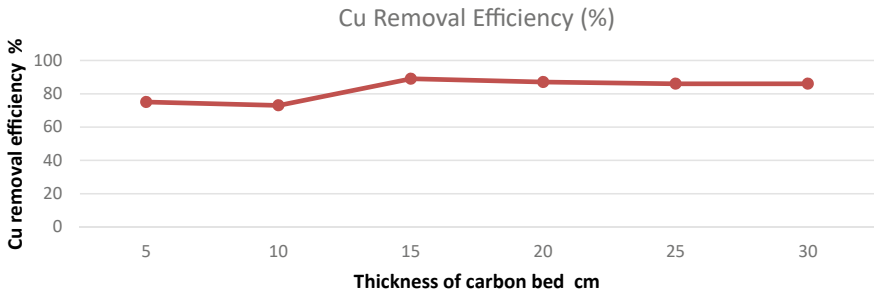


Fig. 7 Graph of Cu removal efficiency verses thickness of carbon bed

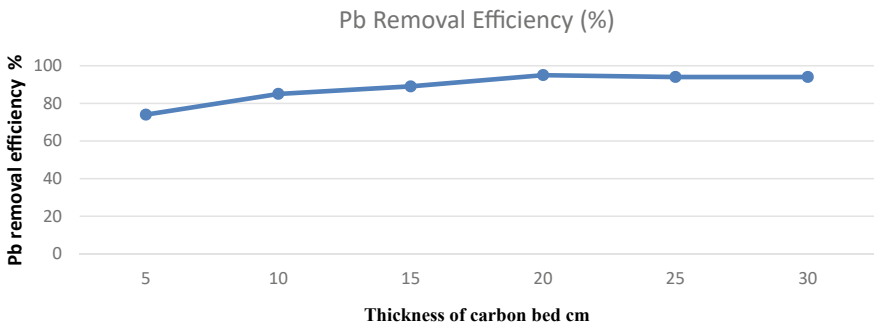


Fig. 8 Graph of Pb removal efficiency verses thickness of carbon bed

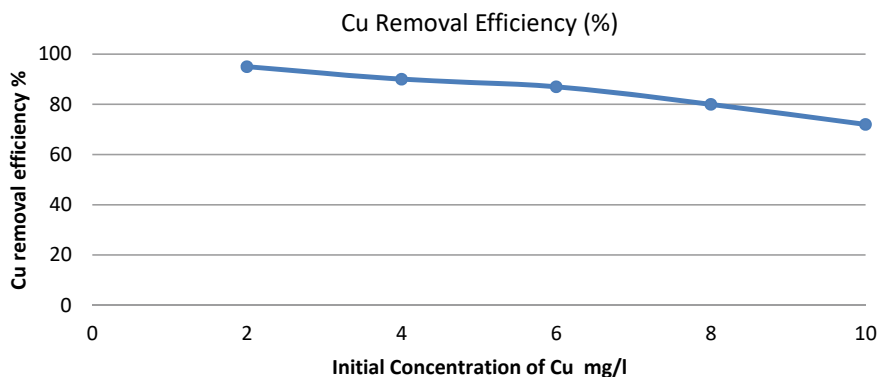


Fig. 9 Graph of Cu removal efficiency versus initial concentration of Cu

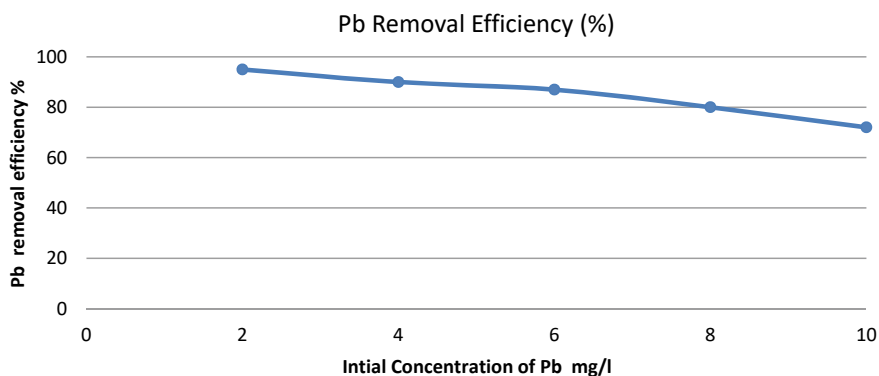


Fig. 10 Graph of Pb removal efficiency versus initial concentration of Pb

## 4 Conclusion

- Banana peel is a cheap and effective adsorbent for the adsorption of Pb ions and Cu ions from industrial wastewater by effectively converting into activated carbon form.
- The solution of HCL when added to banana peel powder helped in giving better efficiency to remove heavy metals.
- Banana peel contains hydroxyl, carboxyl, and glycosidic bond on the banana peels surface. Most of them are organic compounds due to electron richness of their positive charge metal ions bonded by these compound.
- It is concluded from the above results that banana peels give higher efficiency at 40 min for 4 L and a thickness of 15 cm for textile wastewater.

## References

1. Ali A (2017) Environmental nanotechnology, monitoring & management removal of Mn (II) from water using chemically modified banana peels as efficient adsorbent. *Environ Nanotechnol Monit Manag* 7:57–63
2. Thuan T, Thi B, Quynh P, Duy T, Thanh V (2017) Response surface methodology approach for optimization of  $\text{Cu}^{2+}$ ,  $\text{Ni}^{2+}$  and  $\text{Pb}^{2+}$  adsorption using KOH-activated carbon from banana peel. *Surf Interf* 6:209–217
3. Mohammed R, Chong M (2014) Treatment and decolorization of biologically treated palm oil mill effluent (POME) using banana peel as novel biosorbent. *J Environ Manage* 132:237–249
4. Babel S, Kurniawan T (2004) Cr(VI) removal from synthetic wastewater using coconut shell charcoal and commercial activated carbon modified with oxidizing agent and/or chitosan. *Chemosphere* 54(7):951–967
5. Tan W, Ooi S, Lee C (1993) Removal of chromium (VI) from solution by coconut husk and palm pressed fibers. *Environ Technol* 14(3):277–282
6. Mehmet E, Sukru D, Celalettin O, Mustafa K (2007) Heavy metal adsorption by modified oak sawdust thermodynamics and kinetics. *J Hazard Mater* 141(1):77–85
7. Chand D, Aggarwal VK, Kumar P (2005) Removal of hexavalent chromium. *J Appl Sci Environ Mgt* 9(1):123–126
8. Vaishnav V, Daga K, Chandra S, Lal M (2012) Adsorption studies of Zn (II) ions from wastewater using *Calotropis procera* as an adsorbent. *Res J Recent Sci* 1:160–165
9. Gupta VK, Gupta M, Sharma S (2001) Process development for the removal of lead and chromium from aqueous solution using red mud—an aluminum industry waste. *Water Res* 35(5):1125–1134
10. Nhapi I, Banadda N, Murenzi R, Sekomo CB, Wali UG (2011) Removal of heavy metal from industrial wastewater. *Open Environ Eng J* 4:170–180
11. Mallampati R, Adin LXA, Valiyaveetil S (2015) Fruit peels as efficient renewable adsorbents for removal of dissolved heavy metals and dyes. *ACS Sustain Chem Eng* 3(6):117–1124
12. Annadurai G, Juang RS, Lee DJ (2003) Adsorption heavy metals from water using banana and orange peels. *Water Sci Technol* 47(1):185–190
13. Darge A, Mane SJ (2015) Treatment of industrial wastewater by using banana peels and fish scales. *Int J Sci Res* 4(7):600–604
14. Sridhar N, Kumar S, Subburayan MR (2014) Removal of toxic metals (lead & copper) from automotive industry waste water by using fruit peels. *Int J* 1(2):2348–9928
15. Hossain MA, Ngo HH, Guo WS, Nguyen TV (2012) Biosorption of Cu(II) from water by banana peel based biosorbent: experiments and models of adsorption and desorption. *J Water Sustain* 2(1):87–104
16. Mane SJ, Kumbhare P, Pandav A (2024) Experimental study of treatment of kitchen waste water using rice husk ash. *Mater Today Proc*